Vol. 284, No. 1, December 20, 1993 ISSN 0003-2670

ANALYTICA CHIMICA ACTA

An international journal devoted to all branches of analytical chemistry

Editors: Harry L. Pardue (West Lafayette, IN, USA)
Alan Townshend (Hull, Great Britain)
J.T. Clerc (Berne, Switzerland)
Willem E. van der Linden (Enschede, Netherlands)
Paul J. Worsfold (Plymouth, Great Britain)

Associate Editor: Sarah C. Rutan (Richmond, VA, USA)

Editorial Advisers:

F.C. Adams, Antwerp
M. Aizawa, Yokohama
J.F. Alder, Manchester
C.M.G. van den Berg, Liverpool
A.M. Bond, Bundoora, Vic.
S.D. Brown, Newark, DE
J. Buffle, Geneva
P.R. Coulet, Lyon
S.R. Crouch, East Lansing, MI
R. Dams, Ghent
L. de Galan, Vlaardingen
M.L. Gross, Lincoln, NE
W. Heineman, Cincinnati, OH
G.M. Hieftje, Bloomington, IN
G. Horvai, Budapest
T. Imasaka, Fukuoka
D. Jagner, Gothenburg
G. Johansson, Lund
D.C. Johnson, Ames, IA
A.M.G. Macdonald, Birmingham
D.L. Massart, Brussels
P.C. Meier, Schaffhausen
M.E. Meyerhoff, Ann Arbor, MI
J.N. Miller, Loughborough
H.A. Mottola, Stillwater, OK
M.E. Munk, Tempe, AZ
M. Otto, Freiberg
D. Pérez-Bendito, Córdoba
C.F. Poole, Detroit, MI
J. Ruzicka, Seattle, WA
A. Sanz-Medel, Oviedo
S. Sasaki, Toyohashi
T. Sawada, Tokyo
K. Schügerl, Hannover
M.R. Smyth, Dublin
M. Thompson, Toronto
G. Tölg, Dortmund
Y. Umezawa, Tokyo
E. Wang, Changchun
J. Wang, Las Cruces, NM
H.W. Werner, Eindhoven
O.S. Wolfbeis, Graz
Yu.A. Zolotov, Moscow
J. Zupan, Ljubljana

ELSEVIER

ANALYTICA CHIMICA ACTA

Scope. *Analytica Chimica Acta* publishes original papers, *rapid publication letters* and reviews dealing with every aspect of modern analytical chemistry. Reviews are normally written by invitation of the editors, who welcome suggestions for subjects. Letters can be published within **four months** of submission. For information on the Letters section, see inside back cover.

Submission of Papers

Americas

Prof. Harry L. Pardue
Department of Chemistry
1393 BRWN Bldg, Purdue University
West Lafayette, IN 47907–1393
USA

Tel:(+1-317) 494 5320
Fax:(+1-317) 496 1200

Computer Techniques

Prof. J.T. Clerc
Universität Bern
Pharmazeutisches Institut
Baltzerstrasse 5, CH-3012 Bern
Switzerland

Tel:(+41-31) 654171
Fax:(+41-31) 654198

Prof. Sarah C. Rutan
Department of Chemistry
Virginia Commonwealth University
P.O. Box 2006
Richmond, VA 23284-2006
USA
Tel:(+1-804) 367 1298
Fax:(+1-804) 367 7517

Other Papers

Prof. Alan Townshend
Department of Chemistry
The University
Hull HU6 7RX
Great Britain

Tel:(+44-482) 465027
Fax:(+44-482) 466410

Prof. Willem E. van der Linden
Laboratory for Chemical Analysis
Department of Chemical Technology
Twente University of Technology
P.O. Box 217, 7500 AE Enschede
The Netherlands
Tel:(+31-53) 892629
Fax:(+31-53) 356024

Prof. Paul Worsfold
Dept. of Environmental Sciences
University of Plymouth
Plymouth PL4 8AA
Great Britain

Tel:(+44-752) 233006
Fax:(+44-752) 233009

Submission of an article is understood to imply that the article is original and unpublished and is not being considered for publication elsewhere. *Anal. Chim. Acta* accepts papers in English only. There are no page charges. Manuscripts should conform in layout and style to the papers published in this issue. See inside back cover for "Information for Authors".

Publication. *Analytica Chimica Acta* appears in 16 volumes in 1994 (Vols. 281–296). *Vibrational Spectroscopy* appears in 2 volumes in 1994 (Vols. 6 and 7). Subscriptions are accepted on a prepaid basis only, unless different terms have been previously agreed upon. It is possible to order a combined subscription (*Anal. Chim. Acta* **and** *Vib. Spectrosc.*).
Our p.p.h. (postage, packing and handling) charge includes surface delivery of all issues, except to subscribers in the U.S.A., Canada, Australia, New Zealand, China, India, Israel, South Africa, Malaysia, Thailand, Singapore, South Korea, Taiwan, Pakistan, Hong Kong, Brazil, Argentina and Mexico, who receive all issues by air delivery (S.A.L.–Surface Air Lifted) at no extra cost. For Japan, air delivery requires 25% additional charge of the normal postage and handling charge; for all other countries airmail and S.A.L. charges are available upon request.

Subscription orders. Subscription prices are available upon request from the publisher. Subscription orders can be entered only by calendar year and should be sent to: Elsevier Science Publishers B.V., Journals Department, P.O. Box 211, 1000 AE Amsterdam, The Netherlands. Tel: (+31-20) 5803 642, Telex: 18582, Telefax: (+31-20) 5803598, to which requests for sample copies can also be sent. Claims for issues not received should be made within six months of publication of the issues. If not they cannot be honoured free of charge. Readers in the U.S.A. and Canada can contact the following address: Elsevier Science Publishing Co. Inc., Journal Information Center, 655 Avenue of the Americas, New York, NY 10010, U.S.A. Tel: (+1-212) 6333750, Telefax: (+1-212) 6333990, for further information and free sample copy of this or any other Elsevier Science Publishers journal.
Advertisements. Advertisement rates are available from the publisher on request.

US mailing notice – Analytica Chimica Acta (ISSN 0003-2670) is published biweekly by Elsevier Science Publishers (Molenwerf 1, Postbus 211, 1000 AE Amsterdam). Annual subscription price in the USA US$ 3035.75 (valid in North, Central and South America), including air speed delivery. Second class postage paid at Jamaica, NY 11431. *USA Postmasters*: Send address changes to Anal. Chim. Acta, Publications Expediting, Inc., 200 Meacham Av., Elmont, NY 11003. Airfreight and mailing in the USA by Publication Expediting.

ANALYTICA CHIMICA ACTA

An international journal devoted to all branches of analytical chemistry

(Full texts are incorporated in CJELSEVIER, a file in the Chemical Journals Online database available on STN International; Abstracted, indexed in: Aluminum Abstracts; Anal. Abstr.; Biol. Abstr.; BIOSIS; Chem. Abstr.; Curr. Contents Phys. Chem. Earth Sci.; Engineered Materials Abstracts; Excerpta Medica; Index Med.; Life Sci.; Mass Spectrom. Bull.; Material Business Alerts; Metals Abstracts; Sci. Citation Index)

VOL. 284 NO. 1 CONTENTS DECEMBER 20, 1993

Electroanalytical Chemistry and Sensors

Quality classification of grain using a sensor array and pattern recognition
J.R. Stetter, M.W. Findlay, Jr., K.M. Schroeder, C. Yue and W.R. Penrose (Naperville, IL, USA) 1

Electrochemical behaviour of nitrobenzene in aqueous ethanol studied by differential pulse polarography
K.J. Kippax-Davis, M. Bully, A. Economou, P.R. Fielden, A.F.R. Watson and J.F. Alder (Manchester, UK) 13

Amperometric glucose biosensor based on an electrocatalytically bulk-modified epoxy-graphite biocomposite
F. Céspedes, E. Martínez-Fàbregas and S. Alegret (Bellaterra, Spain) 21

Chromatography

Analyte identification in ion chromatography. Electromigration governed chronoamperometric profiles
H. Sato and P.K. Dasgupta (Lubbock, TX, USA) 27

Column chromatographic separation of Y^{3+} from Sr^{2+} by polymeric ionizable crown ether resins
D.J. Wood, S. Elshani, C.M. Wai (Moscow, ID, USA), R.A. Bartsch (Lubbock, TX, USA), M. Huntley and S. Hartenstein (Idaho Falls, ID, USA) 37

Separation, identification and assay of fluradoline hydrochloride in the presence of other tricyclic antidepressants or neuroleptics by spectral and thin-layer and liquid chromatographic methods
J. Joseph-Charles and M. Bertucat (Bordeaux, France) 45

Determination of phenol and monochlorophenols in water by reversed-phase liquid chromatography
B. Makuch, K. Gazda and M. Kamiński (Gdańsk, Poland) 53

Separation of aqueous polythionates by reversed-phase ion-pair liquid chromatography with suppressor–conductivity detection
H. Zou (Dalian, China), Z. Jia (Beijing, China), Y. Zhang and P. Lu (Dalian, China) 59

On-line trace enrichment for the determination of ethacrynic acid in urine by liquid chromatography and column-switching
P. Campíns-Falcó, R. Herráez-Hernández and A. Sevillano-Cabeza (Burjassot, Spain) 67

Chromatographic pattern recognition for the analysis of complex mixtures
M.K. Park, J.H. Cho, N.Y. Kim and J.H. Park (Seoul, South Korea) 73

Chemometrics

Extracting information from complex chromatographic fingerprints for evaluation of organic air pollution
C. Armanino, M. Forina (Genova, Italy), L. Bonfanti (Pisa, Italy) and M. Maspero (Segrate, Italy) 79

Drift correction for pattern classification with neural networks
J.R.M. Smits, W.J. Melssen, M.W.J. Derksen and G. Kateman (Nijmegen, Netherlands) 91

Automatic polarographic elucidation of electrode mechanisms by means of a knowledge-based system. Part 4. Elucidation of mechanisms of newly synthesized compounds
M.J. Pałys, M. Bos and W.E. Van der Linden (Enschede, Netherlands) 107

Studying aerosol samples by non-linear mapping of electron probe microanalysis data
B. Treiger, H. Van Malderen, I. Bondarenko, P. Van Espen and R. Van Grieken (Antwerpen-Wilrijk, Belgium) 119

(Continued overleaf)

- 4 ก.พ. 2537

Contents (continued)

Use of the spectral trace length in determining the concentration of known compounds in complex mixtures
F.R. Burden (Clayton, Vic., Australia) 125
Expert system for the interpretation of infrared spectra
G.N. Andreev, O.K. Argirov and P.N. Penchev (Plovdiv, Bulgaria) 131

Infrared Spectrometry
Chemical composition analysis of carrageenans by infrared spectroscopy using partial least squares and neural networks
S.P. Jacobsson and A. Hagman (Stockholm, Sweden) 137

Kinetic Methods
Micellar effects on reaction kinetics. Part I. Simultaneous determination of chromium(VI), vanadium(V) and titanium(IV)
D. Sicilia, S. Rubio and D. Pérez-Bendito (Córdoba, Spain) 149

Flow Systems
Stopped-flow, air-segmented continuous flow: kinetic determinations of glucose and phosphate in wine and serum samples
Y.-S. Hsieh and S.R. Crouch (East Lansing, MI, USA) 159
Continuous-flow method for the determination of total inorganic carbonate in water
T. Aoki, Y. Fujimaru, Y. Oka and K. Fujie (Sakai, Japan) 167
Flow-injection determination of oxalate by a photoinduced chemiluminescent reaction
T. Pérez-Ruiz, C. Martinez-Lozano, A. Sanz and O. Val (Murcia, Spain) 173
Determination of traces of copper, cadmium and lead in biological and environmental samples by flow-injection isotope dilution inductively coupled plasma mass spectrometry
P.-L. Lu, K.-S. Huang and S.-J. Jiang (Kaohsiung, Taiwan) 181
Determination of dissolved oxygen by use of a spectrophotometric flow-through sensor
A. Sanz-Martínez, A. Ríos and M. Valcárcel (Córdoba, Spain) 189

Spectrophotometry and Fluorimetry
Spectrophotometric determination of antimony after extraction of Brilliant Green hexachloroantimonate(V) with microcrystalline 1,4-dichlorobenzene
D.T. Burns, D. Chimpalee and H.J. Bullick (Belfast, UK) 195
Trace metal determinations by spectrophotometry with a double chromogenic system and a chemometric approach
Y. Ni (Nanchang, China) 199
Sensitive, fluorescent detection of hydrazine via derivatization with 2,3-naphthalene dicarboxaldehyde
G.E. Collins (Fort Washington, MD, USA) and S.L. Rose-Pehrsson (Washington, DC, USA) 207

Electrophoresis
Method development and optimization for the determination of rare earth metal ions by capillary zone electrophoresis
M. Jimidar, T. Hamoir, W. Degezelle, D.L. Massart, S. Soykenç and P. Van de Winkel (Brussels, Belgium) 217

Immunoassay
High sensitive microcapsule immunoassay for protein antigens or antibodies
Y. Ishimori (Kawasaki, Japan) and K. Rokugawa (Tochigi-ken, Japan) 227

Extraction
Selectivity and yields in supercritical fluid extraction of tar-mats and source rocks
M. Skurdal, M. Østbye and T. Greibrokk (Oslo, Norway) 235

Book Reviews 241

ANALYTICA CHIMICA ACTA
VOL. 284 (1993)

ANALYTICA CHIMICA ACTA

An international journal devoted to all branches of analytical chemistry
Revue internationale consacrée à tous les domaines de la chimie analytique
Internationale Zeitschrift für alle Gebiete der analytischen Chemie

Editors: Harry L. Pardue (West Lafayette, IN, USA)
Alan Townshend (Hull, Great Britain)
J.T. Clerc (Berne, Switzerland)
Willem E. van der Linden (Enschede, Netherlands)
Paul J. Worsfold (Plymouth, Great Britain)

Associate Editor: Sarah C. Rutan (Richmond, VA, USA)

Editorial Advisers:

F.C. Adams, Antwerp
M. Aizawa, Yokohama
J.F. Alder, Manchester
C.M.G. van den Berg, Liverpool
A.M. Bond, Bundoora, Vic.
S.D. Brown, Newark, DE
J. Buffle, Geneva
P.R. Coulet, Lyon
S.R. Crouch, East Lansing, MI
R. Dams, Ghent
L. de Galan, Vlaardingen
M.L. Gross, Lincoln, NE
W. Heineman, Cincinnati, OH
G.M. Hieftje, Bloomington, IN
G. Horvai, Budapest
T. Imasaka, Fukuoka
D. Jagner, Gothenburg
G. Johansson, Lund
D.C. Johnson, Ames, IA
A.M.G. Macdonald, Birmingham
D.L. Massart, Brussels
P.C. Meier, Schaffhausen
M.E. Meyerhoff, Ann Arbor, MI
J.N. Miller, Loughborough
H.A. Mottola, Stillwater, OK
M.E. Munk, Tempe, AZ
M. Otto, Freiberg
D. Pérez-Bendito, Córdoba
C.F. Poole, Detroit, MI
J. Ruzicka, Seattle, WA
A. Sanz-Medel, Oviedo
S. Sasaki, Toyohashi
T. Sawada, Tokyo
K. Schügerl, Hannover
M.R. Smyth, Dublin
M. Thompson, Toronto
G. Tölg, Dortmund
Y. Umezawa, Tokyo
E. Wang, Changchun
J. Wang, Las Cruces, NM
H.W. Werner, Eindhoven
O.S. Wolfbeis, Graz
Yu.A. Zolotov, Moscow
J. Zupan, Ljubljana

Anal. Chim. Acta, Vol. 284 (1993)

ELSEVIER, Amsterdam–London–New York–Tokyo

© 1993 ELSEVIER SCIENCE PUBLISHERS B.V. ALL RIGHTS RESERVED

0003-2670/93/$06.00

No part of this publication may be reproduced, stored in a retrieval system or transmitted in any form or by any means, electronic, mechanical, photocopying, recording or otherwise, without the prior written permission of the publisher, Elsevier Science Publishers B.V., Copyright and Permissions Dept., P.O. Box 521, 1000 AM Amsterdam, The Netherlands.

Upon acceptance of an article by the journal, the author(s) will be asked to transfer copyright of the article to the publisher. The transfer will ensure the widest possible dissemination of information.

Special regulations for readers in the U.S.A.–This journal has been registered with the Copyright Clearance Center, Inc. Consent is given for copying of articles for personal or internal use, or for the personal use of specific clients. This consent is given on the condition that the copier pays through the Center the per-copy fee for copying beyond that permitted by Sections 107 or 108 of the U.S. Copyright Law. The per-copy fee is stated in the code-line at the bottom of the first page of each article. The appropriate fee, together with a copy of the first page of the article, should be forwarded to the Copyright Clearance Center, Inc., 27 Congress Street, Salem, MA 01970, U.S.A. If no code-line appears, broad consent to copy has not been given and permission to copy must be obtained directly from the author(s). All articles published prior to 1980 may be copied for a per-copy fee of US $2.25, also payable through the Center. This consent does not extend to other kinds of copying, such as for general distribution, resale, advertising and promotion purposes, or for creating new collective works. Special written permission must be obtained from the publisher for such copying.

No responsibility is assumed by the publisher for any injury and/or damage to persons or property as a matter of products liability, negligence or otherwise, or from any use or operation of any methods, products, instructions or ideas contained in the material herein.

Although all advertising material is expected to conform to ethical (medical) standards, inclusion in this publication does not constitute a guarantee or endorsement of the quality or value of such product or of the claims made of it by its manufacturer.

This issue is printed on acid-free paper.

PRINTED IN THE NETHERLANDS

Analytica Chimica Acta, 284 (1993) 1–11
Elsevier Science Publishers B.V., Amsterdam

Quality classification of grain using a sensor array and pattern recognition

J.R. Stetter, M.W. Findlay, Jr., K.M. Schroeder, C. Yue and W.R. Penrose
Transducer Research, Inc., 999 Chicago Avenue, Naperville, IL 60540 (USA)

(Received 15th September 1992; revised manuscript received 13th July 1993)

Abstract

Measurements using arrays of electrochemical gas sensors, combined with pattern recognition methods, were used to classify wheat samples by quality grade. The classifications corresponded closely to those made by trained grain inspectors. Volatile compounds evolved from warmed samples of grain were passed over a heated noble metal catalyst and then into a series of electrochemical sensors. Signals from four sensors were recorded for four different catalyst temperatures in order to generate 16 signals for each grain odor sample. The 16 sensor signals were treated as a 16-dimensional vector or pattern of responses that was characteristic of the odor sample. The patterns for different grain odor samples were compared using both nearest-neighbor analysis and a commercial neural network simulation (NNS) program. These methods classified the samples correctly by grade with an accuracy of 68% and 65%, respectively. After compensation for instrument parameters, the NNS score improved to 83%; the nearest-neighbor analysis could not be similarly compensated. The robustness of the two algorithms was compared by adding simulated random and systematic errors to the sensor response patterns. The original data were used as the training set, and the patterns with errors added were used as the test set. In these cases, the NNS consistently outperformed the nearest-neighbor method at classification of the grain odor samples.

Keywords: Pattern recognition; Sensors; Grain; Quality classification

All grain exported from the United States must by law be inspected by agents of the Federal Grain Inspection Service (FGIS), US Department of Agriculture, while being loaded into the ships, holds. Additionally, there are inspectors who are certified by the FGIS who may be hired to inspect grain during domestic transfers of custody. A subjective judgment of odor is used by the FGIS as a primary criterion of the fitness of grain for human consumption. An experienced inspector inhales from a sample of the grain and evaluates the grain as Good, Sour, or Musty. Internally, additional designations, such as COFO (commercially objectionable foreign odor) are also used. Should a sample be classified as bad due to odor or any of the other parameters being monitored, loading of the ship is halted, and the grain already on the ship must be unloaded.

Because these evaluations frequently involve large sums of money, there is an appeal process which delays and confuses the task of grain grading. A sample of the grain in question is sent to the FGIS Board of Appeals and Review, where a panel of inspectors grades the sample. The final classification is the average of the individual judgments of the inspectors.

Subjective judgments are difficult to defend in an adversarial environment, and the USDA has searched for more objective means of evaluating the quality of a sample of grain. It is recognized that this is a philosophical contradiction, since

Correspondence to: M. Findlay, Jr., Transducer Research, Inc., 999 Chicago Avenue, Naperville, IL 60540 (USA).

0003-2670/93/$06.00 © 1993 – Elsevier Science Publishers B.V. All rights reserved

the subjective olfactory evaluation is necessarily the "primary standard" in the analysis. Nevertheless, the ability to produce a consistent judgment of grain quality will provide a credible support for the human inspector's judgment – and it would continue to do so even if the inspector has a cold. In addition, concerns have been expressed for the health effects of grain dust and odorous volatiles on the inspectors themselves [1].

Attempts have been made to develop objective estimates of grain odor based on specific analysis of volatiles emitted from grain samples. Gas chromatography (GC) and gas chromatography–mass spectrometry (GC–MS) methods have been used in attempts to correlate specific compounds or groups with subjective odor analyses [2,3]. After analysis of more than 300 samples by GC–MS, "no relationship between the chemical composition and the odor could be found" [2]. The odor classification apparently is not related to the presence of single compounds in quantities large enough to be measured; the large number of volatile compounds emitted even from "good" grain seems to mask the odor-causing con-

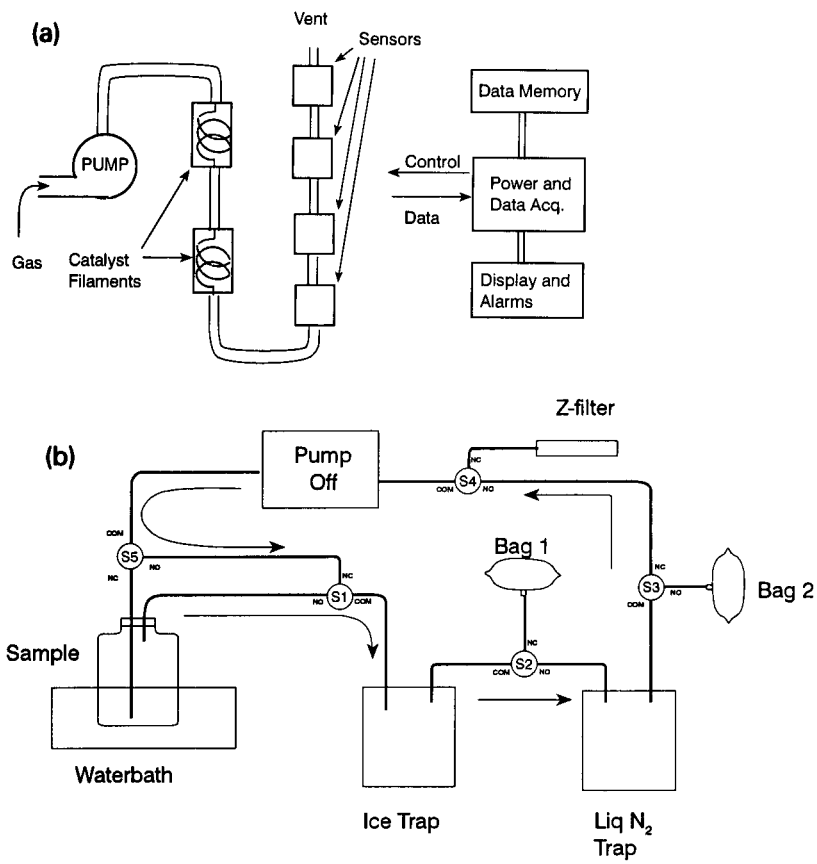

Fig. 1. (a) Schematic of the CPS-100 chemical parameter spectrometer. The sample is drawn in with an air pump at 200 ml/min and passed over a rhodium filament. Four amperometric gas sensors of different selectivities are used to measure the reactive compounds in the gas stream. Sensor 1: platinum sensing electrode at a bias of +1.15 V vs. the SHE; Sensor 2: platinum at a bias of 1.02 V; Sensor 3: thin film gold electrode at a bias of 1.3 V; Sensor 4: high surface area gold electrode at bias of 1.3 V. Data channels are identified as $S_{i,j}$, where i = the filament mode, and j = sensor number. (b) Diagram of sampling apparatus used to fractionate and concentrate grain vapors. The two fractions (ice trap = volatiles; liquid N_2 = non-volatiles) were desorbed into separate bags by raising the traps to 60°C and room temperature, respectively, and purging with 1 l of air.

stituents. Or, perhaps, some of the most important odorous compounds are not amenable to GC or GC–MS analysis.

Olfaction in animals seems to depend on the pattern of responses from a relatively few types of receptors. Attempts have been made to mimic olfaction in artificial systems by correlating the responses of chemical sensors. A solid-state semiconductor (SSS) sensor has been used to estimate the "freshness" of fish [4]; a single sensor can give a measure of intensity, but cannot characterize an odor. Arrays of SSS sensors have been used to characterize and differentiate odors from foods and fragrances [5], and from liquors [6]. Pyrolysis–mass spectrometry and pyrolysis–GC–MS have been used to identify species of grass seeds [7] and even individual cultivars of grains [8]. In all of these methods, pattern recognition at various levels of sophistication were used to perform the actual discrimination. A recent conference was held to summarize the advances in development of artificial olfactory systems [9].

We have previously and successfully explored the use of arrays of electrochemical sensors to identify single compounds and specific mixtures of chemical compounds [10–14]. The sensor array technology (termed chemical parameter spectrometry, or CPS) was used for all the experiments reported here. In CPS, a sample of

dilute vapor is pyrolyzed on a heated catalyst of platinum or rhodium, then passed through an array of four electrochemical gas sensors with different selectivities (Fig. 1). By systematically varying the catalyst metal and temperature, and measuring the resulting sensor outputs, a collection of data points (a "pattern") is obtained on each sample. A simple pattern recognition algorithm, nearest-neighbor analysis, can be used to identify unknowns from a library of known patterns. It appeared that pyrolysis resulted in the formation of electroactive compounds, so that all organic compounds responded on the system, even those that are not normally electroactive. In most cases, the patterns were unique.

The success of the CPS method was limited by the long-term stability of the sensors, as well as the inability of the simple system to identify components of mixtures. Mixtures of two or more compounds gave response patterns that were distinct from those of either of the components of the mixture and that would vary with the ratios of the components [15]. It occurred to us that this limiting phenomenon was similar to olfaction, in which new aromas can be created by mixing oth-

TABLE 1

Samples of wheat used in these experiments and the consensus grades given by panels of USDA inspectors

Sample	Olfactory analysis by GMRL inspectors	Consensus grade	Intensity	Notes [a]
F41	C2/G/G/G	G	-	1
F42	G/G/M1/C2	G	-	
F67	G/M1/G/G	G	-	
F78	G/G/M2/G	G	-	
F128	G/G/G/G	G	-	
F30	I3/I3/I3/I3	I	3.0	
F39	I2/C3/I2/C1	I	2.0	
F69	I1/I2/I2/M3	I	2.0	
F89	I3/I3/I2/S3	I	2.7	
N53	I2/S3/S2/S3	S	2.8	2
N166	S3/S3/S3/S3	S	2.9	2
N168	S2/S3/S2/S2	S	2.6	2

[a] Note 1: Intensities range from 0 for a definite Good grade to 3 for a definite off-odor. Odor descriptors used are: G = Good, M = Musty, I = Insect, S = Sour, and C = COFO (commercially objectionable foreign odor). Note 2: These three samples were also evaluated by five Federal Grain Inspection Service inspectors. The average intensities are for all nine inspectors. Note 3: Deviations from consensus grade occurred 8 of 48 times or 17%, with 83% agreement on consensus grades. Note 4: Data and samples were provided by L. Seitz and D. Saur, Grain Marketing Research Laboratory, Manhattan, KS.

ers. An olfactory response, such as the smell of a sample of grain, is not so different in principle than the response of CPS to a mixture of organic compounds. In addition, the rapid development of small, low-cost computing power and of pattern recognition methodology in recent years has encouraged us to explore more advanced data analysis methods that might overcome the long-term sensor drift problems encountered in early investigations.

This work is the result of a feasibility study of the application of CPS to the mimicking of human olfaction. We have measured the CPS patterns of several grain samples of known quality. Two pattern analysis methods, **K**-nearest-neighbor analysis and a neural network simulation (NNS) program, were used to correlate the patterns with the subjective quality grades. The robustness of each method was tested by introducing random and systematic errors into the patterns.

EXPERIMENTAL

Grain samples

Samples of wheat were provided by the Grain Marketing Research Laboratory (GMRL, U.S. Department of Agriculture, Manhattan, KS). These samples had been graded by one or both of two separate panels of experts (Federal Grain Inspection Service (FGIS) inspectors, and GMRL scientists). The summary of their evaluations is given in Table 1. These evaluations are considered "standards" for the purpose of this study, although it is clear from these data that the experts were rarely unanimous on the quality or intensity of the odor. Because these samples were used for several purposes at GMRL, the number, types, and amounts of samples available to this feasibility study were limited. Three "odor descriptions" (as opposed to official grades) were available, named Good, Insect, and Sour.

Collection of volatiles from grain samples

Samples of grains (40 g) were heated to 60°C in a closed glass container. A total volume of ten liters of air was recirculated continuously through the container as well as through an ice trap and a liquid N_2 trap. The condensed volatiles from each trap were separately evaporated into 600 cc of air and saved in Tedlar gas sample bags. This procedure resulted in an approximately tenfold concentration of the vapors from the original volume of air used to purge the sample. The fractions were labelled NI (not filtered, ice trap) and NL (not filtered, liquid N_2 trap).

For some experiments, a chemically reactive filter was located between the grain chamber and the cold traps. The filter consisted of a $2'' \times 3''$ glass fiber filter (Whatman GF/B), previously wetted with 5% citric acid and dried. The corresponding fractions, from which basic and some neutral components were removed, were labelled FI (filtered, ice trap) and FL (filtered, liquid N_2 trap).

Grain odor pattern measurement

Grain odor patterns were gathered using a Model CPS-100, built by Transducer Research, Inc. All operations during the data collection phase were automatic. The CPS-100 contained an array of four electrochemical sensors, as previously reported [11,13]. Figure 1 illustrates the functional layout of the CPS-100. A rhodium filament (0.1 mm diameter × 8 cm in length) was used as the catalyst. For each sample measurement, the catalyst was operated in four modes of 20 s duration each. In Mode 1, the filament was cold; in Modes 2, 3, and 4, the filament was operated at 450, 700, and 800°C, respectively. At the end of each mode, the outputs of the four sensors were stored in the CPS-100 for later transfer to a desktop computer. Each pattern therefore consisted of 16 responses, or channels. Baseline patterns were run prior to each analysis using zero grade air in order to establish the responses of the system with no sample present. These baseline patterns were subtracted element-by-element from the subsequent sample pattern.

The apparatus was first tested with several concentrations of hydrogen sulfide, carbon monoxide, and ethanol in air, to establish that the sensors and catalysts were giving repeatable and well-behaved responses. From time to time during analysis of the grain odor vapors, patterns

were obtained using hydrogen sulfide samples to monitor the long-term behavior of the sensors. We also considered that the hydrogen sulfide data might later be used to correct for long-term drift (aging) of the sensors.

The odor fractions from the grain samples (ca. 600 cc) were sufficient for at least two replicate analyses in this system. Test runs using sorghum (because the standard wheat samples were scarce) confirmed that the entire process, from vapor generation and collection, to analysis, was repeatable to a precision of approximately 10% or better for each pattern vector element.

Patterns were labelled by the grain sample number and the method of collection (NI, NL, FI, FL). In addition, a 17th element was added to each pattern vector to encode the collection method into the data. This extra element (either 100, 200, 300, or 400) forced the pattern analysis algorithms to treat each fraction as a completely separate sample.

An 18th channel was utilized to indicate the state of the sensor array to the NNS. A 100 was placed in the 18th channel when data acquisition was initiated and was indexed by 100 (i.e., to 200, 300, 400, etc.) whenever a significant change in sensor performance was introduced. Therefore, when a sensor was replaced or its H_2S pattern drifted by more than 10%, the 18th channel was indexed.

K-nearest-neighbor (KNN) analysis

Nearest-neighbor analysis is the simplest case of **K**-nearest neighbor analysis, in which the unknown pattern is compared to each of **K** patterns obtained from each known standard. If $\mathbf{K} = 1$, the method becomes a computationally simple and powerful measure of similarity. The KNN method used with sensor array data has been described extensively [10,13,16].

KNN treats each pattern of 16 numbers as a vector in 16-dimensional space. Analysis consists of normalizing each vector to a constant length and computing the scalar distances between the vector of an unknown compound and each member of a library of normalized vectors derived from known compounds. A short distance presumably identifies the unknown with a likely compound. Moreover, inspection of the list of distances produces a graphic picture of the probability that the identification is correct, relative to other possibilities. Replicate vectors derived from the same compound typically yield very short distances when compared with each other. Because the vectors are normalized, this holds even if the concentrations of the vapors are different.

Our procedure for KNN analysis consisted of the following steps:

(1) Baseline correction. A valid baseline vector is subtracted from the raw sample vector.

(2) Normalization of the vectors. In each vector, the element with the largest absolute magnitude was set to $+127$ or to -127 (if negative). The other elements were scaled proportionately, so that the ratios between pairs of elements were maintained. Normalization had the effect of removing the concentration dependence of the individual responses, and was performed on all vectors, whether for known or unknown samples.

(3) Distance calculations. The scalar distance D was calculated between the vector of the unknown $\mathbf{X}$ $(x_1, x_2, \ldots x_{16})$ and each known compound $\mathbf{Y}$ $(y_1, y_2, \ldots y_{16})$ using the Pythagorean formula:

$$D = \sqrt{\Sigma(x_i - y_i)^2}$$

(4) The unknown is identified with one of the known compounds by selecting the known compound with the shortest distance to the unknown. This identification is tempered by the magnitude of **D**; the shorter the distance, the more definite the identification. If the shortest distance is greater than an arbitrary threshold, the unknown is considered to be associated with none of the known compounds.

The KNN method has proved effective in past work, but it has a major inconvenience. As the responses of the electrochemical sensors to various chemicals drifted with time, the array required complete recalibration; an entirely new library of known vectors had to be recreated from time to time. Moreover, there was no convenient way to cope with discontinuities in data collection, such as sensor replacement.

Neural network simulation (NNS) analysis

Neural network simulations (NNS) are essentially iterative type algorithms which apply weight factors to each channel of data. These algorithms evaluate the relationship between each channel and all other channels, via a network of fit parameters, usually called "nodes" [17]. NNS can handle either quantitative (analog) data where the magnitude of the numbers is of concern, or binary data, where each channel is either "on" or "off".

The features that made them attractive for our application were (1) a decision surface of arbitrary shape, and (2) simple updating of the training to account for drift and changes in the chemical sensors and catalysts. The decision surface in **n**–dimensional space defines the boundary between two possible classifications. The "recognition" in pattern recognition occurs when the unknown vector is located on one side or the other of the decision surface. In most pattern recognition methods, including KNN, the surface is a plane. In NNS analysis, the surface is defined by hyperspheres drawn around each point in the training set which touch only at their surfaces. The relative sizes of the spheres are adjusted during the training operation so that the largest volume of space is filled without overlapping. The decision surface can therefore assume any shape, and need not even be continuous. Adding or replacing data merely adjusts the response surface appropriately. This is a shorter operation than complete recalibration.

The NNS program used was NeuroShell 3.0 (Ward Systems Group, Frederick, MD). This product uses back-propagation, one of the more powerful NNS algorithms, to train the network. Baseline-corrected pattern vectors were submitted to the program as input data.

RESULTS

Sensor array response pattern analysis

The patterns resulting from the analysis of three samples of "Good" wheat are shown in Fig. 2. The raw sample vectors have been normalized and displayed as histograms to better demonstrate the relative variability of the pattern elements. The first four elements represent the responses of the sensors to the unpyrolyzed sample. For all four sensors, the responses were a significant fraction of the strongest response, indicating that the samples contained a large fraction of compounds that were electroactive without pyrolysis. The strong responses of the last two sensors, which do not normally respond to carbon–oxygen compounds, indicated that oxidizable nitrogen or sulfur compounds were probably present. The variation in the sample vectors indicated the range of variability of the Good category of wheat.

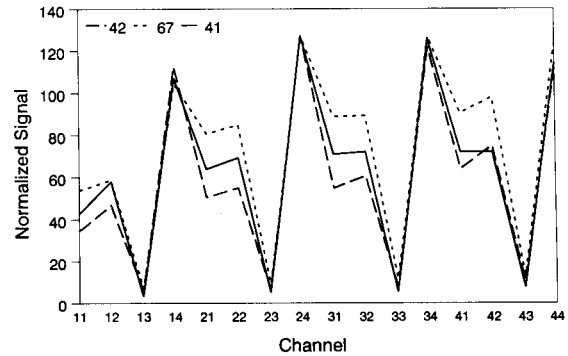

Fig. 2. Patterns produced by three samples of Good wheat, normalized so that the strongest channel is set to +127. See Fig. 1 for an explanation of channel numbers.

By contrast, the patterns from Good, Sour, and Insect grades of wheat displayed very large differences in both the shape and intensity of the resulting histograms (Fig. 3).

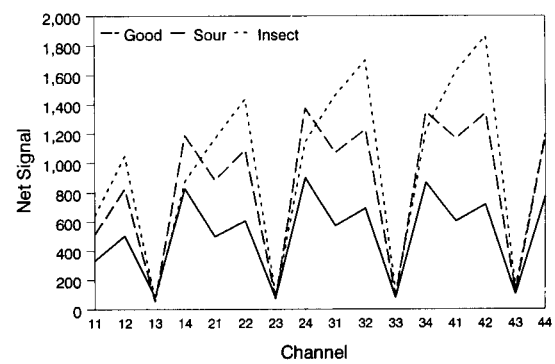

Fig. 3. Patterns from samples of Good, Sour, and Insect grades of wheat, not normalized to show differences in intensity.

TABLE 2

Make-up of data set patterns
[A total of 115 patterns were obtained for the 11 separate wheat samples using four different procedures (fraction types)]

Wheat Sample No.	Consensus grade	Fraction type			
		Liquid nitrogen trap/ filter	Liquid nitrogen trap/no filter	Ice trap/ filter	Ice trap/ no filter
128	Good	3	3	4	2
78	Good	1	3	1	3
42	Good	4	2	4	1
67	Good	2	2	2	2
41	Good	4	1	4	2
53	Sour	1	1	2	2
166	Sour	3	2	4	2
168	Sour	4	2	4	2
30	Insect	4	2	4	2
39	Insect	2	4	2	4
89	Insect	4	2	4	2
Total (115 sample runs)		32	24	35	24

Classification of grain samples by KNN and NNS

The number of grain samples available to us was not large enough to provide a large training data set and an entirely independent test data set. It was not practical, therefore, to calibrate the pattern analysis method on one set of samples, and then to challenge with independently obtained data. Nevertheless, the large differences in the pattern vectors for different wheat grades allowed us to effectively evaluate the CPS method. A total of 115 patterns were obtained for all samples and fractions as identified in Table 2.

The patterns obtained from the grain samples were subjected to several different data treatments. The order of these treatments is shown in Fig. 4. Pattern analysis was carried out on the data after the different treatments. The results of all the pattern analysis experiments are shown in Table 3.

KNN analysis was performed by first assembling a training set of normalized pattern vectors. Hence, each combination of sample and collection method was treated as an independent sample. All runs of the same fraction of a sample in the training set were averaged (element by element); the averaged pattern was used in the training set. When used for the NNS analysis, elements 17 (fraction type) and 18 (sensor changes) were included unless otherwise stated.

If the training set included all the available patterns, and was challenged with the same patterns, the success of identification was 100% for both KNN and NN. In Table 3, line 2, the data set was divided into separate training and test sets by sorting one pattern of each set of replicates into the test set. The training set then contained 55% of all the vectors, since there were usually more than two replicates on a sample. This analysis was performed using only the 16 channel response patterns from the array, the additional channels 17 and 18 were not included. The rate of successful classification by grade was similar for both KNN (68%) and NNS (65%). These scores were statistically significant and indicate that the patterns for different grades are different beyond the signal/noise limit of the measurement and that the pattern is specific for the odor using this sensor array approach.

Because of the nature of KNN, with its planar decision surface, the inclusion of an arbitrary element 17 or 18 to specify the fraction or to compensate for a change in the array make-up was not meaningful. However, in NNS practice, it

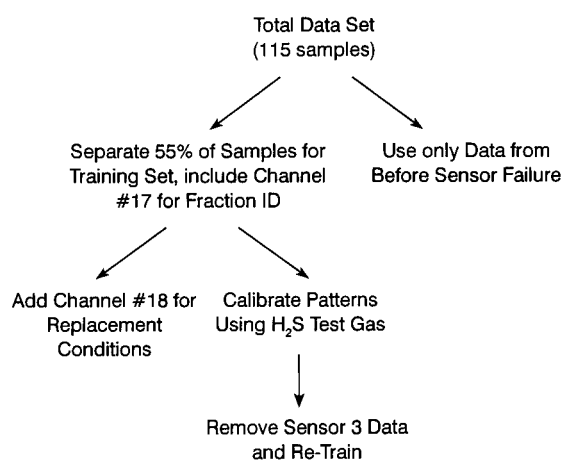

Fig. 4. Diagram of the post-treatment of the analytical data. Effects of these data treatments on the accuracy of the two pattern recognition methods is summarized in Table 3.

is quite easy to add channels of qualitative data to a row of quantitative values. This has the effect of creating new decision surfaces, any one of which can correctly classify an unknown. When the Channel 17 fraction type and Channel 18 sensor replacement parameters were included, the success of NNS classification of the patterns increased to 83%, which is approximately the rate at which human inspectors agreed with the consensus classifications (Table 1, Note 3).

In order to determine the degree to which the KNN classification may have been compromised by the failure of one of the sensors part way through the measurements, the analyses were repeated, with the data sets limited to data taken before the sensor failed (a total of 53 patterns). However, the success of correct classification actually fell to 58% for KNN, but stayed rather constant at 78% for the NNS method.

A second method was investigated for correcting for sensor drift and sensor changes. The array was periodically challenged with a low concentration of hydrogen sulfide, to which all four sensors responded. The change in response to H_2S over the course of the experiments was used to correct the sensitivity of the sensors to that at the beginning of the experiments. This strategy was unsuccessful, and caused a decrease in the rate of classification: 61% for KNN and 70% for NNS.

A final strategy was to eliminate the data from sensor 3. This sensor gave rather weak responses to all samples, and generally exhibited signals proportional to those of Sensor 4. Removal of sensor 3 data had no effect on the rate of correct classification. It is therefore considered redundant.

Tests of robustness to analytical error

Robustness is a measure of the ability of the pattern analysis method to successfully classify the grain sample over the range of variability of the measured patterns. The following discussion illustrates the ability of the two pattern recognition algorithms to accommodate two types of analytical error typically encountered: (a) random error, or signal "noise", and (b) monotonic sensor drift over time, or loss in sensitivity of a given sensor.

Test 1 – robustness to random error. There were not enough graded standard samples available to do a proper measurement of actual pattern variability within all the categories. Random errors were therefore introduced into the patterns that were available in order to carry out these tests. The analysis program was trained on the full set of original 115 patterns. Based on a random number generator, the test set was generated by adding an error of between +5% and −5% to each element of a pattern before classification was carried out. The analysis was repeated with 5% increments of error up to 25%.

The results of KNN and NNS analysis are shown in Figs. 5 and 6. In Fig. 5, the effect of random error on the classification of individual

TABLE 3

Summary of the accuracy of the NNS and K-nearest neighbor algorithms for identification of the wheat vapors
[The entire data set was used as the training set in the first test (self-identification), to ensure the algorithms were correctly analyzing the data]

Data set	Accuracy of identification (%)	
	NNS	K-Nearest neighbor
(1) Train on total data	100	100
(2) Train on 55% of data set	65	68
(3) Add channel for sensor changes	83	N/A
(4) Calibrate channels using H_2S patterns	70	61
(5) Remove S3 data reducing pattern to 12 channels	71	62
(6) Use only data before sensor replaced (no channel 18)	78	58

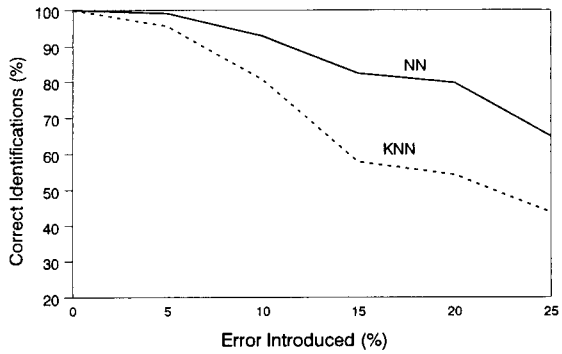

Fig. 5. The effect of adding increasing amounts of random error to the unknown pattern elements on the ability of the KNN and NNS to identify individual patterns.

odor patterns is shown. The ability of KNN to overcome the effect of error on self-identification of patterns drops off very quickly when the error exceeds 5%. The NNS proves to be very robust, even with ±25% error introduced into each element, the classification still was 65% correct.

The purpose of this analytical system, however, is the classification by grade, and not of individual samples. This Grade identification proved to be even more robust (Fig. 6), and classification was more accurate for a given error for both methods. NNS correctly assigned all samples (100%) to their subjectively-determined grade even with 5% error introduced. At the 10% precision expected of the sensor array, NNS performance had degraded only to 93%, while KNN performance had deteriorated to 80%. The performance of KNN and NNS diverged further as the introduced error was increased.

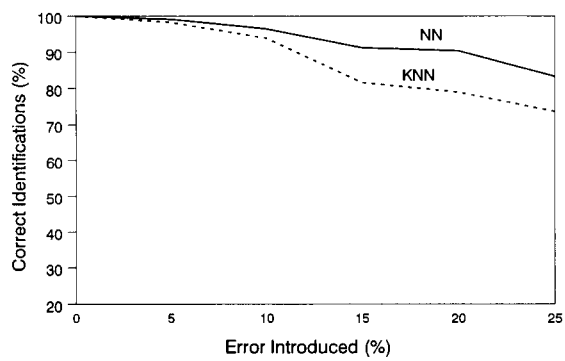

Fig. 6. The effect of adding increasing amounts of random error to the unknown pattern elements on the ability of the KNN and NNS to identify odor categories.

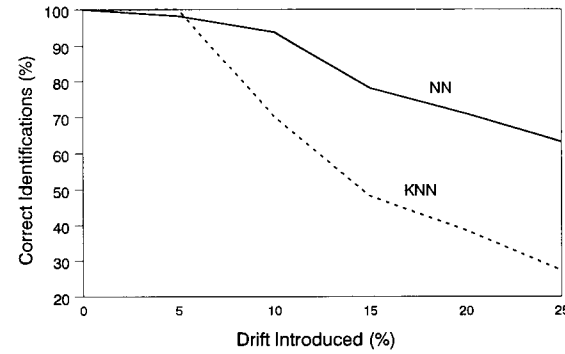

Fig. 7. The effect of adding increasing amounts of negative error to the Sensor 2 elements on the ability of the KNN and NNS to identify individual samples. This test simulates the effect of Sensor 2 drift.

Test 2 – robustness to systematic error (sensor drift). Sensor drift is a quite different parameter than random noise. Electrochemical sensors like many others have a finite lifetime (say 1–2 years). Over that time, there is an initial period of relatively stable signal output, followed by a gradual decrease. At the end of the sensor's life, the signal becomes too small to be useful, or it becomes erratic or noisy. The gradual decrease in signal is referred to as "drift". Drift was simulated in these studies by reducing the four pattern elements due to a given sensor by a fixed percentage. These were used to challenge an analytical system trained with the unaltered data, as before.

Drift of sensor output was simulated by adding increments of "error" from −5% to −25% to the data from individual sensors. The results obtained when drift is added in Sensor 2 are shown in Figs. 7 and 8. Self-identification of individual samples was rapidly affected by drift greater than −5% when KNN analysis was used, but NNS resisted the effects of even −10% drift (Fig. 7). In classification by grade, however, both methods were resistant to drift of −10% with the NNS slightly more resistant at larger values of sensor drift.

The drift experiment was repeated with the Sensor 4 signals. The results were quite different (Figs. 9 and 10). Both KNN and NNS failed

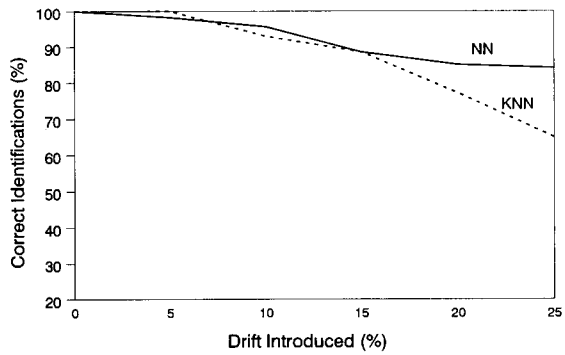

Fig. 8. The effect of adding increasing amounts of negative error to the Sensor 2 elements on the ability of the KNN and NNS to identify by grade.

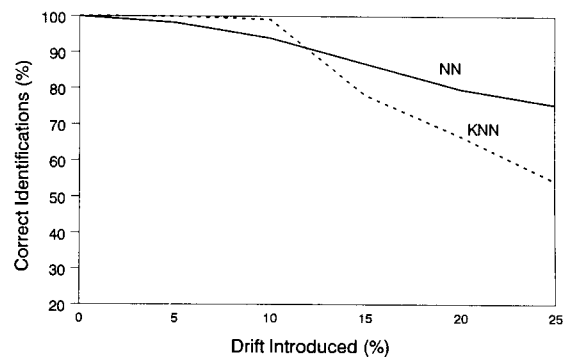

Fig. 10. The effect of adding increasing amounts of negative error to the Sensor 4 elements on the ability of the KNN and NNS to identify by grade.

rapidly in the ability to identify individual samples when the amount of drift exceeded −5% (Fig. 9), but the ability to classify by grade was maintained up to -10% drift by both KNN (99%) and NNS (93%) (Fig. 10) and the NNS slightly better at higher values of drift.

Sampling methods

As discussed earlier, each sample vapor was fractionated using both a cold trap and a sorbent trap. Patterns obtained from all fractions were included in the data set to provide a sufficiently large set for the NNS analysis. However, for a practical analyzer, the desired method would be to analyze a sample only one time, using whichever vapor fraction gave the most accurate grade identification.

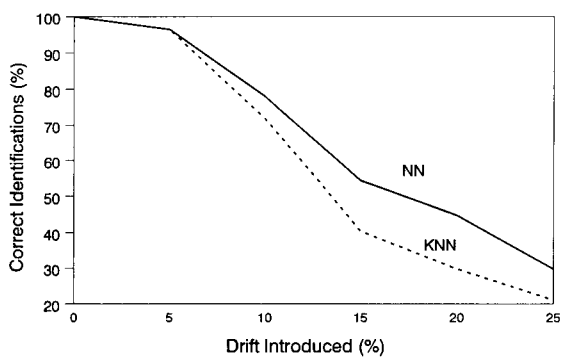

Fig. 9. The effect of adding increasing amounts of negative error to the Sensor 4 elements on the ability of the KNN and NNS to identify individual samples. This test simulates the effect of Sensor 4 drift.

As seen in Table 2, there were 25–33 analyses of each fraction. If one uses the data set which is divided into a 64 run training set and 52 run test ("unknown") set, then the total number of "unknown" runs of each fraction range from 11 to 17. When one examines the accuracy of identification within each fraction, it is seen that the FL fraction yields the highest percent correct, at 100% correct grade ID. The other three fraction had accuracies ranging from 82% to 69%. These results bear more detailed evaluation, on a larger set of grain samples.

DISCUSSION

The chemical composition of grain volatiles is known to be complex [2,3]. More than 50 different components have been identified using GC–MS, and several classes of compounds have been found in higher concentrations in vapors of certain grades than in others (e.g., organic acids in "Sour" grain). However, there is no reason to assume that any one of these 50 or more compounds is actually responsible for the odors.

On the other hand, whichever method of odor analysis is used, it may not be necessary to measure the actual odor-causing components. Any method based on pattern recognition begins with the hypothesis that a pattern can be found that is associated with the odor, i.e., microorganisms that produce a consistent and recognizable odor will also produce a recognizable mixture of other

metabolic products. We have tested this hypothesis directly using chemical parameter spectrometry, i.e., measuring an arbitrary pattern without any pretense of identifying the odor-causing components. The patterns were found to be associated closely with the subjective classification of the grain odor by trained experts.

The major conclusions of this work have been:

(1) For the three types of grain tested (Good, Sour, and Insect), the patterns produced by CPS are clearly different and can be used to classify the samples by type.

(2) Using separate training and test sets of data, the NNS pattern analysis method yields approximately the same performance in terms of classification by sample or by grade as the nearest-neighbor method. The NNS method, however, is much more resistant to random error and drift in sensor signal magnitudes.

(3) The NNS method is more adaptable to events that occur in real analytical situations, such as the failure of an instrument component. For example, the installation of a new sensor can be coded into the data and serves as a signal to the NNS that the marked data is different.

Development of the sensor array coupled with a NNS pattern recognition method appear very possible for the purpose of grain classification. Future work will determine whether this method can be generalized to other grades of grain than Good, Sour, and Insect, as well as other types of grain such as sorghum and corn. The robustness of the method in the face of actual error and spurious hardware problems will also be investigated using an expanded number of grain samples.

This work was sponsored by the US Department of Agriculture, SBIR Agreement NO. 90-33610-5088. We discussed the aspects of the project with several members of the U.S. Department of Agriculture, Federal Grain Inspection Service Technical Center, Kansas City, Kansas. Dr. Donald Koeltzow, the Chief of the FGIS Research and Development Branch, was extremely helpful in providing background information, and directed us to several potential sources of standard grain samples. Dr. Larry Seitz and Dr. David Sauer of the U.S. Grain Marketing Research Laboratory, Manhattan, KS, were extremely helpful in locating and providing the data in Refs. 2 and 3 and in selecting the grain samples for analysis during the course of the project.

REFERENCES

1 NIOH and NIOSH Basis for an Occupational Health Standard: Grain Dust. Health Hazards of Storing, Handling, and Shipping Grain, U.S. Dept. of Health and Human Services, National Institute of Occupational Safety and Health Publication No. 89-126, Cincinnati, OH (1989).
2 D.S. Weinberg, Development of an Effective Method of Detecting and Identifying Foreign Odors in Grain Samples, Final Report, Volume I, USDA Contract No. 53-6395-5-59, SoRI-EAS-86-1208, December 15, 1986.
3 M.C. Ponder and D.S. Weinberg, Development of an Effective Method of Detecting and Identifying Foreign Odors in Grain Samples, Literature and Equipment Survey USDA, Contract No. 53-6395-5-59, SoRI-EAS-85-727, August 5, 1985.
4 K. Fukui, in Proc. 3rd International Meeting on Chemical Sensors, Cleveland, OH, September 24–26, 1990, Pub. Edison Technology Center, Case Western Reserve Univ., p. 48.
5 B.S. Hoffheins and R.J. Lauf, J. Sensory Studies, 5 (1990) 129.
6 T. Aishima, Anal. Chim. Acta, 243 (1991) 293.
7 R.V. Valcarce, G.G. Smith and D.N. Stevenson, Chemom. Intell. Lab. Syst., 9 (1990) 95.
8 R.V. Valcarce, G.G. Smith, J.A. Alberico and R.S. Albrechtsen, J. Anal. Appl. Pyrolysis, 22 (1991) 1.
9 J.W. Gardner and P.N. Bartlett (Eds.), Sensors and Sensory Systems for an Electronic Nose, Kluwer, Dordrecht, 1992.
10 S. Zaromb and J.R. Stetter, Sensors Actuators, 6 (1985) 225.
11 J.R. Stetter, in J.W. Gardner and P.N. Bartlett (Eds.)., Sensors and Sensory Systems for an Electronic Nose, Kluwer, Dordrecht, 1992, p. 273.
12 J.R. Stetter, S. Zaromb, and M.W. Findlay, Jr., Sensors Actuators, 6 (1985) 269.
13 J.R. Stetter, P.C. Jurs and S.L. Rose, Anal. Chem., 58 (1986) 860.
14 J.R. Stetter, in D. Schuetzle, R. Hammerle and J. Butler (Eds.), Fundamentals and Applications of Chemical Sensors, ACS Symposium Series Vol. 309, ACS, Washington, DC, 1986, p. 299.
15 J.R. Stetter, in Transducers'87, Proc. 4th Int. Conf. on Solid-State Sensors and Actuators, Tokyo, Japan, June 2–5, 1987, IEEE Japan Publishers, Tokyo, p. 557.
16 K. Varmuza, Pattern Recognition in Chemistry, Springer Verlag, Heidelberg, 1980.
17 M.M. Nelson and W.T. Illingworth, A Practical Guide to Neural Nets, Addison-Wesley, Reading, MA, 1990.

Analytica Chimica Acta, 284 (1993) 13–19
Elsevier Science Publishers B.V., Amsterdam

Electrochemical behaviour of nitrobenzene in aqueous ethanol studied by differential pulse polarography

Kerry J. Kippax-Davis, Madeleine Bully [1], Anastasios Economou, Peter R. Fielden, Adrian F.R. Watson [2] and John F. Alder

Department of Instrumentation and Analytical Science, UMIST, P.O. Box 88, Manchester M60 1QD (UK)

(Received 18th May 1993)

Abstract

Differential pulse polarographic studies of nitrobenzene in aqueous ethanol reveal complex behaviour involving solvent composition, viscosity and pH. Both reduction potential and peak reduction current are dependent on all three parameters. Limits of detection of ca. 2×10^{-7} M and a linear working range up to 10^{-3} M nitrobenzene in ethanol–water (80:20) at pH 6 were recorded. No adsorptive accumulation of nitrobenzene onto the hanging mercury drop electrode employed was observed under any condition in the aqueous ethanol mixtures.

Keywords: Polarography; Electrochemical behaviour; Nitrobenzene

The electrochemical reduction of nitrobenzene has been extensively studied over many years. The most recent work by Zuman and Fijalek [1] reviews the past literature and puts the rather complex chemistry into perspective. The differential pulse voltammogram of nitrobenzene has two peaks. The reduction proceeds first by protonation of the nitro group:

$$PhNO_2 + H^+ \rightarrow PhNO_2H^+ \quad (1)$$

and then by a series of steps:

$$PhNO_2H^+ + e^- \rightarrow PhNO_2H^{\cdot} \quad (2)$$

$$PhNO_2H^{\cdot} + H^+ \rightarrow PhNO_2H_2^{\cdot+} \quad (3)$$

$$PhNO_2H_2^{\cdot+} + e^- \rightarrow PhN(OH)_2 \quad (4)$$

Correspondence to: J.F. Alder, Department of Instrumentation and Analytical Science, UMIST, P.O. Box 88, Manchester M60 1QD (UK).

[1] Present address: Lab. des Sciences Analytiques, Universite Claude Bernard Lyon 1, Bat. 308, 43 Blvd. du 11 Novembre 1918, F69622 Villeurbanne Cedex (France).

[2] Current address: Dept. Environmental and Geographical Sciences, Manchester Metropolitan University, Manchester M1 5GD (UK).

to the dihydroxylamine species. There follows a dehydration step followed by a 2-electron reduction of the nitrobenzene:

$$PhN(OH)_2 \rightarrow PhNO + H_2O \quad (5)$$

$$PhNO + 2e^- + 2H^+ \rightarrow PhNHOH \quad (6)$$

Steps 1 to 6 give rise to the first peak in the nitrobenzene reduction voltammogram.

The second peak is due to an alternative route from step 2.

$$PhNO_2H^{\cdot} + e^- + H^+ \rightarrow PhN(OH)_2 \quad (7)$$

followed by reactions 5 and 6 [1]. The authors discuss in detail the mechanism and nature of the strong pH dependence of peak currents and reduction potentials of the voltammograms obtained in aqueous–35% dimethylformamide solutions. The shifts of reduction potentials of the first waves are clearly linked to the protonation steps in reaction 1 and decrease in the rate of protonation in reaction 3 gives rise to an observed decrease in the height of the first peak.

In the present study adsorptive stripping from aqueous ethanol was investigated. The original

0003-2670/93/$06.00 © 1993 – Elsevier Science Publishers B.V. All rights reserved

goal was to improve the sensitivity of the determination of nitrobenzene in air. The aim was to employ a scrubber similar to that described by Fielden et al. [2] to determine nitrobenzene vapour in atmospheric samples. As the work progressed, it was clear that adsorptive accumulation of nitrobenzene was not detectable, and a more detailed study of the electrochemistry was undertaken. The effect of pH and solvent composition of the aqueous ethanol mixtures was studied along with the stripping voltammetry parameters.

EXPERIMENTAL

Apparatus

Measurements were carried out using a Princeton Applied Research (PAR) potentiostat/galvanostat Model 273 in conjunction with a PAR Model 303A static mercury drop electrode (EG&G Instruments, Wokingham). This type of electrode served as either a dropping mercury or hanging mercury drop electrode. The cell was fitted with a silver–silver chloride reference electrode and a platinum wire auxiliary electrode. A magnetic stirrer and 'star head' stir bar provided the convective transport during the preconcentration step. Ethanol was from a range of sources, none being particularly better than any other. Certain batches, even from the same supplier, gave problems due to a low concentration of a contaminant, which were removed by eluting through XAD-2 resin and dried chromatographic grade silica prior to use. It was important to ensure that all the reagents employed were made up in the same batch of ethanol.

Solution used for voltammetric studies

A potassium acetate solution (1.0 M) was made from 9.814 g of the salt dissolved in and made up to 100 ml in high purity water. 1.0 M acetic acid was made from 6.005 g of glacial acetic acid diluted to 100 ml with high purity water. For the pH studies at various ethanol fractions, solutions containing 2 ml of 1.0 M potassium acetate and 2 ml of 1.0 M acetic acid, with the required amount of ethanol, and water made up to 10 ml, were employed. The voltammetric cell was then filled with 4 ml of the nominally 0.2 M potassium acetate–ethanol–water mixture and 6 ml of the 0.2 M acetic acid–ethanol–water mixture. The buffer formed contained therefore the same quantities of acid and salt, but different fractions of ethanol and water. For the experiments at constant pH, the solutions made in a similar way were adjusted to pH 4.54 and 4.39 with glacial acetic acid. The amount of 1×10^{-2} M nitrobenzene solution added to the mixture was adjusted proportionately to ensure the nitrobenzene concentration in the final mixture was constant.

Stock solutions of nitrobenzene were prepared at 1×10^{-2}, 1×10^{-3} and 1×10^{-5} M by dissolving 0.123 g of nitrobenzene in 100 ml ethanol then diluting 1 ml of this by 10 and then by 100 with more ethanol. These solutions were stored in the dark between 16°C and 20°C. High purity water and AnalaR grade reagents (BDH) were used.

All volumetric glassware and electrochemical cups were first cleaned with Decon 90 and rinsed with distilled water. This was followed by several washes with concentrated nitric acid and rinsing with distilled water and finally high purity water. The glassware was dried in the oven and then silanised using 2% dimethyldichlorosilane in trichloroethane.

Preparation of supporting electrolyte

Using clean volumetric pipettes 30 cm^3 of ethanol was placed in a clean 100 cm^3 volumetric flask. This was made up to the mark with high purity water. 2 cm^3 of 0.5 M potassium nitrate was added to the electrochemical cup and diluted to 10 cm^3 by the addition of 8 cm^3 of the water–ethanol solution.

General procedures

For accumulation studies the 10 cm^3 of supporting electrolyte in the electrochemical cup was purged for 4 min initially and 30 s before analysis. An accumulation potential of 0.0 V was applied to the cell for a selected accumulation period. The potential chosen was arrived at after experimentation, the accumulation potential being varied between 0 and −0.6 V vs. Ag/AgCl. In the event, no adsorption enhancement was seen over

TABLE 1
Instrument settings

Purge time (s)	120 (30) [a]
Initial potential (mV)	−100 (−350) [a]
Final potential (mV)	−750
Scan increment (mV)	2
Scan rate (mV s^{-1})	2
Step/drop time (s)	1
Pulse height (mV)	100
Pulse width (s)	0.05
Drop size	Large (24 mg Hg)
Reference electrode	Ag/AgCl

[a] For accumulation studies only.

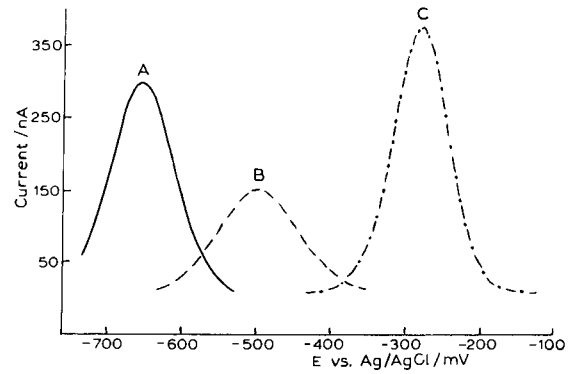

Fig. 1. Differential pulse voltammogram for 10^{-5} M nitrobenzene in (A) 80% ethanol–20% water; (B) 40% ethanol–60% water; (C) 0% ethanol–100% water. For conditions see text.

this potential range. Data are reported for a potential of 0.0 V only. The voltammogram was recorded by applying a negative (cathodic) potential scan in the differential pulse mode. After recording the voltammogram for the blank solution, 5 μl additions of 1×10^{-5} M nitrobenzene in ethanol were made and the adsorptive stripping cycle was repeated after each addition and with a new mercury drop for each analysis, for the same accumulation period. Additions of 5 μl of 1×10^{-5} M nitrobenzene stock solution produced solutions in the range of 5.0×10^{-8} M and 2.0×10^{-7} M. This routine was repeated for varying accumulation times from 0 to 1800 s. Instrument settings are shown in Table 1.

For voltammetric studies no accumulation time was used. The purge time was extended to 120 s, and the initial potential set at −100 mV. Otherwise the instrument parameters were as in the accumulation studies, and are given in Table 1.

RESULTS AND DISCUSSION

Initial studies were undertaken to establish the baseline conditions for nitrobenzene determination by voltammetry, particularly the effect of pH and ethanol–water ratio. Mixtures of nitrobenzene (1×10^{-5} M) in ethanol–water mixtures with potassium acetate buffer were made up as outlined above; the voltammograms obtained are shown in Fig. 1. The effect of the ethanol–water ratio is marked, not only in terms of peak reduction potential, but also in terms of peak current. The peak reduction potential (E_p) was related to the fraction of ethanol in the mixture X (EtOH) by:

$$E_p = -496X(\mathrm{EtOH}) - 278 \ (\mathrm{mV})$$

with a linear correlation coefficient of 0.994 (17 points).

The peak current vs. ethanol fraction is shown in Fig. 2. This shows a complicated relationship which probably has at least three contributory factors. Increasing the fraction of ethanol in the aqueous solution decreases the dielectric constant of the mixture and changes its viscosity. Suppression of the dielectric constant changes the degree of dissociation of the water and alters the dissociation constants of the buffer components leading to change in pH. This was observed

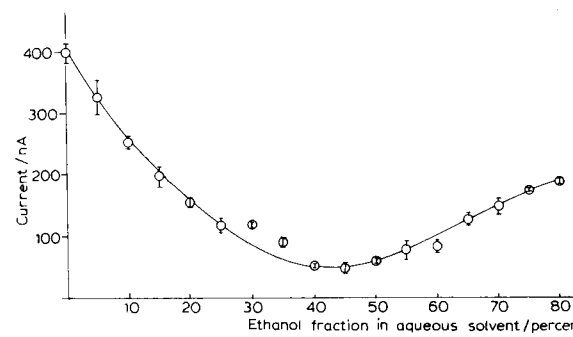

Fig. 2. Peak current vs. fraction of ethanol in the aqueous ethanol solvent. Error bars are standard deviation.

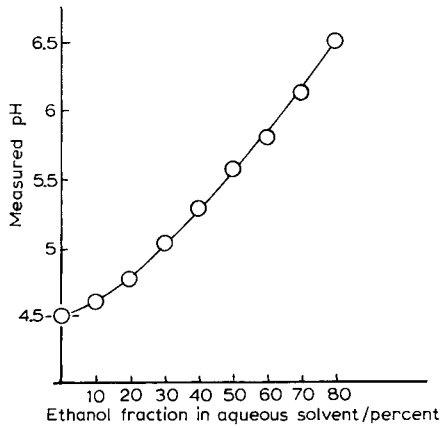

Fig. 3. Measured pH vs. fraction of ethanol in the aqueous ethanol solvent. pH measured with a glass electrode calibrated at pH 4.01 and 7.01.

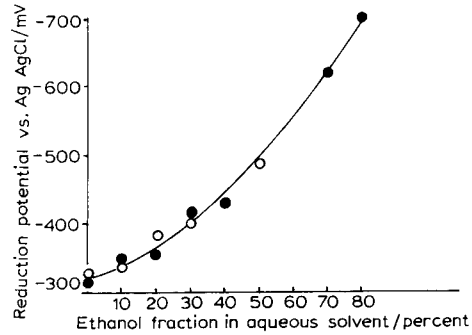

Fig. 5. Reduction potential vs. Ag/AgCl electrode vs. fraction of ethanol in the aqueous ethanol solvent at two values of pH held constant. Open circles (○) pH 4.39, filled circles (●) pH 4.54. Analyte 1×10^{-5} M nitrobenzene; the concentration was adjusted for dilution after buffering to ensure the same concentration at each point.

using a pH glass electrode (Orion 701 Ionanalyser, Cambridge, MA). Figure 3 shows the observed pH as a function of ethanol–water ratio, for the same buffer additions to all solutions, at 23°C. Figure 4 shows the relationship between the reduction potential (E_{red}) of a 1×10^{-5} M nitrobenzene solution and observed pH. The linear portion of the E_{red} vs. pH plot is 240 mV/pH. This value is four times greater than the 60 mV/pH reported by Zuman and Fijalek [1] for nitrobenzene in aqueous–35% DMF solution by d.c. polarography but, as discussed below, the

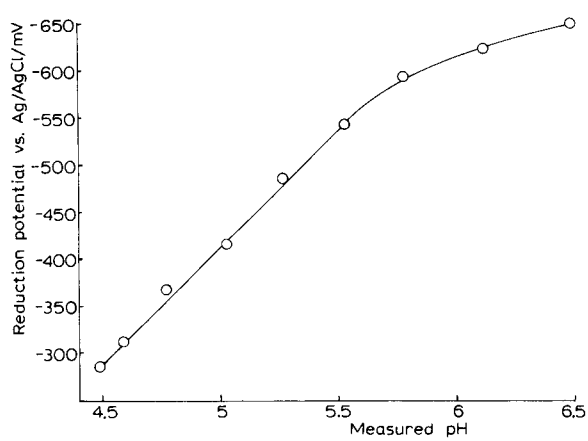

Fig. 4. Reduction potential vs. Ag/AgCl electrode, vs. pH for a 1×10^{-5} M nitrobenzene solution. The pH varied as the ethanol content of the mixture changed, so each point is at a different ethanol fraction, as well as pH (see Fig. 3).

experimental conditions were rather different in this work. The figures emphasise the need to control carefully the solution conditions in order to maintain reproducible electrochemistry.

An experiment was carried out when the pH of the solution was adjusted to a constant value (pH 4.54 and pH 4.39) for different ethanol–water ratios. Reduction potentials of a 1×10^{-5} M nitrobenzene solution were measured and the data plotted in Fig. 5. Although the plot is a smooth curve at ethanol concentrations less than 50%, the points lie reasonably on a straight line at $\geqslant 50\%$ ethanol. The range 0–50% ethanol corresponds to a pH change of about 1.05 pH unit in the mixture where no attempt was made to readjust the buffer (see Fig. 4). One might cautiously suppose therefore that Fig. 4 demonstrates two convoluted phenomena in the region 0–50% ethanol, one is an effect due to pH, the other a secondary effect, possibly permittivity changes, represented in Fig. 5. The difference in the two effects corresponds to about 80 mV/pH unit which explains why the two sets of points in Fig. 4 for the pH 4.54 and 4.39 (difference 0.15) appear to lie on the same curve, because the points scatter is of the same order of magnitude as the expected difference due to pH (12 mV). It is possible to calculate the change in dielectric constant (ϵ) as a function of ethanol–water composition in the mixture. When the data for Fig. 5

were plotted in a log–log format, the gradient of the plot was -1.03 ($\log E_r/\log \epsilon_{mix}$) over the range $\epsilon = 35$ to 78 with the points lying on a gentle curve (Fig. 6). One should be wary of reading too much into this empirical observation as the effects are bulk properties, but one would expect dielectric constant to have some effect on reduction potentials because of the effect on coulombic shielding and dissociation equilibria on species near to the electrode surface.

The results shown in Fig. 2 on the decrease in peak current with changing ethanol fraction is at least partly due to pH effects. It is interesting to note, however, that the viscosity of ethanol–water solutions goes through a maximum at 42% ethanol [3] which corresponds to the minimum in Fig. 2, and it is tempting to relate the two effects. One would expect the maximum diffusion current to be inversely proportional to (viscosity)$^{1/2}$ through the diffusion coefficient of the ethanol–water mixtures. In differential pulse voltammetry the peak current i_p is given by [4]:

$$i_p = \frac{n^2F^2}{4RT} AC\Delta E \left[\frac{D}{\pi\tau}\right]^{1/2}$$

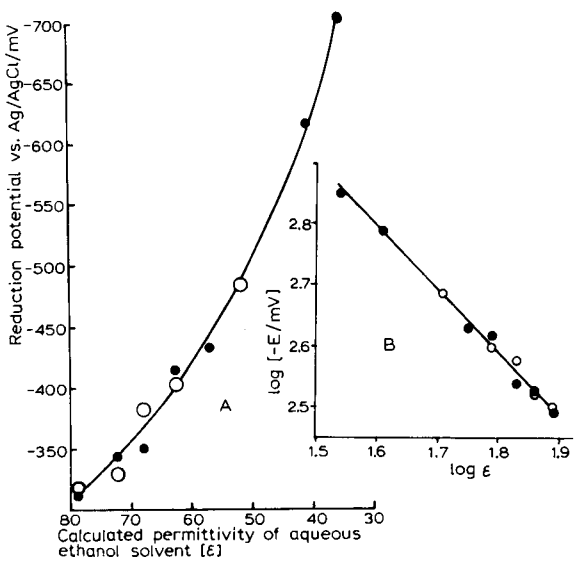

Fig. 6. (A) Reduction potential vs. Ag/AgCl electrode, vs. calculated permittivity (ϵ) of the aqueous ethanol mixture. Data and symbols are as for Fig. 5. (B) Same data as in Figs. 6A and 5 plotted in log–log notation. The gradient of the curve is -1.03.

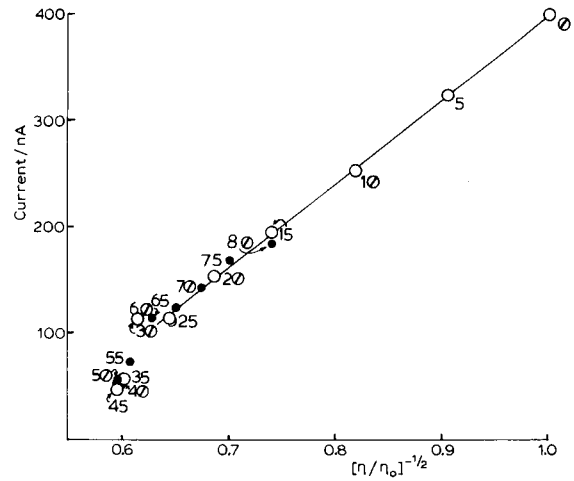

Fig. 7. Plot of observed peak current vs. (calculated viscosity ratio)$^{-1/2}$ of the ethanol water mixture (η) vs. the viscosity of pure water (η_0). Data are the same as for Fig. 2 with the solvent composition plotted as $(\eta/\eta^0)^{-1/2}$. Figures next to the point are the fraction percent of ethanol in the solvent. For clarity, the values less than 50% are in open circles, the values greater than 50% in filled circles.

where π, n, F, R, T have their usual significance, A is the electrode area, C the bulk analyte concentration, ΔE the pulse amplitude, τ the pulse duration and D the diffusion coefficient.

If the viscosity η of a medium at a given temperature changes, one can apply Walden's rule: $\Lambda_m\eta$ = constant [5] modified to $D\eta$ = constant as $\Lambda_m\alpha\eta$ (Λ_m is the molar conductivity). Thus one would expect that as the ethanol concentration of the solution was increased, the ratio $(\eta/\eta_0)^{-1/2}$, where η is the mixture viscosity and η_0 the viscosity of water at the same temperature, plotted against i_p would yield a straight line. The experimental procedures adopted here were not able to prove this by measurement of viscosity, but a plot of observed peak current vs. tabulated values $(\eta/\eta_0)^{-1/2}$ [13] shows empirically a linear relationship over the range 0–30% and 60–80% (v/v) ethanol (Fig. 7). The numbers by the points are the percent fraction (v/v) of ethanol in the mixtures. These results support the proposition that viscosity changes are at least partially responsible for the peak current variation.

Differential pulse voltammetry of nitrobenzene

The conditions chosen for the determination of nitrobenzene were 80% ethanol and pH 6, as

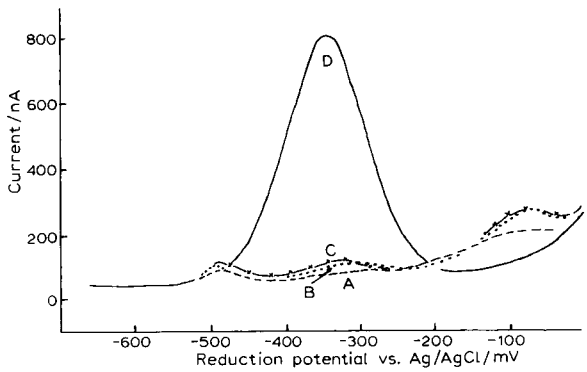

Fig. 8. Differential pulse stripping voltammogram for nitrobenzene. The electrode was immersed in a solution of 1×10^{-4} M nitrobenzene in pure ethanol and 0.0 V vs. Ag/AgCl. After 2, 3 and 5 min, the electrode was removed and placed in the 80% ethanolic, pH 6 test solution and the stripping voltammograms obtained. A (– – –) = 2 min; B (· · ·) = 3 min and C (×–×–×) = 5 min accumulation time. D is a peak due to 4×10^{-6} M nitrobenzene in the test cell. The amount of material accumulated on the electrode is insignificant.

these gave the most reproducible results. Linear calibration graphs were obtained over the concentration range 2×10^{-7} M (limit of detection) to 1×10^{-3} M nitrobenzene. The lower limit corresponded to 3× the standard deviation of the background current. Accumulation studies were carried out over a wide variety of times and conditions. It was found that accumulation effects, however, were very small. If the mercury electrode was immersed in a 1×10^{-4} M nitrobenzene solution in pure ethanol, removed and then stripped in 80% ethanol, pH 6 (see above), the effect of adsorption could just be seen (Fig. 8). At concentrations lower than this, however, no adsorption was apparent. Adsorption accumulation studies in aqueous ethanol media were also carried out, conditions were: 10^{-6} M to 10^{-4} M nitrobenzene in 20%, 40%, 80% ethanol water mixtures at pH 5.6, 6.1 and 6.6 and accumulation voltage 0 V to −0.6 V for periods up to 30 min; no accumulation was observed under these conditions.

The studies were repeated twice by different workers. At no stage was accumulation observed under these conditions. In order to check if the nature of the buffer was a contributory factor a series of studies was undertaken [6] and later repeated. A mixture of 0.1 M aqueous potassium nitrate and 25% ethanol was used as the solvent. Instrument conditions were as in Table 1 with 0.0 V vs. Ag/AgCl accumulation potential. The differential pulse voltammogram of the blank solution showed a small peak at −330 mV vs. Ag/AgCl with 60 s accumulation time, which increased at longer accumulation times up to 1200 s, to about 8 times the peak current and a reduction potential increasing to −400 mV. Addition of nitrobenzene to the blank electrolyte produced another peak at about −200 mV vs. Ag/AgCl which increased from a detection limit of about 2×10^{-7} M nitrobenzene in proportion to the concentration of nitrobenzene added. The magnitude of the reduction peak did not increase with increasing accumulation times up to 1200 s, either at 0 or −200 mV vs. Ag/AgCl accumulation potential.

Conclusions

The work of Zuman and Fijalek [1] describes the behaviour of nitrobenzene in solutions of constant gross composition (water–35% dimethylformamide) where the pH is changed purposely. The work described in this paper is about solutions of altering gross compositions where the pH effects are a consequence of the changes in solvent composition. It is clear that viscosity, and probably also permittivity have an influence on both the reduction potentials and the peak currents observed. The changes in reduction mechanisms are likely therefore to be more complex even than those described by Zuman and Fijalek [1] and clearly solution composition needs to be carefully controlled if reproducible chemical analysis is to be carried out. The electrochemical behaviour of nitrobenzene in ethanol–water mixtures is analytically useful although not particularly sensitive with a detection limit of about 2×10^{-7} M (25 μg l^{-1}). The absence of adsorption accumulation at low concentration was disappointing from the analytical perspective, particularly for the analysis of gaseous atmospheres where concentrations in the range μg m^{-3} nitrobenzene in air are of more interest.

This work was supported by the Procurement Executive, Ministry of Defence. Madeleine Bully was on study leave from the University of Dijon under the Erasmus scheme.

REFERENCES

1 P. Zuman and Z. Fijalek, J. Electroanal. Chem., 296 (1990) 583, 589.
2 P.R. Fielden, A. Cox and C.L.P. Thomas, Analyst, 113 (1988) 1799.
3 J. Weast (Ed.), Handbook of Chemistry and Physics, 66th edn., Chemical Rubber Co., Boca Raton, FL, 1985.
4 E.P. Parry and R.A. Osteryoung, Anal. Chem., 37 (1965) 1634.
5 P.W. Atkins, Physical Chemistry, Oxford University Press, Oxford, 4th edn., 1990, p. 766.
6 K. Johnson, MSc Thesis, Department of Instrumentation and Analytical Science, UMIST, University of Manchester, 1992.

Analytica Chimica Acta, 284 (1993) 21–26
Elsevier Science Publishers B.V., Amsterdam

Amperometric glucose biosensor based on an electrocatalytically bulk-modified epoxy-graphite biocomposite

F. Céspedes, E. Martínez-Fàbregas and S. Alegret

Grup de Sensors & Biosensors, Departament de Química, Universitat Autònoma de Barcelona, E-08193 Bellaterra, Catalonia (Spain)

(Received 15th April 1993; revised manuscript received 16th July 1993)

Abstract

An inexpensive, robust, polishable and easily machinable amperometric glucose transducer was constructed. The biocomposite materials used were graphite, palladium–gold, non-conducting epoxy resin and glucose oxidase. The enzyme retains its bioactivity in the rigid epoxy-graphite matrix. The electrocatalytic oxidation of hydrogen peroxide is enhanced by gold–palladium and it is used as the analytical signal (at 900 mV vs. Ag/AgCl in a pH 7.00 buffered solution with 0.1 M phosphate and 0.1 M KCl). The biosensor exhibits a linear response to glucose in the 0.01–2 mM range and produces steady-state signals within a few seconds (6 s for 95% signal). Simple polishing procedures can be used to generate a fresh bioactive transducer surface.

Keywords: Amperometry; Biosensors; Catalytic methods; Biocomposites; Glucose biosensor; Epoxy-graphite biocomposite

Chemically or physically modified electrodes are very versatile and hold a great promise for electroanalytical applications [1,2]. This is the reason behind the significant research and development efforts seen recently in the field of amperometric devices. The resulting electrodes are increasingly sensitive, selective, stable and inexpensive. They are seen as a viable alternative to bulky and costly analytical equipment, especially in the control and monitoring of biomedical, environmental and industrial processes. In spite of all these advantages, modified amperometric devices have not been widely used as they have not been commercially available. The main reason for this disparity is that modified electrodes are difficult to prepare, especially when activating the surface of the electrode without loss of sensitivity, or when attaching modifiers to the electrode using covalent bonds, adsorption, polymer film coating, etc.

Enzyme-based amperometric sensors are widely studied at present. Such devices can be seen as biologically modified electrodes. Several immobilization methods have been studied for the construction of electrochemical biosensors, depending on the specific biocatalyst. Generally, the biological component is immobilized on the surface of the electrode either by physical (using membranes) or chemical means (using covalent bonding or chemical cross-linking).

Alternatively, the biocomponent can be incorporated to the matrix of the transducer. An example of such bulk-phase modified electrodes is the popular carbon paste electrode. However, the nature of this paste is such that the resulting devices do not show sufficient chemical or me-

Correspondence to: S. Alegret, Grup de Sensors & Biosensors, Departament de Química, Universitat Autònoma de Barcelona, E-08193 Bellaterra, Catalonia (Spain).

0003-2670/93/$06.00 © 1993 – Elsevier Science Publishers B.V. All rights reserved

chanical stability and therefore are hardly applicable in commercial equipments.

Wang and co-workers [3–6] recently proposed the use of a commercial available conductive resin based on epoxy-graphite to develop novel biologically modified electrodes. The modifier is combined with the conductive polymeric matrix, in a similar fashion as in modified carbon paste electrodes, but in this case a rigid and renewable electrode results.

In the present work, the biological modification of a non-commercial conductive resin is presented. The resin is based on epoxy-graphite and has been previously studied [7] and electrochemically characterized [8] in our laboratory. The modification consisted of a dispersion of an enzyme (glucose oxidase) and a H_2O_2 catalyst (Au–Pd) in the resin. Placing the catalyst in the biocomposite allows for the lowering of the hydrogen peroxide detection potential, diminishing the response time and increasing the stability of the signal.

Yang et al. [9] proposed the surface modification of graphite rods using a gold–palladium sputtering technique. The mixing of these metals in the biocomposite is a very simple procedure in the technique reported here, with the additional advantage that a freshly bioactive surface can be produced with a simple polishing procedure.

EXPERIMENTAL

Apparatus

The sensor current was measured with a PRG-DEL amperometric unit (Taccussel, Lyon). Voltage-current curves were recorded using a Polarecord E506 recorder (Metrohm, Herisau). pH was controlled using a Digilab 517 meter (Crison, Barcelona). Responses were recorded with a Labograph E586 recorder (Metrohm).

Reagents and solutions

The electrodes were constructed using graphite powder with a particle size of 50 μm (Merck), Epo-Tek H77 epoxy resin (Epoxy Technology, Billerica, MA), gold power (32, 659-3 [7440-57-5], Aldrich), palladium power (36,666-6 [7440-05-3], Aldrich) and glucose oxidase (GOD)(G-2133 type VII from *Aspergillus niger*, Sigma).

The supporting electrolyte was an aqueous solution buffered at pH 7.00 with 0.1 M phosphate and 0.1 M KCl. Glucose solutions were prepared from a benzoic acid saturated solution (3 g dm^{-3}).

Auxiliary electrodes

To characterize and evaluate the working electrodes, a platinum auxiliary electrode and a double-junction Ag/AgCl reference electrode (Orion 92-02-00) were used. The external reference solution was 0.1 M KCl.

Construction of the amperometric electrode modified with Au–Pd–GOD

The sensitive composite material was prepared from mixing the catalyst, the graphite and the epoxy resin. The mixture ratio was 1:4:16 parts in weight respectively. The catalyst is made of a mixture of gold and palladium in a 3:2 parts in weight, respectively.

For each gram of the resulting composite, 15 mg of the GOD enzyme were added. The paste was thoroughly mixed by hand, until a homogeneous mixture resulted. The inner hollow of a PVC tube (6 mm i.d.) was filled with the biocomposite until a depth of 3 mm had been reached (Fig. 1). The material was cured at a temperature between 35 and 40°C, during a week. In previous reports [8], the hardening process of composite

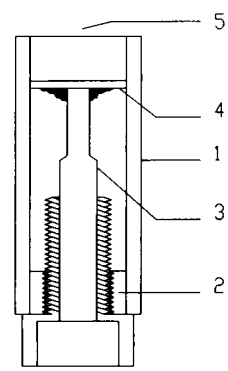

Fig. 1. Construction of the biosensor. 1 = Electrode body; 2 = metallic nut supporting the electrical contact; 3 = electrical contact; 4 = copper contact; 5 = composite material consisting of epoxy-graphite–Au–Pd–GOD.

based amperometric electrodes was carried out at 60°C during 48 h. In the present work, lower temperatures were used to avoid the thermal denaturalization of the enzyme.

The surface of the biosensor was polished using a 3-μm alumina paper (polishing strips 301044-001, Orion) wetted with bidistilled water.

When the biosensor was not being used, it was kept at a temperature of 5°C under dry conditions.

RESULTS AND DISCUSSION

Characteristics of the sensor system

The developed biosensor, built from an epoxy-graphite–Au–Pd–GOD composite, can be classified as a first generation glucose enzyme electrode. This type of biosensors is defined by the biocatalytical generation of an electrochemically active species (hydrogen peroxide) by an enzyme (GOD).

$$\text{D-(+)-glucose} + O_2 \xrightarrow{\text{GOD}} \text{gluonic acid} + H_2O_2 \quad (1)$$

The hydrogen peroxide produced by reaction 1 is measured amperometrically by the direct oxidation on the surface of the biocomposite when a potential E is applied:

$$H_2O_2 \xrightarrow{E} O_2 + 2H^+ + 2e^- \quad (2)$$

The potential E to be applied depends on the catalytical effect of the Au/Pd on the oxidation of hydrogen peroxide, according to Eqn. 2.

Construction of the biosensor based on the composite epoxy-graphite–Au–Pd–GOD

Effect of the amount of Au–Pd in the bulk of the material. When the amount of the catalyst in the bulk of the biomaterial is increased, the analytical signal due to the catalytical oxidation of the hydrogen peroxide also rises. Beyond a content of 20% (w/w) Au–Pd, the analytical signal becomes stable as current density in the electrode reaches a maximum (Fig. 2). This quantity was considered optimal, since an increase in the proportion of the catalyst in the composite raised the cost of the biosensor, without a correspondent electrochemical improvement.

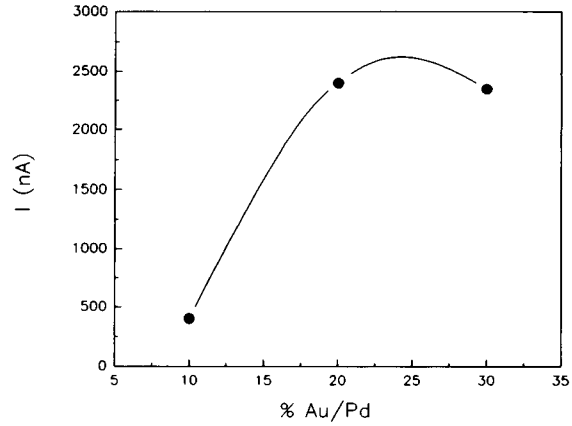

Fig. 2. Effect of Au–Pd content in the biocomposite on the hydrogen peroxide oxidative electrocatalysis.

H_2O_2 oxidation potential. In Fig. 3B linear sweep voltamperograms for the epoxy-graphite–Au–Pd transducer are shown. In these voltamperograms, the characteristic plateau due to the maximum oxidation current for hydrogen peroxide can be observed. This plateau appears at 900 mV vs Ag/AgCl and is 250 mV lower than the optimal working potential (1150 mV) for non-modified epoxy-graphite transducers (Fig. 3A) [8].

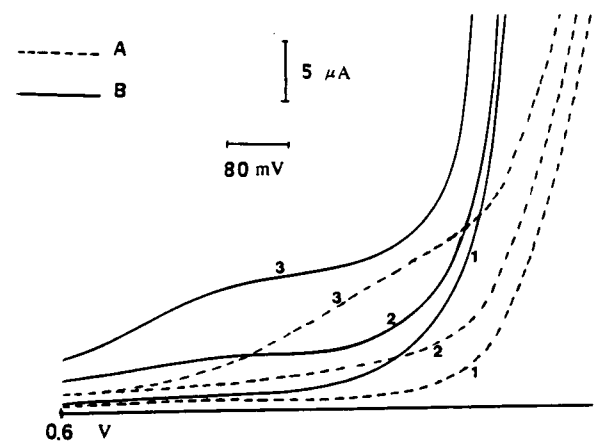

Fig. 3. Linear-sweep voltammetry in a pH 7.00 buffered solution (0.1 M phosphate–0.1 M KCl). Sweep rate, 200 mV min^{-1}. (1) In supporting electrolyte (SE); (2) in SE + 0.2 mM H_2O_2; (3) in SE + 0.6 mM H_2O_2. (A) Epoxy-graphite unit and (B) modified epoxy-graphite unit with a 20% Au–Pd catalyst.

TABLE 1

Relative accuracy in the determination of glucose in aqueous solutions containing some common clinical interferent species using different biosensor devices

Biosensor		Pt–GOD [a]	Epoxy-graphite–GOD	Epoxy-graphite–Au–Pd–GOD
Configuration		Enzymatic membrane	Enzymatic membrane	Biocomposite
Detection		H_2O_2	H_2O_2	H_2O_2
Working potential (mV)		650	1150	900
Glucose concentration (g/l)		1	0.6	1
Added interferent:				
Ascorbic acid	0.1 g/l	> 50%	> 100%	> 100%
Citrate	5.0 g/l	1.4%	– [b]	– [b]
Urea	0.1 g/l	1.2%	– [b]	– [b]
Uric acid	0.1 g/l	−7.5%	> 50%	> 100%

[a] Data from Ref. 10. [b] Imperceptible.

Although this does not solve all interference problems due to the electrochemically active species present in the solution (Table 1), the addition of the Au–Pd catalyst improves the response of the sensor by producing a more stable analytical signal since the potential window where the system is working is sufficiently far from the oxidation potential of the medium used (H_2O).

Electrode stability. When the logarithm of the current and the logarithm of glucose concentration are processed using the method of least-squares, the equation of a straight line results, where a is the value of $\log[I(\text{nA})]$ at the point of intersection with the y-axis, b is the slope of the line (theoretically $b = 1$). For thirteen calibrations, and a 95% confidence level, $a = 6.15 \pm 0.05$ and $b = 1.002 \pm 0.008$ as seen in Table 2. It can be concluded that the enzyme is trapped in the plastic matrix and that its bioactivity is preserved at the surface of the electrode for long periods (longer than 2 months).

A concurrent study was carried out with other devices built from the same biomaterial, observing the effect of the polishing of the surface after each calibration. It was confirmed that the enzyme was trapped in the bulk of the biomaterial and that it kept its bioactivity even when it is dispersed in a rigid polymeric matrix, with properties very different from those of the soft matrices of carbon paste electrodes. An electrode was polished after each calibration and then a new calibration run was performed. Table 3 shows the results of 5 calibration runs under these conditions. The average value of a was 5.6 ± 0.1 and the slope $b = 0.97 \pm 0.02$ for a 95% confidence interval. The same electrode was then used in 6 successive calibrations without the surface polishing procedure and it was observed that $a = 6.13 \pm 0.09$, which is comparable with the values described above for an electrode that was not polished for more than 2 months.

It can be concluded that the surface of the biomaterial evolves when used until a maximum catalytical activity is reached while the stability

TABLE 2

Calibration parameters for biocomposite-based glucose biosensor (The surface of biosensor was not polished between calibrations) [a]

Day	a	b	r
1	5.78	0.99	0.9997
4	5.98	0.99	0.99998
4	6.14	1.02	0.99995
4	6.14	1.01	0.99993
6	6.13	1.00	0.99995
8	6.17	0.99	0.99994
11	6.17	1.00	0.99996
20	6.26	0.98	0.99997
22	6.26	1.00	0.99992
25	6.25	1.00	0.99994
34	6.22	1.01	0.99997
81	6.05	1.01	0.99995
81	6.07	1.03	0.99997

[a] I (nA) = $a + b$ log[glucose] (M).

TABLE 3

Calibration parameters for biocomposite-based glucose biosensors: (1) polished surface and (2) unpolished surface, between calibrations [a]

Calibration number (1)	*a*	*b*	*r*
1	5.71	0.96	0.99990
2	5.69	0.99	0.99996
3	5.75	0.95	0.99991
4	5.50	0.97	0.99996
5	5.50	1.00	0.99990
Calibration number (2)			
1	5.71	0.96	0.99990
2	6.14	1.06	0.99997
3	6.03	1.11	0.99990
4	6.10	1.06	0.9998
5	6.07	0.98	0.99996
6	6.23	1.00	0.99998
7	6.23	1.00	0.99998

[a] I (nA) = $a + b$ log[glucose] (M).

and reproducibility of the resulting analytical signal also rises.

Evaluation of the biosensor based on an epoxy-graphite–Au–Pd–GOD

Electrolyte concentration and pH effects. Based on previous work carried out in our laboratory [8], a pH 7.00 buffered electrolyte (0.1 M phosphate, 0.1 M KCl) was chosen. The conductivity of this solution was found to be sufficiently high to support a reproducible double layer, it stabilizes the migration current and minimizes potential drop IR.

Figure 4 shows the effect of the variation of the pH of the supporting electrolyte has. Observing Eqn. 2 it can be seen that increasing the pH of the solution would cause a shift of the reaction towards the right. Consequently, the current would rise due to increased hydrogen peroxide oxidation. In Fig. 4 the increased analytical current is observed to be directly dependent on pH. The maximum current is attained near pH 9, showing a decrease with higher pH values due to the chemical denaturalization of the enzyme.

Linear range of the response. Figure 5 shows a typical calibration curve using the biocomposite based sensor described here. Using this curve the lower limit of the linear response (LLLR) and the upper limit of the linear response (ULLR) were determined. The systems under study showed a linear response dynamic range between 0.01 mM and 2 mM glucose and an approximate sensitivity of 1400 nA mM^{-1}.

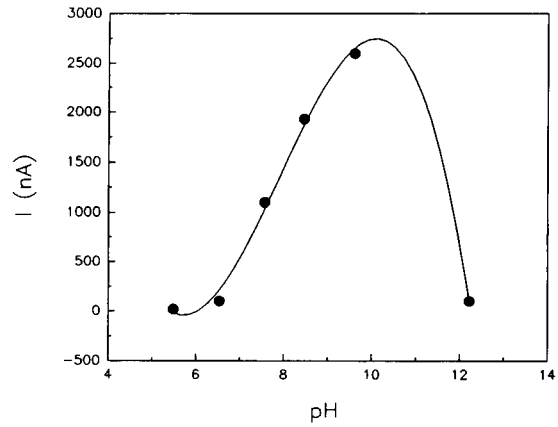

Fig. 4. pH effect on the signal of the glucose biosensor. Glucose concentration is 1 mM.

Response dynamics. When the glucose concentration was taken from 0 to 0.1 mM and from 0.1 mM to 1 mM the time the sensor took to attain a 95% response was 6 s in both cases. This is much lower than the 32 s needed for an amperometric transducer based on an epoxy-graphite transducer on top of which a nylon mesh with immobilized glucose oxidase has been deposited (epoxy-graphite–GOD sensor) [8]. This disparity is also

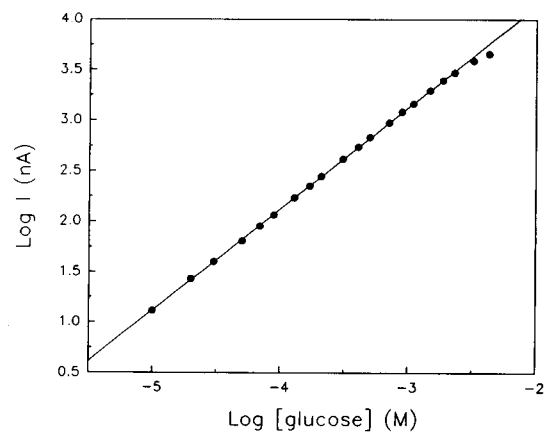

Fig. 5. Dynamic range of the response of the glucose biosensor based on an epoxy-graphite–Au–Pd–GOD biocomposite.

proved by the Michaelis-Menten apparent constants (K_m^{app}) calculated from the graphic depiction of $1/I$ vs. 1/[glucose] (Lineweaver-Burk plot). The value of K_m^{app} for the epoxy-graphite–GOD sensor was 16 mM and for the epoxy-graphite–catalyst–GOD was 7.6 mM. The proximity between the enzyme and the conductive material in biocomposites minimizes the diffusion problems arising at the surface of the electrode among the species involved in the generation of the analytical signal. This helps to reduce the overall response time of the sensor.

On the other hand, the response time is even lower than the one observed in an epoxy-graphite electrode used in the detection of H_2O_2 [8]. The probable cause of this phenomenon is the mixing of the Au–Pd in the biocomposite matrix where it can catalyze the oxidation of hydrogen peroxide at the electrode surface from the kinetic point of view of reaction 2.

Conclusions

A biosensor based on a epoxy-graphite–Au–Pd–GOD composite has been developed. The epoxy-graphite material allows for a simple and straightforward immobilization of the GOD enzyme, which is performed using a dry procedure. The enzyme is directly incorporated into the bulk of the sensor and it maintains its biocatalytical activity on the sensor surface for more than two months. The surface is renewed by a simple polishing procedure. Furthermore, materials such as the composite used, facilitate the blending of substances that enhance the response of the sensor. Such is the case of the addition of gold and palladium, which act as catalysts in the oxidation of hydrogen peroxide, enhancing the stability of the signal, lowering the response time when compared to non-modified epoxy-graphite biosensors, and decreasing the oxidation potential of the hydrogen peroxide by 250 mV. This reduction of the oxidation potential of H_2O_2 is similar to the reduction reported by other authors using Au–Pd modified graphite rods, where more complicated sputtering procedures were used. In any event, the introduction of metal catalysts in the biocomposite does not reduce the effect of common interferent species (ascorbic acid, uric acid, etc.) found in certain types of biological samples.

The polishing of the biosensor surface produces a fresh and reproducible surface since the enzyme and the catalysts are homogeneously blended into the bulk of the sensor.

This work was supported in part by CICYT, Madrid, Spain. F. Céspedes is grateful for the financial assistance in the form of a research scholarship (FPI program) from the Ministerio de Educación y Ciencia, Spain.

REFERENCES

1 V. Stará and M. Kopanica, Electroanalysis, 1 (1989) 251.
2 J. Wang, D.E., Electroanalysis, 3 (1991) 255.
3 J. Wang and K. Varughese, Anal. Chem., 62 (1990) 318.
4 J. Wang and M. Ozsoz, Electroanalysis, 2 (1990) 647.
5 V. Wollenberger, J. Wang, M. Ozsoz, E. González-Romero and F. Scheller, Bioelectrochem. Bioenerg., 26 (1991) 287.
6 J. Wang, E. González-Romero and M. Ozsoz, Electroanalysis, 4 (1992) 539.
7 S. Alegret and E. Martínez-Fàbregas, Biosensors, 4 (1989) 287.
8 F. Céspedes, E. Martínez-Fàbregas, J. Bartrolí and S. Alegret, Anal. Chim. Acta, 273 (1993) 409.
9 X. Yang, G. Johansson and L. Gorton, Mikrochim. Acta, 1 (1989) 9.
10 W. Matuszewski, M. Trojanowicz and A. Lewenstam, Electroanalysis, 2 (1990) 607.

Analytica Chimica Acta, 284 (1993) 27–36
Elsevier Science Publishers B.V., Amsterdam

Analyte identification in ion chromatography. Electromigration governed chronoamperometric profiles

Hisakuni Sato [a] and Purnendu K. Dasgupta

Department of Chemistry and Biochemistry, Texas Tech University, Lubbock, TX 79409-1061 (USA)

(Received 18th May 1993; revised manuscript received 22nd July 1993)

Abstract

If a DC voltage is applied between two electrodes defining the boundaries of a small volume containing a stationary acid electrolyte, the resulting chronoamperogram is characteristic of the anion of the acid and can be used for identification purposes. Factors that affect the results obtained and their reproducibilities have been identified and studied using two 2-electrode cell designs. One parameter that affects the day-to-day reproducibility of the results and is relevant to the use of the technique as an adjunct to suppressed ion chromatography is the impurity level of the eluent. High purity electrodialytically generated eluents constitute one solution. To see if impurity problems could also be circumvented by an alternate experimental arrangement, a cell was devised in which the trapped eluite was subjected to electromigration using a third electrode and a high electric field. While the influence of the impurities on the chronoamperometric profile generated by the analyte ion of interest could not be eliminated under the conditions of the present experiments, it is suggested that this design may have significant utility for future experiments, including tandem ion chromatography–capillary electrophoresis.

Keywords: Chromatography; Electromigration

Ion chromatography (IC) is now a mature technique. As it is used widely, a facile means of eluite ion identification as an adjunct to retention time-based identification is perceived to be increasingly important. In environmental analysis, situations are often encountered where more than one analyte unknowingly coelutes, resulting in an apparently single peak and thus both qualitative and quantitative errors. Also, peaks occassionally elute at times that correspond to no known standard analyte. Okada et al. [1] have shown one possibility of eluite ion identification in IC by measuring the chronoamperometric profile of a trapped eluite band with a DC conductivity cell. The profile is characteristic of the ionic mobility of the anions in the solution but it is also a function of their concentration. Since no direct control can be exercised over the concentration of the samples to be analyzed, the concentration dependence is eliminated by examining isoconductive slices of a chromatographic peak. The effluents eluting from an NaOH eluent suppressed anion chromatography system constitutes a good experimental system since the background effluent is pure water. In the experimental arrangement to practice this technique, the suppressor effluent flows through a 3-way electromagnetic valve and then through a DC conductivity detector. As the analyte of interest elutes and passes through the detector, the detector current increases. At some desired preset detector re-

Correspondence to: P.K. Dasgupta, Department of Chemistry and Biochemistry, Texas Tech University, Lubbock, TX 79409-1061 (USA).

[a] Permanent Address: Yokohoma National University, Faculty of Engineering, Department of Analytical Chemistry, 156 Tokiwa-Dai, Hodagaya-Ku, Yokohama 240 (Japan).

0003-2670/93/$06.00 © 1993 – Elsevier Science Publishers B.V. All rights reserved

sponse level, the electromagnetic valve is actuated to divert the flow to waste so that the eluite band then present in the detector becomes static. The chronoamperometric profile obtained under these conditions is characteristic of the trapped eluite ion and is related to its mobility. Further details are given in Ref. 1. While this approach is relatively simple and straightforward, the results exhibited poor reproducibility on a day-to-day basis. The cause of this was not understood and therefore a solution could not be pursued. It was also apparent that there were several experimental parameters that affected the observed chronoamperogram. Even the basic nature of the profile observed was not fully understood. When voltage is applied to a static electrolyte contained in a finite volume between two closely spaced electrodes, a monotonic decay of the initial current would be expected. Experimentally it was observed that from the moment of flow cessation, the current initially increased to a peak value and then decreased slowly in the expected manner.

In the present paper, the general phenomena and the possibility of ion identification by this approach have been examined in greater detail. Several parameters that affect the chronoamperometric profile were identified, leading to a technique that yields reproducible results.

EXPERIMENTAL

Cell configuration and flow path

Two-electrode linear configuration cell. Two different types (respectively 10-32 and 1/4-28 threaded, male-to-male) of chromatographic unions were utilized for constructing the DC conductivity cells shown in Fig. 1a and b. Electrodes were platinum tubes (50 mm × 0.5 mm i.d.). The distance between the two electrodes was 2 mm in cell 1, and 5 mm in cell 2. With these two cells, the flow scheme was the same as that used by Okada et al. [1]. A 4.6 × 50 mm column, packed with strong acid form cation exchange resin (SCX

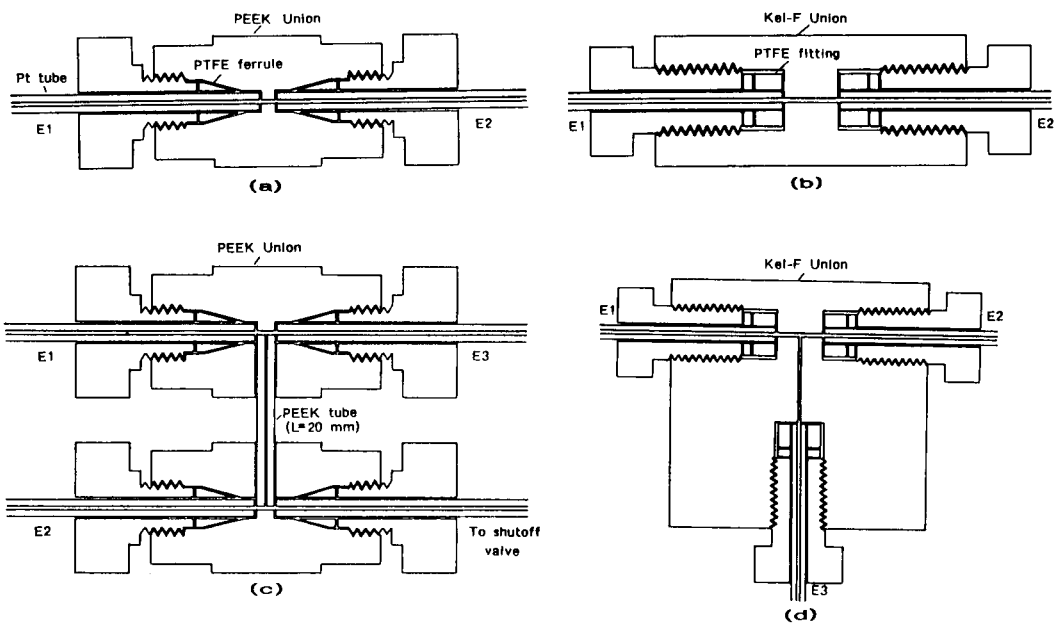

Fig. 1. Cell designs investigated: (a) two-electrode cell (E1 and E2 are tubular Pt electrodes) based on a 10-32 union, (b) two-electrode cell based on a 1/4-28 union, (c) three-electrode cell (E1–E3 are tubular Pt electrodes) of H-configuration, and (d) three electrode cell of T configuration.

gel, TOSOH) was used as a suppressor. An electromagnetic valve (type PSV-100SR, Pharmacia Inc.) was used for flow diversion at some desired preset level of detector current [1].

Three-electrode H- and T-configuration cells. Three tubular platinum electrodes were set up as shown in Fig. 1c and d. Electrodes 1 and 2 (E1 and E2) were used for DC conductivity measurement with an applied voltage of 6 or 12 V. At a preset threshold current level, the flow was diverted and a high voltage, up to 600 VDC, was applied between E1 and E3. Even with this amount of voltage applied, the overall current is at the nA level and over the entire course of experiment, 2–3 μC of charge are transferred. The resulting gas volume is less than 1 nl and readily dissolves in the solution.

The primary goal of this study is to develop a convenient means of identifying pure electrolytes, such as eluite bands from a suppressed IC system with a water background (e.g., one utilizing an NaOH eluent). In such a system the eluite anion appears in the detector as the corresponding acid. The migration path between E1 and E3 is initially filled with pure water (vide infra). When the flow is diverted and voltage is applied between E1 and E3, the acid trapped between E1 and E2 is subjected to electromigration. If E3 is positive with respect to E1, the eluite ions migrate towards E3 and H^+ electrolytically generated at E3 migrates towards E1. In cell 3, a PEEK tube (20 mm × 0.18 mm i.d. × 1.5 mm o.d.) was used as the conduit connecting E1 and E3. The tube can be provided with exterior threads to construct a very low-volume H-union [2]. Cell 4 was a T-union made from Kel-F. The migration path between E1 and E3 was a 10 × 0.3 mm tube.

Figure 2a shows the scheme of the flow path used with the three-electrode cells. A 50 × 4.6 mm i.d. column, packed with conventional mixed-bed demineralizing ion exchange resin, was used for filling the conduit with purified water. With the aid of the two 3-way valves (V1-V3), the flow path was cleaned, and purified water was filled in the conduit before each measurement. Note that depending on how these valves are manipulated,

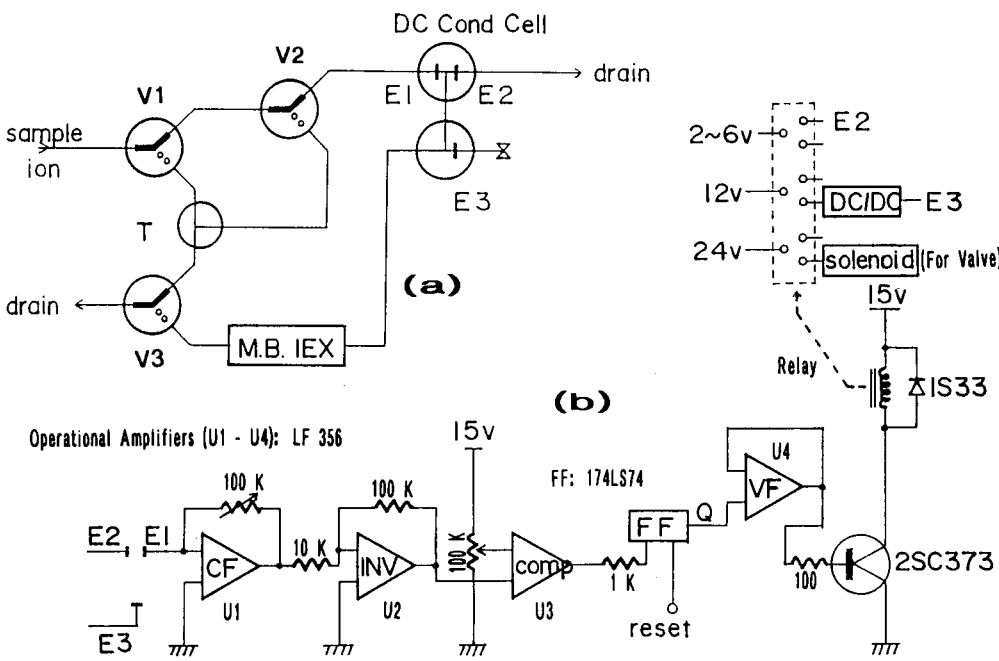

Fig. 2. (a) Flow scheme used with the three electrode cells. V1-V3 are three-way inert flow path solenoid valves, normally flow occurs through the thick lines shown. The mixed bed resin column produces pure water using the flow stream; (b) the electronic circuit used for fully automated operation of the three electrode cell system.

the sample can either proceed though V1 → V2 → E1 → E2 → waste or V1 → (V2) → V3 → waste, or V1 → V3 → demineralizer → E3 → E2 → waste. Typically, the flow proceeds through the thick lines shown schematically in V1-V3. At the current threshold, V2 is actuated and high voltage is applied to E3 to perform the electromigration experiment. At the conclusion of the electromigration study, voltage to E3 is shut off, V1 and V3 are actuated to purge the migration conduit with deionized water.

To perform the desired experiment in an automated manner, the electronic circuit shown in Fig. 2b was used. The current level for flow cessation could be changed by changing the reference voltage to the comparator in Fig. 2b. This is referred to as the threshold level through the rest of this paper. A DC/DC converter (Matsusada Precision, Tokyo) was used as the high voltage source. Operational amplifier U1 acts as a variable gain current follower and converts the cell current into a proportional voltage. Operational amplifier U2 then inverts the sign of the signal. This signal is then input to comparator U3 which compares it to a preset voltage. When U2 output exceeds this preset voltage, U3 output slews from −13 to +13 V and J–K flip-flop FF turns from reset to set. The Q output of the flip-flop is used to turn on the transistor T through a voltage follower U4. The relay R turns on, actuates the 3-way valve, turns on DC–DC high voltage power supply to power E3 and disconnects E2. The chronoamperometric current vs. time data were stored in memory in a XT-type personal computer through an A/D converter, and were processed with an algorithm written in Basic.

Sample solutions were prepared with reagent grade chemicals. The concentrations were 10–20 μM. 100 μl of sample solutions were injected for each experiment.

RESULTS AND DISCUSSION

Chronoamperograms with two-electrode cells

Figure 3 shows the chronoamperograms of SO_4^{2-} and $H_2PO_4^-$. The ordinate and abscissa

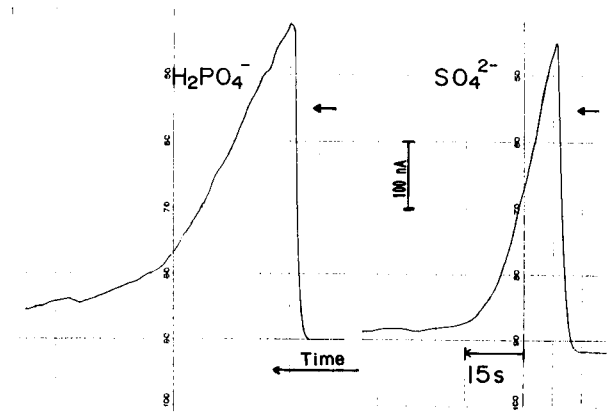

Fig. 3. Typical chronoamperograms obtained with the two electrode cells. Carrier flow-rate 1.5 ml min^{-1}, 10 μM 100 μl sample, 6 V DC applied.

values corresponding to the arrow marks indicate respectively the temporal location and the current threshold level chosen for flow diversion. In an arrangement similar to that previously reported [1], as the analyte enters the cell and the current increases to the threshold level, the electromagnetic valve is actuated, the flow direction is changed and the eluite is trapped in the cell. As previously noted, and as Fig. 3 shows, the observed current initially increases, reaches an apex and then decays. It is now understood that the current peak is related to the nature of valve action. The movement of the valve plunger in either a piston or diaphragm type valve causes the liquid ahead of the valve port to move forward in the cell. Since the system responds on the ascending part of an analyte concentration profile, this liquid movement represents an increased analyte concentration, resulting in an increase in current over the threshold value initially set. Accordingly, the formation and the magnitude of the current peak is very dependent on the nature of valve action and the flow resistance through the cell. The use of a electropneumatic rotary valve and/or increased backpressure to the cell can dramatically alter, even eliminate, the current peak. Thus, the true stopped flow chronoamperometric profile is represented in reality only by the current decay curve past the observed apex and the mobility characteristics of the different analyte ions are reflected on this descending slope.

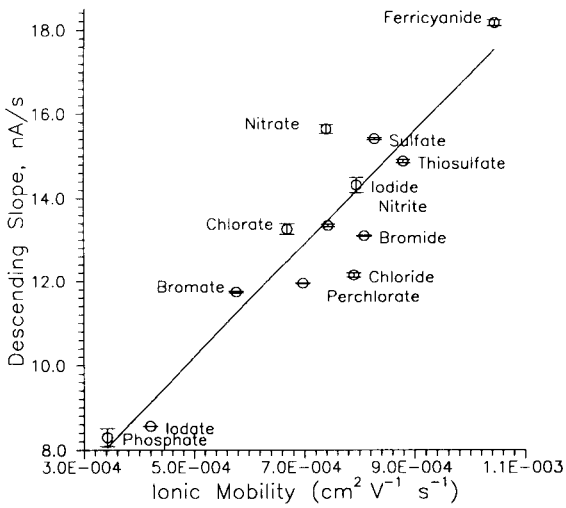

Fig. 4. A plot of the observed value of the slope of the descending portion of the chronoamperogram vs. the known ionic mobility of the test ion. Deionized water was used as the carrier liquid. The error bars represent ±1 standard deviation.

The values of the slope were obtained by the Savitsky-Golay smoothing derivative method [3].

The relationship between the ionic mobility and the experimental slope with deionized water as the carrier is shown in Fig. 4. The anions for which data are shown in this figure are expected to be present essentially completely in the ionic form for which the mobility value is plotted (phosphate is presumed to be present as $H_2PO_4^-$). While the observed relationship is generally linear ($r^2 = 0.93$), the reproducibility of the individual slope values are such (R.S.D. rages from $< 0.04\%$ for iodate to 2.65% for phosphate) that the departure from the best-fit straight line must be taken as real and due to reasons as yet not understood. In any case, the level of reproducibility attained under the above conditions makes it clear that the system is applicable to the identification of an anion in an unknown electrolyte, as long as a single anion is present, without reference to a chromatographic context.

In a real ion chromatographic experiment, pure water cannot obviously be used as the carrier (eluent). In principle, however, once an NaOH eluent is suppressed, it becomes pure water and there should be little difference at the detection stage of the present experimental scheme. Yet, actual experiments with a suppressed NaOH eluent system provided slope values much lower than those obtained with highly purified water as carrier. Further, the day-to-day reproducibility of these values were quite poor. Figure 5 depicts a comparison of the respective data obtained with fresh Mill-Q water, house-deionized water (sub-

TABLE 1

Descending or ascending slopes of current–time curve

Exp. No.	Cell type	Sample ion	Experimental conditions				Experimental results		
			DC voltage	Threshold level (μA)	Temp. (°C)	n	Slope (arb. units²)	R.S.D. (%)	Background current (μA)
1	1	SO_4^{2-}	6	4.0	20	10	4.029	4.8	0.253
2	1	SO_4^{2-}	6	4.0	20	9	4.569	4.0	0.258
3	1	IO_3^-	2	4.0	21	8	3.639	3.2	0.160
4	2	SO_4^{2-}	12	4.0	24.5	5	11.588	1.0	0.086
5	2	SO_4^{2-}	12	4.0	24.5	9	7.081	1.6	0.184
6	2	SO_4^{2-}	12	4.0	24.5	8	4.453	1.2	0.274
7	2	SO_4^{2-}	12	4.0	24.5	3	3.752	0.7	0.291
8	2	IO_3^-	12	4.0	24.5	9	2.543	1.0	0.391
9	2	IO_3^-	12	4.0	24.5	9	2.354	1.0	0.385
10	2	IO_3^-	12	4.0	24.5	8	2.404	1.4	0.275
11	3	SO_4^{2-}	3,550	2.5	24.5	5	4.719	6.6	< 0.05
12	3	IO_3^-	6,550	4.0	24.5	5	4.517	5.6	< 0.05
13	3	IO_3^-	6,550	4.0	24.5	10	4.783	4.1	< 0.05
14	4	SO_4^{2-}	12,550	4.0	26	10	6.135	4.0	< 0.05

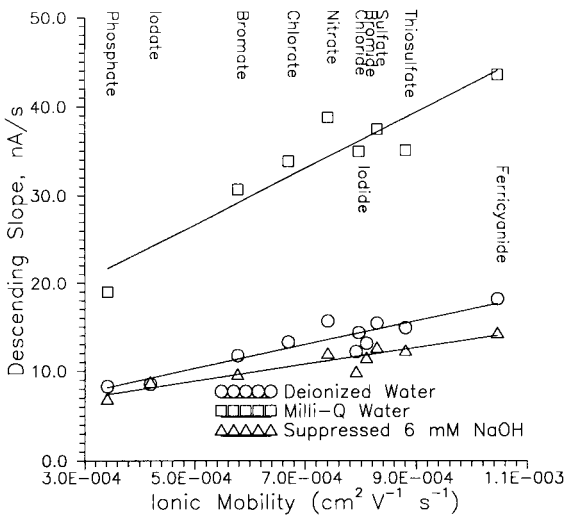

Fig. 5. Observed slope vs. ionic mobility plots obtained with three different carrier liquids.

sequently exposed to the laboratory atmosphere) and a 6 mM NaOH solution. The trend of lower slopes along the series is clearly evident. Some detailed data on the dependence of the observed slope values on cell designs and various other experimental conditions are presented in Table 1. In particular, experimental sets 4–7 were identical except for the choice of the carrier, ranging from Milli-Q water (set 4) to 6 mM NaOH (set 7). A real NaOH eluent always contains dissolved carbonate and even with purified water, dissolved CO_2 is present unless scrupulous care is taken to prevent its intrusion. Thus, varying amounts of H_2CO_3 are present in these solutions after passage through the suppressor and the level of this contamination is reflected in the background current, that increases in the experimental series 4–7. Note that because H_2CO_3 is only weakly ionized, the actual amount of dissolved CO_2 is related approximately to the square of the observed background current [4]. The chronoamperometric slopes obtained in electromigration experiments with weak acids are lower than those of strong acids with a comparable anion mobility. In the weak acid case, a significant portion of the solute is initially unionized and is not subject to electrophoretic migration. It begins to ionize only as the ionic components migrate electrophoretically. For weak acids it is therefore more appropriate for comparisons to use a weighted ionic mobility value in which the true ionic mobility is multiplied by the fraction ionized.

In the present instance with experimental sets 5–7, we have a more complex situation in which the current decay rate of a high mobility anion like sulfate is being measured in the presence of varying amounts of a low mobility anion HCO_3^-, that is weakly ionized. The observed values represent a weighted average, i.e., the true slope of sulfate is corrupted to varying degrees due to the presence of varying level of the contaminants.

If these experiments are done with carbonate or borate eluents, the former likely being the most common eluent used to date in suppressed IC, one would essentially ensure a constant level of background electrolyte in the detector. It is possible to obtain reproducible values for the chronoamperometric slopes for strong acid eluites, using only a limited portion of the initial descending profile. However, this is possible only at relatively high eluite concentrations (such that the eluite dominates any contribution of the background electrolyte and especially during the initial portion of the migration experiment, the presence of the strong acid greatly depresses the ionization of the background electrolyte), and is therefore of limited practical value.

One practical alternative is to ensure minimum background electrolyte contribution through the use of ultrapure eluents, coupled to electrodialytic suppression. The method of on-line electrodialytic generation of ultrapure NaOH eluents (suppressed conductance over a 0–175 mM concentration range of 340 ± 40 nS/cm) has been published and patented [4–9]. This approach may ultimately be the most desirable because such eluents have many advantages over conventional eluents other than the issues relevant to this paper.

Nevertheless, electrodialytic eluent generation systems are not commercially available at this time. We wanted therefore to explore if the effect of the background electrolyte can be eliminated or minimized by changing the physical design of the experiment such that the eluite (and any background electrolyte) are introduced at one

end of a migration conduit, which is filled reproducibly with the same medium. The three electrode cell designs 3 and 4 and the attendant experimental flow scheme were arrived at with such a perspective.

Chronoamperograms with three-electrode cells

As in the case of the two-electrode cell, when analyte ions come into the DC conductivity cell (electrodes 1 and 2), the current increases. At a preset current threshold level, using the arrangement of Fig. 2, the flow was stopped and a high DC voltage is applied between electrodes 1 and 3. Note that the electric field strength of several hundred volts per cm used in these experiments for electromigration is equal to or in excess of typical electric field strengths used in present day capillary electrophoresis (CE). In the migration conduit joining E3 and E1, purified water was deemed a convenient choice as a reproducible medium to be introduced before each experiment. It could be prepared in-line from the chromatographic effluent using the mixed bed resin column. Prior to flow switching, the current is monitored between E1 and E2 using a low applied voltage. Starting from the moment of switching, the applied voltage is between E1 and E3. If the conduit is imagined to be a series of discrete zones, the overall current is related to $\Sigma C_{ij}\lambda_j E_i$ where C_{ij} is the concentration of species j in zone i and λ_j is the mobility of species j and E_i is the electric field in zone i and Σ represents the summation over all i and j values. Because most of the conduit is filled with pure water at this time, much of the applied voltage is dissipated over this high resistance region and the current starts at a very low value. As the eluite anion at one end of the conduit and the electrogenerated H^+ begins to migrate in opposite directions through the conduit, the current begins to increase as the electric field is more uniformly distributed. It reaches a maximum and eventually decreases as the electrolyte accumulates in the electrode region and the central region has little electrolyte. Figure 6 shows the chronoamperograms of some anions. The ascending slope of the chronoamperogram reflects the characteristics of the anion migrating through the conduit. Figure 7

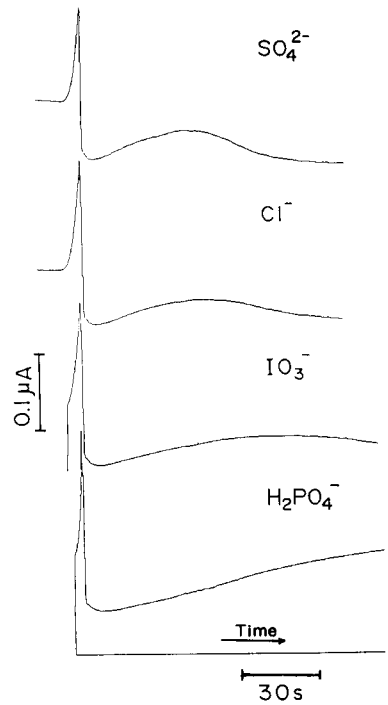

Fig. 6. Chronoamperograms obtained with the three-electrode cells. The results for the different ions has been offset on the y-axis for ready visibility. Carrier flow-rate, 1.0 ml min^{-1}; 10 μM 100 μl sample; E2, 3.0 V; E3, 550 V.

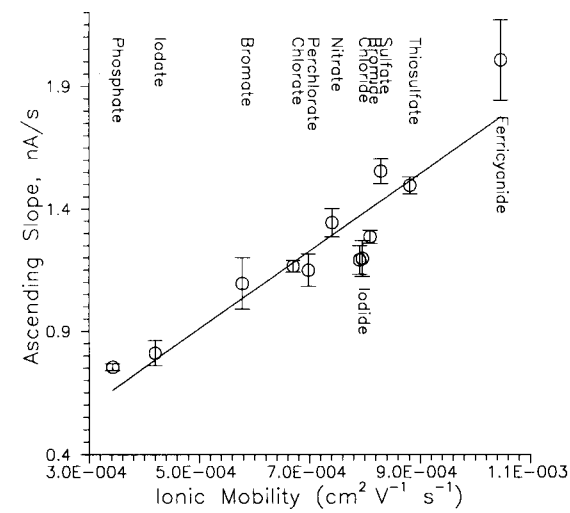

Fig. 7. A plot of the observed slope of the ascending portion of the chronoamperogram vs. the known ionic mobility of the test ion, cell type 3. Milli-Q water as carrier, ±1 standard deviation is shown as the error bar.

shows the ascending slope plotted against the ionic mobility, results similar to those shown previously for the 2-electrode cell design are observed. However, reproducibility is poorer than that observed in the simpler 2-electrode cell arrangement, even with pure water as the carrier (see also results from experimental sets 11–14 in Table 1). Moreover, The 3-electrode cell arrangement did not solve the problem arising from varying purity levels of the eluent background. The eluent contaminant ions affected the slope values observed for the analyte of interest in the same manner as in the 2-electrode cells. One apparent reason may be that the initial distribution of the electrolyte in the conduit, i.e., analyte/contaminant mixture at one end and the rest of the conduit filled with deionized water, results in very little of the applied voltage being available for the electromigrative separation of the analyte from the contaminant. At least with the present approach, the use of the 3-electrode cell leads to no advantage and cannot therefore be recommended.

Reproducibility and effect of various parameters

The descending or ascending slopes of chronoamperograms for different test anions were repeatedly measured with cells 1–4. The experimental data are shown in Table 1. With cell 2, the relative standard deviation (R.S.D.) values are about 1%. With the other cells, the R.S.D. values are about 5%. We believe that reproducibility is adversely affected by the unswept volume in the migration path; cell 2 has minimum dead space. Cell 4 is partly similar in structure to cell 2 but the T-junction itself leads to an appreciable amount of unswept volume.

Table 2 shows the qualitative dependence of the results obtained with the different cell designs upon the experimental parameters. The dependence on flow history possibly originates from the fact that the geometry of the sample bolus, i.e., its radial profile is a function of the flow velocity prior to flow cessation. The use of a flow-through tubular electrode with a part of the analyte contained within the electrode make a priori theoretical evaluations difficult. The dependence is less with the three-electrode design because prior to flow switching, there was no sample flow through one of the measuring electrodes. For similar reasons, we believe that the two electrode geometry shows a dependence on the electrode polarity relative to the flow direction whereas the three-electrode geometry does not. A small continuation of flow in the original direction due to valve action is irrelevant to the 3-electrode cell and thus the nature of the valve or the backpressure to the cell have no effects in

TABLE 2

Qualitative dependence of the chronoamperometric profile on cell design and experimental parameters

	Two electrode system	Three electrode system
Flow-rate of carrier	dependent	less dependent
Electrode polarity (E1–E2)	dependent	not dependent
Back pressure to cell	very sensitive	not sensitive
Mechanism of flow cessation valve	dependent	not dependent
Applied DC voltage (E1–E2)	sensitive	not sensitive
Structure of cell (near electrode)	dependent	dependent
Threshold level for flow cessation	dependent	dependent
Impurity in carrier	influenced	influenced
Distance between E1 and E2	very dependent	less dependent
Conduit size	N/A	very dependent
Applied DC voltage (E1–E3)	N/A	very dependent

this geometry. Diffusive migration from unswept volume near electrodes affect both type of cell designs and in the present type of experiments it is possibly compounded by electrolytic gas evolution in the form of microbubbles at the electrode and/or uneven Joule heating. Chronoamperograms from both cell types are influenced by the choice of the switching threshold and impurity levels in the carrier. As may be expected, the results from the 3-electrode cell are also influenced markedly by the magnitude of the high voltage applied for electromigration and the dimensions of the migration conduit. The spacing of the initial sensing electrodes do not, however, have as much influence on the results with the 3-electrode cell as with the 2-electrode design.

Potential utility of the three-electrode cell geometries

Assuming that radially inserted wires can be used in lieu of tubular electrodes to make a more compact design, minimize unswept volume and thereby improve reproducibility, we believe that the concept of the 3-electrode cell geometry and the associated flow arrangement may have merit for further future investigations. It is clear that to separate the analyte from the eluent contaminant, the applied electric field must be distributed differently than that in the present experiments. Consider a situation where the conduit is filled initially with the sodium salt of a weak acid with a low mobility anion. The concentration of this solution is such that the conductivity is approximately the same as the suppressed eluite conductivity that initiates flow switching. At the beginning of the migration experiment one would then have an acidic solution at one end of the conduit containing the analyte ion and any eluent contaminant and the alkaline electrolyte through the rest of the conduit. The principal charge carrier at one end will be H^+ and at the other end OH^- will be a significant charge carrier. Because of acid–base neutralization at the interface, the conductivity will be the lowest at this point. Comparable experiments in CE suggest that the analyte/contaminant zone will stack to a sharp band [8]. Separation is then expected to take place by further migration. The chronoamperometric profile in such an experiment may not be sufficient by itself to deduce the analyte mobility. However, an alternative is to monitor the conductivity of the fluid in the migration conduit at the appropriate end with an on-line probe. As the high mobility analyte ion zone passes through the probe region and replaces a corresponding amount of the low mobility carrier electrolyte ion, a corresponding decrease in voltage across the probe electrodes will be registered. Many designs of on-line conductivity detectors for CE have been described that will be applicable [9–11]; one particularly simple design recently developed in this laboratory involves the insertion of an insulated bifilar wire through a radial hole in the capillary insulation is removed from all sides of the bifilar wire except that between the two wire elements which serve as the electrodes [12].

The use of membrane-suppressed conductometry, well known in IC, has recently been shown to be a practical detection method for capillary electrophoretic separation systems [13]. Significant electroosmotic flow is an essential ingredient to this approach. It is not difficult to envision a three-electrode cell arrangement in which the migration conduit is a fused silica capillary filled with a borate electrolyte that is both suppressible and provides the necessary electroosmotic flow. Such an arrangement can be the heart of a powerful, two-dimensional, suppressed IC-suppressed CE system.

REFERENCES

1 T. Okada, P.K. Dasgupta and D. Qi, Anal. Chem., 61 (1989) 1387.
2 K. Morris and P.K. Dasgupta, LC–GC Mag., 10 (1992) 149.
3 A. Savitsky and M.J.E. Golay, Anal. Chem., 36 (1964) 1627.
4 D.L. Strong, P.K. Dasgupta, K. Friedman and J.R. Stillian, Anal. Chem., 63 (1991) 427.
5 D.L. Strong and P.K. Dasgupta, J. Membr. Sci., 57 (1991) 321.
6 D.L. Strong and P.K. Dasgupta, J. Chromatogr., 546 (1991) 159.
7 D.L. Strong, P.K. Dasgupta, J.R. Stillian and K. Friedman, US Pat. 5,045,204 (1991).

8 R.-L. Chien and D.S. Burgi, Anal. Chem., 64 (1992) 489A.
9 P. Gebauer, M. Deml, P. Bocek and J. Janak, J. Chromatogr., 267 (1983) 455.
10 X. huang, T.-K.J. Pang, M.J. Gordon and R.N. Zare, Anal. Chem., 59 (1987) 2747.
11 Th.P.E.M. Verheggen, J.L. Beckers and F.M. Everaerts, J. Chromatogr., 452 (1988) 615.
12 S. Kar, H. Liu, P.K. Dasgupta and H. Hwang, 1993, unpublished results.
13 P.K. Dasgupta and L. Bao, Anal. Chem., 65 (1993) 1003.

Analytica Chimica Acta, 284 (1993) 37–43
Elsevier Science Publishers B.V., Amsterdam

Column chromatographic separation of Y^{3+} from Sr^{2+} by polymeric ionizable crown ether resins

D.J. Wood, S. Elshani and C.M. Wai

Department of Chemistry, University of Idaho, Moscow, ID 83843 (USA)

R.A. Bartsch

Department of Chemistry, Texas Tech University, Lubbock, TX 79409 (USA)

M. Huntley and S. Hartenstein

Westinghouse Idaho Nuclear Company, Inc., P.O. Box 4000, Idaho Falls, ID 83415 (USA)

(Received 17th May 1993)

Abstract

Condensation polymers containing subunits of crown ether carboxylic acid monomers are effective stationary phases for the chromatographic separation of Y^{3+} and Sr^{2+}. The pH range and metal loading capacities for the resins have been determined under equilibrium conditions. The resin can be regenerated for repeated use without losing its separation capability. Altering the molecular structure of the monomer (*sym*-dibenzo-16-crown-5-oxyacetic acid) by an alkyl substitution on the macrocyclic cavity decreases the loading capacity of the resin.

Keywords: Chromatography; Crown ethers; Polymers; Strontium; Yttrium

The separation of Y^{3+} and Sr^{2+} is important for the determination of the fission product ^{90}Sr ($t_{1/2}$ = 28.9 years) and its daughter ^{90}Y ($t_{1/2}$ = 64 h) in environmental samples [1]. Extraction of pure ^{90}Y from its precursor ^{90}Sr is also important for new applications of ^{90}Y in nuclear medicine [2]. Any method applied to this type of separation must be accomplished rapidly, conveniently, and efficiently for accurate quantification of the nuclides or for obtaining the short-lived daughter product for medical use.

It has been shown that ionizable crown ethers containing a carboxylic acid functional group are effective for the separation of Y^{3+} and Sr^{2+} by solvent extraction [3]. The extraction is reversible with respect to pH and no specific counteranions are required. While quantitative separation can be readily achieved, solvent extraction has the potential disadvantages of production of organic waste and the consumption of ligand. Chromatographic separation of the isotopes based upon a selective stationary phase would eliminate these disadvantages. Wai and Du [4] recently reported the separation of ^{90}Y from ^{90}Sr by paper chromatography with paper strips impregnated with crown ether carboxylic acids. This method is limited by the fact that the paper strips can only be used for one application. A column chromatographic technique based upon a stationary phase incorporating ionizable crown ethers which may be regenerated for repeated separations of ^{90}Y from ^{90}Sr would be highly desirable.

It has been shown that crown ether carboxylic acids containing two benzo group substituents

Correspondence to: C.M. Wai, Department of Chemistry, University of Idaho, Moscow, ID 83843 (USA).

0003-2670/93/$06.00 © 1993 – Elsevier Science Publishers B.V. All rights reserved

can be polymerized to produce resins which contain the macrocyclic monomers as subunits [5–9]. The polymerization is achieved by condensation of dibenzo crown ether carboxylic acid monomers with formaldehyde in formic acid. These new resins have been utilized for the selective sorption and separation of alkali and alkaline earth metals in aqueous solution. This paper examines the conditions for separation of Y^{3+} from Sr^{2+} using the resins prepared by polycondensation of dibenzo crown ether carboxylic acids.

EXPERIMENTAL

Reagents

The radioactive isotope ^{88}Y ($t_{1/2} = 106.6$ days) was obtained from Isotope Products Lab. of Burbank, California. ^{87m}Sr ($t_{1/2} = 2.8$ h) was obtained by neutron activation of strontium nitrate solutions at the Nuclear Radiation Center at Washington State University. Reagent grade chloroform was obtained from EM Science. The procedures for the synthesis of the crown ether carboxylic acids are given in the literature [6]. The condensation polymers were prepared from the crown ether monomers in our laboratory according to the procedures described in the literature [5]. All other reagents were Baker Analyzed Reagents.

Radioactivity measurements

^{90}Y and ^{90}Sr, which are the isotopes of interest to this report are pure beta emitters. This prevents the simultaneous quantitation of the isotopes. In this study, we used the gamma emitting isotopes ^{88}Y (898 keV) and ^{87m}Sr (388.4 keV), whose energies are sufficiently different to provide simultaneous measurement of the elements by a Ge(Li) detector. The radioactivity measurements in the solvent extraction experiments were performed by gamma spectrometry according to a procedure described previously [11]. Radioactivity measurements in the chromatographic column experiments were performed by counting individual elution fractions in 1-ml volumes by gamma spectrometry. Metal concentrations were determined by comparison to a prepared standard of the same counting geometry. The solutions which resulted from the stripping of the resins in the loading experiments were counted similarly.

pH Dependence of metal loading on resins

The loading of Y^{3+} on the ionizable crown ether resins was studied as a function of pH in batch experiments. Weighed amounts of resin were placed in 30-ml polyethylene bottles which contained 20 ml of 0.05 M sodium acetate spiked with the radioactive tracer ^{88}Y. The containers were shaken for 30 min on a mechanical wrist-action shaker (Burrel Model 75). After the resin had settled to the bottom of the containers, the pH was measured and 1-ml aliquots of the supernatant solutions were removed for gamma counting. Following radioactive measurement, the counted solutions were replaced and the solutions were adjusted to the desired pH with nitric acid and lithium hydroxide for repeated experiments.

Metal loading capacities

The maximum loading capacities of the ionizable crown ether resins was determined under equilibrium conditions. Weighed amounts of the resins were placed into separate glass vials. 2 ml of a 0.05 M sodium acetate solution at pH 6.5, which contained 2.5×10^{-3} M each of Y^{3+} and Sr^{2+} and spiked with ^{88}Y and ^{87m}Sr radioactive tracers, were added to each vial. The solution was then shaken on the wrist-action mechanical shaker for 5 h. After shaking, the loaded resin was filtered, rinsed with a small volume of 0.05 M sodium acetate solution, and dried in an oven. A weighed amount of the dry loaded resin was placed in a 0.1 M nitric acid solution and shaken for 1 h to strip the metals. A measured aliquot of the stripping solution was then removed and counted by gamma spectrometry. Metal concentrations in the stripping solution were determined by comparison to a prepared standard.

Column separation experiments

The elution separation experiments were performed using polyethylene columns (10 cm × 8 mm i.d.) purchased from Pierce (Rockford, IL). Weighed amounts of the crown ether resins (approximately 0.05 g) were placed in the column to serve as an ion-exchange resin. Glass frits which

were provided by the column manufacturer were placed in the column to contain the resin. After the column preparation, the resins were pre-equilibrated with a small volume of an ammonium acetate buffer. The columns were then loaded with a 10-ml aliquot of 0.05 M ammonium acetate which was 1×10^{-4} M each in Y^{3+} and Sr^{2+} spiked with the radioactive tracers.

The loading solution was allowed to pass through the column at a rate of approximately 2 ml min^{-1}. When all the loading solution had exited the column, elution of the metals was started by the addition of successive 1-ml aliquots of 0.05 M ammonium acetate which had been adjusted to a pH of 6.5 with nitric acid. Each 1-ml fraction was collected separately and counted by gamma spectrometry for metal concentration determination. After 10 fractions had been collected, the elution solution was changed to 0.05 M nitric acid. Each 1-ml fraction was collected and counted as before.

Solvent extraction

The organic phase in extraction experiments with the ionizable crown ether monomers **1** and **2** was prepared by dissolving weighed amounts of the macrocycles in chloroform with ligand concentrations of 1×10^{-2} M. The aqueous phase consisted of a 0.05 M sodium acetate buffer solution which was 1×10^{-4} M in each metal.

Equal amounts of the organic and aqueous phases were placed in an extraction container and shaken on a wrist-action shaker for sufficient time for the system to reach equilibrium. The pH of the aqueous phase was measured using an Orion combination semi-micro electrode. Equal amounts of each phase were then removed and counted separately by gamma spectrometry. The ratio of the gamma activity in the phases was used to determine the extraction efficiency of the ligand at the measured pH.

RESULTS AND DISCUSSION

pH Dependence and loading capacity of resins

To determine the viability of a chromatographic separation of ^{90}Y from ^{90}Sr using the polymerized ionizable crown ethers, we have studied the metal loading capacities of resins **3** and **4**. The synthesis of resins **3** and **4** was achieved by a condensation reaction with the corresponding monomers **1** and **2** [5]. The propyl substituted compound **2** was selected because it has been shown to exhibit altered selectivity in the separation of the alkali metals [6]. The loading of Y^{3+} and Sr^{2+} on the ionizable crown ether resins **3** and **4** shown in Fig. 1 are expected to be dependent upon the pH of the aqueous loading solution. This pH dependence has been investigated for resin **3** to determine an appropriate pH range for the separation experiments. Using ^{88}Y as a tracer, our experiments indicate that resin **3** does not retain Y^{3+} in solutions of pH < 3, as shown in Fig. 2. However, as the pH of the loading solution is increased above 3, Y^{3+} is retained on the resin. The percent of the activity which is

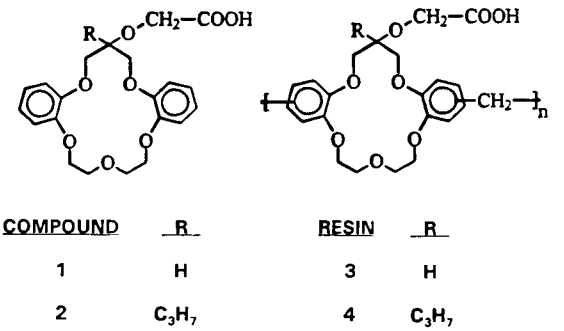

COMPOUND	R	RESIN	R
1	H	3	H
2	C_3H_7	4	C_3H_7

Fig. 1. Molecular structures of crown ether carboxylic acid monomers and polymers.

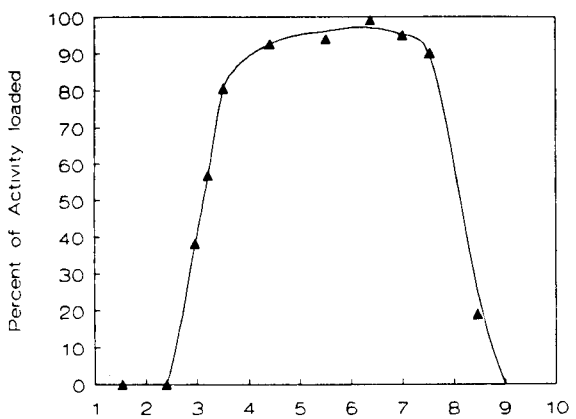

Fig. 2. pH dependence on the loading of Y^{3+} on resin **3**.

TABLE 1

Metal loading capacities of resins

Resin	Loading capacity (mmole g^{-1})		
	Y^{3+}	Sr^{2+}	Y^{3+}/Sr^{2+}
3	0.27	0.05	5.4
4	0.07	0.02	3.5

loaded on the resin becomes quantitative in solutions with pH > 6.0. This result suggests that the maximum loading of the resin should occur in the pH range between 6 and 7, above which hydrolysis of Y^{3+} results in precipitation of the metal ions from solution.

The loading capacity of the condensation polymer resins was determined by equilibrium experiments in which excess amounts of the metals were placed in contact with the resin for an extended period of time. The experiments were performed in an aqueous sodium acetate solution (0.5 M) at pH 6.5. The loading capacities of Y^{3+} and Sr^{2+} on resin **3** were determined to be 0.27 and 0.05 mmoles per gram of resin, respectively. The ratio of the loading capacities of Y^{3+} to Sr^{2+} has a value of 5.4. The propyl substituted resin **4** exhibits a decreased loading capacity from that of **3** for both Y^{3+} and Sr^{2+} as shown in Table 1. The loading capacity for Y^{3+} on resin **4** is 0.07, approximately a factor of 4 less than that on resin **3**. The loading capacity of Sr^{2+} on **4** is 0.02, which is approximately a factor of 3 less than that on resin **3**. The ratio of the loading capacities (Y^{3+}/Sr^{2+}) on **4** has a value of 3.5. The decrease in the value of the loading capacity ratio from resin **3** to **4** suggests that resin **3** will provide a stationary phase for a chromatographic separation which is more selective for Y^{3+} over Sr^{2+} than resin **4**. In addition, the larger loading capacity values for resin **3** will provide a stationary phase with a greater sample capacity than that of **4**.

Chromatographic separation of Y^{3+} and Sr^{2+}

The results of the resin loading capacity experiments suggest that immobilization of the ionizable crown ether resins on a chromatographic column has the potential for offering a rapid and efficient method for the separation of Y^{3+} from Sr^{2+} in solution. The separation of Y^{3+} from Sr^{2+} by selective elution from an ion exchange column with resins **3** and **4** as stationary phases were evaluated experimentally. Figures 3 and 4 show the results of the elution experiments.

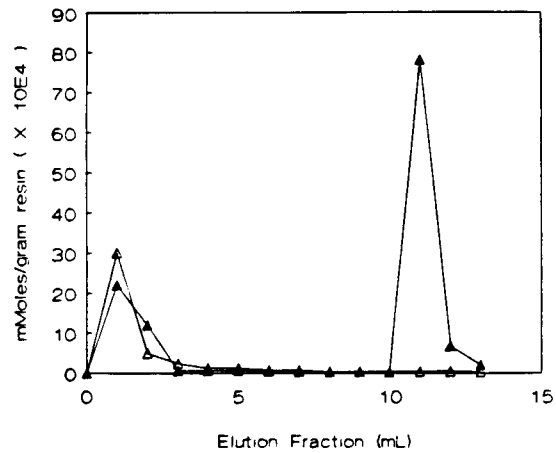

Fig. 3. Column chromatographic separation of Y^{3+} and Sr^{2+} with resin **3** under conditions in which the metal concentrations exceeded the loading capacities of the resin. (▲) Y^{3+} and (△) Sr^{2+}.

The elution experiments were performed by loading a solution of known metal concentrations and eluting immediately. The amount of metal was selected to exceed the loading capacity of the

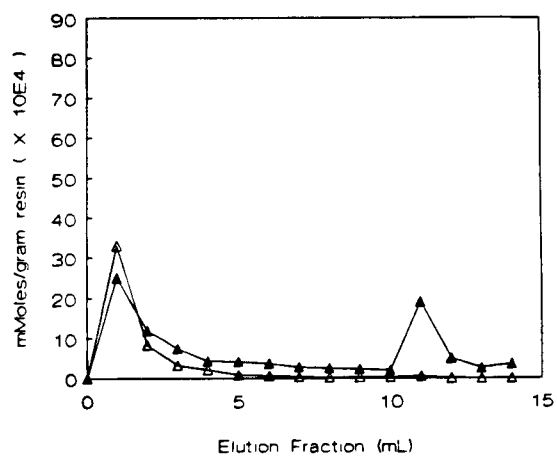

Fig. 4. Column chromatographic separation of Y^{3+} and Sr^{2+} with resin **4** under conditions in which the metal concentrations exceeded the loading capacities of the resin. (▲) Y^{3+} and (△) Sr^{2+}.

column. The columns were not rinsed after loading. This allowed the rate at which unbound metals are washed from the column to be observed. The peak which is found at the start of the elution procedure is due to unbound metal ions which are exiting the column. Resins **3** and **4** exhibit peaks at the start of the elution which are approximately equal in peak area. This initial peak is due to the loading solution containing unbound metal ions which did not exit the column during the loading procedure.

A gradient elution procedure was employed to elute the bound metals from the column. 10 ml of an ammonium acetate solution at pH 6.5 were placed on the column. Each ml of eluent was collected and counted separately. A solution of 0.05 M nitric acid was then employed as a stripping eluent for the bound Y^{3+} ions. The peak found at the end of the elution procedure is due to bound metal ions which have been stripped by the acid eluent. At this concentration of acid, the metals are stripped rapidly. The metal concentrations in the eluent fractions return to background within a few additions. The purity of the Y^{3+} obtained in the fraction located at the apex of the peaks shown in Figs. 3 and 4 was calculated from the ^{88}Y concentrations in the counted fraction. The purity of Y^{3+} was found to be 99.5% and 97.5% for **3** and **4**, respectively. This indicates that ^{90}Y can be obtained in high purity using resin **3**.

The eluted Y^{3+} peak for **4** is much smaller than that of **3**. This decrease in peak size is expected from the loading capacity results given in Table 1. The total concentration of Y^{3+} in the elution peaks is estimated to be 3.3 times greater for **3** than **4**. This result indicates that the placement of the alkyl functional group on the ionizable crown ether **3** has a negative rather than beneficial effect when applied to the separation of Y^{3+} from Sr^{2+}. Our experiments indicate that the resins can be regenerated and used for multiple separations. In some cases, columns containing resin **3** were regenerated for use in 8 to 10 successive experiments with no observable decreases in loading capacity or separation efficiency. It was observed however, that the use of concentrated nitric acid eluents (> 1 M) rapidly

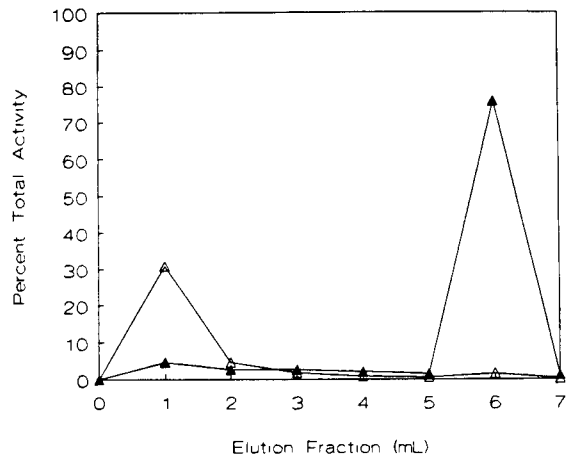

Fig. 5. Column chromatographic separation of trace metals Y^{3+} and Sr^{2+} with resin **3** under conditions in which the metal concentrations did not exceed the loading capacity of the resin. (▲) Y^{3+} and (△) Sr^{2+}.

degraded the resin, which could be visualized as a slightly colored solution exiting the column. Columns loaded with resins **3** and **4** can be stored for later use by placing a few ml of buffered aqueous solution on the resin bed and capping both ends of the polyethylene column.

The chromatographic separation of Y^{3+} and Sr^{2+} under conditions in which the concentration of the metals in the loading solution did not exceed the loading capacity of the resin on the column was performed with resin **3** as shown in Fig. 5. A 10-ml solution of 0.5 M ammonium acetate containing trace amounts of the radioisotopes was placed on the column and the eluent was collected for radioactive measurements. Five individual 1-ml aliquots of 0.5 M ammonium acetate solution at pH 6.5 were then placed on the column and collected for individual radioactive measurements. The remaining metals were then stripped with 1-ml aliquots of 0.05 M nitric acid. The data is plotted in Fig. 4 as the percent of the total activity of each radiotracer as compared to a prepared standard. Approximately 65% of the activity from the Sr^{2+} tracer exited the column with the loading solution prior to the stripping steps. The remaining Sr^{2+} activity was eluted in the first two additions of the stripping solution. The total recovery for Sr^{2+} was quantitative. The activity of the Y^{3+} tracer was retained by the

column until the addition of the nitric acid stripping solution. The activity then exited the column rapidly. This experiment suggests that trace concentrations of Y^{3+} can be separated from Sr^{2+} on the column with less than 10 ml of eluent in a rapid and efficient manner.

Extraction with free ligand

The decrease in loading capacity of resin **4** which contains the alkyl substituted polymer may be due to a change in the conformation of the monomer when an alkyl substituent is present on the macrocyclic cavity. It is interesting to compare the behavior of the polymerized ligands with the free ligands in solvent extraction. For this purpose we performed classical solvent extraction experiments employing the ionizable crown ether monomers as the chelating agents in chloroform. The solvent extraction experiments were performed with compounds **1** and **2** under similar conditions to evaluate the extraction characteristics of each compound for Y^{3+} and Sr^{2+}. The extraction of the metal ions into chloroform as a function of the pH of the aqueous phase is shown in Fig. 6.

The extraction of Y^{3+} into the organic phases becomes observable between pH 4 to 5 and reaches a maximum above pH 6. The extraction of Sr^{2+} by **1** becomes observable at pH 6.5. Sr^{2+} remains negligible in the organic phase over the entire pH range 4–7 for **2**. However, the maximum extraction efficiency of Y^{3+} for **2** is much lower than that for **1**. These observations indicate that placement of the alkyl group on **2** has a two-fold effect on the extraction experiment. (1) It increases the selectivity of Y^{3+} over Sr^{2+} at near neutral pH. (2) It decreases the extraction efficiency of the yttrium into chloroform. This decrease is likely due to an unfavorable conformation produced by the presence of the propyl group on the macrocyclic cavity.

It is of interest to note that the pH range for the solvent extraction of Y^{3+} by macrocycle **1** is higher by approximately two pH units than the pH range for the loading of Y^{3+} on resin **3**. This observation suggests that the requirements for the extraction of Y^{3+} from water into chloroform are different than the requirements for complexation of Y^{3+} by the immobilized crown ether polymer **3**. The energy requirement to facilitate transport of a charged particle into a non polar solvent is large. Therefore, only metal chelates which are neutrally charged may be extracted from water to chloroform. The ion-exchange process is different from the solvent extraction process in that the complexation and adsorption of the metal ions may occur without the charge-balancing requirement. The lower pH range in the loading experiment as compared to the solvent extraction experiment may be explained by the

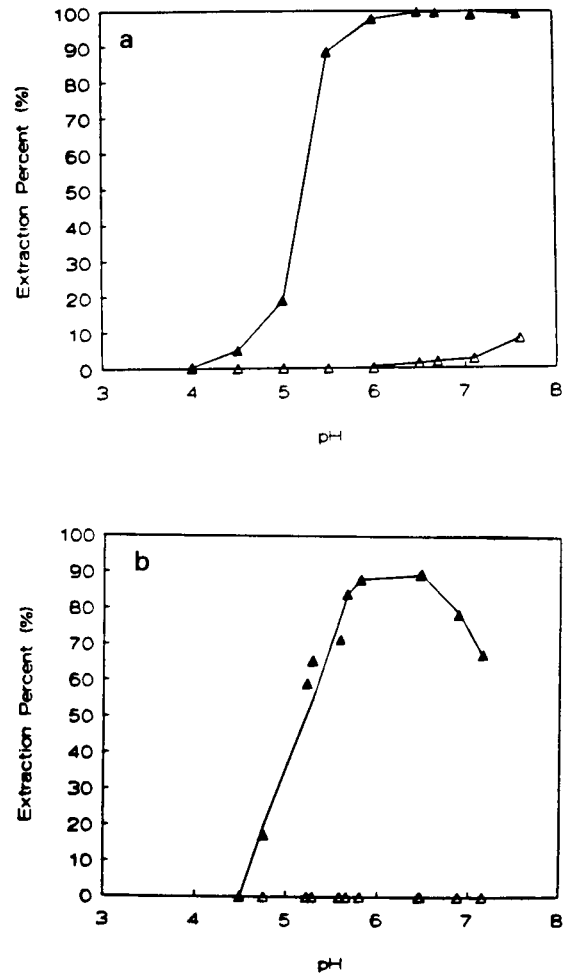

Fig. 6. pH dependence on the extraction of Y^{3+} and Sr^{2+} from aqueous solutions buffered with 0.05 M sodium acetate into chloroform containing 0.01 M (a) **1** and (b) **2**. (▲) Y^{3+} and (△) Sr^{2+}: 1×10^{-4} M each.

ability of the resin to complex Y^{3+} species which occur at low pH and which do not meet the charge-balancing requirement of solvent extraction.

The results from column chromatographic elution experiments indicate that the addition of an alkyl functional group to an ionizable crown ether at the point of the lariat attachment to the macrocyclic cavity decreases the performance of the chelating agent in the separation of Y^{3+} from Sr^{2+} in aqueous solutions. This result is similar to that observed in the solvent extraction experiments in which the substituted monomer displays decreased extraction efficiency from that of the unsubstituted monomer. Thus, the chelation properties of the polymer resins may be inferred from the monomer properties observed from solvent extraction experiments. In summary, our experiments indicate that a polymeric resin containing *sym*-dibenzo-16-crown-5-oxyacetic acid monomer subunits can be used as a stationary phase in ion exchange columns to accomplish efficient separation of Y^{3+} from Sr^{2+} in a rapid elution step. The resin can be regenerated for repeated use up to 10 times without losing its separation capability.

We are grateful to Westinghouse Idaho Nuclear Co. Inc. (WINCO) for their financial support. Neutron irradiations were performed at Washington State University's Nuclear Radiation Center under a Reactor Sharing Program supported by the Department of Energy.

REFERENCES

1 R.F. Wilken and S.R. Joshi, Radioact. Radiochem., 2 (1991) 95.
2 S.C. Srivistava, Radiolabeled Monoclonal Antibodies for Imaging and Therapy, Plenum Press, New York, 1988.
3 D.J. Wood, S. Elshani, H.S. Du, N.R. Natale and C.M. Wai, Anal. Chem., 65 (1993) 1350.
4 C.M. Wai and H.S. Du, Anal. Chem., 62 (1990) 2412.
5 W. Walkowiak, W.A. Charewicz, S.I. Kang, I.W. Yang, M.J. Pugia, and R.A. Bartsch, Anal. Chem., 62 (1990) 2018–2021.
6 T. Hayashita, M.J. Goo, J.C. Lee, J.S. Kim, J. Krzykawsik and R.A. Bartsch, Anal. Chem., 62 (1990) 2283.
7 T. Hayashita, J.H. Lee, C. Shiping and R.A. Bartsch, Anal. Chem., 62 (1991) 1844.
8 T. Hayashita, J.H. Lee, J.C. Lee, J. Krzykawski and R.A. Bartsch, Talanta, 39 (1992) 857.
9 T. Hayashita, J.H. Lee, M.G. Hankins, J.C. Lee, J.S. Kim, J.M. Knobeloch and R.A. Bartsch, Anal. Chem., 64 (1992) 7815.
10 J. Strzelbicki and R.A. Bartsch, Anal. Chem., 53 (1981)1894.
11 H.S. Du, D.J. Wood, S. Elshani and C.M. Wai, Talanta, 40 (1993) 173.

Analytica Chimica Acta, 284 (1993) 45–52
Elsevier Science Publishers B.V., Amsterdam

Separation, identification and assay of fluradoline hydrochloride in the presence of other tricyclic antidepressants or neuroleptics by spectral and thin-layer and liquid chromatographic methods

J. Joseph-Charles and M. Bertucat

Laboratoire de Chimie Analytique Appliquée, UFR des Sciences Pharmaceutiques, Place de la Victoire, F-33076 Bordeaux Cedex (France)

(Received 16th November 1992)

Abstract

Fluradoline hydrochloride is a novel centrally acting analgesic with antidepressant activity. Its UV absorption and emission spectra and thin-layer and liquid chromatographic (TLC and LC) identification are described. The separation of tricyclic antidepressant or neuroleptic compounds including zotepine, amoxapine, loxapine, fluperlapine, clotiapine, nitroxazepine and fluradoline by TLC and LC is reported. The UV spectrophotometric, spectrofluorimetric and LC methods described can be applied to the determination of fluradoline.

Keywords: Fluorimetry; Liquid chromatography; Thin-layer chromatography; UV–Visible spectrophotometry; Fluradoline hydrochloride; Pharmaceuticals

Fluradoline hydrochloride (FLDH) (HP-494), synthesized and pharmacologically evaluated at Hoechst-Roussel Pharmaceutical (Sommerville, NJ), is a tricyclic drug substance [1,2] with analgesic and antidepressant properties. It has been demonstrated to be a very potent analgesic different from the opiates in its action. It has been shown to be free from narcotic action and development of tolerance [3,4]. Its anticonvulsant activity is weak and it shows no anxiolytic activity.

Concerning its antidepressant activity, FLDH is four times more active than imipramine. It is not a monoamine oxidase inhibitor [1]. Unlike earlier tricyclic antidepressants, its structure, 2-fluoro-11-[2-(methylamino)ethylthio]dibenzo[*b*, *f*]-oxepine hydrochloride, contains sulphur in the side-chain. Its structure is similar to that of zotepine (Fig. 1), which is, however, a neuroleptic drug.

FLDH can be expected to be an effective drug as both an antidepressant and an analgesic, so it was of interest to carry out experiments that may serve as a basis for its identification and determination. UV absorption (Fig. 2), and fluorescence excitation and emission spectra (Fig. 3) were obtained. FLDH can be determined by UV spectrophotometry and spectrofluorimetry. Reversed-phase liquid chromatography (LC) with UV detection also permits the determination of FLDH. As psychiatric clinics and hospitals use various antidepressants and neuroleptics, a single method of analysis would be useful. From the toxicological point of view, a rapid analysis that is capable of detecting and determining as many antidepressants as possible is required. Therefore, the separation of FLDH and six other tricyclic molecules

Correspondence to: M. Bertucat, Laboratoire de Chimie Analytique Appliquée, UFR des Sciences Pharmaceutiques, Place de la Victoire, F-33076 Bordeaux Cedex (France).

0003-2670/93/$06.00 © 1993 – Elsevier Science Publishers B.V. All rights reserved

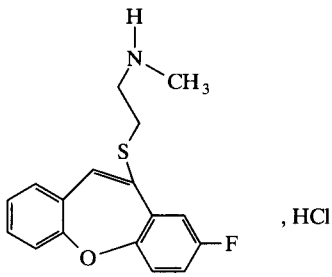

FLDH

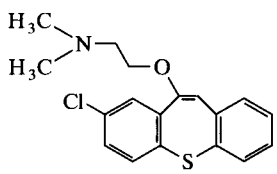

ZOT

Fig. 1. Structures of fluradoline hydrochloride (FLDH) and zotepine (ZOT).

either antidepressants or neuroleptics but structurally analogous, viz., zotepine (ZOT), amoxapine (AMOX), loxapine (LOX), fluperlapine (FLP), clotiapine (CLOT) and nitroxazepine (NITR), was carried out by thin-layer chromatography (TLC) and LC. The methods proposed here permit the simultaneous and rapid identification of these compounds.

EXPERIMENTAL

Equipment

A Perkin-Elmer Model 550 S double-beam UV–visible spectrophotometer was used with 1-cm quartz cuvettes; UV spectra were recorded with a Perkin-Elmer (Norwalk, CT) Model 56 recorder. A Safas Model FL 200 spectrofluorimeter and recorder (Safas, Monaco) permitted spectrofluorimetric analysis. The LC system consisted of a Varian (Walnut Creek, CA) Model 2010 constant-flow pump and a Milton Roy LDC (Riviera Beach, FL) Spectromonitor III variable-wavelength UV detector. The time constant of the detector was set to 0.5 s and the sensitivity range varied between 0.1 and 0.01 absorbance full-scale, depending on the amount of sample. Chromatograms were recorded on a Perkin-Elmer R 50 10-mV chart recorder at a chart-speed of 300 mm h^{-1}. Samples were introduced by an SGE syringe into a Model 7125 injection valve fitted with a 20-μl loop (Rheodyne Berkeley, CA). A 150 × 4.6 mm i.d. stainless-steel column packed with Nucleosil 120 C_{18}, particle size 5 μm (Macherey–Nagel, Düren, Germany), purchased from CIL (Ste.-Foy-la-Grande, France) was used at room temperature. A 20 × 2 mm i.d. Uptight guard column with a 40-μm C_{18} packing (Upchurch Scientific, Oak Harbor, WA) was inserted between the injector and the analytical column. The detection wavelength was 230 nm.

Chemicals, drug standards and materials

All chemicals and reagents were used without further purification.

The tricyclic antidepressants or neuroleptics were kindly supplied by the following companies: FLDH by Hoechst-Roussel (Sommerville, NJ), ZOT by Fujisawa Pharmaceutical (Osaka), AMOX and LOX by Lederle (Oullins, France), FLP by Sandoz (Basle, Switzerland), CLOT by Sandoz (Rueil Malmaison, France) and NITR by Ciba-Geigy (Basle). All the solutions prepared from these samples were kept in light-protected bottles at 4°C.

Methanol and absolute ethanol (RPE-ACS) were obtained from Carlo Erba (Milan). Cyclohexane, ethyl acetate, *n*-butanol, ammonia solution, potassium dihydrogenphosphate, triethylamine and 85% phosphoric acid (Normapur) were obtained from Prolabo (Paris). LC-grade acetonitrile was purchased from Rathburn Chemicals (Walkerburn, UK). Water was freshly distilled from deionized tap water in a glass still.

Glass plates (20 × 20 cm) were coated with silica gel GF_{254} Type 60 (0.3 mm) (Merck, Darmstadt) by means of a Camag (Muttenz, Switzerland) Model 21602 automatic thin layer apparatus. After air drying, the plates were activated in an oven at 110°C for 1 h, then kept in a desiccator before use. Reactivation is necessary if the plates are not used within 48 h. A 215 × 215 × 60 mm (internal dimensions) flat-bottomed tank was obtained from Camag.

Reagents

Lemontey's reagent [5]. Dissolve ammonium cerium(IV) sulphate (0.6325 g) in water (10 ml), then add phosphoric acid (sp.gr. 1.70) (80 ml). After dissolution, dilute to 100 ml with the phosphoric acid.

Xanthydrol reagent [6]. To xanthydrol (20 mg) add hydrochloric acid (1 ml) and dilute to 100 ml with acetic acid.

Dragendorff reagent, as modified by Munier and Macheboeuf. Solution A consists of 0.85 g of bismuth subnitrate (bismuth oxynitrate), 10 ml of acetic acid and 40 ml of water and solution B is 40% (w/v) aqueous potassium iodide. To prepare the spray reagent, mix 5 ml each of solutions A and B with 20 ml of acetic acid and dilute to 100 ml with distilled water.

Potassium iodoplatinate reagent. Mix 100 ml of 6% potassium iodide solution with 100 ml of 0.3% hexachloroplatinic acid hexahydrate solution.

KH_2PO_4–H_3PO_4 buffer. To 40 mM KH_2PO_4 solution add concentrated phosphoric acid until pH 2.0 is reached.

Triethylamine–H_3PO_4 buffer. To 10 mM triethylamine solution add concentrated phosphoric acid to adjust the pH to 2.4.

Colour reactions

FLDH is a white powder, fairly soluble in water and readily soluble in methanol, giving solutions fluorescing at 366 nm. It produces a brown colour with Lemontey's reagent with blue fluorescence and no colour with xanthydrol reagent but with intense yellow fluorescence.

A few mg of FLDH were mixed with 3 ml of the particular reagent solution in a test tube. Lemontey's reaction was carried out at room temperature whereas the xanthydrol reaction required heating on a boiling water-bath for 30 min. A reagent blank is advisable.

Spectra

The UV spectrum (Fig. 2) shows intense absorption at about 230 nm, with a minimum at 254 nm followed by a slight maximum at about 296 nm and by a shoulder at 309 nm. Working standard solutions were prepared from a 0.2 mg ml^{-1} stock standard methanolic solution of FLDH by dilution with methanol. Linear calibration graphs were constructed by plotting absorbance against concentration over the concentration range 1–15 $\mu g\ ml^{-1}$. The least-squares linear equations were $A(230\ nm) = 0.067$ [FLDH ($\mu g\ ml^{-1}$)] – 0.005 ($r = 0.9995$, $n = 12$) and $A(296\ nm) = 0.027$ [FLDH ($\mu g\ ml^{-1}$)] – 0.004 ($r = 0.9996$, $n = 12$).

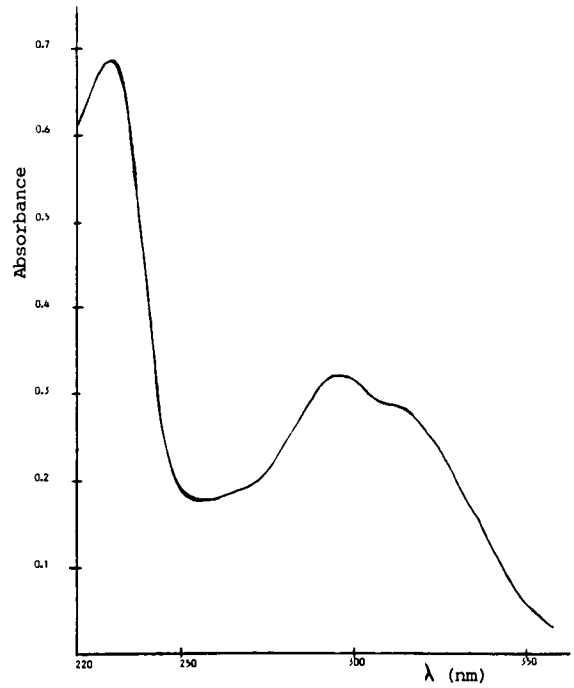

Fig. 2. UV spectrum of FLDH (methanolic solution, 10.0 $\mu g\ ml^{-1}$).

The aromatic structure of FLDH permits the use of a fluorescence detection method. The maximum excitation and emission wavelengths of a 1 $\mu g\ ml^{-1}$ methanolic solution were 338 and 492 nm, respectively (Fig. 3). Measurement of fluorescence intensity (F) gives a linear calibration graph with the least-squares linear equation $F = 0.052$ [FLDH ($\mu g\ ml^{-1}$)] – 0.006 ($r = 0.9996$, $n = 8$) over the range 0.1–1 $\mu g\ ml^{-1}$ FLDH in methanolic solution.

Chromatography

Chromatographic methods permitted the separation of FLDH from six other tricyclic molecules and its detection. These compounds are shown in Fig. 1 and Table 1.

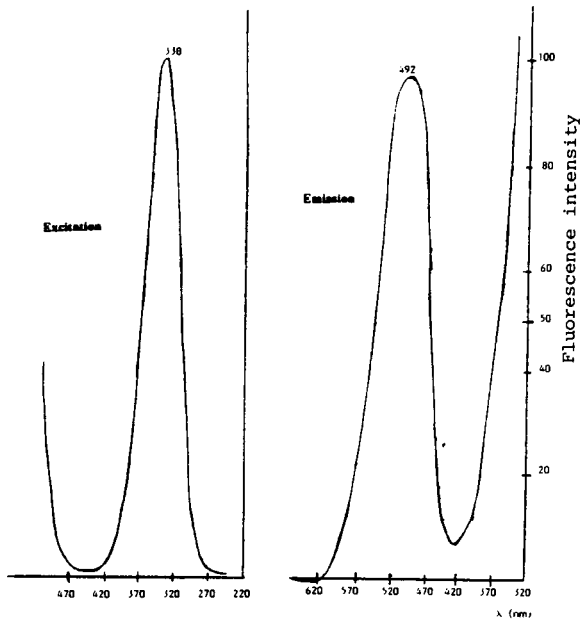

Fig. 3. Excitation and emission spectra of FLDH at a concentration of 1.0 μg ml^{-1} in methanol.

TLC of FLDH and six other tricyclic compounds. The experiments were carried out at room temperature (19°C). Cyclohexane–ethyl acetate–absolute ethanol–*n*-butanol–25% (v/v) ammonia solution (70 + 30 + 10 + 20 + 1) was freshly prepared and used as the developing solvent. The volumes should be measured accurately to maintain reproducibility. No significant change in R_F values was noted with or without pre-equilibration with the solvent system that was used in this study.

A 5-μl volume of a 0.2 mg ml^{-1} methanolic solution of each compound was spotted on the baseline of the plate. After allowing the spots to dry, without heat treatment, the plate was developed in rectangular developing tank until the solvent front had migrated a distance of 15 cm (about 1.5 h).

The plate was removed, air dried and examined under UV radiation (254 and 366 nm). Dragendorff reagent diluted from 1 to 10 ml with 0.1 M hydrochloric acid and then concentrated phosphoric acid sprays were then applied in succession.

Another detection procedure was to spray in succession with potassium iodoplatinate reagent and 50% (v/v) sulphuric acid.

Liquid chromatography. Identification and determination of FLDH are also possible by LC. The mobile phases were vacuum filtered through 0.45-μm Sartolon membranes (Sartorius, Göttingen, Germany) and degassed by ultrasonic vibra-

TABLE 1

Structures of compounds studied [a]

Compound	Formula
Amoxapine	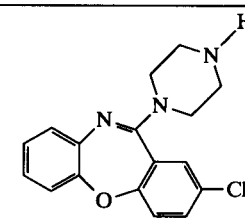
Loxapine	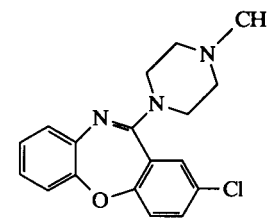
Fluperlapine	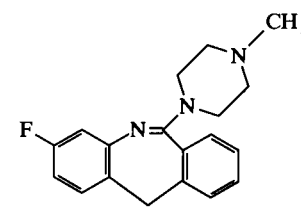
Clotiapine	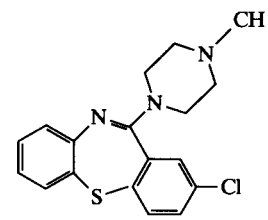
Nitroxazepine	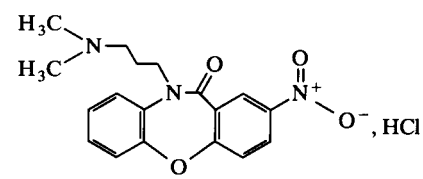

[a] For formulae of FLDH and ZOT, see Fig. 1.

tion for ca. 5 min prior to use. Before any sample was injected into the chromatograph, the system was equilibrated with the mobile phase. In order to increase the lifetime of the column, it was thoroughly cleaned by pumping distilled water and then methanol through it at the end of each day.

LC of FLDH alone. The isocratic mobile phase was prepared by mixing 45 ml of acetonitrile and 40 mM phosphate buffer (pH 2.0) up to 100 ml. The solvent flow-rate was 1.0 ml min^{-1} at 90 atm with the UV detector set at 230 nm. A 0.2 mg ml^{-1} stock standard solution of FLDH was prepared in methanol. Working standard solutions were prepared by serial dilution of the stock solution with the eluent. All the solutions were stored at 4°C between analyses. Two calibration graphs of peak height versus concentration were used, one for 100–1000 ng ml^{-1} and the other for 1–10 μg ml^{-1}.

LC of FLDH and six other tricyclic compounds. A mixture of acetonitrile (35 ml) and 10 mM triethylamine (pH 2.4) (to 100 ml) was used for elution. The flow-rate was 1.0 ml min^{-1} at 90 atm. An appropriate wavelength for detection was selected from the UV spectra of the seven compounds (Fig. 4); 230 nm appeared to be the most suitable wavelength for detection of all these substances.

Stock solutions of each compound in the eluent (0.1 mg ml^{-1}) were prepared. From these solutions, a standard mixture was obtained by diluting with the eluent to achieve a concentration of 10 μg ml^{-1} of each substance.

Figure 5 shows a chromatogram produced under these optimum conditions.

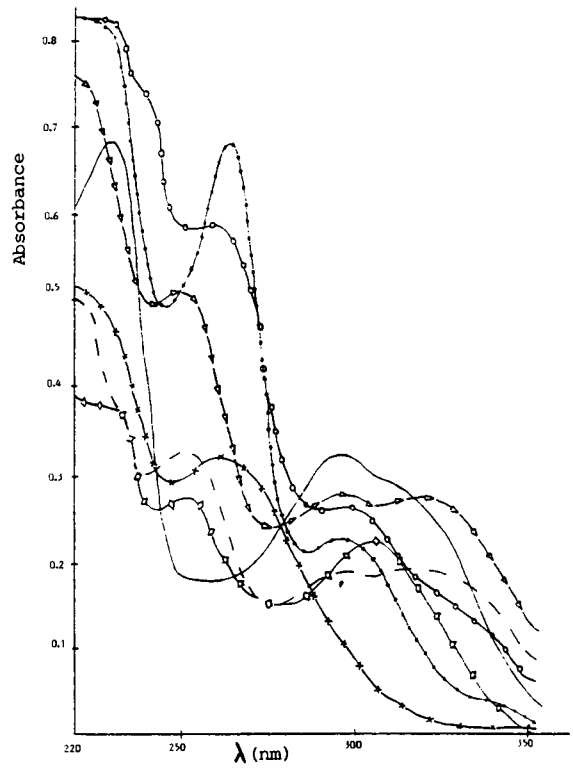

Fig. 4. UV spectra of seven tricyclic compounds in methanolic solution. Solid line without symbols = FLDH; ● = ZOT; dashed line without symbols = AMOX; ▽ = LOX; ◇ = FLP; ○ = CLOT; × = NITR.

RESULTS AND DISCUSSION

UV and spectrofluorimetry

Values of $A_{1\,cm}^{1\%}$ and molar absorptivity equivalent to about 660 and 2.23×10^4 l mol^{-1} cm^{-1} at 230 nm, respectively, were found. Calibration graphs of absorbance versus concentration of FLDH were linear over the concentration range 1–15 μg ml^{-1} at the two absorption maxima (230 and 296 nm). Linearity between fluorescence intensity and concentration of FLDH was found over the range 0.1–1 μg ml^{-1} of methanolic solution. These two spectral methods can be considered suitable for the determination of FLDH over the linear range whenever no interference from another substance is expected.

Thin-layer chromatography

There was a good separation of the seven compounds under the conditions described. Their R_F values are given in Table 2. These values were approximately the same whether the tank was saturated or not. The spots examined at 254 nm were dark on a fluorescent background. At 366 nm, only FLDH showed blue fluorescence. Dragendorff reagent and concentrated phosphoric acid gave an orange colour with all the spots. The colours produced by potassium iodoplatinate reagent and 50% (v/v) sulphuric acid were blue

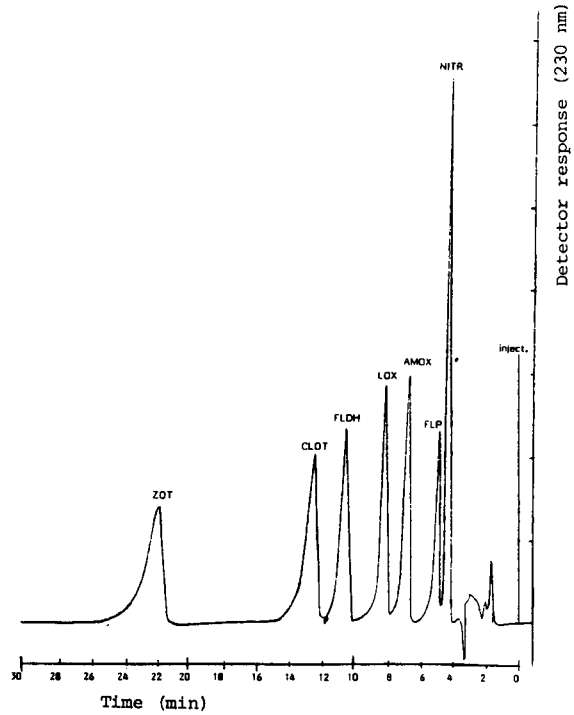

Fig. 5. Chromatographic separation of FLDH and six other tricyclic antidepressants or neuroleptics. Column, Nucleosil 120 C_{18}, 5 μm (150×4.6 mm i.d.); eluent acetonitrile (35 ml)–0.01 M triethylamine (pH 2.4) (to 100 ml); flow-rate, 1 ml min^{-1}; detection, UV absorbance at 230 nm; sensitivity, 0.1 absorbance full-scale; concentration of each drug in mixture, 10 μg ml^{-1} in methanol. For abbreviations, see text.

for FLP, dark violet for LOX and CLOT and purplish pink for the others.

Many solvent systems were tried and the results obtained with some of them are given in Table 3.

TABLE 2

Average R_F values [a] of seven tricyclic antidepressants or neuroleptics

Drug	R_F value
FLDH	0.29
ZOT	0.49
AMOX	0.20
LOX	0.54
FLP	0.37
CLOT	0.61
NITR	0.08

[a] Relative to solvent front at 15 cm.

TABLE 3

Comparison of R_F values of seven tricyclic antidepressants or neuroleptics using different solvents

Compound	Solvent [a]					
	1	2	3	4	5	6 [b]
NITR	0.03	0.06	0.03	0.06	0.02	0.08
AMOX	0.10	0.13	0.12	0.17	0.06	0.20
FLDH	0.13	0.19	0.17	0.21	0.09	0.29
FLP	0.22	0.19	0.23	0.30	0.17	0.37
ZOT	0.29	0.20	0.35	0.39	0.23	0.49
LOX	0.55	0.30	0.37	0.47	0.35	0.54
CLOT	0.58	0.33	0.35	0.51	0.40	0.61

[a] 1 = Cyclohexane–absolute ethanol–*n*-butanol–concentrated ammonia solution (60+20+10+1); 2 = ethyl acetate–absolute ethanol–*n*-butanol–concentrated ammonia solution (60 + 20 + 10 + 1); 3 = cyclohexane–ethyl acetate–absolute ethanol–*n*-butanol–concentrated ammonia solution (70+30 +10+10+1); 4 = cyclohexane–absolute ethanol–*n*-butanol–25% (v/v) ammonia solution (60 + 20 + 20 + 1); 5 = cyclohexane–ethyl acetate–absolute ethanol–25% (v/v) ammonia solution (60+20+10+1); 6 = cyclohexane–ethyl acetate–absolute ethanol–*n*-butanol–25% (v/v) ammonia solution (70+30+10+20+1). [b] The effective solvent system for separation.

This identification method is rapid. The development time was about 1.5 h. One development of the plate was sufficient to isolate FLDH from the six other tricyclic antidepressants or neuroleptics. It requires a readily available sorbent. The plates were coated in the laboratory, but commercial precoated plates can also be used.

Liquid chromatography

Acetonitrile was used as the organic modifier because of its low cut-off wavelength and the moderate pressure it yields.

LC of FLDH alone. Various compositions of acetonitrile and phosphate buffer at different pH values were tried as mobile phases. Different ionic strengths of the buffer component were also evaluated and an ionic strength of 0.04 appeared to be the best. A mixture of acetonitrile (45 ml) and phosphate buffer (40 mM, pH 2.0) (to 100 ml) was found to be the optimum composition of the mobile phase when only FLDH was measured. Under these conditions, the retention time was 4.0 min. A typical chromatogram (Fig. 6) shows a sharp peak that is symmetrical and well

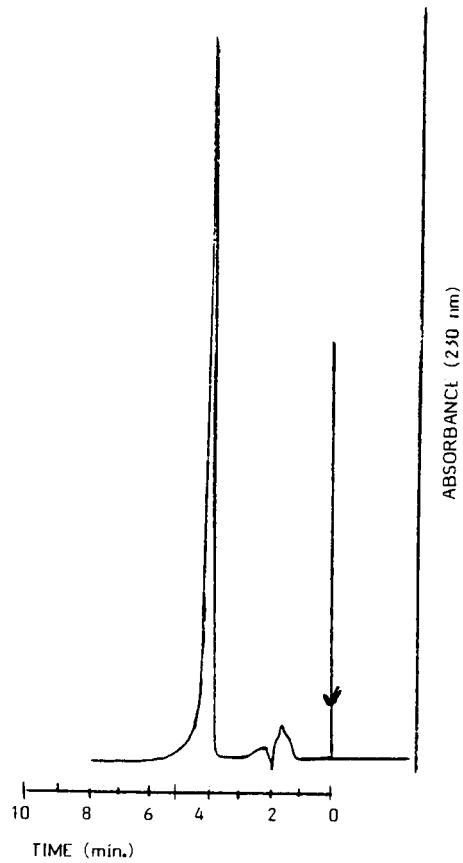

Fig. 6. Chromatogram of FLDH on Nucleosil 120 C_{18} (5 μm). Mobile phase, acetonitrile (45 ml)–40 mM phosphate buffer (pH 2.0) (to 100 ml); flow-rate, 1.0 ml min^{-1}.

defined with respect to the baseline. The limit of detection (2σ) was 100 ng ml^{-1}. Peak heights (H) were plotted against concentration to give a linear calibration graph from 100 ng ml^{-1} to 10 μg ml^{-1}. The least-squares linear equation was $H = 0.058$ [FLDH(μg ml^{-1})] + 0.003 ($r = 0.9998$, $n = 6$).

Solutions of FLDH stored in brown bottles in a refrigerator for several months remained colourless and no apparent degradation product was observed according to chromatographic analysis.

LC of FLDH and six other tricyclic compounds. The use of triethylamine instead of phosphate buffer permitted the separation of the seven substances. Triethylamine improved the peak symmetry, as has been observed by others [7–9] for basic compounds. The pH of the 10 mM triethylamine solution added to acetonitrile appeared to be an important factor in obtaining an adequate separation of the substances, as shown in Table 4. A pH < 2.4 resulted in co-elution or poor separation of NITR and FLP and incomplete separation of FLDH and CLOT. The run time increased and peak broadening occurred at pH > 2.4.

TABLE 4

Effect of pH on retention time in minutes in the LC of the seven tricyclic compounds

Compound	pH of 0.01 M triethylamine			
	2.0	2.2	2.4 [a]	2.6
NITR	4.2	4.2	4.2	4.4
FLP	3.9	4.2	4.8	5.4
AMOX	6.2	6.4	6.6	7.0
LOX	7.6	7.7	8.0	8.5
FLDH	10.1	10.2	10.3	10.8
CLOT	11.2	11.6	12.2	13.1
ZOT	20.8	21.1	21.6	23.0

[a] pH adopted for separation.

Conclusion

There appears to have been no previous report on the identification and determination of FLDH. The present results indicate that the spectral and chromatographic methods reported here can be used to monitor FLDH in its pure form or in future pharmaceutical dosage forms. They are also of interest for analyses in pharmacokinetic and toxicological studies. However, these possibilities are not definitive because of the possible occurrence of metabolites of this compound. Interference studies must be carried out whenever other drugs are used in medication.

The authors are grateful to Hoechst-Roussel, Sandoz, Lederle, Fujisawa and Ciba-Geigy for supplying tricyclic antidepressant and neuroleptic samples.

REFERENCES

1 H.H. Ong, J.A. Profitt, V.B. Anderson, T.C. Spaulding, J.C. Wilker, H.M. Geyer, III, and H. Kruse, J. Med. Chem., 23 (1980) 494.

2 Drugs Future, 10 (1985) 813.
3 Drugs Future, 11 (1986) 887.
4 H. Koch, Pharm. Int., 7 (1986) 27.
5 Y. Lemontey, J. Meunier and P. Lafargue, Clin. Chim. Acta, 30 (1970) 713.
6 T. Özden, A. Brachet-Liermain and M. Bertucat, J. Fac. Pharm. Ankara, 5 (1975) 68.
7 A. Sokolowski and K.G. Wahlund, J. Chromatogr., 189 (1980) 299.
8 M.S. Lennard and J.H. Silas, J. Chromatogr., 272 (1983) 205.
9 J.S. Kiel, S.L. Morgan and R.K. Abramson, J. Chromatogr., 320 (1985) 313.

Analytica Chimica Acta, 284 (1993) 53–58
Elsevier Science Publishers B.V., Amsterdam

Determination of phenol and monochlorophenols in water by reversed-phase liquid chromatography

Bogumiła Makuch, Krystyna Gazda and Marian Kamiński

Faculty of Chemistry, Department of Analytical Chemistry, Technical University, 80-952 Gdańsk (Poland)

(Received 23rd February 1993; revised manuscript received 21st July 1993)

Abstract

Phenol and monochlorophenols were determined by reversed-phase liquid chromatography with LiChrospher RP-18e. A good separation was obtained with this system. The effectiveness of liquid–liquid and solid-phase extractions on Amberlite XAD-2, XAD-4, octadecyl Si 100, Tenax and Polyspher RP-18 were compared. A large loss of phenol and monochlorophenols was found during removal of the solvent after liquid–liquid extraction. The best results were achieved with Polyspher RP-18. Solid-phase extraction on this sorbent was used to monitor phenol and monochlorophenols in drinking and river waters.

Keywords: Liquid chromatography; Chlorophenols; Extraction; Phenol; Waters

The presence of phenols in the environment results from their common use in many branches of industry and to a small extent from metabolic processes. Chlorinated phenols occur in drinking water as products of water chlorination. Because phenol compounds are harmful to living organisms, there is great interest in methods allowing the detection of very low concentrations of these compounds.

A spectrophotometric method for the determination of the concentration of total phenols in water has been used for many years. However, as phenols differ considerably in their toxicity, there is need for information on the concentrations of particular components. This can be achieved by the application of chromatographic methods. As thin-layer chromatography (TLC) is still considered to be a semi-quantitative method, it is hardly used in the determination of phenols in waters. Gas chromatography (GC), using both packed and capillary columns, is often used for the determination of phenols [1–4]. In order to improve either their detection [1] or their chromatographic behaviour [2], phenols are often converted into various derivatives.

In the last two decades, liquid chromatography (LC) has been widely used for the determination of trace contaminants, including the separation and determination of phenols at the ng and pg levels [5–11]. The detection limit achieved in LC with UV detection is in the range 10–100 mg l^{-1} of phenols, which is too high for environmental analyses as the concentrations of these compounds in water and wastes (apart from particular cases) are at the ng l^{-1} level. In order to improve the sensitivity it is necessary to concentrate phenols prior to analysis. This can be achieved by using liquid–liquid extraction (LLE) or solid-phase extraction (SPE) or by the application of membranes [12]. In addition, the sensitiv-

Correspondence to: B. Makuch, Faculty of Chemistry, Department of Analytical Chemistry, Technical University, 80-952 Gdańsk (Poland).

0003-2670/93/$06.00 © 1993 – Elsevier Science Publishers B.V. All rights reserved

ity of the determination of phenols can be improved by postcolumn reaction to form compounds with high absorption coefficients [5] or by precolumn derivatization with dansyl chloride [13,14].

Preconcentration of phenols by LLE is attended by common inconveniences and the final result of analysis depends on numerous parameters related to the extraction procedure. For instance, the extraction efficiency of phenol varies from 37% to over 90%, *o*-chlorophenol from 36 to 93% and *p*-nitrophenol from 93 to 112% [15–17]. Similarly, great differences in extraction efficiency are observed with other phenols.

Preconcentration on solid sorbents allows some of these problems to be eliminated, but considerable differences in efficiency are observed even with the same type of sorbent. Many sorbents have been used to concentrate phenol and its derivatives [17–27] but, based on the published data, it is impossible to conclude unambiguously which of the applied sorbents is the most useful, because different workers obtained very different results. This can best be illustrated with phenol as an example: the recovery from a C_{18} sorbent obtained by Borra et al. [25] was 3%, whereas Larroque et al. [21] obtained recoveries of 91–96%. On applying Amberlite XAD-4, the phenol recovery reached 100.6% [19] and 63–96.7% [20] and differences with respect to carbon were also considerable [25,27]. Differences in recoveries have also been observed with other phenols.

Taking into account the variety of results obtained, it was decided to apply two methods, namely LLE, according to a method reported by Realini [16], and SPE on Tenax, Polyspher RP-18, C_{18} silica and Amberlite XAD-2 and XAD-4, in order to concentrate phenol and monochlorophenols.

EXPERIMENTAL

Reagents and apparatus

Analytical-reagent grade chemicals were used unless indicated otherwise.

Methanol, phosphoric acid, hydrochloric acid and sodium chloride were obtained from POCH (Gliwice, Poland), methylene chloride (pure) from Zakłady Chemiczne (Tarnów, Poland) and tetramethylammonium chloride from Prosynth (Germany). Water was distilled twice in glass. All solvents were distilled before use. Phenol standards were phenol (POCH), *o*-chlorophenol (Koch-Light, Colnbrook, UK), *m*-chlorophenol (Fluka, Buchs, Switzerland) and *p*-chlorophenol (Verd, Germany).

A Merck–Hitachi liquid chromatograph was used, equipped with a Type L 4250 UV–visible detector, an L 6200 pump, a D 2500 integrator and a Rheodyne Model 7125 injection valve with a 20-μl loop. The column (250 × 4.6 mm i.d.) was packed with LiChrospher RP-18e, $d_p = 5$ μm. The extraction columns were Polyspher RP-18 (100 mg) (Merck, Darmstadt, Germany), Tenax (Alltech Associates, Deerfield, IL), $d_p = 0.25$–0.5 mm (200 and 400 mg), Amberlite XAD-2 and XAD-4 (Aldrich-Chemie, Steinheim, Germany), $d_p = 0.25$–0.85 μm (400 mg) and octadecyl Si 100 (Serva, Heidelberg, Germany), $d_p = 30$ μm (400 mg). All the extraction columns, except Polyspher RP-18, were made in the laboratory.

Amberlite resins were purified according to the procedure described by Junk et al. [28].

Monitoring of analyte loss during solvent evaporation

A 0.3-ml volume of methanol containing 2.5 μg of each component was adjusted to pH 14 and tetrabuthylammonium chloride was added. The mixture was diluted with 150 ml with methylene chloride and distilled from a water-bath at 43°C until a volume of 5 ml was reached, then the remaining solvent was removed with a stream of cold nitrogen. From the second sample the solvent was evaporated from a water-bath at 16°C under reduced pressure.

Solid-phase extraction procedure

The overall procedure with respect to the extraction columns was as follows. Before sampling, each column was conditioned with 5 ml of methanol and then with 10 ml of 0.01 M HCl containing 0.5% propan-2-ol. Water samples spiked with different amounts of phenols and containing 0.5% propan-2-ol were adjusted to pH

2 with HCl and 40 g of NaCl were added. The samples were then filtered through the sorbent bed under reduced pressure, followed by washing with 2 × 0.5 ml of 0.01 M HCl containing 0.5% propan-2-ol and aspirating for 10 min under reduced pressure. Phenols were eluted with 1.00 ml of methanol. A 20-μl volume of the eluate was analysed directly by LC. The content of each component was determined on the basis of a calibration graph. This procedure was applied to river water.

RESULTS AND DISCUSSION

Although LC has been widely used to determine phenol and substituted phenols [5–11], it is still a problem to separate *m*- and *p*-chlorophenols. The selection of the separation conditions was based on normal- and reversed-phase systems. To obtain a good separation the reversed-phase system LiChrosorb RP-18e–methanol + 0.001 M H_3PO_4 was chosen. A chromatogram obtained with this system is presented in Fig. 1. The separation of phenol and *m*-chlorophenol on silica gel was not successful.

The selection of a suitable wavelength for detection was based on spectrophotometric curves obtained in the range 200–300 nm. The detection limits for phenol and monochlorophenols are presented in Table 1. The detectability obtained in this study is comparable to values reported elsewhere [16,20,25].

Liquid–liquid extraction

LLE of phenol and monochlorophenols was done according to the procedure described by Realini [16]. Preconcentration was based on ion-pair extraction. The recoveries were lower than those reported, viz., phenol 42% (75% [16]) and *o*-chlorophenol 55% (93% [16]). These values were also lower than those obtained by other workers and with extraction methods under different conditions. The differences in recoveries are probably caused by solvent evaporation losses. In our opinion, the results presented in Table 2 confirm this supposition. From these results, it is considered that the LLE method is inadequate for routine analyses for compounds of this group.

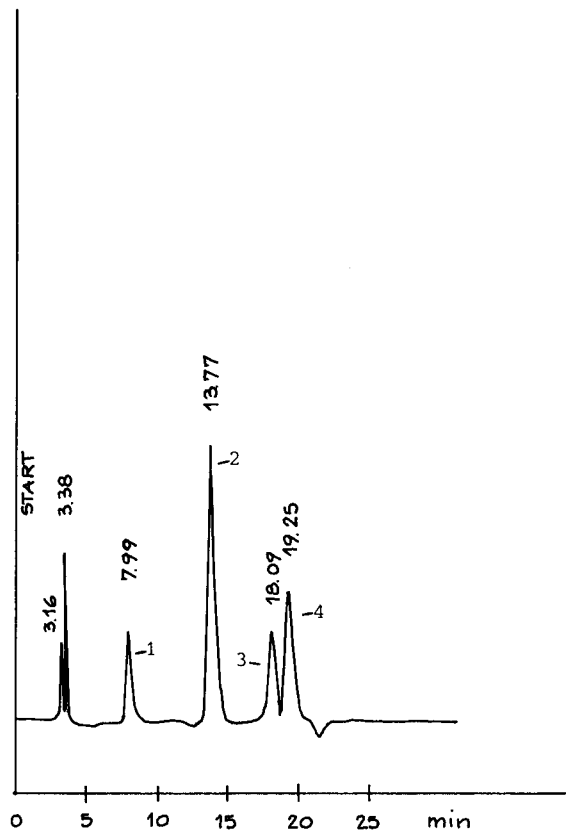

Fig. 1. Chromatogram of standard mixture of phenols. Column, LiChrospher RP-18e, $d_p = 5$ μm; Mobile phase, methanol–0.001 M H_3PO_4 (45+55, v/v); flow-rate, 1.2 ml min^{-1}: detection at 280 nm. 1 = Phenol; 2 = *o*-chlorophenol; 3 = *m*-chlorophenol; 4 = *p*-chlorophenol.

Solid-phase extraction

Table 3 presents the phenol and monochlorophenol recoveries obtained with different sor-

TABLE 1

Detection limits of phenol and monochlorophenols at 280 nm [a]

Compound	Concentration ($\mu g\ \mu l^{-1}$) [b]
Phenol	0.13×10^{-3}
o-Chlorophenol	0.18×10^{-3}
m-Chlorophenol	0.42×10^{-3}
p-Chlorophenol	0.15×10^{-3}

[a] Peak height 2× r.m.s. noise at a detection sensitivity of 0.005 absorbance full-scale. [b] Concentration of analytes injected on to the column. Sample volume, 20 μl.

TABLE 2

Phenol and monochlorophenol losses (%) resulting from solvent removal by distillation + evaporation and evaporation under reduced pressure (mean values calculated for three independent samples)

Compound	Distillation + evaporation	Evaporation under reduced pressure
Phenol	26	34
o-Chlorophenol	19	33
m-Chlorophenol	15	5
p-Chlorophenol	22	28

bents. A comparison of these results with those published by other workers shows differences in the recoveries of phenols. This is particularly apparent with of phenol and *o*-chlorophenol concentrated on Amberlite XAD-2 and XAD-4 [18–20]. It seems that the only explanation for the above differences lies in the fact that the sorbents used were obtained either from different producers or from different production batches, or from the application of different filtration procedures. This is supported by the fact that, e.g., the phenol recovery reported by Bigley and Grob [29] was 52.5% whereas Chladek and Marano [17] achieved 95%, using the same sorbent and a similar preconcentration procedure.

The best results were obtained when the preconcentration was performed with Polyspher RP-18 (this is a macroporous polymer that covalently derivatized with C_{18} functional groups). The advantage of using this sorbent is particularly apparent with phenol and *o*-chlorophenol. A 0.5% concentration of propan-2-ol in water was used instead of the 10% advised by the producer, but nevertheless, no disturbances in the operation of the extraction column were observed. Similarly, poor repeatability of the results arising from poor wettability of the sorbent surface by water was not observed. However, there is one drawback in using this sorbent, namely its high price.

Concentration on Tenax also gave good results for monochlorophenols but unfortunately not so good for phenol. Tenax is rarely used owing to its small specific surface area. However, taking into account the permissible total phenol concentration in waste, which in some countries may be at the level of 0.5 mg l^{-1}, and assuming that there will be several compounds in this group present, it can be said that the concentration of an individual component is about 0.05 mg l^{-1}. In such a case a 20–50-ml volume of waste will be sufficient to achieve a quantitative determination. Raymer and Pellizzari [30] used Tenax for the determination of phenols, filtering 0.35–0.5 l of water that was contaminated to various degrees. Using ODS silica columns, we obtained low but reproducible recoveries for monochlorophenols, but unfortunately the phenol recovery varied over a wide range (9–20%). These results differ from those reported by other workers, which could be expected because the differences in the properties of bonded phases have been widely discussed. The small scatter of the results indicates that it is possible to apply this type of sorbent for the determination of some phenols, but on the condi-

TABLE 3

Recoveries of phenol and monochlorophenols obtained with different sorbents (mean values ± standard deviations calculated for three independent samples)

Analyte	Recovery (%)					
	Amberlite XAD-2 [a]	Amberlite XAD-4 [b]	Octadecyl Si 100 [c]	Polyspher RP-18 [d]	Tenax 1 [e]	Tenax 2 [f]
Phenol	64 ± 2.9	–	9–20	99 ± 0.9	76 ± 3.6	40 ± 6.1
o-Chlorophenol	60 ± 3.2	51 ± 3.8	53 ± 3.2	105 ± 1.1	93 ± 4.7	93 ± 3.0
m-Chlorophenol	82 ± 1.8	82 ± 2.1	70 ± 1.4	99 ± 2.6	98 ± 2.0	93 ± 3.0
p-Chlorophenol	92 ± 1.8	96 ± 1.3	72 ± 0.9	99 ± 2.1	95 ± 2.2	87 ± 3.1

[a] Mass of the sorbent 400 mg, volume of water sample 200 ml. [b] Mass of sorbent 400 mg, volume of water sample 200 ml. [c] Mass of sorbent 400 mg, volume of water sample 100 ml. [d] Mass of sorbent 100 mg, volume of water sample 150 ml. [e] Mass of sorbent 400 mg, volume of water sample 100 ml. [f] Mass of sorbent 200 mg, volume of water sample 100 ml.

tion that the recovery for a given column is determined and is taken into account when calculating the final result. Taking into account the fact that it is a commonly used and relatively cheap sorbent and in addition it does not require a specific clean-up procedure (as for example Amberlite), it seems a useful alternative.

Based on the data in Table 3, Polyspher RP-18 was used to monitor the phenol and chlorophenol contents in drinking and river waters. A 500-ml volume of drinking water was filtered through the sorbent bed (as described under Experimental). This sample did not contain phenol and monochlorophenols (see Fig. 2), which means that their concentrations were lower than 0.26 $\mu g\ l^{-1}$ for phenol, 0.36 $\mu g\ l^{-1}$ for *o*-chlorophenol, 0.84 $\mu g\ l^{-1}$ for *m*-chlorophenol and 0.30 $\mu g\ l^{-1}$ for *p*-chlorophenol. A 200-ml volume of river water was treated as described above. The chromatogram shows that the extract from river water is very contaminated. Fortunately, the main bulk of the impurities appeared at the beginning of the chromatogram. The result was obtained using a column packed with LiChrospher RP-18e because the capacity factors of phenols obtained with this column are higher than those observed with ODS silica. The river water contained 22 $\mu g\ l^{-1}$ of phenol and we did not find any monochlorophenols, which means that their concentrations were lower than 0.9 $\mu g\ l^{-1}$ for *o*-chlorophenol, 2.1 $\mu g\ l^{-1}$ for *m*-chlorophenol and 0.75 $\mu g\ l^{-1}$ for *p*-chlorophenol.

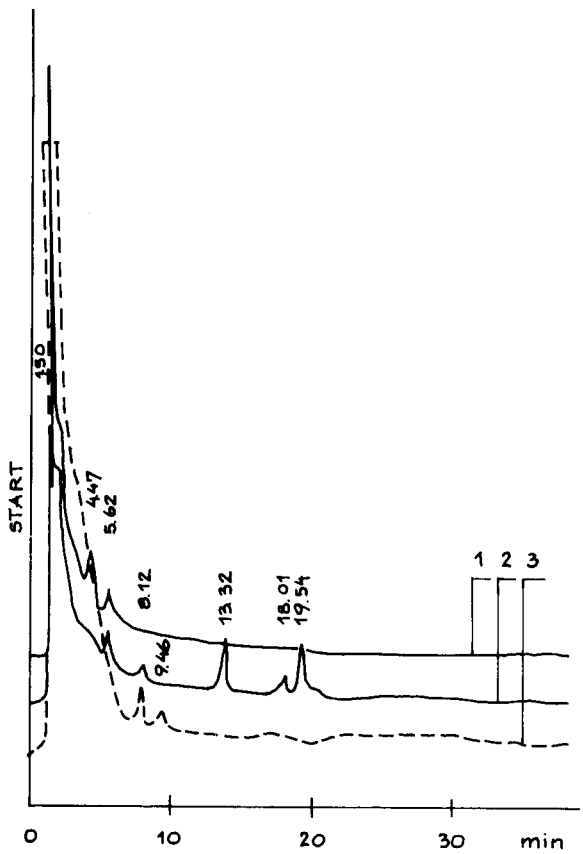

Fig. 2. Chromatogram of preconcentrated extracts. 1 = Drinking water; 2 = drinking water spiked with 0.8 μg of phenol, 2.5 μg of *o*-chlorophenol, 0.9 μg of *m*-chlorophenol and 4.0 μg of *p*-chlorophenol; 3 = river water. Curves 1 and 2 were obtained at 0.01 and 3 at 0.04 absorbance full-scale. Chromatographic conditions as in Fig. 1.

REFERENCES

1 L.L. Lamparski and T.J. Nestrick, J. Chromatogr., 156 (1978) 143.
2 J. Hajšlova, V. Kocourek, J. Zemanova, F. Pudil and J. Davidek, J. Chromatogr., 439 (1988) 307.
3 L. Weber, J. Chromatogr., 574 (1992) 349.
4 F. Mangani and A. Fabbri, Anal. Chem., 58 (1986) 3261.
5 S.K. Ratanathanwongs and S.R. Crouch, Anal. Chim. Acta, 192 (1987) 277.
6 M. Paleologou, S. Li and W.C. Purdy, J. Chromatogr. Sci., 28 (1990) 311 and 319.
7 Ch.H. Risner and S.L. Cash, J. Chromatogr. Sci., 28 (1990) 239.
8 Z. Vasilic, S. Fingler and V. Drevenkor, Fresenius' Z. Anal. Chem., 341 (1991) 732.
9 K. Pekari and A. Aitio, J. Chromatogr., 232 (1982) 129.
10 A.G. Hüsgen and R. Schuster, Hewlett-Packard Application Note No. 12-5952-1548, 1990.
11 J.H. Knox, B. Kaur and B.R. Millword, J. Chromatogr., 352 (1986) 3.
12 R.G. Melcher, D.W. Bakke and G.H. Hughes, Anal. Chem., 64 (1992) 2259.
13 C. de Ruiter, R.R. Otten, U.A.Th. Brinkman and R.W. Frei, J. Chromatogr., 553 (1988) 429.
14 P.J.M. Kwakman, D.A. Kamminga, U.A.Th. Brinkman and G.J. De Jong, J. Chromatogr., 553 (1991) 345.
15 B.K. Afghan, P.E. Belliveau, R.H. Larose and J.F. Ryan, Anal. Chim. Acta, 71 (1974) 355.
16 P.A. Realini, J. Chromatogr. Sci., 19 (1981) 124.
17 E. Chladek and R.S. Marano, J. Chromatogr. Sci., 22 (1984) 313.

18 T.R. Edgerton, R.F. Hoseman, E.M. Lores and L.M. Wright, Anal. Chem., 52 (1980) 1774.
19 B. Gawdzik, J. Gawdzik and U. Czerwińska-Bill, J. Chromatogr., 509 (1990) 135.
20 A. Borys, J. Chromatogr., 216 (1981) 361.
21 M. Larroque, L. Vien and A. Bleise, J. Chromatogr., 407 (1987) 384.
22 L. Renberg, J. Chromatogr., 214 (1981) 327.
23 C. Brage and K. Sjöström, J. Chromatogr., 538 (1991) 303.
24 R.L. Smith and D.J. Pietrzyk, J. Chromatogr. Sci., 21 (1983) 282.
25 C. Borra, A. DiCorcia, M. Marchetti and R. Samperii, Anal. Chem., 58 (1986) 2048.
26 J.J. Sun and J.S. Fritz, J. Chromatogr., 590 (1992) 197.
27 A. Bacaloni, G. Goretti, A. Lagana, B. Petronio and M. Rotatori, Anal. Chem., 52 (1980) 2033.
28 G.A. Junk, J.J. Richard, M.D. Grieser, D. Witiak, J.L. Witiak, M.D. Arquello, R. Vick, H.J. Svec, J. Fritz and S.V. Calder, J. Chromatogr., 99 (1974) 745.
29 F.P. Bigley and R.L. Grob, J. Chromatogr., 350 (1985) 407.
30 J.H. Raymer and E.D. Pellizzari, Anal. Chem., 59 (1987) 1043.

Analytica Chimica Acta, 284 (1993) 59–65
Elsevier Science Publishers B.V., Amsterdam

Separation of aqueous polythionates by reversed-phase ion-pair liquid chromatography with suppressor–conductivity detection

Hanfa Zou

National Chromatographic R&A Centre, Dalian Institute of Chemical Physics, Academia Sinica, Dalian 116011 (China)

Zhongjiang Jia

Institute of Chemical Metallurgy, Academia Sinica, Beijing 100080 (China)

Yukui Zhang and Peichang Lu

National Chromatographic R&A Centre, Dalian Institute of Chemical Physics, Academia Sinica, Dalian 116011 (China)

(Received 27th February 1993, revised manuscript received 21st July 1993)

Abstract

A method for the separation of sulphate, thiosulphate and four polythionates by reversed-phase ion-pair liquid chromatography with supressor–conductivity detection is described. The limits of detection for these inorganic anions varied between 0.01 and 0.30 μg ml^{-1}. The effects of the number of sulphur atoms in polythionates, the ion-pair reagent and the organic modifier concentration on retention were studied. It was observed that the logarithm of the capacity factors decreases linearly with the organic modifier concentration (C_b) and increases with the logarithm of the ion-pair reagent concentration (C_p) and the number of sulphur atoms in the polythionates. The absolute values of intercepts and slopes of the linear relationships of ln k' vs. ln C_p and ln k' vs. C_b increase linearly with increasing number of sulphur atoms in the polythionates. The method developed was applied to the determination of sulphate and polythionates in different gold extract solutions.

Keywords: Ion chromatography; Gold; Sulphate; Polythionates; Thiosulphate

Polythionates are commonly formed as intermediate oxidation products of sulphide minerals at acidic to neutral pH values [1]. Such an oxidation is primarily responsible for the acidic pollution of rivers and lakes receiving drainage from mining activities. However, elucidation of the reaction mechanisms of this process has been impeded by the inability to separate analytically the intermediate sulphur species formed, especially the polythionates. Published methods have been mainly based on cyanolysis or sulphitolysis of thionates to form thiocyanate and/or thiosulphate ions, which are measured spectrophotometerically [2–4]. In recent years, separations of polythionates by ion chromatographic techniques have been studied [5,6]. The limitation with ion chromatography is that the polythionates are hydrophobic anions and strongly retained on anionic resins and seriously asymmetric peaks are therefore usually observed [7].

Correspondence to: H. Zou, National Chromatographic R&A Centre, Dalian Institute of Chemical Physics, Academia Sinica, Dalian 116011 (China).

0003-2670/93/$06.00 © 1993 – Elsevier Science Publishers B.V. All rights reserved

Reversed-phase ion-pair liquid chromatography (RP-IPC) is now widely used for the separation of organic and inorganic ions [8–11]. The retention can be regulated by the properties and the concentration of the organic modifier and counter ion and by a competing ion with the same charge as the analyte [12]. In this study a method for the separation of thiosulphate and four polythionates by RP-IPC with supressor–conductivity detection was developed and the retention behaviour of these anions in RP-IPC was studied. The method was applied to the determination of sulphate and polythionates in gold extract solutions.

EXPERIMENTAL

Materials

Polythionates were prepared by the methods described by Takano et al. [6]; their purity was > 96%. The purity of sulphuric acid H_2SO_4 was > 99.99%. Acetonitrile, sodium carbonate, the ion-pair reagent tetrabutylammonium hydroxide (TBAOH) and other reagents were of analytical-reagent grade. Doubly distilled water was used throughout.

Apparatus

A Dionex Model 2120i ion chromatograph with a supressor-conductivity detector and a column temperature control system was used to separate thiosulphate and polythionates. The separation column used was a Dionex MPIC-NS1 (200 × 3 mm I.D.) with a guard column (Dionex NG1, 50 × 3 mm I.D.). The supressor column (60 × 6.5 mm I.D.) was packed with a strong anion exchanger. The column temperature was kept at 20 ± 1°C in all experiments. Sample solutions were injected by using 50-μl sample loops. The flow-rate in all experiments was 0.8 ml min^{-1}.

RESULTS AND DISCUSSION

Separation of thiosulphate and polythionates

Figures 1 and 2 show the chromatograms of a standard sample under different conditions in

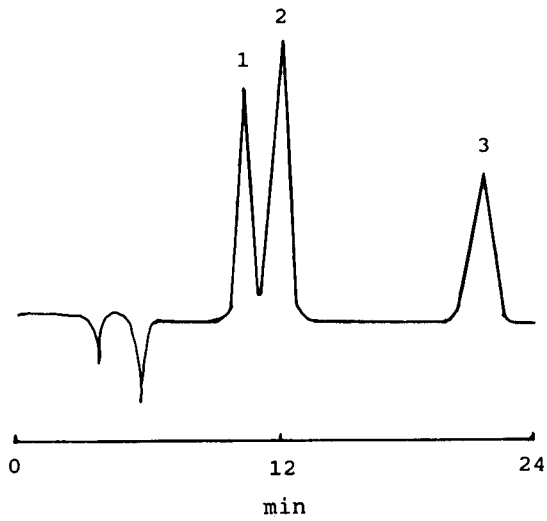

Fig. 1. Chromatogram of a standard solution containing three inorganic anions. The eluent used was acetonitrile–water (10 + 90) containing 2.0 mmol l^{-1} TBAOH ion-pair reagent and 2.0 mmol l^{-1} Na_2CO_3, at a flow-rate of 0.90 ml min^{-1}. For other experimental conditions, see text. Peaks: 1 = SO_4^{2-} (10 μg ml^{-1}); 2 = $S_2O_3^{2-}$ (15 μg ml^{-1}); 3 = $S_2O_6^{2-}$ (25 μg ml^{-1}).

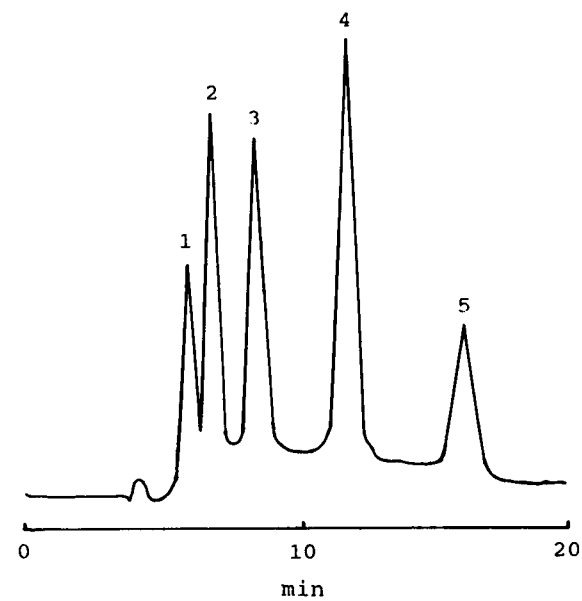

Fig. 2. Chromatogram of a standard solution containing five inorganic anions. The eluent used was acetonitrile–water (26 + 74) containing 3.0 mmol l^{-1} TBAOH ion-pair reagent and 2.0 mmol l^{-1} Na_2CO_3, at a flow-rate of 0.80 ml min^{-1}. For other experimental conditions, see text. Peaks: 1 = SO_4^{2-} and $S_2O_3^{2-}$; 2 = $S_2O_6^{2-}$ (10 μg ml^{-1}); 3 = $S_3O_6^{2-}$ (20 μg ml^{-1}); 4 = $S_4O_6^{2-}$ (30 μg ml^{-1}); 5 = $S_5O_6^{2-}$ (40 μg ml^{-1}).

TABLE 1

Detection limits for sulphate, thiosulphate and polythionates in RP-IPC with supressor–conductivity detection

Solute	Detection limit (μg ml^{-1}) [a]	Range of linearity (μg ml^{-1})
SO_4^{2-}	0.01	0.06– 30
$S_2O_3^{2-}$	0.01	0.10– 40
$S_2O_6^{2-}$	0.04	0.20– 40
$S_3O_6^{2-}$	0.1	1.0 – 80
$S_4O_6^{2-}$	0.3	1.0 –120
$S_5O_6^{2-}$	0.2	5.0 –240

[a] Based on 3σ of blank.

RP-IPC. The peak shape of thiosulphate and polythionates was improved by adding a small amount of Na_2CO_3. To determine the detection limits of the analytes, calibration solutions were prepared by serial dilution and the peak height of each analyte was determined. The linearity range was investigated and also the limit of detection (3σ) for each analyte and the results are given in Table 1. The detection limits of the analytes varied between 0.01 and 0.30 μg ml^{-1}, which are much lower than those observed by Steven and David [13].

Effect of number of sulphur atoms on retention

Tables 2 and 3 gives the capacity factors measured for different organic modifier and ion-pair reagent concentrations in RP-IPC for thiosulphate and polythionates. In RP-IPC, the retention of an ionic solute can be expressed by [14–16]

$$\ln k' = -\left(\Delta G_{iR}^0 + \Delta G_{ie}^0\right)/RT + \ln \phi \qquad (1)$$

TABLE 2

Capacity factors of thiosulphate and polythionates at different acetonitrile concentrations in RP-IPC [a]

Solute	Acetonitrile volume fraction, C_b				
	0.23	0.24	0.25	0.26	0.27
$S_2O_3^{2-}$	1.152	1.054	0.934	0.848	0.684
$S_2O_6^{2-}$	1.728	1.532	1.370	1.193	0.937
$S_3O_6^{2-}$	2.738	2.364	2.066	1.750	1.351
$S_4O_6^{2-}$	5.089	4.228	3.557	2.924	2.222
$S_5O_6^{2-}$	8.373	6.722	5.513	4.351	3.203

[a] The eluent was acetonitrile–water containing 3 mmol l^{-1} TBAOH ion-pair reagent and 0.5 mmol l^{-1} Na_2CO_3. For other experimental conditions, see text.

TABLE 3

Capacity factors of thiosulphate and polythionates at different TBAOH ion-pair reagent concentrations in RP-IPC [a]

Solute	Concentration of TBAOH C_p (mmol l^{-1})				
	1.6	2.0	2.8	3.2	3.6
$S_2O_3^{2-}$	0.938	1.013	1.175	1.250	1.263
$S_2O_6^{2-}$	1.238	1.331	1.588	1.719	1.750
$S_3O_6^{2-}$	1.713	1.938	2.394	2.638	2.763
$S_4O_6^{2-}$	2.688	3.125	4.094	4.351	4.950
$S_5O_6^{2-}$	3.888	4.650	6.400	7.219	–

[a] The eluent was acetonitrile–water (25 + 75) containing different concentrations of TBAOH and 0.5 mmol l^{-1} Na_2CO_3. For other experimental conditions, see text.

where ΔG_{iR}^0 and ΔG_{ie}^0 are the free-energy change contributed by the molecular interaction and the electrostatic interaction between the ionic solute and the mobile and stationary phases, respectively, ϕ is the phase ratio and R and T are gas constant and absolute temperature, respectively. If it is assumed that the negative charges of the polythionates are the same, then the term ΔG_{ie}^0 in Eqn. 1 is constant for the different polythionates, but ΔG_{iR}^0 is linearly related to the number of sulphur atoms under given separation conditions. Therefore, a linear relationship should exist between the logarithm of capacity factors and the numbers of sulphur atoms, N, for polythionates:

$$\ln k' = a + bN \qquad (2)$$

Results of linear regression of $\ln k'$ vs. N at different organic modifier and ion-pair reagent concentrations are shown in Figs. 3 and 4, respectively. There is a good linear relationship. The parameter b is positive, which means that the capacity factors of polythionates increase with increasing number of sulphur atoms.

Effect of organic modifier concentration

As discussed by many workers [14–18], the effect of the organic modifier concentration on retention in RP-IPC can be expressed by

$$\ln k' = \ln k_w + cC_b \qquad (3)$$

where $\ln k_w$ and c are the constants in a given column system and C_b is the organic modifier concentration. Results of the linear regression

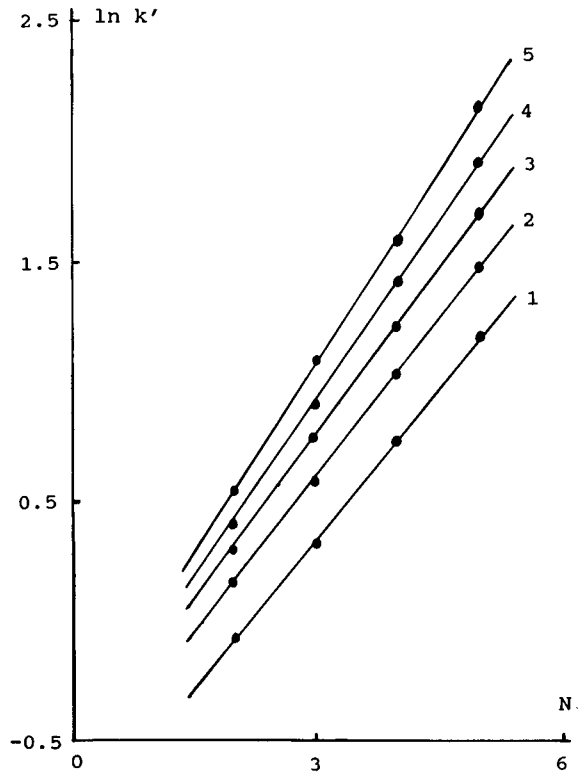

Fig. 3. Linear relationships of ln k' vs. N for the data in Table 2. (1) $C_b = 0.27$, ln $k' = -0.915 + 0.419$ N ($n = 4$, $r = 0.9980$); (2) $C_b = 0.26$, ln $k' = -0.719 + 0.440$ N ($n = 4$, $r = 0.9984$); (3) $C_b = 0.25$, ln $k' = -0.648 + 0.472$ N ($n = 4$, $r = 0.9987$); (4) $C_b = 0.24$, ln $k' = -0.598 + 0.502$ N ($n = 4$, $r = 0.9985$); (5) $C_b = 0.23$, ln $k' = -0.548 + 0.536$ N ($n = 4$, $r = 0.9984$).

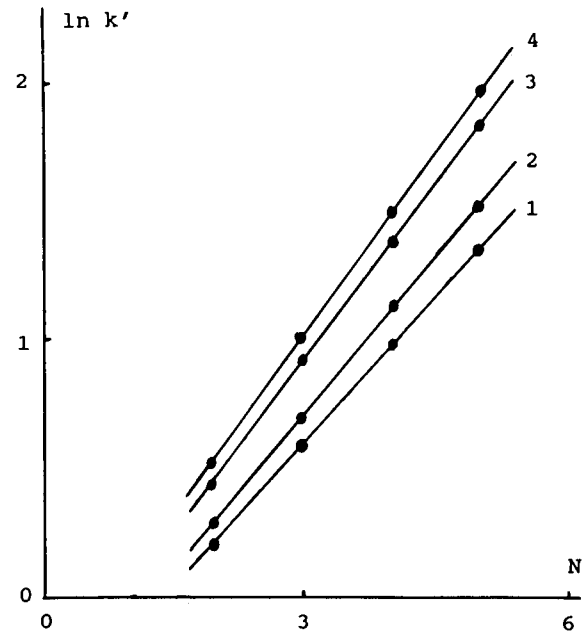

Fig. 4. Linear relationships of ln k' vs. N for the data in Table 3. (1) $C_p = 1.6$ mmol l^{-1}, ln $k' = -0.583 + 0.388$ N ($n = 4$, $r = 0.9983$); (2) $C_p = 2.0$ mmol l^{-1}, ln $k' = -0.575 + 0.423$ N ($n = 4$, $r = 0.9990$); (3) $C_p = 2.8$ mmol l^{-1}, ln $k' = -0.501 + 0.471$ N ($n = 4$, $r = 0.9988$); (4) $C_p = 3.2$ mmol l^{-1}, ln $k' = -0.556 + 0.485$ N ($n = 4$, $r = 0.9991$).

according to Eqn. 3 for the experimental data in Table 2 are given in Table 4. It can be seen that the regression coefficients are between 0.985 and 0.996, supporting the validity of Eqn. 3. The parameter c was always negative, which means that the capacity factors of thiosulphate and polythionates decrease with increasing concentration of organic modifier. The main reason for this phenomenon is that an increase in organic modifier concentration in the eluent causes a decrease in the amount of the ion-pair reagent TBAOH adsorbed, which will decrease the electrical potential on the stationary surface. It has been observed that a good linear relationship exists between ln k_w and c for sulphonic acids [18,19].

TABLE 4

Ln k_w and c in Eqn. 3 and A and B in Eqn. 4

Solute	Ln k_w	c	r	A	B	r
$S_2O_3^{2-}$	3.066	−12.60	0.9846	2.451	0.391	0.9944
$S_2O_6^{2-}$	3.965	−14.74	0.9855	3.149	0.458	0.9940
$S_3O_6^{2-}$	4.966	−17.11	0.9905	4.441	0.607	0.9988
$S_4O_6^{2-}$	6.307	−20.26	0.9955	5.886	0.762	0.9996
$S_5O_6^{2-}$	7.565	−23.56	0.9964	7.155	0.902	0.9994

Such a linear relationship was also obtained for thiosulphate and polythionates:

$$\ln k_w = -2.108 - 0.412c \quad (n = 5,\ r = 0.9998)$$

This linear relationship indicates that solute properties contribute to $\ln k_w$ and c in a parallel way for both thiosulphate and polythionates. A linear regression analysis of $\ln k_w$ and c vs. the number of sulphur atoms N in the polythionates was carried out, and the results obtained were as follows:

$$\ln k_w = 1.451 + 1.214N \quad (n = 4,\ r = 0.9983)$$

$$c = -8.552 - 2.963N \quad (n = 4,\ r = 0.9974)$$

Hence there are good linear relationships between $\ln k_w$ and c and the number of sulphur atom N. Ln k_w increases whereas c decreases with increasing number of sulphur atoms.

Effect of ion-pair reagent concentration on retention

It has been proposed that the effect of the ion-pair reagent concentration in the eluent on retention in RP-IPC can be expressed by [20,21]

$$\ln k' = A + B \ln C_p \qquad (4)$$

where A and B are constants in a given column system and C_p is the ion-pair reagent concentration in the eluent. The results of linear regression analysis according to Eqn. 4 for the experimental data in Table 3 are given in Table 4. It can be seen that the regression coefficients varied between 0.994 and 0.999, which means that Eqn. 4 describes correctly the effect of ion-pair reagent concentration on the retention of polythionates. B always was positive, which implies that the capacity factors of ionic solutes increase with increasing concentration of ion-pair reagent. Linear relationships between A and B and the number of sulphur atoms N in the polythionates were found:

$$A = 0.446 + 1.346N \quad (n = 4,\ r = 0.9997)$$

$$B = 0.162 + 0.149N \quad (n = 4,\ r = 0.9998)$$

According to the electrostatic model of RP-IPC, the value of B in Eqn. 3 is mainly determined by the number of solute charges [20,21]. However, B increases with increasing number of sulphur atoms for polythionates with two apparent negative charges. This phenomenon is difficult to explain. One reason may be that the effective charges of polythionates increase with increasing number of sulphur atoms.

Effect of solution pH on stability of polythionates

Decomposition of polythionates in basic aqueous solution is well known. Figures 5 and 6 show the relative peak heights in RP-IPC vs. time for polythionate solutions [acetonitrile–water (26 + 74) containing 3 mmol l^{-1} TBAOH and 0.5 mmol l^{-1} Na_2CO_3] at different pH values. The h_0 and h values in Figs. 5 and 6 are the peak height of an analyte in the original sample and that at time t, respectively. It can be seen that the polythionate anion $S_3O_6^{2-}$ is stable but the anions $S_4O_6^{2-}$ and $S_5O_6^{2-}$ are not. The decomposition rate of the polythionates $S_4O_6^{2-}$ and $S_5O_6^{2-}$ increases with increasing pH of the solution. Therefore, the solution used to prepare the polythionate samples should not be alkaline. The use of a solution with the same ratio of organic modifier to water

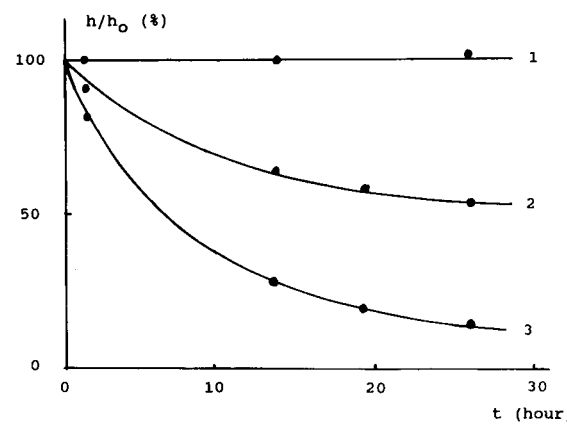

Fig. 5. Relative peak heights (h/h_0) of polythionates $S_3O_6^{2-}$ and $S_5O_6^{2-}$ vs. time t. Chromatographic conditions; eluent, acetonitrile–water (26+74) containing 3 mmol l^{-1} TBAOH and 0.5 mmol l^{-1} Na_2CO_3; detection sensitivity, 30 μS; original concentrations of $S_3O_6^{2-}$ and $S_5O_6^{2-}$ in sample solution, 10 and 40 mg l^{-1} respectively. For other experimental conditions, see text. (1) $S_3O_6^{2-}$ at sample solution pH 8; (2) $S_5O_6^{2-}$ at sample solution pH 7; (3) $S_5O_6^{2-}$ at sample solution pH 8.

TABLE 5

Determination of SO_4^{2-} and polythionates in gold extract solutions [a]

Sample	Dilution	Detection sensitivity (μS)	Anion	Concentration determined (mg l^{-1})
Gold extract solution obtained by $Na_2S_2O_3$ method	2000	30	SO_4^{2-}	5.96
	10000	30	$S_2O_3^{2-}$	9.60
	5000	10	S_3O_6	2.15
Gold extract solution obtained by low-temperature PBS method	20	1	SO_4^{2-}	0.51
	20	1	$S_2O_3^{2-}$	0.09
Gold extract solution obtained by high-temperature PBS method	50	1	SO_4^{2-}	0.15

[a] The eluent used for analysis of a mixture of SO_4^{2-} and $S_2O_3^{2-}$ was acetonitrile–water (10 + 90) containing 2.0 mmol l^{-1} TBAOH and Na_2CO_3 2.0 mmol l^{-1}. The eluent used to determine $S_nO_6^{2-}$ (n = 2–5) was acetonitrile–water (26 + 74) containing 3.0 mmol l^{-1} TBAOH and 0.5 mmol l^{-1} Na_2CO_3. For other experimental conditions, see text. PBS = Polythionate barium salt.

as the mobile phase to prepare the polythionate sample solution is to be prefered.

Application to analysis of gold extract solutions

Apart from the effect of pH on the stability of polythionates, interference of heavy metal cations in the analysis of practical polythionate samples must be taken into account. Heavy metal cations can catalyse the oxidation of inorganic sulphur anions, and can also be precipitated or adsorbed on the packing material during the column separation, which can damage the column and interfere with the determination of analyte anions. Therefore, heavy metal cations should be eliminated by hydroxide precipitation or cation exchange. Table 5 gives the results for the analysis of different gold extract solutions. It can be seen that RP-IPC can be used in separation of polythionates.

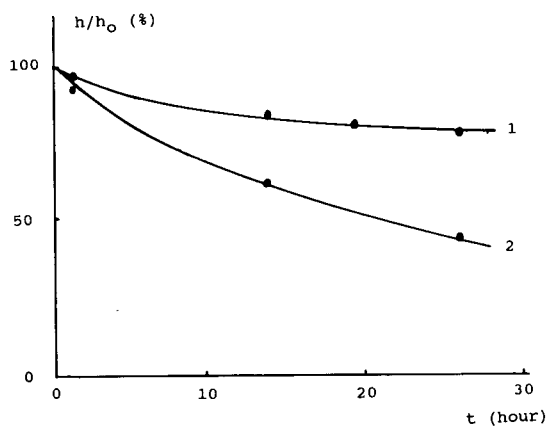

Fig. 6. Relative peak height (h/h_0) of polythionate $S_4O_6^{2-}$ vs. time t. Chromatographic conditions as in Fig. 5; original concentration of $S_4O_6^{2-}$ in sample solution, 20 mg l^{-1}. (1) Sample solution pH 7; (2) sample solution pH 8.

Financial support from the Natural Science Foundation of China for Young Research Fellowships is gratefully acknowledged.

REFERENCES

1 M.B. Goldhaber, Am. J. Sci., 283 (1983) 193.
2 T. Koh and K. Taniguchi, Anal. Chem., 45 (1973) 2018.
3 D.P. Kelly, L.A. Chambers and P.A. Trudinger, Anal. Chem., 41 (1969) 898.
4 M.Y. Nor and M.A. Tabatabai, Soil Sci., 122 (1976) 171.
5 J.N. Story, J. Chromatogr. Sci., 21 (1983) 272.
6 B. Takano, M.A. McKibben and H.L. Barnes, Anal. Chem., 56 (1984) 1594.
7 S.F. Mou and K.L. Liu (Eds.), Ion chromatography, Academic Press, Beijing, 1986 (in Chinese).
8 A. Tilly-Melin, Y. Askemark, K.G. Wahlund and G. Schill, Anal. Chem., 51 (1979) 976.
9 Cs. Horvath, W. Melander and I. Molnar, Anal. Chem., 49 (1977) 2295.
10 B.A. Bidlingmeyer, S.N. Deming, W.P. Price, Jr., B. Sachok and M. Petrusek, J. Chromatogr., 186 (1979) 419.
11 P.C. Lu, H.F. Zou and Y.K. Zhang, Mikrochim. Acta, Part III, (1990) 35.
12 B.A. Bidlingmeyer, J. Chromatogr. Sci., 18 (1980) 525.

13 B.R. Steven and M.S. David, Anal. Chem., 57 (1985) 1130.
14 P. Jandera, J. Churacek and B. Taraba, J. Chromatogr., 262 (1983) 121.
15 A. Bartha, Gy. Vigh and J. Stahlberg, J. Chromatogr., 506 (1990) 85.
16 H.F. Zou, Y.K. Zhang, M.F. Hong and P.C. Lu, J. Chromatogr., 625 (1992) 169.
17 H.F. Zou, Y.K. Zhang and P.C. Lu, J. Chromatogr., 545 (1991) 59.
18 H.F. Zou, Y.K. Zhang, M.F. Hong and P.C. Lu, J. Chromatographia, 32 (1991) 329.
19 H.F. Zou, Y.K. Zhang, M.F. Hong and P.C. Lu, J. Chromatographia, 34 (1992) 14.
20 A. Bartha and J. Stahlberg, J. Chromatogr., 535 (1990) 181.
21 H.F. Zou, Y.K. Zhang, M.F. Hong and P.C. Lu, Chromatographia, 35 (1993) 390.

Analytica Chimica Acta, 284 (1993) 67–71
Elsevier Science Publishers B.V., Amsterdam

On-line trace enrichment for the determination of ethacrynic acid in urine by liquid chromatography and column-switching

Pilar Campíns-Falcó, Rosa Herráez-Hernández and Adela Sevillano-Cabeza

Departamento de Química Analítica, Facultad de Química, Universidad de Valencia, Dr. Moliner 50, 46100 Burjassot, Valencia (Spain)

(Received 12th May 1993; revised manuscript received 21st July 1993)

Abstract

A chromatographic method based on liquid chromatography (LC) using column-switching for the determination of ethacrynic acid in urine samples, is described. The proposed system uses an Hypersil ODS-C18, 30 μm (20 mm × 2.1 mm i.d.) pre-column for the pre-concentration and separation of ethacrynic acid from the biological matrix. Polar urinary compounds are removed by flushing the pre-column with purified water, and the enriched analyte is then switched in back-flush mode onto an HP-LiChrospher RP C18, 5 μm (125 mm × 4 mm i.d.) analytical column, where it is chromatographed using an acetonitrile–acetate buffer gradient elution. The UV detector was set at 275 nm. The recovery of drug was 99 ± 2% in the 0.010–1.0 μg/ml concentration range. The limit of detection was 1 ng/ml, the total analysis time being less than 10 min. The reliability of this study has been tested by analyzing urine samples after minimum single dose (25 mg) administration of ethacrynic acid.

Keywords: Liquid chromatography; Ethacrynic acid; Trace enrichment; Urine

Ethacrynic acid (Fig. 1) is a high-ceiling loop diuretic, primarily used in the treatment of pulmonary oedema when a rapid and potent diuretic action is required. In recent years, this compound has also been misused and abused in sports, in attempts to evade drug testing and to reduce body weight in sports that involve weight categories.

The detection and quantification of ethacrynic acid in biological samples is a very complex problem because of its short time of elimination, and also because it is extensively metabolized. Although gas chromatography (GC) usually provides good sensitivity [1,2] the time taken for analysis is high, and pre-derivatization of the analyte is required. Moreover, GC may be inadequate to analyze large numbers of samples due to the cost involved. The sensitivity reported by most of the proposed liquid chromatographic (LC) assays [3–5] is not suitable for pharmacokinetic studies in urine samples, and LC–UV methods described for the screening of diuretics have not detected ethacrynic acid after a normal single dose ingestion [6]. Ventura et al. [7] have reported the detection of ethacrynic acid in real samples by LC and mass spectrometry (MS), after the ingestion of 50 mg of drug. We have recently described the quantification of ethacrynic acid in spiked urine samples applying solid-phase extraction cartridges for sample clean-up [8], which provides a sensitivity comparable to that reported by GC procedures.

Since high sensitive analytical methods are required for the identification and quantification of

Correspondence to: P. Campíns-Falcó, Departamento de Química Analítica, Facultad de Química, Universidad de Valencia, Dr. Moliner 50, 46100 Burjassot, Valencia (Spain).

0003-2670/93/$06.00 © 1993 – Elsevier Science Publishers B.V. All rights reserved

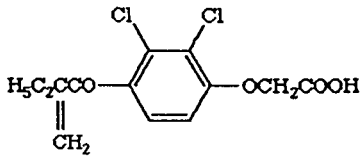

Fig. 1. Chemical structure of ethacrynic acid.

ethacrynic acid in urine samples, we have evaluated the potential of column-switching as an enrichment technique for this diuretic. In addition, the time required for the sample clean-up process by column-switching chromatography is drastically shortened, as minimum off-line sample manipulation is involved. Therefore, this technique can be very useful for doping control tests, where large series of samples must be processed.

EXPERIMENTAL

Apparatus

The chromatographic system used consisted of two quaternary pumps (Hewlett-Packard, 1050 Series, Palo Alto, CA), an automatic sample injector (Hewlett-Packard, 1050 Series) and a high-pressure six-port valve (Rheodyne Model 7000). A diode-array detector (Hewlett-Packard, 1040 series) linked to a data system (Hewlett-Packard HPLC Chem Station) was used for data acquisition and storage. The detector was set to collect a spectrum every 640 ms over the range 200–400 nm, and the chromatographic signal was monitored at 275 nm. All the assays were carried out at ambient temperature.

Reagents

All the reagents were of analytical grade. Methanol and acetonitrile were of HPLC grade (Scharlau, Barcelona). Water was distilled, deionized and filtered in nylon membranes, 0.45 μm (Teknokroma, Barcelona). Ethacrynic acid (Sigma, St. Louis, MO) stocks solutions were prepared by dissolving the pure compound in methanol. Propylamine hydrochloride (Fluka, Buchs), sodium acetate (Panreac, Barcelona) and acetic acid (Probus, Badalona) were also used.

Standard solution

A standard solution of ethacrynic acid was prepared by dissolving 50 mg of the pure compound in 25 ml of methanol (2000 μg/ml), and it was stored in the dark at 2°C. Under such conditions, this standard solution is stable at least for a week. Working solutions were prepared daily by dilution of the stock solution with the appropriate volumes of water.

Columns and mobile phases

The pre-column (20 mm × 2.1 mm i.d.) was dry-packed with an Hypersil ODS-C18, 30 μm (Merk, Darmstadt) stationary phase. Purified water was used as washing solvent to eliminate the biological matrix from the pre-column. The analytical column was an HP-LiChrospher 100 RP 18, 125 mm × 4 mm i.d., 5 μm, column (Merck, Darmstadt). An acetonitrile–0.05 M acetate buffer (pH 4) mixture in gradient elution mode, was used for the analytical separation. The acetate buffer was prepared by dissolving 2 g of sodium acetate in 500 ml of purified water, after the addition of 0.7 ml of propylamine hydrochloride. The pH was adjusted to 4 by adding concentrated acetic acid. The mobile phases were prepared daily, filtered with a nylon membrane, 0.45 μm, (Teknokroma) and degassed with helium before use.

Column-switching operation

At the beginning of each assay 250 μl of sample were injected from the injector to the pre-column. By pumping water, the polar components of the matrix were directly washed-out, whereas the analyte was trapped in the pre-column. At the same time, the analytical column was being re-equilibrated by an acetonitrile–acetate buffer mixture. At $t = 5$ min, the switching valve was rotated, so the analyte was eluted in back-flush mode,from the pre-column to the analytical column with the acetonitrile/acetate buffer eluent. A gradient was used to increase the acetonitrile content from 30% at 0–4 min, to 60% at 8 min. After 8.0 min the acetonitrile content was kept constant. At $t = 9$ min the switching valve is turned back to the original position to regenerate

and re-equilibrate both the pre-column and the analytical column.

Urine samples

Volumes of 1 ml of filtered urine samples were placed into glass injection vials, and 250 μl were directly injected onto the chromatographic system.

Recovery studies

Blank urine samples of 5.0 ml were spiked with ethacrynic acid standard solutions reproducing different concentrations in the 0.01–1.0 μg/ml range. The percentage of drug recovered for a particular injection was calculated by comparing the peak areas obtained for the spiked samples, with the values obtained for a direct injection of 250 μl of an aqueous solution containing different concentrations in the calibration range. Each concentration was assayed in duplicate.

Preparation of standards for calibration

Standards for calibration were prepared by spiking 5.0 ml of urine samples with the appropriate volumes of methanolic ethacrynic acid solution reproducing different concentrations in the 0.01–1.0 μg/ml range. These samples were processed as described above. Peak areas at 275 nm were plotted versus ethacrynic acid concentration, and the resulting calibration curve was used to calculate the ethacrynic acid concentration of the unknown samples.

Human studies

Urinary excretion studies were performed with a human healthy volunteer after a minimum single dose administration of ethacrynic acid (25 mg). Urine samples were collected at appropriate time intervals post-dose, and analyzed as described above.

RESULTS AND DISCUSSION

Chromatography

In order to obtain a satisfactory chromatographic response, an acetonitrile–0.05 M acetate buffer (pH 4) mixture in gradient elution mode was selected for the analytical separation [8]. A back-flush configuration was selected to transfer the analyte from the pre-column to the analytical column, to minimize the dispersion of the sample onto the chromatographic system. In such a way, no peak broadening was observed in comparison to direct injection of the samples onto the analytical column. Typical chromatograms of blank and spiked urine samples are shown in Fig. 2. Under the working conditions, ethacrynic acid is eluted at 2.51 min (7.51 min since the injection of the samples). The baseline at the end of each assay is slightly higher than that observed at times lower than 1.5 min. It is probably due to the adsorption properties of the acetate solution used in the mobile phase for the analytical separation [8]. As can be seen from Fig. 2, there are no urinary endogenous compounds which may interfere with the identification or quantitation of ethacrynic acid.

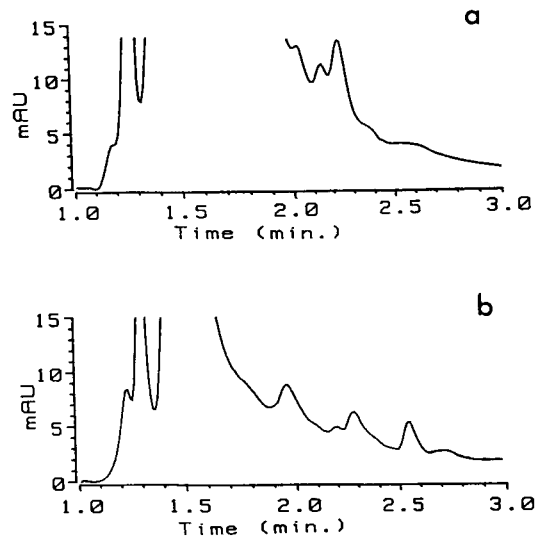

Fig. 2. Chromatograms at 275 nm of (a) blank and (b) spiked with 0.50 μg/ml of ethacrynic acid (retention time 2.51 min) urine samples.

Recovery

In previous studies with different solid phase extraction cartridges, we found that the strongest retention for ethacrynic acid is obtained with apolar materials such as octyl or octadecyl silica packings [9]. This latter packing has been em-

TABLE 1

Recovery percentages of ethacrynic acid at the different concentrations tested ($n = 2$)

Ethacrynic acid concentration (ng/ml)	Recovery (%)
10	100, 98
50	101, 101
100	97, 99
250	102, 101
500	99, 97
1000	98, 98
Mean value	99 ± 2%

ployed for the detection and determination of ethacrynic acid in urine samples. Consequently we have selected an octadecyl-bonded material as stationary phase for the pre-column. The retention obtained for ethacrynic acid when the pre-column is filled with an Hypersil ODS-C18 30-μm packing, is almost complete and independent of the duration of the flushing in the 1.0–10.0 min interval. In this work, the duration of the flush-step was set to 5 min. This was found to be necessary to ensure a satisfactory operative life of the analytical column, as large volumes of samples must be injected if high sensitivity is required.

The extraction recoveries for the different concentrations of ethacrynic acid tested are listed in Table 1. The efficiency and precision obtained in the sample clean-up step is adequate and do not depend on the drug concentration in the interval studied. The mean recovery is of 99 ± 2% (n = 12).

Precision and accuracy

The calibration curves obtained are unbiased and linear over the working interval 0.01–1.0 μg/ml. The mean correlation coefficient was 0.9998. In order to evaluate the precision and accuracy of the method, control urine samples from different volunteers were spiked with ethacrynic acid, and tested in triplicate to determine drug levels. The results obtained are summarized in Table 2. The concentrations found were close to the actual concentrations in all

TABLE 2

Precision and accuracy for ethacrynic acid in urine ($n = 3$)

Subject number	Added concentration (ng/ml)	Determined concentration (μg/ml)
1	25	25 ± 3
	100	107 ± 6
	500	515 ± 8
2	25	24 ± 3
	100	103 ± 4
	500	484 ± 13
3	25	26 ± 2
	100	96 ± 4
	500	485 ± 4

cases tested. From these results it can be derived that the accuracy and precision of the method is suitable, with relative standard deviations ranging between 1% and 12% for concentrations of 0.50 and 0.025 μg/ml, respectively. No differences in the precision were observed when an internal standard was used. Therefore, the addition of a standard is not necessary, and sample dilution was avoided.

Sensitivity

The described column-switching system provides an enrichment factor of about 10 compared to the previously reported off-line sample pretreatment based on the employment of solid phase extraction cartridges [8]; in addition smaller vol-

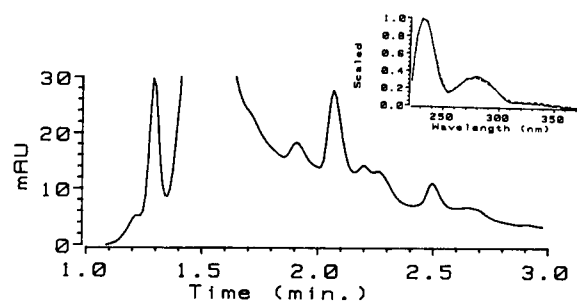

Fig. 3. Chromatogram at 275 nm of a urine sample obtained 5.5 h after a single dose administration of 25 mg of ethacrynic acid (retention time, 2.51 min). Inset: a comparison between the UV spectra of the sample (– – –) and a standard of ethacrynic acid (———).

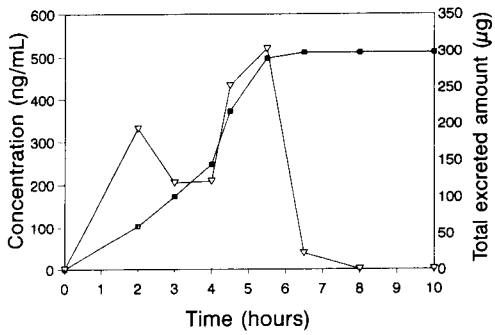

Fig. 4. Urinary excretion–time profile of ethacrynic acid (▽). The figure also shows the cumulative urinary excretion of the drug (■) (dose administered, 25 mg).

umes of sample are required (250 μl vs. 2.0 ml). The injection of volumes greater than 250 μl is not recommended, because urinary endogenous compounds are also concentrated, then increasing the background noise and limiting the operative life of both the pre-column and the analytical column.

The limit of detection (for a signal-to-noise ratio of 3) corresponds to an ethacrynic acid concentration in urine of 1 ng/ml.

Human studies

The described assay has been applied to the measurement of urinary levels of ethacrynic acid after a minimum single dose administration of 25 mg to a human volunteer. Figure 3 shows a chromatogram obtained 5.5 h after the administration of drug, the estimated concentration of drug being 0.43 ± 0.04 μg/ml ($n = 3$). The urinary excretion profile is shown in Fig. 4, which also shows the total amount of drug eliminated. The amount of ethacrynic acid excreted gradually increases in each urine collection from 2 to 5.5 h. However, the concentration of drug in the samples depends on volume of sample eliminated, which explains the concentration time profile observed. Less than 2% of ethacrynic acid is eliminated in the 6.5-h period after administration. The amount of drug excreted after 6.5 h is negligible.

Utility

Although urine samples are directly injected, more than 40 injections can be made without increase of the back-pressure neither in the pre-column or in the analytical column. The pre-column and the analytical column are effectively regenerated and re-equilibrated in a few minutes. With the proposed procedure the analyte can be measured at least 6.5 h after dose. Then, this assay can be used for pharmacokinetic studies, taking into account that ethacrynic acid is active within the 6–8 h period after dose [10], the precision and accuracy being suitable at therapeutical levels. In addition, owing to the minimum sample handling and time required, this procedure can also be useful for doping control tests, where large series of samples must be processed.

The authors are grateful to the CICyT for financial support received for the realization of Project SAF 92-0655.

REFERENCES

1 W. Stüber, E. Mutschler and D. Steinbach, J. Chromatogr., 227 (1982) 193.
2 W.R. Sullivan and K.E. Fox, J. Chromatogr., 452 (1988) 396.
3 A.K. Singh, M. Ashraf, K. Granley, U. Mishra, M. Madhusudana Rao and B. Gordon, J. Chromatogr., 373 (1989) 215.
4 A.K. Singh, Y. Jan, U. Mishra and K. Granley, J. Chromatogr., 568 (1991) 351.
5 F.P. LaCreta, J.M. Brennan, P.W. Tinsley and P.J. O'Dwyer, J. Chromatogr., 571 (1991) 271.
6 R.O. Fullinfaw, R.W. Burry and R.F.W. Moulds, J. Chromatogr., 415 (1987) 347.
7 R. Ventura, D. Fraisse, M. Becchi, O. Paisse, J. Segura, J. Chromatogr., 562 (1991) 723.
8 P. Campíns-Falcó, R. Herráez-Hernández and A. Sevillano-Cabeza, Anal. Chim. Acta, 270 (1992) 39.
9 P. Campíns-Falcó, R. Herráez-Hernández and A. Sevillano-Cabeza, J. Liq. Chromatogr., 14 (1991) 3575.
10 V. Rimbau, Offarm, 10 (1991) 57.

Analytica Chimica Acta, 284 (1993) 73–78
Elsevier Science Publishers B.V., Amsterdam

Chromatographic pattern recognition for the analysis of complex mixtures

Man Ki Park, Jung Hwan Cho, Na Yung Kim and Jeong Hill Park

College of Pharmacy, Seoul National University, Seoul 151-742 (South Korea)

(Received 16th October 1992; revised manuscript received 14th April 1993)

Abstract

A system of pattern recognition for the analysis of complex mixtures was developed using a conventional capillary gas chromatograph and a personal computer with laboratory-written software. Pattern recognition was accomplished by a multiple reference peak identification method and outlier statistics using an on-line data system. Reference peaks were selected as they were well resolved and present in both the sample and reference chromatograms. The resultant area ratios of peaks selected as the nearest neighbours were treated statistically by three kinds of outlier rejection method, Dixon's Q test, the two-sided Grubbs test and Huber's elimination rule. The outlier peak is simply dropped from the averaging and the reported mean becomes more representative of the true value. Huber's elimination rule gave the best results. Repeatability of the results of analysis was examined by a two-sided analysis of variance (ANOVA) test.

Keywords: Gas chromatography; Pattern recognition; Complex mixtures; Essential oils

The nature of a complex mixture is expressed as a multivariate relationship between several independent variables and one or more dependent variables. Nonetheless, in the usual chemical analyses used for complex mixtures, the system is simplified to the relationship of a single independent variable and a single dependent variable for the convenience of experimental procedures and ease of data processing. In this situation, it is usually true that the results of analysis may distort the real nature of a complex mixture. Therefore, the multivariate chemical system should be analysed by a multivariate analytical method [1–10]. A system of pattern recognition with the use of a conventional gas chromatograph and a personal computer was developed and applied to the analysis of complex mixtures.

Correspondence to: J.H. Park, College of Pharmacy, Seoul National University, Seoul 151-742 (South Korea).

Modern capillary gas chromatographs show powerful resolution even for complex mixtures. In particular, essential oils can be effectively separated on a certain stationary phase in a capillary column, showing combinations of patterns consisting of well resolved peaks. These patterns are specific as they can be used as a fingerprint of certain crude drugs containing essential oils, even in complex mixtures with others [11–15]. The recognition of these patterns on the chromatogram can be accomplished with the naked eye by comparing the chromatogram of an unknown complex mixture with that of a standard essential oil, but this kind of recognition may not be reproducible. As a solution to this kind of problem, a chromatographic data processing system was designed for a personal computer which is connected to a capillary gas chromatograph via an analogue-to-digital converter and a digital output device [16]. Using this system, the digitized chromatogram can be used for the identification

0003-2670/93/$06.00 © 1993 – Elsevier Science Publishers B.V. All rights reserved

and quantification of complex mixtures of compounds which together constitute a single entity. In this pattern matching, the analysis of unknown complex mixtures may be complicated by interference with one or more peaks by other compounds that ordinarily are not part of the reference complex mixture. These interfering peaks may be rejected statistically by methods of outlier detection. To accomplish this kind of data processing on-line, two software systems were designed and programmed for an IBM/PC/AT-compatible personal computer.

EXPERIMENTAL

Materials, reagents and instrumentation

A Hewlett-Packard 5890 Series II gas chromatograph used was equipped with a flame ionization detector and interfaced to IBM/PC/AT-compatible personal computer via a PCL-812 analogue-to-digital converter (Advantech, Taiwan). The signal from the gas chromatograph was amplified by a PCLD-789 (Advantech). A fused-silica capillary column (25 m × 0.2 mm i.d.) coated with Carbowax 20M was used for the analysis of essential oils.

Reference lemon oil (Charabot, France) was mixed with eau de cologne (Pacific Chemical, Korea) and/or cinnamon bark oil (Charabot, France) to make synthetic complex mixtures. This synthetic mixture was subjected to steam distillation using a Dean and Stark-type trap [17]. The *n*-hexane of the trap was used to concentrate the essential oils in the aqueous condensate. Acetophenone (Sigma, St. Louis, MO) dissolved in *n*-hexane was used as an internal standard.

Data processing and computer programming

The two software systems designed for the experimental are the main program named ChroMan and the chromatographic data acquisition program named ChroAQ. ChroAQ was written in structured BASIC. Using this data acquisition system, the chromatograms can be acquired in digital form for data processing. The chromatographic data were averaged for every 0.2 s and these averaged data were collected in a data file on magnetic disk. The main program, ChroMan, designed for pattern recognition and written in Pascal, has a sub-program, FindPeak, for the usual functions of a digital integrator. The program recognizes the start point, the apex, the end-point, the precise peak height and area and the full width at half-maximum intensity [18,19]. In addition, the Savitzky–Golay polynomials of quartic transfer function were used for noise reduction of the chromatogram [20]. The size of the convolution block used for this experiment was eleven points of a chromatographic data set. The relative retention time and relative area of the chromatographic peaks were calculated with reference to the retention time and area of an internal standard peak. The pattern recognition system constructed for the actual application of the method uses the retention data provided by the peak recognition system for the matching of chromatographic peaks of the standard and those of the complex sample mixtures by the method of nearest neighbours [21]. The ratios (R_i) of the areas of matched peak pairs are then calculated and subjected to statistical treatment for outlier rejection using Dixon's Q test, the two-sided Grubbs test or Huber's elimination rule [22–27]:

$$R_i = S_{p_{(i)}}/S_{t_{(i)}}$$

where $S_{p_{(i)}}$ = relative peak area of matched peak of sample chromatogram and $S_{t_{(i)}}$ = relative peak area of matched peak of standard chromatogram.

After the rejection of outliers, two kinds of means were calculated with the remaining data of ratios of areas. One was the simple arithmetic mean (M_s) calculated by the usual statistical treatment:

$$M_s = \Sigma R_i/n$$

where ΣR_i = the summation of remaining data of ratios and n = the number of remaining data of ratios. The other was the weighted mean. For the calculation of the weighted mean, the weighting factors (W_i) were determined from the area ratio of the selected peaks on the standard chromatogram

$$W_i = S_{t_{(i)}}/\Sigma S_{t_{(i)}}$$

The weighting factor was multiplied by the corresponding value of the ratio of peak areas, then these values were summed to give the weighted mean (M_w):

$$M_w = \Sigma(R_i W_i)$$

As a result, a large peak on the standard chromatogram contributes more significantly to the value of the mean. The concentration (C_{S_p}) of the sample in the complex mixture was calculated from these mean values (M) and the concentration (C_{S_t}) of the standard used:

$$C_{S_p} = C_{S_t} M$$

All these procedures have been incorporated as sub-programs of ChroMan. The program ChroAQ was designed to be called by ChroMan, which controls the whole procedure of pattern recognition on-line.

Analysis of essential oils

The pattern recognition system consisting of the corresponding hardware and the ChroAQ and ChroMan software was used for the analysis of essential oil mixtures. The concentrations of reference essential oil solutions were 1.0, 2.0, 3.0 and 4.0% (v/v) of lemon oil in 10 ml of *n*-hexane at 25°C. A standard essential oil was mixed with *n*-hexane after steam distillation. The first set of test samples were mixtures of 0.20 ml of reference lemon oil and 2.0, 3.0, 4.0, 5.0 or 6.0 ml of eau de cologne to make 10 ml of final synthetic complex sample mixture after steam distillation. The second set of test samples were the mixtures of 0.20 ml of lemon oil and 0.05, 0.10, 0.15, 0.20 or 0.25 ml of cinnamon bark oil and 2.0 ml of eau de cologne to make 10.0 ml of a more complex mixture after steam distillation. The concentration of acetophenone as an internal standard for these mixtures was 0.3% in the final solution.

The conditions for capillary gas chromatography were as follows: detector and injector temperature, 250°C; column oven temperature, 50°C for 10 min then increased to 200°C (at 5°C min^{-1}); sample injection volume, 2.0 μl; splitting ratio, 50:1; and linear velocity of carrier gas (helium), 25.0 cm s^{-1}.

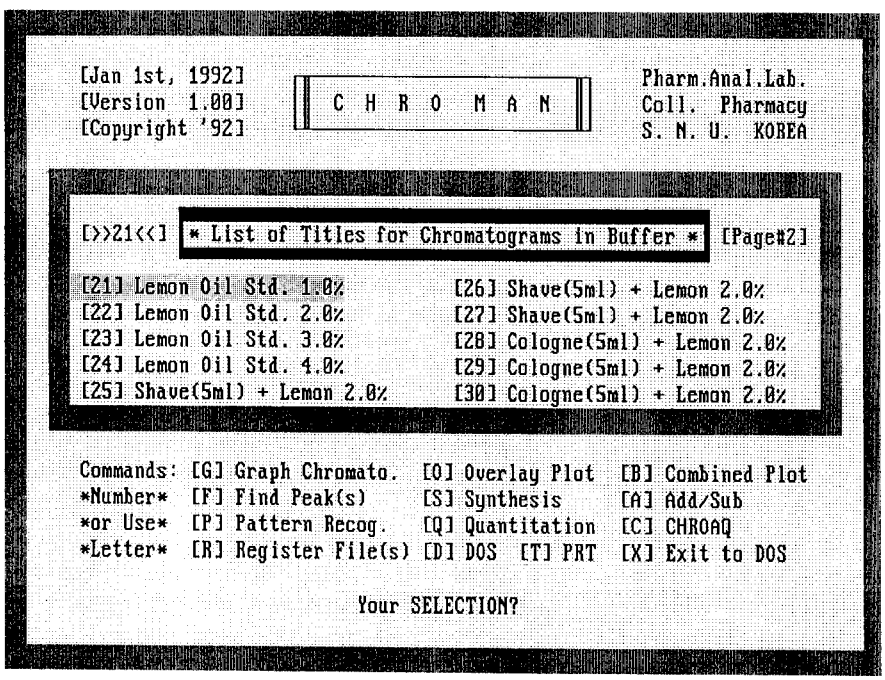

Fig. 1. Opening screen and command processing part of ChroMan system.

RESULTS AND DISCUSSION

The opening screen of ChroMain is shown in Fig. 1. The program supports several graphic card (e.g., Hercules monochrome, CGA, EGA, VGA and IBM 8514) to show chromatograms on a screen with eleven types of display, and this graphical screen can be hardcopied on four different printers (Epson LX, Epson LQ, NEC-P6 and HP Laserjet). Automatic peak picking is available. The synthetic chromatogram can be generated using a Gaussian or Lorentzian distribution model and addition or subtraction between two chromatogram can be calculated with user-specified factors to generate a new chromatogram. The connection between the sub-programs of ChroMan is shown in Fig. 2. All these features of ChroMan facilitated the analytical procedures.

The outlier peaks of the chromatogram result from the interference with one or more peaks by other compounds that normally are not compo-

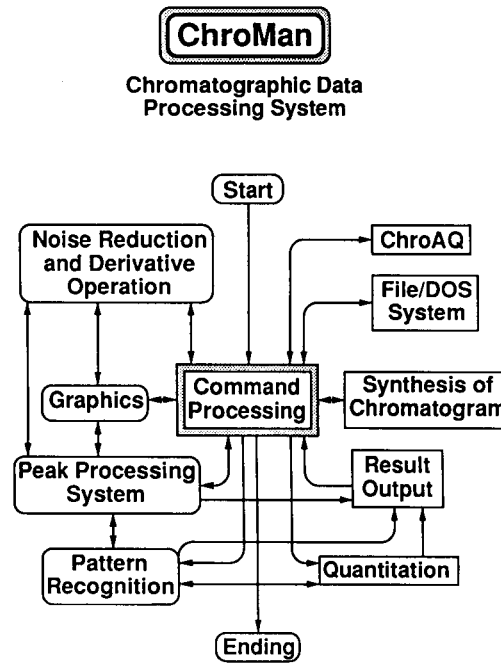

Fig. 2. Connection between sub-programs of ChroMan.

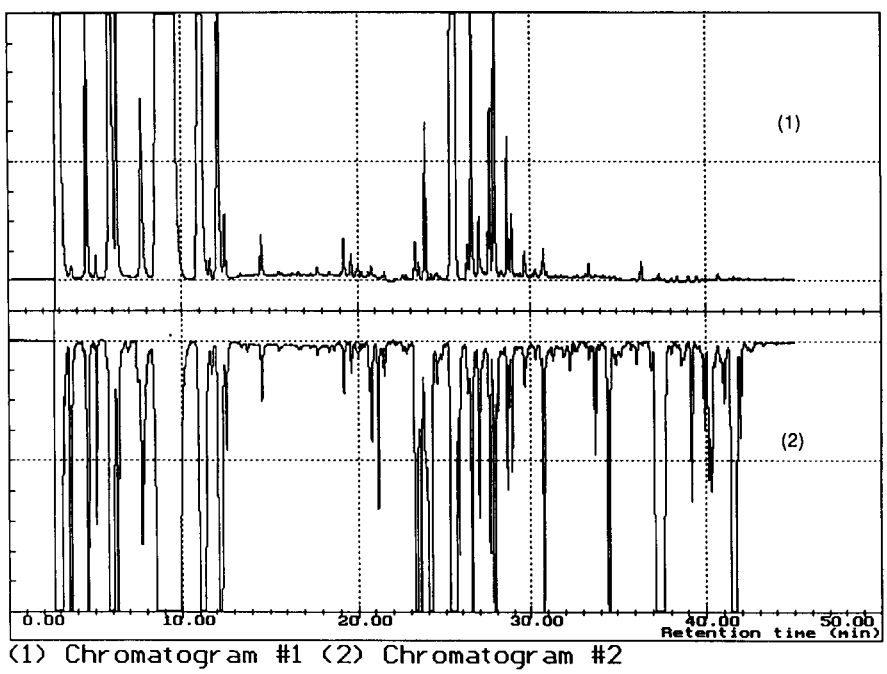

Fig. 3. Example of chromatograms of standard and sample. (1) Standard lemon oil; (2) mixture of lemon oil, cinnamon oil and eau de cologne.

TABLE 1

Recovery (%) of lemon oil in binary mixtures with eau de cologne

Sample [a]	Simple mean			Weighted mean		
	Dixon	Grubbs	Huber	Dixon	Grubbs	Huber
A	138.1	130.9	108.5	104.6	104.6	102.7
B	113.2	101.6	98.4	96.5	94.5	96.9
C	129.2	129.2	108.3	105.1	105.1	102.6
D	117.8	117.4	112.5	95.3	94.7	94.7
E	128.1	120.5	110.9	101.9	101.5	99.8
Mean ($n = 5$)	125.3	119.9	107.7	100.7	100.1	99.3
S.D.	9.9	11.7	5.5	4.5	5.2	3.5

[a] Lemon oil (0.20 ml) was mixed with (A) 2.0 ml, (B) 3.0 ml, (C) 4.0 ml, (D) 5.0 ml or (E) 6.0 ml of eau de cologne.

TABLE 2

Recovery (%) of lemon oil in ternary mixtures with cinnamon bark oil and eau de cologne

Sample [a]	Simple mean			Weighted mean		
	Dixon	Grubbs	Huber	Dixon	Grubbs	Huber
A	104.2	104.2	99.6	98.0	98.0	97.1
B	111.2	111.2	103.4	99.2	99.2	98.9
C	123.7	123.7	105.2	106.9	106.9	103.1
D	131.8	121.6	101.5	103.3	102.4	97.1
E	129.4	112.6	109.6	109.2	103.1	102.6
Mean ($n = 5$)	120.1	114.7	103.9	103.3	101.9	99.8
S.D.	11.9	8.0	3.8	4.8	3.5	2.9

[a] Lemon oil (0.20 ml) was mixed with (A) 0.05 ml, (B) 0.10 ml, (C) 0.15 ml, (D) 0.20 ml or (E) 0.25 ml of cinnamon bark oil and 2.0 ml of eau de cologne.

nents of the standard essential oils. The detection and rejection of outliers among the ratio values calculated from matched peaks was accomplished by three kinds of statistical methods. The results of statistical treatments of data were compared with each other.

Figure 3 shows typical chromatograms of reference lemon oil and a ternary mixture with eau de cologne and cinnamon bark oil. The results of the analysis of binary mixtures are given in Table 1. Lemon oil itself is a complex mixture, showing complicated multiple peaks. The binary mixture of lemon oil and eau de cologne is much more complicated. Nonetheless, the amount of lemon oil in the binary mixture was calculated with a reasonable recovery. In this case, calculation using the weighted mean gave better results than that using the simple mean. Among the three methods used for outlier rejection, Huber's elimination rule was superior, with a smaller standard deviation.

Table 2 gives the results of the analysis of ternary mixtures. As shown in Fig. 3, the chromatogram of a ternary mixture is much more complicated, but the amount of lemon oil in the mixtures can be calculated exactly using Huber's elimination rule and the weighted mean. In general, the results of Dixon's Q test shows greater errors when the chromatogram is more complex, although it can be used when there are smaller number of outliers in the data set. The two-sided Grubbs test rejects the outliers to minimize the resulting standard deviation. This may distort the result when the values of the data set are distributed mainly at points other than the median value or distributed widely around the median value. In contrast to these two methods, Huber's elimination rule showed reasonable results in all cases examined.

To examine the repeatability of the pattern recognition using Huber's elimination rule and the weighted mean, a two-sided analysis of variance (ANOVA) test was performed using three sets of five complex mixtures of 2.0% lemon oil in the 5.0 ml of eau de cologne. The results of the test are given in Table 3. The recoveries of lemon oil in the complex mixtures were not significantly different within each experiment and between three experiments with 95% or 99% confidence. In other words, the results of calculations were repeatable statistically.

Conclusion

Huber's elimination rule is the preferred method for outlier rejection after peak matching by the method of nearest neighbours, especially with more complex mixtures. The weighted mean resulted in more reproducible quantification than the simple arithmetic mean. The quantification results were proved to be statistically repeatable according to a two-sided ANOVA test. It is concluded that the pattern recognition system consisting of the chromatographic data acquisition

TABLE 3

Repeatability [a] of pattern recognition method (Huber's method, weighted mean) by two-way ANOVA

Sample	Experiment No.		
	1	2	3
A	104.1	95.3	95.2
B	114.9	97.2	97.9
C	101.8	102.2	99.9
D	97.1	102.7	98.6
E	98.3	101.3	100.8
Mean ($n = 5$)	101.2	99.7	98.5
S.D.	3.5	2.9	1.9

ANOVA [b]

Source	S.S.	D.F.	M.S.	F
Total	127.9	14		
S.S.T.	18.3	2	9.15	
S.S.E.	109.6	12	9.13	1.00

$F_{0.95} = 3.88$ (not significant)
$F_{0.99} = 6.93$ (not significant)

[a] Repeatability test was carried out on recovery (%) data with samples containing 0.20 ml of lemon oil and 5.0 ml of eau de cologne. [b] S.S. = sum of squares; D.F. = degrees of freedom; M.S. = mean of squares; F = F-statistic; Total = total variation; S.S.T. = variation between experiments; S.S.E. = variation within experiments.

system ChroAQ and the data processing system ChroMan, which utilizes the digital chromatogram provided by ChroAQ, can be used effectively for the quantitative analysis of complex mixtures.

This research was supported, in part, by a grant (91-05-2057) from Daewoo Research–SNU Fund.

REFERENCES

1 G. Kateman, Anal. Chim. Acta, 191 (1986) 125.
2 B.E. Saxberg, D.L. Duewer, J.L. Booker and B.R. Kowalski, Anal. Chim. Acta, 103 (1978) 201.
3 M.E. Parrish, B.W. Good. F.S. Hsu, F.W. Hatch, D.M. Ennis, D.R. Douglas, J.H. Shelton, D.C. Watson and C.N. Reilley, Anal. Chem., 53 (1981) 826.
4 W.J. Goux, J. Magn. Reson., 85 (1989) 457.
5 M. Chien, Anal. Chem., 57 (1985) 348.
6 M.E. Parrish, B.W. Good, M.A. Jeltema and F.S. Hsu, Anal. Chim. Acta, 150 (1983) 163.
7 W.J. Dunn III, D.L. Stalling, T.R. Schwartz, J.W. Hogen, J.D. Petty, E. Johansson and S. Wold, Anal. Chem., 56 (1984) 1308.
8 M.E. Cohen, D.L. Hudson, L.T. Mann, J. Bogaerde and N. Gitlin, J. Chromatogr., 384 (1987) 145.
9 M. Otto and H. Bandemer, Anal. Chim. Acta, 184 (1986) 21.
10 R.E. Lee, R. Bramston-Cook and J. Tschida, Anal. Chem., 55 (1983) 626.
11 M.G. Motto, J. Chromatogr. Sci., 25 (1987) 56.
12 E. Lemberkovics, J. Chromatogr., 286 (1984) 293.
13 V.A. Zamureenko, N.A. Kluyev, L.B. Dmitriev and I.I. Grandberg, J. Chromatogr., 303 (1984) 109.
14 M. Godefroot, P. Sandra and M. Verzele, J. Chromatogr., 203 (1981) 325.
15 E. Lemberkovics and G. Petri, J. Chromatogr., 446 (1988) 267.
16 R.E. Dessy, Anal. Chem., 58 (1986) 678A.
17 S.K. Poole, T.A. Dean, J.W. Oudsema and C.F. Poole, Anal. Chim. Acta, 236 (1990) 3.
18 W. Kipiniak, J. Chromatogr. Sci., 19 (1981) 332.
19 A.N. Papas and M.F. Delaney, Anal. Chem., 59 (1987) 55A.
20 M.K. Park and J.H. Cho, Arch. Pharm. Res., 10 (1987) 1.
21 S.B. Tejada and J.E. Sigsby, Jr., J. Chromatogr. Sci., 26 (1988) 494.
22 R.B. Dean and W.J. Dixon, Anal. Chem., 23 (1951) 636.
23 N.R. Draper and J.A. John, Technometrics, 23 (1981) 21.
24 P.L. Davies, Fresenius' Z. Anal. Chem., 331 (1988) 513.
25 H. Streuli, Fresenius' Z. Anal. Chem., 303 (1980) 406.
26 W. Rechenberg, Fresenius' Z. Anal. Chem., 311 (1982) 590.
27 D.B. Rorabacher, Anal. Chem., 63 (1991) 139.

Analytica Chimica Acta, 284 (1993) 79–89
Elsevier Science Publishers B.V., Amsterdam

Extracting information from complex chromatographic fingerprints for evaluation of organic air pollution

Carla Armanino and Michele Forina

Istituto Analisi Tecnologie Farmaceutiche Alimentari, via Brigata Salerno, 16147 Genova (Italy)

Loretta Bonfanti

ENEL – Centro Ricerche Termiche Nucleari, via A. Pisano 120, 56100 Pisa (Italy)

Mario Maspero

CISE, via Reggio Emilia 39, 20090 Segrate (Italy)

(Received 3rd May 1993; revised manuscript received 5th July 1993)

Abstract

The gas chromatographic profiles of 47 samples of airborne particulate matter, obtained by flame ionization detection, were synchronized and quantified into variables by an automatic procedure, avoiding peak recognition and identification. Pattern recognition methods of principal components and clustering were used to extract information from the variables and seasonal similarities were established. Multivariate regression with the partial least squares method found predictive relationships between the profiles and other variables determined by different methods: extractable organic material, carbon preference index of the *n*-alkane homologous series (computed from gas chromatographic–mass spectrometric determinations) and mutagenicity. The predictive power was between 68% and 81%, and so the usefulness of the extracted information was verified; the profile obtained by flame ionization detection contains information related to the quality of air. The procedure is also suitable for different kinds of complex matrices, provided that synchronization is realized: it gives a first general knowledge of sample characteristics which may be used to address further analysis.

Keywords: Gas chromatography; Multivariate calibration; Pattern recognition; Air; Chemometrics

The evaluation of atmospheric pollution by organic compounds generally requires a detailed chemical study of complex matrices, which can be performed only by applying sophisticated and laborious analytical techniques.

Often the sample to be investigated is a very dilute solution obtained by extraction of the original matrix with an organic solvent. This extract contains several hundred organic compounds which are present at trace levels and covering a wide range of concentrations (often ranging over 5–6 orders of magnitude).

Gas chromatography (GC) is the technique most widely used to separate these complex mixtures into their components. Often it must be combined with detection techniques having a sensitivity and selectivity that need to be higher the more complex and dilute the sample solution is,

Correspondence to: C. Armanino, Istituto Analisi Tecnologie Farmaceutiche Alimentari, via Brigata Salerno, 16147 Genova (Italy).

0003-2670/93/$06.00 © 1993 – Elsevier Science Publishers B.V. All rights reserved

otherwise laborious clean-up procedures are necessary. The extracted organic material provides a "fingerprint", the chromatogram, which constitutes the raw data set from which all the information on the chemical composition of the mixture is drawn. Classical utilization of the chromatogram requires the recognition of the resolved peaks, their identification from the retention times and their quantification by a suitable response factor. Both identification and quantification require previous establishment of which compounds are to be searched for, the availability of standard solutions of these compounds and repetition of the GC analysis on each individual standard or on mixtures of standards, in order to determine the retention time and the specific response factor for each compound.

When the absolute retention time is poorly reproducible, often it has to be corrected using relative retention indices, otherwise more specific detection techniques must be used (e.g., mass spectrometric detection). A well known way to make the retention time more significant is to use of Kováts retention indices [1], allowing its correction with respect to a homologous series of internal standards which has to be added to the sample. Usually *n*-alkanes (C_xH_{2x+2}) are used.

The detailed description of the chemical composition of a complex mixture is, in any case, an ambitious aim which requires long analytical times, hard work and seldom the application of expensive instrumental techniques.

Within a study devoted to the evaluation of urban atmospheric pollution, several samples of urban air were characterized; the observations made on the chromatographic fingerprints of their organic extracts, combined with the information obtained from their chemical characterization, suggested the present study, which led to a non-classical utilization of the chromatograms, considered as simple fingerprints of the samples.

A method based on pattern recognition techniques was developed to evaluate the similarities of these fingerprints and to obtain information related to the quality of urban air as far as organic compounds are concerned.

The chromatogram was conceived as a pure profile, overcoming peak recognition, identification, calibration and, in some respects, also resolution.

The only requirement is to single out in the chromatograms a homologous series of compounds and to identify just one or two of them. This allows the synchronization of chromatograms, reducing the error associated with retention times. This essential condition, on the other hand, can be easily satisfied for all the organic extracts derived from terrestrial air samples; in fact, *n*-alkane homologous (n-A) can be derived from both anthropogenic and biogenic sources. The anthropogenic n-A are emitted from combustion processes, petroleum and coal refining, etc. [2], whereas biogenic n-A are mainly produced by vegetation [3].

Further, the concentration profiles of this set of compounds can also give information about their origin [4] and can be related to air quality. Hence a homologous series of *n*-alkanes can be always found in airborne particulate samples, providing a set of "natural internal standards" suitable for synchronization. They can easily be recognized, as all the members of the homologous series are always present and, in the chromatogram, their peaks generally show a characteristic intensity distribution and they are typically spaced out on the time scale.

Pattern recognition methods have been successfully applied to interpret spectroscopic and chromatographic fingerprints of complex mixtures [5–11]. In this work, quantification of the original profile based on its integral was used. The main purpose was to demonstrate the usefulness of the information extracted from GC profiles with flame ionization detection (FID) by this method and to verify its relationships with the information carried by the usual chemical characterization of the GC profile.

EXPERIMENTAL

Air particulate samples were collected in the centre of Milan 25 m above street level during the period September 1986–November 1988. Forty-seven samples of airborne particulate matter were obtained by filtering large volumes of

TABLE 1

Sampling characteristics
W (mg) = weight of particulate; V (m^3) = volume of strained air; A (m^3 h^{-1}) = delivery capacity of the air intake

Sample		Date	W	V	A
Index	Name				
1	O186F	31/10/86	122	2200	50
2	N186F	2/11/86	142	1180	50
3	D186F	1/12/86	87	675	50
4	D286F	10/12/86	75	885	50
5	m187W	16/03/87	102	820	17
6	M187P	14/05/87	81	1085	23
7	L187S	16/07/87	78	704	15
8	L287S	23/07/87	77	1073	22
9	A187S	6/08/87	56	1142	24
10	S187S	3/09/87	113	862	18
11	S287F	10/09/87	101	1094	23
12	S387F	24/09/87	124	780	16
13	O187F	8/10/87	117	1014	21
14	O287F	29/10/87	101	1055	22
15	N187F	19/11/87	115	501	10
16	D187F	3/12/87	76	702	15
17	D287F	17/12/87	97	365	8
18	a188P	6/04/88	95	587	24
19	a288P	13/04/88	68	582	24
20	a388P	20/04/88	65	594	25
21	a488P	27/04/88	84	588	25
22	M188P	4/05/88	65	575	24
23	M288P	11/05/88	46	588	25
24	M388P	19/05/88	32	558	23
25	M488P	25/05/88	63	507	21
26	J188P	8/06/88	50	555	23
27	J288P	15/06/88	27	566	24
28	J388S	23/06/88	72	547	23
29	L188S	20/07/88	84	848	29
30	L288S	27/07/88	63	596	22
31	A188S	3/08/88	50	592	23
32	A288S	11/08/88	40	550	23
33	A388S	18/08/88	34	564	24
34	A488S	25/08/88	30	530	22
35	A588S	31/08/88	38	540	23
36	S188S	8/09/88	43	540	23
37	S288S	15/09/88	30	577	24
38	S388S	20/09/88	70	546	23
39	S488F	29/09/88	13	431	18
40	O188F	5/10/88	57	568	24
41	O288F	12/10/88	17	579	24
42	O388F	19/10/88	51	552	23
43	O488F	26/10/88	80	545	23
44	N188F	4/11/88	106	789	21
45	N288F	10/11/88	80	228	7
46	N388F	17/11/88	197	728	20
47	N488F	23/11/88	69	689	17

ambient air (500–2200 m^3) through a glass-fibre filter for 24–48 h. Table 1 gives some characteristics of the samples, which are identified by a five-component label: the first is the sampling month (m = March, a = April, M = May, J = June, L = July, A = August, S = September, O = October, N = November, D = December), the second is the index within the month, the third and fourth are the year and the fifth is the season [P = spring, S = summer, F = autumn (fall), W = winter].

The filters were Soxhlet extracted with dichloromethane for 24 h. The organic extracts were concentrated to 1 ml and characterized by GC techniques. The total extractable organic material (EOM) was determined by a microgravimetric method [12] using a Sartorius S4 microbalance.

GC–FID analyses were carried out on a Varian Model 3600 gas chromatograph equipped with an on-column injector. A 1-μl volume of each extract was injected in the splitless mode and separated on an SPB-5 capillary column (film thickness 0.25 μm; 30 m × 0.25 mm i.d.) (Supelco) under the following conditions: injection mode, 100°C for 0.1 min, then to 300°C at 250°C/min; carrier gas, helium at a flow-rate of 2.5 ml min^{-1} (at 100°C); oven programme, 100°C for 1 min, then increased to 300°C at 6°C min^{-1}; detection, FID; detector temperature, 320°C; sensitivity, 8 × 10^{12} mV A^{-1}; run time, 50 min. As the injection of these extracts involves a progressive accumulation of substances on the column head, an initial section of column (5–10 cm) was removed whenever necessary.

All the GC–FID profiles, as electrical signals from the detector versus the run time, were acquired by a Spectra-Physics Model 4270 integrator and transferred to an IBM-AT computer. The points acquired for each run were then reduced 10:1 by conversion software (Spectra-Physics). For synchronization of GC profiles and their quantitative description a series of unpublished programs were used.

The determination of n-A was achieved after calibration with a standard mixture of 25 C_{12}–C_{36}

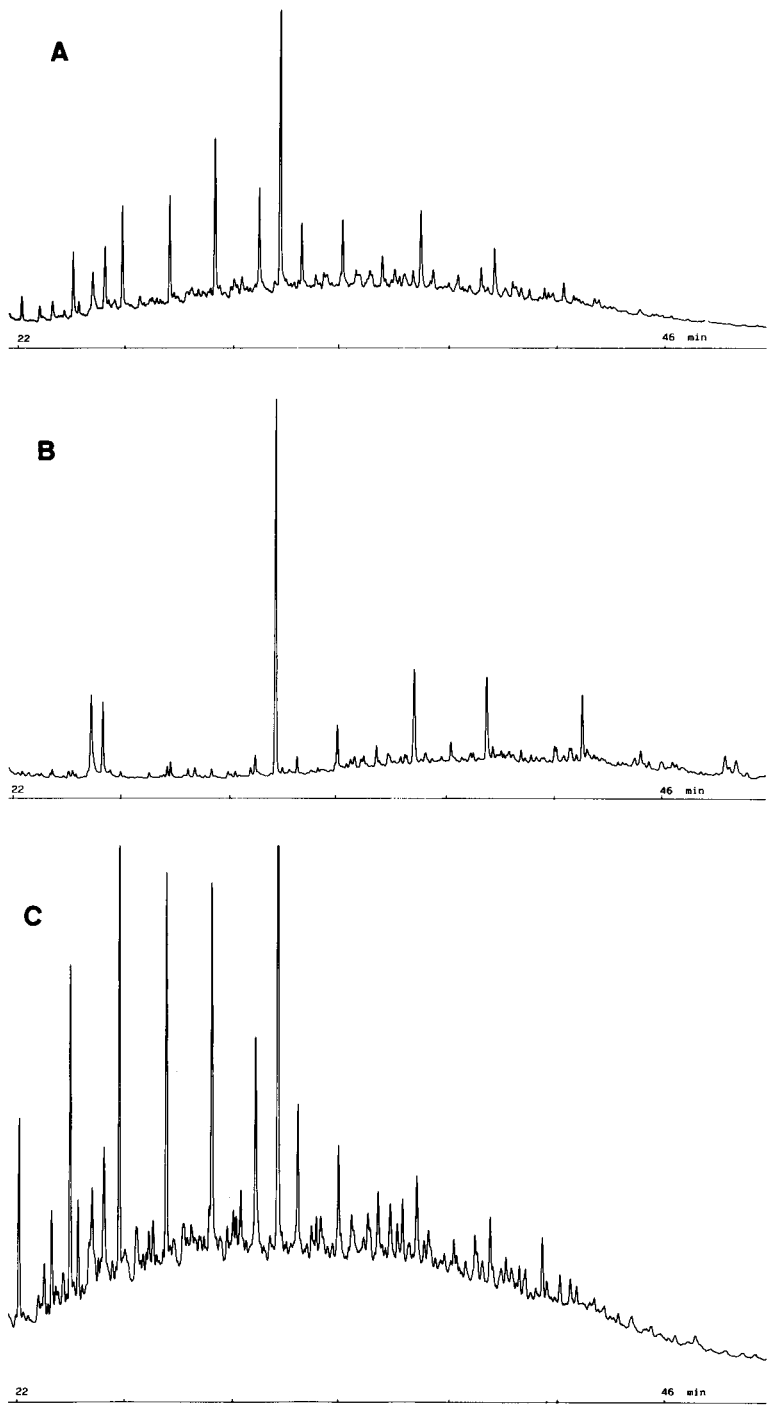

Fig. 1. Gas chromatograms (flame ionization detection) of extracts from 3 out of the 47 samples. (A) Sample collected on 12–14th May 1987; (B) sample collected on 14–16th July 1987; (C) Sample collected on 15–17th December 1987.

n-A. Resolvable chromatographic matter (RCM) was calculated as the sum of all the peaks acceptably resolved by the GC method. Each peak was integrated by considering the unresolvable complex mixture (UCM) profile as the baseline. The UCM was integrated with respect to the baseline without considering column bleeding.

GC analyses with mass spectrometric (MS) detection were performed using an HP 5890A Series II gas chromatograph coupled with an HP 5970B quadrupole mass spectrometer for determinations of n-A. The selected-ion monitoring (SIM) mode was used by selecting one or two specific mass fragments for each compound; the carbon preference index (CPI), defined as the ratio of the total amount of n-A with odd carbon numbers to those with even carbon numbers, was computed from the GC–MS determinations of n-A.

The mutagenicity of the ambient air particulate matter was measured on eighteen samples: an aliquot of the extracts was tested for mutagenicity by the Ames procedure [13], using the strains TA98 and TA100, with and without the metabolizing system S9, in order to evaluate the presence of direct or indirect mutagens in the extracts.

RESULTS AND DISCUSSION

Quantification

To be examined by pattern recognition methods, profiles (formed by thousands of data points) have to be reduced to a smaller number of variables which carry the same information as held by the original signal.

The procedure used to quantify the chromatograms was undertaken after the knowledge of several classical characterizations (GC–FID and GC–MS) of air particulate profiles had been acquired; on this basis it was known that all the examined GC profiles have, in fact, common characteristics and they are differentiated especially in quantitative aspects. Most of them show a "hump", constituted by a large number of compounds that cannot be separated under the applied conditions, which changes its pattern, intensity, amplitude and position on the time scale with different samples. This "hump", named UCM (unresolved complex mixture), is related to air pollution [14]. Therefore, the UCM contains information to be considered.

The main components of the organic mixtures extracted from air particulate matter are homologues C_{17}–C_{36} n-A. They exhibit a typical concentration pattern and are easily recognized on the time scale, owing to their regular distribution. They are also present when the air quality is good, because they can be produced also from natural sources. The homologues having less than seventeen carbon atoms are probably also present, but owing to the long sampling periods they were preferentially lost during sampling.

The final part of the chromatogram is also poorly significant, owing to high bleeding and poor efficiency of the column at high temperatures. A few large peaks were easily recognized in all the chromatograms as contaminants introduced by the plastics of the vessels. In fact they were also present in the solvent blank and were identified by GS–MS as phthalate esters. They were deleted from the profile before the quantification into variables.

Figure 1 shows the profiles of three samples collected in different seasons: differences in shape and amount are present. The study was then focused on the central part of the retention time axis, discarding the beginning (before C_{20}) and the end (after C_{33}) of the chomatograms.

For quantification purposes, usually the heights or areas of several selected peaks are considered as variables. When, as here, overlapping peaks are present and it is desired to by-pass peak resolution and identification in order to have a rapid overview of the samples, it is useful to obtain a decreased number of variables from the total profile areas, as has already been done [15,16] by the maximum entropy method, avoiding subjective variable selection.

According to the procedure developed in this paper, suitable for air particulate samples, the profiles are submitted to a three-step treatment involving synchronization, partition into upper (resolved) and lower (unresolved) profiles and subdivision of the two parts into variables.

Synchronization was verified by displaying the profiles together with one out of the 47 chosen as references; when necessary, the synchronization was made perfect by referring to the peaks of homologous *n*-alkanes.

Partition was carried out by a simple algorithm for baseline correction [17]; the resolved peak part and unresolved complex mixture part are shown in Fig. 2.

For subdivision into variables, from the upper part 100 variables were obtained by dividing the retention time axis (from C_{20} to C_{33}) into 100 equal intervals and computing the area of the peaks within each interval. Then, dividing the retention time axis into fifteen intervals and computing the area of the unresolved lower part, fifteen values were obtained. The number of variables obtained by the subdivision could be changed; the results did not vary substantially provided that the number of variables was greater than 50 in the resolved part and 10 in the unresolved part.

Regarding the GC–FID profile, each of the 47 samples is now described by 115 quantitative variables. Hence a data matrix with 47 rows and 115 columns was obtained that was submitted to chemometric analysis, which was done entirely with the package Parvus [18], the latest edition of which includes partial least squares (PLS), among other multivariate regression methods.

Pretreatments

Each row vector was normalized with respect to the extract concentration and particulate weight, in such a way the quality of suspended particulate was studied rather than air quality.

The variable distributions were inspected by histograms; they were all positively skewed (as commonly happens with chromatographic data), then a logarithmic transformation was applied and data more centrally distributed were obtained.

Subsequently, the data were centred, subtracting the column averages, and block-wise scaled so that the total variance was the same within each of the two groups of 100 and 15 variables. The block-wise scaling was achieved dividing the data by the variable standard deviation multiplied by the square root of the number of variables in the block.

The variance–covariance matrix was computed; several pairs of variables showed the highest correlation ($r > 0.8$) and indeed, redundant information is usually retained in profiles from

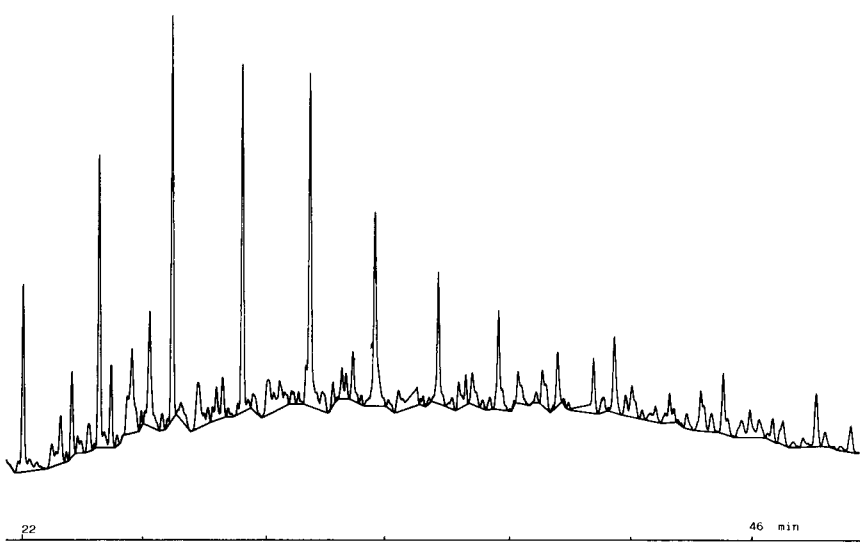

Fig. 2. Gas chromatogram of the sample collected on 17th December 1987. The resolved and the unresolved part are separated by a baseline. The resolved part was quantified into 100 variables and the unresolved lower part into 15 variables.

complex samples. On the other hand, as a small number of phenomena influence the variations in these profiles, this means that a few latent variables, related to environmental phenomena, can explain these variations.

Principal component analysis is a powerful tool to reduce dimensionality, retaining only the useful information.

Principal component analysis

The eigenvectors of the variance–covariance matrix were computed; 115 eigenvectors were computed from the 115 variables. By the double cross-validation method [19], the first six were found to be significant, retaining 91% of the total variance. The remaining 109 eigenvectors held minor information or noise; they were discarded and the dimensionality was reduced to the six uncorrelated new variables, the first of which were used to give a display of the data matrix. Plotting the objects in the plane of the first two components (eigenvectors), 79% of the total variance is displayed (Fig. 3; the samples are represented by their sampling season, i.e., the last digit of their names).

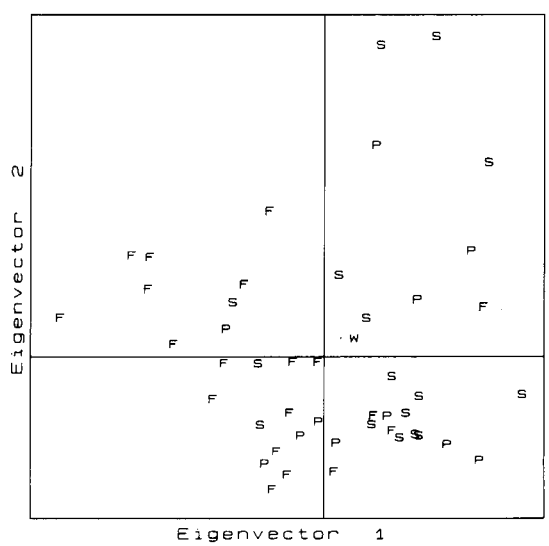

Fig. 3. The 47 samples are projected in the plane of eigenvector 1 and eigenvector 2. The objects are shown according to their sampling season: F (autumn), W (winter), P (spring) or S (summer). 79% of the variance is explained: 67% by the first and 12% by the second eigenvector.

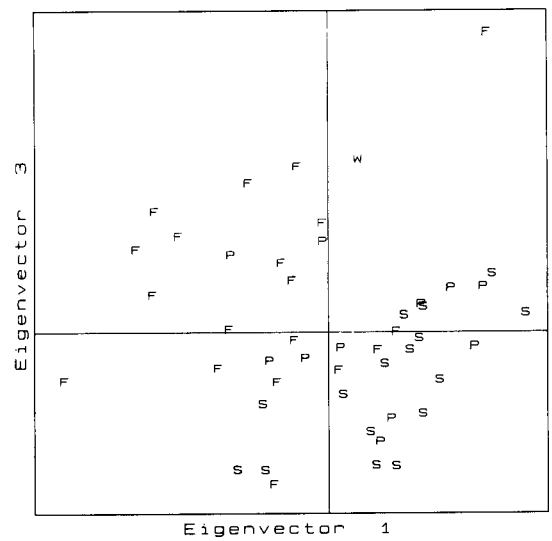

Fig. 4. The objects are projected in the plane of eigenvector 1 and eigenvector 3. The objects are shown according to their sampling season: F (autumn), W (winter), P (spring) or S (summer). 74% of the variance is explained: 67% by the first and 7% by the third eigenvector.

In the eigenvector 1–eigenvector 3 plane (Fig. 4), 74% of the total variance, a seasonal discrimination, is displayed. By plotting the eigenvector score of each sample against the sampling week (three years are simultaneously present, even though, unfortunately, no samples were collected in the first 8 weeks of the year), a time-dependent relationship for eigenvector 1 (Fig. 5) and eigenvector 3 (Fig. 6) seems to be present; the scores of eigenvector 2 did not show any time dependence. That could be related to the sampling temperature and procedure; in fact, the method of sample collection involved a simple filtration of the atmospheric particulates, without any collection of organic compounds present as vapour in the air or those which were lost from the filter during aspiration.

Indeed, the ratio between organic compounds in the particulate phase, collected on the filter, and those in vapour phase, collected on adsorption resins or other suitable sampling devices, is dependent on the sampling temperature. The proportion of organic compounds in the vapour phase increases with increase in temperature and sampling period and, during spring and summer,

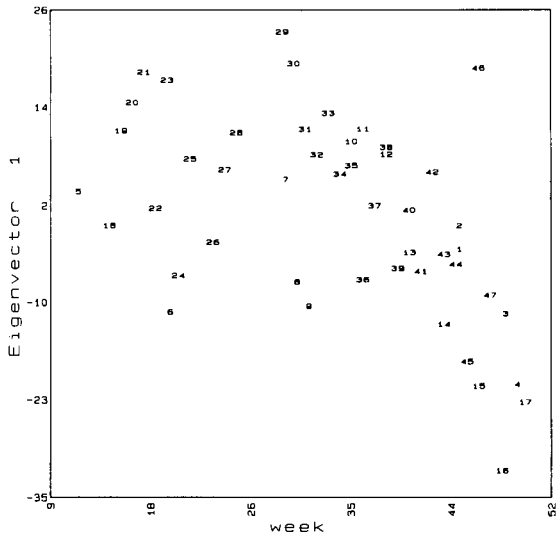

Fig. 5. The scores of the objects on eigenvector 1 are reported versus the number of the week (from the beginning of the year) in which they were collected. They are shown according to their indices in the first column in Table 1.

the measurement accuracy and precision for the organic compounds in the particulate phase are strongly reduced. This dependence should be made more evident and better defined by sampling simultaneously both particulate and vapour phases.

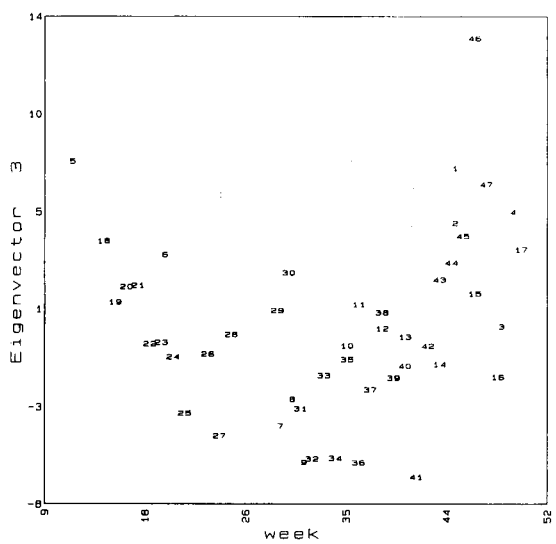

Fig. 6. The scores of the objects on eigenvector 3 are reported versus the number of the week (from the beginning of the year) in which they were collected. They are shown according to their indices in the first column in Table 1.

Clustering

To evaluate the overall significant information held by the first six eigenvectors, a cluster analysis was done. By the average linkage unweighted criterion of clustering [20], applied to the euclidean distances among the samples in the space of the scores of the first six eigenvectors, the similarities of samples were computed and are represented by the dendrogram in Fig. 7, where the samples are represented by their names (Table 1).

At similarity level 0.6 two clusters of 25 and 21 objects and one singleton are present. The seasonal differentiation singled out by the first 3 eigenvector plot is confirmed: 18 out of the 25 samples in the first cluster (left in Fig. 7) are autumn or winter samples, whereas 16 out of the 21 in the second (right in Fig. 7) are spring or summer samples.

Prediction

The unsupervised pattern recognition methods of principal component analysis and clustering

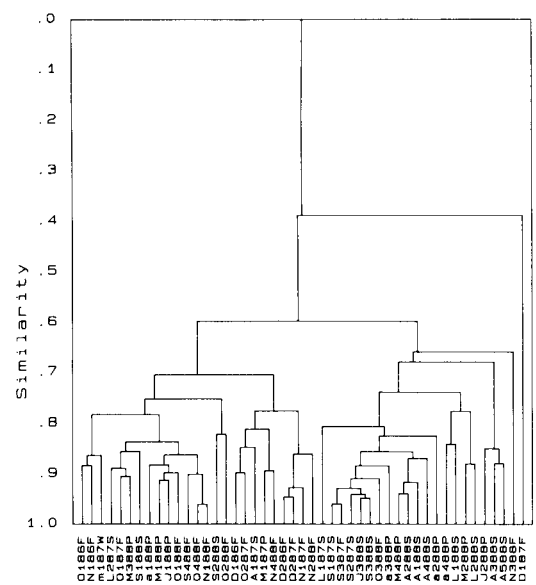

Fig. 7. Dendrogram of similarities among samples. Clustering method of average linkage applied to the scores of the first six significant eigenvectors. Samples are reported according to their names in the second column in Table 1.

were applied to understand the complex multi-dimensional profiles, searching for recognizable patterns; a seasonal differentiation was shown. Subsequently a multivariate regression study was carried out to determine the predictive relationships between the blocks of variables in which the FID profile had been quantified and the chemical analysis results on the same samples. The PLS method for multivariate linear regression [21] was applied, searching for the prediction (by the "leave-one-out" procedure) of the EOM, CPI (computed from *n*-alkane peaks measured by GC–MS) and mutagenicity of the samples.

EOM and FID profile. PLS was used to verify whether linear relationships were present between the dependent variable EOM and the block of independent variables (115 variables from the FID profile, or only the 100 variables from the resolved upper part). The relationship between measured, "found", EOM and the predicted value from the 115 variables obtained from the FID profile, when a three-component PLS model is used, explains 80% of predicted variance. In addition, in the relationship between measured EOM values and the predicted values from the upper resolved part of the FID profile (100 variables, Fig. 8), 81% of the variance is explained in the prediction procedure by the three-component PLS model. This means that the variables derived from the unresolved part do not add information related to the EOM determinations.

It can be concluded that the EOM values are predictable by the FID profile information; this means that most of the organic extractable material may be determined by GC–FID.

CPI and FID profile. First, it is emphasized that the CPI is not a directly measured value, but a ratio among groups of original variables (*n*-alkane peaks) accurately measured by GC–MS or GC–FID. The relationship between the GC–MS ratio (response) and the FID profile was studied by PLS.

In Fig. 9 the relationship between the found CPI values and the values predicted by PLS is shown; when the first four components, computed from the 100 variables of the resolved part of the FID profiles, and the leave-one-out procedure of cross-validation were used, the variance

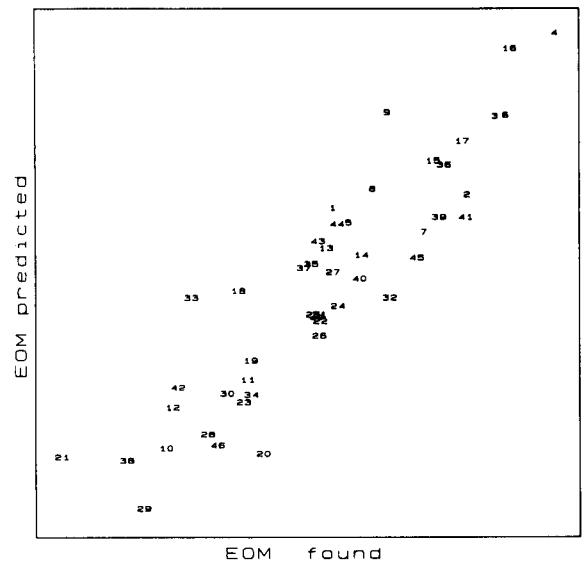

Fig. 8. EOM (extractable organic material) of the samples predicted by the PLS method plotted against the EOM measured by the microgravimetric method. The first three PLS components explain the 81% of the predicted variance. The samples are shown according to their indices in the first column of Table 1.

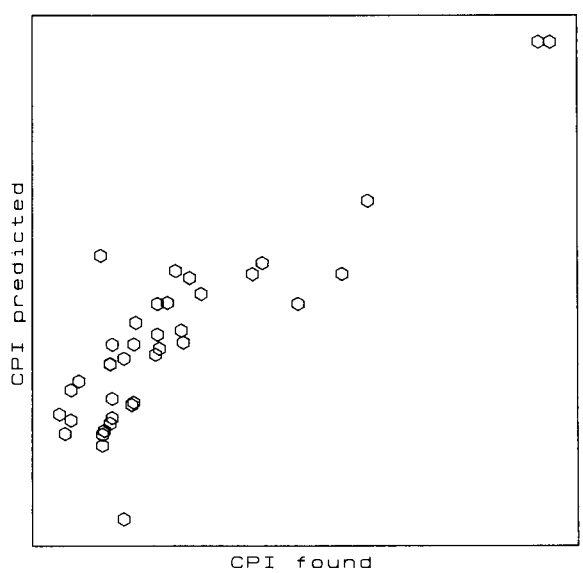

Fig. 9. CPI (carbon preference index) of the samples predicted by the PLS method plotted versus the CPI values computed from the *n*-alkane peaks measured by GC–MS. 77% of the variance is explained.

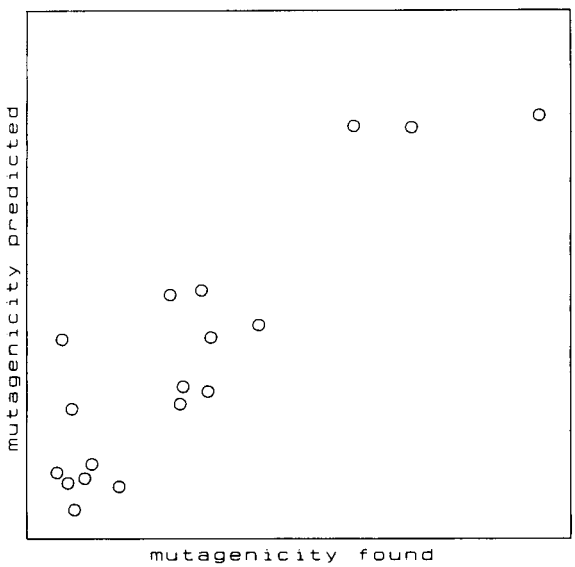

Fig. 10. Mutagenicity found versus mutagenicity predicted (TA100) by the first two PLS components. 68% of the predicted variance is explained.

explained in the prediction relationship was 77%. It remained almost the same (78%, four components), when the 115 variables were the predictors. It can be stated that the information on the CPI accurately computed from GC–MS data is predictable by the information contained in the FID profile.

Mutagenicity and FID profile. Only eighteen samples were tested for mutagenicity. In spite of the small number of objects and the large number of predictor variables, owing to the basic characteristic of PLS, i.e., the compression of information into a few components, it was possible to study the prediction of mutagenicity by using PLS with the leave-one-out procedure of cross-validation.

The best prediction of the mutagenicity was found between TA100 (without S9) and the PLS components of the 100 variables derived from the upper resolved part of the FID profile. In Fig. 10 a linear relationship between the found and predicted mutagenicity of the eighteen samples is shown; it was produced by the first two PLS components and explains 68% of the total variance, whereas the unresolved part of the FID profile had a low linear relationship with mutagenicity at best explaining 41% of the total variance in the prediction of TA100 (without S9) by the first PLS component.

As expected, strong linear relationships were found between the FID profile and the other measured variables (*n*-alkane peaks, UCM, RCM), as they are measured on the FID profile itself.

Conclusions

The methodological approach described in this paper can be used also for different kinds of complex matrices in order to evaluate the similarities of chromatographic fingerprints produced under the same experimental conditions. The method is applicable provided that a homologous series of compounds, sufficiently far apart on the time scale and easily recognizable, may be found in all the samples to allow synchronization.

The unsupervised pattern recognition of the information extracted by this procedure from the FID profiles increases the knowledge of the samples before they are submitted to further qualitative and quantitative analyses.

The total extractable organic matter and the carbon preference indices of the samples can be predicted by the information extracted from the FID profile by this procedure, avoiding microgravimetric determinations and GC analyses of individual *n*-alkanes to calculate the CPI.

In the same way, the mutagenicity of the air particulate can also be predicted, giving an immediate measure of toxicity.

This work received financial support from the Education Department (MPI 40% and 60%).

REFERENCES

1 E. Kováts, Adv. Chromatogr., 1 (1965) 229.
2 W. Cantrels and K. Van Canwenberghe, Water Air Soil Pollution, 6 (1976) 103.
3 B.R.T. Simoneit and M.A. Mazurek, Atmos. Environ., 16 (1982) 2139.
4 K. Kawamura and I.R. Kaplan, Atmos. Environ., 20 (1986) 115.
5 F.J. Knorr and J.H. Futrell, Anal. Chem., 51 (1979) 1236.

6 P. Gillette, J.B. Lando and J.L. Koenig, Anal. Chem., 55 (1983) 630.
7 R.E. Lea, R.B. Bramston-Cook and J. Tschida, Anal. Chem., 55 (1983) 626.
8 O.M. Kvalheim, D.W. Aksnes, T. Brekke, M.O. Eide and E. Sletten, Anal. Chem., 57 (1985) 2858.
9 O.M. Kvalheim, Chemometr. Intell. Lab. Syst., 4 (1988) 11.
10 T. Brekke, O.M. Kvalheim and E. Sletten, Chemometr. Intell. Lab. Syst., 7 (1989) 101.
11 T. Alsberg, S. Hakansson, M. Strandell and R. Westerholm, Chemometr. Intell. Lab. Syst., 7 (1989) 143.
12 A. Lafleur, P.A. Monchamp, E.F. Plummer and E.L. Kruzel, Anal. Lett., 19 (1986) 2103.
13 D.M. Maron and B.N. Ames, Mutat. Res., 113 (1983) 173.
14 K. Kawakamura and I.R. Kaplan, Environ. Sci. Technol., 17 (1983) 497.
15 T.V. Karstang and R.J. Eastgate, Chemometr. Intell. Lab. Syst., 2 (1987) 209.
16 A.A. Christy, R.A. Velapoldi, T.V. Karstang, O.M. Kvalheim, E. Sletten and N. Telnaes, Chemometr. Intell. Lab. Syst., 2 (1987) 199.
17 J. Zupan, Algorithms for Chemists, Wiley, New York, 1989, pp. 82–85.
18 M. Forina, R. Leardi, C. Armanino and S. Lanteri, PARVUS: an Extendable Package of Programs for Data Exploration, Classification and Correlation, Elsevier Scientific Software, Amsterdam, 1988.
19 S. Wold, Technometrics, 20 (1978) 397–406.
20 D.L. Massart and L. Kaufman, The Interpretation of Analytical Chemical Data by Use of Cluster Analysis, Wiley, New York, 1983, p. 90.
21 P. Geladi and B. Kowalsky, Anal. Chim. Acta, 185 (1986) 1.

Analytica Chimica Acta, 284 (1993) 91–105
Elsevier Science Publishers B.V., Amsterdam

Drift correction for pattern classification with neural networks

J.R.M. Smits, W.J. Melssen, M.W.J. Derksen [1] and G. Kateman

Laboratory for Analytical Chemistry, Faculty of Science, Catholic University of Nijmegen, Toernooiveld 1, 6525 ED Nijmegen (Netherlands)

(Received 3rd May 1993)

Abstract

A neural network may be used as a pattern classifier to assign objects, which are characterized by different variables, to certain classes (J.R.M. Smits et al., Chemom. Intell. Lab. Syst., in press). One of the problems that might be encountered with pattern classification is instrumental drift. Drift may cause the neural network to misclassify the objects, if the clusters of the different classes lie relatively close to each other. Therefore it is necessary to calibrate the analytical instrument that is used to measure the variables. However, calibration of an instrument is not always straightforward. Correction of the measurements for drift would make it permissible to calibrate less often. In this paper the effects of different drift correction strategies are studied. Simulated data sets are used, with different amounts of drift of a non-linear nature. A multi-layer feed-forward neural network is used to classify the simulated objects. The performance of the neural network is determined for three situations: no drift correction, correction for the drift by subtracting it, and correction for the drift by using the amount of drift as an extra input variable for the neural network. For the type of non-linear drift used in this study, the last drift correction strategy appears to give the best results.

Keywords: Chemometrics; Drift correction; Neural networks; Pattern classification

In pattern classification problems, a decision has to be made to which class an object belongs, based on certain measured characteristics of that specific object. Multi-layer feed-forward (MLF) neural networks [1,2] may be applied as pattern classifiers [3,4].

One of the problems that might be encountered with pattern classification is instrumental drift, i.e., the change of a variable value in time, due to instrumental changes. Each object is characterized by a set of variable values. These variables are measured with analytical instruments, and these instruments may cause slight changes of the variable values in time, due to different and often uncontrollable causes, like aging, wear, temperature, humidity, etc. The pattern classifier is usually trained on data which do not show drift. If the classifier is used for real measurements and the deviations in these measured variables become too large, the pattern classifier is no longer able to predict the correct class. Therefore the instruments will have to be calibrated from time to time with calibration samples, i.e., samples of which the characteristics are known. Often the following calibration procedure is applied: a calibration sample is measured at set times, in between the measurements of the real samples. If the values for the calibration sample measured by the instrument differ from the known

Correspondence to: J.R.M. Smits, Laboratory for Analytical Chemistry, Faculty of Science, Catholic University of Nijmegen, Toernooiveld 1, 6525 ED Nijmegen (Netherlands).
[1] Present address: Organon International, P.O. Box 20, 5340 BH Oss (Netherlands).

0003-2670/93/$06.00 © 1993 – Elsevier Science Publishers B.V. All rights reserved

values, a certain amount of drift is present. If the deviations are too large, one may choose between

(i) calibrating the instrument, i.e., adjusting or tuning the instrument in such a way that the correct values for the calibration samples are obtained;

(ii) compensation for the drift by correcting the measurements of the real samples with the amount of drift found for the calibration sample.

The choice when to measure calibration samples is a compromise between efficiency and costs on one hand, and reliability on the other hand. If it is complicated or a lot of effort to calibrate the instrument, but relatively easy to just measure one or more calibration samples from time to time, correcting for the drift is worthwhile: if it is possible to compensate for drift, it will no longer be necessary to calibrate the instrument very often to obtain reliable values.

Different strategies are possible for drift correction, but usually these strategies are based on the assumption that the drift of a variable is uniform or depends only on the value of the specific variable. However, drift may be of a somewhat more complex nature: drift in one variable may depend on the value of other variables too. Most papers issueing drift correction procedures deal with *calibration* instead of *classification* problems, and usually the drift that is addressed is relatively simple. One of the methods that may be used to predict and compensate for drift is the Kalman filter [5,6]. In this paper an alternative approach for drift correction is proposed.

A neural network used for pattern classification defines boundaries between two ore more neighboring clusters. Based on these boundaries the neural network decides to which cluster a particular object belongs. However, drift causes the clusters to shift, and if the drift is such that the clusters move in time across these boundaries, the neural network will misclassify objects. This is more likely to happen if the clusters are lying relatively close to each other. One may compensate for drift by means of correction of the measurements, or by means of correction of the decision boundaries. In effect, these two approaches are equal.

An analytical instrument which may exhibit a relatively complex form of drift is a flow cytometer. A special type of flow cytometer has been developed for the measuring of algae in surface waters [7,8]. This flow cytometer is able to detect automatically algal particles in water. It measures a set of variables for each particle individually, which characterizes the specific particle. Analysis of these data shows a clustering of the different algal species in the multi-dimensional space spanned by the variables (variable space) [3]. However, some of the clusters tend to show considerable overlap and posses irregular shapes.

The data of a flow cytometer may be interpreted by using a neural network [3,9,10]. In such studies, measurements from a calibrated instrument are taken. However, a flow cytometer is an optical system, and measurements performed with it may show drift, often of a non-linear nature. This makes it necessary to calibrate the flow cytometer from time to time. However, the calibration is not straightforward, while on the contrary the measurement of a calibration sample is relatively easy. Calibration samples provide an indication of the drift the measurements exhibit in the different variables. If the measurements for the real samples made with the flow cytometer could be corrected for drift, it will be possible to use the flow cytometer without having to calibrate it often.

If calibration of the instrument is not performed often, drift causes the clusters to overlap. In this paper, different types of drift and some correction strategies are described. A possible drift correction procedure is a mathematical correction, like subtraction of the amount of drift from the measurements. This might reduce the overlap between the clusters, but for specific types of drift the problem will not be solved entirely. Therefore, an alternative approach is proposed: the amount of drift incorporated in a variable value, is derived from the measurement of a calibration sample, and added as an extra variable. This may be done for every variable that is subject to drift, i.e., per variable an extra variable may be added. Such an additional variable increases the dimension of the variable space, and this enables a separation of the clusters. How-

ever, the decision boundary that is created in this way between the clusters will, in general, be a non-linear one. For this reason, a non-linear pattern classification method has to be applied, like an MLF neural network.

To investigate the effect of the latter drift correction procedure, three experiments are carried out. Several data sets (containing two clusters of objects) are generated, in which different amounts of a specific type of non-linear drift are incorporated. This classification problem is tackled according to different correction strategies. In the first experiment, no drift correction is applied. In the second one, the amount of drift is subtracted, a procedure which is applied often. In the third experiment the amount of drift is not subtracted, but it is used as an additional variable to describe the objects with. Since non-linear decision boundaries are expected, a multi-layer feed-forward neural network is applied for object classification.

THEORY

Neural networks

Nowadays, MLF neural networks are the most popular neural networks. They are applied for a wide variety of problems, e.g., classification problems [4].

Network structure and signal propagation. An MLF network consists of three or more layers of units: one input layer, one output layer and one or more intermediate (hidden) layers. A unit in one layer is connected to all units in the next layer (feed-forward). In Fig. 1 a possible network structure is shown.

A unit receives and/or sends signals from and to other units or the outside world via the network connections. Each signal is weighted by a weight factor that is associated with a connection. The input of a unit is determined by the incoming (weighted) signals, the output of the unit is a function of the input. Often a sigmoid transfer function is chosen.

Training the network. Adequate functioning of a neural network is highly dependent on the way the signals are propagated through the network. This signal propagation is determined by the weights of the connections. In general, however, a proper weight setting is not known beforehand and therefore initially the weights are given a random value. The process of updating the weights to a correct set of values is called training or learning.

A correct weight set usually is achieved by means of supervised learning. Often the back-propagation learning rule [1] is used. According to this learning rule, in e.g., a three-layer network first the weights from the hidden layer to the

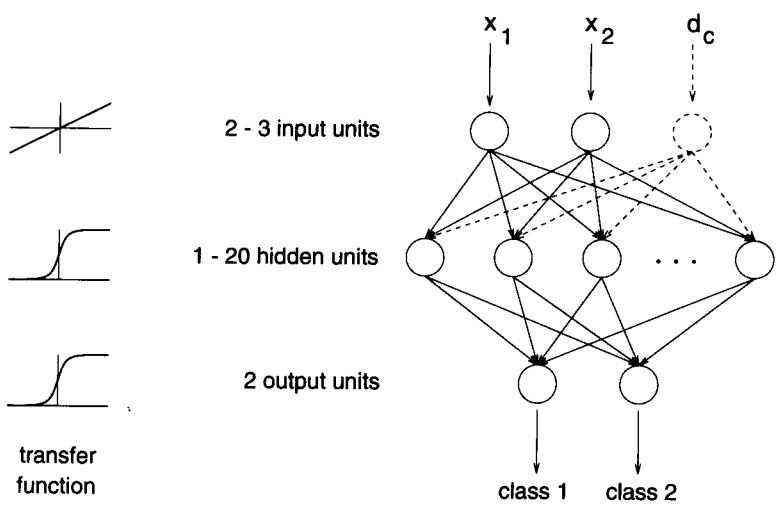

Fig. 1. Network structure as used in the experiments. The network shown on the right has one input layer, one hidden layer and one output layer. The transfer functions that are used per layer are shown on the left.

output layer are adapted, and next the weights from the input layer to the hidden layer. The weight adaptations are given by

$$\Delta w_{ji}(n+1) = \eta \delta_j o_i + \alpha \Delta w_{ji}(n) \quad (1)$$

in which Δw_{ji} denotes the adaptation of the weight from unit i to unit j in the next layer, o_i is the output of unit i, and η is the learning rate. To limit the danger of oscillations, a so-called momentum term α is invoked. If the layer is the output layer, the error correction term δ_j is a function of the transfer function used and the difference between desired and obtained output. For the hidden layer, δ_j is a function of the transfer function used and the weights and error correction terms of the output layer.

Testing the network. During and after training, the performance of the network has to be tested. This is done with a test set consisting of other examples, comparable to the set of examples that was used for training the network [4].

In the testing phase the input patterns are fed to the network, and the desired output patterns are compared with the output patterns produced by the neural network. The (dis)agreement of the two output pattern sets gives an indication of the performance of the network. When the performance meets the requirements specified in advance, the network is ready for real analysis purposes.

For more information on the theory and the use of MLF neural networks, the reader is referred to, e.g., Refs. 1 and 4.

Pattern classification

A pattern classifier has to distinguish between different classes of objects. The variables with which the objects are characterized, have to be discriminative enough to make this distinction possible. If this is the case, objects belonging to different classes will form separable clusters in the variable space.

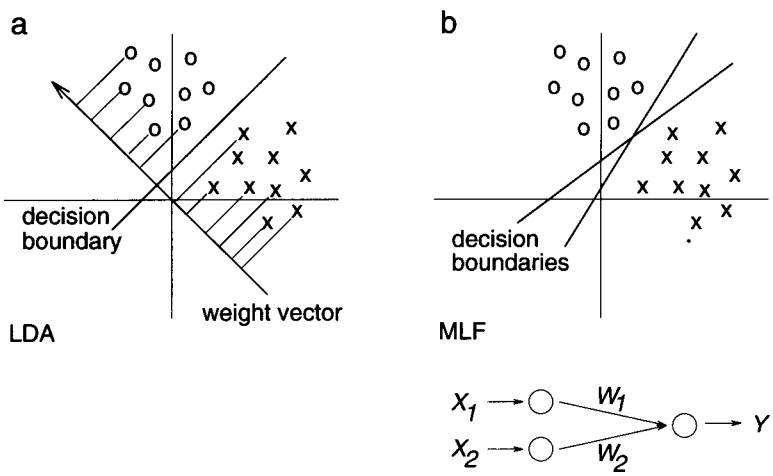

Fig. 2. A classification problem. (a) Division of the objects in two classes by LDA. Only one decision boundary is found. (b) Division of the objects in two classes by an MLF network. A possible network structure is shown in addition. The two input units are flow-through units, the transfer function of the output unit is a threshold function. The net input for the output unit is given by $net = w_1 x_1 + w_2 x_2$. The output of the output unit, y, is given by

$$y = \mathrm{f}(net) = \begin{cases} 1 & \text{if } net \geq t \\ 0 & \text{if } net < t \end{cases}$$

in which t denotes the threshold. The value of y indicates to which class (represented by '0' and '1') the object belongs. The equation for the decision boundary is given by $w_1 x_1 + w_2 x_2 = t$. Two possible decision boundaries are drawn that are equally probable regarding the criterion of the network. With the network shown, only linear separable clusters may be separated. If the decision boundaries are curved lines, a more complex network structure has to be used.

A pattern classifier that is trained supervised, e.g., a neural network, is given a training set with examples. Based on these examples, the pattern classifier defines decision boundaries in the variable space, which separate the different clusters from each other. If an unknown object is presented to the pattern classifier, the classifier will assign this object to a specific class. This decision is based on the position of this object in the variable space with respect to the decision boundaries. Various pattern classifiers are based on this principle, e.g., linear discriminant analysis (LDA, [11]) and MLF neural networks.

If, in a two-dimensional space, the decision boundaries that separate the clusters are straight lines, the clusters are said to be linearly separable. Analogous, for three or more dimensions the decision boundaries will then be (hyper)planes. In such cases, LDA may be applied to classify the objects. An example of a classification problem is shown in Fig. 2. In LDA, the objects are all projected on a weight vector (Fig. 2a). The direction of the weight vector is chosen in such way that the within-class variance of the projected objects is minimized, whilst the between-class variance is maximized. The decision boundary is defined to be perpendicular to this weight vector.

An MLF network also defines a decision boundary to separate the classes, but in a different way. The neural network tries to find the decision boundary for which the network error is minimal. The obtained decision boundary is determined by the weights. During the training phase these weights are adapted, and different decision boundaries may result from different initial weight settings (Fig. 2b). LDA is a parametric technique, based on the assumption that the distribution of the different classes is more or

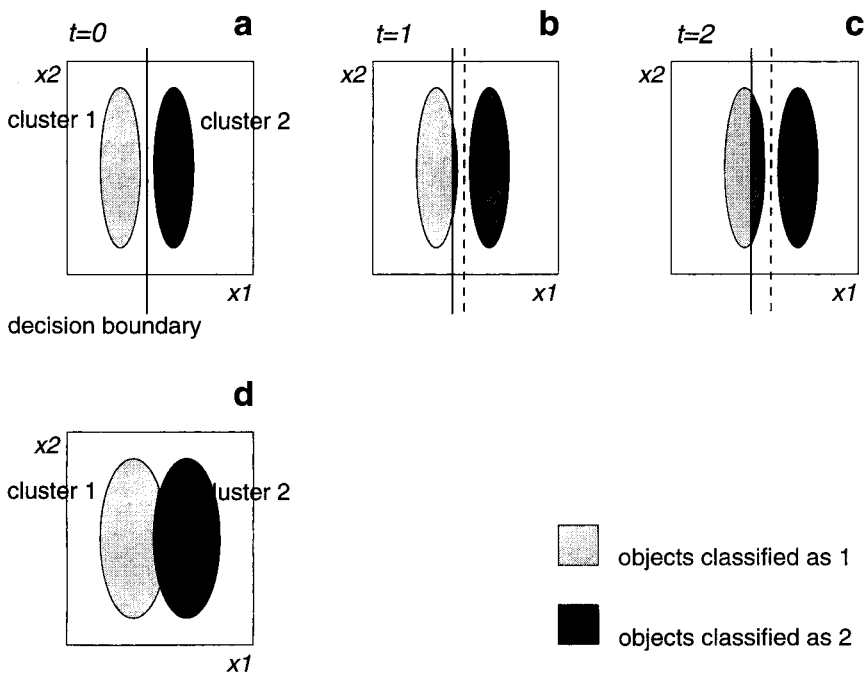

Fig. 3. The effect of drift on the classification. (a), (b) and (c) give the position of two clusters at time $t = 0$, $t = 1$ and $t = 2$, respectively. The clusters show drift in variable x_1. If the data set without drift, shown in (a), is used for training a neural network, a decision boundary as shown may result. If the network is now used to classify the objects of (b) or (c), measured at time $t = 1$ or $t = 2$, respectively, part of cluster 1 will be classified as 2. It is seen that, due to the drift, the clusters cross the decision boundary the network has built based on the data shown in (a). The dotted lines show the decision boundaries as they should be positioned for the specific data sets to achieve a good classification. Back-translation of the clusters to (a) solves the problem. (d) If data measured on different points in time [like in (a), (b) and (c)] are merged, the clusters may overlap (black region).

less the same. It is relatively sensitive to outliers. If the conditions are not ideal, or the problem is not linearly separable, MLF networks usually will perform better.

Drift

An MLF neural network is trained in a supervised way. In case of supervised learning, a training set has to be selected to train the network. If such a training set contains only measurements in which no or only a small amount of drift is incorporated, the neural network may only be used for classifying objects which also show no or only a small amount of drift. This drift makes a lot of calibration in between measurements necessary, to ensure working in the data domain the network is trained for.

No calibration. If the instrument is not calibrated often, the performance of the pattern classifier might decrease (Fig. 3a–c). To prevent the clusters from crossing the decision boundaries, the training set can be composed of measurements performed on different points in time, i.e., with different amounts of drift incorporated. In this way one has to calibrate less often, but in effect the clusters are spread out. The resulting training set will contain larger clusters, which may even overlap partially (Fig. 3d). If these clusters are used to train the network, it will not be able to define a good decision boundary and the overlap will result in a decreasing performance.

Types of drift. Drift can be incorporated in every variable value. In the sequel, only drift

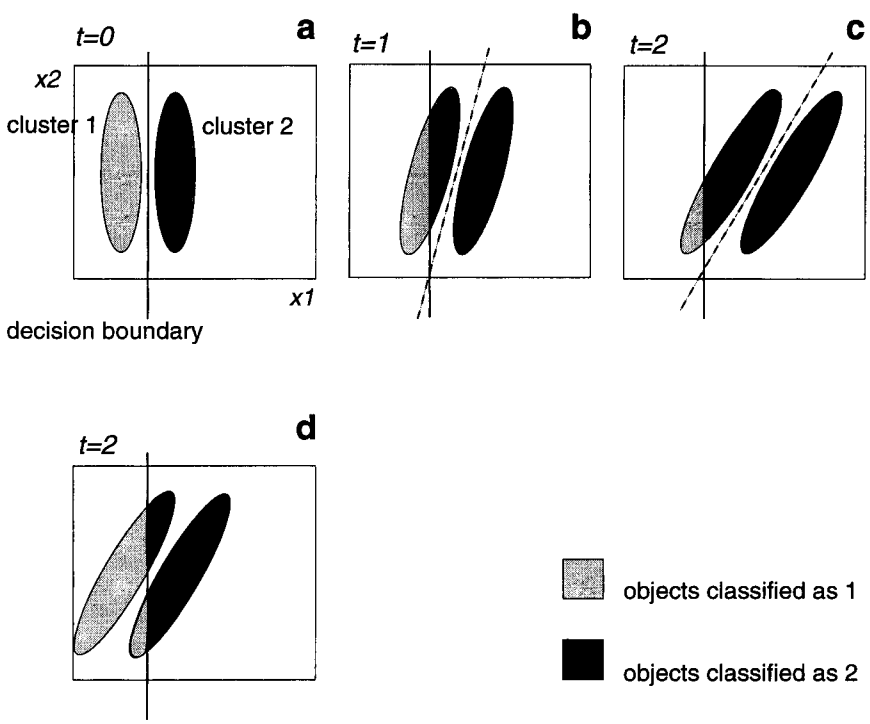

Fig. 4. The effect of complex drift on the classification. (a), (b) and (c) give the position of the two clusters at time $t = 0$, $t = 1$ and $t = 2$, respectively. The amount of drift incorporated in variable x_1 depends on the value of variable x_2. If the data set shown in (a) is used for training a neural network, a decision boundary as shown may result. If the network is now used to classify the objects of (b) or (c), part of cluster 1 again will be classified as 2. The dotted lines show the decision boundaries as they should be positioned for the specific data sets to perform a good classification. (d) Simple back-translation of the clusters of (c) does not solve the problem entirely.

incorporated in one variable value is considered. In case more variable values are subjected to drift an analogous approach may be taken.

Drift is a function of time. However, the aim of this paper is not to study the drift behavior as function of the time. The time is enclosed implicitly in the amount of drift. The following describes the behavior of drift as function of different variable values, measured at one specific point in time. Different types of drift are possible:

(1) The drift is uniform, i.e., the amount of drift incorporated in a variable value is the same for all measurements, over the entire range of this variable. Such a type of drift results in a translation of the clusters in the variable space (like in Fig. 3a–c). The relative positions of the clusters are retained, and the decision boundaries between the clusters are translated. In a two-dimensional case (variables x_1 and x_2) the drift in x_1 may be expressed as

$$d_{x_1} = C$$

where C is a constant.

(2) The amount of drift incorporated in a variable value depends on the value of this variable. For different measurements, which are distributed over the domain of the specific variable, the amount of drift may differ considerably. This dependency may be linear as well as non-linear. This type of drift will not only result in a translation of the clusters, but the clusters (and, accordingly, the space in between) may also be changed in shape. Data points may be pulled apart or pushed together, but, again, the decision boundaries are just translated. In a two-dimensional case the drift in x_1 may be expressed as

$$d_{x_1} = \mathrm{f}(x_1)$$

(3) The amount of drift incorporated in a variable value depends not only on the value of the specific variable, but also on the value of another variable. This results in a change in *orientation* of the clusters and, hence, the decision boundaries (like in Fig. 4a–c). In a two-dimensional case the drift in x_1 may be expressed as

$$d_{x_1} = \mathrm{f}(x_1, x_2)$$

Drift correction. To be able to correct for drift, the drift has to be described first. A calibration sample is measured from time to time, and the difference between the measured and the known variable value for the calibration sample is an indication of the amount of drift incorporated in the specific variable value at that point in the variable domain. A measurement of a calibration sample may include multiple measurements (e.g., in duplo) measured at one point. In such cases, the mean value is taken.

If the drift in a variable is known to be more or less uniform over the entire domain of this variable (the first type of drift listed above, $d_{x_1} = C$), characterization of the drift is easy: the measurement of only one calibration sample, positioned anywhere in the domain of the variable, is sufficient to enable a description of the drift. Due to this (uniform) drift, the clusters are shifted, and the decision boundaries between the clusters are shifted along with the clusters. Correction of the drift is possible by subtracting the amount of drift in a variable from the variable value of the real measurements. This is in fact analogous to a simple back-translation of the clusters with their decision boundaries.

If the drift is not uniform, but dependent on the variable value (second type of drift listed above), subtraction of the amount of drift measured at only one variable value will to some extent still solve the problem, provided the amount of drift only changes a little as function of the variable value $[d_{x_1} = \mathrm{f}(x_1) \approx C]$. If this correction is not sufficient, measurement of more calibration samples, at different positions in the variable domain, might be necessary to get a better description of the drift. For example, if this drift is known to be linear, i.e. the change of the amount of drift as function of the variable value is constant $[d_{x_1} = \mathrm{f}(x_1) = Cx_1]$, measurement of two calibration samples, positioned at different points in the domain of the specific variable, will be enough to describe the drift entirely. If the drift is of a non-linear nature, three or more calibration samples, distributed over the entire variable domain, have to be measured to describe the drift. The amount of drift to be subtracted may in both cases be determined by means of interpolation of the calibration sample measurements.

If the drift in one variable depends on the value of another variable [third type of drift listed above, $d_{x_1} = f(x_1, x_2)$], even more measurements of calibration samples, distributed over the domains of both variables, will be necessary to get a description of the drift. A simple back-translation (subtraction of the amount of drift), based on only one or a few calibration samples will no longer be sufficient to correct for the drift, as is depicted in Fig. 4d.

Summarizing, it appears to be possible to correct for the drift by subtracting the amount of drift, which is derived from calibration sample measurements, from the variable value of a real measurement. To get a good correction for non-linear types of drift, the drift has to be described in detail. If this is not the case, subtraction will not entirely solve the problem: the clusters may still overlap partially, due to the drift. Depending on the type of drift and knowledge about which types may be manifest, characterization of the drift may involve measurements of a lot of calibration samples. The more complex the function f, the more calibration samples have to be measured at different points in the variable space to obtain a detailed description of the drift. It would be desirable, however, to perform drift correction based on as few measurements as possible.

An alternative approach to correct for drift is addition of the amount of drift as an extra characteristic of the object. This increases the dimensionality of the variable space, and the clusters are less likely to overlap if drift occurs. In this case the drift does not have to be described in full detail: even a rough indication of the amount of drift may be enough to solve the problem. This means that less knowledge has to be available on the type of drift, and less measurements of calibration samples are necessary. In this paper, the effect of this correction procedure is determined and compared with the effect of subtraction of the drift, for data sets subject to the third type of drift described above.

MATERIALS AND METHODS

Data set

As was already stated, classification problems originating from drift occur only if the clusters in the data are lying close together. In the simulated data set used in this study the clusters border on

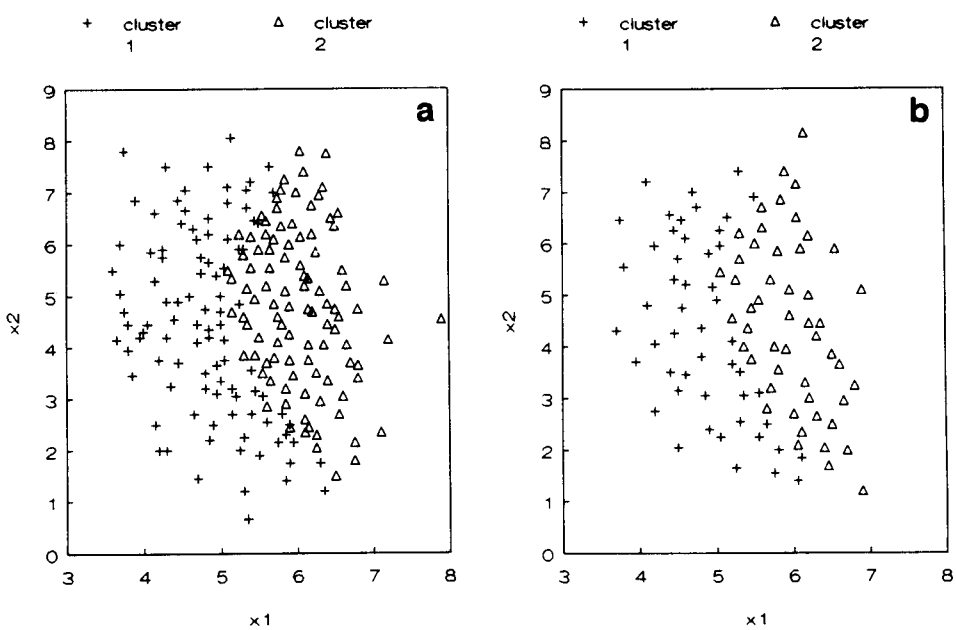

Fig. 5. The simulated basic data set, set A. (a) The training set. (b) The test set. The clusters are not linearly separable.

TABLE 1

Composition of the different data sets

Data set	t (Eqn. 2)	No. of examples	
		Training set	Test set
A	0	200	100
B	0 and 1	400	200
C	0, 1 and 2	600	300
D	0, 1, 2 and 3	800	400
E	0, 1, 2, 3 and 4	1000	500
F	0, 1, 2, 3, 4 and 5	1200	600

each other closely to emphasize the effect of the different correction strategies on the performance of the neural network. The basic data set contains two clusters and is split in two sets: a training set and a test set. The objects are described by two variables: x_1 and x_2. The training set contains 200 examples (100 examples per cluster), the test set contains 100 examples (50 examples per cluster). In Fig. 5 both sets are shown.

Based on this basic data set (training set and test set, hereafter referred to as data set A) five other data sets (sets B to F) are generated, with different amounts of drift in one variable, x_1. This amount of drift depends on the value of the other variable, x_2. The new (drifted) variable x_1' is given by

$$x_1' = x_1 + 0.1tx_2 \quad (2)$$

in which t denotes symbolically an elapsed time period since the last calibration. Sets B to F are derived from set A according to Eqn. 2. In Table 1 the composition of the different data sets is summarized. These sets refer to different situations: data set A contains data points measured just after calibration of the instrument, i.e., without any drift incorporated ($t = 0$). Data set B also contains these data points, and, in addition, data points measured after some elapsed time period as well, i.e., a small amount of drift is incorporated ($t = 1$). Going from set C to F, the elapsed time period since the last calibration increases. This leads to a spred of the clusters, like is shown in Fig. 3d. An example of how the data sets are composed is given in Fig. 6.

Only one calibration sample (positioned somewhere in the middle of the two clusters) is used in the experiments to correct for this non-linear type of drift.

Representations

For the representation of the input objects, input patterns consisting of the variables x_1 and x_2 are used. In accordance with this particular object representation, the input layer of the neural network consist of two input units. In case the drift in the variable x_1 is given as extra variable, an additional input is necessary and in that case three input units are used. The input values are autoscaled per variable according to

$$x_s = \frac{x_u - \bar{x}}{\sigma_x} \quad (3)$$

in which x_s is the scaled value, x_u is the unscaled value, $\bar{x}$ and σ_x are the mean and standard

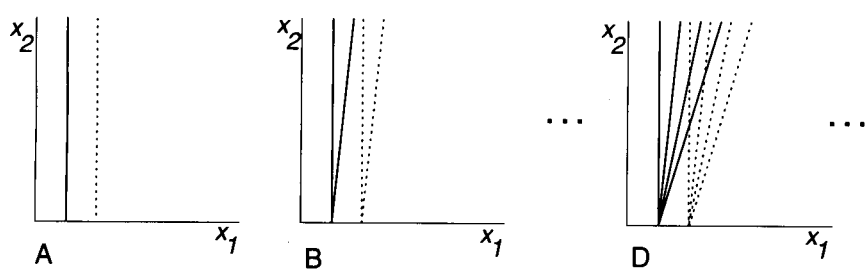

Fig. 6. Schematical composition of different data sets. Since the drift in variable x_1 depends only on the value of variable x_2, every data set is represented symbolically with only x_2 values, i.e., each cluster is shown as a straight line. Data sets A, B and D are shown schematically. As is seen, e.g., in set D, every cluster is a fan of measurements measured at different times t. The more different times are included (i.e., the longer the calibration of an instrument is postponed), the more the two clusters overlap. ———, Cluster 1; - - - - - -, cluster 2.

deviation, respectively, of all values for the specific variable.

In case of classification, for the representation of the class to which the input object belongs (the output) often a sequence of binary values (0 and 1) is taken. Every class is represented by one value and associated with one unit. In this study an output of (1 0) represents the first class, and (0 1) represents the second class.

Neural networks

The MLF neural network used in this study (Fig. 1) has two or three input units, depending on the drift correction strategy followed, and two output units, equal to the number of classes. The number of hidden units is varied between one and twenty, in order to monitor the performance of the network as function of the number of hidden units.

The learning rate η and momentum term α (Eqn. 1) are set to 0.4 and 0.2, respectively. The transfer function of the input layer is given by $f(x) = x$, hence the input units operate as flow-through units. For the hidden layer and the output layer the output o_j of unit j is a sigmoid function of the input net_j to unit j, and is given by

$$o_j = f(net_j) = \frac{1}{1 + e^{-(net_j + \theta_j)}} \quad (4)$$

in which θ_j is a bias term which influences the horizontal offset of the sigmoid, and net_j is given by

$$net_j = \sum_i w_{ji} o_i \quad (5)$$

In this equation i refers to the units in the previous layer, w_{ji} is the weight from unit i to unit j, and o_i indicates the output of unit i. Obviously, the outputs of both the hidden units and the output units range from 0 to 1.

During every iteration first a training set is presented to train the network, and subsequently a test set is presented to enable monitoring of the generalization capabilities of the network. The optimal number of iterations appears to depend on the specific problem, but, in general, after some 30 iterations most of the runs show a satisfactory degree of convergence. Overtraining, i.e., an increasing test error in combination with a decreasing training error, has not been encountered during the experiments.

The experiments have been performed on a Sun Sparc workstation with the software package ANNET (Artificial Neural Network Experimentation Toolbox, Lab. for Analytical Chemistry, University of Nijmegen).

Interpretation of the output

The network output values are used to indicate to which class the input pattern belongs to. However, the output unit values usually are not exactly equal to 0 or 1, but take a value somewhere in between. Moreover, since an input pattern is defined to belong to only one class, only one output is expected to be high. Therefore, an interpretation criterion has to be defined which determines to which class a given input pattern belongs to.

In this study different classification criteria were tried, and, finally, the following criterion was used in the experiments: the pattern is said to belong to the class associated with the unit with the highest value. This simple 'one-highest' criterion gave good overall results.

The performance of the networks is expressed in a percentage: the number of correct classifications divided by the total number of examples in the presented set, times 100%. If the presented set is a training set, this percentage is called the recognition performance; if the presented set is the test set, this percentage is called the prediction performance.

EXPERIMENTS AND RESULTS

First, the basic training and test set (set A) is used. Nine different network configurations, with 1, 2, 3, 4, 6, 8, 10, 15 or 20 hidden units, respectively, are each trained and tested with the sets of set A. For every network configuration the training and testing procedure was repeated six times, and each time a different initial (random) setting of the weights is used. The results of these runs are given in Fig. 7.

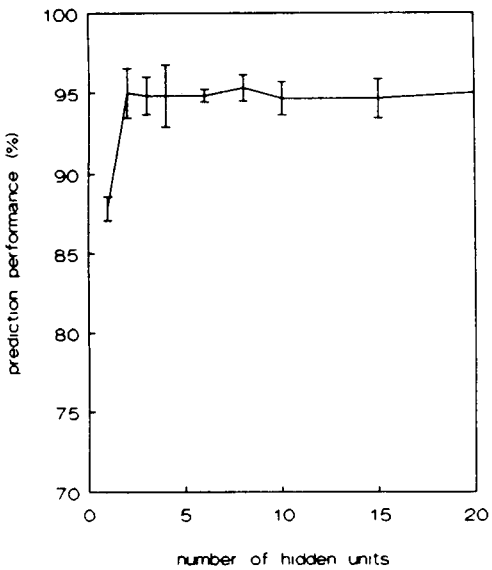

Fig. 7. Mean performance as function of the number of hidden units. For every network structure the mean prediction performance and the standard deviation of the six runs is given for the test set of set A. For the training set analogue results were found. One hidden unit appears not to be enough; for two or more hidden units the performance remains more or less constant.

For every drift correction strategy the same experiment is performed with each of the five 'drift' sets, B to F. For every experiment only results for the test set (prediction performance) are shown. For the training set (recognition performance) comparable results were observed.

No correction

In the first experiment, no correction for the drift is applied. For every drift set (B to F), again nine different network structures are each trained six times. The prediction performances for these uncorrected runs are given in Fig. 8b–f. It is seen that going from Fig. 7 and Fig. 8b–f the prediction performance decreases.

Due to the drift, the clusters show gradually more and more overlap going from set A to F (like in Fig. 3d). The prediction performance decreases considerably because the clusters are lying close to each other.

Subtracting the drift

In the second experiment, the applied drift correction strategy is subtraction of the drift. A calibration sample is defined, and the amount of drift found in variable x_1 for this sample is subtracted from the value of the variable x_1 of every data point. For specific instruments, like the flow cytometer, one calibration measurement is the measurement of a single sample, containing an entire cluster of calibration particles. In such a case the drift of the mean value of the cluster is taken. Since the data is simulated, it is not necessary to define an entire calibration cluster: a simulated mean value suffices.

The drift in x_1 depends on the value of variable x_2 (see Eqn. 2). Therefore, the single calibration sample is positioned somewhere around the mean of variable x_2, i.e., $x_{2,c} = 4.5$ (see Fig. 5). The amount of drift of the calibration sample does not only depend on $x_{2,c}$, but also on the time t. This is expressed by

$$d_c = 0.1tx_{2,c} = 0.45t \quad (6)$$

For each drift set the drift can be determined with Eqn. 7 (the values of time t are shown in Table 1). The drift, d_c, is now subtracted from the values of x_1, for every data point in the particular drift set [a]. The effect of this correction procedure on data set E is shown in Fig. 9.

Again for every drift set nine network structures are each trained six times. The results for these experiments are depicted in Fig. 8b–f, respectively. It is seen that going from Fig. 7 and Fig. 8b–f the prediction percentages still decreases a little, but not so much as was the case without the correction procedure.

It is seen that 'measurement' of only a single calibration sample is not sufficient to describe the non-linear drift detailed enough. If a better correction is desired, more calibration examples have to be measured to obtain a more detailed de-

[a] In this case, t could have been taken directly as extra variable, instead of the drift, since the relation between the drift and the time is simple. However, in general, it is not known exactly in which way the drift depends on the time.

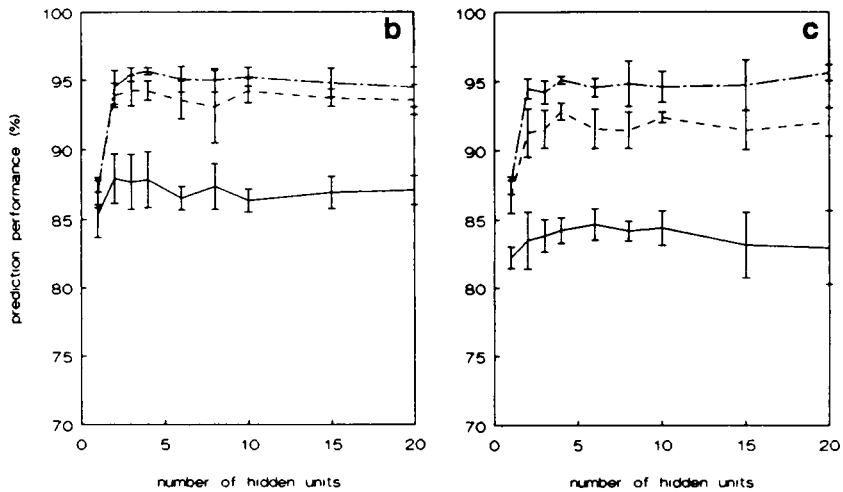
b
prediction performance (%)
number of hidden units

c
number of hidden units

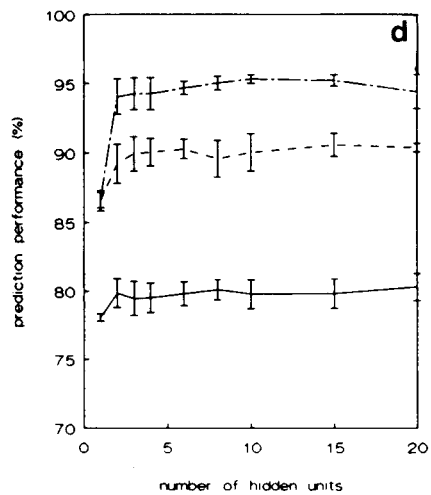
d
prediction performance (%)
number of hidden units

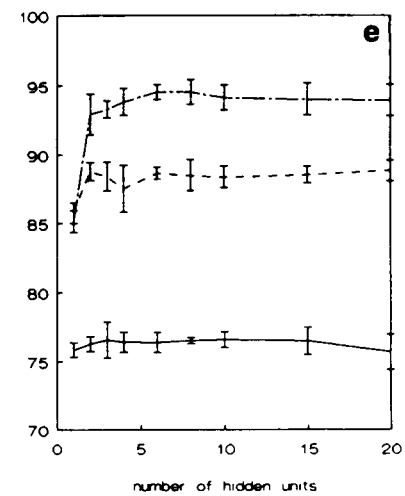
e
number of hidden units

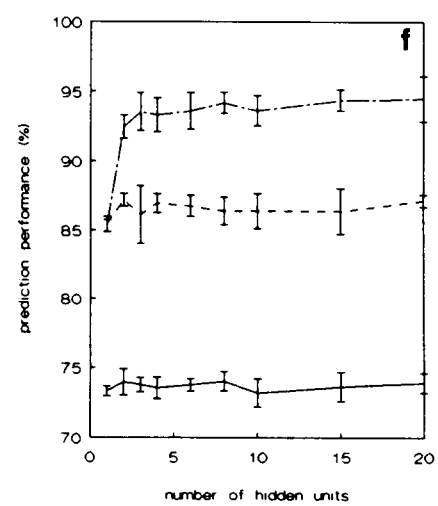
f
prediction performance (%)
number of hidden units

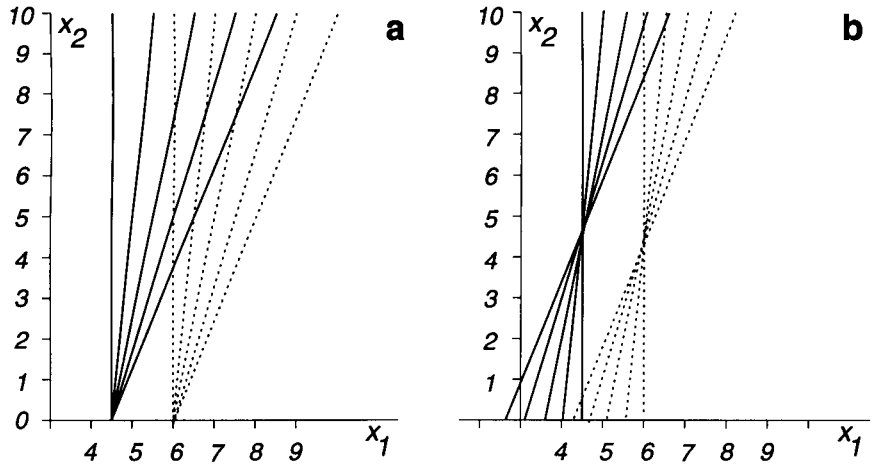

Fig. 9. Effect of subtraction of drift. (a) Schematical composition of uncorrected data set E. The fan-like clusters show considerable overlap. (b) Schematical composition of data set E after subtraction of the drift of the calibration sample. The overlap is decreased, but it has not disappeared entirely. ———, Cluster 1; - - - - - -, cluster 2.

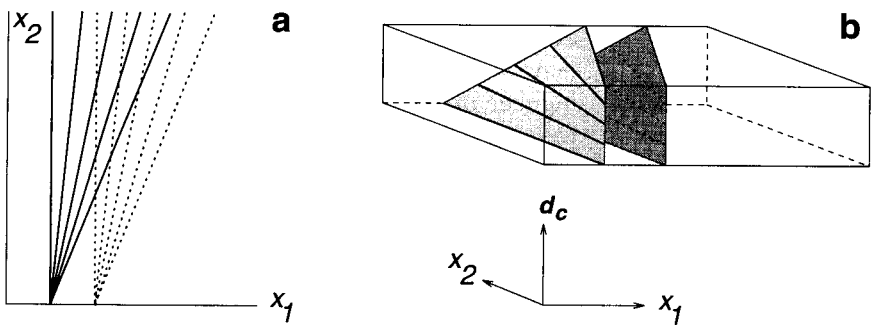

Fig. 10. Effect of drift as extra variable. (a) Schematical composition of uncorrected data set E, with considerable overlap between the clusters. (b) Schematical composition of data set E if the drift of a calibration sample, d_c is given as extra variable. The merged measurements measured at different times t do not form fans any more, but combine more or less like the steps of a spiral staircase. Whereas in (a) the two fan-like clusters show overlap, in (b) the two spiral-like clusters are well separated: the overlap has disappeared completely, due to the introduction of the extra dimension (d_c). The decision boundary between these two clusters is non-linear. ———, Cluster 1; - - - - - -, cluster 2.

scription. The amount of drift at a specific position in the variable space may in this case be determined by means of an interpolation procedure applied on the calibration sample measurements.

Drift as extra variable

In the third experiment, the drift of a single calibration sample is used as an extra input variable: for every object not only the values for the variables x_1 and x_2 are given, but in addition

Fig. 8. Results of the three experiments with the drift sets. (b) to (f) For every network structure the mean prediction performance and the standard deviation of the six runs is given for the test set of sets B to F, respectively. (———) gives the prediction performance without any drift correction, (· · · · · ·) gives the prediction performance if the drift is subtracted, and (· – · – ·) gives the prediction performance if the drift is given as extra parameter.

also the drift d_c (Eqn. 7). The effect of this correction procedure is shown in Fig. 10. The results for these experiments are shown in Fig. 8b–f, respectively. It can be observed that, going from Fig. 7 and Fig. 8b–f, the prediction percentages stay high.

Due to the addition of the third dimension, i.e., the variable d_c, the clusters remain separated in the extended variable space, this despite of the drift. In this case the decision boundary is not a straight line anymore, but a curved plane. The clusters are shifted parallel to this plane and, hence, do not cross it.

It is seen that only a singe calibration sample suffices; it is not necessary to describe the drift in more detail. However, if the drift is extremely variable, even for this procedure more than one calibration sample measurements will be necessary.

Conclusions

If a neural network, trained with data measured with a calibrated instrument, is used to classify measurements containing a certain amount of drift, it may perform badly. Due to the drift, the clusters may cross the decision boundaries the network derived from the training data. This phenomenon is more likely to happen if the clusters are relatively close to each other.

If calibration is not performed often, and measurements containing drift are used to train the network, the clusters are spred out and adjacent clusters may start to overlap. To prevent this, a drift correction procedure has to be applied. The amount of drift on a specific time may be determined by measuring calibration samples in between real measurements. Different correction strategies were applied: no correction, subtraction of the drift, and drift as extra variable.

If the drift is of a relatively simple nature, i.e., the clusters are only translated, subtraction of the drift will be sufficient to correct for it. If the drift is more complex, i.e., the clusters are not only translated but the shape or even the orientation has changed also, subtraction of the drift might not suffice. An alternative drift correction strategy is to use the drift as an additional variable to describe the object. This increases the dimensionality of the variable space (and of the decision boundaries), and drifting (spred) clusters are less likely to overlap. However, the resulting decision boundaries will be non-linear, e.g., curved planes instead of straight lines. Therefore a non-linear pattern classifier like a neural network has to be used in combination with this correction procedure. This paper demonstrates the effect of the described drift correction strategies on the performance of a neural network. The simulated data sets which are used exhibited a specific non-linear type of drift, and drift corrections were based on only a single calibration sample. The latter strategy, adding drift as an extra variable, appeared to give the best overall results.

The simulated data sets contained only drift in one variable, so only this variable had to be corrected for drift. Of course, one may correct for drift in every variable in a similar way, i.e., for every variable an extra drift correction variable may be used. This may lead to a doubling of the number of input variables. If there is not much training data available, this may cause problems with training the neural networks [4].

If the drift is such that the clusters are starting to overlap even if data is taken which is measured at one specific point in time, correction will not be possible anymore. In this case calibration of the instrument is the only remedy to retain the performance of the network.

If drift correction is applied, the network still may only be used to classify objects with maximally the same amount of drift in their variables as was present in the data points the network was trained with. If the drift of the instrument exceeds this maximal amount after some time, again, calibration will be necessary.

The described method may not only be applied in case a neural network is used as pattern classifier, but it is also applicable in combination with other non-linear pattern classifiers.

Summarizing, subtraction of the drift is a good strategy, provided the drift is simple to describe. If the drift is more complex, more calibration samples will be necessary to enable correction for the drift with subtraction. In this case, correction with an extra drift variable is often sufficient,

even if this correction is based on only one calibration sample.

Although the proposed correction procedure (addition of the amount of drift as extra variable) is only tested on a specific type of non-linear drift, it may be a promising method for correction of other types of non-linear drift also.

The authors would like to thank L.M.C. Buydens and J.W. Hofstraat for their evaluation of the manuscript.

REFERENCES

1 D.E. Rumelhart, J.L. McClelland and the PDP Research Group, Parallel Distributed Processing, Explorations in the Microstructure of Cognition, Vol. 1, Foundations, MIT Press, London, 1986.
2 R.P. Lippmann, IEEE ASSP Mag., 4 (1987) 4.
3 J.R.M. Smits, L.W. Breedveld, M.W.J. Derksen, G. Kateman, H.W. Balfoort, J. Snoek and J.W. Hofstraat, Anal. Chim. Acta, 258 (1992) 11.
4 J.R.M. Smits, W.J. Melssen, L.M.C. Buydens and G. Kateman, Chemom. Intell. Lab. Syst., in press.
5 P.C. Thijssen, S.M. Wolfrum, G. Kateman and H.C. Smit, Anal. Chim. Acta, 156 (1984) 87.
6 S. Rutan, J. Chemometr., 1 (1987) 7.
7 G.B.J. Dubelaar, A.C. Groenewegen, W. Stokdijk, G.J. Van den Engh and J.W.M. Visser, Cytometry, 10 (1989) 529.
8 J.C.H. Peeters, G.B.J. Dubelaar, J. Ringelberg and J.W.M. Visser, Cytometry, 10 (1989) 522.
9 D.S. Frankel, R.J. Olson, S.L. Frankel and S.W. Chisholm, Cytometry, 10 (1989) 540.
10 H.W. Balfoort, J. Snoek, J.R.M. Smits, L.W. Breedveld, J.W. Hofstraat and J. Ringelberg, J. Plankton Res., 14 (1992) 575.
11 D.L. Massart, B.G.M. Vandeginste, S.N. Deming, Y. Michotte and L. Kaufman, Chemometrics: A Textbook, Elsevier, Amsterdam, 1988.

Analytica Chimica Acta, 284 (1993) 107–118
Elsevier Science Publishers B.V., Amsterdam

Automatic polarographic elucidation of electrode mechanisms by means of a knowledge-based system

Part 4. Elucidation of mechanisms of newly synthesized compounds

M.J. Pałys [1], M. Bos and W.E. van der Linden

Laboratory for Chemical Analysis, Department of Chemical Technology, Twente University of Technology, P.O. Box 217, 7500 AE Enschede (Netherlands)

(Received 22nd March 1993; revised manuscript received 2nd July 1993)

Abstract

After validation, the previously described expert system has been employed in the investigation of reduction mechanisms of two metallomacrocyclic compounds that have not been electrochemically studied before: a nickel salen derivative and a binaphthyl–uranyl salen crown ether. The system has found that on a mercury electrode in DMSO, under experimental conditions (concentration in the range of 5×10^{-4}–2×10^{-3} M, time scale corresponding to scan rates 0.15–8.0 V s^{-1}) the nickel salen derivative undergoes a reversible electron transfer followed by a fast, reversible chemical reaction. Additional experiments performed outside the expert system suggest that another very slow chemical step takes place, either subsequent or parallel, resulting in a product accumulated on the electrode surface. In the chemical processes most probably traces of water, oxygen or other impurities are involved. For binaphthyl–uranyl salen crown ether the elucidated mechanism is a fast, reversible electron transfer followed by a weak adsorption of the reduction product (studied concentration range 2×10^{-4}–2×10^{-3} M, time scale corresponding to scan rate 0.11–5.0 V s^{-1}). In both cases the expert system provided results which supported a single hypothesis about the mechanism much more than all others, giving a clear, unambiguous conclusion. The full elucidation cycle took approximately one working day.

Keywords: Polarography; Expert system; Knowledge-based system; Schiff bases

In three previous papers in this series [1–3] a knowledge-based (expert) system for the automatic elucidation of electrode reaction mechanisms has been described: its structure, its functioning and the criteria underlying the set of rules for the determination of mechanisms. This system has been validated using a number of compounds for which the mechanism of the reaction on the electrode is well known and has been extensively studied. The scope of this paper is to evaluate the performance of this expert system in a real-world situation: elucidation of the mechanism for a compound that has not been studied yet.

We have chosen two compounds recently synthesized in the Laboratory of Organic Chemistry of the University of Twente: a nickel salen derivative (Fig. 1) [4] and a binaphthyl–uranyl salen crown ether (Fig. 2) [5]. These compounds are interesting from the point of view of their complexation capabilities, but their electrochemical

Correspondence to: M.J. Pałys, Laboratory for Chemical Analysis, Dept. of Chemical Technology, Twente University of Technology, P.O. Box 217, 7500 AE Enschede (Netherlands).
[1] On leave from the Department of Chemistry, University of Warsaw.

0003-2670/93/$06.00 © 1993 – Elsevier Science Publishers B.V. All rights reserved

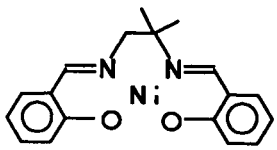

Fig. 1. Structure of nickel salen derivative studied: [1,2-(2,2-dimethyl)ethylenebis(nitrilomethylidyne)bis(2-phenolato]-(2−)-*N,N',O,O'*]nickel.

properties have not been systematically investigated yet.

For complexes of transition metals with salen [*N,N'*-ethylenebis(salicylideneaminato)dianion] a simple one-electron transfer is usually observed, with a stable anion as a product, with the metal in the lower oxidation level [6–8]. The presence of the radical as an intermediate is very probable [9]. This mechanism has been observed for a broad range of salen derivatives, metal cations and solvents [7,10]. The electron transfer is moderately fast leading to reversible, quasi-reversible or sometimes irreversible voltammograms [7,9]. Complexes with a similar ligand, salophen [*N,N'*-phenylenebis(salicylideneaminato)dianion] are reduced to relatively stable radicals that undergo fast dimerization [11,12]. The dimer can be reoxidized, probably in an ECE process, yielding the original complex [12]. The presence of alkali cations promotes dimerization.

It has been observed, that traces of molecular oxygen react very rapidly with the radical formed in the first step leading to a stabilisation of the radical, affecting the electrochemical behaviour of nickel–Schiff bases complexes [6].

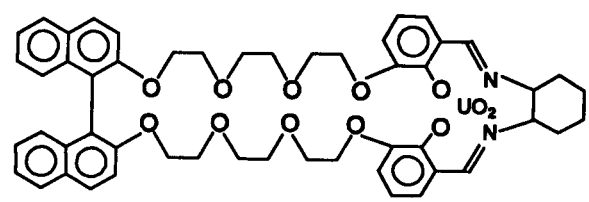

Fig. 2. Structure of binaphthyl–uranyl salen crown ether studied: [*cis*-4,5,7,8,10,11,19a,20,21,22,23,23a,32,33,35,36,38,39-Octadecahydro-13,17:26,30-dimethenobenzo[*f*1]dinaphth-[2,1-*k*:1',2'-m] [1,4,7,10,15,18,21,24,31,34]octaoxadiazacyclotetracontine-51,52-diolato(2−)-N^{19},N^{24},O^{51},O^{52}]dioxouranium.

Electrochemical literature on complexes of dioxouranium(VI) with salen and salen derivatives is very scarce. Taking into account the generality of the electron transfer mechanism observed in complexes of nickel, cobalt, copper and other transition metals it can be expected that also in this case a simple electron transfer should be the most probable mechanism.

EXPERIMENTAL

The expert system was run on an Olivetti M24 personal computer (IBM PC-compatible, 8086 CPU and 8087 numerical coprocessor), controlling the Autolab-100 General Purpose Electrochemical System (Eco Chemie, Utrecht) that carried out the experiments. All measurements were made using the static mercury drop electrode (Metrohm VA-663), the Hg drop radius used was approx. 0.25 mm. Reported potentials were measured with respect to an Ag/AgCl (3 M KCl) reference electrode (Metrohm). A glassy carbon rod served as auxiliary electrode.

Oxygen was expelled with polarographic grade nitrogen (Hoekloos). Mercury for the filling of the electrode (commercial grade), has been successively purified by shaking with ethanol, 2 M sodium hydroxide and 2 M nitric acid and finally has been doubly distilled at low pressure.

0.25 M solution of tetrabutylammonium perchlorate (Fluka, puriss. electrochemical grade) in DMSO (Janssen, spectrophotometric grade) was used as a supporting electrolyte. Nickel salen and binaphthyl–uranyl salen crown ether (both used as received) were dissolved in supporting electrolyte giving stock solutions with concentrations of 1.31×10^{-2} M and 10^{-2} M, respectively.

In experiments with the nickel salen derivative the concentration of the compound in the cell was varied from 0.5×10^{-3} to 2.0×10^{-3} M. The electrochemical behaviour was studied in the potential range from −0.8 V to −2.0 V, scan rates were varied from 0.15 V s^{-1} up to 5.0 V s^{-1}. Step height in staircase voltammetry was 2.44 mV. In chronocoulometry the potential of the electrode was kept at −0.8 V for 1 s (preconditioning) followed by two periods of 0.4 s at potentials

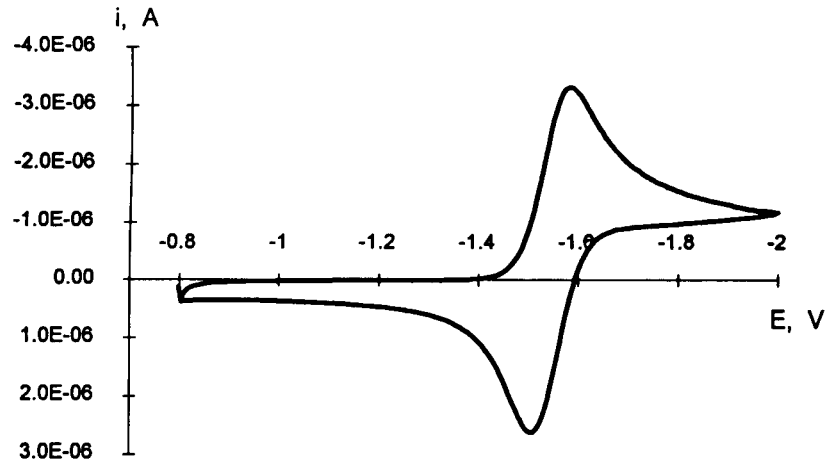

Fig. 3. Voltammogram of nickel salen derivative in 0.25 M tetrabutylammonium perchlorate in DMSO, background corrected. Concentration: 1.4×10^{-3} M, scan rate 0.935 V s^{-1}. Vertical scale in A.

−2.0 V and −0.8 V, respectively; charge was sampled with intervals of 6.1 ms.

The respective experimental parameters for binaphthyl uranyl salen crown ether were: concentration range 2.0×10^{-4} to 2.0×10^{-3} M, voltammetric potential range −0.6 V to −1.6 V, scan rates range 0.11 V s^{-1} up to 8.0 V s^{-1}, step height 2.44 mV; chronocoulometry at potentials −0.6, −1.6, −0.6 V with the same time regime as in the case of the previous compound.

All voltammograms and chronocoulograms were background-corrected.

The set of rules for the elucidation was the same as described previously [2,3]. The expert system shell was slightly modified: instead of the rather complicated statistical test for trend used

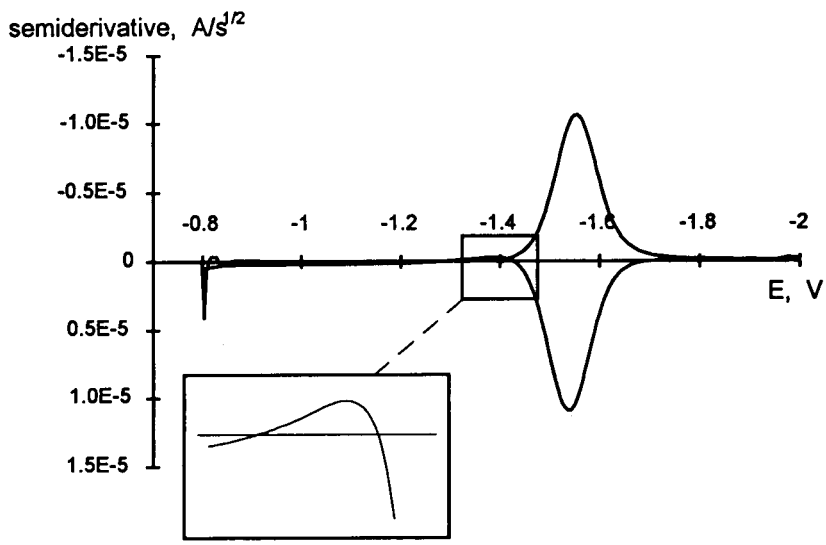

Fig. 4. Semiderivative of voltammogram from Fig. 3; semidifferentiation carried out using G0 algorithm [13]. Enlarged fragment: the descending branch of the anodic peak.

till now, a more straightforward and a better theoretically sound Kendall τ-test was applied.

RESULTS AND DISCUSSION

Reduction of the nickel salen derivative

The expert system run. In the first step, the expert system tried to determine the number of separate electron transfer steps by recording the staircase (SCV) voltammogram with three half-cycles. It was found, that there was only one peak in each branch and no secondary peak appeared (see Fig. 3), examination of the semiderivative of this voltammogram (Fig. 4) proved, that there are no overlapping peaks nor hidden signals. Conclusions of these experiments excluded whole classes of mechanisms, i.e., all mechanisms with only one irreversible electron transfer step, ECE mechanisms with $E_2^{0'} \ll E_1^{0'}$, all EE, as well as "square-" and "triangle scheme" mechanisms.

In the second step the presence of the net reaction was investigated. The obtained result, namely a supporting pair with values close to [0,1], means that it is completely unclear whether a net reaction takes place or not.

The next phase consisted of the investigation of various suggestions for the mechanisms of the observable electron transfer steps, followed by the determination of the factors controlling the transport to the electrode. Measured characteristics of the system can be found in Figs. 5 and 6.

All results for the different features of the electrochemical behaviour [2] of nickel salen derivative are collected in Table 1. On the basis of these features a ranking list of mechanisms, ordered according to decreasing support, has been compiled and is reported in this table: the most supported mechanism is an ECr one (fast, uncomplicated electron transfer followed by a fast, reversible chemical reaction), the second one on the list is an ErCrEr mechanisms with both electron transfer steps taking place at very close potentials.

Interpretation of results. The first feature that attracts attention is the presence of a net (irreversible) reaction in the system, a feature that acquired an unusual support very close to [0,1],

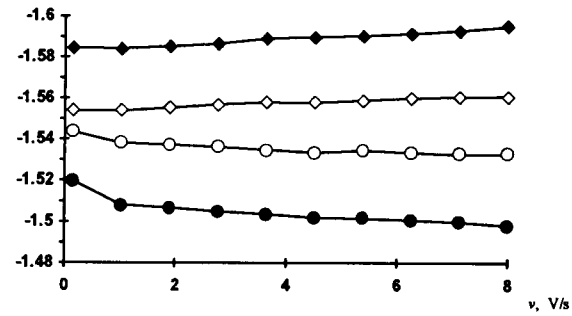

Fig. 5. Dependence of peak potentials on scan rate in staircase and semiderivative voltammetry of nickel salen derivative. (♦) SCV cathodic peak, (●) SCV anodic peak, (◇) semiderivative cathodic peak, (○) semiderivative anodic peak, x axis: scan rate, V s^{-1}; y axis: peak potential.

i.e., almost complete ambiguity about this fact. The presence of a net reaction in this type of systems is detected by the investigation of the

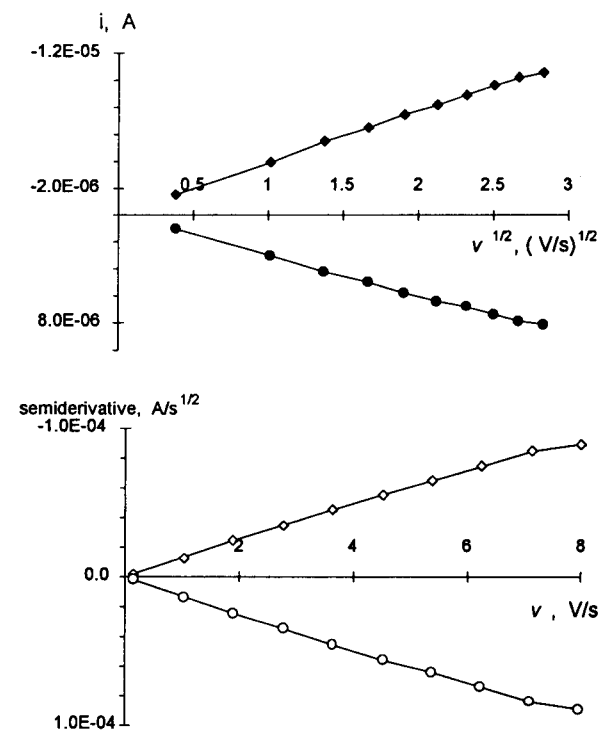

Fig. 6. Dependence of peak height on square root of scan rate (in staircase) and on scan rate (in semiderivative) voltammetry of nickel salen derivative. (♦) Cathodic SCV peak, (●) anodic SCV peak, (◇) cathodic semiderivative peak, (○) anodic semiderivative peak.

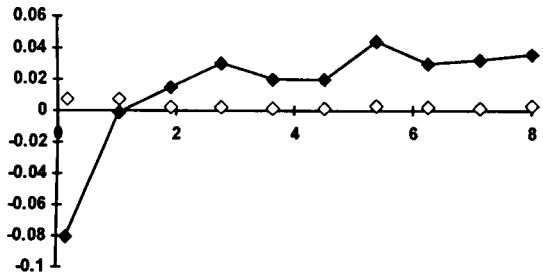

Fig. 7. Nickel salen derivative: plot of the relative semi-integral value at the end of the second branch of the voltammogram (♦) vs. scan rate. Semi-integral is normalized to its maximal value during the scan. Semi-integration carried out using the spherical convolution algorithm (see [14]) under assumption of diffusion coefficient $D = 9 \times 10^{-10}$ m^2 s^{-1}. Open clubs mark the standard deviation of corresponding values.

semi-integral value at the end of the second branch of the voltammogram (normalized to the largest negative semi-integral value during the scan): it should be equal to zero if no chemical consumption takes place, or greater than zero if a part of the reduction product is irreversibly consumed [3]. A plot of the relative semi-integral value vs. scan rate (Fig. 7) shows, that it actually changes sign with the increase of scan rate. This change is significantly larger than the experimental error so the statistical test used decides, that there is a total ambiguity about the hypothesis that the semi-integral is larger than zero.

A closer examination of the semiderivative curves (see Fig. 4) provides an explanation for this strange behaviour: the descending branch of the semiderivative anodic peak crosses the zero line suggesting accumulation of the product at the electrode surface. Accumulation of reduction products, better visible at low scan rates, causes the value of the relative semi-integral to change the sign. This effect becomes less significant at higher scan rates and the effect of the net reaction prevails. The conclusion is that there is a slight net reaction in the system, at long experimental times obscured by the accumulation effect.

To check the hypothesis about the accumulation of the reduction product, a series of experiments with very slow scan rates has been carried out outside the expert system (these scan rates lie below the range currently available for the experimental module of the system). Voltammograms observed at scan rates of 25 and 5 mV s^{-1} (Fig. 8a and b) clearly show additional peaks rising from the anodic one. Especially one sharp, small peak visible at 5 mV s^{-1} has a symmetric form characteristic for reoxidation of surface-accumulated product. These experiments proved, that at least one other chemical step, either following or concurrent to the first one, gives a product that is accumulated on the electrode surface. The nature of this step could be explained using observations done at low concentrations (approx. 10^{-5} M): under such circumstances the anodic peak becomes very small and the consumption of the reduction product becomes more evident. The fact that this effect is better visible at low concentrations suggests that either water or other impurities are involved in this process.

The mechanism of the reduction is not in complete agreement with the one suggested by, e.g., Gosden et al. [6], where no chemical step following the electron transfer is reported. In our case, the support for the hypothesis that the mechanism of the reduction is an uncomplicated electron transfer (mechanism Er or Es) is substantially lower (resp. $[4.28 \times 10^{-9}, 0]$ and $[6.64 \times 10^{-16}, 0]$, see Table 1). The feature that is responsible for this low support is the variation of the cathodic peak potential with scan rate: very clearly, a cathodic shift is observed upon increase of ν, but its rate does not fit the theoretical prediction of slow electron transfer. Actually, the value of the shift is rather small (ca. 10 mV for 50-fold increase in the scan rate) suggesting a very small influence of chemical kinetics on the reduction process. This can be explained by the presence of traces of water and oxygen (reported to modify the electrochemical behaviour [6]) in the solution and a slow homogeneous process mentioned above. Nevertheless, the conclusion of the expert system that under investigation conditions the mechanism has ECr character is correct and justified by the experimental data.

It should be noticed, that though differences in support for different hypotheses on the ranking list in Table 1 are large, the absolute values of

supporting pair elements are small. The reason for it can be found by inspection of Table 2 that collects the features with the largest influence on the final support for a hypothesis about the reaction mechanism (rules for the elucidation usually consist of conjunctions of conditions to be satisfied, so the feature with the lowest support determines the overall support). The low absolute value of the support for the ECr mechanism is caused by a demand, that the height of the reoxidation peak should vary characteristically for the mixed linear diffusion and a kinetic effect. The ranking list in Table 1 shows, that the most supported hypothesis for the reoxidation process is the mixed limited and semiinfinite linear diffusion, an effect due to the mentioned accumulation phenomenon. The low support for the demanded type of the transport results in low overall support for mechanism hypothesis.

Reduction of binaphthyl–uranyl salen crown ether

The expert system run. In the series of experiments with the second compound, the order of reasoning steps and experiments carried out was principally identical to the previous case. The

TABLE 1

Features and their support obtained during the elucidation of the reduction mechanism of nickel salen derivative in DMSO (Acronyms: F = signal in the forward branch, B = signal in the backward branch. For explanations of other symbols refer to [2,3])

F = 1, B = 1	[1.000, 1.000]	Secondary peak(s) present	[0.000, 0.000]
Net reaction present	[5.55E-16, 1.000]	Hidden peak(s) present	[0.000, 0.000]
Suggestion for the type of the ETS:			
F1: EiCat	**[0.634, 0.998]**	B1: EiCat	**[0.855, 0.984]**
F1: ECr	**[0.634, 0.999]**	B1: CEr	**[0.855, 0.992]**
F1: E	[0.049, 0.124]	B1: BrCat	[0.855, 0.984]
F1: ErCat	[6.03E-5, 0.364]	B1: E	[0.002, 0.011]
F1: Es	[1.36E-10, 0.17]	B1: ECi, CEi	[7.5E-5, 0.130]
F1: ECi, CEi	[0.000, 8.72E-4]	B1: Es	[7.2E-6, 0.519]
F1: CEr	[0.000, 3.2E-4]	B1: ECr	[0.000, 0.001]
Transport to the electrode:			
F1: LIN	**[0.872, 0.872]**	B1: LIM-LIN	**[0.566, 0.578]**
F1: LIN-KIN	[0.337, 0.337]	B1: LIN	[0.483, 0.483]
F1: ADS	[0.000, 0.001]	B1: LIN-KIN	[0.102, 0.126]
F1: ADS-LIN	[0.000, 0.001]	B1: ADS	[0.000, 0.150]
F1: LIM-LIN	[0.000, 5.3E-4]	B1: ADS-LIN	[0.000, 0.073]
F1: KIN	[0.000, 0.000]	B1: KIN	[0.000, 0.000]

System mechanism:	
ECr	**[0.056, 0.000]**
ErCrEr, $E_2^{0'} \gg E_1^{0'}$	[0.014, 0.000]
Er	[4.28E-9, 0.000]
Es	[6.64E-16, 0.000]
ErCrEi, $E_2^{0'} \gg E_1^{0'}$	[6.13E-17, 0.154]
ErCrEi, $E_2^{0'} \gg E_1^{0'}$	[6.13E-17, 0.154]
ErCiEi, $E_2^{0'} \gg E_1^{0'}$	[6.13E-17, 0.154]
ErCiEi, $E_2^{0'} \gg E_1^{0'}$	[6.13E-17, 0.154]
ErCiEr, $E_2^{0'} \gg E_1^{0'}$	[1.1E-17, 0.0336]
EAw	[0.000, 0.063]
EiCEr, $E_2^{0'} \gg E_1^{0'}$	[0.000, 0.009]
AwE	[0.000, 6.28E-4]
ErCat	[0.000, 2.08E-6]
CEs	[0.000, 3.04E-7]
other	[0.000, 0.000]

system behaviour has been found to follow a single reduction and reoxidation step, no overlapping or hidden peaks were detected. The staircase and semiderivative voltammograms of the investigated compounds are shown in Figs. 9 and 10, respectively. Similarly to nickel salen derivative, the support for the hypothesis that there is a net chemical reaction observed in cyclic voltammetry of the compound reflects a large uncertainty. Characteristics of the system, obtained during determination of the type of the electron transfer and factors controlling the transport to the electrode can be found in Figs. 11 and 12.

The ranking list of mechanisms, produced by the expert system on the basis of separate features, clearly places the EAw mechanism (fast, reversible electron transfer with fast, weak adsorption of the reaction product) on the first place. The next hypothesis suggesting an uncomplicated, fast electron transfer has a support which is approx. 10^{11} times less.

Interpretation of results. There is a strong support for the hypothesis, that the reduction of the binaphthyl–uranyl salen crown ether proceeds in a single step, the product being adsorbed on the electrode. This is supported by the ranking list of factors controlling the transport: linear diffusion in the case of the reduction peak and the linear diffusion (highest support) and adsorption (highest but one) in the case of reoxidation peak.

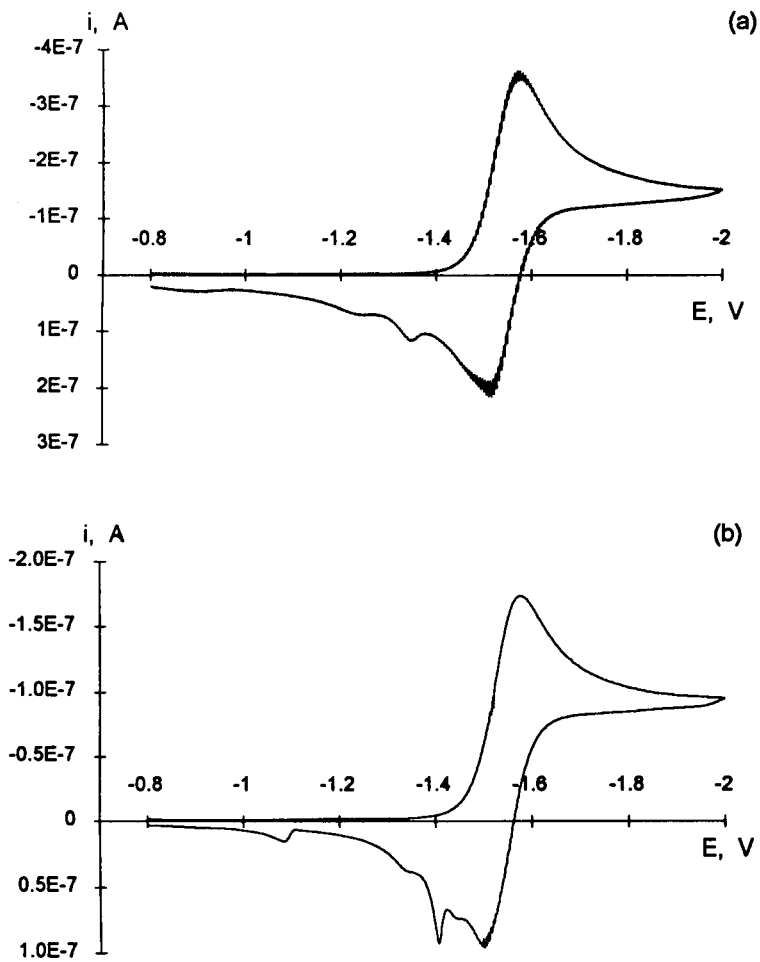

Fig. 8. Voltammogram of nickel salen derivative at the scan rates 25 (a) and 5 mV s^{-1} (b). concentration 1.4×10^{-3} M.

TABLE 2

Features with the strongest influence on the support pair for hypotheses about the reaction mechanism for the reduction of nickel salen derivative (F, B = number of peaks in forward and backward branches of the SCV voltammogram. For explanations of other symbols refer to [2,3])

Er	Trend in semiderivative peak potential difference
Es	Sugg. for the type of the electron transfer
Ei	F, B
CEr, CEs	Sugg. for the type of the electron transfer
CEi	F, B
ECr	Type of transport to the electrode (anodic process)
ECi	F, B
Ercat	Presence of a net reaction
EiCat, ErCrEr ($E_2^{0'} \ll E_1^{0'}$)	F, B
ECrEr ($E_2^{0'} \approx E_1^{0'}$)	Type of transport to the electrode
ErCrEr ($E_2^{0'} \gg E_1^{0'}$), ErCiEr ($E_2^{0'} \ll E_1^{0'}$)	F, B
ErCiEr ($E_2^{0'} \approx E_1^{0'}$)	Presence of a net reaction
ErCiEr ($E_2^{0'} \gg E_1^{0'}$), ErCrEi ($E_2^{0'} \ll E_1^{0'}$)	F, B
ErCrEi ($E_2^{0'} \approx E_1^{0'}$, $E_2^{0'} \gg E_1^{0'}$)	Presence of a net reaction
ErCiEi ($E_2^{0'} \ll E_1^{0'}$)	F, B
ErCiEi ($E_2^{0'} \approx E_1^{0'}$, $E_2^{0'} \gg E_1^{0'}$)	Presence of a net reaction
EiCEr ($E_2^{0'} \ll E_1^{0'}$)	F, B
EiCEr ($E_2^{0'} \approx E_1^{0'}$)	Trend in semiderivative peak height ratio
EiCEr ($E_2^{0'} \gg E_1^{0'}$), EiCEi ($E_2^{0'} \ll E_1^{0'}$, $E_2^{0'} \approx E_1^{0'}$, $E_2^{0'} \gg E_1^{0'}$)	F, B
AwE	Type of transport to the electrode
EAw	Type of transport to the electrode (anodic process)
ErEr, ErEs, ErEi, EiEr, EiEs, E ⇔ E, E ⇄ E	F, B

Location of semi-infinite linear diffusion before adsorption on the list can suggest that the adsorption effect is not very well visible at this concentration level; the difference in support for these two hypotheses is, however, relatively small compared to other supports. The evidence of adsorption can be derived from the fact that the descending branch of the semiderivative anodic peak crosses the zero line (see enlarged fragment of Fig. 10) and that the anodic peak grows faster

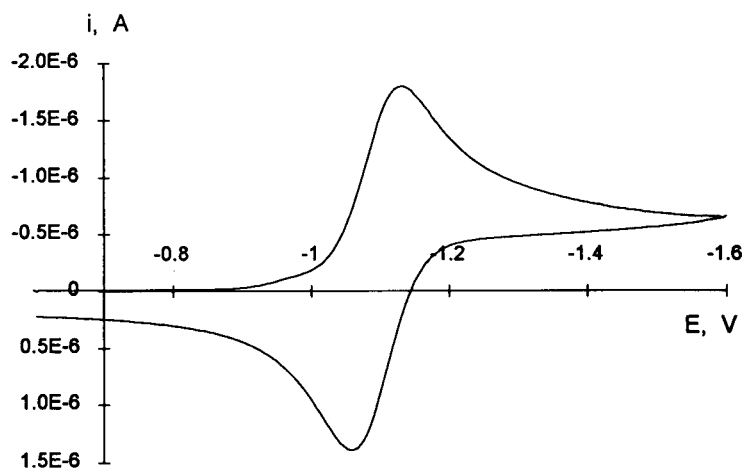

Fig. 9. Voltammogram of binaphthyl–uranyl salen crown ether in 0.25 M tetrabutylammonium perchlorate in DMSO. Concentration 1.28×10^{-3} M, scan rate 0.610 V s^{-1}.

than the square root of the scan rate. This last effect is too small to be observable on the i_p vs. ν plot, but it is detectable using statistical tests.

Because of the very scarce literature on the electrochemistry of uranyl salen complexes, the comparison with results for similar compounds is difficult. However, assuming that uranyl complexes should exhibit much similarity with nickel and cobalt salen complexes, the EAw mechanism leading to the formation of dioxouranium(V) complex is acceptable.

Conclusions, performance of the expert system

The elucidation of mechanisms of the electrochemical reduction of the studied metallomacrocycles delivered a list of possible mechanisms with corresponding supporting pairs. In both cases there were clear differences in support between the first mechanism on the list and the other ones, justifying the decision which mechanism is chosen as the correct one.

The time spent on the elucidation was approximately one working day per compound. The exact measurement of the time was difficult because the addition of solutions to the cell was done by hand: available quantities of metallomacrocyclic compounds were much too small to use burettes.

In the case of the nickel salen derivative the obtained mechanism differs from the literature data for similar compounds. Backtracking the

TABLE 3

Features and their support obtained during the elucidation of the reduction mechanism of binaphthyl uranyl salene crown ether in DMSO (Acronyms: F = signal in the forward branch, B = signal in the backward branch. For explanations of other symbols refer to [2,3])

F = 1, B = 1	[1.000, 1.000]	Secondary peak(s) present	[0.000, 0.000]
Net reaction present	[5.55E-16, 1.000]	Hidden peak(s) present	[0.000, 0.000]
Suggestion for the type of the ETS:			
F1: EiCat	**[0.184, 0.955]**	B1: EiCat	**[0.314, 0.519]**
F1: ErCat	[0.138, 0.911]	B1: CEr	[0.191, 0.539]
F1: E	[0.115, 0.388]	B1: ErCat	[0.191, 0.396]
F1: ECr	[0.052, 0.839]	B1: ECi, CEi	[0.184, 0.529]
F1: Es	[4.55E-11, 0.138]	B1: E	[0.160, 0.0.168]
F1: CEr	[0.000, 0.018]	B1: Es	[4.48E-18, 0.207]
F1: ECi, CEi	[0.000, 0.016]	B1: ECr	[0.000, 0.140]
Transport to the electrode:			
F1: LIN	**[0.740, 0.740]**	B1: LIN	**[0.814, 0.814]**
F1: LIN-KIN	[2.73E-4, 2.97E-4]	B1: ADS	[0.715, 0.857]
F1: ADS	[0.000, 0.075]	B1: ADS-LIN	[0.579, 0.695]
F1: ADS-LIN	[0.000, 0.055]	B1: LIM-LIN	[0.000, 3.92E-6]
F1: LIM-LIN	[0.000, 2.41E-5]	B1: KIN-LIN	[0.000, 3.92E-6]
F1: KIN	[0.000, 0.000]	B1: KIN	[0.000, 0.000]

System mechanism:	
EAw	**[0.429, 0.514]**
Er	[5.80E-11, 0.000]
ErCat	[3.19E-22, 2.92E-5]
AwE	[0.000, 0.045]
CEs	[0.000, 6.63E-7]
EiCEr, $E_2^{0'} \gg E_1^{0'}$	[0.000, 1.08E-9]
ErCrEi, $E_2^{0'} \gg E_1^{0'}$	[0.000, 8.05E-11]
ErCrEi, $E_2^{0'} \gg E_1^{0'}$	[0.000, 8.05E-11]
ErCiEr, $E_2^{0'} \gg E_1^{0'}$	[0.000, 8.05E-11]
ErCiEi, $E_2^{0'} \gg E_1^{0'}$	[0.000, 8.05E-11]
ErCiEi, $E_2^{0'} \gg E_1^{0'}$	[0.000, 8.05E-11]
other	[0.000, 0.000]

TABLE 4

Features with the strongest influence on the support pair for hypotheses about the reaction mechnnism for the reduction of binaphthyl–uranyl salen crown ether (F, B = Number of peaks in forward and backward branches of the SCV voltammogram. For explanations of other symbols refer to [2,3])

Er	Sugg. for the type of the electron transfer
Es	Trend in semiderivative peak potential difference
Ei	F, B
CEr, CEs	Sugg. for the type of the electron transfer
CEi	F, B
ECr	Type of transport to the electrode (anodic process)
ECi	F, B
ErCat	Presence of a net reaction
EiCat, ErCrEr ($E_2^{0'} \ll E_1^{0'}$)	F, B
ErCrEr ($E_2^{0'} \approx E_1^{0'}$)	Type of transport to the electrode (anodic process)
ErCrEr ($E_2^{0'} \gg E_1^{0'}$), ErCiEr ($E_2^{0'} \ll E_1^{0'}$)	F, B
ErCiEr ($E_2^{0'} \approx E_1^{0'}$)	Trend in semiderivative peak height ratio
ErCiEr ($E_2^{0'} \gg E_1^{0'}$), ErCrEi ($E_2^{0'} \ll E_1^{0'}$)	F, B
ErCrEi ($E_2^{0'} \approx E_1^{0'}$, $E_2^{0'} \gg E_1^{0'}$)	Trend in semiderivative peak height ratio
ErCiEi ($E_2^{0'} \ll E_1^{0'}$)	F, B
ErCiEi ($E_2^{0'} \approx E_1^{0'}$, $E_2^{0'} \gg E_1^{0'}$)	Trend in semiderivative peak height ratio
EiCEr ($E_2^{0'} \ll E_1^{0'}$)	F, B
EiCEr ($E_2^{0'} \approx E_1^{0'}$)	Trend in semiderivative peak height ratio
EiCEr ($E_2^{0'} \gg E_1^{0'}$), EiCEi ($E_2^{0'} \ll E_1^{0'}$, $E_2^{0'} \approx E_1^{0'}$, $E_2^{0'} \gg E_1^{0'}$), EAs, AsE	F, B
AwE, EAw	Type of transport to the electrode
ErEr, ErEs, ErEi, EiEr, EiEs, E ⇔ E, E ⇄ E	F, B

elucidation process allowed to find the feature responsible for it: the slight variation of cathodic peak potential with scan rate. Taking into account that this effect is rather small it can be concluded, that it may be due to the presence of water and traces of oxygen in the solution. This does not violate the conclusion that the ECr is the most probable mechanism of the reduction under the given conditions.

The inspection of the measured curves also allowed us to find the explanation for the small absolute values of supporting pairs assigned to the hypotheses about the mechanisms. This inspection also revealed, that criteria for the detec-

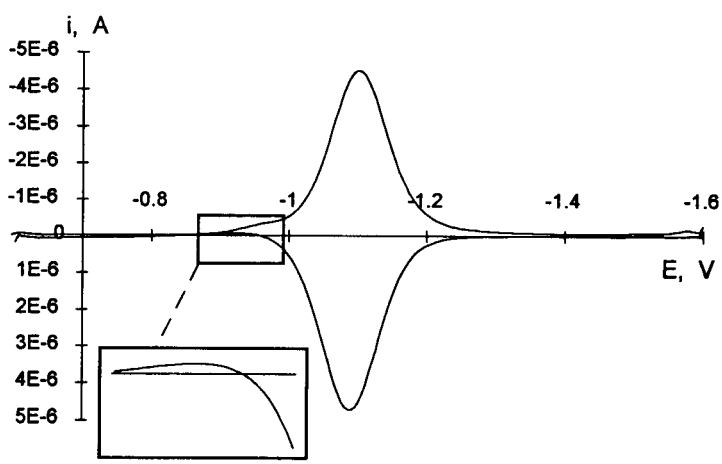

Fig. 10. Semiderivative of the voltammogram from Fig. 9. Algorithm G0. Enlarged fragment: the descending branch of the anodic peak.

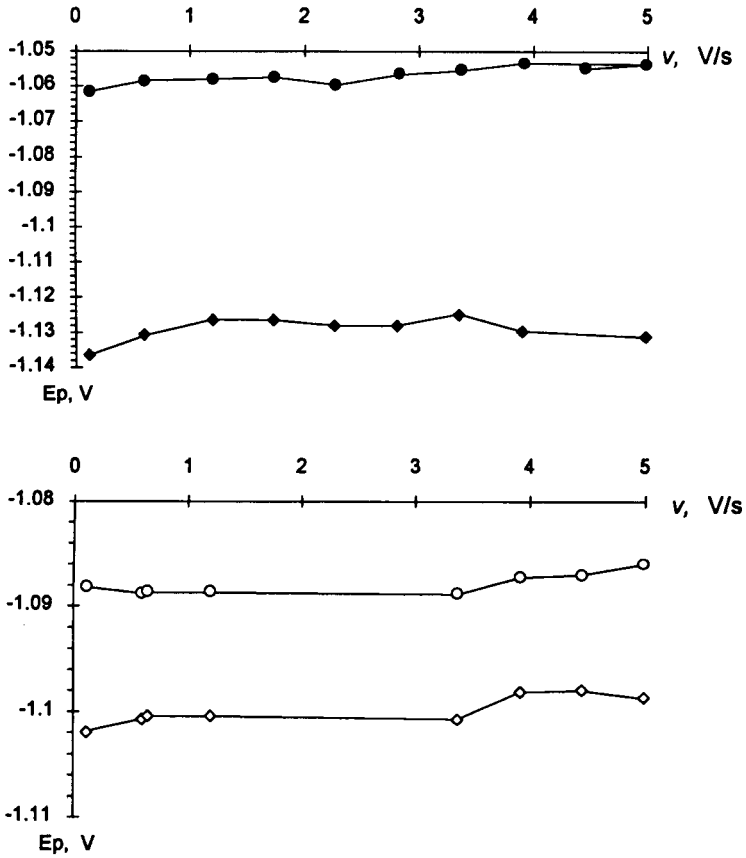

Fig. 11. Variation of the peak potential with the scan rate in staircase and convolution voltammetry of binaphthyl–uranyl salen crown ether. Concentration 1.28×10^{-3} M. (●) Cathodic peak in SCV, (◆) anodic peak in SCV, (○) cathodic semiderivative peak, (◇) anodic semiderivative peak.

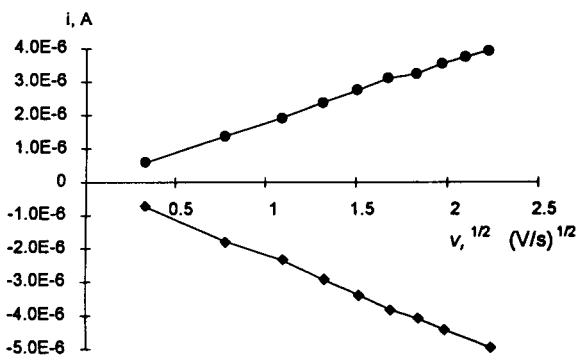

Fig. 12. Variation of the peak height with the square root of scan rate in staircase voltammetry of binaphthyl–uranyl salen crown ether, concentration 1.28×10^{-3} M. (●) Cathodic peak, (◆) anodic peak.

tion of the presence of the net reaction should account for the possibility of a combination of two effects: a slow consumption by a follow-up reaction and the accumulation of its products on the electrode surface. These criteria could be possibly improved in the future.

It can be concluded that these two runs of the expert system proved that it is possible to use it for real-world problems: automatic elucidation of mechanisms of electrochemical reaction of compounds, that have not been studied yet, without using broad electrochemical knowledge and experience. On the other hand, if the set of rules is further improved, the performance of the system, expressed as unambiguity of answers, could even be better.

The expert system's possibility to show its reasoning process to the user, in order to examine and check the obtained conclusions, was used in this paper to explain results obtained for nickel salen derivative. This feature of expert systems is very important: the system is not a "black box" that can be trusted or not – the findings of the system can be always verified.

Therefore the knowledge-based system built and validated so far can therefore be considered to be an intelligent electrochemical apparatus, giving electrochemists a completely new tool to carry out automated research. The appearance of this type of instruments and its importance to electroanalysis have already been foreseen by He et al., who wrote in their paper on one of the first modern computer-controlled electrochemical instruments "... *The ability to achieve skilled decision making within an instrument [...] is poorly developed. When more is learned about the way to achieve it, there will be spectacular results. It is already clear, that we are not far from seeing instruments, that will carry out scientific investigations, not just measurements*" [15].

We would like to thank A.M. Reichwein and F.C.J.M. van Veggel from the Laboratory of Organic Chemistry of the University of Twente for providing us with samples of binaphthyl–uranyl salen crown ether and nickel salen derivative, respectively. M. Palys also owes thanks to F. van Veggel for making available his unpublished electrochemical information regarding the nickel salen compound.

REFERENCES

1 M. Pałys, M. Bos and W.E. Van der Linden, Anal. Chim. Acta, 231 (1990) 59.
2 M. Pałys, M. Bos and W.E. Van der Linden, Anal. Chim. Acta, 248 (1991) 429.
3 M. Pałys, M. Bos and W.E. Van der Linden, Anal. Chim. Acta, 283 (1993) 811.
4 F.C.J.M. van Veggel, unpublished results.
5 A.M. Reichwein, Ph.D. thesis, University of Twente, 1993; and A.M. Reichwein, W. Verboom and D.N. Reinhoudt, Recl. Trav. Chim. Pays-Bas, 112 (1993) 358.
6 C. Gosden, J.B. Karr, D. Pletcher and R. Rosas, J. Electroanal. Chem., 117 (1981) 101.
7 A. Kapturkiewicz and B. Behr, Inorg. Chim. Acta, 69 (1983) 247.
8 A. Kapturkiewicz and B. Behr, J. Electroanal. Chem., 163 (1984) 189.
9 G. Cros, J.-P. Costes and D. de Montauzon, Polyhedron, 3 (1984) 585.
10 E. Reisenhofer and G. Costa, Inorg. Chim. Acta, 49 (1981) 121.
11 S. Gambarotta, F. Urso, C. Floriani, A. Chiersi-Villa and C. Guashini, Inorg. Chem., 22 (1983) 3966.
12 A.A. Isse, A. Gennaro and B. Vianello, Electrochim. Acta, 37 (1992) 113.
13 K.B. Oldham, J. Electroanal. Chem., 121 (1981) 341.
14 S.O. Engblom and K.B. Oldham, Anal. Chem., 62 (1990) 625.
15 P. He, J.P. Avery and L.R. Faulkner, Anal. Chem., 54 (1982) 1313A.

Analytica Chimica Acta, 284 (1993) 119–124
Elsevier Science Publishers B.V., Amsterdam

Studying aerosol samples by non-linear mapping of electron probe microanalysis data

B. Treiger [1], H. Van Malderen, I. Bondarenko [1], P. Van Espen and R. Van Grieken

Department of Chemistry, University of Antwerp (UIA), 2610 Antwerpen-Wilrijk (Belgium)

(Received 19th May 1993; revised manuscript received 12th July 1993)

Abstract

One of the graphical methods of multivariate data analysis, namely non-linear mapping, is applied to the processing of the results of electron probe x-ray microanalysis of individual aerosol particles. A method of representation of the results of non-linear mapping in the form of triplot is proposed. It is shown that it can be used for the fast evaluation of the data structure. The results for aerosol samples from the Lake Baikal are discussed.

Keywords: Multivariate calibration; Chemometrics; Aerosols; Electron probe microanalysis; Environmental analysis

Non-linear mapping (NLM) is known to be one of the most powerful techniques enabling to visualize the structure of multivariate data. It is widely used in social and life sciences but hitherto it was used in analytical aims rather rarely (see, e.g. [1]). However, it can be very useful if one needs to process a large amount of information.

This is the case if we deal with single particle analysis of aerosol samples. This type of analysis has proven to be a very useful tool for solving different problems in aerosol science, especially the problem of apportionment of the different aerosol sources which have an impact on a certain airshed [2].

The interest to the analysis of aerosols from Lake Baikal is explained by the significance of this lake which contains, with its 23000 km^3, almost 22% of all the freshwater on earth. Lake Baikal is scientifically enormously interesting for biologists (the lake has 1500 endemic species) and geologists (it is over 25 million years old), but also in the context of environmental chemistry, air pollution and study of atmospheric aerosols. The largest part of the lake is rather far from the sources of industrial pollution and according to the first drawn data, the aerosol there can be considered as a "background" or "baseline" continental one, i.e., the aerosol which should occur in natural circumstances and on which, as far as composition goes, all pollution is superimposed. Also, in winter, several thousand km around the lake are snow covered and the ocean is far away. Hence soil and seaspray particles are absent. Every characterization of individual aerosol particles is, in these circumstances, by definition limited to the most interesting particles, namely those which are transported in the air over long distances and the pollution particles.

EXPERIMENTAL

Sampling

A set of 40 samples was collected during a 14-day cruise over the total area of Lake Baikal in the month of June 1992. Sampling took place

Correspondence to: R. Van Grieken, Department of Chemistry, University of Antwerp (UIA), 2610 Antwerpen-Wilrijk (Belgium).
[1] On leave from Pedagogical Institute, Kirovograd, Ukraine.

0003-2670/93/$06.00 © 1993 – Elsevier Science Publishers B.V. All rights reserved

from the upperdeck of the research vessel Balkash, approximately 10 m above the water line. Total airborne particulate matter was collected using a 47 mm diameter, 0.4 μm pore size Nuclepore polycarbonate membrane filter (aerosol-grade). This filter was placed in a plexiglass filter holder with a hat-type cover to protect the filter from rain or wet drops created by the ship through wave braking under high winds. The filter holder was connected to a vacuum pump, which was operated at a flow-rate of approximately 50 l min^{-1}, and equipped with an automatic timer system and a flow meter.

Proper precautionary measures were taken in order to prevent contamination of the samples from sources on the ship (exhaust fumes, corrosion products, dust or dirt particles,...). Therefore sampling only took place when the relative wind direction to the ship was between an angle of $-45°$ to 45°. Also under low wind conditions sampling was discontinued. After collection the filters were stored in airtight Millipore petri dishes.

The cruise started in Listvyanka, a little port on the southwestern shore, where a part of the Limnological Institute is housed, then all the way up to Severobaikalsk, a town in the north, then back to the south to the city of Baikalsk, to return two weeks later back to Listvyanka. Throughout all of the trip, samples were taken over a 2-h period, resulting in a proper loading of the filter for single particle analysis.

The surface water temperature of the lake is around 4°C in June. During the cruise the weather was mostly sunny with only one short rain event.

Electron probe x-ray microanalysis

Electron probe x-ray microanalysis (EPXMA) is a fast and reliable analytical method which allows to obtain chemical and morphological information of micrometer-sized particles. EPXMA has been succesfully automated, so that, in a couple of hours, a few hundred particles can be analyzed. In that way, an enormous amount of data is obtained so that some way of data reduction is needed. Multivariate methods combined with automated EPXMA are therefore a useful and efficient tool for the analysis of aerosols.

For the 40 samples taken in Baikal the analysis of in total 16000 (400 per sample) individual particles was performed by EPXMA on a 733 Superprobe (JEOL, Tokyo) equipped with a 10-mm^2 energy-dispersive Si(Li) detector, secondary electron and transmission electron detectors for visualisation and a backscattered electron detector for automated particle localization. This apparatus is also connected to a TN-2000 system (Tracor Northern) that controls the automated analysis of the samples. Typical working parameters for our analysis were an accelerating voltage of 25 kV, a beam current of 1 nA and a magnification of 1200×. For every particle an x-ray spectrum of 20 s was accumulated. Detection limits for EPXMA are around 1000 ppm. For the automatic analysis of single particles we used a self-modified version of a particle recognition and characterization program (PRC, Tracor Northern). In this program localisation of a particle is obtained by succesive horizontal scanning with the electron beam. Whenever a signal higher than a preset value is detected contour pixels of the particles are stored into memory. When all contour pixels have been stored, perimeter and diameter are calculated. Henceforth an x-ray spectrum is accumulated and all this information is stored on disk. Typically minimum detectable particle size of EPXMA is around 0.2 μm, but since our samples were collected on 0.4 μm pore size Nuclepore filters only particles bigger than 0.4 μm were analyzed.

NONLINEAR MAPPING

Automated EPXMA of all aerosol particles was conducted on 15 elements (Na, Mg, Al, Si, P, S, Cl, K, Ca, Ti, Cr, Mn, Fe, Zn, Pb). Also the average diameter of the particles was determined. In other words, each aerosol particle was represented by a point in N-dimensional ($N = 16$) data space. Useful information can be obtained if one can reveal the structure of such an N-dimensional space. In order to do this we propose to apply NLM.

NLM is really a set of multivariate graphical techniques which try to find a projection of an

N-dimensional data space onto a plane which preserves the structure of the initial space as much as possible. Usually it is not a simple thing especially if one takes into account the large number (≈ 400) of data points. Therefore a simplified method to conduct NLM was used; it has been described in detail elsewhere [3]. Its main idea is to introduce in an N-dimensional space three pairs of specially chosen reference points and then try to find such projections of N-dimensional space into three linear independent straight lines which preserve the relative distances between the data points and the pairs of reference points. In other words, after application of NLM each data point is characterized by three parameters (p_1, p_2, p_3).

We used just three pairs of reference points because it seems to be a reasonable compromise between the unavoidable distortion of the projected data structure in comparison with the initial one, and visuality of the projection. However, there also exists a very simple way of representation of three-dimensional data on a plane. It is similar to the Trilogplot proposed by Lewi [4] and we called it triplot. If we consider an equilateral triangle and a point lying inside of it, then it can easily be proved that the sum of the distances of the points to the sides of the triangle is constant for all points and equal to the height of the triangle (see Fig. 1). Thus if we consider an equilateral triangle with unit height, the sum of distances of every point lying inside of it equals 1. If we have a point in 3-dimensional space with coordinates, say, p_1, p_2 and p_3, then we can normalize these coordinates as follows:

$$p_1^* = \frac{p_1}{p_1 + p_2 + p_3}$$

$$p_2^* = \frac{p_2}{p_1 + p_2 + p_3}$$

$$p_3^* = \frac{p_3}{p_1 + p_2 + p_3}$$

It is clearly seen that now the constraint

$$p_1^* + p_2^* + p_3^* = 1$$

is satisfied and three-dimensional points can be drawn lying inside some equilateral triangle, i.e.,

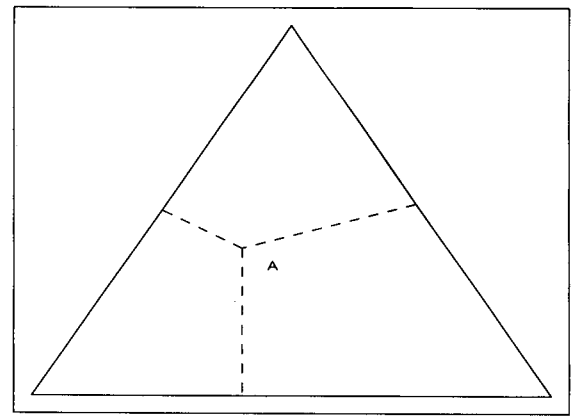

Fig. 1. Example which shows the main idea of triplot.

the results of NLM are presented in the form of triplot. It should be noted that such representation is not a completely new thing. Nearly the same ideas were proposed by Gower [5], who however, used not initially independent data, but data which satisfied some type of constraint.

RESULTS AND DISCUSSION

According to the appearance of triplots, all aerosol samples can be divided into two main groups: (1) those containing Pb or Zn (including 75% of all samples, of which approximately 56% contain lead; usually in such samples 1 or 2 particles of 400 analyzed per sample contain Pb or Zn), and (2) those without these elements (25%). Typical examples of these two groups are shown in Figs. 2 and 3.

A typical triplot for a sample, containing Zn or Pb is shown on Fig. 2. The particle No. 367 in the left bottom corner of triangle is Zn-containing. A black rectangle on the right side of the triangle consists of organic particles. The appearance of just a black rectangle is due to the fact that all of them appear just in the same point on the border of the triangle and their numbers are printed one over another. Four different classes of the particles are also clearly seen. Three of them are comparatively compact. Class 1, consisting of particles enriched mainly in Si and Al, originates from soil dispersion. Class 2, enriched by S and P,

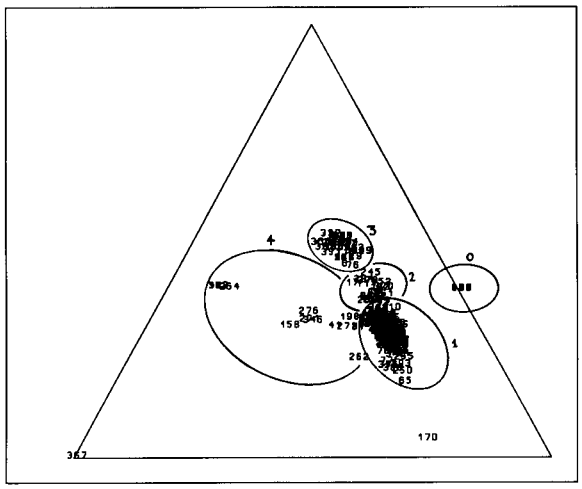

Fig. 2. Typical triplot for a sample containing Pb-rich particles. Here and in subsequent figures the following designation was used for classes of particles enriched in: (1) Si and Al; (2) S and P (or Cl); (3) Ca; (4) Fe. Organic particles are designated as 0.

can be assigned to vegetation as it has been done before [6]. The presence of S could be also connected to the paper mill which produces high amounts of SO_2 or to the heavy industry near Irkutsk. Class 3, enriched with Ca, embraces Ca-containing silicates as well as gypsum particles. Gypsum is frequently found in atmospheric aeosols both in remote [6,7] and polluted [8,9]

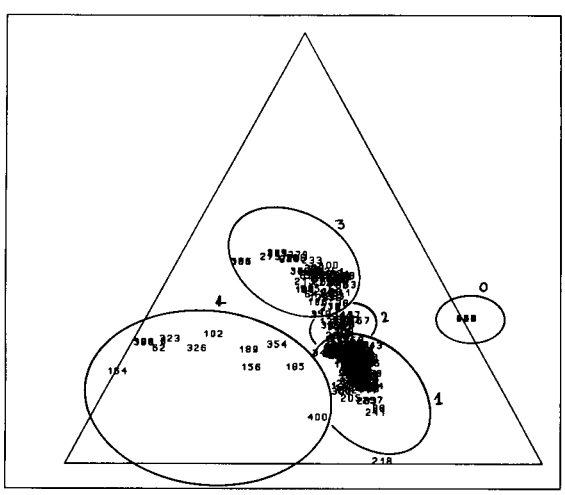

Fig. 3. Typical triplot for a sample without particles containing Pb- or Zn-rich particles.

environments. Class 4, consisting of Fe-containing particles, is rather elongated. This elongation is the consequence of large compositional variations of this group of particles in comparison with the 3 other groups, because this group is a mixture of Fe-containing aluminosilicates and some minerals with high Fe contents such as Fe oxide, olivine and mixed ilmenite [10]. The presence of these minerals is rather typical for desert areas [11]. The occurence of these particles here is not surprising since the Gobi desert in Mongolia is only a few 100 km distant. There are also particles (the most evident example is particle No. 170) lying aside of the main groups. It is due to the presence in addition to the main group-forming elements (Si and Al, S and P, Ca, and Fe), of minor elements, such as Mg in the case of point No. 170.

Nearly the same picture can be seen in Fig. 3, where the typical example of a triplot for a sample, which does not contain Zn or Pb, is shown. The group of organic-containing particles, seen in the form of the filled-in rectangle, is again standing far from others. The group of Fe-containing particles is again elongated. The rather compact groups of Al- and Si-; S-, Cl-, and K-; and Ca-containing particles are also seen. Point No. 218 is situated far from the main Al- and Si-containing group due to the presence of Na (just as point No. 170 in Fig. 2 was situated far from the main Al- and Si-containing group due to the presence of Mg).

The direct comparison of Figs. 2 and 3 shows that the main structure of the samples of two different aerosol groups from Lake Baikal is the same. There are four main groups: containing (1) Si and Al (mainly silicates and aluminosilicates); (2) S and P (or Cl) (connected with vegetation or industrial pollution); (3) Ca (primarily Ca-containing silicates and gypsum); and (4) Fe (Fe-containing silicates and non-silicate minerals). There is also a number of points which do not belong to any of the above mentioned groups and form intermediate groups.

The main difference between the two triplots shown in Figs. 2 and 3 is the presence or absence of Zn or Pb. (It is interesting to note that in the samples with Pb-containing particles the triplot is

"compressed" in comparison with the samples with Zn-containing particles; see Fig. 4.) However it is clear that this difference is not essential; the structure of the samples remains constant. This is true for all samples which were studied except for sample No. 39. This sample was taken in the middle of the lake, rather far from the shores, under very low wind conditions. The triplot for this sample is shown in Fig. 5. First of all it is seen that there are no organic particles (black rectangle on the right border of a triangle is absent), which is understandable if we take into account the origin of this sample. The Pb-containing particle No. 235 is not situated in the bottom left vertex as usually, due to the presence of Ca. Although the classes of Fe-, Ca-, Al- and Si-containing particles are present, a number of the other intermediate classes are also observed. In the whole, this triplot is less "compressed" in comparison with previously shown due to the absence of organic particles and particles consisting only of pure Pb or Zn.

Just the same triplots as were considered above for the composition of the individual particles can be constructed also for the variables, i.e., for the chemical elements (the average diameter of the particles is also included). Such triplots visualize the clustering of variables. An example of a variables' triplot is given in Fig. 6. It is evident that

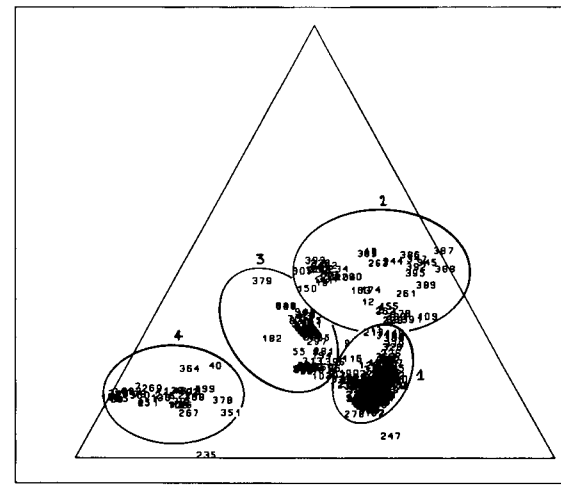

Fig. 5. Triplot showing the data structure of the sample No. 39.

the set of variables can be considered as consisting of several groups. The main group-forming elements Al, Ca and Fe belong to one group, while Si and S belong to another. It is interesting to note that the positions of points corresponding to the contents of Pb and to the average diameter of the particles nearly coincide. This indicates the existing interrelation between them.

The triplots for all samples but sample No. 39 are just the same. The triplot for this sample is shown in Fig. 7. Its structure apparently differs

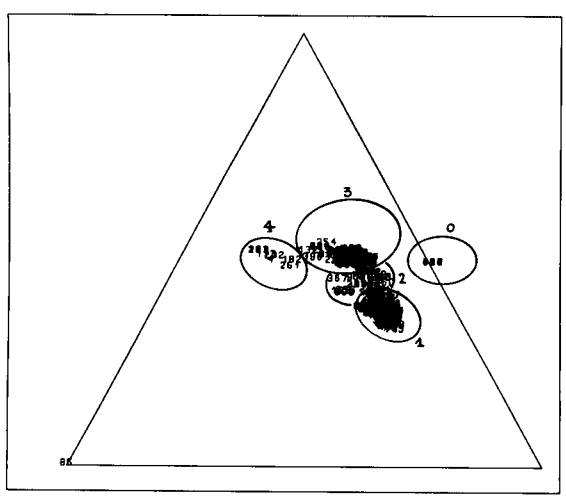

Fig. 4. Typical triplot for a sample containing Zn-rich particles (cf. Fig. 2).

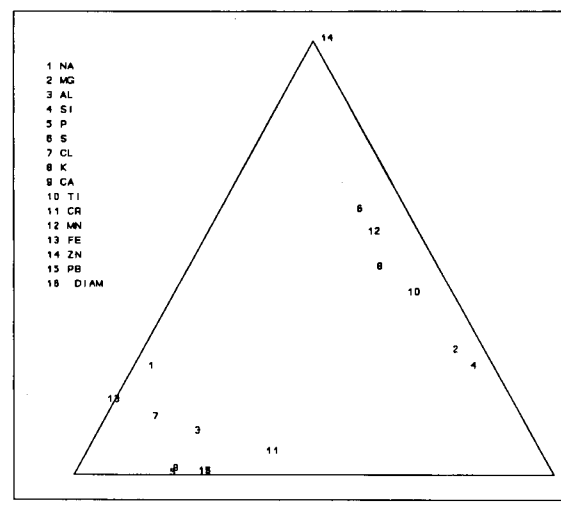

Fig. 6. Clustering of chemical elements for sample No. 3 (see Fig. 2).

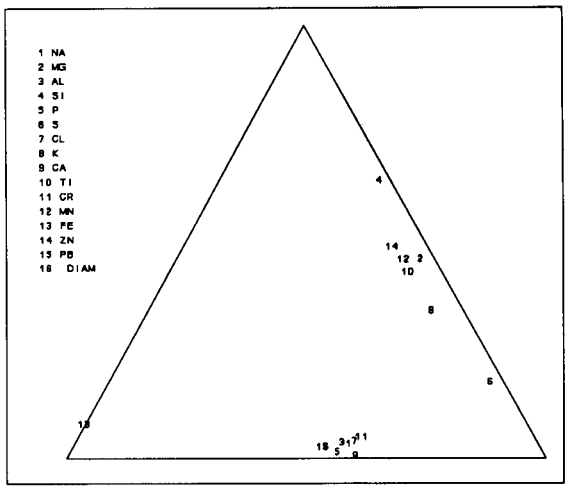

Fig. 7. Clustering of chemical elements for sample No. 39 (see Fig. 5).

from that of Fig. 6 reflecting the differing composition of sample No. 39.

Conclusions

Representation of the results of NLM of the EPXMA of individual aerosol particles in the form of triplots is an efficient method for the fast evaluation of the data structure. It is shown that all but one Lake Baikal aerosol samples consist of five main groups of particles: (1) Si- and Al-containing; (2) S- and P- (or Cl-) containing; (3) Ca-containing; (4) Fe-containing, and (5) organic particles. In one sample, a number of groups with intermediate compositions was also clearly observed.

Triplots built for variables allow to reveal the interrelations between the contents of different chemical elements and average diameter of particles.

One of the authors (B.T.) is indebted to National Science Foundation of Belgium (NFWO) for financial support during his stay at UIA. Sampling of aerosols on Lake Baikal was made possible by the logistical support of Prof. M. Grachev and Dr. T. Khodger (Limnological Institute, Irkutsk) and by financial support (via Prof. J. Klerkx) in the framework of a collaboration agreement between the Belgian Ministry of Science Policy and the Siberian Branch of the Russian Academy of Sciences.

REFERENCES

1 M. Meloun, J. Militki and M. Forina, PC-Aided Statistical Data Analysis, Horwood, New York, 1992.
2 C.M. Rojas and R.E. Van Grieken, Atmos. Environ., 26A (1992) 1231.
3 B. Treiger, J. Injuk, I. Bondarenko, P. Van Espen, L. Breitenbach, U. Wätjen and R. Van Grieken, Analyst, submitted for publication.
4 P.J. Lewi, Multivariate Data Analysis in Industrial Practice, RSP, Chichester, 1982.
5 J.C. Gower, in P. Legendre and L. Legendre (Eds.), Developments in Numerical Ecology, Springer, Berlin 1986, p. 3.
6 P. Artaxo, H. Storms, F. Bruynseels, R. Van Grieken and W. Maenhaut, J. Geophys. Res., 93 (1988) 1605.
7 M.O. Andreae, R.J. Charlson, F. Bruynseels, H. Storms, R. Van Grieken and W. Maenhaut, Science, 232 (1986) 1620.
8 C. Xhoffer, P. Bernard, R. Van Grieken and L. Van der Auwera, Environ. Sci. Technol., 25 (1991) 1470.
9 H. Van Malderen, C. Rojas and R. Van Grieken, Environ. Sci. Technol., 26 (1992) 750.
10 I. Bondarenko, H. Van Malderen, B. Treiger, P. Van Espen and R. Van Grieken, Chemom. Intell. Lab. Syst., in press.
11 T.W. Shattuck, M.S. Germani and P.R. Buseck, Anal. Chem., 63 (1991) 2646.

Analytica Chimica Acta, 284 (1993) 125–130
Elsevier Science Publishers B.V., Amsterdam

Use of the spectral trace length in determining the concentration of known compounds in complex mixtures

Frank R. Burden

Chemistry Department, Monash University, Clayton, Victoria 3168 (Australia)

(Received 6th April 1993; revised manuscript received 27th July 1993

Abstract

The principal of minimum length of a spectral trace has been used to determine the concentration of a known compound in a mixture of other unknown compounds when the unknown compounds are not available for study without the known compound mixed in with them. This method works where the spectrum of the unknown compounds approximates a quadratic curve and does not have spectral peaks in a region where there are spectral peaks of the known compound.

Keywords: Chemometrics; Spectral trace length; Mixtures

A common problem for a chemical analyst is to estimate the concentration of a known, and available, compound in a mixture of other unknown compounds, where the unknown compounds are never available without some of the known compound mixed with them. Unless there are particular chemical or physical methods whereby the known compound can be readily separated from the mixture, the problem is not easily resolved. In this paper a new procedure is proposed which makes use of the *length* of the signal trace of a spectrum rather than the peak heights or areas under the signal. The method is not confined to infrared (IR) spectra but it is most easily demonstrated by this technique.

Such mixture resolutions have been tackled by a variety of methods [1,2] the most well-known of which is that of factor analysis [3,4]. Of course many such problems may be solved by the astute analyst picking an appropriate IR absorbance of the known compound where it can be readily ascertained by direct examination of the mixture spectrum that the unknown compounds are unlikely to be producing confounding absorbances. Factor analysis, when producing concentrations rather than elucidating pure component spectra, relies on the boundary conditions of non-negative concentrations and extinction coefficients.

The method presented here, in making use of the *length* of the signal trace as well as assuming the applicability of Beer's law, is relying on producing a minimum in the signal *length* to produce the concentration of the known component. It is a variant of baseline correction methods [5,6] adapted to situations where the data is stored digitally but avoids the need to fit polynomials and other functions to the observed signals, a procedure which can easily lead to spurious results [7].

The method is presented algebraically together with some operating rules which set the boundaries of the methods' usefulness. This method is then illustrated by using a theoretical example similar to that used in reference [2].

Correspondence to: F.R. Burden, Chemistry Department, Monash University, Clayton, Victoria 3168 (Australia).

0003-2670/93/$06.00 © 1993 – Elsevier Science Publishers B.V. All rights reserved

METHOD

General

Consider a mixture, M, of two components, K and U, where K represents a known and available compound and where U is an unknown compound or mixture of unknown compounds. It is desired to ascertain the concentration of K in the mixture using only the spectra of K and M with no knowledge of the spectrum of U in the absence of K.

Let $A(\lambda)$ be the absorbance at wavelength λ so that

$$A_M(\lambda) = A_U(\lambda) + A_K(\lambda) \quad (1)$$

which can be written as

$$A_M(\lambda) = \{C_U U(\lambda)\} + C_K K(\lambda) \quad (2)$$

where C_U and C_K are the concentrations and, $U(\lambda)$ and $K(\lambda)$ are the absorbances at unit concentration of U and K.

The term $\{C_U U(\lambda)\}$ in Eqn. 2 can be written as $\underline{U(\lambda)}$ since the concentration is not of interest, or is even undefined, here. Eqn. 2 becomes

$$A_M(\lambda) = \underline{U(\lambda)} + C_K K(\lambda) \quad (3)$$

Equation 3 may be differentiated with respect to λ to give

$$A'_M(\lambda) = \underline{U'(\lambda)} + C_K K'(\lambda) \quad (4)$$

Using the formula for the length of a curve the length of the spectral trace $L_M(\lambda_1, \lambda_2)$ from λ_1 to λ_2 is given by

$$L_M(\lambda_1, \lambda_2) = \int_{\lambda_1}^{\lambda_2} \left[1 + A'_M(\lambda)^2\right]^{\frac{1}{2}} d\lambda \quad (5)$$

and the concentration C_K is found by searching for a minimum in $L_M(\lambda_1, \lambda_2)$. Differentiating Eqn. 5 with respect to C_K gives

$$\frac{dL_M(\lambda_1, \lambda_2)}{dC_K} = \int_{\lambda_1}^{\lambda_2} \frac{A'_M(\lambda) K'(\lambda)}{\left(1 + A'_M(\lambda)^2\right)^{\frac{1}{2}}} d\lambda \quad (6)$$

$$= \int_{\lambda_1}^{\lambda_2} \frac{U'(\lambda) K'(\lambda)}{\left(1 + A'_M(\lambda)^2\right)^{\frac{1}{2}}} d\lambda + C_K \int_{\lambda_1}^{\lambda_2} \frac{K'(\lambda) K'(\lambda)}{\left(1 + A'_M(\lambda)^2\right)^{\frac{1}{2}}} d\lambda \quad (7)$$

and these two terms can be represented by I_1 and I_2

$$\frac{dL_M(\lambda_1, \lambda_2)}{dC_K} = I_1 + I_2 \quad (8)$$

If the condition $\frac{dL_M(\lambda_1, \lambda_2)}{dC_K} = 0$ can be found, by numerically subtracting increasing amounts of $K(\lambda)$ from $M(\lambda)$, and the first term, I_1, of Eqn. 8 is zero then C_K is the amount of K subtracted from M. This condition will occur when $U'(\lambda) =$ a constant, i.e., $U(\lambda)$ is linear, and $\int_{\lambda_1}^{\lambda_2} K'(\lambda) d\lambda = 0$.

Linear background

The main variable that is available is to choose the range λ_1 to λ_2. This choice can be made by examining the spectrum of the known compound, K, to pick out some clearly defined absorbances. The integral $\int_{\lambda_1}^{\lambda_2} K'(\lambda) d\lambda$ should be zero which means in practice that the absorbances should effectively reduce to zero, or be equal, at the boundaries λ_1 and λ_2.

If the background is linear, i.e., $\underline{U}(\lambda) = a + b\lambda$ and $U'(\lambda) = b$ then both terms of Eqn. 8 will approach zero as the amount of K subtracted from M approaches C_K, i.e., the shortest distance between two points is a straight line.

Non-linear background

If the background is quadratic, i.e., $\underline{U}(\lambda) = a + b\lambda + c\lambda^2$ and $\underline{U}'(\lambda) = b + 2c\lambda$ the first term of Eqn. 8, I_1, will not become zero unless c can be set to zero. Higher order traces in $\underline{U}(\lambda)$ would prove less suitable though a Lorentzian trace of the type $\frac{\Delta v^2}{(\lambda - \lambda^0)^2 + \Delta v^2}$ can be expanded in a Taylor series with the coefficients of λ^n being $\frac{\Delta v^2}{(\lambda^0)^{2n}}$ when $\Delta v \ll (\lambda - \lambda^0)$ which will be the case for the tail of a Lorentzian. The cubic term $\frac{\Delta v}{(\lambda^0)^6}$ is then likely to be sufficiently small.

IMPLEMENTATION

Using the above arguments, the following strategy may be utilised on instruments where the spectral trace is held in a computer memory in digitisied form. It is assumed that Beer's law applies to K(λ) at low concentrations.

(A) The spectrum, M(λ), of the mixture M must be recorded and stored.

(B) The spectrum, K(λ), of the known compound K must be recorded at a measured concentration. This may be achieved by adding some K to the mixture M and then subtracting the spectrum of M as recorded under A above.

(C) Definitive peak absorbances of K must be identified in the mixture M in a region λ_1 to λ_2 where there are no identifiable spectral maxima due to U(λ).

(D) For the chosen peak absorbances of K the integral $\int_{\lambda_1}^{\lambda_2} K'(\lambda)d\lambda$ should be numerically evaluated. The range λ_1 to λ_2 should be adjusted until the integral differs insignificantly from zero.

(E) The spectrum of K, in known quantity C_K (estimated), should be numerically subtracted form M until the resultant trace has a minimum length, i.e.,

$$\frac{dL_M(\lambda)}{dC_K(\text{estimated})} = 0$$

If the resultant trace is linear then U(λ) must be linear and therefore the concentration, C_K, of K in the mixture M will equal C_K (estimated). The linearity of the resultant trace is easily tested by using the initial slope at λ_1 and continuing the line to λ_2. Variance from linearity is then ascribed to the quadratic term, c, in $\underline{U}(\lambda) = a + b\lambda + c\lambda^2$.

(F) If the quadratic coefficient, c, is non-zero then the spectral trace M(λ) may be initially modified by numerically subtracting $c\lambda^2$ from it. This may be represented by

$$M_1(\lambda) = M_0(\lambda) - c_0\lambda^2 \quad (9)$$

where the subscript 1 represents the first iterative attempt to remove the quadratic term from M(λ).

Steps (E) and (F) may now be applied to $M_1(\lambda)$ so producing $M_2(\lambda)$ and c_1. These steps are then re-applied until c_i is close enough to zero. If c_i is sufficiently close to zero then the amount of K subtracted from M in the last cycle will equal the unknown concentration.

If the final value of c_i in the last cycle differs significantly from zero then the trace of U(λ) in the range from λ_1 to λ_2 cannot be closely fitted to a quadratic. In this circumstance either the range λ_1 to λ_2 must be varied or another peak absorbance of K(λ) tried.

This procedure will work best where the chosen spectral peak of K(λ) lies on a linear or gently curved portion of $\underline{U}(\lambda)$. It will be at its worst, as will a straight application of Beer's law, where the chosen spectral peak of K(λ) lies directly above a similar peak of U(λ). In this case the concentration will be estimated as being too high to the extent of the absorbance of $\underline{U}(\lambda)$. Recourse to more than one peak spectral absorbance of K(λ) is the appropriate safeguard.

EXAMPLES

The method was tested with a theoretical model similar to that of reference [2] using the programming language Mathematica [8] on an IBM style personal computer as well as with a practical illustration using a mixture of toluene and benzene.

For the theoretical model three spectral peaks

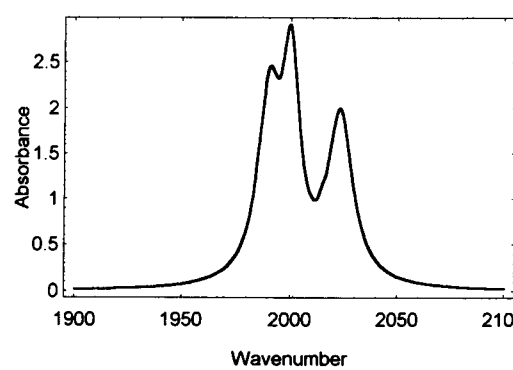

Fig. 1. The three Lorentzian peaks derived from the data in Eqn. 10 and Table 1.

TABLE 1

Lorentzian peak parameters for Fig. 1

	Peak 1	Peak 2	Peak 3
A	0.57	0.67	0.55
Δv	6	5	7
λ^0	1990	2000	2023

shown in Fig. 1 were derived using the data in Table 1 and a Lorentzian spectral shape given by

$$K(\lambda) = \sum_{i=1}^{3} A_i \frac{\Delta v_i^2}{(\lambda - \lambda_i^0)^2 + \Delta v_i^2}$$

where, for peak i, A_i, is the relative absorbance at unit concentration, Δv_i is the peak width at half height and λ_i^0 is the location of the peak maximum.

Figure 2 shows the three peaks of K(λ) superimposed on a background function

$$U(\lambda) = 0.001(1900 - \lambda) + 0.00012(1900 - \lambda)^2 \quad (10)$$

with an arbitrary concentration C_K of K at 3.34 mol dm^{-3}. Equation 10 was chosen to represent a strongly curved baseline which would demand more than one iteration to produce C_K which itself was deliberately specified to 3 significant figures for testing purposes. After a single minimization of the spectral trace length the value of C_K (estimated) was found to be 3.30 and the quadratic term of the remaining curve, c, calculated to be 0.000118. A second pass gave C_K (estimated) at 3.34 with the quadratic term at 2×10^{-6}, which is effectively zero.

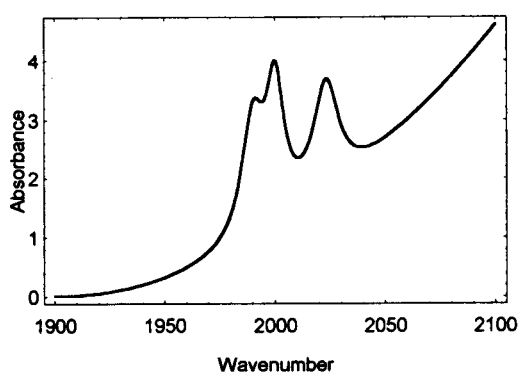

Fig. 2. The Lorentzian peaks plus background.

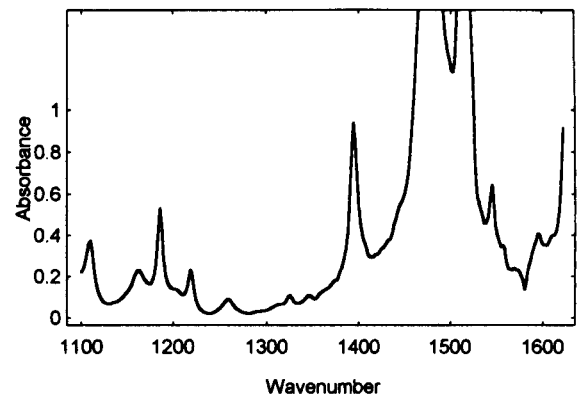

Fig. 3. Toluene.

Although this example represents a single instance in a noise free environment it is sufficient to show a universal applicability. Noise will be partially cancelled by virtue of the integration of Eqn. 5.

For the practical example a mixture of toluene and benzene was made up to a mole fraction of benzene of 0.43, $X_{benzene} = 0.43$. IR spectra were taken of the two pure compounds and of the mixture on a Fourier transform IR spectrometer and the files converted to a form suitable for being read by Mathematica. Although toluene was taken to be the unknown compound, with benzene as the known one, the spectrum of each, and the mixture, are shown in Figs. 3–5 in the

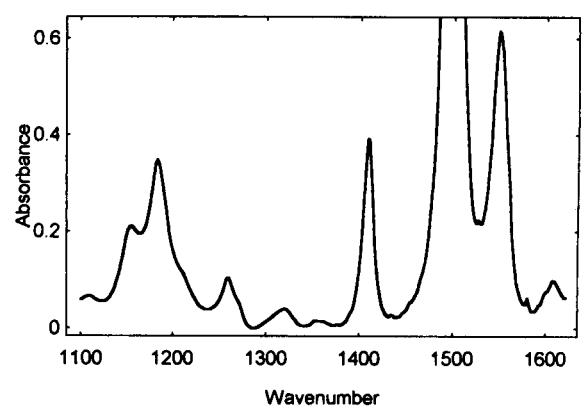

Fig. 4. Benzene.

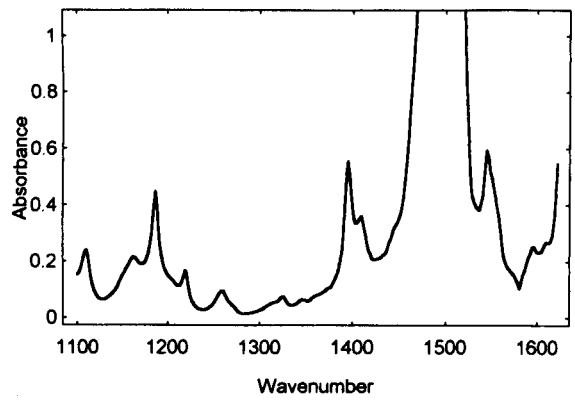

Fig. 5. Mixture.

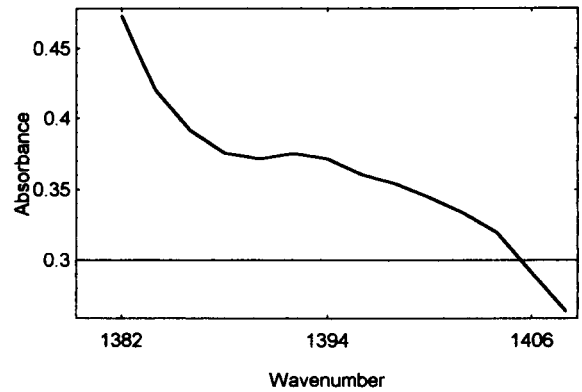

Fig. 7. The mixture spectrum minus the quadratic function.

range 1000 cm^{-1} to 1600 cm^{-1}. The peaks near 1400 cm^{-1} were chosen to illustrate the method and the spectrum from 1360 cm^{-1} to 1420 cm^{-1} is shown in Fig. 6 where the benzene peak is the smaller of the two. The resolution of the two peaks is not as good as in the theoretical example and therefore constitutes a more severe test of the method; the range 1382 cm^{-1} to 1408 cm^{-1} was selected to meet the integration requirement, D, of the implementation section.

To ensure convergence a damping factor of 0.2 was used and convergence was then achieved to $X_{\text{benzene}} = 0.43$, (the exact answer) at the 10th iteration. Figure 7 shows the mixture spectrum with the final quadratic function subtracted and the fact that it deviates from a straight line implies that the toluene trace in the chosen range is of higher order than a quadratic. This must occur because the absorbances of toluene and benzene are insufficiently resolved though it should be noted that the correct result was, nevertheless, produced.

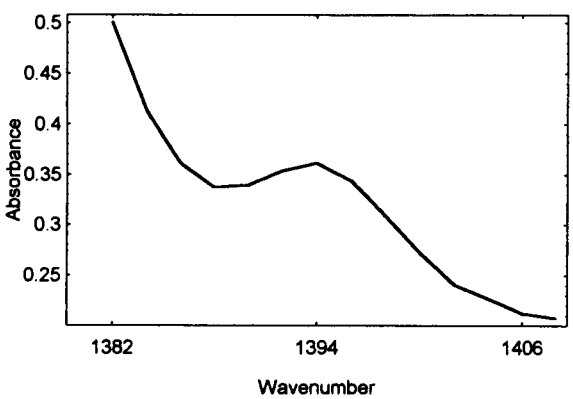

Fig. 6. The toluene and benzene absorbances used in the analysis.

Conclusion

A method has been presented whereby the concentration of a known substance in a mixture with unknown substance can, in many circumstances, be extracted from knowledge of the spectra of the known substance and the mixture alone. It has the strength that it can be automated when coupled with a few rules regarding the selection of the known spectral peak absorbance and the range of integration about this peak.

A weakness of the method relates to overlapping peak absorbances of the known and unknown compounds. If these have exactly the same central wavelength then the problem is not resolvable. However even if they do not have exactly the same central wavelength there is a dividing line at which the problem is potentially resolvable. This line occurs when the underlying part of the unknown spectrum can be reasonably fitted to a quadratic curve in terms of the wavelength, though it would be possible to allow for higher order terms in principle. Whether or not this occurs is testable and to some extent manipulable by defining an appropriate range for the integration about the peak of the known compound.

REFERENCES

1 Y.-C. Ling, T.J. Vickers and C.K. Mann, Appl. Spectrosc., 39 (1985) 463.
2 J. Liu and J.L. Koenig, Appl. Spectrosc., 41 (1987) 447.
3 E.R. Malinowski, Factor Analysis in Chemistry, Wiley, New York, 1991.
4 P.J. Gemperline, S.E. Boyette and K. Tyndall, Appl. Spectrosc., 41 (1987) 454.
5 M.A. Raso, J. Tortajada, D. Escolar and F. Accion, Comput. Chem., 11 (1987) 125.
6 M.A. Raso, J. Tortajada and F. Accion, Comput. Chem., 15 (1991) 29.
7 W.F. Maddams, Appl. Spectrosc., 34 (1980) 245.
8 Mathematica Program Version 2.0, Wolfram Research, 1991.

Analytica Chimica Acta, 284 (1993) 131–136
Elsevier Science Publishers B.V., Amsterdam

Expert system for the interpretation of infrared spectra

G.N. Andreev, O.K. Argirov and P.N. Penchev
Department of Chemistry, University of Plovdiv, 4000-Plovdiv (Bulgaria)

(Received 7th December 1992; revised manuscript received 30th March 1993)

Abstract

An expert system for the interpretation of infrared spectra EXPIRS was created. The main features of EXPIRS are: hierarchical organization of the characteristic groups, realized by frames; registration of the multiple use of spectral bands; taking into account the solvent absorption and the chemical inconsistencies; documenting the interpretation course and providing explanations on request. The ten most important heuristics used by an expert for interpretation of infrared spectra were formulated and some of them were tested with EXPIRS.

Keywords: Infrared spectrometry; Expert systems; Frames; Heuristics; Organic compounds

Computer-assisted interpretation of infrared (IR) spectra has drawn the attention of scientists for more than a decade. Several different approaches have been applied, including the utilization of correlation tables [1–5], symbolic [6–8] and fuzzy [9] logic, expert systems based on rules [10–14 and refs. cited therein] and table-driven procedure [15], frames [16] and, recently, neural networks [17–19]. Most of the authors have formulated their results in the terms of probability predictions for the characteristic groups in the studied compound. These systems produce results in the form of tables: functional groups vs. probability. The final decision for the presence of a given substructure was left to the user. In the general case, however, the user is not a specialist in IR spectroscopy.

An alternative approach is to base the interpretation rules on classical logic, leading to decisions clearly formulated by an expert. This can be achieved using the heuristic knowledge of a human expert in conjunction with the positive characteristics of computers.

The present work deals with the formulation of the principle heuristics used by an expert to interpret IR spectra and the implementation of some of them in an expert system.

Correspondence to: G.N. Andreev, Department of Chemistry, University of Plovdiv, 4000-Plovdiv (Bulgaria).

BASIC CONCEPTS OF THE EXPERT

Until now, we have not found in the literature clear formulated heuristics used by an expert for the interpretation of vibrational spectra. Our experience in structural elucidation of organic compounds by IR spectroscopy and the practice with EXPert in InfraRed Spectroscopy (EXPIRS) have led to the following ten most important heuristics:

(1) Taking into consideration the preliminary information about the studied sample.

(2) Correction of the spectral band intensities, when some of the bands are "obviously too intensive".

0003-2670/93/$06.00 © 1993 – Elsevier Science Publishers B.V. All rights reserved

(3) Comparison between the parameters of the spectrum bands (position, intensity, width) and characteristic group data.

(4) Discussion of the alternatives for the functional group combinations, possibly existing in the compound at hand, satisfying the spectral data.

(5) Discussion of the alternatives for the explanation of spectrum bands' origin: normal vibrations, overtones, combinations, Fermi resonances.

(6) Excluding from consideration the bands used during the interpretation of every alternative, i.e. single use of each band by discussion of every alternative.

(7) Taking into consideration the band shapes as well as the whole spectrum or any of its sectors.

(8) Taking into consideration the absorption of moisture and carbon dioxide.

(9) Taking into consideration spectrum registration conditions: physical condition (influence upon characteristic group intervals and band intensities), solute–solvent interactions, blocking of spectrum intervals caused by solvent absorption, sample concentration (hydrogen bonds), sample thickness, pressure, etc.

(10) Taking into consideration non-spectral reasons: chemical inconsistencies of the functional groups simultaneously predicted in a given alternative; chemical interaction between the solvent used and the predicted functional groups.

It should be noted that this enumeration is not in order of importance because the neglection of any heuristic can lead to wrong conclusions. Furthermore, such an order should not be accepted as and algorithm, because some of the heuristics must be repeatedly applied in the course of interpretation, depending on the nature of the studied molecule.

The third heuristic is the only heuristic used in all expert systems developed for the interpretation of IR spectra. Most of these also use some of the other heuristics described above. However, we have not found any utilization of heuristics 5, 7, 8 and 10 whereas 2 and 6 have been used but not in the same manner as an expert would use them.

The band of each characteristic group has a different relative intensity depending on the other groups included in the same molecule. For example, γ(CH) modes are very strong in the IR spectra of aromatic hydrocarbons but they often appear medium to strong in the spectra of aromatic carbonyl compounds. The common solution for this problem of the system for automated interpretation is enlargement of the intensity interval in the knowledge base. However, this automatically brings one to the so-called "hyperprediction". On the other hand, the expert detecting the presence of the "very strong" ν(CO) modes "expands" the intensity of the other spectrum bands instead of extending the intensity intervals in his mind. The application of this principle in the expert system will avoid the hyperprediction. Heuristic 2 takes into account the latter approach.

The results obtained from EXPIRS testing pointed out that the most significant reduction of the hyperprediction can be achieved by the application of heuristic 6.

EQUIPMENT AND MATERIALS

EXPIRS was developed on an IBM-PC compatible computer with 640 kbyte RAM and the program was written in PASCAL (the system is available on request). 200 spectra from the Sadtler Fourier transform (FT)-IR library were used to test the system as well as spectra registered in our laboratory on a Perkin Elmer 1750 FT-IR spectrometer with a resolution of 2 cm^{-1}.

More than 70 characteristic groups containing the elements C, H, O and N were incorporated in the system and the appropriate rules for their interpretation were programmed.

Program description

The expert system is based on the concept of "characteristic group intervals". [20]. There are three levels in EXPIRS (Fig. 1). The first two levels involve the process of interpretation; the third one (documentation) is designed to register the interpretation course and the number of spectrum peaks used during the work of the program.

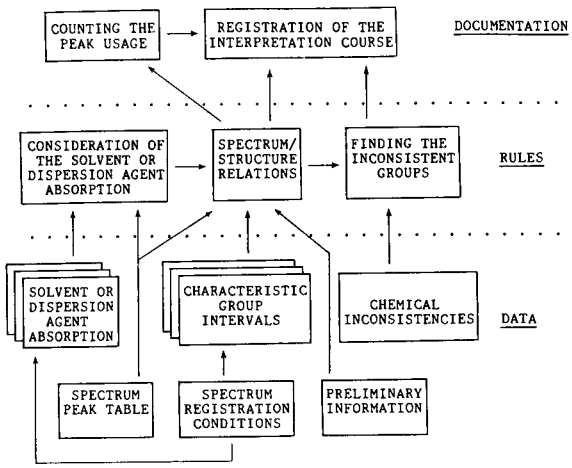

Fig. 1. Flow chart of EXPIRS.

The data for the characteristic intervals, solvent absorption and chemical inconsistency were realized as arrays of the appropriate variables.

Analysis of the literature, combined with our experience, reveals that the groups are best organized hierarchically. Such an approach avoids repeating the interpretation of the spectral intervals. For example, the primary $-CH_2-OH$, secondary $>CH-OH$ and tertiary $\geq C-OH$ alcohols have a common interval at 3600–3200 cm^{-1} due to the stretching vibration of the hydroxyl group $\nu(OH)$. The triple verification of this interval can be avoided if the characteristic OH group, which determines this interval, is used as a "parent group". In this case, the rules for the different alcohols (primary, secondary and tertiary) must take into account not only the entire spectrum, but also the status of the parent group OH. Such an approach was utilized in the description of other characteristic groups, including alkanes, alkenes, amines, aldehydes, etc. This type of group organization corresponds to the chemist's knowledge that the primary, secondary and tertiary alcohols are special cases of the concept "alcohol". In other words such an organization reflects the different levels of abstraction of the chemical structure in the chemist's mind.

We have used frames to realize the hierarchical organization of the characteristic groups in our expert system (Fig. 2). The principal frame in

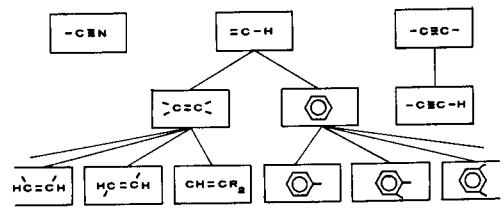

Fig. 2. Hierarchical organization of the frames in EXPIRS.

the program is the frame "Characteristic group"; two specifications of this frame are given in Fig. 3 for the groups sp^3C-H and CH_2.

When the system checks for the presence of the methylene group CH_2 it needs data for its parent group sp^3C-H. If the status of the parent group has yet to be discovered, the procedure starts with its frame, etc. There are no limitations to the depth of such parent group checks. This makes the system independent on the group order in the data base and on the user's range of demand, which differentiate EXPIRS from the approaches utilized elsewhere [10,16,21].

One can readily see (Fig. 3) that the parent group and its "generics" belong to the same frame and the hierarchy mentioned above is de-

Characteristic group:	
Name:	sp^3CH
String for the screen:	sp3C-H
Conclusion for presence:	Received by a procedure based on data for the characteristic intervals, spectrum, solvent absorption.
Parent group:	
Name:	Absent
Conclusion for presence	Absent
Characteristic intervals:	
Interval No 1:	3000-2800 cm^{-1} weak to strong
Characteristic group:	
Name:	CH_2
String for the screen:	CH2
Conclusion for presence:	Received by a procedure based on data for the parent group, characteristic intervals, spectrum, solvent absorption.
Parent group:	
Name:	sp^3CH
Conclusion for presence	Received
Characteristic intervals:	
Interval No 1:	1480-1430 cm^{-1} weak to strong

Fig. 3. Two entities from the frame "characteristic group": sp^3C-H and CH_2.

termined not as frame hierarchy, but by means of the connection "parent group" between the different specifications of the same frame "characteristic group".

Operation of the system

The interaction between the user and the system is determined by the appropriate menus. There are three main options: INTERPRETATION, CONCLUSIONS, SAVING THE RESULTS.

In the option INTERPRETATION the user:

- puts in the name of the spectrum file; interaction mode can be selected;
- defines the intensity margins for strong, medium and weak peaks;
- puts in the solvent or the disturbing media for the measured sample;
- gives preliminary information (based on analysis or the origin of the sample) for the absence of some groups as well as the kind of the groups of interest.

The option CONCLUSIONS provides information on the groups whose presence in the studied molecule is positive, negative or uncertain. The user can request explanation about the arguments on which the conclusion is based. Additional information on positively predicted groups which are not chemically coincident is available.

In the option SAVING THE RESULTS the user can save on disk or print the results of the interpretation.

RESULTS AND DISCUSSION

We have obtained excellent to satisfactory agreement between the predicted and existing characteristic groups by testing the developed expert system with the IR spectra, measured in our laboratory or included in the Sadtler FT-IR library.

The following examples of EXPIRS' work illustrate the importance of some heuristics described above.

The interpretation of the spectrum of DL-2-methylbutanoic acid [$CH_3CH_2CH(CH_3)COOH$] gives a report for the presence of the following characteristic groups: sp^3C–H, CH_2, CH_3, COOH, alkyl–COOH. As seen EXPIRS identifies all three functional groups of the studied substance. It further specifies that the carboxylic group is aliphatic. The presence of C–H with sp^3-hybridized carbon atom is also mentioned.

Along with the correct predictions we also received some incorrect answers by the spectral interpretation. The latter can be divided into two different types: (1) negative statement for a characteristic group existing in the studied molecule; (2) positive statement for a characteristic group that is absent in the studied compound.

We found that one could eliminate the first kind of incorrect answers by improving the data base. The errors of the second type, which appear more frequently (hyperpredictions), could not be avoided by the same manner. The latter are connected with the multiple use of the same bands in the course of interpretation. Our program was supplied with a counter in order to register the multiplicity of band usage.

The hyperprediction will be illustrated by the interpretation of the spectrum of isopropylbenzene. EXPIRS reveals the existence of the following characteristic groups: sp^3C–H, CH_2, CH_3, i-Pr, =C–H, C=C, *cis*-CH=CH, aryl, Ph–, *o*-aryl.

This interpretation is based on the spectrum bands given in the following format: wavenumber(bandwidth) – multiplicity of band's usage: 3083(m) – 1, 3064(m) – 1, 3029(s) – 1, 2963(s) – 1, 2929(s) – 1, 2889(s) – 1, 2873(s) – 1, 2802(m) – 1, 1949(m) – 0, 1872(w) – 0, 1804(m) – 1, 1744(w) – 0, 1665(w) – 1, *1605(m) – 2*, 1533(w) – 0, 1496(m) – 0, 1465(s) – 1, 1451(s) – 1, 1386(m) – 3, 1364(m) – 3, 1320(m) – 1, 1300(m) – 1, 1279(m) – 1, 1208(w) – 0, 1102(m) – 0, 1079(m) – 1, 1048(m) – 2, 1027(m) – 2, 921(m) – 0, 905(m) – 0, 777(w) – 0, *761(s) – 4*, *697(s) – 4*, 531(m) – 1, where s = strong, m = medium and w = weak.

The multiple use of the 1605, 761 and 697 cm^{-1} bands is the reason for the C=C, *cis*-CH=CH and *o*-aryl groups hyperprediction. Obviously, one could eliminate such incorrect predictions by tak-

ing into account the multiple use of each spectral band.

The ability of EXPIRS to take into consideration the influence of the solvent or dispersion agent used will be illustrated by the interpretation of the spectrum of D-glucose measured in nujol mull (wavenumber/relative intensity bandwidth): 3408/0.810, 3306/0.833br, 2925/0.905, 2855/0.828, 1459/0.720, 1376/0.662, 1340/0.630, 1296/0.568, 1224/0.568, 1203/0.570, 1149/0.695, 1111/0.751, 1078/0.611, 1050/0.753, 1024/0.824, 996/0.798, 916/0.597, 838/0.592, 775/0.559, 723/0.531, 614/0.709.
The following message appears after the interpretation:

(1) There are spectral data for PRESENCE of the following groups: OH, RCH_2–OH, R_2CH–OH, R_3C–OH, Ar–OH, R–O–R, R–O–Ar, > N–H;

(2) The presence of the following groups is UNCERTAIN: sp^3C–H, CH_2, $(CH_2)_4$, CH_3, i-Pr, *t*-Bu, Ar–NH.

The second report deals with the groups whose characteristic intervals overlap with those of the dispersion media (or solvent used).

An important feature of EXPIRS is that the user can follow the logic of the interpretation upon request. If the user wants to provide an explanation for any of the above results, he can use the option EXPLANATION. He goes to the option CONCLUSIONS and designate the correspoding group of interest. For example, the following messages will appear for the groups R_2CH–OH and CH_2:

```
R2CH-OH .....
REPORT: The conclusion for presence of OH is
        POSITIVE
        Is there a strong band between 1120
        and 1080?
        YES: 1111 (s)
        There are spectral evidences for pres-
        ence of R2CH-OH
Press any key to continue...

CH2.....
REPORT: The conclusion for presence of sp3C-
        H is UNCERTAIN
        TOTAL OVERLAPPING WITH
        THE SOLVENT BANDS
        The presence of the CH2 is UNCER-
        TAIN
Press any key to continue...
```

This possibility makes the expert system appropriate for educational purposes as well.

The authors wish to thank the Bulgarian National Fund of Research at the Ministry of Education and Science for partial financial support through Grant No. X-124/91.

REFERENCES

1 T. Visser and J.H. van der Maas, Anal. Chim. Acta, 122 (1980) 363; Anal. Chim. Acta, 133 (1981) 451.
2 M. Farkas, J. Markos, P. Szepesvary, I. Bartha, G. Szalontai and Z. Simon, Anal. Chim. Acta, 133 (1981) 19.
3 G. Szalontai, Z. Simon, Z. Csapo, M. Farkas and Gy. Pfeifer, Anal. Chim. Acta, 133 (1981) 31.
4 B. Debska, J. Duliban, B. Guzowska-Swider and Z. Hippe, Anal. Chim. Acta, 133 (1981) 303.
5 W.-R. Leupold, C. Domingo, W. Niggemann and B. Schrader, Freszenius' Z. Anal. Chem. 303 (1980) 337.
6 L.A. Gribov and M.E. Elyashberg, J. Mol. Struct., 5 (1970) 179; J. Mol. Struct., 50 (1978) 351.
7 L.A. Gribov, M.E. Elyashberg and L.A. Moscovkina, J. Mol. Struct., 9 (1971) 357.
8 K. Funatsu, Y. Susuta and S. Sasaki, Anal. Chim. Acta, 220 (1989) 155.
9 T. Blaffert, Anal. Chim. Acta, 161 (1984) 135.
10 H.B. Woodruff and G.M. Smith, Anal. Chem., 52 (1980) 2321.
11 S.A. Tomellini, D.D. Saperstein, J.M. Stevenson, G.M. Smith, H.B. Woodruff and P.F. Seelig, Anal. Chem., 53 (1981) 2367.
12 S.A. Tomellini, R.A. Hartwick and H.B. Woodruff, Appl. Spectrosc., 39 (1985) 330.
13 B.J. Wythoff, C.F. Buck and S.A. Tomellini, Anal. Chim. Acta, 217 (1989) 203.
14 H.J. Luinge, Vib. Spectrosc., 1 (1990) 3.
15 M.O. Trulson and M.E. Munk, Anal. Chem., 55 (1983) 2137.
16 P. Edwards and P.B. Ayscough, Chemom. Intell. Lab. Syst., 5 (1988) 81.
17 E.W. Robb and M.E. Munk, Mikrochim. Acta (Wien) I, (1990) 131.
18 M.E. Munk, M.S. Madison and E.W. Robb, Mikrochim. Acta (Wien) II, (1991) 505.
19 K.J. Fessenden and L. Gyorgyi, J. Chem. Soc. Perkin Trans 2, (1991) 1755.

20 N.B. Colthup, L.H. Daly and S.E. Wiberlay, Introduction to Infrared and Raman Spectroscopy, Academic Press, New York, 1975; L.J. Bellamy, The Infrared Spectra of Complex Molecules, Methuen, London, 1964; K. Nakanishi, Infrared Absorption Spectroscopy, Holden-Day, San Francisco, CA, and Nankodo, Tokyo, 1962.
21 H.J. Luinge and J.H. van der Maas, Anal. Chim. Acta, 223 (1989) 135.

Analytica Chimica Acta, 284 (1993) 137–147
Elsevier Science Publishers B.V., Amsterdam

Chemical composition analysis of carrageenans by infrared spectroscopy using partial least squares and neural networks

Sven P. Jacobsson [1] and Anders Hagman [2]

Kabi Pharmacia AB, S-112 87 Stockholm (Sweden)

(Received 25th January 1993; revised manuscript received 15th April 1993)

Abstract

The use of partial least squares and neural networks is described for the multivariate analysis of the chemical composition of carrageenans by infrared spectroscopy. The content of κ-, ι- and λ-carrageenan is determined in standard mixture samples and in production batches of carrageenans. Various models of PLS and neural networks are examined using a designed ternary mixture of different carrageenan forms and the use of up to 36 independent variables selected from the infrared spectrum of the carrageenans. Both models can be applied for an accurate and rapid chemical composition analysis, although the neural networks model performs slightly better and appears to be more consistent.

Keywords: Infrared spectrometry; Chemometrics; Carrageenans; Neural networks

Carrageenan is a generic term for a group of commercially important galactan sulfates extractable with hot water from some members of the class *Rhodophyceae* (red seaweed). Carrageenans are used extensively in the food and pharmaceutical/cosmetic industry as viscosity/gel or texture enhancers, stabilisers, etc. The backbone of the polysaccharide is formed of alternating α-1,3- and β-1,4-linked D-galactopyranose units. The carrageenans are classified according to the presence of the 3,6-anhydro-D-galactose on the 1,4-linked residue and the position and the number of sulfate groups. Three primary forms (κ-, ι-, λ-) of carrageenan are identified based on the modification of the disaccharide repeating unit resulting from the occurrence of ester sulphate, or anhydride formation in the 4-linked residue. κ- and ι-carrageenans contain the 3,6-anhydro unit and form thermoreversible gels in solution while λ-carrageenan with only galactose units yield highly viscous solutions that do not gel. There are considerable differences in substitution patterns from the idealised carrageenan forms, and this masks the repeating units.

Structural characterisation and chemical analysis of carrageenans can be performed in a number of ways ranging from spectroscopic analysis with IR, NMR, classical light scattering to chromatographic or hyphenated techniques as pyrolysis GC–MS and size-exclusion chromatography [1–8]. Other techniques are gel breaking strength measurements, gravimetric sulfate determinations, immunologic and enzymatic methods [2].

Correspondence to: S.P. Jacobsson, Kabi Pharmacia Therapeutics AB, S-751 82 Uppsala (Sweden).

[1] Present address: Kabi Pharmacia Therapeutics AB, S-751 82 Uppsala (Sweden).

[2] Present address: Kabi Pharmacia Peptide Hormones, S-112 87 Stockholm (Sweden).

0003-2670/93/$06.00 © 1993 – Elsevier Science Publishers B.V. All rights reserved

Chemical composition analysis of carrageenans can be carried out using classical chemical polysaccharide analysis, i.e., hydrolysis and derivatization followed by gas chromatographic analysis of the formed derivatives. This methodology discloses detailed information on the chemical composition but is to some extent too lengthy and cumbersome to be implemented for routinely performed pharmaceutical raw material analysis.

NMR spectroscopy has some powerful features with respect to chemical structure analysis of polysaccharides [6]. For carrageenans the NMR technique could be conveniently used for structure analysis of κ- and ι-carrageenans. For λ-carrageenan, however, especially at higher concentrations necessary for carbon-13 work, NMR is not applicable due to the low molecular mobility of the carrageenan in the highly viscous solution [9]. A straightforward way to circumvent this difficulty is to use solid state NMR for structural characterisation of carrageenans [9]. The availability of NMR, especially solid state NMR is, however, quite low.

Infrared spectroscopy is routinely used in pharmaceutical analysis, mainly for identification purposes. IR spectroscopy is also one of the standard techniques used for characterisation of carrageenan and a number of studies have been conducted in which the different structure elements of carrageenan are assigned to different absorption bands [1,3,4]. The IR technique is rapid, non-destructive and needs only a few mg of sample.

There are several infrared absorption bands which provide information about characteristic structural elements in carrageenan. The presence of for example 3,6-anhydrogalactose (928–940 cm^{-1}), ester sulfate (1240 cm^{-1}), 3,6-anhydrogalactose-2-sulfate (805 cm^{-1}) [2] and galactose-4-sulfate (850 cm^{-1}) [1] in carrageenans could be provided. In the work published by Rocchas et al. [3] IR has been used to determine the sulfate content of carrageenans and agars. The ratio of absorbance at 1370, 1250, 845, 805 cm^{-1} to 2920 cm^{-1} provides a rapid method for the estimation of sulfate content from IR spectra of agars and carrageenan, thus providing indirect information of the chemical composition of carrageenan. Anderson et al. (e.g., Ref. 1) have used IR extensively as a structural determination tool. Throughout the above given works the assignment of structure and structure elements in carrageenan is based on precise absorption bands/peaks on an univariate level. This approach is based on the assumption that these bands are unique and not confounded. However, as pointed by Anderson et al. [1] it seems doubtful whether the precise positions of the infrared bands of carbohydrate sulfates can in general be safely predicted and that it is necessary to examine the spectra of model compounds for each sulfate ester of interest.

Multivariate data analysis has shown to be a very powerful tool in spectroscopy for the selectivity and reliability enhancement, especially when the information in the spectrum is diffuse and the absorption bands, as in UV and near-IR, show overlap [10]. Especially, principal component regression (PCR) and partial least squares (PLS) have received considerable attention in the chemometrical literature [10]. The high degree of collinearity of the IR absorbances data is an advantage in calibration since the inclusion of redundant information in the form of covarying or overlapping signals makes the model more stable towards noise and eases the task of detecting outliers. Essentially, more information is available and low-dimensional projections of the variable and object space usually can be found which are representative for the major sources of variation (information) in the data. One other attractive feature of multivariate data analysis based on the latent variable approach is that no a priori information on correlation between the dependent and the independent variable needs to exists. Furthermore, there are less limitations in the proportion on objects to variables in comparison to classical statistical analysis. However, PCR and PLS are linear techniques, and are thus limited to linear regression problems. Although the inclusion of extra principal components or latent variables in the model, have been shown to be able to model slight deviations from linearity [11].

Feed-forward neural networks (NN) have, on the other hand, shown to be able to approximate

any linear or non-linear continuous function with arbitrary accuracy [12]. A widespread interest in neural networks has emerged during the last years within the chemistry field, resulting in numerous applications including pattern recognition of chromatographic data [13], continuous learning using sequential processing of spectroscopic data [14], non-linear multivariate calibration [11], identification [15], and infrared spectrum interpretation [16]. Neural networks resemble to some extent PLS, but lack some of the diagnostics and explanatory tools available in PLS and PCR, e.g., latent variable projections.

In this work the combination of infrared spectroscopy and partial least squares or neural networks is examined with the purpose to develop a mathematical relationship between spectral measurements and the relative chemical composition of carrageenans. This would allow us to predict the relative concentration of the principal constituents of different carrageenans, in a short and accurate manner, by a rapid IR analysis of a production batch. Furthermore, indications of the chemical structure are evidently of use in the evaluation of the production behaviour of different batches of carrageenans.

Although the relationship between IR absorbance and concentration is basically a linear calibration problem, the effects of saturation, peak shifts, inconsistent peak assignment, and noise may introduce non-linearity on the correlation of spectral data to concentration. Slight deviations, due to certain effects, from linearity are possible to model by introduction of extra components in the PLS model, but effects such as peak shifts and poor peak assignment are probably less successfully adjusted for. However, the main motive for this study was to impartially examine neural networks as an alternative to PLS. Since, in this study as it was performed, the non-linearity effects given above are less likely to impair on the linear relation on IR absorbance and the carrageenan concentration.

A designed ternary data set of carrageenans has been used for training and testing, and for the evaluation of the predictive performance/capability of PLS and NN. Furthermore, a comparison of the results generated on seven production batches of carrageenans are presented and discussed.

THEORY

The theory and applications of partial least squares (PLS) in the field of analytical chemistry are nowadays well established [10], and since the PLS work carried out in the present study utilises a commercial software package, which has been described elsewhere [17], this brief theory part is solely focused on the feed-forward neural networks implemented in this study. For a more comprehensive description of neural networks there are several reviews and books available, see for example [18–21].

Artificial neural networks consist of simple processing elements, nodes, see Fig. 1. These nodes can be thought of as neurones, their biological counterpart. The output y of the node is given as;

$$y = \mathrm{f}\left(\sum_{i=1}^{n} w_i x_i + w_0 \right) \tag{1}$$

where $x = (x_1, \ldots, x_n)$ is the input to the node, the vector $w = (w_1, \ldots, w_n)$ gives the weight, and $f(\cdot)$ is the transfer function at the output. The term w_0 is here called bias and it is responsible for accommodating non-zero offsets in the data. The transfer function could be any function, but virtually all that have been used in analytical chemical context are sigmoids. The use of functions as the sigmoid function [2] allows the standard feed-forward network architecture to model virtually any function of interest to any degree of accuracy [12].

$$\mathrm{f}(x) = \frac{1}{1 + \mathrm{e}^{-(x)/\theta_0}} \tag{2}$$

The sigmoid function has a output in the range from 0 to 1, where x is the weighted sum of the inputs plus the bias, and θ_0 is the gain. The value of the gain modifies the slope of the sigmoid function.

In the training phase a set of input patterns/objects with their corresponding expected output

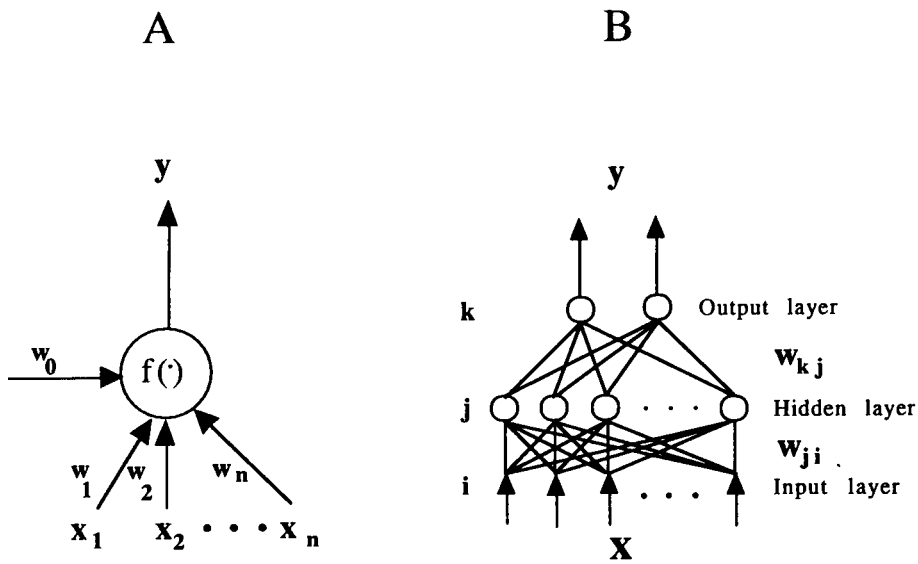

Fig. 1. (A) A node, the basic computational element of neural networks. $x = (x_1, \ldots, x_n)$ input/independent variables, $w = (w_1, \ldots, w_n)$ the corresponding weight factors, w_0 = bias. (B) A two layer neural network.

values are presented in an iterative fashion to the network. After each presentation the network adjusts the set of weights in the connection links and also all the bias in the nodes. This process continues either until the accuracy between the expected and the actual output ceases to improve, the maximum number of iterations is reached or the predetermined level of prediction precision (err_goal) of the average system or of the individual objects is reached.

In general, for each pattern/object the output $\{o_k\}$ differs from the expected or target values $\{t_k\}$. For each pattern/object the squares of the error is,

$$E = \sum_k (t_k - o_k)^2 \tag{3}$$

and the average sum-squared error is,

$$E_{pk} = \frac{1}{P} \sum_p \sum_k (t_{pk} - o_{pk})^2 \tag{4}$$

where t_{pk} is the expected output for pattern p at node k, and o_{pk} is the actual output from the net for pattern p at node k.

In the generalised delta rule formulated by Rumelhart et al. [19] for learning the weights and bias, convergence toward improved values in the weights and bias is achieved by taking incremental changes Δw_{kj} proportional to $-\partial E/\partial w_{kj}$ that is,

$$\Delta w_{kj} = -\eta \frac{\partial E}{\partial w_{kj}} \tag{5}$$

where η is the learning rate and Δw_{kj} is the change in the weight between output node k and the node j in the previous layer, see Fig. 1.

The partial derivative $\partial E/\partial w_{kj}$ can be evaluated using the chain rule [21], assuming that the error, E, is expressed in terms of the output o_k at node k. That is,

$$o_k = f\left(\sum w_{kj} o_j\right) \tag{6}$$

where $\sum w_{kj} o_j$ is the output to the kth node and is the weighted linear sum of all the outputs from the previous layer.

Using the definition,

$$\delta_k = -\frac{\partial E}{\partial\left(\sum w_{kj} o_j\right)} \tag{7}$$

it could be stated that for any output layer node k, that,

$$\Delta w_{kj} = \eta (t_k - o_k) f_k'\left(\sum w_{kj} o_j\right) o_j = \eta \delta_k o_j \tag{8}$$

where Δw_{kj} is the change in weight between node k in the output layer and node j in the hidden layer. When the output transfer function is a sigmoid the output layer error is given by,

$$\delta_k = (t_k - o_k)o_k(1 - o_k) \quad (9)$$

where δ_k is the error term at node k. For the hidden layer the corresponding error term is,

$$\delta_j = o_j(1 - o_j)\sum_k \delta_k w_{kj} \quad (10)$$

where δ_j is the error term at the hidden node j, and o_j the output from node j. The bias is learned in the same manner as of the other weights, assuming that the bias always has an output node of unity.

In order to improve the system error of the net, the error terms from the output and hidden layer are back-propagated through the net at each iteration by making adjustments to the weights of their respective layer. Weight adjustments, or delta weights are calculated as,

$$\Delta w_{ji}(n + 1) = \eta(\delta_j o_i) + \alpha \Delta w_{ji}(n) \quad (11)$$

where the term $n + 1$ and n indicates the present iteration and the previous iteration, respectively and α is the momentum term. By the introduction of the second term in expression [11] a degree of similarity is specified in the weight adjustment of the present step to the previous step [19].

The first step in the learning/training procedure is to set the weights to random values, choosing one of the training set objects, and using that object as input, evaluating the output(s) in a feed-forward manner. Using the back propagation procedure each object in the training set sequentially contributes to the change of the weights in the net. After complete presentation of the objects in the training set, a new set of weights are obtained, and new outputs are evaluated in a feed-forward manner. This proceeds iteratively until the predetermined level of precision is reached (err_goal), or the maximum number of iteration is reached. The outcome of the net with respect to calibration will be dependent on the net architecture, i.e., the number of nodes, the number of hidden layers, the values chosen for the learning rate and momentum term and the degree of precision wanted. The predictive capability of the net is not only dependent on these factors but also strongly reflects how well the training set is representative of the test set.

EXPERIMENTAL

Two different batches of κ-, ι-, and λ-carrageenan (Sigma, St. Louis, MO) were used without further purification. Production batches of carrageenans with unknown chemical composition (A–D) and known chemical composition (E–G) (Table 1) were supplied by different suppliers. The water content and sulfate content of the carrageenans were determined by weight loss and gravimetrically as barium sulfate, respectively (see Table 1).

KBr tablets (300 mg) with approximately 5 mg of carrageenan were subjected to IR analysis. A Perkin-Elmer dispersive IR instrument, Model 580B, was used. The IR spectrum was manually, by using a ruler, converted to a data table, consisting of two subsets, using normalised peak height and by use of two different baseline criteria as outlined in Table 2.

Independent variables 1–18 (subset 1) are based mainly on defining peaks in the absorption spectrum of carrageenan, whereas independent variables 19–36 (subset 2) are based on distances

TABLE 1

Content of water and sulfate in the carrageenan batches

Carrageenan	Water content (%, w/w)	Sulfate content of dry carrageenan (%, w/w)
κ- [a]	13.9; 11.6	32.1
ι- [a]	13.6; 14.2	37.4
λ- [a]	9.5; 10.5	36.0
Batch A	9.0	31.1
Batch B	5.9	28.6
Batch C	4.2	30.5
Batch D	3.6	31.5
Batch E	5.9	n.d.
Batch F	n.d. [b]	n.d.
Batch G	n.d.	n.d.

[a] Two different batches, sulfate content on only one batch.
[b] n.d. = not determined

TABLE 2

Absorption bands and baseline criteria used to convert the IR spectrum to a data table form using peak height or distance to a common baseline

Variable No.	Peak (cm^{-1})	Baseline (cm^{-1})
1	2960	3025–2750
2	2930	3025–2750
3	2910	3025–2750
4	1260	1340–1180
5	1155	1180–1140
6	970	980–955
7	930	955–900
8	890	900–875
9	845	875–815
10	825	875–780
11	805	815–780
12	770	785–760
13	730	760–720
14	700	720–680
15	1070	1350–660
16	1035	1350–660
17	1010	1350–660
18	980	1350–660
19	1260	1350–660
20	1230	1350–660
21	1155	1350–660
22	1070	1350–660
23	1035	1350–660
24	1010	1350–660
25	980	1350–660
26	955	1350–660
27	930	1350–660
28	890	1350–660
29	875	1350–660
30	845	1350–660
31	825	1350–660
32	815	1350–660
33	805	1350–660
34	770	1350–660
35	730	1350–660
36	700	1350–660

to a common baseline. In the first set the variables are normalised to variable 3 and in set 2 to variable 19, thus reducing the effect on variation in sample preparation, since only the relative concentrations of κ-, ι-, and λ-carrageenan were of interest in the present work. For the calibration an experimental design with 24 samples was set up to span the relative concentration range (0–100%) of each carrageenan form (Table 3). The samples were prepared by dry-mixing the individual carrageenan forms. The calibration set was used for training of the PLS and neural networks models used for prediction of the relative carrageenan composition of the seven production batches, constituting the test set.

To allow for a more in-depth comparison between PLS and neural networks, the prediction of the concentration of κ-, ι-, and λ-carrageenan in five samples constituting the validation set were examined. Samples 4, 8, 14, 15, and 18 were chosen as validation objects, from the designed ternary mixture of different carrageenan forms, see Table 3. The remaining 19 objects constituted the training set. The validation set was chosen so as to allow a good agreement between the training and validation set of κ-carrageenan, i.e., the concentration space is well spanned for the training set and the concentration of κ-carrageenan in

TABLE 3

Relative chemical composition of carrageenans in the calibration set

Sample No. [a]	κ-Carrageenan (%)	ι-Carrageenan (%)	λ-Carrageenan (%)
1	100	0	0
2	0	100	0
3	0	0	100
4	49.9	32.9	17.2
5	16.8	49.6	33.6
6	33.1	17.3	49.6
7	89.8	10.2	0
8	90	0	10
9	0	10.3	89.7
10	9.6	0	90.4
11	100	0	0
12	0	100	0
13	0	0	100
14	11.3	77.4	11.3
15	67	20.4	12.6
16	10.3	11.4	78.3
17	32	31.5	36.5
18	31	18.6	50.4
19	53.4	30.6	16
20	0	90	10
21	90.7	9.3	0
22	49	51	0
23	52.4	0	47.6
24	0	51	49

[a] Samples 1–10 have different Sigma batch origins than samples 11–24.

the validation set covers almost equal distance in the concentration range 0 to 100 percent. For the ι and λ forms the agreement between training and validation set was less apparent. In the following the relative composition of the carrageenan forms will be given corrected for the content of water, contrary to what is given in Table 3. The prediction capability is calculated according to Eqn. 4, i.e., the average sum-squared error.

To build the best predictive PLS model, several combinations of data may be examined and sometimes principal components of the spectra can be used as variables in the model. However, a straight forward PLS regression procedure was carried out on the calibration set and training set. These sets are modelled by selecting an optimal number of PLS components to represent the complexity of the systems without overfitting the model. This is done by utilising cross-validation. However, it is also of importance to use spectral peaks/data that show large variance and high correlation with concentration. Otherwise, the non-correlated peaks introduce a noise into the model and the predictive capability is decreased. In this study, however, the PLS models of the different carrageenan forms contained all of the variables in Table 2, in order to facilitate a comparison of the neural networks model and the PLS models. The PLS models were trained by using the three different carrageenan forms, i.e., dependent variables, simultaneous (PLS 2) or separately (PLS 1).

Principal component analysis and partial least squares were run on a SIRIUS data package (Pattern Recognition Systems Ltd., Norway). The regression analysis was performed after correction for content of water. The whole data set was autoscaled, i.e., each variable was scaled to zero mean and unit variance.

For neural networks the same calibration, training, validation, and test sets were used, although the independent variables 1–36 were not standardised, i.e., not mean centred and scaled to unit variance.

The net architecture utilises all of the independent variables as input, and learning is carried out for one carrageenan form at the time. The analysis was performed after correction of water content, and scaling of the carrageenan concentration to the range 0.1 to 0.9 by adding an offset and multiplying by a constant.

The feed-forward neural networks program was written in-house using C (Borland Turbo C + +) but essentially follows the program outlined by Pao [21] and utilises the generalised delta rule as learning algorithm. The program was modified so as to allow use of script files, more efficient and larger data set handling, and improved result generation and presentation.

The data analysis was run on a Dell 425E personal computer (Dell, Austin, TX).

RESULTS AND DISCUSSION

The optimisation of neural networks with regard to the prediction capability is by itself a multivariate optimisation problem. The prediction ability is dependent to varying degrees on the following factors constituting elements in the feed-forward neural networks algorithm; the number of hidden layers, the number of nodes in the hidden layers, learning rate, momentum term, the error goal of individual patterns/objects, and the error goal of the average system. As in PLS the aim is to balance the fitting of the training set with the predictive ability of the model. For example, the prediction capability expressed as the average sum-squared error (Eqn. 4) of a neural network with one hidden layer and only one node in that layer, is relatively stable and low in a region of relatively small values of learning rates and momentum terms. Outside this region the prediction error, i.e., the average system error of the validation data set changes rapidly and is much less favourable. Figure 2 illustrates the complexity of such a neural network. However, using more nodes than two in the hidden layer minimised such drastic changes of the prediction error.

The number of nodes has been considered to be roughly analogous to the number of latent variables in PLS [22]. Our results do not support a too strict relationship on number of significant latent variables in the PLS model and the num-

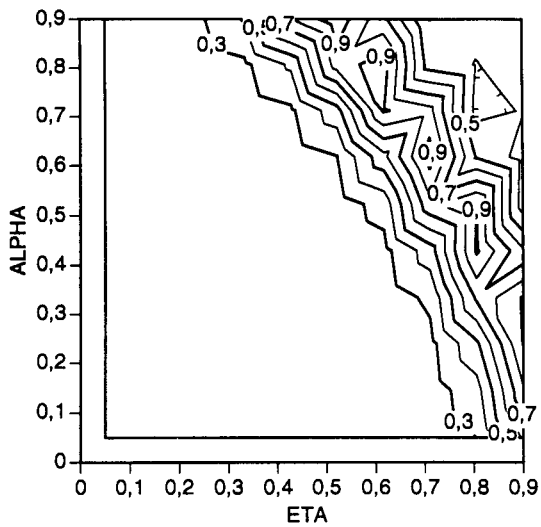

Fig. 2. The average sum-squared error of the validation data set of κ-carrageenan as a function of the learning rate (η) and the momentum term (α) in the back-propagation algorithm. The average sum-squared error in the contour plot is given for a neural networks with one hidden layer containing one node.

ber of nodes in a prediction error optimised neural networks. For the neural networks model of κ-carrageenan the optimal number of nodes in the hidden layer is in the range of 8–10 nodes, see Fig. 3. The corresponding number of significant latent variables, as determined using cross-validation, is four in the PLS model of κ-carrageenan.

To determine the attainable levels of prediction ability it is important to know the expected level of precision of the calibration/training set and the test or validation set to be examined. Our results indicate that convergence to a predetermined precision of $< 6\%$, at the concentration level of 50%, of the training set implies little changes of the achievable prediction capability of the validation data set. This effect is illustrated in Fig. 4. We interpret this result, that the training set variation on average is in the vicinity of 6% or lower and that further training is of little use. However, the neural networks model seems robust enough to accommodate the overfitting achieved if higher precision are converged to. Since the carrageenans were dry mixed, a variation of the concentration of ca. 6% or lower appears likely. This variation of concentration also includes the contribution of the inaccuracies of using manual integration.

From the studies conducted on different architecture of the net, the following neural networks architecture was chosen: learning rate = 0.1; momentum = 0.1; gain 1.0; error goal of the system

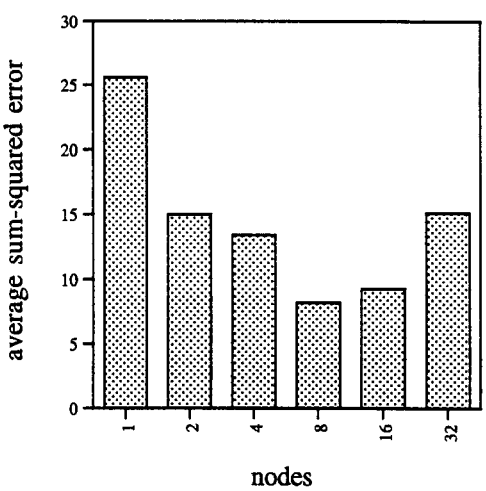

Fig. 3. The average sum-squared error calculated on the predicted concentration of the validation set of κ-carrageenan for different numbers of nodes in the hidden layer.

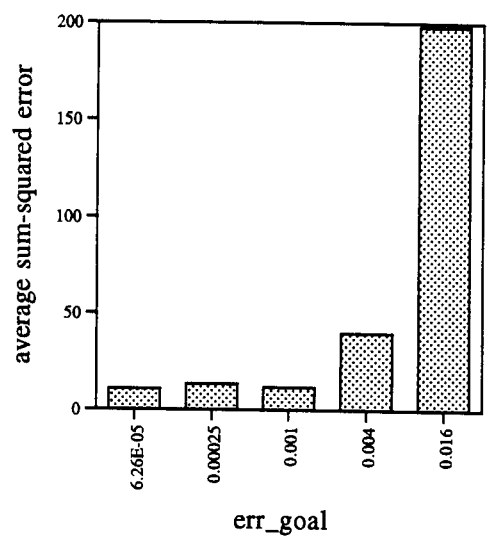

Fig. 4. The average sum-squared error calculated on the predicted concentration of the validation set of κ-carrageenan for different predetermined levels of average sum-squared error for convergence (err_goal).

TABLE 4

Neural networks (NN) and PLS modelling of the carrageenan data generated by infrared spectroscopy. The results are given as the average sum-squared error of the predicted carrageenan concentration (%) of the validation set

Input variables [a]	Model	Carrageenan		
		κ	ι	λ
1–36	NN	8.2	25.2	16
	PLS 1	29.2	22	22.2
	PLS 2	31	23.8	18.2
1–18	NN	26	34	38.8
	PLS 1	31	103.8	34.6
	PLS 2	117.6	44.4	39.2
19–36	NN	68	41.8	38.8
	PLS 1	56.4	23.4	92.2
	PLS 2	60.8	42	13.2

[a] For variable description, see Table 2.

= 0.0004: error goal of separate objects = 0.00004; maximum number of iterations = 20 000; one hidden layer with 8 nodes. The results obtained with this neural networks and the PLS model of the validation set are summarised in Table 4. Using the PLS model the best predictions are obtained for the ι- and λ-carrageenans. For ι and λ the predictive ability of the neural networks and PLS models appears to be equal, at least for the use of the full-scale input variable data set (i.e., variables 1–36), whereas for κ-carrageenan the neural networks model performs better in comparison to the PLS models.

The good prediction obtained for κ-carrageenan using the neural networks model for the full variable input, is probably due to that the parameters of the net architecture have been optimised on the κ-carrageenan. However, in all other cases where the neural networks model has been applied, the same net architecture as for κ-carrageenan, has been used without any attempt of a similar optimisation. For the PLS models separate optimisations have been carried out in each separate case.

In general, the prediction capability deteriorates on the use of reduced variable data set. The PLS model appears to some extent be more sensitive to the examined changes of the variable data set than the neural networks model.

Since neural networks utilise a steepest descent approach in adjusting the weights in the connections and the first step of the training procedure starts with weights set to random values, the actual weights in the connections varies slightly from a complete training to another. The results given for the neural networks model in Table 4 are the average sum-squared error of five to six trainings. For the κ-carrageenan concentration determinations by the neural networks model, using variables 1–36 as input, an average standard deviation of 2.7 (range 1.1–3.8) is generated. For ι- and λ-carrageenan average standard deviations of 1.4 (range 0.4–2.0) and 0.58 (range 0.3–0.8) are obtained, respectively. Since the convergence of the present NN model is determined by the err_goal of average system, an absolute value, generally higher precisions are generated for the higher concentration determinations than for the concentration in the lower range.

A typical plot on predicted versus actual concentration of the κ-carrageenans by the neural networks model and PLS 1 is given in Fig. 5. The correlation coefficient is 0.993. The correspond-

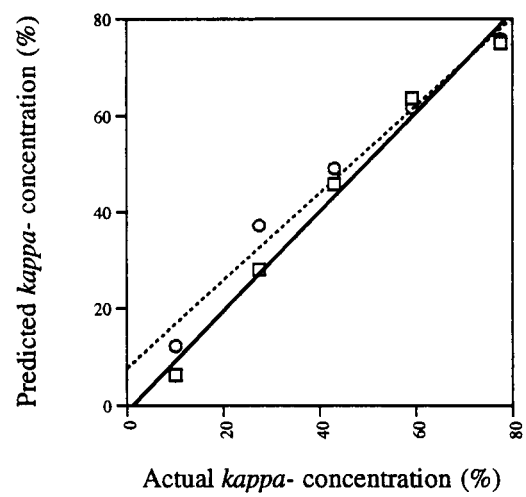

Fig. 5. Actual versus predicted concentration of the κ-carrageenans of the validation data set by neural networks (□, solid line) and PLS 1 (○, dotted line). The correlation coefficient of the neural networks model was 0.993 and the corresponding value for the PLS 1 model 0.989. For the neural networks model the following linear regression equation was obtained; $y = -1.22 + 1.04x$. The corresponding equation for the PLS 1 model was; $y = 7.86 + 0.91x$.

ing correlation coefficient by the PLS 1 model was also 0.989. The slight curvature of graph of the neural networks model may be due to the use of the sigmoid transfer function as discussed by Long et al. [22]. However, since also the curve for the PLS 1 model exhibits a similar curvature, this effect may instead relate to the variation of the concentration of the κ-carrageenan in the validation set.

In general, at least when the average sum-squared error is used as estimate of the prediction capability on the validation set, the neural networks model performs equally good or slightly better than the PLS models. However, both models could be further improved. For instance, the PLS models by exclusion of input/independent variables with little or no information content, use of cross terms, and quadratic terms. Furthermore, as is indicated in Table 4, in general the PLS models are favoured by an increase of the number of input/independent variables, e.g., the use of the complete IR spectrum as input to the PLS models would probably be beneficial. The neural networks model would probably benefit from a larger number of input variables as well, although at the cost of increased computional demands. Moreover, separate optimisation of the neural network models for the different carrageenan forms and variables input could also have an impact on the prediction ability.

The results generated by the neural networks and PLS on the test set (batch A–G, Table 1) are summarised in Fig. 6. In general, the agreement between the two models is acceptable. Of the production batches A–D, batches A–C are acceptable from a production view, whereas batch D does not qualify. The relative chemical composition of batch D is substantially different, containing a larger proportion of λ-carrageenan than batch A to C.

Batch E, F and G are according to the supplier pure ι-, κ-, and λ-carrageenan, respectively. Our results shows that batch E and F are pure ι- and κ-carrageenan, respectively, but that batch G does not qualify as pure λ-carrageenan. The agreement between the neural networks and PLS models are as follow: The best correlation between the neural networks model and the PLS model is generated for the κ-carrageenan, with a correlation coefficient of 0.984 and a correlation equation of PLS 2 = 8.03 + 1.016NN. The correlation coefficient for ι-carrageenan is 0.976 and for λ-carrageenan 0.947. The corresponding equations are PLS 2 = −2.80 + 1.058NN (ι) and PLS 2 = −3.90 + 0.777NN (λ).

Neural networks are in general considered to be computational demanding, however, studies on the relatively small matrices as in this study is quiet feasible using a 486 processor. Convergence to an average system error corresponding to a

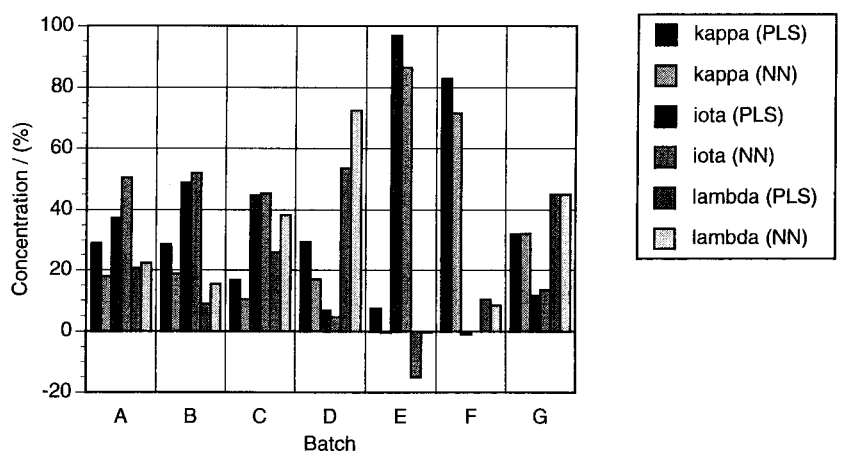

Fig. 6. The relative chemical composition of the test set (batches A–G) as generated by neural networks and PLS 2.

relative precision of ±2% at the 50% κ-carrageenan concentration is obtained within 5–10 min for data matrix consisting of 19 samples and 36 independent variables, and the use of 32 nodes in the hidden layer.

The present study was conducted on manually digitised spectra, although the objective is to use the complete digital spectrum in routine analysis.

However, since this study was conducted on a variable space consisting of up to 36 independent variables, this study also has relevance for the use of the complete digital IR spectrum (> 200 input variables). In conclusion, although the neural networks generate a slightly better prediction, as judged by the validation set, than PLS, both models appear to be appropriate for the purpose, i.e., to provide means for a rapid and accurate determination of the relative chemical composition of production batches of carrageenans by IR spectroscopy.

REFERENCES

1 N.S. Anderson, T.C.S. Dolan, A. Penman, D.A. Rees, G.P. Mueller, D.J. Stancioff and N.F. Stanley, J. Chem. Soc. C, (1968) 602.
2 J.S. Craigie and C. Leigh, Handbook Phycological Methods: Physiological and Biochemical Methods, Cambridge Univ. Press, London, 1978, p. 109.
3 C. Rochas, M. Lahaye and W. Yaphe, Botanica Marina, XXIX (1986) 335.
4 P.S. Belton, B.J. Goodfellow and R.H. Wilson, Marcomolecules, 22 (1989) 1636.
5 L.-G. Ekström, J. Kuivinen and G. Johansson, Carbohydrate Res., 116 (1983) 89.
6 C. Bodeau-Bellion, Physiol. Vég., 21 (1983) 785.
7 R.J. Helleur, E.R. Hayes, J.S. Craigie and J.L. McLachlan, J. Anal. Appl. Pyrol., 8 (1985) 349.
8 G. Sworn, W.M. Marrs and R.J. Hart, J. Chromatogr., 403 (1987) 307.
9 C. Rochas and M. Lahaye, Carbohydrate Polym., 10 (1989) 189.
10 H. Martens and T. Naes, Multivariate Calibration, Wiley, Chichester, 1989.
11 P.J. Gemperline, J.R. Long and V.G. Gregoriou, Anal. Chem., 63 (1991) 2313.
12 K. Hornik, M. Stinchcombe and H. White, Neural Networks, 2 (1989) 359.
13 J.R. Long, H.T. Mayfield, M.V. Henley and P.K. Kromann, Anal. Chem., 63 (1991) 1256.
14 P.A. Jokinen, Chemom. Intell. Lab. Syst., 12 (1991) 121.
15 K. Tanabe, T. Tamura and H. Uesaka, Applied Spectrosc., 46 (1992) 807.
16 M. Meyer and T. Weigelt, Anal. Chim. Acta, 265 (1992) 183.
17 O.M. Kvalheim and T.V. Karstang, Chemom. Intell. Lab. Syst., 2 (1987) 235.
18 J. Zupan and J. Gasteiger, Anal. Chim. Acta, 248 (1991) 1.
19 D.E. Rumelhart, J.L. McClelland and the PDP Research Group, Parallel Distributed Processing: Explorations in the Microstructure of Cognition, Vol. 1, MIT Press, Cambridge, MA, 1986.
20 R.P. Lippmann, IEEE ASSP Mag., 3 (1987) 4.
21 Y.H. Pao, Adoptive Pattern Recognition and Neural Networks, Addison-Wesley, Reading, MA, 1989.
22 J.R. Long, V.G. Gregoriou and P.J. Gemperline, Anal. Chem., 62 (1990) 1791.

Analytica Chimica Acta, 284 (1993) 149–157
Elsevier Science Publishers B.V., Amsterdam

Micellar effects on reaction kinetics

Part I. Simultaneous determination of chromium(VI), vanadium(V) and titanium(IV)

Dolores Sicilia, Soledad Rubio and Dolores Pérez-Bendito

Department of Analytical Chemistry, Faculty of Sciences, University of Córdoba, 14004 Córdoba (Spain)

(Received 22nd March 1993; revised manuscript received 26th July 1993)

Abstract

A method for the simultaneous resolution of ternary mixtures of chromium(VI), vanadium(V) and titanium(IV) by reaction with Pyrogallol Red in aqueous dodecyltrimethylammonium bromide (DTAB) micelles was developed. The effects of DTAB on the three reactions were control of reaction paths, micellar catalysis and alteration of the spectral features of the reaction products, all of which were exploited for the simultaneous determination of the analytes. Resolution was accomplished by measuring absorbance at three wavelengths (520, 620 and 760 nm) and a fixed time of 5 min. The analysis of ternary mixtures of chromium(VI), vanadium(V) and titanium(IV) over the concentration ranges 0.2–0.8 μg ml^{-1}, 0.2–1.6 μg ml^{-1} and 0.2–1.0 μg ml^{-1}, respectively, was achieved with relative errors less than 6% in most instances.

Keywords: Kinetic methods; Chromium; Micellar medium; Titanium; Vanadium

Micellar media have long been known to alter reaction rates [1,2]. Several quantitative kinetic treatments have been developed for assessing the intrinsic reactivity of substances in micelles; irrespective of the model used, enhancements in the rates of bimolecular reactions appear to arise solely from concentration of the reagents on the micellar surface. The fact that surfactant micelles can accelerate reactions has been increasingly frequently exploited in the last few years to improve the features of both catalytic [3–5] and non-catalytic [6] kinetic methods.

One interesting aspect of these organized media in relation on reaction kinetics is that reagent organization in, and the different microenvironments provided by, micellar media open up the possibility of controlling pathways leading to specific products, altering reaction mechanisms and effecting selective micellar catalysis of two or more species interacting with a common reagent [7]. These assets of micellar systems have been advantageously used in photochemistry [8,9]; as well as to hinder or avoid undesirable side reactions in order to stabilize drugs, foodstuffs, pesticides and light- or oxygen-sensitive materials [10]; and for enantiomeric and isotopic enrichment [11]. *Micellar control of reaction products* occurs when a given substrate can undergo two reactions, one of which is inhibited by micelles. There are various documented examples [7] where micelles substantially alter product distribution. *Micelles can also alter reaction mechanisms*. One example is the decomposition of 3-bromo-3-phenylpropionate ion [12]. The rate determining step

Correspondence to: D. Pérez-Bendito, Department of Analytical Chemistry, Faculty of Sciences, University of Córdoba, 14004 Córdoba (Spain).

0003-2670/93/$06.00 © 1993 – Elsevier Science Publishers B.V. All rights reserved

for this reaction in an aqueous medium is the formation of a zwitterionic carbonium ion which rapidly decarboxylates with elimination to yield styrene as the major product. In the presence of micellar 1-hydroxyethyl-2-dimethylalkylammonium bromide, the nucleophilic substitution reaction (SN_1) is replaced with an elimination mechanism (E_2) and transcinnamate ion becomes the major product. *Selective micellar catalysis* is of aid for discriminating enantiomeric reactants [11]. Chiral resolution is accomplished provided there is a substantial difference in either the binding constants for the enantiomers with the micelle and/or the specific rate constants of formation of the respective products.

The effects of micelles on reaction kinetics can be conveniently exploited for kinetic multicomponent determinations. To our knowledge, only two applications of this type have so far been reported. Thus, Ni(II) and Co(II) were simultaneously determined by complex formation with 5-octyloxymethyl 8-quinolinol in Triton X-100 [13]. The non-ionic surfactant inhibited both reactions and permitted the determination of the two ions by using a stopped-flow spectrophotometer. On the other hand, selective micellar catalysis has been used for the determination of cyanide, sulphide and sulphite in binary mixtures, by reaction with 5,5′-dithiobis(2-nitrobenzoic acid) (DTNB) in the presence of the cationic surfactant cetyltrimethylammonium bromide (CTAB) [14]. The anion mixture could not be resolved by conventional differential kinetic analysis in an aqueous medium because of the similar reactivity of sulphide and sulphite ions and the slowness of the reaction between cyanide and DTNB (it took ca. 100 min to complete). The dependences obtained by plotting the observed rate constants, k_{exp}, of the reactions between the three ions and DTNB as a function of the CTAB concentrations showed that, by selecting an appropriate concentration of surfactant, adequate differences between the rate constants could be obtained in order to resolve binary mixtures of the anions at micromolar concentrations.

This paper reports a study on the influence of dodecyltrimethylammonium bromide (DTAB) micelles on the kinetics of reaction between Pyrogallol Red (PGR) and Cr(VI), V(V) and Ti(IV) ions that was aimed at accomplishing the simultaneous determination of the three ions in the micellar medium. These reactions were selected for two reasons: first, resolving the ions simultaneously in an aqueous medium was impossible because Cr(VI) and V(V) oxidized PGR at a similar rate and Ti(IV) interfered with the individual determinations of Cr(VI) and V(V) by forming a complex with PGR [15]; second, although oxidized PGR is the main product for the PGR–Cr(VI) and PGR–V(V) systems, a complex between V(V) and PGR was also formed as reaction product, to a lesser extent, under the working reaction conditions. We thus investigated the potential of micelles for selectively altering reaction pathways as a means of accomplishing the simultaneous resolution of the ions. The effects of DTAB micelles on the reactions considered included control of the reaction paths, micellar catalysis and changes in the spectral features of the reaction products, all of which were exploited for the analysis of ternary mixtures of the analytes.

EXPERIMENTAL

Apparatus

Absorbance measurements were made on a Hewlett Packard 8452A diode array spectrophotometer furnished with 1-cm quartz and glass cells. The spectrophotometer cell compartment was thermostated by circulating water from a Neslab RTE bath featuring a temperature stability of ± 0.1°C through it. A classical stalagmometer was used for surface tension measurements in order to determine the critical micelle concentration (cmc) of the surfactant [16].

Reagents

All reagents used were of analytical grade and utilized as purchased, without further purification. Bidistilled water was used throughout. A stock aqueous solution of Cr(VI) (1.92×10^{-2} M) was prepared from $K_2Cr_2O_7$ (Merck). Another stock aqueous solution of V(V) (1.96×10^{-2} M) was prepared from NH_4VO_3 (Aldrich). Working

solutions of Cr(VI) (1.92×10^{-4} M) and V(V) (1.96×10^{-4} M) were prepared daily by appropriate dilution. A stock Ti(IV) solution (2.09×10^{-2} M) was made by dissolving 0.1 g of titanium metal (Merck) in 10 ml of HCl (1:1) with warming; after cooling, the solution was made up to 100 ml with HCl (1:1). Working solutions of this metal (2.09×10^{-4} M) were prepared daily by appropriate dilution with further bidistilled water. The pH of these solutions was adjusted to 1.6–1.7 with NaOH. A 7.0×10^{-4} M solution of Pyrogallol Red (PGR) (Aldrich) was made by dissolving 0.0280 g of the reagent in 100 ml of 5.84×10^{-2} M aqueous dodecyltrimethyl ammonium bromide (DTAB). This solution was stable for at least three days. A 0.1 M phthalate buffer of pH 3.5 was also prepared. A DTAB (Sigma) solution (9.73×10^{-2} M) was made by dissolving the required amount of surfactant in bidistilled water. The other surfactants tested, viz. cetyltrimethylammonium bromide (CTAB) (Sigma), cetylpyridinium chloride (CPC) (Serva), sodium dodecylsulphate (SDS) (Aldrich), Triton X-100 (Serva) and *N*-dodecyl-*N*,*N*-dimethylammonium-3-propane-sulphonate (SB-12, sulphobetaine) (Serva) were prepared similarly. Less readily soluble surfactants were dissolved with warming.

Procedure

In a 10-ml standard flask were placed, in sequence, 3.0 ml of phthalate buffer (0.1 M, pH 3.5), 1.0 ml of Pyrogallol Red–DTAB solution, appropriate volumes of chromium(VI) (1.92×10^{-4} M), and vanadium(V) (1.96×10^{-4} M) and titanium(IV) (2.09×10^{-4} M) standard solutions to give final chromium(VI), vanadium(V) and titanium(IV) concentrations between 0.2 and 0.8 μg ml^{-1}, 0.2 and 1.6 μg ml^{-1} and 0.2 and 1.0 μg ml^{-1}, respectively. The stopclock was then started and the mixture was diluted to the mark with bidistilled water. An aliquot of this reaction mixture was transferred to a thermostated cell at 25 ± 0.1°C and its absorbance spectrum was recorded exactly 5 min after the stopclock was started. Absorbance values at 520, 620 and 760 nm were acquired from the absorbance spectrum and substracted a blank containing no Cr(VI), V(V) or Ti(IV).

The dependence of the absorbance at these wavelengths and time on the concentration of the analytes in ternary mixtures was found to conform to the following functions:

$$A(520) = \beta_0 - \beta_1[\text{Cr(VI)}] + \beta_2[\text{V(V)}] + \beta_3[\text{Ti(IV)}] \quad (1)$$

$$A(620) = \beta_0' + \beta_2'[\text{V(V)}] + \beta_3'[\text{Ti(IV)}] \quad (2)$$

$$A(760) = \beta_0'' + \beta_2''[\text{V(V)}] + \beta_3''[\text{Ti(IV)}] \quad (3)$$

with $\beta_1 > \beta_3 \gg \beta_2$; $\beta_3' > \beta_2'$ and $\beta_2'' \gg \beta_3''$, for absolute values of the coefficients. The concentration of the analytes was expressed in μg ml^{-1}. Coefficients β were estimated by multiple linear regression (MLR) from 20 ternary mixtures containing Cr(VI), V(V) and Ti(IV) in the above-mentioned ranges using a laboratory developed FORTRAN 77 program. The expression for the MLR for eqs. 1, 2 and 3 in matrix notation is:

$$y = X\beta + e$$

where y is the measurement vector [A(520), A(620) or A(760)], e the residual vector, β the parameter vector and X the independent variable matrix. The least-squares estimates of $\beta(b)$ were obtained from $b = (X',X)^{-1}X'y$, where X' is the transpose of X and $(X'X)^{-1}$ the inverse of $X'X$. Once the coefficient estimates were obtained, unknown samples were analysed by substituting the measured parameters A(520), A(620) and A(760) into eqs. 1, 2 and 3, and calculating the analyte concentrations by using another laboratory-developed FORTRAN 77 program.

RESULTS AND DISCUSSION

Pyrogallol Red [4,5,6-trihydroxy-3-oxo-9-(phenyl-*o*-sulphonic acid) xanthene] has been used as a metallochromic indicator and spectrophotometric reagent, as well as in kinetic spectrophotometric determinations by oxidation in uncatalysed and catalysed reactions [17]. Several kinetic methods for the individual determination of trace amounts of Cr(VI) [15] and V(V) [18] (detection limits for both ions 50 ng ml^{-1}) based on their oxidation of PGR have been reported. The decrease in the absorbance of this reagent at 490

nm at fixed times of 10 and 5 min are dependent on the concentration of V(V) and Cr(VI), respectively. On the other hand, Ti(IV) has been determined by formation of a 1:1 or 1:2 complex with PGR [19] that absorbs maximally at 610 nm (detection limit, ca. 30 ng ml^{-1}). The determination of V(V)–Cr(VI) in mixtures by using PGR is unsatisfactory because of the similar reaction rates of the systems involved. Titanium(IV) introduces excess errors in the individual determinations of Cr(VI) and V(V) [15,18].

Figure 1A shows absorption spectra for the PGR (curve 1) and PGR–V(V) (curve 2), PGR–Cr(VI) (curve 3) and PGR–Ti(IV) (curve 4) systems, in an aqueous medium at a reaction time of 5 min. They were recorded under experimental conditions given under Experimental. As can be concluded from these spectra the simultaneous determination of Cr(VI)–V(V)–Ti(IV) in an aqueous medium is unfeasible. Absorbance signals at about 610–620 nm correspond to the V(V)–PGR (curve 2) (as will be proved below) and Ti(IV)–PGR complexes (curve 4). Signals for Cr(VI) at these wavelengths were negligible, which suggests that only Cr(VI) and PGR reacted under the selected experimental conditions. The

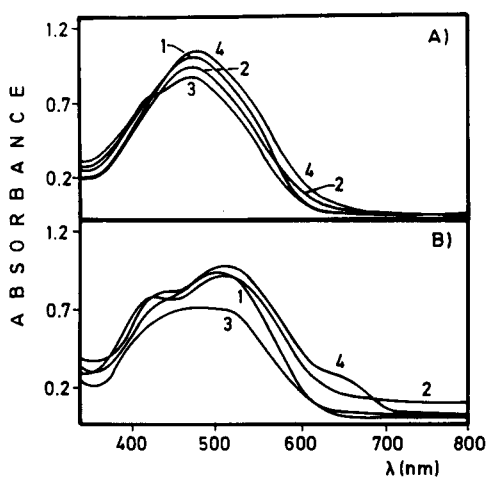

Fig. 1. Influence of DTAB on the absorption spectrum of Pyrogallol Red, recorded 5 min after mixing reactants in the presence of (1) no metal, (2) 0.5 $\mu g\ ml^{-1}$ vanadium(V), (3) 0.5 $\mu g\ ml^{-1}$ chromium(VI), (4) 0.5 $\mu g\ ml^{-1}$ titanium(IV), in the absence (A) and presence (B) of 5.84×10^{-3} M DTAB. For experimental conditions, see *Procedure*.

AQUEOUS MEDIUM

PGR → Cr(VI) → Oxidation product

PGR → V(V) → Oxidation product + PGR-V(V) complex
[Oxidation product] > [PGR-V(V) complex]

PGR → Ti(IV) → PGR-Ti(IV) complex (λ_{max} = 580 nm)

CATIONIC MICELLAR MEDIUM

PGR → Cr(VI) → Oxidation product

PGR → V(V) → PGR-V(V) complex

PGR → Ti(IV) → PGR-Ti(IV) complex (λ_{max} = 620 nm)

Scheme 1.

reaction products formed between the analytes [Cr(VI), V(V), Ti(IV)] and PGR in an aqueous medium under the experimental conditions are shown in Scheme 1.

Selection of the micellar system. Influence on the reactions between pyrogallol red and titanium(IV), vanadium(V) and chromium(VI)

The effect of micelles on the reactions considered was investigated in order to check whether these organized media facilitated the simultaneous resolution of titanium(IV), vanadium(V) and chromium(VI). Taking into account that the partitioning of reactants and/or reaction products between the micellar and aqueous phase is essentially determined by electrostatic and hydrophobic interactions between species and the micelles, one must consider the type of charge the reactants and/or reaction products bear in order to choose and appropriate micellar medium for the system concerned. At the reaction pH (3.5), chromium(VI) and vanadium(V) are likely to be present almost entirely as $Cr_2O_7^{2-}$ and $HV_2O_7^{3-}$, respectively. On the other hand, PGR is also negatively charged so, these reactants can be concentrated on the surface of cationic micelles. Inasmuch titanium(IV) bears a positive charge (the most likely forms present in the reaction medium are TiO_2^{2+}/TiO_2H^+), it can also be concentrated on the micellar surface of cationic surfactants since the PGR–Ti(IV) complex pre-

serves the negative charge of the ligand and the functional groups face the sulphonic group. The PGR–V(V) complex also preserves the negative charge of the ligand so it can be retained at the micellar surface when formed.

The cationic (DTAB, CTAB, CPC) and zwitterionic (SB-12) surfactants selected for this study were tested at three different concentrations, namely, below, close to and above their cmc. Neither anionic (SDS) nor non-ionic (Triton X-100) surfactants had any effect on the reactions studied. On the other hand all the cationic and zwitterionic surfactants tested influenced the three investigated systems in the same way: they accelerated the reaction between Cr(VI) and PGR, they suppresed the oxidation reaction between V(V) and PGR almost completely (thereby altering product distribution compared with that in water); and they caused a bathochromic shift and a hyperchromic effect on the absorption spectrum of the Ti(IV)–PGR complex.

The most pronounced effect was exerted by DTAB, which was thus chosen for subsequent experiments. Scheme 1 shows the reaction products formed in cationic micellar media assayed. Also, Fig. 1B shows the absorption spectra for the PGR (curve 1) and PGR–V(V) (curve 2), PGR–Cr(VI) (curve 3) and PGR–Ti(IV) (curve 4) systems in the DTAB micellar medium at a reaction time of 5 min. From the spectra it follows that each analyte features a spectral region where its contribution to the overall absorbance signal is significantly higher than those of the others. Thus, Cr(VI), Ti(IV) and V(V) contribute maximally to the signal obtained at 520, 620 and 760 nm, respectively. On the other hand, the contribution of Cr(VI) to the signals at 620 and 760 nm and that of V(V) to the signal at 520 nm are insignificant.

Influence of the DTAB concentration

Figure 2 shows the influence of DTAB concentration on the absorbance of the systems considered at the three selected wavelengths (520, 620 and 760 nm) and fixed reaction time of 5 min (time by which the oxidation reaction between Cr(Vl) and PGR had developed to at least 70%) and three ion concentrations (0.2, 0.5 and 0.8 μg

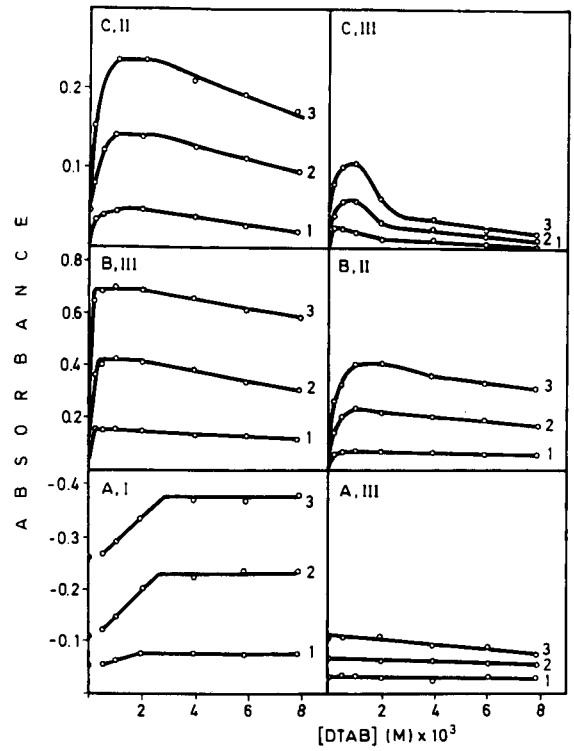

Fig. 2. Influence of the DTAB concentration on the absorbance of the metal–pyrogallol Red system at a fixed time (5 min) and three different metal concentrations: (1) 0.2 μg ml^{-1}, (2) 0.6 μg ml^{-1}, (3) 1.0 μl ml^{-1}; at (A) 520 nm (B) 620 nm and (C) 760 nm for Cr(VI) (curves in I), V(V) (curves in II) and Ti(IV) (curves in III). For experimental conditions, see *Procedure*.

ml^{-1}). Results for Cr(VI) at 620 and 760 nm, and for V(V) at 520 nm, were not plotted because of the negligible absorbance values obtained at any DTAB concentration tested. The reactions were scarcely affected by surfactant concentrations below the cmc (9.2×10^{-5} M, calculated under our reaction conditions); however, concentrations slightly above the cmc resulted in increased absorbance values for the PGR–V(V) and PGR–Ti(IV) complexes up to a maximun value above which they decreased with increasing DTAB concentration, the final absorbance decrease being the result of dilution of the reactants offsetting the effect of the increasing concentration of micelles in solution. The oxidation reaction between Cr(VI) and PGR was accelerated at surfactant concentrations above ca. 5×10^{-4} M, so micelles

were also required in order to observe some effect of DTAB on this reaction. Because of the increased absorbance values resulting from the presence of DTAB, the determination of the analytes was more sensitive than in an aqueous medium. Thus, the maximum signal ratio between the obtained in the presence and absence of surfactant was about 50 for V(V) and Ti(IV) at 760 nm; about 10 and 3.5 for V(V) and Ti(IV), respectively, at 620 nm; and about 1.5 for Cr(VI) at 520 nm. The DTAB concentration at which the maximum absorbance was reached was dependent on the Cr(VI) concentration (Fig. 2, AI): the number of micelles required for optimum reaction development increased with increase in the Cr(VI) concentration.

Optimization of the reaction conditions

The chromium(VI), vanadium(V) and titanium(IV) systems were optimized by changing each experimental variable in turn while keeping all others constant. The three measured parameters used to resolve ternary mixtures of the analytes (absorbances at 520, 620 and 760 nm at a fixed reaction time) were found to be additive throughout the analytes concentration ranges tested. Blank reactions involving no analytes were also examined. In order to achieve the highest possible accuracy and sensitivity in the determination, the reactant concentrations should meet two requirements, namely: that the A[Cr(VI)]/A[Ti(IV)], A[Ti(IV)]/A[V(V)] and A[V(V)]/A[Ti(IV)] ratios at 520, 620 and 760 nm, respectively, should be maximal, and that the absolute measured absorbance values for the Cr(VI)–PGR system and Ti(IV)–PGR and V(V)–PGR complexes at 520, 620 and 760 nm, respectively, should also be maximal. If either condition was not fulfilled at a given value of the studied parameter, then the selected values were that which resulted in the maximum A[V(V)]/A[Ti(IV)] ratio at 760 nm since absorbance values at this wavelength were always smaller than those at 520 and 620 nm.

The PGR–Ti(IV) and PGR–V(V) complexes formed inmmediately after the reactants were mixed. Oxidation of PGR by Cr(VI) gave a first quick stage up to about 120 s, followed by a lower

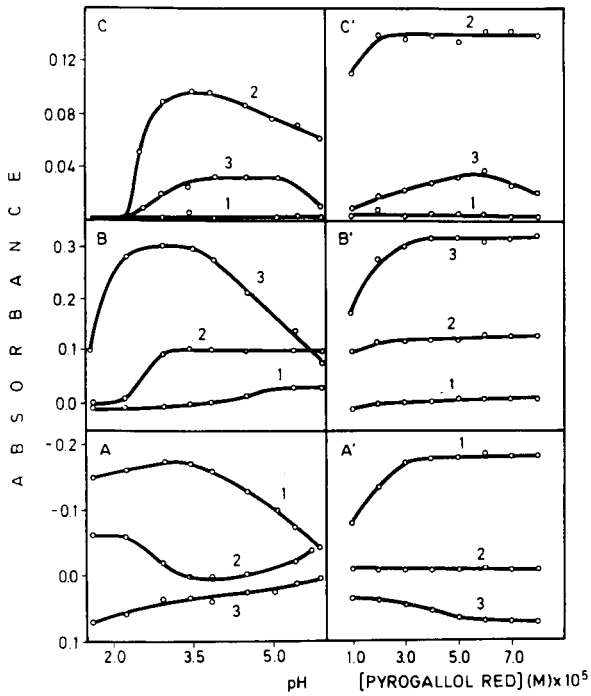

Fig. 3. Influence of pH (A, B, C) and the Pyrogallol Red (A', B', C') concentration on the absorbance of metal–pyrogallol Red systems at a fixed time (5 min) [Metal: (1) Cr(VI), (2) V(V) and (3) Ti(IV); wavelength: (A, A') 520 nm, (B, B') 620 nm, (C, C') 760 nm]. Metal concentration 0.5 μg ml^{-1}. For experimental conditions, see *Procedure*.

stage. A time of 5 min was selected as a compromise between maximun sensitivity and rapidity in the measurements. The reaction developed to ca. 70% over that interval.

Figure 3 shows the variation of the absorbance as a function of pH (A, B, C) and the PGR concentration (A', B', C') for the Cr(VI)–PGR (1), V(V)–PGR (2) and Ti(IV)–PGR (3) systems at the three wavelengths selected. The study of the influence of pH was performed over the range of 1–6. Higher pH values were not tested because of the reagent instability. Oxidation of PGR by Cr(VI) occurred preferentially at the most acids pH values (Fig. 3, A1). Above pH $\approx$ 4.5, some absorbance signals were significantly different from zero for the PGR–Cr(VI) system at 620 nm (Fig. 3, B1), although the formation of a complex could not be ascertained. Oxidation of PGR by V(V) was almost completely suppressed

pH ≈ 3 (Fig. 3, A2). The variation of the absorbance of the V(V) complex with pH was found to be dependent on the measuring wavelength (Fig. 3, B2 and C2), and the positive interference of Ti(IV)–PGR complex at 520 nm decreased as the pH increased (Fig. 3, A3). On the basis of these results, pH 3.5 was chosen as the working value, since, the absorbance signals for the Cr(VI)–PGR, V(V)–PGR and Ti(IV)–PGR systems at 520, 620 and 760 nm, respectively, were maximal. Likewise, the above absorbance ratios were also found to be maximal. A 0.03 M phthalate/phthalic acid buffer was used to adjust the pH of the solutions to the required value. The concentration of buffer was found not to affect any of the systems studied up to about 0.03 M. Higher concentrations increased the absorbance signals obtained for the PGR–Ti(IV) complex at any of the three measuring wavelengths, so the A[V(V)]/A[Ti(IV)] ratio at 760 nm decreased as a result.

The influence of the Pyrogallol Red concentration on the three reactions considered was studied in the range $(1.0–8.0) \times 10^{-5}$ M. Concentrations above 4.0×10^{-5} M provided maximum absorbance signals for the V(V)–PGR (Fig. 3, C'2), Ti(IV)–PGR (Figure 3, B'3) and Cr(VI)–PGR (Figure 3, A'1) systems at 760, 620 and 520 nm, respectively. A value of 7.0×10^{-5} M was selected.

The effect of the temperature was investigated over the range 20–60°C; this parameter was found to affect the three reactions differently. Thus, it hardly had any influence on the oxidation rate of PGR by chromium(VI), and increased only slightly the absorbance signals for the PGR–Ti(IV) complex. However, it significantly altered product distribution for the PGR–V(V) reaction. Thus, above 30°C, the oxidation product/complex ratio increased as the temperature was raised. A temperature of 25°C was chosen as optimal for resolving the ternary mixture.

The ionic strengh, which was adjusted with sodium chloride and potassium nitrate, had no influence on the PGR–V(V) or PGR–Cr(VI) system and resulted in slightly increased absorbance signals for the PGR–Ti(IV) system, at least up to an electrolyte concentration of 1 M. The effect of the dielectric constant on the reactions was studied by using methanol as solvent. Increasing methanol contents up to about 20% had no influence on the PGR–Ti(IV) system. However, decreasing the dielectric constant had a more pronounced effect on the PGR–Cr(VI) and PGR–V(V) systems. Thus, methanol contents above 5% decreased the rate of oxidation of PGR by Cr(VI) and increased the absorbance signals for the PGR–V(V) complex.

Finally, the order of addition of reactants had no influence on the absorbance signals at any of the measuring wavelengths.

Features of the proposed analytical method

Calibration graphs for chromium(VI), vanadium(V) and titanium(IV) were constructed by plotting absorbance values measured at a reaction time of 5 min and the three selected wavelengths, as a function of the analyte concentration. The graphs for the individual determinations were linear over the range 0.2–1.6 μg ml^{-1} analyte concentration (Fig. 4) and confirmed that the contribution of Cr(VI) to the absorbance at 620 (Fig. 4, B1) and 760 (Fig. 4, C1) nm was nil

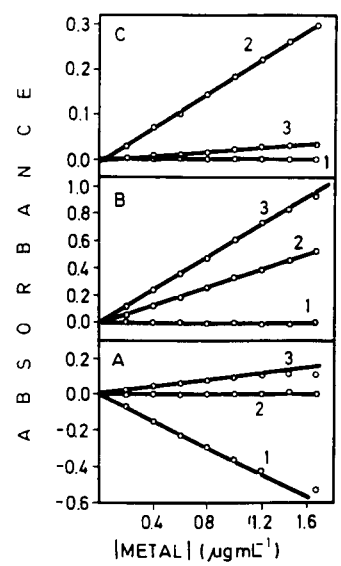

Fig. 4. Calibration curves obtained for individual analytes [(1) Cr(VI), (2) V(V) and (3) Ti(IV)] at (A) 520 nm, (B) 620 nm and (C) 760 nm. For experimental conditions, see *Experimental*.

TABLE 1

Quantitative performance of the proposed method for the determination of ternary mixtures of chromium(VI), vanadium(V) and titanium(IV)

Measured parameter	Coefficients of Eqns. 1 and 2				r [a]	S.E.E. [b]
	$(\beta_0, \beta_0'$ or $\beta_0'') \pm$ S.D.	$\beta_1 \pm$ S.D.	$(\beta_2, \beta_2'$ or $\beta_2'') \pm$ S.D.	$(\beta_3, \beta_3'$ or $\beta_3'') \pm$ S.D.		
$A(520)$	$-(3.3 \pm 0.6) \times 10^{-2}$	$-(33.5 \pm 0.8) \times 10^{-2}$	$(1.3 \pm 0.4) \times 10^{-2}$	$(8.0 \pm 0.6) \times 10^{-2}$	0.994	9.1×10^{-3}
$A(620)$	$-(4.2 \pm 0.9) \times 10^{-2}$		$(33.7 \pm 0.7) \times 10^{-2}$	$(57.9 \pm 0.9) \times 10^{-2}$	0.997	1.4×10^{-2}
$A(760)$	$-(2.7 \pm 0.3) \times 10^{-2}$		$(19.6 \pm 0.2) \times 10^{-2}$	$(3.9 \pm 0.3) \times 10^{-2}$	0.998	4.6×10^{-3}

[a] Correlation coefficient ($n = 20$). [b] Standard error of the estimate.

and that of V(V) to the absorbance at 520 (Fig. 4, A2) nm was insignificant. The absence of synergistic effects ensured that the absorbances values obtained for a mixture of the three analytes were the sums of the absorbance values obtained for each individual analyte.

In order to calculate the concentration of chromium(VI), vanadium(V) and titanium(IV) in the mixture, Eqns. 1, 2 and 3 (see Experimental) were solved by using a straightforward, laboratory-developed FORTRAN 77 program. Coefficients β in the equations were estimated by multiple linear regression from 20 observations of variables $A(520)$, $A(620)$ and $A(760)$ on 20 samples containing different combinations of analyte concentrations. The results obtained are shown in Table 1, which includes the statistical parameters for the equations. The precision of the proposed method, expressed as the relative standard deviation (%), was 1.3% for chromium(VI), 0.7% for vanadium(V) and 1.4% for titanium(IV) in a 1:1:1 mixture containing 0.5 μg ml^{-1} of each.

TABLE 2

Multiple linear regression predictions for ternary mixtures of Ti(IV), V(V) and Cr(V)

Analyte proportions Cr(VI):V(V):Ti(IV)	Actual concentration (μg ml^{-1})			Relative error (%)		
	Cr(VI)	V(V)	Ti(IV)	Cr(VI)	V(V)	Ti(IV)
1:1:1	0.6	0.6	0.6	2.0	−0.2	5.5
1:3:1	0.2	0.6	0.2	−2.5	1.0	−6.5
1:5:1	0.2	1.0	0.2	5.0	−2.1	−5.0
1:1:5	0.2	0.2	1.0	4.5	−1.5	−2.6
1:3:5	0.2	0.6	1.0	−9.5	9.5	1.7
2:1:1	0.4	0.2	0.2	0.8	7.0	−1.0
2:3:1	0.4	0.6	0.2	−1.5	−1.3	0.0
2:1:3	0.4	0.2	0.6	3.2	−2.5	−1.2
2:1:5	0.4	0.2	1.0	5.5	−8.5	−1.9
2:3:3	0.4	0.6	0.6	1.0	−5.2	7.2
2:3:5	0.4	0.6	1.0	0.0	5.3	−1.0
2:5:3	0.4	1.0	0.6	0.8	−0.8	3.2
2:5:1	0.4	1.0	0.2	6.5	−0.3	−5.0
3:1:1	0.6	0.2	0.2	−2.0	8.5	−0.5
3:3:1	0.6	0.6	0.2	0.5	3.2	3.5
3:1:3	0.6	0.2	0.6	1.8	7.0	−1.2
3:3:5	0.6	0.6	1.0	−6.8	−1.2	−0.1
3:5:1	0.6	1.0	0.2	0.3	−0.2	1.0
4:5:1	0.8	1.0	0.2	−2.2	−0.2	−3.0
4:1:3	0.8	0.2	0.6	2.4	−5.5	0.8
4:1:5	0.8	0.2	1.0	2.1	−2.3	−4.5
4:3:3	0.8	0.6	0.6	−2.5	0.0	3.5
4:3:1	0.8	0.6	0.2	0.5	−2.0	1.0

The predictive ability of indirect calibration by MLR for the ternary mixtures was tested by using 23 mixtures containing the analytes in different ratios as unknown samples and making measurements under the same experimental conditions as those used for calibration. Table 2 summarizes the results obtained from Eqns. 1, 2 and 3 at the different analyte ratios tested. Relative errors less than 6% were obtained in most of the analyte determinations, which confirms the good accuracy of the proposed method.

Conclusions

Micelles possess a high potential for multicomponent analysis. Micellar systems are known to possess some unique features and properties that should prove very useful in helping one to overcome many of the analytical problems encountered in this context. These organized media can be used in various ways to obtain the selectivity required for simultaneous determinations of species. Thus, micelles can alter reaction kinetics through their rate, control pathways, change reaction mechanisms and/or the observed rate constant ratio of two or more species interacting with a common reagent. Micelles are also known to alter the physico-chemical properties of solubilized compounds by causing wavelength shifts, changing molar absorptivities and equilibrium constants, etc. Taking into account that different reagents can organize differently in micelles and the also different microenvironments provided by these organized media, micelles can enable discrimination in some chemical systems and hence permit the species involved to be simultaneously resolved.

The authors gratefully acknowledge financial support from the CiCyT (Project No. PB91-0840).

REFERENCES

1 C.A. Bunton, F. Nome, F.H. Quina and L.S. Romsted, Acc. Chem. Res., 24 (1991) 358.
2 M. Gratzel and K. Kalyanasundaram, Kinetics and Catalysis in Microheterogeneous Systems, Marcel Dekker, New York, 1991.
3 M.L. Lunar, S. Rubio and D. Pérez-Bendito, Anal. Chim. Acta, 237 (1990) 207.
4 D. Sicilia, S. Rubio and D. Pérez-Bendito Talanta, 38 (1991) 1147.
5 D. Sicilia, S. Rubio and D. Pérez-Bendito, Anal. Chem., 64 (1992) 1490.
6 E. Athanasiou-Malaki, M.A. Koupparis, Anal. Chim. Acta, 219 (1989) 295.
7 J.H. Fendler, Membrane Mimetic Chemistry, Wiley, New York, 1982, pp. 293–338.
8 N.J. Turro, M. Grätzel and A.M. Braun, Angew. Chem. Int. Ed. Eng., 19 (1980) 675.
9 J.H. Fendler, J. Phys. Chem., 84 (1980) 1485.
10 P.H. Elworthy, A.T. Florence and C.B. Macfarlane, Solubilization of Surface Active Agents, Chapman and Hall, London, 1968.
11 W.L. Hinze, Ann. Chim., 77 (1987) 167.
12 C.A. Bunton, A.A. Kamego and P. Ng, J. Org. Chem., 39 (1974) 3469.
13 S. Tagashira, K. Onove, Y. Murakami and Y. Sasaki, Anal. Sci., 8 (1992) 307.
14 V. González, B. Moreno Cordero, D. Sicilia, S. Rubio and D. Pérez-Bendito, Anal. Chem., 65 (1993) 1897.
15 J. Medina-Escriche, A. Sevillano-Cabeza and M. de la Guardia-Cirugeda, Analyst, 110 (1985) 719.
16 P. Mukerjee and K.J. Hysels, Critical Micelle Concentrations of Aqueous Surfactant Systems, NSRDS-NBS 36, U.S. Department of Commerce, Washington, DC, 1971.
17 J. Medina-Escriche, A. Sevillano-Cabeza and M. Lobat, Quím. Anal., 5 (1986) 229.
18 J. Medina-Escriche, A. Sevillano-Cabeza and M. de la Guardia-Cirugeda, Analyst, 108 (1983) 1402.
19 D. Abromaityte and S. Ramonaite, Liet TSR Mokyly Mokslo Darbai, Chemija ir Chem. Technol., Nauch. Tr. Vyssh. Ucheb. Zavedenii Lit SSR. Khimiya i Khim. Tekhnol., (1975) 5.

Analytica Chimica Acta, 284 (1993) 159–166
Elsevier Science Publishers B.V., Amsterdam

Stopped-flow, air-segmented continuous flow: kinetic determinations of glucose and phosphate in wine and serum samples

Yun-Sheng Hsieh and S.R. Crouch

Department of Chemistry, Michigan State University, East Lansing, MI 48824 (USA)

(Received 14th June 1993; revised manuscript received 23rd August 1993)

Abstract

The feasibility of using the stopped-flow technique with an air-segmented continuous-flow analysis system has been investigated. Kinetic determinations of glucose and phosphate are used to evaluate the potential of this approach. The effects of such instrument characteristics as delay time and flow-rate on the observed reaction rates are discussed. The results of determining glucose and phosphate in wine and serum samples are reported.

Keywords: Flow system; Air-segmented continuous-flow analysis; Glucose; Stopped-flow technique; Phosphate; Serum; Wine

The advantages of using kinetic-based determinations over equilibrium-based methods in biological and other complicated samples have been pointed out in many reviews [1–4] and monographs [5,6]. Flow injection (FI) [7,8] and air-segmented continuous-flow (ASCF) [9,10] analysis are frequently employed for kinetic-based determinations with slow reactions, such as many enzymatic reactions. Flow-based kinetic measurements can generally be divided into the multiple flow cell approach [11], the single detector approach using a pH gradient or split streams [12], the flow reversal or recycle approach [13], the dispersion-correction approach [14] and the stopped-flow approach [15]. Of these techniques, stopped-flow measurements by normal injection [15] and sequential injection [16,17] are quite promising for future development due to such practical advantages as instrumental simplicity, the lack of dispersion after the flow is stopped, and the ease of automation of the instrument operation and data handling. In the stopped-flow mode, samples are injected into a reagent-containing stream, and the flow is stopped to allow rate measurements to be made on a selected portion of the sample zone trapped inside the flow cell. Despite the many applications of stopped-flow FI, there are very few references for using the stopped-flow method for kinetic determinations in ASCF systems. Here the air segmentation should be advantageous in minimizing dispersion and in promoting mixing prior to stopping the flow. Two previous reports used the stopped-flow technique in conjunction with an air-segmented continuous flow system to simultaneously diagnose and evaluate reactor stages [18] and to quantitatively determine creatinine [19]. However, there has not been an extensive study of this methodology for kinetic-based determinations.

In this work, the performance of the stopped-flow ASCF technique with both an enzymatic and

Correspondence to: S.R. Crouch, Department of Chemistry, Michigan State University, East Lansing, MI 48824 (USA).

0003-2670/93/$06.00 © 1993 – Elsevier Science Publishers B.V. All rights reserved

a non-catalytic reaction is examined. The effects of delay time and flow-rate on measured reaction rates are described. The stopped-flow ASCF approach is demonstrated by determining glucose and phosphate without deproteinization in wine and serum samples. Analytical results on standard serum samples are compared with manufacturer's values.

EXPERIMENTAL

Apparatus

Schematic diagrams of the ASCF systems employed in this work are shown in Fig. 1. Physical debubbling prior to the flow cell was employed. The composite reagent for the enzymatic reaction was stored in a thermostated water bath for control of temperature. The reagents, samples and air were introduced into the system and pumped into the manifold by a 12-channel peristaltic pump (Ismatec). The flow-rates of reagents and samples were selected by appropriate choice of pump setting numbers and tubing. Flow-rated pump tubing (Technicon) was used as reported elsewhere [20]. The colorimeter was constructed locally [21,22]. Absorbance signals were obtained at 510 nm and at 660 nm for spectrophotometric measurements of glucose and phosphate respectively.

Data collection

The output signals were recorded either with a strip chart recorder or an IBM PC computer equipped with a commercial data acquisition board (Model RTI-815 Analog Devices, Nor-

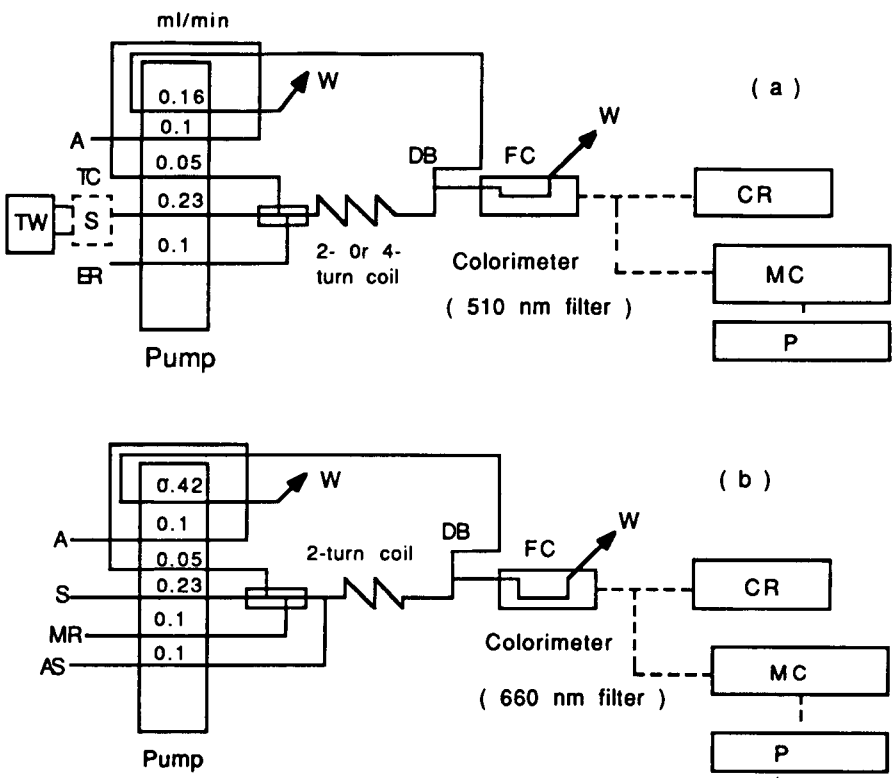

Fig. 1. Diagrams of stopped-flow ASCF instruments for (a) the determination of glucose and for (b) the determination of phosphate. A = air, S = samples, ER = composite enzyme reagent, MR = acid–molybdate reagent, AS = ascorbic acid solution, DB = debubbler, FC = flow cell, CR = strip chart recorder, MC = microcomputer, W = waste, TC = temperature-controlled chamber, TW = thermostated water-bath. Flow-rates are at the nominal pump speed setting of 44.

word, MA). In the former, the absorbance signals from a log-ratio amplifier [22] were recorded directly. With computer data acquisition, absorbances were calculated from transmittances by the computer. The computer system and software have been described previously [21]. Data were processed and plotted by a commercial spreadsheet program, EXCEL (Microsoft).

Reactions used

The enzymatic determination of glucose with glucose oxidase was used to illustrate the performance of the system. The Trinder reaction [21,23] was used to convert the hydrogen peroxide formed into an absorbing red dye whose concentration is directly proportional to the original glucose concentration with an absorption maximum at 510 nm. The rate of the color-forming reaction was much faster than that of the enzymatic reaction.

Spectrophotometric procedures for the nonenzymatic determination of phosphate have been based on the formation of the yellow heteropoly acid [24,25] (measured at ~ 360 nm) or on the reduced heteropoly blue product [26–31] (measured at ~ 660 nm). The latter method is widely applied in clinical determinations. It was used here for investigating the feasibility and analytical performance of the stopped-flow method. Ascorbic acid served as a reducing reagent. For the determination of inorganic phosphate in serum, deproteinization is often used to eliminate interferences from proteins. However, a method for determining serum inorganic phosphorus without deproteinization or dialysis, based on dilution (with sulfuric acid), has been proposed [27]. Here we adopted the dilution method for determining inorganic phosphorus in untreated blood serum. The serum sample was diluted by a factor of 20 with 1% sulfuric acid before the determination.

Reagents and samples

All solutions were prepared in distilled, deionized water. All chemicals (reagent grade) were used without additional purification. For the glucose determinations, glucose (Sigma) standards were made from a 1 g/l stock solution containing 0.5 g/l benzoic acid as a preservative. The glucose oxidase enzyme solution was prepared by dissolving 0.06 g of glucose oxidase (Sigma, Type VII, from *Aspergillus niger*) in 50 ml distilled water. It was subsequently refrigerated. The composite reagent solution consisted of 10 ml of glucose oxidase solution, 5 ml of 10 mM 4-aminoantipyrine (Sigma), 5 ml of 10 mM 3,5-dichoro-2-hydroxyphenyl sulfonic acid (Sigma), about 12 mg of horseradish peroxidase (Sigma, Type II), and 20 ml of 0.05 M phosphate buffer mixed together in an amber bottle before use. A 0.1 M phosphate buffer solution (pH ~ 7.1) was prepared by mixing 13.609 g of KH_2PO_4 and 14.196 g of Na_2HPO_4 in 2 l of distilled water containing a few drops of Brij-35. The serum standard, Monitrol I (Dade) was dissolved and handled as recommended by the manufacturer and diluted with 0.1 M phosphate buffer solution before the determination. The wine samples were buffered and diluted with phosphate buffer.

For the phosphate assay, the phosphate standard solution was prepared by dissolving 0.2195 g of KH_2PO_4 in 1 l of distilled water. This solution contains 50 mg/l phosphorus. A solution of 1% sulfuric acid was prepared for dilution of the serum sample by mixing 10 ml of concentrated sulfuric acid in 1 l of distilled water. Ammonium molybdate solutions (2 g/l) were made 0.3 M in sulfuric acid. These solutions were stable at room temperature. A 5% ascorbic acid solution was prepared by dissolving 5 g of ascorbic acid in 100 ml of distilled water containing 1 ml of glycerine.

Procedures

In the stopped-flow air-segmented continuous flow experiment, samples, reagents, and air were aspirated manually through the pump into the manifold. The absorbance of the flow stream was monitored by continuously drawing a portion of the stream down through the flow cell while the air bubbles and a small amount of liquid passed into a waste container. For kinetic measurements, the stream was halted by turning off the pump manually for a period of time after the absorbance of products reached a plateau. The plateau is a function of aspiration times, tubing lengths and flow-rates as shown in Fig. 2. After stopping the flow, the rate of change of absorbance for a trapped segment can be observed.

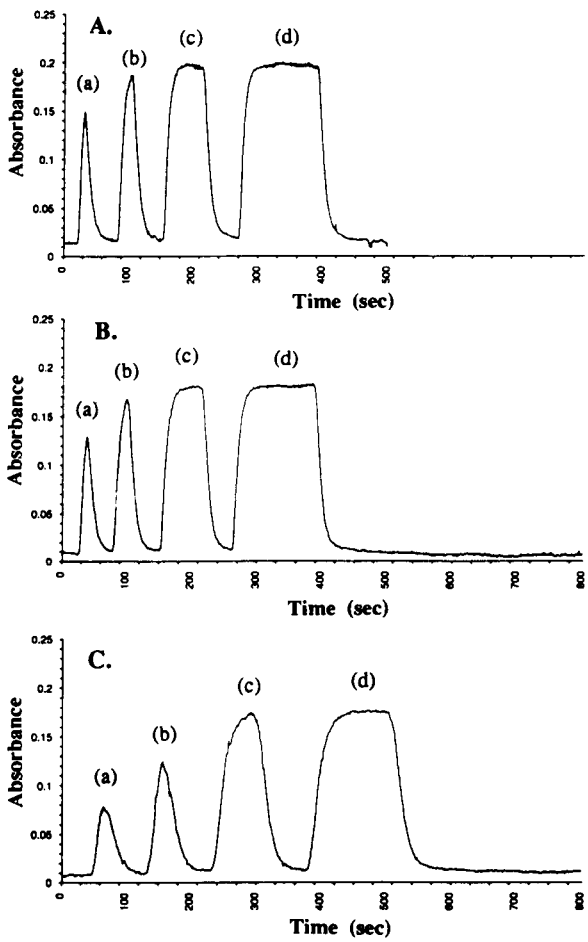

Fig. 2. Response curves as a function of aspiration time with different pump settings and tubing lengths. (A) 2-turn coil at pump setting 82; (B) 4-turn coil at pump setting 82; and (C) 4-turn coil at pump setting 42. All curves recorded with aspiration times of (a) 10, (b) 20, (c) 60 and (d) 120 s, respectively. Samples aspirated are the red dye collected from the waste solution of glucose oxidase/Trinder reaction at 510 nm.

Reaction rates were obtained by measuring the slope of the absorbance versus time plots after the flow was halted. Sample solution was washed out of the system by buffer solution after measurement. For replicate determinations, the stream was pumped through the flow cell after the first stopping period. Consequently, the absorbance signal reached the plateau again, after which the flow was halted. The reactions used for determinations were run at ambient temperature. The diluted wine and serum samples mixed with the composite enzyme reagent were tested here at different pump settings and tubing lengths (2-turn and 4-turn coil). For phosphate measurements only one length of tubing (a 2-turn coil about 12 cm) was employed.

RESULTS AND DISCUSSION

In order to investigate the characteristics of stopped-flow, air-segmented continuous flow, several studies were made. The effect of the time delay before stopping the flow was investigated along with the influence of flow-rate and tubing length.

Effect of delay time

An important factor in the stopped-flow method is the delay time prior to stopping the flow. To characterize this effect, sample and reagent were continuously aspirated into the manifold and the product was monitored. Figure 3 illustrates the important times in a stopped-flow, air-segmented continuous flow experiment. At the start, sample and reagent are introduced into the system and the mixtures are transported to the detector (transport time). The period of time from the absorbance plateau until the flow is stopped is termed the delay time (Fig. 3). During the transport and delay times, the reaction mix-

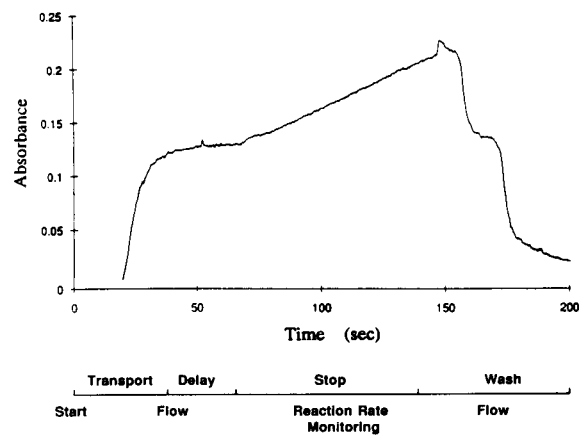

Fig. 3. Typical absorbance versus time curve for stopped-flow ASCF system.

ture is flowing. During the stop time, the flow is stopped, and the kinetics of the reaction are monitored. After the stop time a wash solution is introduced until the absorbance returns approximately to its initial baseline value. Figure 4 shows the effect of delay time on the rate of absorbance change with time. It is found that the slopes of the curves after stopping are essentially independent of delay time in contrast to results obtained from flow injection [15] which are highly dependent on delay time. This independence of delay time is not surprising because when the absorbance plateau is reached, the reaction mixtures arriving in the flow cell have resided in the flow system for the same time. In the experiment illustrated in Fig. 4, sample and reagents are aspirated continuously into the manifold. Even in an ordinary ASCF determination with a fixed amount of sample, the delay time is unimportant as long as the product concentration is on the plateau of the profile. As a result of this effect, when the flow is resumed and the reaction mixture is removed from the optical path (accompanied by a continuous decrease in absorbance), the detector signal returns to the plateau again before the wash solution reaches the detector (Fig. 3). The effect of carryover is negligible for most measurements as indicated in Fig. 5A. For slow reactions, the height of the plateau, as can be expected, is a function of the residence times

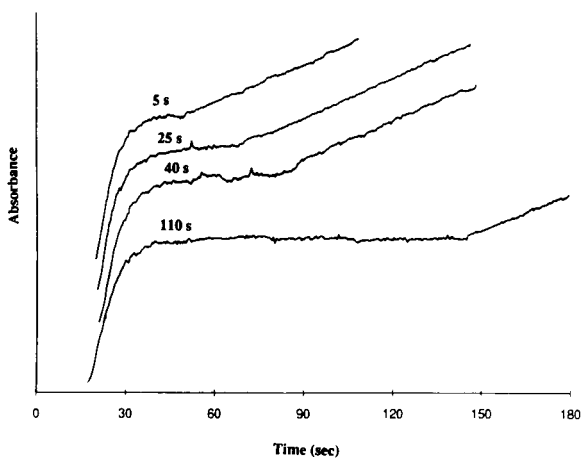

Fig. 4. Effect of delay time on rate measurement for stopped-flow/ASCF system with glucose aqueous standard solution.

which are associated with flow-rates and tubing lengths, as shown in Fig. 5B, and reaction rates are determined by residence times, concentrations of reagents, and reaction temperatures.

Effect of flow-rate and tubing length

Figure 6 shows the effect of flow-rate and tubing length on the reaction rate measurements. Here the same glucose standard solution was used with different residence times. The more turns in the reaction coil and the lower pump settings (proportional to flow-rate), the longer the residence times. For the glucose determination, the reaction rate at longer residence times is slightly higher than that at shorter residence times. However, for the phosphate determination the opposite was found.

For the glucose oxidase reaction, a lower rate is observed at short residence times if the enzyme reaction is still in its induction period. If the residence time is long enough that the reaction is proceeding at its maximum velocity, there is little effect of flow-rate and tubing length until the residence time gets so large that substantial amounts of substrate have reacted prior to the mixture reaching the detector. At these very long residence times, lower rates would be expected. Hence, the rate versus residence time plot should show a maximum. For the molybdenum blue reaction, there is very little induction period [30]. Hence, the lower rate at longer residence times is indicative that the reactant concentrations have changed significantly from their initial values. The reaction temperatures also affect the absorbance plateau which corresponds to the concentration of product as a function of reaction time. The plateau height reaches its maximum value as the reaction temperature increases up to about 40°C and then it decreases gradually.

Calibration curves

The calibration curves for glucose and phosphorus show excellent linearity (for glucose, $r = 0.998$, standard error of estimate $= 0.078$, standard error relative to mean y value $= 3.0\%$; for phosphate, $r = 0.999$, standard error of estimate $= 0.036$, standard error relative to mean y value $= 3.6\%$) under the conditions used. The concen-

tration ranges used were in the clinically relevant range for blood serum monitoring (glucose 10–80 ppm, phosphate 1–10 ppm).

Glucose measurements in wine and serum samples

One of the goals of this study was to apply the proposed procedure in practical determinations. Therefore the kinetic determination of glucose in wine and serum samples was performed at different pump settings and tubing lengths. To evaluate the precision and accuracy of the method, reproducibility tests were performed and measurements were made on spiked sample solutions as well as standard serum samples. To obtain results for 5 replicate measurements required about 5 min during a typical run. Results are given in Table 1 for wine samples and Table 2 for serum samples. Good agreement can be found between values found and manufacturer's values.

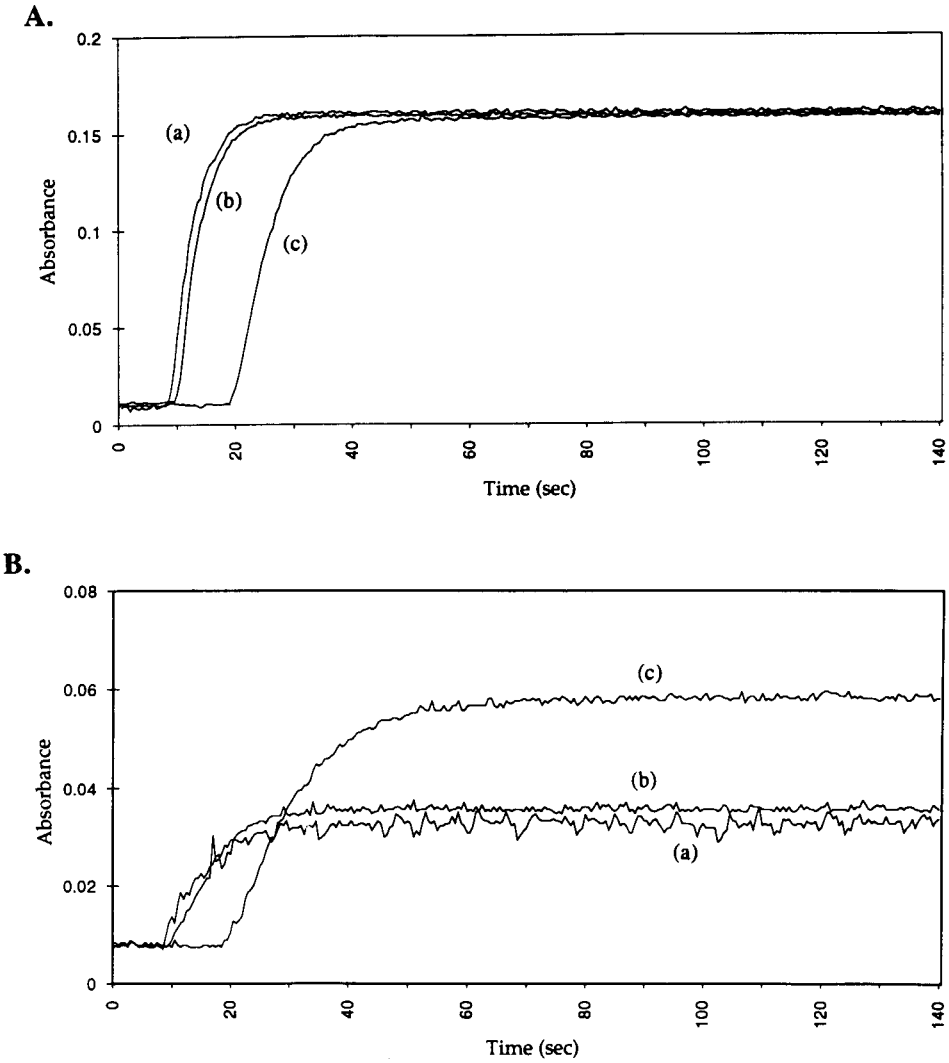

Fig. 5. Response curves; (A) without chemical reaction as the red dye samples are continuously aspirated into the system; (B) with glucose oxidase/Trinder reaction. The plateau height on both parts as a function of residence times at (a) pump setting 82 for 2-turn coil (b) pump setting 82 for 4-turn coil (c) pump setting 42 for 4-turn coil.

TABLE 1

Determination of glucose in wine samples
(Average values of triplicate run for each sample. The relative standard deviation was not more than 4%)

Samples	Conditions [a]	Glucose added (μg/ml)	Glucose expected (μg/ml)	Glucose found (μg/ml)	Recovery (%)	Concentration of glucose (%)
Dry white wine [b]	(1)	0.0		60.1		
		32.0	92.1	92.1	100	
	(2)	0.0		60.7		0.3
		32.0	92.7	91.8	99	
	(3)	0.0		59.8		
		32.0	91.8	90.8	99	
Semi-dry red wine [c]	(1)	0.0		51.9		
			19.5 [d]	18.7	96	
	(2)	0.0		51.4		1.03
			19.5	17.6	90	
	(3)	0.0		51.7		
			19.5	20.4	105	

[a] (1) at pump setting 42 with 4-turn coil, (2) at pump setting 82 with 4-turn coil. (3) at pump setting 82 with 2-turn coil. [b] Dilution factor of 50. [c] Dilution factor of 200. [d] Synthesised solution by mixing 3 ml sample with 2 ml 20 ppm standard solution and 5 ml distilled water.

Phosphate measurements in serum sample

Previous workers [31] have discussed the difficulty of getting consistent results for the determination of inorganic phosphate in serum samples.

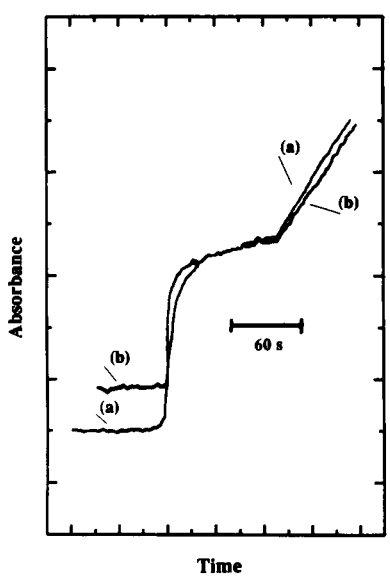

Fig. 6. Recorder tracing for the effect of flow-rates and tubing lengths on reaction-rate measurement with glucose oxidase/Trinder reaction at (a) pump setting 42 for 4-turn coil and (b) pump setting 82 for 2-turn coil.

In untreated serum, high phosphate results are frequently obtained because of interference by high concentrations of paraprotein and other chemical materials [31]. Therefore, most serum samples are treated by dialysis or by precipitation of proteins. Care must be taken because acid treatment can enhance the risk of hydrolysis of labile phosphate bonds. Recently, satisfactory results were obtained by using direct methods [27] with untreated serum. The results obtained here by the dilution method are given in Table 3 and illustrate good agreement with the stated value. These results obtained for glucose and phosphate measurements demonstrate the suitability of the stopped-flow technique in ASCF system for enzy-

TABLE 2

Determination of glucose in serum sample
(Sample was diluted with 0.1 M phosphate buffer solution)

Sample	This work (mg/dl)	Stated mean value (mg/dl)	Range (mg/dl)
Moni-Trol I	81 ± 6 [a]	78 [c]	62–94
Moni-Trol I	80 ± 3 [b]		

[a] At pump settinq 82, average of 7 measurements. [b] At pump settinq 42, averaqe of 8 measurements. [c] Average of 23 certified values.

TABLE 3

Determination of phosphorus in serum sample

Sample	This work (mg/dl)	Stated mean value (mg/dl)	Range (mg/dl)
Moni-Trol I	2.8 ± 0.1 [a]	2.9 [b]	2.3–4.5

[a] Average of 5 measurements. [b] Average of 15 certified values.

matic and non-catalytic reactions. The entire system can be automated by rearrangement of manifolds and by combining these with differential dilution or dialysis systems [27] for clinical analysis.

REFERENCES

1 S.R. Crouch, Chemom. Intell. Lab. Systems, 8 (1990) 259.
2 H.L. Pardue, Anal. Chim. Acta, 216 (1989) 69.
3 H.A. Mottola and D. Perez-Bendito, Anal. Chem., 64 (1992) 407R.
4 D. Perez-Bendito, Analyst, 115 (1990) 689.
5 D. Perez-Bendito and M. Silva, Kinetic Methods in Analytical Chemistry, Ellis Horwood, Chichester, 1988.
6 H.A. Mottola, Kinetic Aspects of Analytical Chemistry, Wiley, New York, 1988.
7 J. Ruzicka and E.H. Hansen, Flow Injection Analysis, Wiley, New York, 2nd edn., 1988.
8 E.H. Hansen, Anal. Chim. Acta, 261 (1992) 125.
9 L.Snyder, J. Levine, R. Story and A. Conetta, Anal. Chem., 48 (1976) 942A.
10 E.B. Townsend and S.R. Crouch, Trends Anal. Chem., 11 (1992) 90.
11 D.J. Hooley and R.E. Dessy, Anal. Chem., 55 (1983) 313.
12 M.D.L. de Castro and M.V. Cases, Analyst, 109 (1984) 413.
13 M. Romero-Saldana, A. Rios and M. Valcarcel, Fresenius' J. Anal. Chem., 342 (1992) 547.
14 H.K. Chung and J.D. Ingle, Jr., Anal. Chem., 62 (1990) 2547.
15 J. Ruzicka and E.H. Hansen, Anal. Chim. Acta, 99 (1978) 37.
16 J. Ruzicka, Anal. Chim. Acta, 261 (1992) 3.
17 J. Ruzicka and T. Gubeli, Anal. Chem., 63 (1991) 1680.
18 B.J. Compton, J.R. Weber and W.C. Purdy, Anal. Lett., 13 (1980) 861.
19 A.S. Olamsky and S.N. Deming, Clin. Chem., 24 (1978) 2115.
20 C.L.M. Stults, A.P. Wade and S.R. Crouch, Anal. Chim. Acta, 192 (1987) 301.
21 C.L.M. Stults, A.P. Wade and S.R. Crouch, Anal. Chem., 59 (1987) 2245.
22 C.J. Patton and S.R. Crouch, Anal. Chim. Acta, 179 (1986) 189.
23 D. Barham and P. Trinder, Analyst, 97 (1972) 142.
24 E. Amador and J. Urban, Clin. Chem., 18 (1972) 7.
25 E.H. Hansen and J. Ruzicka, Anal. Chim Acta, 78 (1975) 145.
26 J. Ruzicka and J.W.B. Stewart, Anal. Chim. Acta, 79 (1975) 79.
27 E.H. Hansen and J. Ruzicka, Anal. Chim. Acta, 87 (1976) 353.
28 M.S. McCracken and H.V. Malmstadt, Talanta, 26 (1979) 467.
29 J.D. Ingle, Jr. and S.R. Crouch, Anal. Chem. 43 (1971) 7.
30 S.R. Crouch and H.V. Malmstadt, Anal. Chem., 40 (1968) 1901.
31 M. Sonnenblick, U. Eylath, R. Brisk, C. Eldad and C. Hershko, Clin. Chem., 32 (1986) 1537.

Analytica Chimica Acta, 284 (1993) 167–171
Elsevier Science Publishers B.V., Amsterdam

Continuous-flow method for the determination of total inorganic carbonate in water

Toyoaki Aoki

Laboratory of Environmental Chemistry, College of Engineering, University of Osaka Prefecture, Gakuen-cho, Sakai 593 (Japan)

Yoshiko Fujimaru, Yuko Oka and Kimiko Fujie

Laboratory of Environmental Science, Department of Natural Science, Osaka Womens University, Daisen-cho, Sakai 590 (Japan)

(Received 18th February 1993; revised manuscript received 12th July 1993)

Abstract

A double-tube separation system with an inner tube of microporous PTFE and an outer tube of PTFE is proposed for the continuous determination of total inorganic carbonate (TIC) in natural waters. Carbon dioxide produced by mixing a sample with 0.5 M sulphuric acid in the outer tube permeates through the microporous PTFE wall and dissolved in 5 mM sodium hydroxide solution in the inner tube. The inner stream passes two electrical conductivity (EC) detectors, one before and the other after the double-tube separator, and TIC in the sample is measured as the difference in the signals obtained from the two detectors. The relative electrical conductivity was proportional to the concentration of TIC in the range 5×10^{-5}–5×10^{-3} M. The limit of detection (signal-to-noise ratio = 3) was 1.0×10^{-5} M. The time required for a 98% response was 2 min. Sulphide interfered but was completely decomposed by using chromate. The method was applied to the determination of TIC in lake waters.

Keywords: Flow system; Carbonate; Membrane separation; Waters

Inorganic carbonates play a major role in regulating the chemical composition of natural waters. Therefore, the distribution of carbonates needs to be accurately quantified in order to understand their effects on natural waters [1–3].

There are many methods for the determination of total inorganic carbonate (TIC) in water. However, they are batch methods and time consuming, and are not suitable for in situ measurements [4,5].

Correspondence to: T. Aoki, Laboratory of Environmental Chemistry, College of Engineering, University of Osaka Prefecture, Gakuen-cho, Sakai 593 (Japan).

Carlson [6] reported a continuous-flow method for the determination of dissolved carbon dioxide by a membrane separation. The method was based on the transfer of carbon dioxide by diffusion through silicone-rubber hollow fibres into a flowing stream of deionized water, followed by electrical conductivity (EC) detection.

We previously reported continuous-flow methods for the determination of free chlorine [7], ammonia [8] and total trihalomethanes [9] in water by membrane separation with a microporous PTFE membrane. In this paper, the application of this technique to the determination of TIC with EC detection is presented. The sensitivity of this method is about 100 times greater than that reported by Carlson [6].

0003-2670/93/$06.00 © 1993 – Elsevier Science Publishers B.V. All rights reserved

EXPERIMENTAL

Reagents

All reagents were of analytical-reagent grade. Distilled, deionized water was used in the preparation of all solutions. A stock standard solution of TIC was prepared from sodium carbonate, which was dried at 410°C. Working standard solutions were prepared by serial dilution of the stock standard solution just before use.

Apparatus and procedure

A schematic diagram of the apparatus used in the determination of TIC is shown in Fig. 1. A sample (S) was mixed with sulphuric acid (H) and then allowed to flow into the outer tube (T2) of the membrane separation unit (M). The construction of the separation unit was as described previously [7]. Molecular carbon dioxide, liberated by mixing the sample with sulphuric acid, permeates through a microporous membrane (T1) to dissolve in a stream of sodium hydroxide solution (R) whose electrical conductivity was measured with two EC detectors (D1, D2), one before and the other after the membrane separator. TIC in a sample was determined from the difference in the two EC values. In this system, conductivity decreased with increase in TIC owing to neutralization of sodium hydroxide by absorption of carbon dioxide in the inner tube.

Unless mentioned otherwise, the flow-rates of the sample, hydrogensulphate solution and sodium hydroxide solution was adjusted to 5.1, 1.5 and 1.5 ml min^{-1}, respectively, with a peristaltic pump (P; Master Flex type). The system, except for the pump (P), was thermostated (C) at 5°C. The length of the separation unit was 50 cm. T1 was made of microporous PTFE (1.8 mm o.d., 1.0 mm i.d., maximum pore size 3.5 μm) (Japan GoreTex) and T2 was made of PTFE (4.0 mm o.d., 3.0 mm i.d.). The electrodes of the conductivity cells were made of stainless steel and the gap between the electrodes of each cell was 1.0 mm.

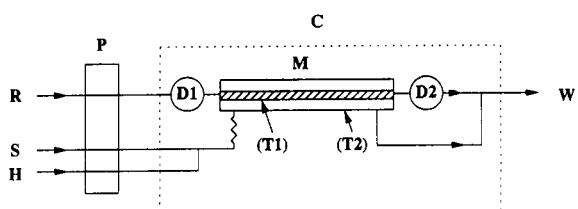

Fig. 1. Schematic diagram of continuous-flow system for determination of TIC in water. S = sample; H = 0.5 M sulphuric acid; R = 5 mM sodium hydroxide; M = membrane separation unit; T1 = microporous PTFE tube; T2 = PTFE; C = thermostat; D = electrical conductivity detector; P = peristaltic pump; W = waste.

RESULTS AND DISCUSSION

Effect of pH on permeation

Inorganic carbonate exists in natural waters as H_2CO_3 (CO_2), HCO_3^- and CO_3^{2-}. The pH of natural water is usually in the range 6–8. In this range, carbonate exists primarily in the anionic form, HCO_3^-, which cannot permeate through the microporous PTFE membrane. Therefore, the conversion of HCO_3^- into H_2CO_3 (CO_2) was studied by measuring the change in the conductivity at various pH values (adjusted with 0.1 M phosphate buffer solution) of sample solutions fed into the system as shown in Fig. 1.

The relative conductivity increased with decrease in the pH of the sample solutions and became constant below pH 3, as shown in Fig. 2. The distribution of HCO_3^- and H_2CO_3 is also shown in Fig. 2 as a function of pH. The equilibrium constant used for the calculation was taken from Sillén and Martell [10]. The theoretical distribution agrees very closely with those obtained experimentally. In subsequent experiments, sample solutions were acidified to pH < 3 by addition of 0.5 M H_2SO_4. When sea water was used as the sample, the pH of a mixture with 0.5 M H_2SO_4 was 1.05.

Effect of sodium hydroxide

The sensitivity of the method depends to a great extent on the concentration of sodium hydroxide flowing in the inner tube. Figure 3 shows the relationships between concentration of TIC and concentration of sodium hydroxide. When the concentration of sodium hydroxide decreases, the relative conductivity starts to level off at lower concentrations of TIC. This may be due to

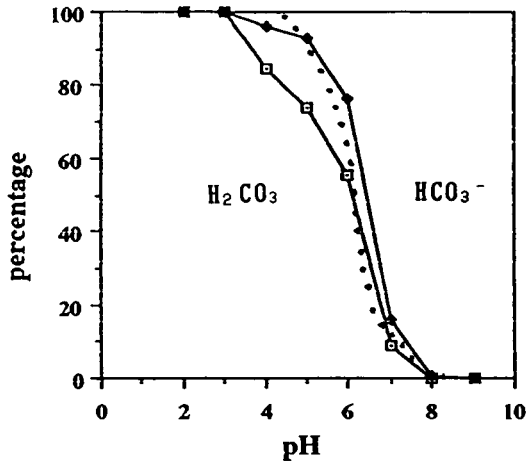

Fig. 2. Relative conductivity and calculated distribution (dotted line) of inorganic carbonate species in aqueous solution as a function of pH. □ = 0.3 mM TIC; ■ = 0.6 mM TIC.

the consumption of sodium hydroxide by neutralization with a large amount of carbon dioxide for higher concentrations of TIC. On the other hand, the precision became worse with increase in concentration of sodium hydroxide. The relative standard deviations ($n = 5$) at 3 mM TIC were 1.0% at 2.5 mM, 1.5% at 5.0 mM, 5.6% at 7.5 mM and 5.4% at 10.0 mM sodium hydroxide. As a compromise, the concentration of sodium hydroxide was selected as 5.0 mM. Under these conditions, TIC in natural waters can usually be determined by this method.

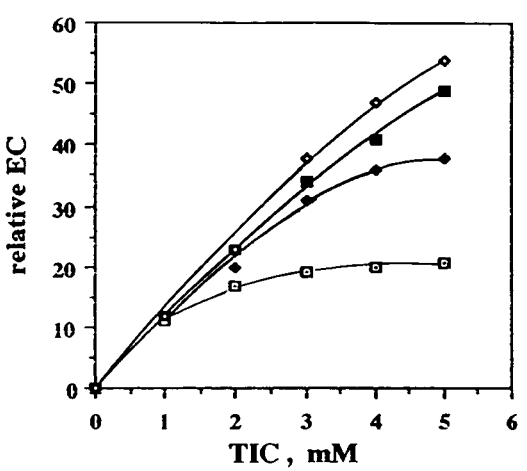

Fig. 3. Effect of concentration of NaOH in inner tube on calibration graphs for TIC. □ = 2.5 mM NaOH; ◆ = 5.0 mM NaOH; ■ = 7.5 mM NaOH; ◇ = 10 mM NaOH.

Effect of temperature

The relative conductivity increased with increase in temperature of the thermostat (C). In the temperature range 5–25°C at 0.5 mM TIC, the change in conductivity was 1.4 μS cm^{-1} °C^{-1} and corresponded to 1.33% of the signal response. This is probably due to the decrease in the solubility and increase in the permeation rate of carbon dioxide through the membrane separator with increase in temperature. Therefore, it is necessary to keep the temperature of the system constant. At high temperatures, however, many air bubbles were produced which entered the EC detector causing a fluctuation of the baseline. Consequently, the system was held at 5°C, which was low compared with the usual water temperature.

At 5°C, the transfer rate of carbon dioxide produced from TIC in the sample solution to the sodium hydroxide solution (5 mM) was 47 ± 3% in the TIC concentration range 0.1–2.0 mM.

Analytical performance

The sensitivity of the method depends to a great extent on the dimensions of the separation unit (M). If the length of the microporous PTFE tube was shorter, response time was shorter but sensitivity was lower. For a tube length of 50 cm, it took 2.5 min after the sample solution began to flow into the system to reach a constant relative conductivity. The time required to reach 98% of the constant signal was 2.0 min. The relative conductivity was linearly proportional to TIC concentration from 5×10^{-5} to 5×10^{-3} M. The relative standard deviations ($n = 5$) were 3.4% at 0.1 mM TIC and 1.8% at 0.6 mM TIC. The detection limit (signal-to-noise ratio = 3) was 0.01 mM.

Typical daily changes in the calibration graph in the TIC concentration range 0.2–1.0 mM was as follows:

(Jan. 21, 1993) $y = 7.56x - 0.06$ ($R = 0.98$)

(Jan. 23, 1993) $y = 7.57x - 0.03$ ($R = 0.99$)

(Jan. 25, 1993) $y = 7.07x - 0.02$ ($R = 0.98$)

TABLE 1

Results obtained with sodium hydroxide solution and distilled water as the flowing stream in the inner tube

TIC (mM)	Relative conductivity	
	NaOH solution [a]	Distilled water [b]
0.3	142	1.5
0.6	290	2.8
0.9	380	3.5
1.2	490	4.2
1.5	580	4.9

[a] In this system, TIC was determined in samples under the conditions of 5 mM NaOH as the flowing stream, 0.5 M H_2SO_4 as acid and temperature 5°C. [b] The conditions were the same as for the NaOH system except for the use of distilled water instead of NaOH solution.

TABLE 2

Interference of foreign species with the determination of TIC [a]

Species	Concentration of species (mM)		
	1	2	3
Sodium chloride	97	97	98
Sodium nitrate	102	98	97
Sodium sulphate	97	97	102
Ammonium chloride	96	98	97
Glycine	97	101	100
Sucrose	105	99	101
Citric acid	104	100	100
Acetic acid	101	98	99

[a] Concentration of TIC = 0.3 mM. Results are recovery (%) compared with TIC alone.

where y, x and R are the relative signal response, concentration of TIC and correlation coefficient, respectively. The linearity of the calibration graphs was satisfactory.

As mentioned, Carlson [6] determined TIC using a membrane separation system that was based on the transfer of carbon dioxide by diffusion through silicone-rubber hollow fibres into a flowing stream of deionized water. With the present system, TIC was determined in samples by using distilled water instead of sodium hydroxide solution in the inner tube (T1). The results are compared with those obtained by using sodium hydroxide solution in Table 1. The sensitivity of the present method was about 100 times larger than that using distilled water for the flowing stream in the inner tube.

Interference studies

Table 2 lists levels of interference with 0.3 mM TIC for various species that occur in natural waters. The concentrations of each species in this study were much higher than those in natural waters. These species did not interfere with the determination of TIC in this method, as none of them could permeate through the microporous PTFE membrane.

Under anaerobic conditions in natural waters, sulphide is produced by sulphate reduction, which occurs not only as an assimilation process but also as a respiratory process [11]. Sulphide is converted into volatile H_2S in acidic media and can pass as such through a microporous membrane.

Figure 4 shows calibration graphs for both sulphide and TIC under the same analytical conditions. The calibration equations are

$$y = 3.25x_a + 0.022 \quad (R = 0.99)$$

$$y = 1.88x_b + 0.024 \quad (R = 0.99)$$

where y, x_a, x_b and R are the relative signal response, concentration of TIC, concentration of sulphide and correlation coefficient, respectively. Hence the sensitivity for the determination of TIC was 1.73 times larger than that for sulphide.

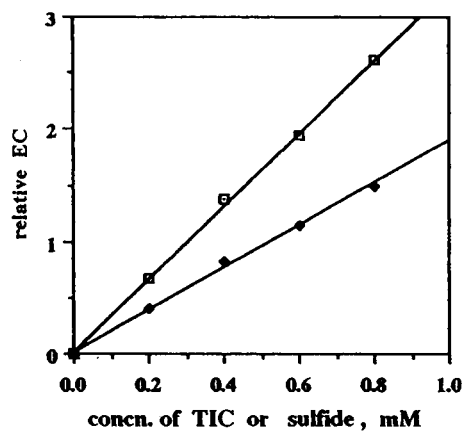

Fig. 4. Calibration graphs for (□) TIC and (♦) sulphide. Inner solution in separator and acidic reagent were 5.0 mM NaOH and 0.5 M sulphuric acid, respectively.

In the determination of TIC in samples containing sulphide, it is necessary to decompose the latter. Various oxidizing reagents were tested such as Cr(VI), Mn(VII) and H_2O_2, which are non-volatile. Cr(VI) was the best with respect to decomposition rate. Figure 5 shows the decomposition rate of sulphide using Cr(VI) which was dissolved in 0.5 M H_2SO_4 (H). In this case, various lengths of reaction coils (PTFE, 3.0 mm o.d. and 2.0 mm i.d.) were inserted before the membrane separation unit after mixing the sample with 0.5 M H_2SO_4 containing Cr(VI). When using 0.1 M Cr(VI), 0.6 mM sulphide was completely decomposed in less than 5 min.

Application

Continuous determinations of TIC were performed at Akanoi, Lake Biwa using the proposed method. At the same time, lake water was taken from the same sampling site and analysed in duplicate within 6 h with a non-dispersive infrared (NDIR) spectrometer (Shimazu, Model TC500) by catalytic combustion. The results are given in Table 3. For all samples, the concentrations of TIC obtained by the proposed method were in agreement with those given by the NDIR method, within experimental error.

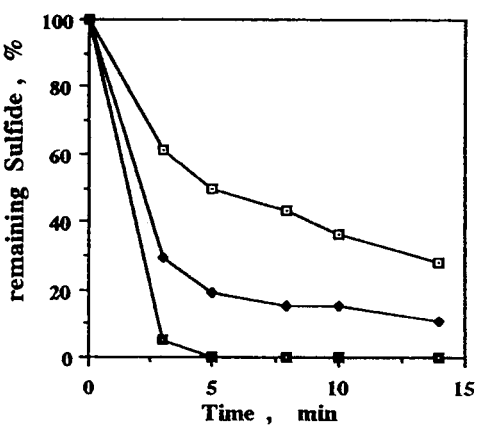

Fig. 5. Decomposition of sulphide using chromate. Experimental conditions are given in the text. □ = 0.01 M Cr(VI); ◆ = 0.05 M Cr(VI); ■ = 0.10 M Cr(VI).

TABLE 3

Comparison of the proposed and NDIR methods for determination of TIC in lake water [a]

Date	Concentration of TIC (mM)	
	Proposed method	NDIR method
5th Aug. 1991	0.58, 0.56	0.56, 0.55
19th Aug. 1991	0.54, 0.55	0.55, 0.56
20th Aug. 1991	0.63, 0.62	0.65, 0.64

[a] Samples were taken at Akanoi, Lake Biwa.

Studies on the changes in TIC concentration in lake water and sea water using this method are in progress.

The authors thank the Rikoh Kagaku Labs. for the construction of the TIC analyser. We also thank K. Kawamoto, K. Ohta, S. Tatsumi in Valves R&D, Kubota, for financial support. Acknowledgement is made to Dr. M. Nakanishi (Centre for Ecological Research, Kyoto University) and Dr. M. Kumagai (Lake Biwa Research Institute) for helping to obtain samples at Akanoi, Lake Biwa.

REFERENCES

1 J.J. Bisogni, Jr. and S.L. Arroyo, Water Res., 25 (1991) 185.
2 A. Lerman and W. Stumm, Water Res., 23 (1989) 139.
3 A.L. Herczeg and R.H. Hesslein, Geochim. Cosmochim. Acta, 98 (1984) 837.
4 American Public Health Authority, American Water Works Association and Water Pollution Control Federation, Standard Methods for the Examination of Water and Wastewater, APHA, Washington, DC, 17th edn., 1989, 4–13.
5 J.F. Dye, J. Am. Water Works Assoc., 50 (1958) 812.
6 R.M. Carlson, Anal. Chem., 50 (1978) 1528.
7 T. Aoki and M. Munemori, Anal. Chem., 55 (1983) 1620.
8 T. Aoki, S. Uemura, and M. Munemori, Environ. Sci. Technol., 20 (1986) 515.
9 T. Aoki and K. Kawakami, Water Res., 23 (1989) 739.
10 L.G. Sillén and A.E. Martell (Eds.), Stability Constants of Metal-Ion Complexes, Chemical Society, London, 1964.
11 H.L. Ehrlich, Geomicrobiology, Marcel Dekker, Basle, 1990, pp. 449–513.

Analytica Chimica Acta, 284 (1993) 173–179
Elsevier Science Publishers B.V., Amsterdam

Flow-injection determination of oxalate by a photoinduced chemiluminescent reaction

Tomás Pérez-Ruiz, Carmen Martinez-Lozano, Antonio Sanz and Otilia Val

Department of Analytical Chemistry, Faculty of Chemistry, University of Murcia, 30071 Murcia (Spain)

(Received 7th May 1993; revised manuscript received 12th July 1993)

Abstract

A new approach for the sensitive determination of oxalate was developed. Iron(II) generated in the photochemical decomposition of iron(III)–oxalate complex was measured by its catalysis of the chemiluminescent luminol reaction in the abscence of added oxidant. A flow-injection configuration is proposed for the determination of oxalate over a concentration range of 1.0×10^{-7}–1.0×10^{-4} M with a throughput of 30 samples/h. The effect of a large number of potential interferents was investigated and a method devised for the determination of oxalate in urine.

Keywords: Flow injection; Chemiluminescence; Oxalate; Urine

Photochemical reactions have long been used to enable the sensitive determination of photoactive analytes in complex matrices because of their selectivity and sensitivity, which can easily be enhanced by modifying the wavelength of the light used for irradiation and by increasing the lamp power [1–4].

The application of chemiluminescence (CL) to quantitative analysis has recently received much attention because of the several substantial advantages it has over other spectrometric techniques. One major advantage is that it does not suffer from problems of light scattering or background emission because no external radiation source is used. A wavelength selector is usually not required, and so a photomultiplier tube directly views the CL without wavelength discrimination so that it is possible to detect low light levels in CL analysis. Other advantages of CL reactions include linear working ranges of several orders of magnitude and simplified instrumentation that requires virtually no optics for operation [5–7].

Both CL detection and flow-injection analysis (FIA) are cheap, compact and simple from a technical point of view. FIA can provide the exact reproducibility of sample and reagent mixing that is so essential for precise CL studies. The combination of FIA and CL detection has received the considerable attention of several groups, including Townshend and co-workers [8–10] and Nakagama et al. [11], who have published a number of papers on the development of flow-injection systems for the determination of organic and inorganic analytes.

Recently, it has been established that the irradiation of photoreactive analytes leads to the formation of species that can be detected by CL. However, until now, such photochemical-chemiluminescence detectors have rarely been used in simple hydrodynamic systems such as FIA [12].

The photochemistry of the iron(III)–oxalate complex (ferrioxalate) has been thoroughly investigated [13]. It is the most widely used actinometer solution [14,15] and has also been used for the

Correspondence to: T. Pérez-Ruiz, Department of Analytical Chemistry, Faculty of Chemistry, University of Murcia, 30071 Murcia (Spain).

0003-2670/93/$06.00 © 1993 – Elsevier Science Publishers B.V. All rights reserved

photochemical determination of iron and oxalate using different approaches [16–22].

The determination of oxalate in body fluids has attracted the attention of many workers [23] because of clinical interest in the diagnosis of hyperoxaluria and genetic disorders of oxalate metabolism [24]. Several enzymatic and non-enzymatic flow-injection methods have been published for the determination of oxalate using amperometric, photometric, fluorimetric and CL detection [21,22,25–27].

In this paper, a new method based on FIA coupled to photochemically induced chemiluminescence is described for the determination of oxalate. The method uses the photochemical decomposition of ferrioxalate, and the iron(II) generated is determined by the production of CL in a luminol system in the absence of added oxidant. Levels as low as 1×10^{-7} M oxalate can easily be determined by measuring the intensity of the light produced.

EXPERIMENTAL

Apparatus

A shielded and separately housed SLM-Aminco Model JD490 photomultiplier tube (PMT) was used as a light detection system. The PMT output was amplified and quantified by an SLM-Aminco Series 2 spectrofluorimeter connected to a personal computer fitted with the SLM-Aminco Data Manager software (designed for handling luminescence data). A Gilson Minipuls-4, an Omnifit rotary valve and an Eurolight tungsten halogen lamp (500 W, 250 V) were also used. Except for the pump tube (Tygon), PTFE tubing (0.5 mm i.d.) was used through the manifold. The CL cell was a Hellma 170. QS flow cell placed in a thermostated cell holder immediately in front of the PMT, with a mirror behind; the volume of the cell was 80 μl exposing a large surface area to the adjacent PMT. Extreme precautions were necessary to ensure that the sample compartment and PMT were light-tight, in view of the high instrument gain settings used.

The photoreactor was a 250-cm PTFE tubing (0.5 mm i.d.) coiled around a glass tube of 0.5 cm diameter placed inside a Pyrex cylinder with a double-walled well through which cooling water continuously flowed. This ensemble was housed in a metal box to protect it from light other that of the lamp. The inside of the box was covered with aluminium foil to permit maximum reflectance of the light from the lamp.

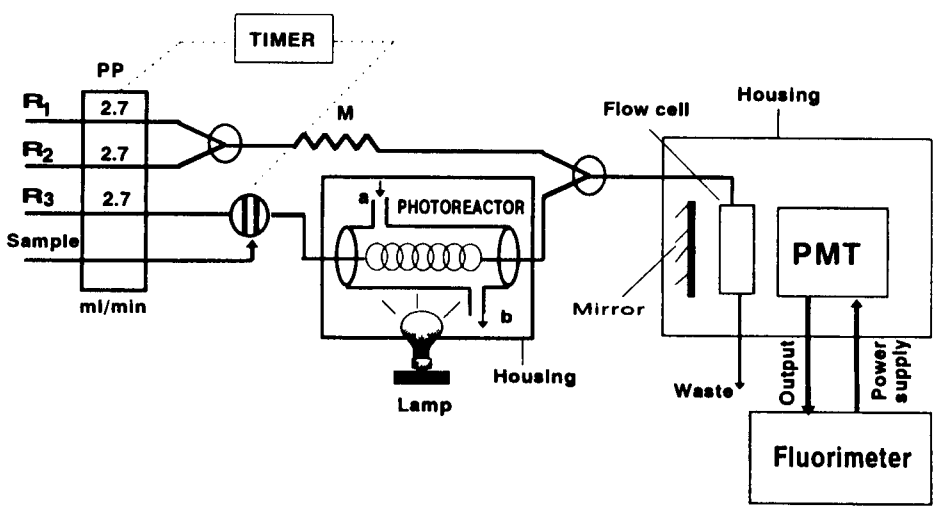

Fig. 1. Manifold for the determination of oxalate. PP = Peristaltic pump (with flow-rate given in ml min^{-1}); R_1 = 1 M borate buffer pH 11; $R_2 = 5 \times 10^{-4}$ M luminol; $R_3 = 5 \times 10^{-4}$ M iron (III) in 0.01 M sulphuric acid concentration and 0.01% PVA (w/v); M = mixing coil; a and b = inlet and outlet of water respectively. Dashed lines represent synchronous control line.

A timer synchronized to the injection system, allowed the flow to be stopped at any delay time and for any length of stop time.

Manifold

The schematic diagram of the instrumental setup is shown in Fig. 1 with optimum conditions as stated. The sample was injected into the iron(III) stream with the aid of a rotary valve having a 235-μl loop. When the sample zone was located in the photochemical reactor the flow was stopped and the irradiation was carried out with the halogen lamp placed at a distance of 10 cm from the reactor. After irradiation, the pump was triggered by the timer and the Fe(II) generated in the photochemical decomposition of the Fe(III)–oxalate complex merged with the buffered luminol stream at the Y-piece in front of the flow cell. The distance between the Y-piece and the flow cell was 10 cm (minimum distance achieved). The light emitted by the Fe(II)–luminol system was detected with a PMT with no wavelength discrimination and amplified by the spectrofluorimeter. The PMT voltage used ranged from 600 to 850 V and the results obtained were always normalized to a PMT voltage of 700 V.

The tubes of the luminol and buffer streams and that leading from the photoreactor to the flow cell were covered with black insulating tape, to prevent a fibre optic effect introducing stray light into the detector.

Reagents

All chemicals were of analytical reagent grade and were used without further purification. Doubly distilled water was used throughout.

A 1×10^{-2} M oxalate standard solution was prepared from sodium oxalate dried at 100°C and stored in a desiccator over calcium chloride. Working standard solutions were prepared by appropriate dilution immediately before use.

Iron(III) stock solutions were prepared from iron(III) sulphate in 0.01 M sulphuric acid. These solutions also contained 0.01% poly(vinyl alcohol) in order to hinder the Fe(III) precipitation in the manifold.

Borate buffers were prepared from 0.25 M sodium tetraborate and sufficient 5 M sodium hydroxide or hydrochloric acid to give the desired pH.

RESULTS AND DISCUSSION

Basis of the method

The irradiation of solutions containing iron(III) and oxalate in aqueous acidic media yield iron(II) [13–15]. The excellent photosensitivity of this system is partly due to the high quantum efficiency ($\phi \approx 1$ at 254–500 nm). Other important features which have led to the system being so widely used are its degree of stability and reproducibility.

Oxalate may be determined conveniently by measuring the Fe(II) produced in this photochemical reaction. It has traditionally been detected by measuring the absorbance after complexation with 1,10-phenanthroline [19] or the current intensity with a glassy carbon electrode polarized to +0.9 V against Ag/AgCl [22,23]. However, there has been no mention of the CL detection of such Fe(II) based on its catalytic effect on the oxidation of luminol although it is very sensitive [28,29].

The photochemical determination of oxalate using CL detection may be described by the following reactions:

$$2Fe(C_2O_4)^+ \xrightarrow{h\nu} 2Fe^{2+} + 2CO_2 + C_2O_4^{2-}$$

$$\text{Luminol} + O_2 + 2OH^- \xrightarrow{Fe^{2+}} \times 3\text{-aminophthalate} + N_2 + 2H_2O + h\nu$$

The reactions have to be carried out in different conditions, an acidic medium for the photochemical reaction and a basic medium for the CL reaction, which is why a flow system is a very appropriate approach.

CL reaction. Knowing the speed of the CL reaction and the effect of mixing reagents on CL intensity is of great importance for the design of the flow system. In general, the mixing order and mixing time interval of the reagent solutions play a key role in achieving good sensitivity in flow CL analysis because transient light emission is monitored.

It was found that the emission intensity was dependent of the way of mixing the reagents

[buffer, Fe(II) and luminol solutions]. The greatest CL signal was obtained when the buffer and luminol streams were mixed within the flow system prior to merging with the Fe(II) stream. The light emission occurred very rapidly and reached maximum intensity within 1 s. This clearly suggests that the sample and reagent stream should be mixed as close as possible to the flow cell.

Photochemical reaction. The photochemical reduction of ferrioxalate to produce iron(II) ions must be carried out in acidic medium in order to obtain reproducible results. This situation is more critical for cases where the iron(III)/oxalate ratio is > 1. A sulphuric acid concentration over the range 0.1–0.01 M is sufficient to avoid the deleterious action of oxygen.

Manifold design. The manifold shown in Fig. 1 was designed taking into account the characteristics of the CL and photochemical reactions. The solution emerging from the photoreactor contains small amounts of Fe(II) in the presence of a large amount of Fe(III); when this solution merges with the alkaline buffered luminol solution, the precipitation of hydrated iron(III) occurs with accompanying instability of the CL signal and blocking of the tubes. The precipitate is colloidal and can be stabilized by addition of surfactants. In addition to overcoming the solubility problem, their presence also alters the pathway of the chemical and photophysical processes and can be an effective means of enhancing the photochemical and CL reactions [30,31]. Thus, the effects of aqueous micellar systems of each charge type (i.e., cationic, anionic, zwitterionic, or nonionic) were studied in order to eliminate the solubility problem and improve sensitivity and precision.

The surfactants employed were hexadecyltrimethylammonium bromide and chloride, sodium dodecyl sulphate, triton X-100, poly(vinyl alcohol), 3-(*N*-dodecyl-*N*,*N*-dimethylammonium)-propane-1-sulphonate and Span-20. Poly(vinyl alcohol) (PVA) gave the best results as regards sensitivity and reproducibility, and was chosen for further study.

Optimization of manifold parameters

The variables studied were flow-rate, volume injected and time of irradiation. The reagent concentrations used in these experiments were as follows: iron(III) line, 4×10^{-4} M Fe^{3+}, 0.01 M H_2SO_4 and 0.02% PVA; luminol line, 6×10^{-4} M; buffer line, 1 M borate buffer pH 10.5; sample solution 2×10^{-5} M. The mixing ratio between the luminol line and buffer line was always 1 : 1. The irradiation time used was 24 s.

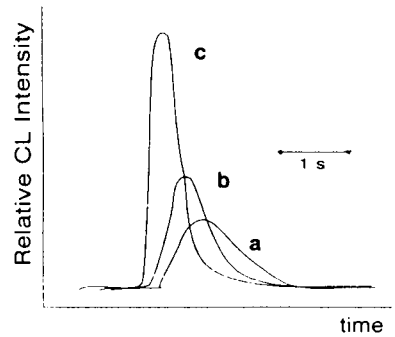

Fig. 2. Signal profiles for a total flow-rate of: (a) 6; (b) 8; (c) 12 ml min^{-1}. Conditions: sample injected, 200 μl of 2×10^{-6} M oxalate; irradiation time 24 s.

Determination of the total flow-rate is important because the time taken to transfer the irradiated sample to the photon counter is critical for obtaining a high CL intensity. The signal profiles obtained at different flow rates are shown in Fig. 2. These results indicate that the CL reaction is very fast; the intensity reaches a maximum less than 1 s after the irradiated sample stream merges with the buffered luminol stream. However, a stopped flow experiment revealed that the time to reach maximum intensity is < 0.05 s, which corresponds to the time required to travel from the mixing point to the inlet of the flow cell only when the total flow-rate is 20 ml min^{-1}. Thus, there is no increase in signal when the stream at a flow-rate of 20 ml min^{-1} is suddenly stopped. At total flow-rates higher than 14 ml min^{-1} the signal became noisy and irreproducible. A flow-rate of 12 ml min^{-1} was chosen as a compromise between sensitivity and reproducibility.

The sample volume was varied between 35 and 285 μl. The peak heights increased with increasing volumes injected up to 235 μl, above which they remained virtually constant. A sample volume of 235 μl was chosen for further experiments.

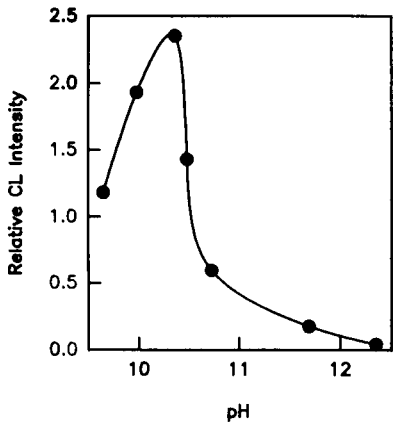

Fig. 3. Effect of pH on the CL intensity for 2×10^{-6} M oxalate.

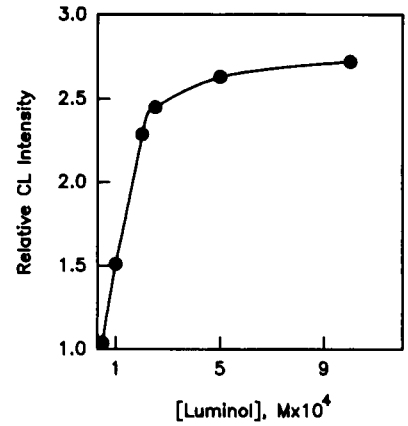

Fig. 4. Effect of the luminol concentration on the CL intensity for 2×10^{-6} M oxalate.

The photoreactor length selected was 250 cm, of which 200 cm was irradiated with the lamp located 10 cm from the reactor.

Special attention was paid to the influence of the irradiation time on the CL signal. Different irradiation times were achieved by halting the flow when the sample was located in the photoreactor and then irradiating it for different times. The extent of the photochemical reaction increased with the length of the irradiation time. An irradiation time of 60 s was chosen as a compromise between sensitivity and sampling rate.

Optimization of reagent concentration

The pH of the solution in the flow cell has a great influence on peak height (Fig. 3), the maximum CL intensity being obtained at pH 10.5. Of the several buffers tested, borate buffer exhibited the best properties although its buffering capacity is low at that pH. The sulphuric acid concentration of the iron(III) solution should be the lowest of the recommended range (0.01 M) so that the pH after mixing with the luminol stream remains as close as possible to the optimum value. Taking all these points into consideration, a 1 M borate buffer pH 11 was chosen to obtain a pH of around 10.5 in the flow cell.

The effect of the concentration of luminol and iron(III) solutions on CL intensity is shown in Fig. 4 and Fig. 5 respectively; 5×10^{-4} M luminol and 5×10^{-4} M iron(III) are recommended and were used throughout.

The influence of the concentration of PVA added to the iron(III) solution was studied over the range 0–0.2%. Reproducible CL intensities were obtained only when the PVA concentration was higher than 0.005%. The concentration adopted in the procedure was 0.02% (w/v).

Calibration graph and reproducibility

A series of standard solutions were injected into the manifold under the optimized conditions to test the linearity of the calibration graph. The

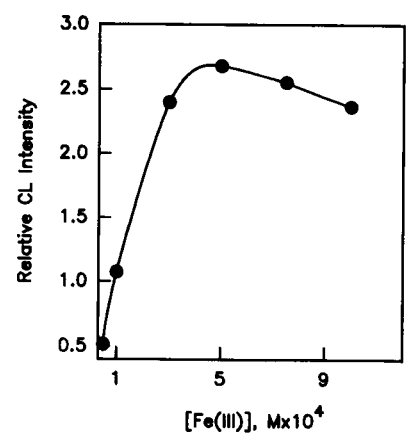

Fig. 5. Effect of the iron(III) concentration on the CL intensity for 2×10^{-6} M oxalate.

calibration graph was linear from 1.0×10^{-7} to 1.0×10^{-4} M. The sampling rate was about 30 samples/h. The statistical study performed on 10 sets of triplicate injections of 5.0×10^{-5}, 5.0×10^{-6} and 5.0×10^{-7} M oxalate yielded relative standard deviations of 0.66%, 1.3% and 1.9%, respectively.

The method was tested for several synthetic samples of oxalate. Some of the analytical results are given in Table 1 and, as can be seen, the errors of these determinations were always less than 3%.

Interferences

An extensive interference study with a view to determining oxalate in body fluids was performed. Samples containing a fixed concentration of oxalate and various concentrations of the foreign substance were injected into the flow system. A substance was considered not to interfere if the variation in the peak height of oxalate was less than ±3%.

The results are shown in Table 2. There are at least three types of interference. The first acts on the CL reaction; the second on the photochemical reaction and the third by reducing Fe^{3+} to Fe^{2+}.

The interferences of Cu^{2+}, Mn^{2+}, Cr^{3+} and Ni^{2+} are possibly due to catalytic effect on the oxidation of Fe^{2+} to Fe^{3+}, while Co^{2+} interference is due to its activity as a catalyst of the CL reaction [28,29,32].

The hydroxy acid anions (tartrate, citrate and lactate) form photochemically active complexes and interfere by producing Fe^{2+} in a competing reaction [1].

The interference of ascorbic acid can be minimized by incorporating a mini-column containing ascorbate oxidase. The sample is passed through the column prior to injection into the flow system.

Determination of oxalate in urine

The proposed method was applied satisfactorily to the determination of oxalate in urine. A prior separation of the analyte by precipitation with calcium chloride is recommended. The precipitation was carried out following the recommendations of Koch and Strong [33]. The precipitate of calcium oxalate was washed with saturated calcium chloride solution and dissolved in 0.1 M sulphuric acid. The resulting solution was suitably

TABLE 1

Determination of oxalate in synthetic samples

Sample	Taken (ng ml^{-1})	Found [a] (ng ml^{-1})	Error (%)
1	8.8	9.0	+2.27
2	17.6	17.5	−0.56
3	44.0	44.6	+1.36
4	176	172	−2.27
5	880	872	−0.90
6	8800	8730	−0.80

[a] Average of four determinations.

TABLE 2

Tolerance to different ions in the determination of oxalate [a]

Species added	Maximum tolerable mole ratio
NO_3^-, SO_4^{2-}, Cl^-, acetate, formate, barbituric acid,urea, K^+,Na^+, Mg^{2+}, Ca^{2+}, Ba^{2+}, Cd^{2+}, Zn^{2+}	500 [b]
PO_4^{3-}, glucose, hippuric acid, malonate, acetylsalicylic acid	100
Succinate, salicylate	20
Cr^{3+}, Ni^{2+}	10
Picrate, lactate	2
Tartrate, citrate, Co^{2+}, Mn^{2+}	0.1
Cu^{2+}, uric acid, ascorbic acid	0.01

[a] Oxalate concentration 4×10^{-6} M. [b] Maximum ratio tested.

TABLE 3

Determination of oxalate in urine

Sample	24-h urine volume (l)	Proposed method [a] (mmol day^{-1})	Sigma oxalate–oxidase method [b] (mmol day^{-1})
1	1.20	0.15	0.16
2	1.50	0.20	0.19
3	0.90	0.14	0.15
4	0.95	0.42	0.40
5	1.05	0.32	0.34
6	1.10	0.33	0.31

[a] Average of four determinations.

TABLE 4

Recovery of oxalate from urine

Sample	Added (mM)	Found (mM)	Recovery (%)
1	–	0.125	
	0.600	0.693	94.7
	0.900	0.994	96.5
2	–	0.133	
	0.600	0.710	96.2
	0.900	1.003	96.7
3	–	0.155	
	0.600	0.725	95.0
	0.900	1.040	98.3
4	–	0.442	
	1.000	1.424	98.2
	1.400	1.807	97.5
5	–	0.305	
	1.000	1.290	98.5
	1.400	1.683	98.4
6	–	0.300	
	1.000	1.256	95.6
	1.400	1.682	98.7

diluted to the required volume with water in a calibrated flask.

The results obtained for the analysis of six samples of urine using the proposed method and the Sigma oxalate–oxidase method are summarized in Table 3. As can be seen the results of both methods are in good agreement. The recoveries obtained by adding two aliquots of a standard solution of oxalate to each urine sample ranged between 94 and 98% (Table 4).

This investigation was supported by a grant from the Spanish DGYCT (PB90-0008).

REFERENCES

1 J.M. Fitzgerald, Analytical Photochemistry and Photochemical Analysis, Marcel Dekker, New York, 1971.
2 A. Peter and J. Csányl, Acta Phys. Chem., 21 (1975) 37.
3 T. Pérez-Ruiz, C. Martínez-Lozano and V. Tomás, Quím. Anal. 6 (1987) 119.
4 A.M. Braun, M.T. Maurette and E. Oliveros, Phothochemical Technology, Wiley, New York, 1991.
5 A. Townshend, Analyst, 115 (1990) 495.
6 W.R. Seitz, C.R.C. Crit. Rev. Anal. Chem., 13 (1981) 1.
7 K. Robards and P.J. Worsfold, Anal. Chim. Acta., 266 (1992) 147.
8 J.L. Burguera and A. Townshend, Anal. Chim. Acta, 114 (1980) 209.
9 A.A. Alwarthan and A. Townshend, Anal. Chim. Acta, 185 (1986) 635.
10 S.A.Al-Tamrah and A. Townshend, Anal. Chim. Acta, 202 (1987) 247.
11 T. Nakagama, M. Yamada and S. Suzuki, Anal. Chim. Acta, 217 (1989) 371.
12 S. Suzuki, H. Nakazawa, M. Fujita, Anal. Chim. Acta, 261 (1992) 39.
13 C.A. Parker and C.G. Hatchard, J. Phys. Chem., 63 (1959) 22.
14 C.G. Hatchard and C.A. Parker, Proc. Roy. Soc. (London), A235 (1956) 518.
15 C.A. Parker, Photoluminescence of Solutions, Elsevier, Amsterdam, 1968, pp. 208–214.
16 G.G. Rao, G. Aravamudan and N.C. Venkatamma, Z. Anal. Chem., 146 (1955) 161.
17 G.G. Rao and G. Aravamudan, Anal. Chim. Acta, 13 (1955) 328.
18 G.G. Rao and G. Aravamudan, Anal. Chim. Acta, 13 (1955) 415.
19 W.M. Riggs and C.E. Bricker, Anal. Chem., 38 (1966) 897.
20 R.J. Lukasiewicz and J.M. Fitzgerald, Anal. Lett., 2 (1969) 159.
21 L.E. Leon, A. Rios, M.D. Luque de Castro and M. Valcarcel, Anal. Chim. Acta, 234 (1990) 227.
22 L.E. León, A. Rios, M.D. Luque de Castro and M. Valcarcel, Analyst, 115 (1990) 1549.
23 M.D. Luque de Castro, J. Pharm. Biomed. Anal., 6 (1988) 1.
24 M. Peacock, J.P. Heyburn and K.G. Robertson, Br. J. Urol., 50 (1978) 449.
25 K. Uchikura, Bunseki Kagaku, 39 (1990) 326.
26 A.M. Almuaibed and A. Townshend, Anal. Chim. Acta, 218 (1959) 1.
27 J.A. Infantes, M.D. Luque de Castro and M. Valcarcel, Anal. Chim. Acta, 242 (1991) 179.
28 W.R. Seitz and D.M. Hercules, Anal. Chem., 44 (1972) 2143.
29 E.G. Sarantonis and A. Townshend, Anal. Chim. Acta, 184 (1986) 311.
30 J.H. Fendler, Membrane Mimetic Chemistry, Wiley, New York, 1982.
31 T.E. Riehl, C.L. Malchorn and W.L. Hinze, Analyst, 111 (1986) 931.
32 L.L. Klopf and T.A. Nieman, Anal. Chem., 55 (1983) 1080.
33 G.H. Koch and F.M. Strong, Anal. Biochem., 27 (1969) 162.

Analytica Chimica Acta, 284 (1993) 181–188
Elsevier Science Publishers B.V., Amsterdam

Determination of traces of copper, cadmium and lead in biological and environmental samples by flow-injection isotope dilution inductively coupled plasma mass spectrometry

Pei-Ling Lu, Kuang-Shie Huang and Shiuh-Jen Jiang

Department of Chemistry, National Sun Yat-Sen University, Kaohsiung 804 (Taiwan)

(Received 5th June 1993; revised manuscript received 21st July 1993)

Abstract

Flow-injection isotope dilution inductively coupled plasma mass spectrometry (ICP-MS) was applied to the determination of Cu, Cd and Pb in several biological and environmental reference materials. The isotope ratios for each injection were calculated from the areas of the flow-injection peaks. The precision for the isotope ratio determination was better than 1%. Detection limits were 45, 25 and 58 ng l^{-1} for Cu, Cd, and Pb, respectively. The flow-injection isotope dilution method was successfully applied to the determination of Cu, Cd and Pb in a urine reference sample (NIST SRM 2670). A preconcentration system was used for the separation of Na and Mg matrix elements and preconcentration of traces of Cu, Cd and Pb in SLRS-2 riverine water and CASS-2 open ocean sea-water reference samples.

Keywords: Flow injection; Inductively coupled plasma mass spectrometry; Isotope dilution methods; Biological samples; Cadmium; Copper; Environmental analysis; Lead

Inductively coupled plasma mass spectrometry (ICP-MS) is used for trace multi-elemental and isotopic analyses of solutions [1–4]. It is applicable to a wide range of samples, although highly saline solutions can cause both spectral interferences and matrix effects [5,6]. Spectral overlaps are seen from polyatomic ions derived from matrix elements such as Na, Ca and Cl. Changes in analyte count rates are observed with high levels of salts or heavy matrix ions. Orifice plugging is also a problem for samples with high solid contents ($> 0.5\%$) [7,8].

Several calibration methods have been adapted to ICP-MS to deal with matrix effects. Matrix matching and standard addition techniques have been used sucessfully with several sample types [9–11]. Internal standardization [12,13] and isotope dilution [10,14,15] can also provide significant improvements in both the precision and accuracy obtained. Various correction techniques for circumventing polyatomic ion interferences have been described [16–18]. The matrix interference problems can also be overcome by separating the analytes from the matrix [10,14,15,19].

Flow-injection analysis (FIA) is a simple, rapid technique that has been applied previously to ICP-MS [20,21]. The principal advantages of FIA include high sample throughput, the ability to analyse small sample volumes and a decrease in the amount of solid material that is introduced into the instrument from solutions containing high matrix concentrations. The use of FIA can also

Correspondence to: S.-J. Jiang, Department of Chemistry, National Sun Yat-Sen University, Kaohsiung 804 (Taiwan).

0003-2670/93/$06.00 © 1993 – Elsevier Science Publishers B.V. All rights reserved

reduce the problem of matrix interferences in ICP-MS [22].

Isotope dilution (ID) is well recognized as a definitive technique for the determination of trace elements. Because another isotope of the same element represents the ideal internal standard for that element, isotope dilution results are expected to be highly accurate even when the sample contains high concentrations of concomitant elements.

In this work, flow-injection ID–ICP-MS was used to determine the concentrations of Cu, Cd and Pb in biological and environmental samples. The influence of instrument operating conditions, flow-injection system, matrix effects, and spectroscopic interferences due to matrix elements on the precision and accuracy of isotope ratio determinations was also investigated. The objective of this investigation is the development of a rapid multi-element method utilizing the stable isotope dilution technique for the analysis of environmental and biological samples using an inductively coupled plasma mass spectrometer with flow-injection sample introduction.

EXPERIMENTAL

ICP-MS device and conditions

An Elan 5000 ICP-MS instrument (Perkin-Elmer Sciex, Thornhill, ON, Canada) was used. It was equipped with a corrosion-resistant sample-introduction system, consisting of a Ryton spray chamber with a Ryton cross-flow nebulizer and end-tip. The injector tube was made of alumina with a large orifice (2.0 mm diameter). The aerosol gas flow-rate was controlled by a mass flow controller.

ICP operating conditions were selected so as to maximize the sensitivity for the isotopes of interest. The operating conditions used throughout are summarized in Table 1.

Data acquisition parameters used for isotope ratio measurements are given in Table 2. Version 2.0 of the Elan 5000 software was used. The measurements were made by peak hopping rapidly from one mass to another, staying only a short time (dwell time) at each mass. After the completion of one sweep, additional sweeps are made until the sum of the accumulated dwell times equalled the required measurement time. Under the combinations of dwell time and sweeps/reading, normally a data point could be obtained in less than 1 s for each isotope. The isotope ratios for each element in each injection were calculated from the areas of the flow-injection peaks. The mean isotope ratio and relative standard deviation (R.S.D.) were calculated from

TABLE 1

Equipment and operating conditions

ICP-MS instrument	Perkin-Elmer Sciex Elan 5000
ICP system:	
Outer gas flow-rate	14 l min^{-1}
Auxiliary gas flow-rate	0.9 l min^{-1}
Nebulizer gas flow-rate	0.85 l min^{-1}
R.f. power	1.0 kW
Mass spectrometer:	
Sample cone orifice	1.14 mm
Skimmer cone orifice	0.89 mm
Lens voltages:	
Photon stop (S2)	−6.04 V
Bessel box barrel	+12.04 V
Einzel lenses 1 and 3 (E1)	+1.97 V
Bessel box and lens (P)	−65.9 V
FIA system:	
Sample delivery pump	Gilson Minipuls 2
Sample loop volume	200 μl
Flow-injection valve	Rheodyne Type 50

TABLE 2

Data acqusition parameters [a] for isotope ratio measurements

Parameter	FIA [b]	Tracecon [c]
Resolution	High	High
Baseline time (ms)	1200	16300
Points per spectral peak	1	1
Number of replicates	1	1
Readings per replicate	53	155
Sweeps per reading	7	7
Dwell time (ms)	20	20
Replicate time (ms) [d]	7420	21700
Transfer frequency	Replicate	Replicate

[a] Definitions and descriptions of these terms are given in user manuals. [b] Sample was introduced by the flow-injection method. [c] Sample was introduced with the Tracecon preconcentration system. [d] replicate time = (dwell time) × (sweeps per reading) × (readings per replicate).

isotope ratios measured from several repeated injections.

Flow injection

A simple FIA system was assembled from a six-port injection valve (Rheodyne Type 50) with various sample loops. The carrier phase (1% HNO_3) was delivered through the system with a peristaltic pump (Gilson Minipuls 2). Switching between FIA and continuous-flow analysis (CFA) was accomplished simply by removing the injection valve and the excess tubing between the peristaltic pump and the nebulizer.

Preconcentration system

A Tracecon sample pretreatment system (Knapp Logistic Automation) was used to separate traces of analytes from matrix elements. During this study an SO_3-CM quinolin-8-ol–cellulose column was used. At suitable pH, commonly encountered matrix components such as alkali and alkaline earth elements are not strongly retained on the ion-exchange materials and are separated from the elements of interest. The operating principle of Tracecon have been published previously [23–25]. The operating parameters of Tracecon used in this experiment are given in Table 3. The preconcentration system was connected to the nebulizer with PTFE tubing (60 cm × 0.8 mm i.d.).

Reagents

All acids were of trace metal grade (Fisher). Enriched ^{65}Cu, ^{111}Cd and ^{204}Pb isotopes were purchased from the Oak Ridge National Laboratory. These stable isotopes were received as metals or oxide (lead as nitrate). Stock solutions of ca. 500 mg l^{-1} of each were prepared by dissolution of an accurately weighed amount of the material in nitric acid and dilution to volume. The concentrations of the spike solutions were verified by reverse spike isotope dilution ICP-MS.

Sample preparation

Riverine water reference material SLRS-2 and sea-water reference material CASS-2 (National Research Council of Canada, Ottawa) were obtained to demonstrate the applicability of the method to real samples. A 75-ml aliquot of these acidified reference materials was adjusted to pH

TABLE 3

Preconcentration system and operating conditions

Preconcentration device	Tracecon, Knapp Logistic Automation
Column	SO_3-CM quinolin-8-ol–cellulose column
Buffer solution	0.2 M ammonium acetate (pH 4.1)
Eluent	0.5 M HNO_3–0.5 M HCl
Flow-rates of pumps 1–3:	
Pump 1 (sample)	7.73 ml min^{-1}
Pump 2 (buffer)	6.53 ml min^{-1}
Pump 3 (eluent)	1.18 ml min^{-1}

Preconcentration method:

Step	Pump in operation	Valve in open position	Solution volume (ml)	Duration (s)
1	P-2	V-2	2.0	18
2	P-2	V-3	3.0	28
3	P-1	V-2	1.5	12
4	P-1	V-3	15.0 [a]	116
5	P-2	V-3	3.0	28
6	P-3	V-3	0.5	25
7	P-3	V-1	5.0	255
8	P-2	V-2	1.0	9
9	P-2	V-3	3.0	28

[a] For sea-water analysis, sample volume was increased to 22 ml.

4.10 with 20 ml of 0.2 M purified ammonium acetate buffer solution. After a suitable amount of enriched isotope had been added, this solution was diluted to 100 ml with distilled deionized water.

Another standard reference material of high salinity (NIST SRM 2670 Toxic Metals in Freeze-Dried Urine) was also analysed. The solid provided was digested by the following procedure. The contents of one sample bottle were reconstituted with a suitable amount of enriched isotope and 20 ml of water and poured into a closed Teflon PFA vessel and 5 ml of nitric acid were added. This solution was heated inside a microwave oven (CEM MDS-2000). After cooling for 30 min at room temperature, the digest was poured into a 50-ml volumetric flask and diluted to volume with distilled, deionized water. This solution was used as the stock solution for the following experiments. For flow-injection isotope dilution analysis, 5 ml of stock solution were diluted to 20 ml with water. For Tracecon isotope dilution analysis, 20 ml of buffer solution were added to 25 ml of stock solution and diluted to 100 ml with water.

Isotope dilution calculation

The analyte concentration in the sample was calculated using the equation

$$c = K \times \frac{W(A' - rB')}{M(rB - A)}$$

where K = natural atomic weight of the element/atomic weight of the spike isotope, W = mass of the isotopically enriched material added, M = weight or volume of the sample, A, B = natural abundances of sample isotopes a and b (a = reference element isotope of the sample, b = reference isotope in enriched isotope solution), A', B' = isotopic abundances of a and b in the spike and r = ratio of isotope a to isotope b measured in the sample.

Owing to the mass discrimination effect, intensities obtained during isotope ratio determinations were used to calculate the isotopic abundance of each element.

RESULTS AND DISCUSSION

Selection of ICP-MS and flow-injection operating conditions

Various factors can influence the precision and accuracy of isotope ratios measured by ICP-MS. Both the mass spectrometer and ICP operating conditions can affect the accuracy and precision of measured isotope ratios [26,27]. Other parameters, such as counting statistics, spike mass and optimum value of r (ratio of isotope a to isotope b), could also play an important role in the accuracy and precision of isotope ratio determination [28].

Under normal operating conditions with continuous nebulization (steady-state signal), a precision of R.S.D. 0.1–1% in the isotope ratio was obtained on a routine basis. Extending the measurement period could improve the precision of isotope ratio determinations when the counting statistics are the limiting factor of the precision.

In contrast, one cannot afford long integration times when determining isotope ratios on transient signals. Figure 1 shows typical flow-injection peaks of ^{114}Cd and ^{116}Cd during a flow-injection analysis. In order to obtain good isotope ratio results during FIA, a systematic study of the effect of operating conditions on the measured

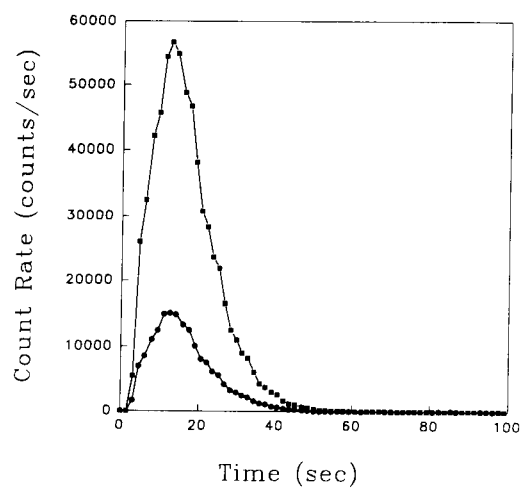

Fig. 1. Flow-injection peaks of (■) ^{114}Cd and (●) ^{116}Cd. Carrier flow-rate, 1.0 ml min^{-1}; sample loop, 200 μl; concentration of Cd, 100 $\mu g\ l^{-1}$.

TABLE 4

Isotope ratios of Cu, Cd and Pb in various matrices with different analysis methods [a]

Sample	$^{63}Cu/^{65}Cu$			$^{114}Cd/^{111}Cd$			$^{208}Pb/^{207}Pb$		
	CFA	FIA	Matrix separation	CFA	FIA	Matrix separation	CFA	FIA	Matrix separation
5 $\mu g\ l^{-1}$ Cu, Cd, Pb	2.12 ± 0.05	2.11 ± 0.09	2.09 ± 0.01	2.36 ± 0.02	2.34 ± 0.10	2.34 ± 0.04	2.34 ± 0.03	2.35 ± 0.06	2.33 ± 0.03
5 $\mu g\ l^{-1}$ Cu, Cd, Pb + 2200 mg l^{-1} Mg	2.04 ± 0.18	1.99 ± 0.05	2.10 ± 0.02	2.36 ± 0.12	2.34 ± 0.09	2.31 ± 0.02	2.35 ± 0.04	2.35 ± 0.07	2.35 ± 0.03
5 $\mu g\ l^{-1}$ Cu, Cd, Pb + 5000 mg l^{-1} Na	5.79 ± 0.18	4.39 ± 0.17	2.10 ± 0.01	2.35 ± 0.12	2.35 ± 0.12	2.32 ± 0.03	2.34 ± 0.02	2.35 ± 0.09	2.35 ± 0.01
5 $\mu g\ l^{-1}$ Cu, Cd, Pb + 2200 mg l^{-1} Mg + 5000 mg l^{-1} Na	3.42 ± 0.54	4.43 ± 0.18	2.12 ± 0.03	2.30 ± 0.03	2.31 ± 0.15	2.32 ± 0.04	2.32 ± 0.06	2.33 ± 0.08	2.33 ± 0.03

[a] CFA sample flow-rate = 1 ml min^{-1}; FIA carrier flow-rate = 1 ml min^{-1}; 200-μl sample loop. Preconcentration system (Tracecon); 5 $\mu g\ l^{-1}$ Cu, Cd and Pb in 0.2 M CH_3COONH_4–CH_3COOH solution (pH 4.16), sample flow-rate = 7.68 ml min^{-1}, eluent = 0.5 M HNO_3–0.5 M HCl, flow-rate = 3.20 ml min^{-1}. Results are means of five measurements ± standard deviations.

isotope ratio is necessary. Although not shown, it was demonstrated in a separate experiment that the ICP operating conditions did not affect the measured value of the isotope ratio significantly. This work was therefore concentrated on the effect of operating conditions of the mass spectrometer and flow-injection system on the isotope ratio determination.

Isotope ratios of Cu, Cd and Pb were determined by measuring the areas of the flow-injection peaks for different dwell times and carrier flow-rates, and were compared with those measured during continuous-flow analysis (CFA). Stable isotope ratios were obtained for different dwell times and carrier flow-rates as long as the dwell time was not too long. The dwell time must be sufficiently short to allow the Graphics routine of the Elan software to acquire data points at a rate sufficient to avoid distortion of the peak shape for each isotope. As the signal measurements for the two isotopes of each element are not made simultaneously, too long a dwell time could have a disastrous effect on the accuracy of isotope ratio measurements for a transient signal. A 20-ms dwell time was therefore used in the following experiments. Further, there was no obvious difference in isotope ratios with CFA and FIA measurement methods. Therefore, the spike isotope ratios were measured by CFA to increase the integration time in the following experiments.

Ion settings could affect the relative sensitivity of heavier and lighter isotopes and the measured isotope ratio [29]. Although not shown, ion optical settings of the mass spectrometer were found to play a major role in determining isotope accuracy. Therefore, ion lens combinations must be set at fixed values so as not to affect isotope dilution determinations. The count rate had a great effect on the precision obtained owing to its counting statistics. Therefore, the plasma conditions and ion lens settings were adjusted in order to maximize the sensitivity for the isotope of interest.

Matrix effect and spectroscopic interferences

Table 4 shows the results of adding various concentrations of NaCl and $Mg(NO_3)_2$ to a test solution containing 5 $\mu g\ l^{-1}$ Cu, Cd, and Pb. As shown, Na and Mg matrix elements did not affect the Cd and Pb isotope ratios. However, the $^{63}Cu/^{65}Cu$ ratio was increased when 5000 mg Na l^{-1} were added, which indicated an interference at m/z 63 from $ArNa^+$. Moreover, the $^{63}Cu/^{65}Cu$ ratio was decreased when 1500 mg Mg l^{-1} were added, which indicated an interference at m/z 65 from $ArMg^+$. Table 4 shows that FIA could reduce the amount of $ArNa^+$ and $ArMg^+$ formation compared with CFA. However, it could still affect the measurement of the Cu isotope ratio. Table 4 also shows that a stable $^{63}Cu/^{65}Cu$ ratio could be obtained when Na and Mg were separated from the sample with a preconcentration device. Hence for the analysis of highly saline samples, Na and Mg must be separated before Cu is determined.

Although the matrix could affect the determination of the Cu isotope ratio owing to molecular ion interferences, the precision (R.S.D. ca. 1%), shown in Table 4, was similar to that obtained for isotope ratio measurements during continuous introduction of aqueous solutions [30,31]. As is usually the case, with ICP-MS the precision of isotope ratio measurement tended to be worse than the counting statistics by a factor of 1–5.

TABLE 5

Flow-injection isotope dilution ICP-MS analysis of freeze-dried urine NIST SRM 2670 [a]

Element	Elevated level			Low level		
	FIA	Tracecon	Certified value	FIA	Tracecon	Certified value
Cu	0.40 ± 0.04	0.38 ± 0.02	0.37 ± 0.03	0.144 ± 0.004	0.14 ± 0.01	0.13 ± 0.02
Cd	0.074 ± 0.016	0.085 ± 0.006	0.088 ± 0.003	0.00036 ± 0.00023	0.00059 ± 0.00018	(0.0004)
Pb	0.112 ± 0.013	0.111 ± 0.005	0.109 ± 0.004	0.0098 ± 0.022	0.0096 ± 0.0023	(0.01)

[a] Results are means of five measurements ± standard deviations (mg l^{-1}).

TABLE 6

Calibration parameters (0.5–800 $\mu g\ l^{-1}$) for Cu, Cd and Pb with FIA system [a]

Parameter	Cu	Cd	Pb
Slope (counts per $\mu g\ l^{-1}$)	2010	1430	980
Regression coefficient	0.9997	0.9997	0.9998
Detection limit ($ng\ l^{-1}$)	45	25	58

[a] Sample loop = 200 μl; carrier solution = 1% HNO_3; carrier flow-rate = 1.00 ml min^{-1}.

The slight but reproducible differences between the found and expected values are similar to those commonly seen in isotope ratio measurements with ICP-MS and were probably caused by some mass discrimination in ion extraction, focusing, mass analysis and detection [32].

Flow-injection isotope dilution ICP-MS

Concentrations of Cu, Cd and Pb were determined by flow-injection isotope dilution ICP-MS in the freeze-dried urine reference sample NIST SRM 2670. The results are given in Table 5. This experiment indicated that Cu, Cd and Pb could be readily determined by isotope dilution using the flow-injection procedure. No obvious molecular ion overlap interference was observed for Cu determinations. Sample dilution could be the factor for the alleviation of molecular ion interference. Detection limits based on the definition of the concentration of the analyte yielding a signal equivalent to three times the standard deviation of the blank signal were 45, 25 and 58 $ng\ l^{-1}$ for Cu, Cd and Pb, respectively (Table 6). Dilution and band broadening could be the causes of the degradation of the detection limits with flow-injection sample introduction.

Flow-injection isotope dilution ICP-MS after preconcentration

When the concentrations of sought elements in the original material or the prepared solution are too low to be measured directly by mass spectrometry or when matrix elements interfere with the determination, a preconcentration and separation sample pretreatment process is needed in order to obtain accurate, reliable and sensitive results. As shown in Table 4, after the high-salt samples had passed through Tracecon preconcentration system, the isotope ratio of Cu remained at a stable value. This indicates that most of the Na and Mg in the samples had been separated from analyte. Therefore, isotope dilution experiments were done on traces of Cu, Cd, Pb in the riverine water reference material SLRS-2 and open ocean sea-water reference material CASS-2. A buffer solution of lower pH (4.10) and careful washing of the column with buffer solution were used to decrease the retention of alkaline earth metal ions when analysing sea-water samples [23,24]. A higher eluent flow-rate could result in narrower elution peaks, but the peak heights were decreased owing to the degradation of the nebulization efficiency. An eluent flow-rate of 1.18 ml min^{-1} was therefore used. Under the operating conditions of the preconcentration system, the peak widths for the flow-injection peaks were ca. 20 s, which is equivalent to 0.66 ml; this means that with an injection volume of 15 ml a preconcentration factor of 23 could be obtained. The detection limits for the elements studied were decreased to the low $ng\ l^{-1}$ range with this preconcentration system [23].

The ICP-MS results for the standard reference materials are given in Table 7. All the results for

TABLE 7

ICP-MS results for reference materials [a]

Element	CASS-2		SLRS-2	
	Found	Expected	Found	Expected
Cu	0.725 ± 0.091	0.675 ± 0.039	2.96 ± 0.07	2.76 ± 0.17
Cd	0.022 ± 0.004	0.019 ± 0.004	0.029 ± 0.005	0.028 ± 0.004
Pb	0.021 ± 0.020	0.019 ± 0.006	0.100 ± 0.020	0.129 ± 0.011

[a] Results are means of five measurements ± standard deviations ($\mu g\ l^{-1}$)

Cu, Cd and Pb were in good agreement with the accepted values.

This research was supported by a grant from the National Science Council of the Republic of China.

REFERENCES

1 R.S. Houk, V.A. Fassel, G.D. Flesch, H.J. Svec, A.L. Gray and C.E. Taylor, Anal. Chem., 52 (1980) 2283.
2 R.S. Houk and J.J. Thompson, Mass Spectrom. Rev., 7 (1988) 425.
3 R.S. Houk, Anal. Chem., 58 (1986) 97A.
4 D.J. Douglas and R.S. Houk, Prog. Anal. At. Spectrosc., 8 (1985) 1.
5 S.H. Tan and G. Horlick, Appl. Spectrosc., 40 (1986) 445.
6 S.H. Tan and G. Horlick, J. Anal. At. Spectrom., 2 (1987) 745.
7 J.A. Olivares and R.S. Houk, Anal. Chem., 58 (1986) 20.
8 D.J. Douglas and L.A. Kerr, J. Anal. At. Spectrom., 3 (1988) 749.
9 J.D. Dean, R. Massey and L.J. Ebdon, J. Anal. At. Spectrom., 2 (1987) 369.
10 J.W. McLaren, A.P. Mykytiuk, S.N. Willie and S.S. Berman, Anal. Chem., 57 (1985) 2907.
11 D. Beauchemin, J.W. McLaren, A.P. Mykytiuk and S.S Berman, Anal. Chem., 59 (1987) 778.
12 J.J. Thompson and R.S. Houk, Appl. Spectrosc., 41 (1987) 801.
13 D. Beauchemin, J.W. McLaren and S.S. Berman, Spectrochim. Acta, Part B, 42 (1987) 467.
14 D. Beauchemin, J.W. McLaren, A.P. Mykytiuk and S.S. Berman, J. Anal. At. Spectrom., 3 (1988) 305.
15 J.W. McLaren, D. Beauchemin and S.S. Berman, J. Anal. At. Spectrom., 2 (1987) 277.
16 C.W. McLeod, A.R. Date and Y.Y. Cheung, Spectrochim. Acta, Part B, 41 (1986) 169.
17 A.R. Date, Y.Y. Cheung and M.E. Stuart, Spectrochim. Acta, Part B, 42 (1987) 3.
18 F.A. Lichte, A.L. Meier and J.G. Crock, Anal. Chem., 59 (1987) 1150.
19 E.M. Heithmar, T.A. Hinners, J.T. Rowan and J.M. Riviello, Anal. Chem., 62 (1990) 857.
20 J.J. Thompson and R.S. Houk, Anal. Chem., 58 (1986) 2541.
21 R.C. Hutton and A.N. Eaton, J. Anal. At. Spectrom., 3 (1988) 547.
22 G.H. Vickers, B.S. Ross and G.M. Hieftje, Appl. Spectrosc., 43 (1989) 1330.
23 K.-S. Huang and S.-J. Jiang, Fresenius' J. Anal. Chem., 1993, in press.
24 P. Schramel, L.Q. Xu, G. Knapp and M. Michaelis, Mikrochim. Acta, 106 (1992) 191.
25 H.-J. Yang, K.-S. Huang, S.-J. Jiang, C.-C. Wu and C.-H. Chou, Anal. Chim. Acta, 282 (1993) 437.
26 H.P. Longerich, B.J. Fryer and D.F. Strong, Spectrochim. Acta, Part B, 42 (1987) 39.
27 J.R. Garbarino and H.E. Taylor, Anal. Chem., 59 (1987) 1568.
28 H.P. Longerich, At. Spectrosc., 10 (1989) 112.
29 D.C. Gregoire, Anal. Chem., 59 (1987) 2479.
30 R.E. Serfass, J.J. Thompson and R.S. Houk, Anal. Chim. Acta, 188 (1986) 73.
31 G.P. Russ, III and J.M. Bazan, Spectrochim. Acta, Part B, 42 (1987) 49.
32 S.-J. Jiang, M.D. Palmieri, J.S. Fritz and R.S. Houk, Anal. Chim. Acta, 200 (1987) 559.

Analytica Chimica Acta, 284 (1993) 189–193
Elsevier Science Publishers B.V., Amsterdam

Determination of dissolved oxygen by use of a spectrophotometric flow-through sensor

Antonio Sanz-Martínez [1], Angel Ríos and Miguel Valcárcel

Department of Analytical Chemistry, Faculty of Sciences, University of Córdoba, E-14004 Córdoba (Spain)

(Received 15th March 1993)

Abstract

A simple flow-injection method for the automatic photometric determination of low concentrations of dissolved oxygen in waters was developed. The method uses Methylene Blue immobilized on a cationic exchange resin packed into a flow-cell located in the spectrophotometer, where the leuco form of the dye is formed by flowing a dithionite solution. The flow-through sensor thus prepared provides a response, the reliability of which depends on the oxygen content in the sample concerned. The linear calibration range accomplished was 0.9 to 5.5 mg l^{-1} oxygen, with a relative standard deviation of 2.2–0.6% over this range; the sampling frequency was 18–22 h^{-1}.

Keywords: Flow injection; Spectrophotometry; Sensors; Oxygen, dissolved; Flow-through sensor

Reagent immobilization technology is widely used in constructing chemical sensors, particularly recently developed flow-through sensors [1,2], where reaction (retention) and detection are integrated in a flow-injection system (e.g., Refs. 3 and 4). In order to ensure proper performance, the reaction system must meet several basic requirements such as reversibility, stability of the immobilized reagent, fast kinetics, and compatibility between the support and the detection system used. Some interesting applications have recently been developed in this way including the automatic determination of different analytes [1]. This type of sensor can be manufactured in the laboratory and used in conventional spectrophotometric and spectrofluorimetric detectors. They have aroused increasing interest lately on the grounds of their high sensitivity, selectivity and simplicity.

The significance of dissolved oxygen measurements is clearly reflected in the large number of papers and monographs (e.g., Ref. 5) published on the subject. A wide range of methods based on electrochemical measurements have been used to develop in situ measuring probes. Colorimetric methods are seemingly applicable to fairly clean samples only; this shortcoming however, can be circumvented by placing filters in continuous-flow manifolds. Such is the case of the spectrophotometric procedure based on the oxidation of the leuco form of Methylene Blue, which was originally developed in Russia many years ago [6] and later adapted for use by a Technicon AutoAnalyzer [7,8]. In this work, we immobilized the dye on exchange material and packed it in a cell in order to develop a stable, sensitive and selective flow-through sensor for dissolved oxygen. Peterson et al. [9], and Li and Narayanaswamy [10,11] recently developed oxygen sensors based on optical fibres. The proposed method is simpler and

Correspondence to: M. Valcárcel, Department of Analytical Chemistry, Faculty of Sciences, University of Córdoba, E-14004 Córdoba (Spain).

[1] Permanent address: Department of Analytical Chemistry, Faculty of Sciences, University of Murcia, Murcia (Spain).

0003-2670/93/$06.00 © 1993 – Elsevier Science Publishers B.V. All rights reserved

uses affordable instrumentation typically available at small control laboratories.

EXPERIMENTAL

Reagents

Aqueous solutions of 10^{-4} M Methylene Blue (C.I. 52015, Aldrich), 1% (w/v) sodium dithionite (Merck), and 0.1 M Na_2SnO_2 (prepared by mixing 0.1 M tin(II) chloride in excess NaOH) were used. All these solutions were prepared daily and stocked in stoppered vessels after removing the dissolved oxygen by blubbling nitrogen gas through them. Aqueous solutions of saturated oxygen at 25°C were also prepared, the amount of dissolved oxygen being adjusted by adding an appropriate amount of sodium sulphite. A Dowex 50×8-200 cation-exchange resin (Sigma) was used to immobilize the Methylene Blue reagent.

Apparatus

Photometric measurements were made on a Unicam 8625 spectrophotometer connected to a Knauer TY recorder. A YSI-58 dissolved oxygen-meter furnished with a YSI-5740 probe were used for oxygen measurements. A Gilson Minipuls-3 peristaltic pump, a Rheodyne 5041 rotary valve and a 138-OS Hellma flow cell were also used. The PTFE tubes used were covered with epoxy-gum in order to avoid oxygen diffusion across.

Immobilization and flow cell packing

The cation exchangers were washed with water and conditioned with 4 M NH_4Cl and water, which converted the resin to its ammonium form [12]. About 0.4 g of exchanger was mixed with 25 ml of 2×10^{-5} M Methylene Blue with stirring until a colourless liquid was obtained. The supernatant liquid was decanted and the exchanger was rinsed several times with water. A special flow-cell (Fig. 1a) of inner volume ca. 40 μl was packed with the exchanger up to half height (8 mm), so that the light beam would cross the upper part of the resin when the flow-cell was placed in the spectrophotometer. The resin required conditioning by passing the carrier (sodium dithionite) through the cell for 30 min. In this way, the leuco form of Methylene Blue was retained in the exchanger.

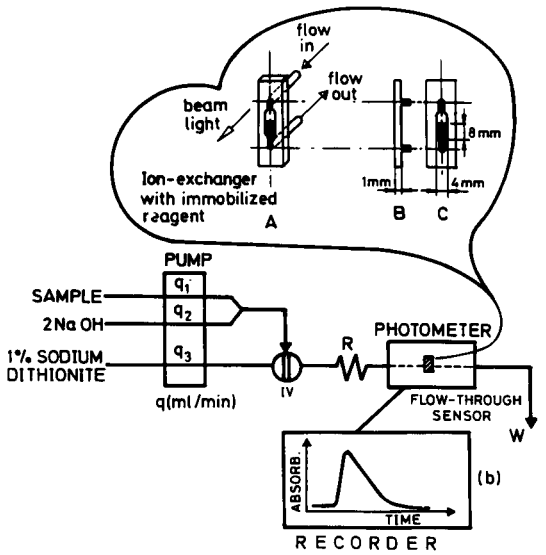

Fig. 1. Flow-injection manifold used (IV = injection valve, R = reactor), showing details of the flow cell employed for packing the exchanger with the reagent (a) (A = general view; and side, B, and front, C, views of the flow-cell), and the type of recording obtained (b).

Manifold and procedure

The manifold used is depicted in Fig. 1. A 1% (w/v) sodium dithionite solution in 1 M NaOH carrier stream was passed at 1.0 ml min^{-1} through the packed flow-cell in order to assure all the Methylene Blue remained in its leuco form. The packed flow-cell thus prepared acted as a flow-through sensor. The sample (water) was continuously merged with a 2 M NaOH stream before reaching the injection loop. A volume of 970 μl of this mixture was injected into the carrier stream. As this injected sample plug passed through the flow cell, a dramatic increase in the absorbance (at 670 nm) was recorded as a result of the leuco form of Methylene Blue being partially oxidized. Then, the baseline was restored by passing the reducing carrier stream. A typical recording is shown in Fig. 1b.

RESULTS AND DISCUSSION

Preliminary batch assays showed that both the oxidized (blue, absorbing at 670 nm) and the

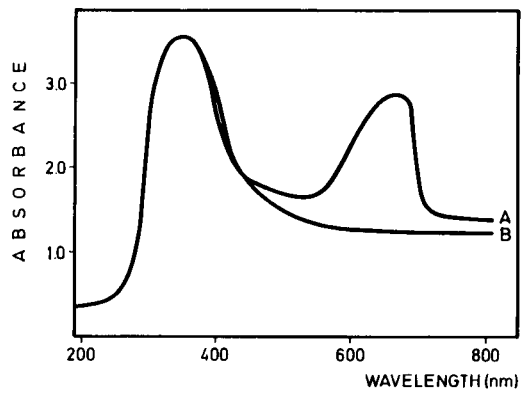

Fig. 2. UV–visible spectrum for Methylene Blue (curve A) and its leuco form (curve B), both immobilized on Dowex 50X-8-200 cation-exchange resin.

reduced (colourless) form of Methylene Blue were strongly retained by the cationic exchanger, probably because of the aromatic character of these forms, in addition to their being positively charged. As can be seen in Fig. 2, the UV–visible spectra of the packed exchanger with the leuco form and its oxidation product absorb differently in the 600–700 nm region. The maximum absorbance at 670 nm was used to perform measurements. The flow-through sensor worked accurately for at least two months.

Influence of chemical variables

Appropriate selection of the reductant to be used as carrier was quite important. A strong reductant was needed to restore the baseline in as short a time as possible following each injection of sample. Cation reductants [tin(II) in an acidic medium was the most efficient] were progressively bound to the resin, partially displacing the leuco form of Methylene Blue from it. Among anionic reagents, dithionite provided the best results ($E_0 = -1.12$ V). Figure 3 illustrates the effect of various reductants on the sensor response. The sodium dithionite solution must be alkaline in order to ensure stability (a 1 M NaOH alkaline medium was optimal in this respect). The $Na_2S_2O_4$ solution prepared in this medium was quite stable and resulted in good repeatability and a rapid baseline restoration (Fig. 3c). In order to avoid changes in the pH of the flow-

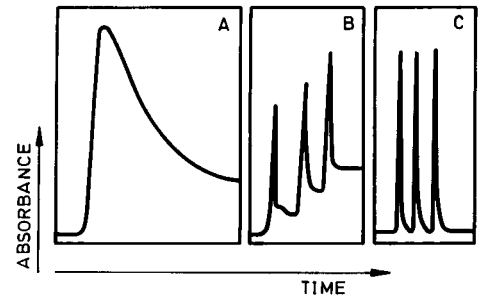

Fig. 3. Absorbance–time recordings obtained by using Sn(II) in an acidic medium (A), SnO_2^{2-} (B), and sodium dithionite (C) as reducing carrier reagent for regeneration of the sensor response.

through sensor, the manifold used (Fig. 1) allowed the water sample to merge with a 2 M NaOH solution before the sample was injected. Dissolved oxygen in this alkaline medium must be removed by bubbling nitrogen gas before use.

The concentration of dithionite was a key variable in this method: the sensitivity decreased dramatically as the concentration was increased [no response from the sensor was detected for a 2% (w/v) sodium dithionite carrier solution]; on the other hand, too low a concentration of this reagent resulted in sluggish baseline restoration and hence in poor throughput. Figure 4 illustrates both effects of the sodium dithionite concentration. As can be seen the optimum concentration was ca. 1% (w/v).

Influence of FIA variables

The sensitivity was found to increase on decreasing length of reactor R in Fig. 1. Thus, a 30

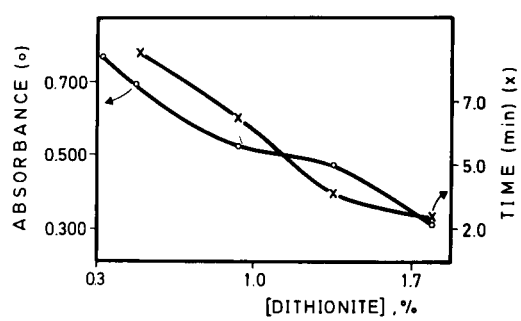

Fig. 4. Effects of sodium dithionite concentration on the: (○) absorbance, i.e., sensitivity and (×) sample throughput time.

cm × 0.5 mm i.d. tubing was employed. The flow-rate was significant in order to ensure enough time of contact between the sample and immobilized reagent so that almost all the oxygen in the sample could react. Thus, the sensitivity increased with decreasing flow-rate. A flow rate of 1.0 ml min^{-1} was selected in order to avoid a low sampling frequency. On the other hand, small-sample injected volumes yielded no detector response because the dissolved oxygen in the sample was reduced by the dithionite carrier solution. At least 350–400 μl were needed to obtain a minimum response. Nevertheless, too high sample volumes dramatically increased the baseline restoration time. An injected volume of 970 μl was choosen as a compromise. Under these experimental conditions, a sampling frequency of 18–22 h^{-1} was achieved.

Determination of dissolved oxygen

The calibration graph was constructed by using different standard solutions of sodium sulphite, a well known oxygen-trapping compound [13]. After each solution was made, dissolved oxygen was measured by using an electrochemical oxygen probe (described in Experimental) and then injected into the flow-system. The equations obtained were:

$$[O_2] = 6.18 - 10.56[Na_2SO_3]$$

measured by the oxygen probe and

$$A = 0.338 - 0.458[Na_2SO_3]$$

for the flow-injection system, where A is the peak absorbance, the oxygen concentration is expressed in mg ml^{-1}, the sodium sulphite concentration in g l^{-1}, and the temperature was 25°C. By correlating both equations, the following calibration function was obtained:

$$A = 7.20 \times 10^{-2} + 4.26 \times 10^{-2}[O_2]$$

$$(r = 0.9984,\ n = 5)$$

The determination range was 0.9–5.5 mg l^{-1} dissolved oxygen, the 3σ detection limit being 0.4 mg l^{-1}. The precision, expressed as relative standard deviation (R.S.D. for $n = 11$), was 0.6% for 5.2 mg l^{-1} and ±2.2% for 0.9 ml l^{-1} oxygen.

Applications

In order to validate the proposed method, it was used to analyse several synthetic and real samples. The results obtained are listed in Table

TABLE 1

Determination of dissolved oxygen in various types of water samples

	O_2 measured by using the electrochemical probe (mg l^{-1})	O_2 measured by the proposed method (mg l^{-1})	Error (%)
Synthetic samples	2.35	2.28	−2.9
	3.86	3.73	−3.3
	0.90	0.94	+3.8
	3.01	2.93	−2.6
	5.21	5.10	−2.1
	4.07	4.11	+0.9
Type of water	O_2 by using the electrochemical probe (mg l^{-1})	O_2 measured by the proposed method (mg l^{-1})	Error (%)
Real samples			
Well (20 m deph)	4.05	4.17	+2.9
Swimming pool	4.92	4.78	−2.8
Tap	5.58	5.40	−3.2
Guadalquivir river:			
Incoming flow	3.93	4.05	+3.0
Outcoming flow	1.77	1.83	+3.3

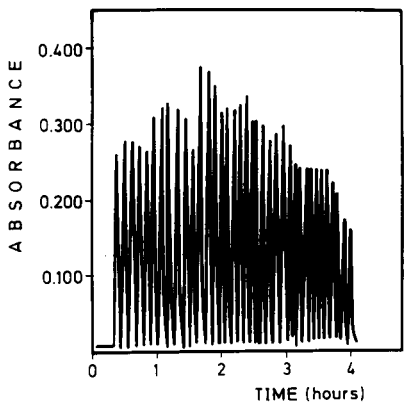

Fig. 5. Simulated quasi-continuous monitoring of the dissolved oxygen content in water samples.

1. As can be seen, the results provided by the flow-sensor methodology are consistent with those obtained by the electrochemical dissolved oxygen-meter. Only strongly reducing species (e.g., S^{2-}), and oxiding compounds (H_2O_2, Cr^{VI}, Mn^{VII}) interfere with the sensor response.

The proposed method can be used to automatically monitor dissolved oxygen in various types of water for environmental or biotechnological studies. By way of example, Figure 5 shows a simulated quasi-continuous monitoring of this parameter. The well water sample of Table 1 was used for this purpose. A volume of 1 l of sample was placed in a 2-l container. Two vessels containing tap water and a 0.2 g l^{-1} Na_2SO_3 solution, respectively, were attached to the tank. Periodically, different volumes of either solution were added to the container in such a way that the dissolved oxygen level was altered.

Conclusions

Automatic methods based on flow-through sensors offer interesting assets such as simplicity, rapidity, low cost and flexibility. The proposed method is an useful approach to the on-line automatic determination of a key environmental and aquacultural parameter production, where oxygen levels play a decisive role in both contexts, so they require periodical measuring. Spectrophotometric detection simplifies calibration and dispenses with the careful handling of electrochemical dissolved oxygen probes.

The CICyT is acknowledged for financial support (Grant No. PB90/0925). One of the authors (A.S.-M.) also gratefully acknowledges financial support from the Comunidad Autónoma de Murcia.

REFERENCES

1 M. Valcárcel and M.D. Luque de Castro, Analyst, 118 (1993) 593.
2 M.D. Luque de Castro and M. Valcárcel, Trends Anal. Chem., 10 (1991) 114.
3 F. Lázaro, M.D. Luque de Castro and M. Valcárcel, Anal. Chim. Acta, 214 (1988) 217.
4 F. Lázaro, M.D. Luque de Castro and V. Valcárcel, Anal. Chim. Acta, 219 (1989) 231.
5 M.L. Hitchman, Measurement of Dissolved Oxygen, Wiley, New York, 1978.
6 V.P. Rotshtein and V.N. Shemyakin, Teploénergetika, 2 (1962) 1105.
7 G.I. Goodfellow and H.M. Webber, Analyst, 104 (1979) 1105.
8 G.I. Goodfellow, D.F. Libaert and H.M. Webber, Analyst, 104 (1979) 1119.
9 J.I. Peterson, R.V. Fitzgerald and D.K. Buckhold, Anal. Chem., 56 (1984) 62.
10 P.Y.F. Li and R. Narayanaswamy, Analyst, 114 (1989) 663.
11 P.Y.F. Li and R. Narayanaswamy, Analyst, 114 (1989) 1191.
12 M. Marhol, Ion Exchangers in Analytical Chemistry: Their Properties and Use in Inorganic Chemistry. Elsevier, Amsterdam, 1982, p. 85.
13 H.A. Laitinen and I.M. Kolthoff, J. Phys. Chem., 45 (1941) 1079.

Analytica Chimica Acta, 284 (1993) 195–198
Elsevier Science Publishers B.V., Amsterdam

Spectrophotometric determination of antimony after extraction of Brilliant Green hexachloroantimonate(V) with microcrystalline 1,4-dichlorobenzene

D. Thorburn Burns, D. Chimpalee [1] and H.J. Bullick

Department of Analytical Chemistry, The Queen's University of Belfast, Belfast BT9 5AG (UK)

(Received 26th May 1993)

Abstract

Antimony ($\leqslant 20$ μg) can be determined spectrophotometrically at 640 nm after its adsorptive extraction as Brillant Green hexachloroantimonate(V) with microcrystalline 1,4-dichlorobenzene after dissolution of the solid phase in toluene. The effects of reagent concentration, order and timing of addition, diverse ions and masking studies are reported. The system has been applied to the determination of antimony in steels.

Keywords: Spectrophotometry; Antimony; Brilliant Green; Solid phase extractions

The use of Brilliant Green permits sensitive and precise determination of several elements in anionic form [1,2] provided that care is taken in method development and their routine operation. It is necessary to allow for the effects of the acid–base equilibria [2–4], purity [2–5], surface adsorption properties [6] and possible dimerisation [7] of the reagent, and in the case of antimony determination, the nature of the oxidant [2]. Brilliant Green methods for cobalt as tetrathiocyanate cobaltate(II) [8], rhenium as perrhenate [9] and perchlorate [10] have been adapted for use with microcrystalline solid phase organic extractants. The only solid phase extraction for antimony, so far available is that based on extraction of antimony(III) morpholine-4-carbodithioate with naphthalene followed by replacement by copper [11].

Correspondence to: D.T. Burns, Department of Analytical Chemistry, The Queen's University of Belfast, Belfast BT9 5AG (UK).

[1] Present address: Department of Chemistry, Silpakorn University (Thailand).

The present paper reports on the novel adsorptive extraction of Brilliant Green hexachloroantimonate(V) with microcrystalline 1,4-dichlorobenzene based on earlier liquid–liquid extraction studies [2,3].

EXPERIMENTAL

Apparatus

Pye Unicam SP 8-400 and SP 6-550 UV–visible spectrophotometers were used for recording absorption spectra and for routine measurements, respectively, with matched 1-cm quartz cells. pH measurements were made with an EIL Model 39A pH meter.

Reagents and solutions

Brilliant Green (Aldrich, dye content ca. 95%) was used as supplied. Elemental analysis gave 66.9% C, 7.0% H, 5.6% N (theor. for $C_{27}H_{34}N_2O_4S$: 67.2% C, 7.1% H, 5.8% N). A 0.5% (w/v) solution was prepared in pure ethanol, and stored in a dark brown glass bottle.

0003-2670/93/$06.00 © 1993 – Elsevier Science Publishers B.V. All rights reserved

A stock antimony(III) (200 μg ml^{-1}) was prepared by dissolving 0.2669 g of antimony potassium tartrate (AnalaR, BDH) in 500 ml of water in a volumetric flask. More dilute solutions were prepared daily, as required.

A cerium(IV) solution (0.1 M) was prepared by dissolving 6.33 g of diammonium cerium(IV) sulphate (AnalaR, BDH) in 100 ml of 1 M sulphuric acid.

Hydroxylammonium chloride solution (1% w/v AnalaR, BDH), was freshly prepared, as required in water.

1,4-Dichlorobenzene was used as a 20% (w/v) solution in acetone.

All other reagents were of analytical grade and doubly distilled water was used throughout.

General procedure

Place an aliquot of antimony(III) solution (ca. 6 μg Sb) in a cooled (5°C) conical flask fitted with a ground glass stopper containing 3 ml of concentrated hydrochloric acid and 4 ml of 50% (v/v) hydrochloric acid. Add 10 drops of cerium(IV) solution and mix the solutions for 1 min. Reduce the excess of cerium(IV) by dropwise addition of hydroxylammonium chloride solution until the yellow colour disappears. Without delay, dilute the mixture with 25 ml of ice-cold water, add 0.5 ml of Brilliant Green solution, mix and add immediately 3 ml of 1,4-dichlorobenzene solution. Shake vigorously for 1 min. Filter the separated solid through a sintered glass filter (No. 2), wash with a small volume of distilled water and suck dry. Dissolve the solid in toluene and make up to 25 ml in a volumetric flask. Remove any residual water by addition of 0.2 g of anhydrous sodium sulphate. Cover the flask with aluminium foil to protect the contents from light. Measure the absorbance at 640 nm against a reagent blank prepared in the same way.

Procedure for steel samples

For samples containing 0.007–0.07% (w/w) of antimony dissolve accurately weighed 0.5-g samples in 10 ml of concentrated hydrochloric acid in 250-ml conical flasks. Oxidise by addition of 1 ml of concentrated nitric acid and boil to expel nitrous fumes. Cool and if necessary filter (Whatman No. 541) into a 100-ml (larger or smaller according to the antimony content) volumetric flask. Wash the residual solids (silica) with concentrated hydrochloric acid, add the washings to the sample solution and dilute to volume with concentrated hydrochloric acid. Complete the analysis within 1 h as follows. Place a 3-ml aliquot of the sample solution in a cooled (ice bath) conical flask containing 3 ml of water and 4 ml of 50% (v/v) hydrochloric acid. Add 10 drops of cerium(IV) solution and mix for 1 min. Continue as in the general procedure except use 25 ml of ice-cold 10% w/v) sodium hexametaphosphate solution in place of water in the dilution stage, to mask iron(III).

Prepare a calibration graph over the range 0–20 μg antimony, adding aliquots of high-purity iron equivalent to the sample weight of steel samples and proceed as for the steel samples.

Examination of the main experimental variables

Naphthalene, diphenyl, benzophenone and 1,4-dichlorobenzene were each examined as extractants for 6 μg of antimony as in the general procedure for their adsorptive–extractive properties using the microcrystalline solid formation precedure from acetone solution. 1,4-Dichlorobenzene gave the highest apparent molar absorptivity in toluene and a low (0.015 absorbance) reagent blank. The separated solid was easy to dry so that it required little drying agent.

Various solvents with a range of functional group types, including alcohols, ketones, esters, ethers, and chlorinated and aromatic hydrocarbons were examined for dissolving the ion-pair and the 1,4-dichlorobenzene. Lower reagent blanks were found using aromatic hydrocarbons. Solutions in xylene were unstable; toluene and benzene gave the same molar absorptivity (λ_{max} = 640 nm). Toluene was chosen on grounds of its lower toxicity.

In earlier work [2,3] it was recommended that the extracting solvent be added prior to the Brilliant Green to reduce the effect of reagent protonation. For solid phase extraction the reverse order is necessary in order to achieve precise results. The effect of protonation of Brilliant Green in 1.7 M hydrochloric acid with time prior

to extraction was examined by introducing a variable time delay after the addition of Brilliant Green prior to extraction. Absorbances decreased with protonation time (25% loss in 8 min), but the effect can be neglected provided extraction takes place within 0.5 min. The effect of hydrolysis of hexachloroantimonate(V) upon dilution of the acid to 1.7 M was studied similarly by introducing a time delay between dilution prior to addition of Brilliant Green. Absorbances decreased with hydrolysis time (20% loss in 8 min). The effect can be neglected provided that the Brilliant Green is added with 0.5 min of sample dilution. The absorbance of extracts was found to be independent of oxidation time over 0.5–2.0 min but to decrease slightly thereafter; it was independent of the amount added (0.2–1.0 ml). A 1-min oxidation time with 0.5 ml of cerium(IV) solution was used subsequently. The extent of extraction was independent of the concentration of Brilliant Green solution added, over the range 0.2–0.8% (w/v); 0.5% (w/v) was chosen for further use. Absorbances were found to increase with the volume of 1,4-dichlorobenzene solution added up to 2 ml and remained constant thereafter, so 3 ml was adopted for the general procedure. The extracts dissolved in toluene were found to be stable for up to 8 h in diffuse daylight but fade slowly in direct sunlight.

TABLE 1

Effect of diverse ions on the determination of antimony (6 μg)

Ion [a]	Ion/Sb ratio (w/w)	Absorbance change (%) [b]
Na, K, Mg(II), Al(III), Ca(II), As(III), Co(II), Mn(II)	500	< 3
Zn(II), Pb(II), Mo(VI), Ni(II), Se(IV), Nb(V)	100	< 3
Cu(II)	500	−5
	200	< 3
NH_4^+, HPO_4^{2-}, SO_4^{2-}, NO_3^-, Cl^-	2000	< 3
F^-	2000	−32
Fe(III)	500	< 3
	1000	+7
	2500	+13
	2500 [c]	< 3
	5000 [c]	+6

[a] Cations added as chloride, sulphate or nitrate; anions added as sodium salts. [b] Ions causing less than a 3% change in absorbance are regarded as non-interfering. [c] 25 ml of 10% (w/v) sodium hexametaphosphate solution added instead of water in the dilution step.

TABLE 2

Determination of antimony in steel samples

BCS steel No.	Antimony in steel (%, w/w)	
	Certified [a]	Found [b]
456	0.011 (0.010–0.013)	0.0107 ± 0.0005
457/1	0.038 (0.036–0.040)	0.0372 ± 0.0014
458	0.07 (0.063–0.082)	0.0646 ± 0.0019
459	0.007 (0.006–0.008)	0.0067 ± 0.0003

[a] With certified range in parentheses. [b] Mean ± 95% confidence limits for 6 replicates.

The composition of the complex was established spectrophotometrically by Job's method of continuous variations [12] and by the mole ratio method [13] to be 1:1.

RESULTS AND DISCUSSION

A linear calibration graph was obtained over the range 0–20 μg of antimony at 640 nm (apparent molar absorptivity 9.89×10^4 l mol^{-1} cm^{-1}). For the determination of 6 μg of antimony the relative standard deviation was 1.35% (ten results).

The possible interferences of a number of cations and anions was checked for the determination of 6 μg of antimony under the conditions of the general procedure. The results are summarised in Table 1. Iron(III) was the only ion to interfere significantly and this was largely overcome by masking with sodium hexametaphosphate. The results for the determination of antimony in British Chemical Standard Steel (unalloyed) samples (Table 2) were in good agreement with the certified values. The method is rapid and more convenient than the only previously described liquid–solid extraction of antimony [11].

REFERENCES

1 A.G. Fogg, C. Burgess and D.T. Burns, Talanta, 18 (1971) 1175.

2 A.G. Fogg, C. Burgess and D.T. Burns, Analyst, 98 (1973) 347.
3 A.G. Fogg, J. Jillings, D.R. Marriott and D.T. Burns, Analyst, 94 (1969) 768.
4 A.G. Fogg, C. Burgess and D.T. Burns, Analyst, 95 (1970) 1012.
5 G.O. Kerr and G.R.E.C. Gregory, Analyst, 94 (1969) 1036.
6 D.T. Burns, A.G. Fogg and A. Willcox, UV Group Bull., 2 (1974) 23.
7 A.G. Fogg, A. Willcox and D.T. Burns, Analyst, 101 (1976) 67.
8 D.T. Burns and N. Tungkananuruk, Anal. Chim. Acta, 189 (1986) 383.
9 D.T. Burns and N. Tungkananuruk, Anal. Chim. Acta, 204 (1988) 359.
10 D.T. Burns and N. Tungkananuruk, Anal. Chim. Acta, 199 (1987) 237.
11 B.K. Puri, C.L. Sethi and M. Satake, Chim. Acta Turc., 12 (1984) 123.
12 P. Job, Ann. Chim. (Paris) 9 (1928) 113.
13 J.H. Yoe and A.L. Jones, Ing. Eng. Chem. Anal. Ed., 16 (1944) 111.

Analytica Chimica Acta, 284 (1993) 199–205
Elsevier Science Publishers B.V., Amsterdam

Trace metal determinations by spectrophotometry with a double chromogenic system and a chemometric approach

Yongnian Ni

Department of Chemistry, Jiangxi University, Nanchang 330047 (China)

(Received 3rd May 1993; revised manuscript received 28th June 1993)

Abstract

A procedure for the simultaneous spectrophotometric quantitative analysis of multi-component systems was developed. A chemical approach with two parallel chromogenic spectrophotometric systems was used to obtain more information, and multivariate calibration techniques, classical least-squares, principal component regression and partial least-squares regression were applied to the processing of absorbance data. As an example, the simultaneous determination of cobalt, nickel, copper, zinc and iron with a double system 2-(5-bromo-2-pyridylazo)-5-diethylaminophenol and 4-(2-pyridylazo)resorcinol as chromogenic reagents by using multivariate calibration methods is described. The predicted results show that the methods with a double system and multivariate calibration methods based on factor analysis are more precise than those with a single system and the classical least-squares method.

Keywords: Multivariate calibration; UV–Visible spectrophotometry; Double chromogenic system; Trace metals

Recently, quantitative spectrophotometry has been greatly improved by the use of a variety of multivariate statistical method, such as classical least-squares (CLS), inverse least-squares (ILS), principal component regression (PCR) and partial least squares (PLS) [1–11]. Multivariate calibrations are effective in spectrophotometric analysis because the simultaneous inclusion of multiple spectral intensities can greatly improve the precision and applicability. With multivariate calibration methods, empirical models are developed that relate the multiple spectral intensities from a set of calibration samples to the known analyte concentration of the samples. These empirical relationships can then be used in multivariate prediction analyses of spectra of unknown samples to predict the analyte concentrations rapidly.

Correspondence to: Y. Ni, Department of Chemistry, Jiangxi University, Nanchang 330047 (China).

In very complex samples, however, spectral overlap is often a serious problem, because the information of each component obtained from the overlapping spectra is very limited and the condition number of the absorbance coefficient matrix is too large to give satisfactory results [6]. Recently, a method for the simultaneous spectrophotometric determination of metal ions by means of a two-component reagent consisting of Tiron and 2-pyridinealdoxime was reported [12]. Limitations and some chemical problems arise, however, from the necessity of finding compromise conditions with respect to the existence of absorbing metal complexes in the then highly complex chemical systems. Because of these complicated metal–ligand equilibria it is difficult to adjust the suitable experimental condictions.

In this work, an alternative chemical approach with a double chromogenic system was selected in order to obtain more information on the components from the training set and improve the ana-

0003-2670/93/$06.00 © 1993 – Elsevier Science Publishers B.V. All rights reserved

lytical precision. In this situation, however, there is a lot of data to be processed as more than one system is employed and errors are easily introduced. To avoid this disadvantage, a suitable chemometric approach for calibration of double systems in quantitative spectrophotometric analyses of multi-component systems was developed and was applied to the analysis of mixtures of trace metals.

THEORY

Two equal sets of mixed standards with the same composition are prepared which contain the analytes at known concentration levels. Their composition can be represented as a matrix $\boldsymbol{C}$ identically with m rows (number of mixture samples) and l columns (number of components).

Spectrophotometric analysis is applied to one of the two sets with the first chromogenic system, and the second chromogenic spectrophotometric analysis is made on another set of mixed standards. Two matrices of absorbance, $\boldsymbol{A}_1$ and $\boldsymbol{A}_2$, respectively, are then obtained. $\boldsymbol{A}_1$ has m rows and k_1 columns (number of wavelengths in the first system) and $\boldsymbol{A}_2$ has m rows and k_2 columns (number of wavelengths in the second system). There is a relationship (Beer's law) between absorbances and concentrations. Two equations are then obtained:

$$\boldsymbol{A}_1 = \boldsymbol{C}\boldsymbol{K}_1 \tag{1}$$

$$\boldsymbol{A}_2 = \boldsymbol{C}\boldsymbol{K}_2 \tag{2}$$

where $\boldsymbol{K}_1$ and $\boldsymbol{K}_2$ are the matrices of absorptivity of the two systems and $\boldsymbol{K}_1$ and $\boldsymbol{K}_2$ can be obtained by applying the least-squares method to Eqns. 1 and 2, respectively. If $\boldsymbol{K}_1$ or $\boldsymbol{K}_2$ is known, the concentration in unknown samples can be easily obtained according to one of the following equations:

$$\boldsymbol{c}^t_{unk} = \boldsymbol{a}^t_{1,unk}\boldsymbol{K}^t_1\left(\boldsymbol{K}_1\boldsymbol{K}^t_1\right)^{-1} \tag{3}$$

$$\boldsymbol{c}^t_{unk} = \boldsymbol{a}^t_{2,unk}\boldsymbol{K}^t_2\left(\boldsymbol{K}_2\boldsymbol{K}^t_2\right)^{-1} \tag{4}$$

To improve the procedure, $\boldsymbol{A}_1$ is combined with $\boldsymbol{A}_2$, and then matrix $\boldsymbol{A}$, with m rows and $k_1 + k_2$ columns, is obtained, i.e., $\boldsymbol{A} = (\boldsymbol{A}_1, \boldsymbol{A}_2)$. According to Beer's law, we can obtain the following equation:

$$\boldsymbol{A} = \boldsymbol{C}\boldsymbol{K} \tag{5}$$

As in Eqn. 3 or 4, the concentration of the unknown can be written as

$$\boldsymbol{c}^t_{unk} = \left(\boldsymbol{a}^t_{1,unk}, \boldsymbol{a}^t_{2,unk}\right)\boldsymbol{K}^t\left(\boldsymbol{K}\boldsymbol{K}^t\right)^{-1} \tag{6}$$

where $\boldsymbol{K}$ is the coefficient matrix with l rows and $k_1 + k_2$ columns. Unfortunately, the inversion of $\boldsymbol{K}\boldsymbol{K}^t$ (and also $\boldsymbol{K}_1\boldsymbol{K}^t_1$ and $\boldsymbol{K}_2\boldsymbol{K}^t_2$ in Eqns. 3 and 4, respectively) will result in almost singular matrices and no statistical solution can be obtained when much complex mixtures are analysed.

PCR and PLS are factor analysis multivariate statistical tools that have been successfully applied to spectrophotometric analyses of multi-component mixtures. Both of these methods involve spectral decomposition. The PCR decomposition is based entirely on spectral variations without regard for the component concentrations. PCR decomposition is significantly influenced by variations which have no relevance to the analyte concentrations. In PLS, the spectral decomposition is weighted to the concentration. The major difference in the predictive abilities of these two methods is that PLS seems to predict better than PCR when there are random linear baselines or independently varying major spectral components which overlap with the spectral features of the analytes [13]. In this work, PCR and PLS were also applied to the resolution of the spectra of double spectrophotometric systems.

The PCR is done by decomposition of $\boldsymbol{A}$ into latent matrices:

$$\boldsymbol{A} = \boldsymbol{T}\boldsymbol{P} \tag{7}$$

where $\boldsymbol{T}$ is the score matrix of $\boldsymbol{A}$ with m rows and d columns (d is the number of principal components of the combined system) and $\boldsymbol{P}$, the loading matrix of matrix $\boldsymbol{A}$, has d rows and $k_1 + k_2$ columns. A regression equation of $\boldsymbol{C}$ and $\boldsymbol{T}$ can be written as

$$\boldsymbol{C} = \boldsymbol{T}\boldsymbol{G} \tag{8}$$

The concentration of the unknown can then be obtained:

$$c^t_{unk} = \left(a^t_{1,unk}, a^t_{2,unk}\right)P'G \quad (9)$$

The PLS method is carried out by decomposing the matrices A and C at the same time:

$$A = TP \quad (10)$$

$$C = UQ \quad (11)$$

where T is the absorbances score matrix with m rows and d columns (number of dimensions) and P represents the absorbance loading matrix with d rows and $k_1 + k_2$ columns. U is the $m \times d$ concentration score matrix and Q is the $d \times l$ loading matrix.

Relating the score matrices U and T, one obtains a diagonal regression matrix B according to

$$U = TB \quad (12)$$

The concentration of an unknown, c_{unk}, can be obtained by an iterative method [10] or calculated with the following equation [6]:

$$c^t_{unk} = \left(a^t_{1,unk}, a^t_{2,unk}\right)(U'A)^{t}BQ \quad (13)$$

EXPERIMENTAL

Apparatus

Spectrophotometric measurements were made on a Lambda 17 UV–visible spectrophotometer (Perkin-Elmer). The pH of the solutions was measured with a Model SA720 pH meter (Orion). The computations were made on a GW 286 EX/16 computer (GW Computer Corp.). All the programs in the computing process were written in BASIC.

Reagents

All solutions were prepared with analytical-reagent grade reagents. Solutions of cobalt, nickel, copper, zinc and iron ions (10.0 μg ml^{-1}) were prepared from their nitrate or chloride salts according to the classical method. Solutions of 2-

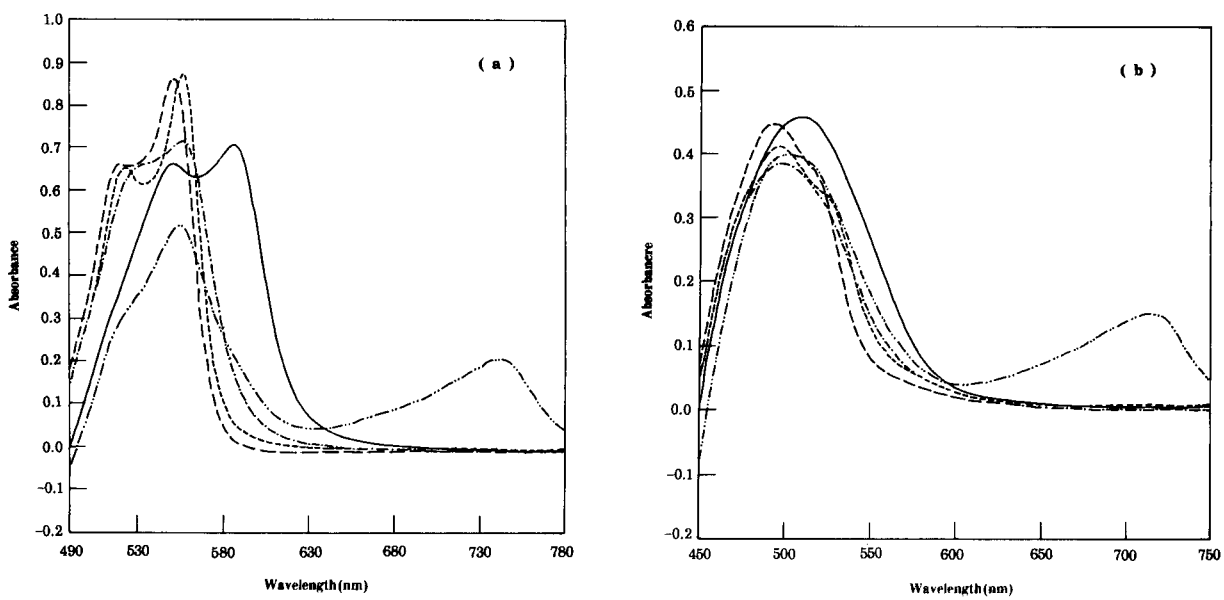

Fig. 1. Absorption spectra of five metal ions in (a) 5-Br-PADAP and (b) PAR systems with borate buffer (pH 9.2). Concentration, 10.0 μg of each ion in 25 ml. ———, Cobalt; - - - - - -, nickel; ·—·—·, copper; — — — zinc —·—·—, iron.

(5-bromo-2-pyridylazo)-5-diethylaminophenol (5-Br-PADAP) (0.02%) and 4-(2-pyridylazo)resorcinol (PAR) (0.05%) were prepared by dissolving the reagents in ethanol. Buffer solution (pH 9.2) was prepared by dissolving sodium borate in distilled water.

Procedure for analysis with 5-Br-PADAP

Analysis with 5-Br-PADAP was performed by pipetting a suitable amount of sample solution (mixture of metal ions), 5.0 ml of 5-Br-PADAP solution, 5.0 ml of ethanol and 5.0 ml of buffer into a flask and diluting with distilled water to 25.0 ml. After 20 min, the absorbance of this mixture was measured in 1.0-cm cuvettes between 490 and 780 nm at 2-nm intervals with respect to a reagent blank.

Procedure for analysis with PAR

Analysis with PAR was carried out by pipetting the same amount of samples as above, 2.0 ml of PAR solution and 5.0 ml of buffer and diluting to 25.0 ml with water. After 20 min, the absorbances were recorded in 1.0-cm cuvettes from 450 to 750 nm at 2-nm intervals with respect to a reagent blank.

RESULTS AND DISCUSSION

Figure 1 shows the spectra of cobalt, nickel, copper, zinc and iron obtained with the chromogenic reagents 5-Br-PADAP and PAR.

Composition of the calibration set and the error criterion

Sixteen mixtures of cobalt, nickel, copper, zinc and iron were selected as the calibration set (Table 1). Their composition was orthogonally designed in order to obtain maximum information on each metal from the calibration procedure. Their concentrations were represented as matrix $\boldsymbol{C}$, and the absorbances measured with 5-Br-PADAP and PAR were used as the calibration matrices $\boldsymbol{A}_1$ and $\boldsymbol{A}_2$, respectively, to establish the models according to the description in the Theory section. These models included CLS, PCR and PLS methods with double and single systems. The prediction error of a single component in the mixture was calculated as the relative standard deviation (R.S.D.) of the predicted concentration:

TABLE 1

Compositions of calibration samples

Sample No.	Concentration (μg per 25 ml)				
	Cobalt	Nickel	Copper	Zinc	Iron
1	4.00	1.00	2.00	4.00	1.00
2	4.00	2.00	1.00	2.00	4.00
3	4.00	4.00	4.00	1.00	2.00
4	4.00	1.00	1.00	1.00	2.00
5	1.00	2.00	2.00	4.00	4.00
6	1.00	4.00	4.00	2.00	1.00
7	1.00	1.00	4.00	1.00	4.00
8	1.00	2.00	2.00	2.00	1.00
9	2.00	4.00	1.00	4.00	2.00
10	2.00	1.00	4.00	2.00	2.00
11	2.00	2.00	1.00	4.00	1.00
12	2.00	4.00	2.00	1.00	4.00
13	10.00	0.00	0.00	0.00	0.00
14	0.00	10.00	0.00	0.00	0.00
15	0.00	0.00	10.00	0.00	0.00.
16	0.00	0.00	0.00	10.00	0.00
17	0.00	0.00	0.00	0.00	10.00

$$\text{R.S.D. (\%)} = \left[\frac{\sum_{i=1}^{n} \left(\hat{C}_{ij} - C_{ij}\right)^2}{\sum_{i=1}^{n} \left(C_{ij}\right)^2} \right]^{1/2} \qquad (14)$$

where C_{ij} is the concentration of the jth component in the ith mixture and $\hat{C}_{ij}$ its estimated

TABLE 2

Compositions of test samples

Sample No.	Concentration (μg per 25 ml)				
	Cobalt	Nickel	Copper	Zinc	Iron
1	0.50	2.00	3.00	2.00	1.50
2	1.50	2.50	3.50	0.50	2.50
3	0.50	1.50	2.50	3.50	3.50
4	2.50	0.50	1.00	1.00	0.50
5	1.50	3.50	0.50	1.50	1.00
6	3.50	1.00	1.50	0.50	3.00
7	2.00	3.50	0.50	3.00	1.00
8	1.50	1.00	3.00	2.50	1.50
9	0.50	2.50	2.50	0.50	3.50
10	3.50	1.50	1.50	1.00	0.50
11	2.00	2.50	2.00	1.50	0.50
12	3.00	0.50	2.00	3.50	3.00

concentration. The total prediction error of the mixtures was calculated as

$$\text{R.S.D. (\%)} = \left[\frac{\sum_{i=1}^{n} \sum_{j=1}^{m} \left(\hat{C}_{ij} - C_{ij}\right)^2}{\sum_{i=1}^{n} \sum_{j=1}^{m} \left(C_{ij}\right)^2} \right]^{1/2} \quad (15)$$

Prediction of synthetic mixtures with a double system by multivariate calibration methods

In this work, twelve five-component metallic ion mixtures (their compositions are given in Table 2), were analysed with the double chromogenic system as described under Experimental. The absorbance spectra were investigated using CLS, PCR and PLS methods. The trace concentrations of each component in these mixtures were in the range 0.025–0.14 μg ml^{-1}. The results of the prediction are summarized in Table 3. It can be seen that both the PCR and PLS methods give satisfactory results. Poor results were obtained by CLS, especially for nickel and copper. This is because the former methods are based on factor analysis and the disadvantage of collinearities of the absorbance spectra can be overcome.

Table 4 gives the results for the analysis of the samples listed in Table 2 with a single chromogenic system. Comparison with those in Table 3 shows that most of the results in Table 3 using any multivariate calibration method with the double system are better than those with a single system in Table 4, except for the CLS method with 5-Br-PADAP. This is because with the double system more information is used to establish the calibration models and then to predict the

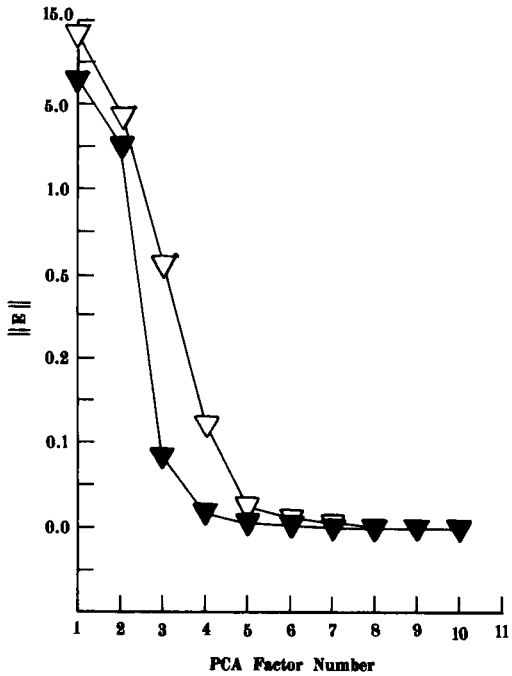

Fig. 2. Plot of squares of residual absorbance, $\|E\|$ vs. the number of principal components in different system. ▽ = 5-Br-PADAP system; ▼ = PAR system. $E = A\text{-}t_h p_h$ (t_h is a column vector of scores for matrix A, factor h; p_h is a row vector of loadings for matrix A, factor h (see Eqn. 10); h is a dummy index for counting principal components or factors).

TABLE 3

Relative standard deviations of prediction results for the test set with the double chromogenic system

Component in mixture	CLS method		PCR method		PLS method	
	Recovery (%) (mean) [a]	R.S.D. (%) (single) [b]	Recovery (%) (mean) [a]	R.S.D. (%) (single) [b]	Recovery (%) (mean) [a]	R.S.D. (%) (single) [b]
Cobalt	100.8	6.5	107.9	5.3	91.2	4.7
Nickel	111.0	20.3	109.5	5.8	93.6	9.2
Copper	91.3	29.7	101.7	8.7	99.9	6.5
Zinc	79.8	12.8	85,7	10.2	93.3	7.9
Iron	108.0	9.5	103.7	4.0	114.3	10.1
R.S.D. total (%) [c]		18.0		7.1(8) [d]		7.9(8) [d]

[a] Recovery(%) = $100\Sigma_{i=1}^{n}(\hat{C}_{ij}/C_{ij})/n$, where C_{ij} is the true concentration of the jth component in the ith mixture and $\hat{C}_{ij}$ its estimated concentration. [b] Calculated according to Eqn. 14. [c] Calculated according to Eqn. 15. [d] Values in parentheses are the number of factors used for prediction.

TABLE 4

Relative standard deviations of prediction results for the test set with a single chromogenic system

Component in mixture	5-Br-PADAP system						PAR system					
	CLS method		PCR method		PLS method		CLS method		PCR method		PLS method	
	Recovery (%) (mean) [a]	R.S.D. (%) (single) [b]	Recovery (%) (mean) [a]	R.S.D. (%) (single) [b]	Recovery (%) (mean) [a]	R.S.D. (%) (single) [b]	Recovery (%) (mean) [a]	R.S.D. (%) (single) [b]	Recovery (%) (mean) [a]	R.S.D. (%) (single) [b]	Recovery (%) (mean) [a]	R.S.D. (%) (single) [b]
Cobalt	110.4	2.4	102.4	2.9	88.3	6.5	145.5	29.8	106.9	8.2	78.1	21.8
Nickel	104.2	13.1	102.0	4.3	92.6	6.6	112.4	17.6	105.9	12.9	117.4	16.5
Copper	103.5	16.1	87.6	9.1	85.1	9.8	81.5	73.1	89.2	18.5	68.2	36.2
Zinc	79.1	16.2	68.7	17.3	77.2	15.9	113.8	30.3	100.2	12.0	152.3	32.4
Iron	101.8	8.8	115.3	7.6	137.0	20.4	105.4	10.8	109.3	7.1	106.1	16.8
R.S.D. (total) (%) [c]		12.4		9.5(7) [d]		13.0(7) [d]		39.3		12.4(11) [d]		26.0(10) [d]

[a–d] See Table 3.

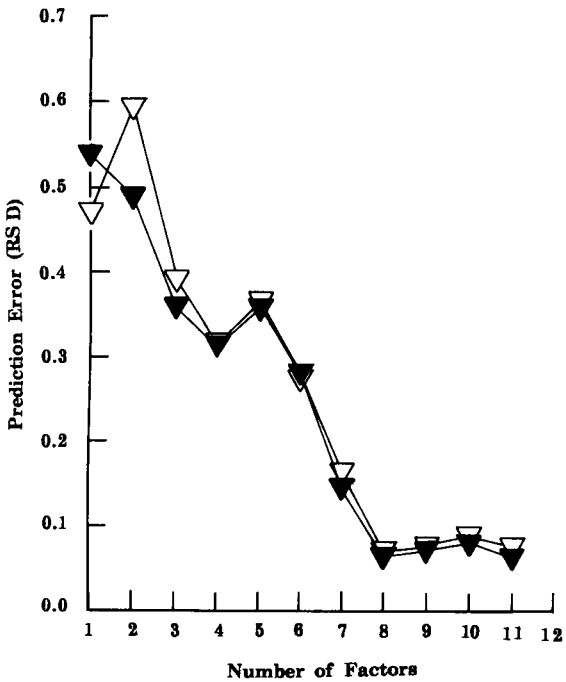

Fig. 3. Plot of predicted error, R.S.D. (total), vs. the factor number in the (▼) PCR and (▽) PLS methods.

concentrations of unknown components successfully. The CLS method is strongly affected by the correlativity of the overlapping spectra, so errors can easily be introduced and satisfactory results will not be obtained.

Extraction of information from each chromogenic system

The amount of information obtained from each chromogenic system can be investigated by principal component analysis. Figure 2 shows the variation of the residual absorbance of these two chromogenic systems. It shows that the sum of the squares of the residual absorbance decreases more quickly in the PAR system than in the 5-Br-PADAP system. This means that the PAR system gives less effective information than the 5-Br-PADAP system owing to the serious overlapping of the spectra.

Choice of the number of factors in double chromogenic systems

It is very important to select a suitable number of factors (i.e., dimensions or principal components) in multi-component analysis methods based on factor analysis. Figure 3 gives the variation of the total prediction error (R.S.D.) with the number of factors in PCR and PLS methods. It shows that the R.S.D. will be smallest when the number of factors is seven in both the PCR and PLS methods with the double system.

Conclusions

A double chromogenic system is an effective approach for multi-component spectrophotometric analysis. More quantitative information can be obtained by using the described method, so the selectivity of determination of multiple components in mixtures can be improved, especially when there is serious spectral overlapping (which has very bad conditioning in a mathematical sense). Chemometric approaches with suitable multivariate calibration methods are used for absorbance data processing and reduction, and satisfactory results can be obtained.

The author thanks Mr. Xinming Yin for his contribution to the experimental work and the Natural Science Foundation of China and Jiangxi Provincial Science Foundation for financial support.

REFERENCES

1 P. Jochum and E.L. Schrott, Anal. Chim. Acta, 157 (1984) 211.
2 C.W. Brown, P.F. Lynch, R.T. Obremski and D.S. Lavery, Anal. Chem., 54 (1982) 1472.
3 S.M. Donahue, C.W. Brown and M.J. Scott, Appl. Spectrosc., 44 (1990) 407.
4 Y. Iida, K. Goto, M. Furukawa and S. Shibata, Bunseki Kagaku, 32 (1983) 401.
5 Y. Ni and X. Chen, Fenxi Huaxue, 18 (1990) 618.
6 M. Otto and W. Wegscheider, Anal. Chem., 57 (1985) 63.
7 Y. Ni, Gaodeng Xuexiao Huaxue Xuebao, 11 (1990) 1016.
8 W. Lindberg, J.-A. Persson and S. Wold, Anal. Chem., 55 (1983) 6643.
9 D. Haaland and E. Thomas, Anal. Chem., 60 (1988) 1193.
10 P. Geladi and B.R. Kowalski, Anal. Chim. Acta, 185 (1986) 1.
11 B.R. Kowalski and M.B. Seasholtz, J. Chemometr., 5 (1991) 129.
12 M. Otto and W. Wegscheider, Anal. Chem., 61 (1989) 1847.
13 E. Thomas and D. Haaland, Anal. Chem., 62 (1990) 1091.

Analytica Chimica Acta, 284 (1993) 207–215
Elsevier Science Publishers B.V., Amsterdam

Sensitive, fluorescent detection of hydrazine via derivatization with 2,3-naphthalene dicarboxaldehyde

G.E. Collins

Geo-Centers, Inc., 10903 Indian Head Highway, Fort Washington, MD 20744 (USA)

S.L. Rose-Pehrsson

Naval Research Laboratory, Chemistry Division, Code 6110, Washington, DC 20375-5342 (USA)

(Received 17th May 1993; revised manuscript received 19th July 1993)

Abstract

The derivatization of hydrazine with 2,3-naphthalene dicarboxaldehyde (NDA) followed by fluorescence detection is shown to be an effective method for the selective determination of extremely low concentrations of hydrazine in solution. Kinetic studies of the reaction between hydrazine and NDA indicate that the reaction is first order in both hydrazine and NDA, and is dependent upon an acidic pH (optimum pH = 2.5) for the formation of the fluorescent derivative. The NDA–hydrazine derivative is readily formed (time response < 5 min) and is strongly fluorescent in the green (λ_{ex} = 403 nm and λ_{em} = 500 nm). A linear concentration dependence is observed over a dynamic range from 50 ng/l to 500 μg/l of hydrazine (correlation coefficient, $r > 0.999$), with a signal-to-noise ratio of 3:1 for 50 ng/l of hydrazine. The selectivity of the NDA reagent is examined with respect to several possible interferents, including ammonia, and is shown to be a highly specific reagent for hydrazine.

Keywords: Fluorimetry; Hydrazine; Naphthalene dicarboxaldehyde

Interest in the development of new methods for the detection of hydrazine, N_2H_4, has paralleled its increasing number of applications as both a primary industrial chemical as well as a hypergolic fuel propellent. Hydrazine is an important building block essential to the synthesis of a number of polymers, pesticides, pharmaceuticals, and chemotherapeutic tools [1,2]. Because of the strong reducing capability of hydrazine in basic solution and the fact that its oxidation products are nitrogen and water, electric utilities employ hydrazine as an effective chemical for preventing the corrosion of boilers by dissolved oxygen and metal oxides [3]. The Department of Defense and NASA have taken advantage of the hypergolic properties of hydrazine for a number of years as propellants for the space shuttle, satellites, and aircraft auxiliary-power units.

Recent medical studies have indicated that there are various toxicological problems associated with hydrazine exposure. Hydrazine is suspected to result in a number of adverse effects in man, including: damage to the liver, kidneys, and other internal organs; production of various blood abnormalities; irreversible damage to the nervous system; an alteration in the behavior of those exposed; and numerous teratogenic and mutagenic effects [4–6]. Because of the health hazards associated with hydrazine, the American Conference of Governmental Industrial Hygienist

Correspondence to: S.L. Rose-Pehrsson, Naval Research Laboratory, Chemistry Division, Code 6110, Washington, DC 20375-5342 (USA).

0003-2670/93/$06.00 © 1993 – Elsevier Science Publishers B.V. All rights reserved

(ACGIH) has recommended that the threshold limit value (TLV) for hydrazine be lowered from 100 ppb to 10 ppb in air [7]. The TLV is a time-weighted average concentration of permissible exposure within a normal eight hour workday. In order to effectively monitor the working environment at these levels, NASA and the U.S. Air Force have solicited the development of new sensor technologies. We have been working in cooperation with NASA/Kennedy Space Center on the development of a highly sensitive detector for hydrazine intended for use in a new satellite payload spin test facility (PSTF). The specifications for this sensor mandate that it be continuously operable for 90 days (maintenance free), with a detection limit of 10 ppb for hydrazine and a response time (the time necessary for a 90% change in the total response) less than ten minutes. This type of sensitive and selective, on-line monitor for hydrazine, operating at the new TLV level, would likely be applicable to a number of industrial situations, also.

Several different methods have been developed for the detection of low levels of hydrazine, although none of the techniques described below completely fulfills the analytical requirements set for the PSTF. The Naval Research Laboratory, along with Geo-Centers, Inc., has developed two passive dosimeter systems for hydrazine detection. The first is referred to as a citrate sampler and is reliant upon a citric acid coating to trap and stabilize the hydrazines for subsequent analysis by wet chemical techniques [8,9]. The second method is a colorimetric technique which incorporates both 2,4-dinitrobenzaldehyde and vanillin (3-methoxy-4-hydroxybenzaldehyde) as separate detectors onto a single badge, allowing for the simultaneous quantitation of both hydrazine and unsymmetrical dimethylhydrazine (UDMH) [10,11]. While these badges are effective passive sampling devices, we have been exploring active sampling methods which will allow for a sensitive and continuous real-time monitor of the hydrazine concentration. The colorimetric reactions that take place between hydrazine and a number of different benzaldehydes (i.e., *para*-dimethylbenzaldehyde, salicaldehyde) have also been utilized in various flow-injection analysis schemes [12,13]. The detection limits for these absorbance techniques are ultimately limited by the nature of the absorbance measurement to be approximately 5–10 μg/l of hydrazine in solution, a fact which makes this approach inadequate for our purposes. While potentiometry and coulometry are useful electrochemical techniques for the detection of hydrazine, their sensitivity, detector lifetime limitations, and/or inappropriateness as real-time continuous monitors of hydrazine concentration have been the limiting problems for these techniques [14,15]. Some mass spectrometric methods have also been employed for the detection of hydrazine, with the expense and operator expertise associated with these techniques being the primary disadvantages [16]. The ion mobility mass spectrometer has seen some success in the measurement of hydrazine vapor concentrations, although the selectivity and expense of this instrument limits its applicability [17,18]. To our knowledge, there are only a few reported cases where fluorescence has been employed for the detection of hydrazine [19–21]. These examples suggest that fluorescence may be well suited for the sensitive determination of hydrazine, providing that a suitable derivatization scheme can be developed.

It is important to bear in mind, though, that while our efforts have centered upon the development of methods for the sensitive determination of hydrazine levels present within a working environment (e.g., ppb in air), a flow-through fluorometric technique actually monitors the concentration of hydrazine present in solution (e.g., μg/l of solution). Imperative to developing a liquid-based fluorescence scheme for the detection of hydrazine, then, is the capability for efficiently scrubbing trace amounts of hydrazine vapor from the ambient into an aqueous medium. Preliminary studies suggest that a counter-current gas–liquid scrubber using acidic water will give nearly complete recovery of the hydrazine from the vapor phase into the liquid phase. Using the ideal gas law and assuming 100% extraction of hydrazine from a 5 l/min air stream into a 15 ml/min aqueous stream, the concentration of hydrazine in air (ppb) is 2.3 times the concentration of hydrazine in solution (μg/l). In order to

meet a 10 ppb detection limit for hydrazine in air, the fluorometric method will then require a 4.4 μg/l detection limit in solution.

Thinking of hydrazine, N_2H_4, as an NH_3 molecule with one of the hydrogen atoms replaced by an $-NH_2$ group, it is reasonable to presume that many of the reagents designed for the fluorescent derivatization of amines, amino acids, and peptides might also be applicable to the trace analysis of hydrazine. Among the different derivatizing agents developed for use in fluorescent amino acid analysis, particular emphasis has been placed in recent years upon the use of the dicarboxaldehydes, *o*-phthalaldehyde (OPA) and naphthalene–2,3-dicarboxaldehyde (NDA) [22–24]. OPA and NDA react with peptides and primary amino acids in the presence of nucleophiles, such as 2-mercaptoethanol and the cyanide ion, respectively, to form highly fluorescent isoindole rings. The alkylthiolisoindole derivatives produced from the OPA/RSH reaction are relatively unstable and possess lower fluorescence quantum yields when compared to the NDA/CN^- derivatives. Therefore, we have concentrated our efforts on the use of NDA in the fluorescent detection of hydrazine.

The reaction mechanism shown in Scheme 1 is proposed to explain the formation of the intensely fluorescent derivative, VI, the conjugate acid of 2,3-diazaanthracene (V), which is the product formed in the reaction between hydrazine and NDA. The reaction is acid catalyzed and readily takes place in the absence of any added nucleophiles (i.e., CN^- or thiol). The incorporation of hydrazine into the naphthalene framework as an additional, fused, six-membered heterocycle, results in the formation of a highly efficient fluorophore that emits maximally in the green. We have found this fluorescent derivatization reaction to be a highly sensitive and selective method for the trace determination of hydrazine levels in solution.

EXPERIMENTAL

Apparatus

All fluorescence measurements were made on an SLM-8000 double-beam, scanning spectrofluorometer with a 450 W Xenon arc lamp excitation source. Fluorescence intensities were corrected for instrument response and fluctuations in the lamp by dividing the sample fluorescence intensity by the fluorescence intensity observed from a reference cell containing Rhodamine B. In all cases, a slit width of 4 mm (spectral bandpass = 8 nm) was used for both the excitation and emission monochromators. A magnetic stir-bar within the quartz cuvette allowed the injection of various aliquots of hydrazine directly into the cuvette. The absorbance measurements were made using a double beam Bausch and Lomb Spectronic 2000, using either a deuterium or tungsten–halogen lamp and a spectral slitwidth of 2 nm.

Chemicals and stock solutions

All chemicals were used as received from the suppliers. Naphthalene–2,3-dicarboxaldehyde (NDA) was obtained from Molecular Probes, Inc. (99%), and used to prepare 10^{-2} M stock solutions in anhydrous ethanol (Warner Graham Co.). All aqueous solutions were prepared using purified water (Millipore). Hydrazine standard solutions were prepared by diluting anhydrous hydrazine (Olin Co.) in 0.1 M H_2SO_4 to give the following concentrations: 1 μg/l, 10 μg/l, 100 μg/l, 1 mg/l, 10 mg/l, and 1000 mg/l. The hydrazine stock solutions were prepared in acid solution (with the exception of the kinetic investigation into the effect of pH on reactivity), in order to ensure the integrity of these concentrations for several days. All buffer solutions were prepared from 0.1 M NaH_2PO_4 (Aldrich) and adjusted to the appropriate pH with either NaOH or H_2SO_4. Those acid solutions with a pH less than one, were prepared using either concentrated HNO_3 or H_2SO_4 acid. Stock solutions of the interferents were prepared such that a 100 μl injection into 2 ml of the NDA reagent would approximate the exposure of twice the threshold limit value as determined by the National Institute for Occupational Safety and Health (NIOSH) [25]. These reagents include: 30 mM NH_4OH (GFS Chemicals), 0.57 M Freon 113 (Dupont), 0.23 M isopropyl alcohol (Mallinckrodt), and 0.11 M methyl ethyl ketone (Fischer Scientific). An

aqueous solution of 23 mM NaCN was also prepared, in order to examine the effect of the nucleophilic CN^- anion in the NDA–hydrazine derivatization reaction.

Procedure

In general, 2.0 ml of buffer solution were pipetted into a quartz cuvette (10 mm lightpath), along with 10 to 100 μl (Eppendorf microburette) of NDA stock solution (0.05–0.5 mM). The solution was mixed and then transferred to the spectrofluorometer or spectrophotometer. The subsequent addition of hydrazine and/or the different interferents was accomplished using a 100 μl variable microburette. Except as noted, all fluorescence measurements were made with the excitation and emission monochromators set to 403 and 500 nm, respectively.

Following derivatization of the NDA reagent with hydrazine, a GC–MS spectrum was recorded using a Varian gas chromatograph/quadrupole ion trap ITS40, giving the following m/z (%) peaks: 180 (100), 153 (20), and 126 (70). These results are consistent with the formation of 2,3-diazaanthracene, $C_{12}H_8N_2$ (product V in Scheme 1). The hydrazone, shown as molecule III in Scheme 1, was also observed in the GC–MS spectrum, exhibiting the following m/z (%) peaks: 198 (25), 186 (12), 154 (36), and 126 (100).

Kinetic investigations

Kinetic studies of the reaction between NDA and hydrazine were accomplished by monitoring the rate of fluorescent product formation using the spectrofluorometer. The reaction dependence of NDA was investigated at a pH of -0.3, with the concentration of NDA (4.8×10^{-5} to 5.9×10^{-3} M) in significant excess with respect to the concentration of hydrazine (7.4×10^{-7} M). Under similar conditions ([NDA] = 2.4×10^{-4} M and $[N_2H_4] = 7.4 \times 10^{-7}$ M), the catalytic effect of the hydrogen ion concentration on the reaction between NDA and hydrazine was characterized. The kinetic order of hydrazine was evaluated at a pH of 3.0, with the concentration of hydrazine (1.5×10^{-4} to 2.8×10^{-3} M) substantially larger than the concentration of NDA (2.4×10^{-8} M).

RESULTS AND DISCUSSION

Reaction characteristics

The absorption spectra obtained from an aqueous 4.8×10^{-4} M solution of the NDA reagent (pH 3) both before and after the addition of 455 μg/l of hydrazine are shown in Fig. 1. Note that the addition of hydrazine results in a significant red-shifting (35 nm) of the absorbance spectrum from a λ_{max} of 362 nm for NDA to 397 nm for the NDA–hydrazine derivative. In addition, the NDA–hydrazine derivative has a significantly larger molar extinction coefficient (8×10^4 cm^{-1} M^{-1} at 397 nm) compared to that of the non-derivatized NDA (1.2×10^3 cm^{-1} M^{-1} at 362 nm). Both of these characteristics can be attributed to an increase in the extent of conjugation and delocalization of π electrons within the NDA–hydrazine derivative. While it is apparent that absorbance methods could be used in the detection of hydrazine with NDA, fluorescence is clearly a significantly more sensitive technique (see below).

A direct comparison can be made between the absorbance spectra shown in Fig. 1 and the fluorescence excitation (Fig. 2) and emission (Fig. 3) spectra obtained from an identical concentration of the NDA reagent both before and after the addition of 4.3, 25 and 105 μg/l of hydrazine. The excitation spectra were obtained by setting the emission monochromator to the λ_{max} for fluorescence emission from the NDA–hydrazine

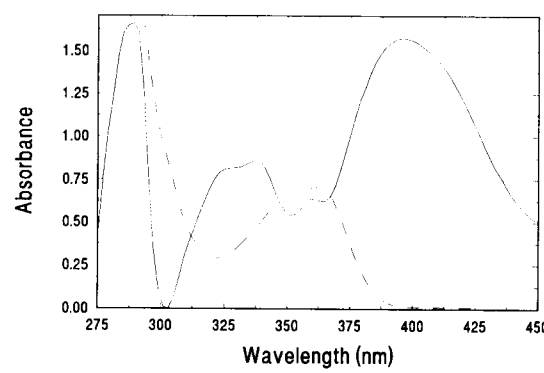

Fig. 1. Absorbance spectra obtained for a 4.8×10^{-4} M solution of NDA (pH 3) before (dashed line) and after (solid line) the addition of 455 μg/l of hydrazine.

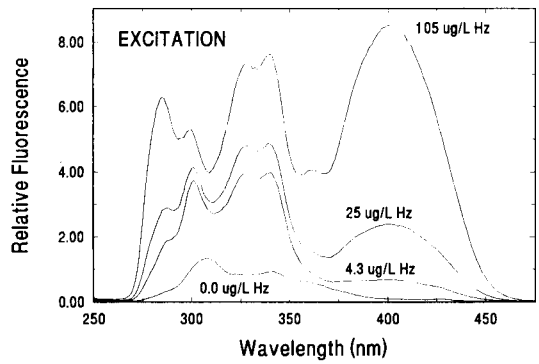

Fig. 2. Excitation spectra obtained with λ_{em} set to 500 nm for a 4.8×10^{-4} M solution of NDA (pH 3) before and after the addition of 4.3, 25 and 105 μg/l of hydrazine.

derivative at 500 nm. The emission spectra were measured by setting the excitation monochromator to 403 nm. It is evident from Fig. 3 that the apparent fluorescence emission of the NDA prior to the addition of hydrazine is minimal and nearly within the noise of the background. The NDA–hydrazine derivative, on the other hand, is intensely fluorescent and characterized by a broad fluorescence emission (FWHM = 80 nm for the 105 μg/l hydrazine addition) centered at approximately 500 nm. The excitation spectrum for NDA prior to the addition of hydrazine has some similarities to the absorption spectrum shown in Fig. 1, with both spectra showing λ_{max} at 362 nm. The additional peaks evident in the excitation spectrum at 308 and 341 nm are likely due to those wavelengths possessing higher fluorescence quantum efficiencies. Following the addition of only 4.3 μg/l of hydrazine, we note the growth of a 400 nm band arising due to the formation of the NDA–hydrazine derivative. This peak ultimately dominates the excitation spectrum, as the amount of hydrazine is increased to values above 105 μg/l of hydrazine (FWHM = 60 nm for the 105 μg/l hydrazine addition). As expected, the excitation spectrum following the addition of 105 μg/l of hydrazine is nearly identical to the absorbance spectrum of the reaction product shown in Fig. 1, with spectral maxima, λ_{max}, at 402, 363, 327, 339, and 286 nm.

From an analytical standpoint, the NDA reagent is ideal in that prior to its derivatization by hydrazine, there is no fluorescence background at 500 nm (providing that the excitation wavelength is approximately 400 nm). The benefit of using fluorescence detection over absorbance techniques is that there is a distinct advantage to measuring a small, fluorescent signal set upon a dark background, as opposed to measuring an equally small difference in signal set upon a large signal background (i.e., absorbance).

Formation kinetics

The importance of pH in the reaction between NDA and hydrazine is demonstrated in Fig. 4, which is a plot of k_{obs} versus log [H^+] under conditions such that [Hz] $\ll$ [NDA] and [H^+]. The reaction rate measured for the formation of

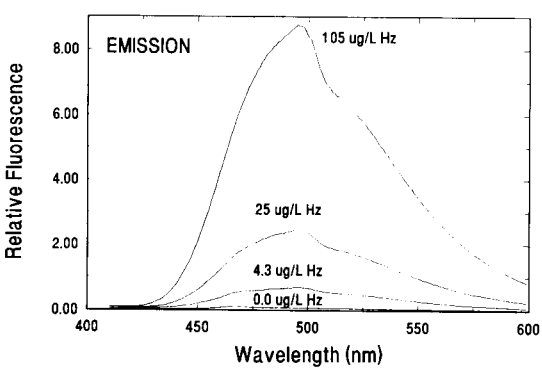

Fig. 3. Emission spectra obtained with λ_{ex} set to 403 nm for a 4.8×0^{-4} M solution of NDA (pH 3) before and after the addition of 4.3, 25 and 105 μg/l of hydrazine.

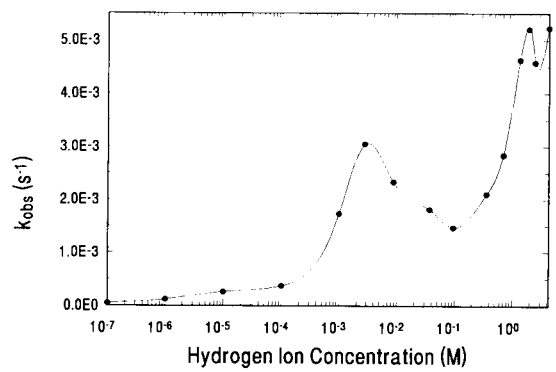

Fig. 4. Dependence of the observed rate constant on the hydrogen ion concentration in solution for the reaction between NDA and hydrazine.

the fluorescent NDA–hydrazine derivative reaches a maximum at a pH of 2.5, as well as at concentrations of H^+ above 1.9 M. It should be pointed out, though, that as the concentration of H^+ goes above 0.7 M, the overall sensitivity toward hydrazine decreases due to a progressive decrease in the fluorescence intensity seen for a given concentration of hydrazine.

Two separate experiments were conducted to evaluate the overall reaction kinetic order with respect to both NDA and hydrazine. Under conditions of analytical application interest, i.e., [Hz] $\ll$ [NDA] and [H^+], the reaction is apparently first order in NDA, with a plot of k_{obs} versus [NDA] showing good linear behavior (regression data: $n = 7$, $m = 5.98\ M^{-1}\ s^{-1}$, $\sigma_m = 0.38\ M^{-1}\ s^{-1}$, $b = 2.17 \times 10^{-4}\ s^{-1}$, $\sigma_b = 2.00 \times 10^{-4}\ s^{-1}$, $\sigma = 2.84 \times 10^{-4}$, $r = 0.98$). While the derivatization rate is proportional to the concentration of NDA, the background fluorescence (or scattering due to undissolved reagent) and the concentration of undesirable side products will also increase in the presence of a large excess of NDA. The optimum concentration of NDA is 100 to 500 μM. The dependence of k_{obs} on the concentration of hydrazine (with [NDA] $\ll$ [Hz] and [H^+]) also exhibits a first order dependence with respect to hydrazine and an excellent linear correlation (regression data: $n = 8$, $m = 5.94\ M^{-1}\ s^{-1}$, $\sigma_m = 0.17\ M^{-1}\ s^{-1}$, $b = 4.30 \times 10^{-4}\ s^{-1}$, $\sigma_b = 2.50 \times 10^{-4}\ s^{-1}$, $\sigma = 4.13 \times 10^{-4}$, $r > 0.99$).

Scheme 1 shows the proposed mechanism for the formation of the NDA–hydrazine derivative, 2,3-diazaanthracene (V). The lone pair of electrons on one of the nitrogen atoms of the hydrazine helps initiate the addition of the nucleophilic hydrazine to one of the carbonyl groups of the NDA, a reaction resulting in the formation of an unstable (and likely unisolateable), alcoholic intermediate, II. The subsequent loss of a water molecule from II is aided by the nonbonding electron pair on the adjacent nitrogen atom, yielding the hydrazone intermediate, III. In a manner similar to that seen in the first step (I → II), the tail end of the hydrazone reacts with the adjacent carbonyl group of the NDA to form an unstable intermediate, IV. Loss of a second molecule of H_2O leads to the formation of an additional heterocycle extending the naphthalene backbone. This product, 2,3 diazaanthracene (V), as well as the hydrazone intermediate, III, have both been verified by GC–MS (see Experimental section).

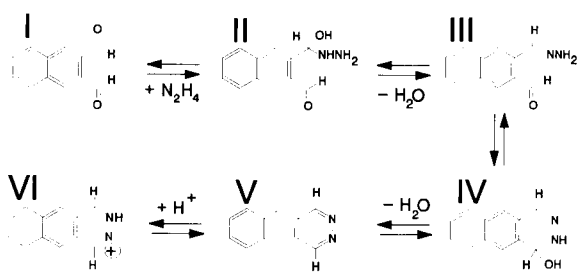

Scheme 1. Diagram indicating the proposed mechanism for the formation of the highly fluorescent NDA/hydrazine derivative.

Protons are known to catalyze condensation reactions of amines with carbonyls in two different catalytic pathways. The first is based upon the protonation of either of the carbonyl groups of the NDA to form a functional group that is more susceptible to attack by the nucleophilic hydrazine (I → II). This same catalysis pathway can also take place later on in the scheme, by protonation of the second aldehyde group of the NDA (III → IV). Clearly, these catalysis pathways are ultimately dependent upon the first and second acid dissociation constants for NDA. The second type of catalytic pathway is manifested in steps II → III and IV → V in Scheme I, both of which rely upon the loss of a molecule of water to form a hydrazone. These steps can be catalyzed by protonating the hydroxyl group in either of the intermediates, II or IV, thereby, forming a much better leaving group in the form of the weakly basic, $-OH_2^+$ group.

Further examination has demonstrated that the NDA–hydrazine derivative formed is actually a fluorescent, pH indicator that is non-fluorescent under basic conditions (pH > 6), and fluorescent under acidic conditions (pH < 6). We propose that the fluorescent derivative actually monitored in this analytical scheme is the conjugate acid of 2,3-diazaanthracene (V), or molecule VI as seen in Scheme 1. It is possible that protonation of the azine group within 2,3-diazaanthracene (V),

causes the $n\pi^*$ excited state levels of the derivative to increase in energy. If the energy of the triplet and singlet electronic states, $T_{n\pi^*}$ and $S_{n\pi^*}$, of 2,3-diazaanthracene become higher than that of the $S_{\pi\pi^*}$ state, the probability for intersystem crossing will be low and the fluorescence quantum efficiency will, therefore, increase [26].

Figure 4 shows an extremely complex behavior with respect to the dependence of the observed rate constant on the hydrogen ion concentration. There are apparently several different rate limiting steps taking place as a function of the pH in solution. It is important to remember that the observed rate constant is being determined with respect to the formation of the fluorescent, NDA–hydrazine derivative, VI, and not with respect to the formation of the non-fluorescent derivative, 2,3-diazaanthracene (V). We have recently demonstrated that the reaction to form V is actually optimum under slightly basic conditions (pH 8–10), in addition to bearing an observed rate constant that is as much as 1000 times that shown in Fig. 4 [27]. These results suggest that performing the reaction under acidic conditions may actually suppress the formation of 2,3-diazaanthracene. This conclusion is supported by the fact that at a pH of 5.0 and below, more than 99% of the hydrazine in solution is present in the singly protonated form, $N_2H_5^+$; at low pH values, then, the reaction step III → IV will likely be inhibited by the absence of a lone pair of electrons on the second nitrogen atom. The optimal pH measured for the formation of 2,3-diazaanthracene (V) is a cross between the hydrogen ion concentration necessary to catalyze the condensation reactions, and that essential to preventing protonation of hydrazine and the formation of a weaker nucleophilic species. We are currently pursuing the possibility of substantially increasing the fluorescent reaction rate by performing the hydrazine derivatization reaction with NDA under basic conditions, and subsequently adding an appropriate amount of acid in order to form the fluorescent conjugate acid, VI.

In summary and with reference to the plot shown in Fig. 4, at high pH values (i.e., pH $\geqslant$ 5) the formation of the fluorescent NDA–hydrazine, VI, is ultimately limited by the pK_a for 2,3-diazaanthracene (V). The observed rate constant increases until pH 2.5, at which point the rate decreases, presumably due to the increasing concentration of $N_2H_5^+$ in solution. Finally, as the acid concentration is increased to very high levels ($[H^+]$ greater than 1 M), the catalytic pathways become increasingly important, and the rate increases once again. Ultimately, though, the addition of too much acid may reduce the overall reaction rate, due to: (1) a reduction in the overall nucleophilicity of hydrazine with the formation of the doubly protonated, $N_2H_6^{2+}$; (2) a resultant suppression of the loss of protons from various intermediates within this scheme (e.g., steps I → II and II → III); or, (3) the formation of various, undesirable and non-fluorescent side products.

Analytical characteristics

In order to characterize the NDA reagent in the fluorescent detection of hydrazine, a series of analytical examinations were performed. For our purposes, it was imperative that the NDA reagent respond linearly to the addition of hydrazine from 0–1000 ppb and that we obtain a minimum detection limit of $\leqslant$ 10 ppb hydrazine in air. Because the fluorescence measurements are made in solution, as opposed to within the vapor phase, the necessary linear dynamic range is actually 0–435 μg/l of hydrazine, with a detection limit of $\leqslant$ 4.4 μg/l (see the Introduction). The fluorescence response seen following the sequential addition of hydrazine from 100 ng/l to 500 μg/l (or 230 ppt to 1000 ppb) was examined as a function of time, with a portion of these data shown in Fig. 5. Note that the response time necessary to give 90% of a full-scale response is $<$ 5 min. With each subsequent addition of hydrazine, the fluorescence at 500 nm increases proportionally. The inset figure is a plot of the fluorescence changes seen in this figure as a function of the concentration of hydrazine added. The NDA reagent gives excellent linear response to hydrazine at these low levels, as well as at significantly higher hydrazine concentrations. A linear dynamic range with respect to the detection of hydrazine has been demonstrated from 50 ng/l up to 500 μg/l. The sensitivity was calculated to be 14.9 (μg/l)/ΔF,

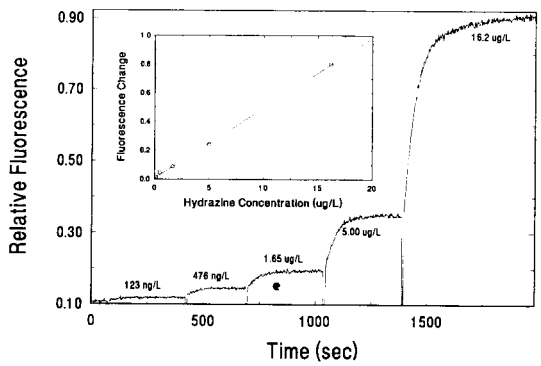

Fig. 5. Fluorescence response of the NDA reagent following repeated additions of hydrazine. The inset is a plot of these fluorescence changes as a function of concentration of hydrazine added.

with an intercept of 4.2 μg/l and a correlation coefficient, $r > 0.999$ (other regression data include: $n = 9$, $\sigma_m = 0.3$ (μg/l)/ΔF, $\sigma_b = 3.0$ μg/l, $\sigma = 8.0$).

Following an optimization of the experimental variables, the detection limit (assuming a signal-to-noise ratio of 3:1) was determined to be approximately 50 ng/l (or 115 ppt). The hydrazine detection limit using the NDA reagent is nearly two orders of magnitude better than the design goal of 10 ppb N_2H_4 in air, a characteristic which will enable the use of simpler, less expensive instrumentation for the monitoring application.

We examined several likely interferents, including NH_3, Freon 113, isopropyl alcohol, ethanol, and methyl ethyl ketone. Each of these different interferents was evaluated at a concentration of twice the threshold limit value. In all cases, there was no measurable or detectable fluorescent response at 500 nm. It is particularly noteworthy that NH_3 is not an interferent. Apparently, at the pH being used (pH 2–3), and without the presence of added nucleophiles such as the cyanide ion or thiol, ammonia does not form a fluorescent derivative with NDA. Because of the nature of the reaction between NDA and hydrazine, and the fact that we can monitor a particular fluorescent wavelength, this reaction appears to be highly selective towards hydrazine.

Application and conclusions

Our results indicate that the fluorescent tagging of hydrazine using NDA is a highly sensitive and selective method for the detection of hydrazine. In terms of the instrumentation required, fluorescence detection can be a relatively inexpensive technique, particularly when the chemistry for the derivatization reaction has been determined and the excitation and emission wavelengths have been established. Rather than employing a fluorescence spectrometer, a relatively inexpensive filter fluorometer can be used, consisting simply of a high intensity light source, the appropriate focussing optics, a set of two filters for isolating the excitation and emission wavelengths of 403 and 500 nm, a flow-through cell, and a detector. Due to the proximity of the excitation wavelength for the NDA/hydrazine derivative to one of the intense spectral lines arising from either a low pressure Hg lamp or a Xe/Hg arc lamp (at 404 nm), it may be possible to boost the sensitivity simply through the proper choice of a lamp.

We would like to thank Dr. Dave Kidwell for his thoughtful advice and for kindly allowing the use of his spectrofluorometer. Thanks also to Dr. Anne Kusterbeck for permitting the use of her spectrofluorometer. This research was supported by NASA/Kennedy Space Center (DL-ESS-24, CC-82360A).

REFERENCES

1 H.W. Schiessl, in K. Othmer (Ed.), Encyclopedia of Chemical Technology, Vol. 12, Wiley, New York, 3rd edn., 1980, p. 734.
2 E.W. Schmidt, Hydrazine and its Derivatives: Preparations, Properties, Applications, Wiley, New York, 1984.
3 Technical Bulletin, Hydrazine for Wet-Lay-up of Boilers, Olin Chemicals, Stamford, CO, 1979.
4 J.A.E. Hannum, Recent Developments in the Technology of Propellant Hydrazines, Chemical Propulsion Information Agency, CPTR 82-15, June 1982.
5 Committee on Toxicology, Emergency and Continuous Exposure Guidance Levels for Selected Airborne Contaminants (Vol. 5), Board on Toxicology and Environmental

Health Hazards, Commission on Life Sciences, National Research Council, National Academy Press, Washington, DC, 1985.
6 E.H. Vernot, J.D. MacEwen, R.H. Bruner, C.C. Haun, E.R. Kinkead, D.E. Prentice, A. Hall III, R.E. Schmidt, R.L. Eason, G.B. Hubbard and J.T. Young, Fundamental and Applied Toxicology, 5 (1985) 1050.
7 American Conference of Governmental Industrial Hygienists (ACGIH) report on proposed current changes to TLV and BEI lists, May 21, 1989.
8 J.R. Holtzclaw, S.L. Rose, J.R. Wyatt and C.M. Hawkins, U.S. Pat. 4,780,282 (1988).
9 S.L. Rose-Pehrsson, J.R. Wyatt, K.P. Crossman, P.T. Carver, S.W. Brown, A.R. Thurow and J.C. Travis, Am. Ind. Hyg. Assoc. J., (1992) in press.
10 P.A. Taffe and S.L. Rose-Pehrsson, U.S. Pat. 4,900,681 (1990).
11 S.L. Rose-Pehrsson and K.P. Crossman, Development of a Dosimeter System for UDMH, MMH, and Hydrazine, CPIA 588, Proceedings of the 1992 JANNAF Safety and Environmental Protection Subcommittee Meeting, Monterey, CA, 10–14 August, 1992, Naval Postgraduate School, August, 1992.
12 G.D. George and J.T. Stewart, Anal. Lett., 23 (1990) 1417.
13 W.D. Basson and J.F. Van Staden, Analyst, 103 (1978) 998.
14 J.R. Stetter, K.F. Blurton, A.M. Valentine and K.A. Tellefsen, J. Electrochem. Soc., 125 (1978) 1804.
15 E.C. Olson, Anal. Chem., 32 (1960) 1545.
16 B.E. Knox and E.J. McHale, Anal. Chem., 38 (1966) 487.
17 C.S. Leasure and G.A. Eiceman, Anal. Chem., 57 (1985) 1890.
18 J.H. Cross, T.F. Limero, S.W. Beck, J.T. James, N.B. Martin, H.T. Johnson, R.C. Young and C.B. Mattson, Monitoring Hydrazines in the Space Shuttle Airlock with a Proof-Of-Concept Ion Mobility Spectrometer, CPIA 588, Proceedings of the 1992 JANNAF Safety and Environmental Protection Subcommittee Meeting, Monterey, CA, 10–14 August, 1992, Naval Postgraduate School, August, 1992.
19 S. Vickers and E.K. Stuart, Anal. Chem., 46 (1974) 138.
20 N.D. Danielson and C.M. Conroy, Talanta, 29 (1982) 401.
21 R.W. Weeks, Jr., S.K. Yasuda and B.K. Dean, Anal. Chem., 48 (1976) 159.
22 M. Roth, Anal. Chem., 43 (1971) 880.
23 P. de Montigny, J.F. Stobaugh, R.S. Givens, R.G. Carlson, K. Srinivasachar, L.A. Sternson and T. Higuchi, Anal. Chem., 59 (1987) 1096.
24 S.M. Lunte and O.S. Wong, LC–GC, 7 (1989) 908.
25 NIOSH Pocket Guide to Chemical Hazards, U.S. Department of Health and Human Services, June, 1990.
26 B.M. Krasovitskii and B.M. Bolotin, in V.G. Vopian (Ed.), Organic Luminescent Materials, VCH, Weinheim, 1988, p. 8.
27 G.E. Collins and S.L. Rose-Pehrsson, Analyst (1993) submitted for publication.

Analytica Chimica Acta, 284 (1993) 217–225
Elsevier Science Publishers B.V., Amsterdam

Method development and optimization for the determination of rare earth metal ions by capillary zone electrophoresis

M. Jimidar, T. Hamoir, W. Degezelle and D.L. Massart

Farmaceutisch Instituut, Vrije Universiteit Brussel (VUB), Laarbeeklaan 103, B-1090 Brussels (Belgium)

S. Soykenç and P. Van de Winkel

Cyclotron, Vrije Universiteit Brussel (VUB), Laarbeeklaan 103, B-1090 Brussels (Belgium)

(Received 5th July 1993; revised manuscript received 10th September 1993)

Abstract

The separation of rare earth metal ions by capillary zone electrophoresis in the presence of creatinine as UV-absorbing background electrolyte and the complexing agent 2-hydroxyisobutyric acid was investigated. The separation is mainly influenced by the pH of the buffer and the concentration of the complexing agent. Both parameters were used in a central composite design to determine optimal conditions. After modelling of the migration behaviour, the optimal conditions were selected using a multi-criteria approach in which separation coefficient (α), sensitivity and analysis time were considered. Finally, the method was validated regarding its detection limit, linearity and reproducibility.

Keywords: Electrophoresis; Capillary zone electrophoresis; Central composite design; Indirect detection; Lanthanides; Rare earths

Capillary ion analysis (CIA), a capillary zone electrophoresis (CZE) technique, was recently proposed for the determination of inorganic ions [1] and appears to be very promising for the detection of low level concentrations [2]. This method is based on indirect photometric detection [1–4].

Owing to its extremely high separation efficiency, CIA has proven to be a powerful tool for the analysis of complex mixtures of ions. An interesting complex mixture is the group of rare earth (RE) metal ions, also called the lanthanides.

The lanthanides have already been determined by chromatographic [5] and spectroscopic [6] techniques and by activation analysis [7]. Recently, CZE was introduced for the separation of the RE [8]. The separation was enhanced by α-hydroxyisobutyric acid (HIBA) as a chelating agent to increase the difference in electrophoretic mobility between the rare earths.

For the prediction of the migration of ions in CIA, knowledge about the variables influencing the selectivity is required. The aim of this study is to develop a method for the determination of RE metal ions, especially terbium (Tb) and gadolinium (Gd). The developed method will be used for

Correspondence to: D.L. Massart, Farmaceutisch Instituut, Vrije Universiteit Brussel (VUB), Laarbeeklaan 103, B-1090 Brussels (Belgium).

0003-2670/93/$06.00 © 1993 – Elsevier Science Publishers B.V. All rights reserved

quality control of RE bulk solutions (mainly Gd and Tb) in a feasibility study for the application of rare earth labelled radiopharmaca for tumour diagnostics and treatment. A group of four RE ions was chosen for this study, namely Gd, Tb, lanthanum (La) and cerium (Ce) as possible internal standards. The influence of several variables will be investigated to select the most important ones for further optimization.

For the optimization experimental statistical design is used. The selection of the optimum conditions will be done by using a multi-criteria approach after applying a central composite design [9].

EXPERIMENTAL

Chemicals

All solutions were prepared using Milli-Q water (Millipore, Bedford, MA). Sodium and potassium hydroxide, sodium dihydrogenphosphate, phosphoric acid, acetic acid, nitric acid (ultra pure), lanthanum nitrate, cerium nitrate, creatinine, citric acid and hydrochloric acid were purchased from Merck (Darmstadt). The α-hydroxyisobutyric acid (HIBA), terbium oxide, gadolinium oxide and also creatinine were obtained from Aldrich (Steinheim).

Preparation of solutions

All buffers were prepared in 100-ml aliquots and filtered through a 0.2-μm membrane filter (Schleicher and Schüll, Dassel). The buffers were adjusted to the final pH using acetic acid (10%, v/v) or 0.001 M sodium hydroxide or 0.01 M hydrochloric acid.

Stock solutions of 1000 mg l^{-1} of lanthanum and cerium, were prepared in Milli-Q water using the nitrate salt of these ions. Terbium oxide and gadolinium oxide were first dissolved in an excess of ultra pure nitric acid and evaporated to dryness. The residue was redissolved in Milli-Q water to obtain a 1000 mg l^{-1} stock solution. Standard solutions of the rare earths were prepared daily.

The buffers were adjusted to the pH required using a WTW (pH 537) Microprocessor pH Meter.

Instrumentation

The analysis was carried out on a Waters Quanta-4000 capillary electrophoresis system equipped with a positive power supply. The capillaries were ordinary fused-silica capillaries (Waters AccuSep®, 60 cm capillaries) of 75 μm i.d. $\times$ 52 cm (length measured from the point of sample introduction to the point of detection). The electrophoresis zones were detected with a fixed-wavelength UV detector at 214 nm. Both injection systems, hydrostatic and electromigration, available on the Quanta system were used. The electropherograms were recorded and integrated with a Waters 810 data workstation equipped with a 'W51-watchdog' interface. This interface converts the digital signal from the detector into a format readable for the data workstation.

Software

For the calculation of the responses for relative migration, peak heights and analysis time, a spreadsheet developed in Microsoft Excel (version 3.0) was used.

The coefficients for the models and the regression statistics for the calibration curves were calculated using the SPSS-PC + Statistics™ version 4.0 software package.

Preparation of the capillary

Each day before starting analysis, the capillary was purged with potassium hydroxide (KOH) 0.1 M and Milli-Q water each for 5 min, followed by the running buffer also for 5 min. Between each run the capillary was flushed with 0.1 M KOH for 1 min, Milli-Q water and the running buffer each for 2 min. Before shut-down the capillary was flushed with Milli-Q water and purged 2 min with air.

RESULTS AND DISCUSSION

Detection optimization

When applying indirect photometric detection one should work at as high a background electrolyte concentration as possible, to obtain the highest separation efficiency [10]. However, the

detection limit can then increase because of more noise. According to Foret et al. [11] a background electrolyte with low concentration and high molar absorptivity results in lower detection limits. Wang and Hartwick [12] demonstrated that in some cases lower background concentration and in other cases higher molar absorptivities can result in lower detection limits. This depends on the noise produced by the concentration fluctuation of the background electrolyte during a run and the noise produced by the detector. If the noise of the background electrolyte is higher than the noise of the detector, then the detection limit is not improved with higher molar absorptivities, but lowering the background electrolyte concentration will result in better detection limits. The opposite occurs when the noise of the detector is higher than the noise of the background electrolyte. The concentration of the background electrolyte is limited by the linear dynamic range of the detector. As proposed by Foret et al. [8] creatinine was selected as background electrolyte with the following initial conditions for the buffer: pH 4 and 4 mM HIBA. Creatinine was added in increasing concentration and the absorbance was measured. A concentration of 10 mM creatinine was selected for further experimentation.

Separation parameters

Because the selection of an optimization procedure depends on a number of important parameters, their influence was investigated. The considered parameters were: buffer type, pH, concentration of HIBA, effect of glycerol and effect of methanol. A mixture of the four rare earths, each in a concentration of 10 mg l^{-1}, was injected hydrostatically for 10 s during these experiments.

Buffer electrolyte

Phosphate and citrate buffer electrolytes both lead to an unstable baseline. It was also checked whether the pH of the creatinine–acetate buffer could be adjusted with hydrochloric acid or sodium hydroxide instead of acetic acid. However the noise-level of the baseline increased considerably, probably due to the increased current. Hence, it was concluded that a weak acid such as acetic acid must be employed to obtain a good baseline. The creatinine–acetate buffer is used in further experiments. This limits the pH to values below 5.

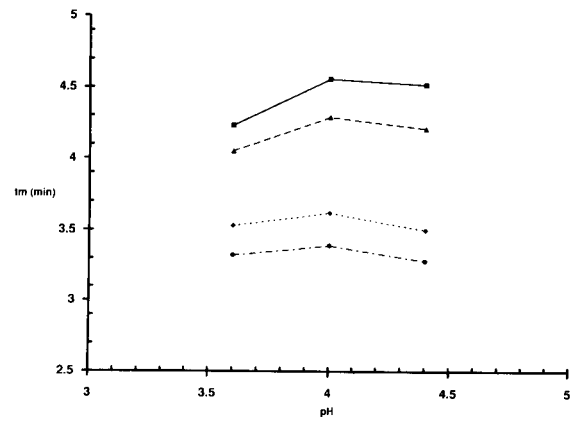

Fig. 1. The effect of pH on the migration of the rare earths. A 10 mg l^{-1} mixture of the rare earths was injected hydrostatically for 10 s. The buffer consisted of 10 mM creatinine, 5 mM HIBA. The running voltage was 30 kV. Key: ● = lanthanum; ◆ = cerium; ▲ = gadolinium; ■ = terbium.

The pH can have an important effect on the separation, owing to the effect on acid–base equilibria. In this application, this concerns the dissociation of HIBA and the ionization of the background electrolyte. At increasing pH the peaks of Gd and Tb tail, owing probably to the interaction with the increasing negative charge of the wall or to the decreased dissociation of creatinine, leading to larger differences in mobilities between analytes and background electrolyte [1]. The effect of the pH was examined at pH 3.6, 4.0 and 4.4 with a concentration of HIBA of 5 mM. The results are presented in Fig. 1. As can be observed, the migration of the components decreases from pH 3.6 to 4.0 and increases when the pH is further increased. The explanation of this effect probably is that when the pH increases, the dissociation of HIBA ($pK_a = 3.97$) increases, leading to the enhancement of complex formation. The charge of these complexes depends on the amount of chelating agent (L^-) [7]:

$$M^{3+} + L^- \Leftrightarrow ML^{2+} \quad (1)$$

$$ML^{2+} + L^- \Leftrightarrow ML_2^+ \quad (2)$$

$$ML_2^+ + L^- \Leftrightarrow ML_3 \quad (3)$$

$$ML_3 + L^- \Leftrightarrow ML_4^- \quad (4)$$

where M represents a RE ion. The positive charge of the complexes decreases or can even become negative with increasing amounts of L^-, due to the dissociation of HIBA at higher pH, leading to lower migration mobilities. This results in an increase of migration time (t_m) for the RE ions. The endosmotic flow (EOF) also increases with increasing pH, due to the increased dissociation of the silanol groups of the capillary wall. At a certain point the effect on the EOF is more important than the effect of the complex formation, leading to decreasing migration times (see Fig. 1).

HIBA effect

The effect of HIBA was examined with a creatinine–acetate buffer at pH 4.0. The employed concentrations of HIBA were: 1.00, 5.00 and 9.00 mM. The results of these experiments are presented in Fig. 2. HIBA has an important effect on the separation of the rare earths as was expected. At low concentration Gd and Tb comigrate, while at higher concentration of HIBA the separation improves to the expense of higher migration times. At the employed pH of 4.0 the dissociation of HIBA is ±50%. Increasing the concentration of HIBA means increasing the amount of ligand resulting in an increase of complex formation. In the experimental domain the highest level of HIBA results in highest complex formation. The separation of the RE improves with increasing concentrations of HIBA due to the formation of complexes.

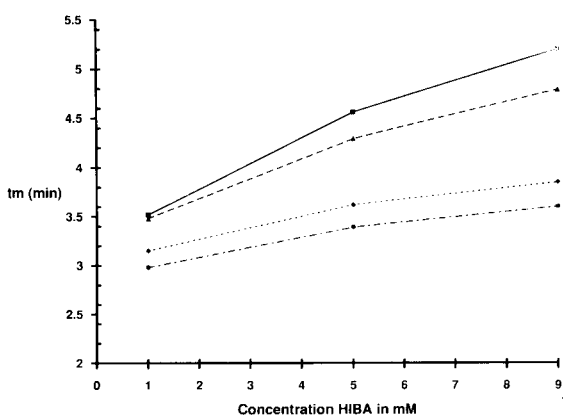

Fig. 2. The effect of the concentration of HIBA on the migration of the rare earths. The buffer consisted of 10 mM creatinine, pH 4.0 and different concentrations of HIBA. For other experimental conditions see Fig. 1. Key to symbols as in Fig. 1.

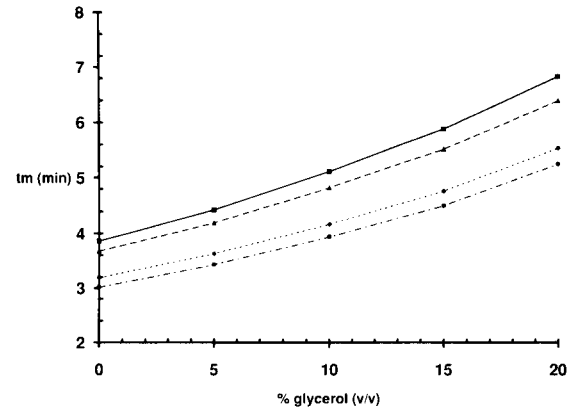

Fig. 3. The effect of the concentration of glycerol on the migration of the rare earths. The buffer consisted of 10 mM creatinine, pH 4.0 and 4.0 mM HIBA and different concentrations of glycerol. For other experimental conditions see Fig. 1. Key to symbols as in Fig. 1.

Effect of glycerol

Organic solvents and polyols have successfully been used in adjusting selectivity in CZE [13–14]. We selected methanol and glycerol, as representative examples. Increasing concentrations of glycerol were added to a creatinine (10 mM)–acetate buffer, pH 4 and 4 mM HIBA (Fig. 3). As expected, an increase in migration time accompanied by an increase in peak tailing occurs for all the four components, because of the increased viscosity. The tailing of the peaks was most noticeable for the late migrating peaks. Nevertheless, the separation of the rare earths improved a little with increasing amounts of glycerol.

Effect of methanol

For the investigation of the effect of methanol on the separation of the rare earths the same buffer was employed as for glycerol. Increasing concentrations of methanol were added to the buffer. As shown in Fig. 4, the migration time of

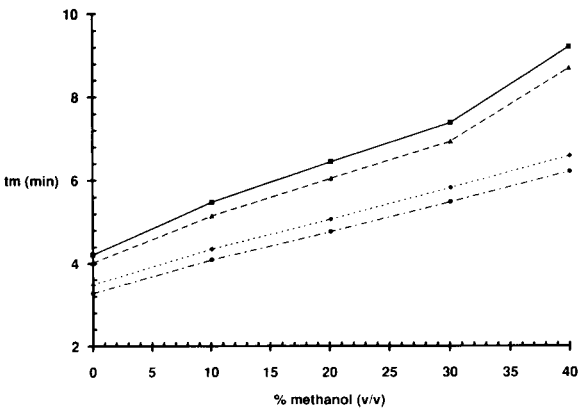

Fig. 4. The effect of the concentration of methanol on the migration of the rare earths. The buffer consisted of 10 mM creatinine, pH 4.0 and 4.0 mM HIBA and different concentrations of methanol. For other experimental conditions see Fig. 1. Key to symbols as in Fig. 1.

the components increased with higher concentrations of methanol. The separation of the components improved a little, but the peak tailing increased with higher methanol concentrations. In addition the resolution between the pair La/Ce and the pair Gd/Tb increased with higher concentrations of methanol.

Selection of optimum conditions

Two parameters have an important effect on the separation of the four rare earths, namely the concentration of HIBA and the pH. Glycerol and methanol increased the analysis time and also the tailing of the peaks, but have a much smaller effect on separation quality and are therefore not considered further. Hence, the concentration of HIBA and the pH were selected as the variables to obtain the optimum separation conditions for the four rare earths.

For an optimization with two parameters one has the choice between different statistical experimental designs. The factorial design, the Doehlert design and the central composite design are possible alternatives. The factorial design, which only needs four experiments, is more appropriate for deciding which effects are important, but is limited to linear response surfaces. The Doehlert and the central composite designs need more experiments but they are to be preferred for modelling as they can allow the use of quadratic response surfaces. Although the Doehlert design is less time-consuming (for two parameters one has to carry out 7 experiments with the Doehlert design and 9 with the central composite design), the central composite design was selected, because of the short analysis times in CIA.

From the preliminary experiments, the following upper and lower limits were selected: the parameter pH ranged from 3.58 (lowest level) to 4.42 (highest level), and HIBA concentration from 0.74 mM (lowest level) to 9.24 mm (highest level). The experimental conditions for the central composite design are presented in Table 1. A 10 mg l^{-1} mixture of the four rare earths was injected for 10 s with electromigration as injection system at 30 kV. All the runs were performed with a running voltage of 30 kV. The experiments of the design were carried out in a random order (using randomized tables [15]) and in duplicate.

For the selection of optimal conditions one should not only consider the separation, but also take into account the analysis time and the sensitivity. For this purpose different optimization criteria were considered. These were the extent of separation (expressed by the separation coefficient α), the sensitivity (expressed in peak height) and the migration time of the last peak. The model was a second order polynomial:

$$Y = b_0 + b_1X_1 + b_2X_2 + b_{11}X_1^2 + b_{22}X_2^2 + b_{12}X_1X_2 \quad (5)$$

TABLE 1

The central composite experimental design

Run	X_1	pH	X_2	[HIBA]
1	−1	3.70	−1	2.000
2	+1	4.30	−1	2.000
3	−1	3.70	+1	8.000
4	+1	4.30	+1	8.000
5	−1.673	3.58	0	5.000
6	+1.673	4.42	0	5.000
7	0	4.00	−1.673	0.737
8	0	4.00	+1.673	9.243
9	0	4.00	0	5.000

where X_1 = pH and X_2 = [HIBA]. The regression coefficients (Table 2) were calculated using multiple regression analysis.

When applying modelling techniques in separation science, one should normally model migration time and from the model predict the separation coefficient. Indeed, the quadratic model cannot accurately describe the separation coefficient (or the resolution), when cross-overs (changes in elution order) occur. However, for the RE the elution order does not change, so that there are no cross-overs. In such cases one can model directly the separation coefficient. The three separation coefficients ($\alpha_1 = t_m\text{Ce}/t_m\text{La}$, $\alpha_2 = t_m\text{Gd}/t_m\text{Ce}$ and $\alpha_3 = t_m\text{Tb}/t_m\text{Gd}$) were calculated and modelled.

As can be seen in Table 3, the relative difference expressed in percent deviation of the predicted and experimentally found values at each run is generally situated under 1%. Therefore the models for the separation coefficients are considered to be good and can be used for further selection of optimal conditions. The minimum separation coefficients ($\alpha_{\text{min.}}$) were selected and are presented in Fig. 5a in function of pH and [HIBA]. As can be seen $\alpha_{\text{min.}}$ increases with increasing HIBA concentration and decreasing pH values. The region with the following limits pH < 4.2 and [HIBA] > 1.75 mM shows α_{min}-values higher than 1.03, which allows an acceptable separation.

The same modelling procedure was performed for the peak heights of the four rare earths and for the migration time of the last peak (Tb). The coefficients of all the models are shown in Table 2. The predicted peak heights presented in Table 2, are found to be in agreement with the experimental results. The response surfaces for the peak heights of La and Tb are shown in Fig. 5b and c, Ce and Gd have more or less the same profile as La and Tb, respectively. For La (limit for peak height: > 0.006 V) and for Ce (limit > 0.007 V) the region pH > 3.6 and < 4.4; [HIBA] > 1 mM was selected as optimal region, while for Gd (limit > 0.006) and Tb (limit > 0.005) the region with pH > 3.6 and < 4.2; [HIBA] < 4 mM was selected.

For the last criterion, the analysis time, the limit was set at maximum 4 min. Figure 5d presents the migration time of the last peak (Tb). As can be seen, the analysis time is lower than 4 min. in the region with pH < 4.3 and [HIBA] < 4 mM. From Table 4 it can be observed that the model for the migration time of Tb is not very good. However, it is good enough for our purpose.

TABLE 2

Calculated coefficients for the models of the responses [a]

Response	b_0	b_1	b_{11}	b_2	b_{22}	b_{12}
α_1	0.625	0.200	−0.024	0.017	−0.0003	−0.003
α_2	−0.352	0.635	−0.069	0.065	−0.0002	−0.011
α_3	−0.045	0.469	−0.052	0.046	−0.0008	−0.008
H La	−10.390	5.609	−0.717	−0.024	−0.0030	0.017
H Ce	−13.681	7.282	−0.939	0.039	−0.0122	0.026
H Gd	−7.065	4.363	−0.590	−0.250	0.0045	0.036
H Tb	−2.612	2.017	−0.301	−0.222	0.0014	0.043
t_m for Tb	−20.819	11.376	−1.355	0.852	−0.010	−0.142

[a] $\alpha_1 = t_m\text{Ce}/t_m\text{La}$; $\alpha_2 = t_m\text{Gd}/t_m\text{Ce}$; $\alpha_3 = t_m\text{Tb}/t_m\text{Gd}$. *H* = Peak height.

TABLE 3

Experimentally found and predicted values of the separation coefficient (α) and migration time of the last peak (Tb) [a]

Run	α_1	Pred. [b]	α_3	Pred.
1	1.055	1.058	1.069	1.075
2	1.048	1.051	1.035	1.039
3	1.045	1.047	1.013	1.015
4	1.058	1.060	1.044	1.046
5	1.051	1.049	1.018	1.015
6	1.062	1.061	1.062	1.063
7	1.060	1.055	1.071	1.061
8	1.068	1.064	1.091	1.084
9	1.065	1.066	1.076	1.077

Run	α_2	Pred.	t_mTb	Pred.
1	1.225	1.241	3.629	4.179
2	1.133	1.141	3.312	3.529
3	1.094	1.102	3.174	3.232
4	1.157	1.166	3.917	4.031
5	1.120	1.104	3.505	3.309
6	1.183	1.190	4.198	4.205
7	1.220	1.190	4.274	3.799
8	1.297	1.272	5.110	4.697
9	1.235	1.243	4.593	4.730

[a] $\alpha_1 = t_m\text{Ce}/t_m\text{La}$; $\alpha_2 = t_m\text{Gd}/t_m\text{Ce}$; $\alpha_3 = t_m\text{Tb}/t_m\text{Gd}$.
[b] Predicted by the model.

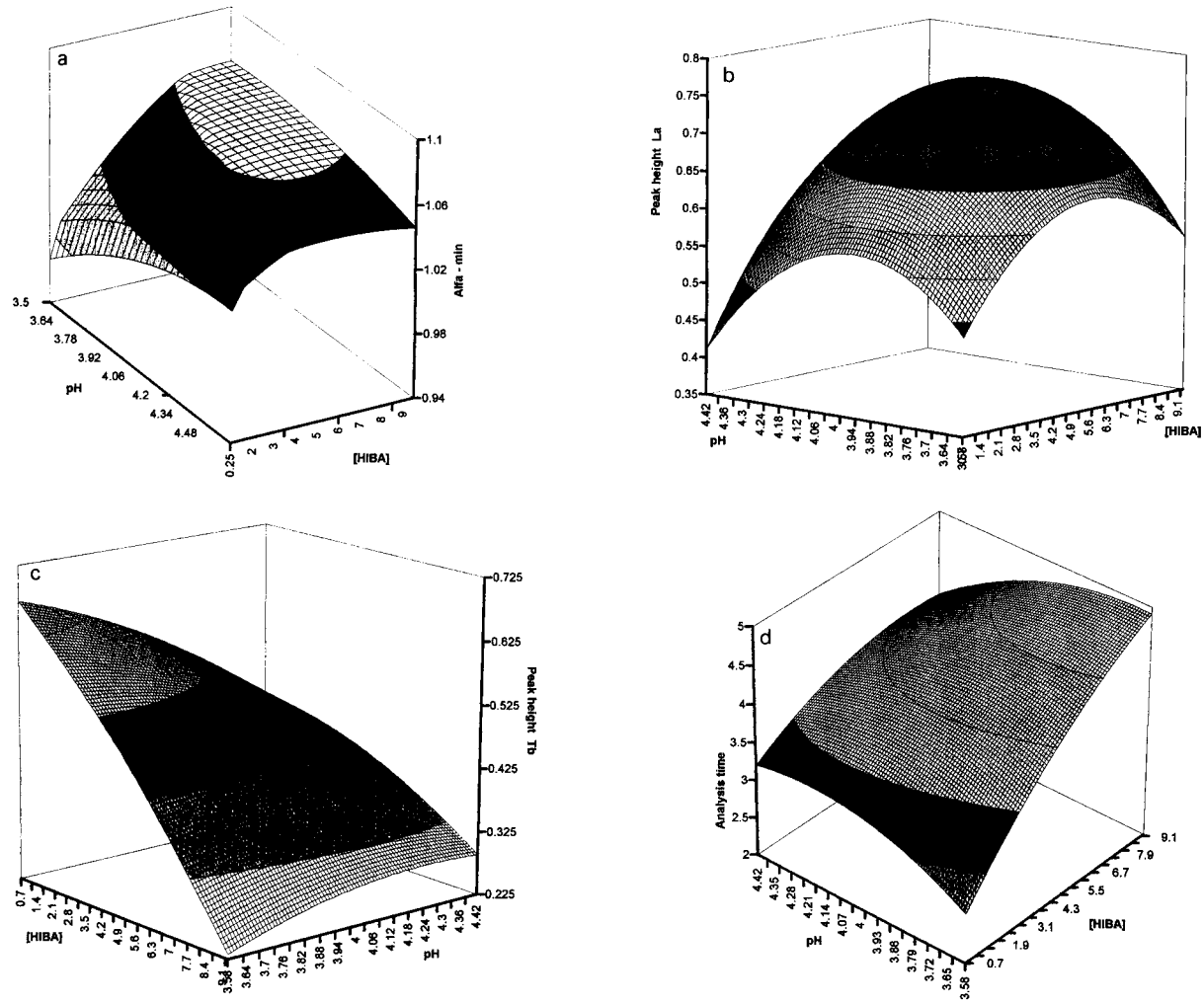

Fig. 5. Response surfaces in function of pH and concentration of HIBA. (a) Minimum separation coefficient (α_{min}), (b) Peak height of La; (c) peak height of Tb and (d) analysis time.

TABLE 4

Experimentally found and predicted peak heights (H) in 10^{-2} V of the 4 rare earth metal ions

Run	La		Ce		Gd		Tb	
	Hexp.	Hpred.	Hexp.	Hpred.	Hexp.	Hpred.	Hexp.	Hpred
1	0.697	0.702	0.763	0.750	0.365	0.363	0.346	0.337
2	0.551	0.565	0.539	0.544	0.634	0.567	0.504	0.472
3	0.580	0.573	0.512	0.511	0.593	0.668	0.548	0.580
4	0.622	0.628	0.720	0.729	0.534	0.558	0.473	0.480
5	0.599	0.601	0.632	0.633	0.754	0.696	0.623	0.603
6	0.747	0.747	0.853	0.853	0.558	0.557	0.462	0.458
7	0.640	0.628	0.698	0.702	0.436	0.473	0.372	0.395
8	0.708	0.714	0.678	0.702	0.298	0.286	0.289	0.289
9	0.674	0.666	0.718	0.701	0.347	0.354	0.325	0.327

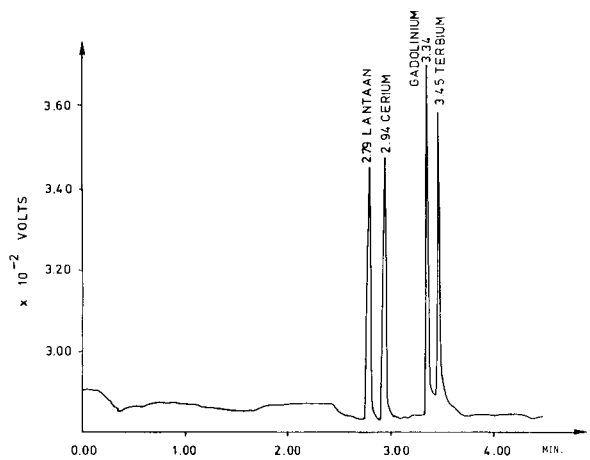

Fig. 6. Electropherogram of the RE at the predicted optimal conditions: creatinine 10 mM–acetate buffer with pH 4.10 and [HIBA] = 2 mM. A 10 mg l^{-1} mixture of the rare earths was injected 20 s by electromigration at 30 kV, the running voltage was 30 kV (± 20 μA). Peaks: 1 = La, 2 = Ce, 3 = Gd, 4 = Tb.

The optimal separation conditions for the four rare earths was derived by overlaying all the calculated response surfaces of the different criteria. Taking all the optimal regions of the criteria into account, the optimum is situated around pH 4.10 and [HIBA] = 2 mM. An electropherogram obtained at these conditions is shown in Fig. 6. As can be seen, a good separation is obtained within 3.5 min. The sensitivity of Gd and Tb also improved compared with the conditions based on the work of Foret et al. [8]. The peaks of Gd and Tb were much smaller than those of La and Ce before optimization. After optimization all the peaks are of about equal peak height (Fig. 6). The current at 30 kV (optimal conditions) was ± 20 μA. By working in a thermostatic environment (20 ± 0.5°C) and with the low current, temperature effects can be neglected.

Validation

Detection limit. The detection limit can be estimated as being a signal 3 times higher than the baseline noise. It is usual in CZE to use the factor 2, but we prefer to conform to IUPAC rules and apply the factor 3. Because of the possibility of increasing the amount injected by electromigration as injection system, either by increasing the injection time or increasing the injection voltage, one can detect very low concentrations. In this case, an injection time of 20 s and an injection voltage of 30 kV resulted in a detection limit of about 40 μg l^{-1}. When the injection time was further increased, an overloading effect was observed.

Linearity. The linear range of the method was investigated with and without internal standard. Without internal standard the response was not linear. This effect was corrected by the use of an internal standard. When using Ce in a 5 mg l^{-1} concentration as internal standard, the method was found to be linear or nearly linear for La, Gd, and Tb up to 5 mg l^{-1}. There may be a slight downwards curvature for Gd and Tb, but this is too small to be of practical importance. The

TABLE 5

Regression statistics for the calibration curves of La, Gd and Tb [a]

Parameter	Calibration La	Calibration Gd	Calibration Tb
Slope	0.20258	0.186675	0.17865
C.I. slope	0.19852–0.20664	0.17998–0.19337	0.17096–0.18634
S.E. slope	0.001463	0.002410	0.00277
Intercept	0.01805	0.019923	0.023036
C.I. intercept	0.00573–0.03038	−0.000383–0.04023	−0.000302–0.04638
S.E. intercept	0.004439	0.007314	0.008406
Standard error	0.0057	0.009399	0.01080
r	0.9999	0.99967	0.99952
Number of points	6	6	6

[a] C.I. = Confidence interval; S.E. = standard error; r = correlation coefficient.

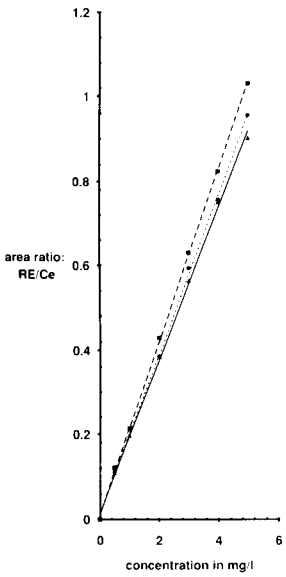

Fig. 7. Calibration curves for La, Gd and Tb, Ce is used as internal standard. The experimental conditions were the predicted optimal conditions. Key: ■ = La/Ce, ——— = La/Ce pred.; ● = Gd/Ce, - - - - - - = Gd/Ce pred.; ▲ = Tb/Ce, ——— = Tb/Ce pred.

regression statistics are presented in Table 5 and the calibration curves are shown in Fig. 7.

Repeatability. Because electromigrative injection resulted in better detection limits, and low detection limits are required in the practical application of this method, this injection system was used during the optimization with the design. Therefore, only electromigration was considered during the validation. The within day precision (repeatability) was examined at three concentration levels, namely 5, 1 and 0.1 mg l^{-1}. The relative standard deviations (R.S.D.s) of the method, with and without the internal standard are presented in Table 6. As can be seen the use of an internal standard greatly improves the repeatability, resulting in acceptable R.S.D.s. In accordance to what was expected the R.S.D. values increased with decreasing concentration levels.

TABLE 6

Repeatability of the method determined with and without an internal standard at 3 concentration levels

	R.S.D. (%)					
	Without internal standard ($n = 6$)			With an internal standard ($n = 6$)		
	RE					
	5.0 mg l^{-1}	1.0 mg l^{-1}	0.1 mg l^{-1}	5.0 mg l^{-1}	1.0 mg l^{-1}	0.1 mg l^{-1}
La	33.0	12.0	1.6	2.2	4.3	5.5
Gd	34.7	8.9	9.1	0.8	3.1	3.5
Tb	35.0	9.9	8.8	1.2	2.2	4.4

The authors would like to thank P. Fernandes de Aguiar and B. Bourguignon for their assistance with the software, and Prof. M. Khots for his encouragements.

REFERENCES

1 P. Jandik, W.R. Jones, A. Weston and P.R. Brown, LC-GC, 5 (1992) 20.
2 G. Bondoux, P. Jandik and W.R. Jones, J. Chromatogr., 602 (1992) 79.
3 W.R. Jones and P. Jandik, J. Chromatogr., 546 (1991) 445.
4 M. Jimidar, M.S. Khots, T.P. Hamoir and D.L. Massart, Quim. Anal., 12 (1993) 63.
5 A. Hrdlicka, J. Havel and M. Valiente, J. High. Resolut. Chromatogr., 15 (1992) 423.
6 M.I. Rucandio, Anal. Chim. Acta, 264 (1992) 333.
7 D.L. Massart and J. Hoste, Anal. Chim. Acta, 28, (1963) 378.
8 F. Foret, S. Fanali, A. Nardi and P. Bocek, Electrophoresis, 11 (1990) 780.
9 D.L. Massart, B.G.M. Vandenginste, S.N. Deming, Y. Michotte and L. Kaufman, Chemometrics: a Textbook, Data Handling in Science and Technology, Vol. 2, Elsevier, Amsterdam, 1st edn., 1988, pp. 283–287.
10 G.J.M. Bruin, A.C. van Asten, X. Xu and H. Poppe, J. Chromatogr., 608 (1992) 97.
11 F. Foret, S. Fanali, L. Ossicini and P. Bocek, J. Chromatogr., 470 (1989) 299.
12 T. Wang and R.A. Hartwick, J. Chromatogr., 607 (1992) 119.
13 M. Jimidar, T.P. Hamoir, A. Foriers and D.L. Massart, J. Chromatogr., 636 (1993) 179.
14 S.F.Y. Li, Capillary Electrophoresis; Principles and Applications, Journal of Chromatography Library, Vol. 52, Elsevier, Amsterdam, 1st edn., 1992, pp. 219–223.
15 W.H. Beyer, Handbook of Tables for Probability and Statistics, CRC Press, Boca Raton, FL, 2nd edn., 1968, pp. 479–483.

Analytica Chimica Acta, 284 (1993) 227–234
Elsevier Science Publishers B.V., Amsterdam

High sensitive microcapsule immunoassay for protein antigens or antibodies

Yoshio Ishimori

Research Laboratory II, Materials and Devices Research Laboratories, Toshiba Research and Development Center, Komukai Toshiba-cho, Saiwai-ku, Kawasaki 210 (Japan)

Kyuji Rokugawa

Medical Systems Division, Medical Engineering Laboratory, Toshiba Corporation, Nasu Works, 1385 Shimoishigami, Otawara-shi, Tochigi-ken 329-26 (Japan)

(Received 17th May 1993; revised manuscript received 26th July 1993)

Abstract

Microcapsule immunoassay (MCIA), a novel homogeneous immunoassay system, involving protein-bearing liposome-encapsulated carboxyfluorescein as a release marker is reported. This system was applied for the determination of protein antigens such as ferritin, etc., in human serum samples by use of a sandwich assay technique. Liposomal lysis was observed in many samples, even though no second antibody was added to the reaction mixture. It was demonstrated that this phenomenon was related to the functional groups used to immobilize an antibody on liposomes. Stable liposomes in human sera could be prepared by incorporating bromoacetyl (BrAc) groups instead of the dithiopyridyl groups as used previously. A good correlation ($\gamma = 0.98$, range = $10 - 2000$ $\mu g\ l^{-1}$) with data by radio immunoassay (RIA) was obtained in the ferritin measurement of 53 patients' sera by using these liposomes. To increase the sensitivity for the measurement of other tumor markers such as α-fetoprotein and carcinoembryonic antigen (CEA), the augmentation in the amounts of an antibody immobilized on the liposomal surface in MCIA was investigated. Based on the assumption that steric hindrance from liposomes would limit the immobilization of an antibody, the length of spacer between the antibody and the liposomal surface was optimized. The liposomes containing a BrAc-spacer-lipid ($n = 5$) showed a 50% increase in the antibody (Fab') immobilized, as compared with those without spacer molecules. CEA in the concentration of 0.1 $\mu g\ l^{-1}$ in human sera could be detected, although correlation to RIA dropped to $\gamma = 0.86$ in 60 samples because of the increase in the nonspecific liposomal lysis based on human sera. The analyses of lipid monolayers using the Langmuir-Blodgett technique imply that the fluidity of lipid membranes may be related to instability of liposomes to human sera.

Keywords: Immunoassay; Liposomes; Microcapsule; Carcinoembryonic antigen

Rapid and easy operations are attractive in the field of clinical immunoassay especially for hormones and tumor markers such as carcinoembryonic antigen (CEA), where automated instrumentation is indispensable.

Synthetic lipid bilayer vesicles (liposomes) have been widely used for model biomembranes, drug carriers, and other purposes. They are also applicable as homogeneous analytical tools of immunological reactions. Kinsky [1] devised an elegant method based on the complement-depen-

Correspondence to: Y. Ishimori, Research Laboratory II, Materials and Devices Research Laboratories, Toshiba Research and Development Center, Komukai Toshiba-cho, Saiwai-ku, Kawasaki 210 (Japan).

0003-2670/93/$06.00 © 1993 – Elsevier Science Publishers B.V. All rights reserved

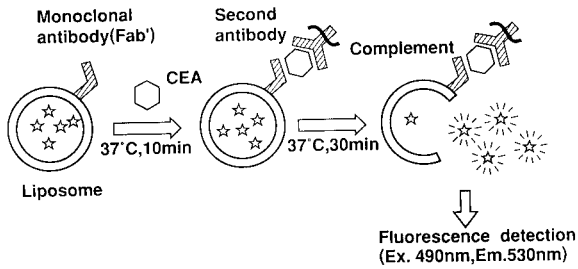

Fig. 1. Principle of microcapsule immunoassay (MCIA). The liposomes immobilized monoclonal anti-CEA antibody and encapsulated carboxyfluorescein (CF) were incubated in the sample solution containing adequate amounts of CEA for 10 min at 37°C. After the addition of a second antibody and complement, the reaction mixture was reincubated for 30 min at 37°C. The sandwich structure of antibody, CEA, and complement was formed on the liposomal surface. The fluorescence from the liposomes lysed by the action of activated complement was detected with a fluorescence spectrophotometer (excitation: 490 nm, emission: 530 nm), since CF entrapped in liposomes was not fluorescent because of the self-quenching phenomenon. The other detailed experimental conditions are shown in the procedure section.

dent liposome immune lysis to study the interaction of antibodies with various lipid antigens (complement stands for a heat-sensitive complementary compound in blood serum). Similar methods were developed by other investigators [2–5].

We previously reported a novel homogeneous immunoassay system in which protein-bearing liposome-encapsulated carboxyfluorescein (CF) was used as a release marker [6]. Proteins were immobilized on liposomes through cross-linking functional groups (dithiopyridyl) (DTP) bound to phosphatidylethanolamine. This assay system, called microcapsule immunoassay (MCIA), was rapid, simple, reproducible, and highly sensitive for the detection of protein antigens or antibodies. The principle of MCIA is outlined in Fig. 1. However, we also observed liposomal lysis independent of the antigen concentration in the measurements of many human sera. This phenomenon is denoted as "nonspecific liposomal lysis". We investigated the causes of the nonspecific liposomal lysis and a preparation of stable liposomes in human sera [7]. We implied that a functional group (DTP group) used for the immobilization of an antibody on liposomes was responsible for this phenomenon. The use of liposomes with bromoacetyl (BrAc) groups allowed the measurement of ferritin in the range of 10 – 2000 $\mu g\ l^{-1}$ in human sera with a good correlation to radio immunoassay (RIA) ($\gamma = 0.98$). But, the BrAc liposomes were not available for the measurements of CEA because the concentration of normal human sera is about a couple of $\mu g\ l^{-1}$ and a detection limit of 0.1 $\mu g\ l^{-1}$ is required for precise measurements.

Steric hindrance from a solid support plays an important role in determining the quantity and the remaining activity of immobilized species [8,9]. The increase in the amounts of the immobilized antibody may lead to the improvement of sensitivity in MCIA. Our study revealed that an optimal spacer was inserted between an antibody and the liposomal surface and thus the sensitivity of MCIA was improved.

EXPERIMENTAL

Reagents

Buffers. The borate-buffered saline solution (BBS) was prepared as follows: 6.18 g of H_3BO_3 and 8.00 g of NaCl were dissolved in ca. 800 ml of H_2O. After the pH of the solution was adjusted to 9.00 with 1 M NaOH, water was added up to 1000 ml.

A gelatin barbital-buffered saline (GBS^-) was prepared according to the method reported by Yasuda et al. [10]. GBS^- was supplemented with 35 mM $MgCl_2$ and 0.15 mM $CaCl_2$ for assay procedures (GBS^{2+}). GBS^- and GBS^{2+} were kept at 4°C until use.

Lipids. Dipalmitoylphosphatidylcholine (DPPC), cholesterol and dipalmitoylphosphatidylethanolamine (DPPE) were purchased from Sigma (St. Louis, MO). Dithiopyridyl (DTP)-DPPE was prepared by the method of Leserman et al. [11], with minor modifications. BrAc-DPPE was synthesized according to the method reported previously [7].

Syntheses

Spacer-inserted DPPE. As a typical example, a procedure of aminohexyl (NH_2–C_6)-DPPE is

shown here. The same procedure was essentially applicable for the syntheses of other spacer-inserted DPPEs. The reagents for syntheses were commercially available grade and were used without any purifications.

1.31 g (10.0 mmol) of 6-aminocaproic acid (Aldrich, Milwaukee, WI) was dissolved in 3 ml (ca. 20 mmol) of triethylamine (TEA; Wako, Osaka) and water (10 ml) was added to the solution. 2.7 g (11 mmol) of 2-*tert*-butoxycarbonyloxyimino-2-phenylacetonitrile (Boc-ON) (Peptide Institute, Osaka) were dissolved in 10 ml of dioxane. These solutions were mixed and stirred at room temperature for 3 h. After the reaction, the solvent was removed by rotary evaporation. A pale yellow crystal (Boc-6-aminocaproic acid) resulted from the sequential extraction using ethyl acetate, 5% $NaHCO_3$ aq. and a 5% citric acid solution (yield; ca. 70%). 0.262 g (1.00 mmol) of Boc-6-aminocaproic acid prepared above was dissolved in 20 ml of chroloform, and then 0.13 g (1.10 mmol) of *N*-hydroxysuccinimide (HSI) and 0.25 g (1.20 mmol) of *N*-dicyclohexylcarbodiimide (DCCD) (Peptide Institute) were added to the solution. The reaction mixture was stirred at room temperature for 3 h. After evaporation, the product was dissolved again in 30 ml of ethyl acetate and the precipitate generated was removed by filtration. The filtrate was evaporated to dryness and dissolved in 5 ml of chloroform again. The concentration of the solution prepared (Boc-6-aminocaproic acid succinimide ester) was conveniently assumed to be about 0.2 M.

70 mg (0.101 mmol) of DPPE was suspended in 20 ml of chloroform. The suspension was stirred overnight at 20°C after the addition of 50 μl (ca. 0.3 mmol) of TEA and 1 ml (ca. 0.2 mmol) of the solution described above. A clear solution was obtained. The oily product which was generated by evaporation was dissolved in 1.5 ml of 1 M HCl–acetic acid. The reaction mixture was kept at room temperature for 1 h. The Boc groups were hydrolyzed completely since the value of the retardation factor of the product lowered and a ninhydrin purple spot based on a free amino group in the lipid appeared in thin layer chromatographic experiments (no. 5721 plate, Merck, Darmstadt). After concentration with a rotary evaporator, repeated washings with methanol and chloroform lead to the complete elimination of HCl and acetic acid from the reaction mixture. The product (NH_2–C_6–DPPE) was purified with preparative thin layer chromatography (No. 5717 plate, Merck). The development solvent used was chloroform–methanol (7:3, v/v). The mass spectroscopic data of NH_2–C_6–DPPE were as follows: *m/z* (%) 805 $[M + H]^+$, 551, 295, 255, 157; calculation implied $C_{43}H_{86}N_2O_9P$ for the molecular formula of the product. The recovery was ca. 60%. Bromoacetyl-aminohexyl (BrAc–NH–C_6)-DPPE was synthesized as follows: 140 mg (1.00 mmol) of bromoacetic acid (Wako) were dissolved in 30 ml of chloroform. 140 mg (1.20 mmol) of HSI and 250 mg (1.20 mmol) of DCCD were added to the reaction mixture and stirred at room temperature for 3 h. After the solvent was evaporated with a rotary evaporator, 30 ml of ethyl acetate was added. The precipitate was removed by filtration. The addition of 10 ml of chloroform resulted in a ca. 100 mM solution of bromoacetyl succinimide ester after the second evaporation. 0.05 mmol of NH_2–C_6–DPPE, 1 ml (0.1 mmol) of the bromoacetyl succinimide ester solution and 50 μl of TEA were reacted overnight at room temperature. The reactive product (BrAc–NH–C_6–DPPE) was purified with preparative thin layer chromatography as shown above. The overall recovery of BrAc–NH–C_6–DPPE was about 30%. A 2.0 mM solution of BrAc–NH–C_6–DPPE was prepared by adding an adequate volume of chloroform (determined after calculating the phosphorus concentration in the BrAc–NH–C_6–DPPE solution according to the method of Gerlach and Deuticke [12]). Each lipid solution was stored at −20°C in a test tube with a PTFE stopper.

Immunoassay reagents

Human CEA and rabbit anti-CEA antibody were purchased from Dako (Kyoto). Monoclonal anti-CEA antibody was donated by Green Cross (Osaka). Guinea pig serum was used as a source of complement, which means a heat-sensitive complementary substance in blood serum. Lyophilized complement was obtained from Denka Seiken (Tokyo).

Preparation of antibody-bearing liposomes

Preparation of liposomes. Liposomes were generally prepared according to the method described previously [7]. The lipid components of liposomes were as follows; DPPC : cholesterol : modified DPPE = 100 : 100 : X (molar ratio). The liposomes were finally suspended in BBS.

Modification of monoclonal antibody. Ten milligrams of monoclonal anti-CEA antibody dissolved in 1 ml of 0.1 M acetate buffer (pH 3.6) was mixed with 1 mg of pepsin (Sigma) and incubated for 10 h at 37°C. The reaction was stopped by adding 25 μl of 2 M Tris–HCl buffer (pH 8.0) and 150 μl of 0.5 M NaOH. The reaction mixture was filtered through a Millex filter (pore size: 0.22 μm, Millipore, Bedford, MA) and then applied to a LC column (TSK-Gel, G-3000SW, Toyo Soda, Tokyo). The purified $F(ab')_2$ of the antibody was collected and condensed with a protein concentrator (Centriprep 10; Amicon, Danvers, MA). The final concentration of the modified antibody was about 3 g l^{-1} in 0.1 M phosphate buffered saline (pH 6.0). We then added 10 mg (88.0 mmol) of 2-mercaptoethylamine hydrochloride (Nakarai Tesque, Kyoto) to 1 ml of the $F(ab')_2$ solution and incubated this for 30 min at 37°C. The reaction mixture was loaded on a commercially available gel filtration column (PD-10, Pharmacia, Uppsala) and eluted with BBS. The concentration of the Fab′ solution prepared was about 1 g l^{-1} in BBS.

Coupling of modified antibody to liposomes. The liposome suspension (1 ml) and the Fab′ antibody solution (1 ml) were mixed and reacted at room temperature for 20 h under a nitrogen gas atmosphere while being slowly rotated. The liposomes were collected by centrifugation under the same conditions as those described in [7]. The liposomes were resuspended in 2 ml of GBS^- containing NaN_3 (0.5 g l^{-1}) and stored in a refrigerator. Protein assay of liposome suspensions before and after the coupling reaction (we used a protein assay reagent from Bio-Rad, Richmond, CA) indicated that about 100 mg of the antibody (Fab′) per liter was bound to the liposomes that did not have spacer molecules. Therefore, ca. 20% of Fab′ that had reacted was actually immobilized on liposomes. The same analytical technique as mentioned above was adopted for the liposomes containing other spacer lipids.

Standard assay system. Into each well of a microtiter plate (Nunc, Roskilde), we put 10 μl of a serum solution and 10 μl of the liposome suspension (both diluted 10-fold with GBS^{2+}) and incubated for 10 min at 37°C. After adding 25 μl of a second antibody and complement (both diluted 10-fold with GBS^{2+}), we incubated this for another 30 min at 37°C. To stop the reaction, we added to each well 100 μl of a 10 mM sodium ethylenediaminetetraacetic acid–barbital-buffered saline solution (EDTA–BS).

The fluorescence of each well was automatically measured with a fluorescence spectrophotometer (Model MTP-32, Corona Electric, Katsuta), with excitation at 490 nm, and emission measured at 530 nm. The total releasable CF in liposomes was determined by lysing with 100 μl of water instead of EDTA–BS. The specific liposomal lysis was calculated as follows: lysis (%) = (experimental release − liposomal background) × 100/total release, where liposomal background means the fluorescence of the suspension containing liposomes solely [that is, diluted liposomal suspension (10 μl) + GBS^{2+} (60 μl) + EDTA–BS (100 μl)].

RESULTS AND DISCUSSION

At first, we investigated spacer molecules which had a bromine atom at the end (i.e., $Br–C_n–COOH$) because of easier synthetic procedures. However, no antibody was immobilized when n was more than two, although thin layer chromatographic data supported that spacer molecules were successfully attached to DPPE. We supposed that these results could be attributed to the activity of the bromine atom at the end of the spacer molecule. Therefore, we modified DPPE introduced spacer molecules ($NH_2–C_n–CONH–$DPPE) with bromoacetic acid for the immobilization of an antibody on liposomes.

We synthesized DPPEs having spacers of various chain lengths (n = 3, 4, 5, 6, 8 and 12) and with a bromoacetic (BrAc) group at the end. The liposomes containing 5 mol% of each modified

TABLE 1

Effect of spacer length on the amounts of IgG (Fab') immobilized on the BrAc–NH–C_n–liposomes

Spacer length (n =)	0	3	4	5	6	8	12
Immobilized IgG (μg/ml) [a]	100	130	140	150	170	180	170

[a] The amounts of IgG (Fab') immobilized in 1 ml of the liposomal suspensions are shown.

DPPE were prepared and reacted with an Fab' fraction of human immunoglobulin (Ig) G as a model molecule of an antibody. The reaction conditions were similar to the procedure described in the experimental section. The amounts of IgG (Fab') immobilized on liposomes are shown in Table 1. Longer chain length resulted in larger immobilized amounts of IgG (Fab'). These results show that steric hindrance from the liposomal surface could limit the immobilization of an antibody and the insertion of spacer molecules between liposomes and an antibody would lead to an increase in the amounts of immobilized antibody.

The degree of lyses of these liposomes in a high concentration complement solution (25.0 CH_{50}) was listed in Table 2. Unfortunately, the liposomes became more unstable to complement with increasing the chain length of spacers. In the liposomes of $n = 12$, the amounts of IgG (Fab') immobilized were almost the same as those in $n = 8$. In Refs. 13–15 it was reported that an optimal length of spacer arms exists in hapten–antibody reactions with regard to liposomes. A similar relation might exist in complement-antigen (or antibody) reactions. That is, the spacer length of $n = 12$ has become too long for complement to attack the liposomal membrane. Thus, $n = 5$ was chosen as the optimal spacer length in

TABLE 2

The lyses of the liposomes immobilized IgG (Fab') through BrAc–NH–C_n–DPPE in a high concentration complement solution (25.0 CH_{50})

Spacer length (n =)	0	3	4	5	6	8	12
Lysis (%)	3.5	4.0	5.0	40.5	41.0	61.5	4.0

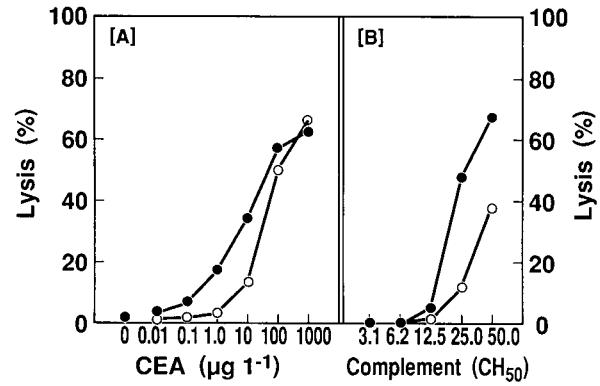

Fig. 2. Calibration curves of both CEA in human serum [A] and complemental dose responses [B] using the liposome-loaded Fab'-antibody through BrAc–DPPE or BrAc–NH–C_5–DPPE. The CEA concentration shows the value before the 10-fold dilution. The CEA-free serum was prepared with affinity chromatography using rabbit-anti CEA antibody-bearing agarose beads. For details of the liposomal preparation and the measurement procedure, see the experimental section in the text. ○ = BrAc–DPPE, ● = BrAc–NH–C_5–DPPE.

view of the immobilization quantity and the liposomal stability to complement.

Figure 2 shows both the CEA [A] and the complemental [B] dose responses of antibody (Fab')-bearing liposomes containing BrAc–NH–C_5–DPPE (DPPC : cholesterol : BrAc–NH–C_5–DPPE, molar ratio, 100:100:5). The standard solutions were prepared by the addition of adequate amounts of pure human CEA to human sera in which CEA was removed by affinity chromatography in advance [16]. The CEA concentration of 0.1 μg l^{-1} could be measured with antibody (Fab')-bearing liposomes containing BrAc–NH–C_5–DPPE [0.1 μg l^{-1}: mean lysis = 6.5%, S.D. = 0.61%, $n = 10$; 0.01 μg l^{-1}: mean lysis = 3.1%, S.D. = 0.58%, $n = 10$]. In the liposomes without spacer molecules, the detection limit was 2 μg l^{-1} [1.0 μg l^{-1}: mean lysis = 3.1%, S.D. = 0.63%, $n = 10$; 2.0 μg l^{-1}: mean lysis = 6.0%, S.D. = 0.60%, $n = 10$]. The detection limit was defined as a concentration in which the difference between signal and blank values was 2S.D. or above. On the other hand, the liposomal stability to complement was reduced with regard to the liposomes without spacer. The 10-fold dilution of complement ($CH_{50} = 25.0$) was not available for

the measurements of CEA in practice (a 20-fold dilution was adopted). The stability of these liposomes against human sera was investigated using 60 human sera obtained from Toshiba Hospital (Oimachi, Tokyo). A second antibody was not added to the reaction mixture. An antibody was not bound to liposomes in this experiment so that the influence of the antibody on this phenomenon was excluded. The liposomes containing BrAc–NH–C_5–DPPE (DPPC : cholesterol : BrAc–NH–C_5–DPPE, 100 : 100 : 5) showed nonspecific liposomal lysis in 10 human sera (lysis over 10%) whereas only two sera broke the BrAc-(no spacer) liposomes. The stability of the spacer-inserted ($n = 5$) liposomes against human sera dropped drastically. A correlation to RIA in these sample sera of 0.86 was observed in the case of the liposomes immobilizing an antibody (Fab') through BrAc–NH–C_5–DPPE (see Fig. 3). The antibody (Fab')-bearing liposomes without spacer molecules were not applicable for the precise CEA measurements of these samples because of the lack of sensitivity (see Fig. 2A).

The presence of functional groups in the modified DPPE for the immobilization of an antibody to liposomes was related to the stability of liposomes against complement and human sera [7]. We investigated whether BrAc groups on the surface of liposomes were blocked with SH compounds such as mercaptoethanol (ME) or mercaptoethylamine (MEA). The liposomes without an antibody were studied at first. The liposomal pellet (30 mg each) was suspended in 1 ml of BBS, 1 mM ME (in BBS) and 1 mM MEA (in BBS), respectively. The suspensions were stirred for 36 h at 20°C. The dose responses to complement were shown in Fig. 4. The liposomes reacted with ME were more stable to complement than the control liposomes. The optimum concentration of ME in the treatment was 5 mM (data not shown).

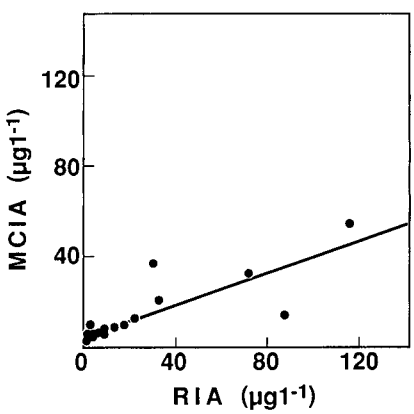

Fig. 3. Correlation between RIA and MCIA in the measurement of CEA in 60 human sera using the liposomes immobilizing an antibody (Fab') through BrAc–NH–C_5–DPPE. The reaction conditions are mentioned in Experimental.

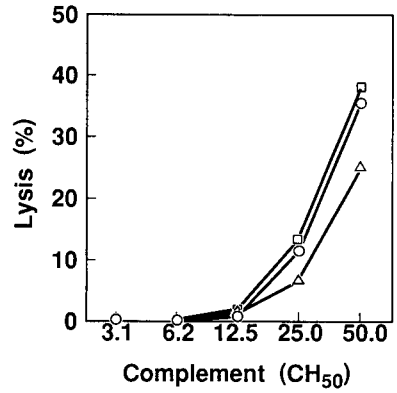

Fig. 4. Blocking of BrAc groups in liposomes without an antibody based on the treatment with SH compounds. The detailed treatment conditions are described in Experimental. The dose responses of liposomes to adequate diluted complement were measured. ○ = 10 mM borate buffered saline (BBS), △ = 5 mM mercaptoethanol in BBS, □ = 5 mM mercaptoethylamine in BBS.

Next, we tried the BrAc group-blocking with 5 mM ME in the antibody (Fab')-bearing liposomes. The treatment conditions were the same as those described above except for the ME concentration (5 mM). The complemental stability of the ME-treated liposomes was unexpectedly reduced although no elimination of antibody and no decrease in sensitivity to CEA were observed (data not shown). The reasons for these results are still unknown. After all, the blocking treatment of remaining BrAc groups with SH compounds was not useful for the improvement of the liposomal stability to complement.

The Langmuir–Blodgett (L–B) technique [17] is one of the methods used to analyze the characteristics of lipid monolayers. To study the stability of liposomes against human sera in the presence

of complement, we measured curves for surface pressure (π) vs. surface area (A) for lipid membranes containing various modified lipids. We investigated the effects of BrAc–NH–C_5–DPPE contents on the π–A curve of lipid monolayers. We used a commercially available L–B membrane preparation equipment (FSD-20, USI, Fukuoka) for experiments at 25°C. The lipid solutions in chloroform contained DPPC, cholesterol, and BrAc–NH–C_5–DPPE (molar ratio = 100:100:X). As Fig. 5 shows, the increase in the content of BrAc–NH–C_5–DPPE shifted the π–A curve to the right. These results imply that the fluidity of membranes containing a higher ratio of BrAc–NH–C_5–DPPE will increase and the hardness of membranes may decrease. The stability of liposomes in human sera in the presence of complement could be related to the fluidity of lipid bilayer in the liposomes.

We also studied the effects of changing the kinds of functional lipids in the liposomes. The molar ratio of functional lipids was fixed at $X = 5$. In the cases of both DPPE and BrAc–DPPE, the curves were similar to those without functional lipids (Fig. 6). In fact, the π–A curve of the lipid monolayer containing BrAc–NH–C_5–DPPE moved markedly to the right. Besides, spacer-linked (NH_2–C_5–) DPPE showed almost the same π–A curve as BrAc–NH–C_5–DPPE. These results may mean that the fluidity of the lipid monolayers without BrAc–NH–C_5–DPPE is low and thus the liposomes incorporating BrAc–NH–C_5–DPPE are very unstable in human sera. The data obtained from the L–B technique are those for lipid monolayers, however, the characteristics of lipid bilayers such as liposomes differ from those of monolayers. Therefore, the liposomal stability in human sera may not be explainable solely by the hardness or strength of the liposomal membrane.

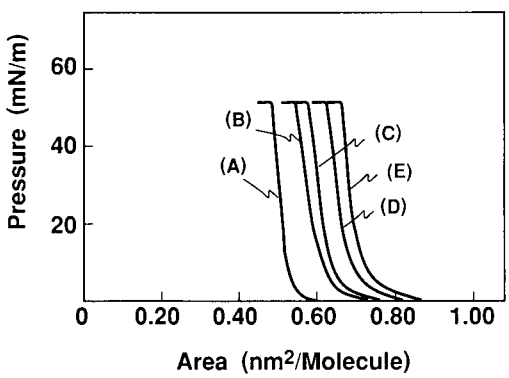

Fig. 5. π–A curves of L–B membranes containing various amounts of BrAc–NH–C_5–DPPE. The lipid contents (molar ratio) of L–B membranes were as follows; DPPC: cholesterol: BrAc–NH–C_5–DPPE = 100:100:X, where $X = 0$ (A), 1.25 (B), 2.50 (C), 3.75 (D), and 5.00 (E). The measurements were performed at 25°C.

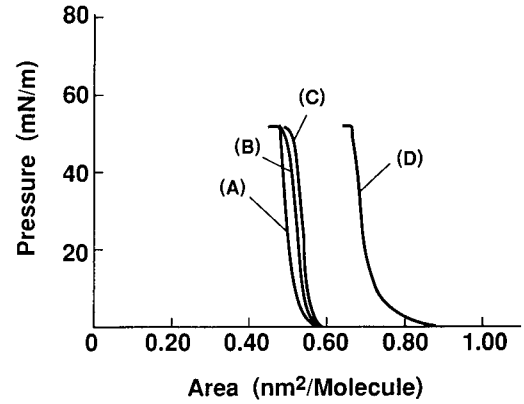

Fig. 6. π–A curves of L–B membranes containing different kinds of functional lipids The lipid contents (molar ratio) of L–B membranes were as follows; DPPC:cholesterol:X = 100:100:5, where X = (A) no additional functional lipid, (B) DPPE, (C) BrAc–DPPE, or (D) BrAc–NH–C_5–DPPE.

In conclusion, we have shown that both the amounts of an antibody bound to liposomes and the liposomal sensitivity are related to the spacer length of the functional group used for the immobilization. The liposomes containing BrAc–NH–C_5–DPPE showed the best sensitivity, however, they became more susceptible to human sera in the presence of complement. The practical measurements of CEA in human sera did not show a good correlation to RIA ($\gamma = 0.86$) in the liposomes containing BrAc–NH–C_5–DPPE, although 0.1 $\mu g\ l^{-1}$ of CEA could be detected. The L–B analyses of lipid monolayers did not clarify the reasons why the spacer-modified liposomes were unstable. Further detailed investigations of the instability of the liposomes to human sera in the presence of complement are required before this analytical system can be applied commercially.

REFERENCES

1 S.C. Kinsky, Biochim. Biophys. Acta, 265 (1972) 1.
2 G.K. Humphries and H.M. McConnell, Proc. Natl. Acad. Sci. USA, 71 (1974) 1691.
3 H.R. Six, W.W. Young and S.C. Kinsky, Biochemistry, 13 (1974) 4050.
4 M. Smolarsky, D. Teitelbaum, M. Sela and C. Gitler, J. Immunol. Methods, 15 (1977) 255.
5 K. Uemura, M. Yuzawa-Watanabe, N. Kitazawa and T. Taketomi, J. Biochem. (Tokyo), 87 (1980) 1641.
6 Y. Ishimori, T. Yasuda, T. Tsumita, M. Notsuki, M. Koyama and T. Tadakuma, J. Immunol. Methods, 75 (1984) 351.
7 Y. Ishimori and K. Rokugawa, Clin. Chem., 39 (1993) 1439.
8 J. Porath and R. Axén, Methods Enzymol., 44 (1976) 19.
9 J.L. Alves and M.A. Ditzler, Anal. Chim. Acta, 274 (1993) 361.
10 T. Yasuda, Y. Naito, T. Tsumita and T. Tadakuma, J. Immunol. Methods, 44 (1981) 153.
11 L.D. Leserman, P. Machy and J. Barbet, Nature (London), 293 (1981) 226.
12 E. Gerlach and B. Deuticke, Biochem. Z., 337 (1963) 477.
13 K. Kimura, Y. Arata, T. Yasuda, K. Kinosita and M. Nakanishi, Immunology, 69 (1990) 323.
14 N. Ohyama, T. Hamano, N. Hamakawa, K. Inagaki and M. Nakanishi, Biochemistry, 30 (1991) 1154.
15 K. Kimura, Y. Arata, T. Yasuda, K. Kinosita, Jr. and M. Nakanishi, Biochim. Biophys. Acta, 1104 (1992) 9.
16 J. Porath and T. Kristiansen, in H. Neurath, R.L. Hill and C.-L. Boeder (Eds.), Proteins, Vol. 1, Academic Press, New York, 3rd edn., 1975, p. 95.
17 K.S. Birdi, Lipid and Biopolymer Monolayers at Liquid Interfaces, Plenum Press, New York, 1989, p. 27.

Analytica Chimica Acta, 284 (1993) 235–240
Elsevier Science Publishers B.V., Amsterdam

Selectivity and yields in supercritical fluid extraction of tar-mats and source rocks

M. Skurdal, M. Østbye and T. Greibrokk

Department of Chemistry, University of Oslo, PB 1033 Blindern, 0315 Oslo (Norway)

(Received 20th May 1993; revised manuscript received 28th June 1993)

Abstract

Extraction of tar-mats and a petroleum source rock with supercritical carbon dioxide has been performed in an attempt to obtain class fractionation by multistage extractions. Depending on the experimental conditions the total yields were similar to or higher than the yields obtained with solvent extraction. The tar-mats were extracted with a 3-stage procedure and the bulk of the hydrocarbon biomarkers was found in the second fraction. The source rock was extracted first with a 5-stage, then with a 2-stage process. The 2-stage extraction contained the biomarkers in the first fraction, and the process was more rapid than the 5-stage extraction, although the yields were slightly reduced. Collection on C_{18} sorbent cartridges was performed both with and without water flow and compared to collection in a solvent. Cartridge collectors equipped with a small vacuum at the outlet were easy to use, free for solvent vapors, but resulted in loss of the volatile end of the extract.

Keywords: Supercritical fluid extraction; Tar-mats; Source rocks

Solvent extraction is commonly used in conventional analysis of source-rock bitumen, either as Soxhlet extraction or as the more rapid flow-blending technique [1]. In both cases substantial amounts of organic solvents, usually chlorinated hydrocarbons, are required. Because of the favourable mass transfer characteristics of supercritical fluids, supercritical fluid extraction (SFE) has been demonstrated to have the ability to replace solvent extraction for sediments [2–4]. Solubility in supercritical fluids is a function of the density of the fluid, which is a function of the pressure and the temperature. The temperature has additional effects on the migration velocity in porous materials and on the vapour pressure of the analytes. Thus, increasing temperatures decrease density, but increase migration rates and partial vapour pressures [5]. Depending on the pressure and the temperature, potentially high selectivity can be obtained in SFE by utilizing multistep extractions, reducing the need for other purification methods prior to analysis.

In a recent study of multistage extraction of a Posidonia shale source rock [6], with 15–20 g samples, the extractions took several hours at each stage, at an extraction rate of approximately 0.5 ml/min CO_2 (measured as liquid). Tar-mats are sedimentary rocks containing heavy, asphaltene-rich oil. With asphaltene proportions around 50%, such samples are potentially even more difficult candidates for rapid extraction than source rocks. This paper includes investigations on the selectivity versus yields of tar-mats, attempts to reduce the extraction time of the shales and examinations of the procedures for collecting the extract.

Correspondence to: T. Greibrokk, Department of Chemistry, University of Oslo, PB 1033 Blindern, 0315 Oslo (Norway).

0003-2670/93/$06.00 © 1993 – Elsevier Science Publishers B.V. All rights reserved

EXPERIMENTAL

Three different tar-mats from the Ula field in the North Sea were obtained from BP-Norway. A sample of Posidonia shale (E38) from a quarry near Dotternhausen, southwest Germany, was obtained from KFA, Jülich, Germany. This sample is a KFA-internal reference material which recently was used for investigating SFE of source rocks [6].

Carbon dioxide, grade 4.8 (99.998%), from AGA/Norgas, Norway, was delivered by an Isco μLC-500 pump equipped with a cooling mantle at -5°C (Isco, Lincoln, NE). Carbon dioxide with 5% 2-propanol (w/w) and a helium head was supplied as a gift by Hydro Gas (Norsk Hydro, Norway). Tetrahydrofuran (THF) was introduced in the last stage by connecting a six-port switching valve to the outlet from the pump. A stainless steel tube with a volume of 0.4 ml, which was connected to the valve, was filled with solvent. By switching the valve from load to inject position, 3×0.4 ml of solvent was included in the carbon dioxide stream.

The 0.5 ml extractor, EX-60105, obtained from Suprex (Pittsburgh, PA), was heated in an old gas chromatograph oven. The linear fused silica restrictor had an i.d. of 30–40 μm.

Solvent collection was performed by immersing the restrictor into a solvent (7 ml of hexane) contained in a glass vial equipped with a cap and a gas outlet. The vial was carefully heated only to prevent restrictor plugging by solid CO_2.

The sorbent collection was performed with a C_{18} Sep-Pak cartridge (Waters/Millipore, Milford, MA) which was connected to a Y-piece glass tube, as described in Ref. 6. The restrictor was connected to one end, and a flow of distilled water at 50°C to the other end. The restrictor ended in the inlet of the cartridge. The cartridge was connected to a water aspirator giving a slight vacuum which was adjusted to give a distilled water flow of approximately 25 ml/min. The purpose of the flowing water was to aid in transferring the extract to the collector, to heat the restrictor to prevent plugging and to remove water soluble modifiers. Highly water-soluble components will be lost by this procedure. Due to the efficient heat transfer a water temperature of 50°C was sufficient to prevent restrictor plugging. By positioning the linear restrictor at the inlet of the Sep-Pak cartridge, a flow of 0.5 ml/min liquid carbon dioxide was maintained. After each stage, the cartridge was replaced by another cartridge. Each cartridge was air dried for 10 min, then flushed in the opposite direction with 3 ml of tetrahydrofuran in a syringe to elute the extract.

Collection on the cartridges without flowing water was obtained by connecting the cartridge to the end of the restrictor, which was heated in a heating block to 75°C. The vacuum from the water aspirator was connected to the outlet of the cartridge. Collection in a solvent was performed at the temperature created by the expanding CO_2, while carefully heating the vial to avoid plugging the restrictor.

The 1-g tar-mat samples were extracted in a 3-stage procedure, starting at 11 MPa and 60°C (0.36 g/ml), then increasing the pressure to 31 MPa (0.84 g/ml) and then at the same pressure with addition of THF in the final stage.

The 1 g shale samples were extracted first with plain CO_2 in four stages at 24 MPa and 50°C (0.83 g/ml), at 24 MPa and 100°C (0.57 g/ml), at 45 MPa and 50°C (0.94 g/ml) and at 45 MPa and 100°C (0.79 g/ml). In the fifth stage, THF was included 3 times, 0.4 ml each time, while pressure and temperature were kept at 45 MPa and 100°C. Each step consisted of 30 min extraction. In the 2-stage extraction, the first stage consisted of 30 min at 45 MPA and 100°C (0.79 g/ml) and the last stage (with THF) as with the 5-stage extraction. The flow-rate of liquid CO_2 was measured on the pump. All samples were extracted in triplet.

The extracts from the first stages were analyzed by GC on a Varian 3400 instrument equipped with a 30 m $\times$ 0.25 μm i.d. DB-1 fused silica column and flame ionization detector (FID). The column temperature was held at 40°C for 3 min, then to 160°C at 10°C/min, then to 270°C at 6°C/min and held at 270°C for 10 min. This instrument and a Hewlett-Packard 5921A atomic emission detector were used to control that the fractions collected at each step were approxi-

mately equal in content compared to the fractions collected with larger sample sizes [6], based on FID and carbon line emission. The fractions were evaporated to constant weight to determine the yields gravimetrically.

The distribution of saturated, aromatic and polar compounds was determined with an Iatroscan TH-10 Mk IV thin layer chromatograph equipped with FID and a Perkin Elmer LCI-100 integrator.

The samples were applied on silica rods (Chromarod-S III, pore diameter 60 A, particle size 5 μm) and eluted first with *n*-hexane, then toluene. The consumption of pure hydrogen was 180 ml/min and of air 2.1 l/min. The software was dedicated to separating the samples into 4 fractions, saturated, aromatic, polyaromatic and polar compounds. However, the separation between the last two groups was not unequivocal, and the results for the two fractions were pooled (as polar compounds).

RESULTS AND DISCUSSION

Tar-mats

A constant temperature of 60°C was chosen initially for extracting 1-g samples of tar mats. At 60°C, a 3-stage extraction was performed with CO_2 at 11 MPa in the first stage, 31 MPa in the second stage and addition of tetrahydrofuran (THF) in CO_2 (at 31 MPa) in the third stage.

The yields were 21.9, 20.9 and 17.7 mg/g for the 3 tar-mats, compared to 22.0, 18.9 and 13.6 mg/g which were obtained [7] by Soxhlet extraction with dichloromethane and methanol (93 + 7, v/v).

The pressure of the first stage was selected as low as 11 MPa (density 0.36 g/ml) in order to determine the amount of material which could be extracted before the expected bulk of the biomarkers (in the second stage). Pressures above 30 bar did not increase the yields substantially (Table 1). In the first step *n*-alkanes up to C_{24}

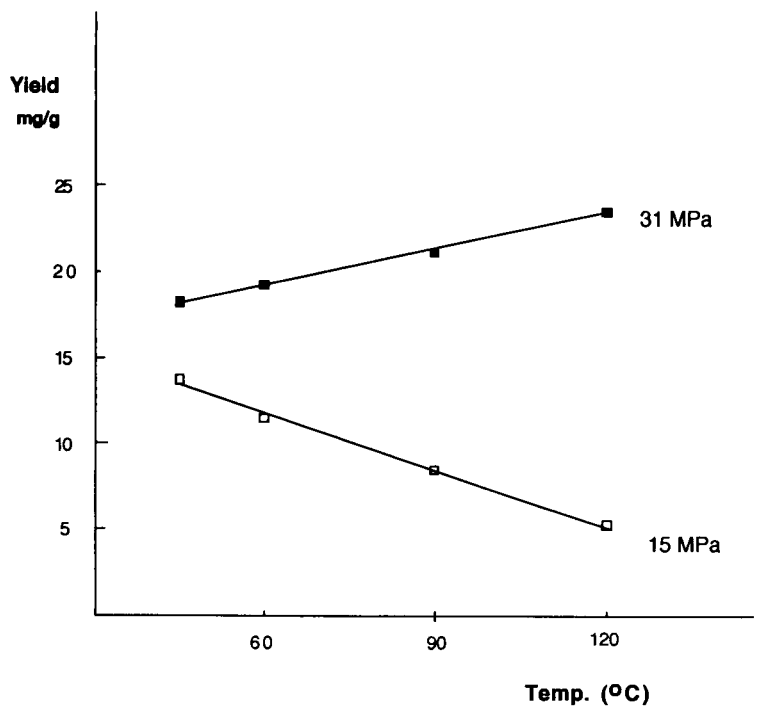

Fig. 1. The yields of SFE of tar-mat as a function of the temperature at low pressure (15 MPa) and at high pressure (31 MPa).

TABLE 1

Extraction yields (mg/g) of tar mats at different pressures (densities) at 60°C (mean ± S.D., $n = 4$)

11 MPa (0.36 g/ml)	21 MPa (0.74 g/ml)	31 MPa (0.84 g/ml)	45 MPa (0.90 g/ml)
5.3 ± 0.7	17.9 ± 0.5	20.0 ± 0.1	21.0 ± 0.1

were extracted, with a peak at C_{19}. The first fraction contained 24–32% of weight of the whole extract with a similar distribution of saturates, aromatics and polars in the three tar-mats (Table 2). In the second step *n*-alkanes up to C_{37} were found, with a peak at C_{23}. Saturated compounds were in large excess (Table 2). Important biomarkers such as steranes, hopanes, monoaromatic steroids and methylphenanthrenes were found in fraction 2, by GC-FID and by GC-mass spectrometry(MS).

The effect of varying the extraction temperature was examined at 2 different pressures. The yields decreased with increasing temperature at 15 MPa, which is due to the significant reduction in the fluid density. At 31 MPa the yield increased with increasing temperature (Fig. 1). At this pressure the reduction in the density of the fluid is small, making the influence of increased migration rate and increased volatility more important to the extraction yields.

A volume of 96 ml of liquid CO_2 per g rock was required for quantitative extraction; a high figure compared to the volumes needed for the source rocks.

Source rock

With large sample sizes of source rocks [6], long extraction times were required since the collector was unable to handle more than 0.5–0.8 ml/min of CO_2 (measured as liquid on the delivery pump). By decreasing the sample size to 1 g, maintaining a flow-rate of 0.5 ml/min, the extraction time was reduced to 30 min at each step, corresponding to 7.5 ml of CO_2/g rock.

In order to examine the possibility of selective fractionation, the shale samples were extracted first with plain CO_2 in four stages at 24 MPa and 50°C, 24 MPa and 100°C, 45 MPa and 50°C and at 45 MPa and 100°C. In a fifth stage, THF was included. The selected pressures were based on earlier extractions of similar samples [6]. The continued extractions at higher temperature at constant pressure resulted in increased yields, without any significant changes in selectivity.

Since the first 4 stages did not result in any complete class separations, a simplified 2-stage procedure was developed to separate a fraction containing the bulk of the saturated and aromatic biomarkers from the polar components. In the 2-stage extraction, the first stage consisted of 30 min at 45 MPa and 100°C and the last stage (with THF) as with the 5-stage extraction.

At a density of 0.79 ($P = 45$ MPa, $T = 100$°C) at the first step, polycyclic compounds like steranes and hopanes, naphthalenes, anthracenes, benzothiophenes and dibenzothiophenes were included in this fraction, as demonstrated earlier [6].

The yields of the last step were little affected by the decrease in extraction time (Table 4) and the selectivity changes were small but noticable, probably due to the less effective extraction of the first step(s). The last stage (with THF) contained 74–86% polar compounds.

With the 5-stage extraction, starting with plain CO_2, a total yield of 6.0 mg/g was obtained (Tables 3 and 4), utilizing almost 40 ml CO_2/g rock. After the 5-stage procedure had been replaced by a 2-stage extraction in order to reduce extraction time, almost the same yield was obtained (4.9 mg/g) as with Soxhlet extraction (5.4 mg/g), but now utilizing only 15 ml CO_2/g rock.

The effect of a modifier was studied. 2-Propanol was selected in order to have an alcohol with good solubility for hydrocarbons. With a mixture of 5% of 2-propanol in CO_2, the total

TABLE 2

Distribution (mg/g) of saturated (SAT), aromatic (ARO) and polar (POL) compounds in the SFE fractions of 3 different tar mats (aromatic compounds were not found in fraction 3)

Tar mat	Fraction 1			Fraction 2			Fraction 3		
	SAT	ARO	POL	SAT	ARO	POL	SAT	ARO	POL
A	2.2	1.8	1.5	6.3	1.2	1.8	1.8	–	5.3
B	2.9	1.9	1.9	6.7	1.1	1.8	1.0	–	3.6
C	1.6	1.1	1.4	5.5	1.1	1.6	1.4	–	3.9

TABLE 3

Distribution (%, w/w) of saturated, aromatic and polar compounds in the combined first 4 steps of the 5-step extraction, compared with the first step of the 2-step extraction of Posidonia shale, after extraction with plain CO_2 and CO_2 modified with 5% 2-propanol (the extraction time was 30 min for each step)

Extraction	Fluid	MPa	%SAT	%ARO	%POL	Yield (mg/g rock)
5-step	CO_2	24–45	65	24	11	3.6
2-step	CO_2	45	66	31	3	2.4
2-step	CO_2	35	nd	nd	nd	2.4
5-step	CO_2 + 2-Pro	24–45	48	32	20	4.8
2-step	CO_2 + 2-Pro	45	44	27	29	3.7

yield increased to 7.6 mg/g in the 5-step procedure and to 6.7 mg/g in the 2-step process, but the selectivity was reduced compared to plain CO_2 (Table 3).

With the purpose of including most of the biomarkers in one fraction which could be separated rapidly from the bulk of polar and high molecular weight compounds, the first step of a 2-step extraction was compared to the combined 4 fractions of the 5-step procedure (Table 3).

Since extractions at 45 MPa require good fittings and tight joints, lower pressures are recommended for regular use. By reducing the pressure to 35 MPa, at the same temperature, the density was reduced from 0.79 to 0.73. Extractions under these conditions gave approximately the same yield as at 45 MPa.

TABLE 4

Distribution (%, w/w) of saturated (SAT), aromatic (ARO) and polar (POL) compounds and yields in the last step of the 5-step extraction, compared with the second step of the 2-step extraction of Posidonia shale, after extraction with plain CO_2 and CO_2 modified with 5% 2-propanol, with a pressure of 45 or 35 MPa and a temperature of 100°C (the extraction time was 30 min for each step)

Extraction	Fluid	MPa	%SAT	%ARO	%POL	Yield (mg/g rock)
5-step	CO_2	45	6	8	86	2.4
2-step	CO_2	45	8	17	75	2.5
2-step	CO_2	35	3	23	74	2.4
5-step	CO2 + 2-Pro	45	20	9	71	2.8
2-step	CO2 + 2-Pro	45	15	22	63	3.0

Thus, the 2-step procedure reduced the total extraction time for 1 g samples from 150 min to 60 min, while still obtaining approximately the same yield as with liquid extraction, but now utilizing only 15 ml CO_2/g rock.

The last step in all the extractions contained batch inclusion of THF in CO_2 in order to extract everything not extracted in the previous step(s). THF is known to be an excellent solvent for high molecular weight compounds and for polar components. THF is also soluble in water and could be removed from the extract by collecting on solid sorbents in a stream of water. Since peroxides may form in THF in the presence of light and oxygen, another good solvent of similar properties, but with less peroxide forming ability, methyl *tert*-butyl ether (MBE), was tried in the last step. The extraction yield was, however, reduced to half of the yield obtained with THF, with only 41% polar compounds, demonstrating the difficulty in finding a good replacement for THF. Combined with collection on solid sorbents in water, peroxide formation, however, is not expected to be of any importance.

Collection

In off-line SFE the most common method of collecting the extract is by placing the restrictor in a receiving solvent. Either the restrictor or the solvent must be heated to avoid plugging by solid CO_2. In order both to avoid solvent vapors and also to remove the THF during extraction, the method of collecting on a solid sorbent in water was developed [6]. When this method was compared to collection in a solvent (Table 5), the volatile end below C_{14} disappeared using the sorbent collector. To see whether this was due to the flowing water, collection on a dry cartridge

TABLE 5

Loss of *n*-alkanes C_{14}, C_{13}, C_{12} and C_{11} relative to C_{20} for collection on sorbents compared to collection in hexane (n.d. = not determined due to small amounts of C_{11} and C_{12})

Collector	C_{14}/C_{20}	C_{13}/C_{20}	C_{12}/C_{20}	C_{11}/C_{20}
Hexane	1.6	1.5	1.0	0.5
Sorbent with water	1.0	0.24	n.d.	n.d.
Sorbent without water	1.0	0.10	n.d.	n.d.

from a separately heated restrictor was examined. The volatile end was still missing (Table 5), indicating that the volatiles were not lost by dissolving in the flowing water, but by passing through the sorbent in the gas phase together with the CO_2. Collection on a dry sorbent had the advantage compared to the water–sorbent collection that no water remained in the sorbent. Even after air drying, traces of water are difficult to remove, requiring solvents like THF to elute the extract from the sorbent. Thus, where the volatile end of the sample ought to be collected, solid sorbent collection should be exchanged with collection in a small volume of a proper solvent.

The authors wish to thank D. Leythaeuser, M. Radke, B. Krooss, H. Willsch, A. Wilhelms and S.R. Larter for providing the shale and the tarmats and for cooperating throughout the study. The project was supported by the German–Norwegian VISTA program.

REFERENCES

1 M. Radke, D.H. Welte and H. Willsch, Org. Geochem., 10 (1986) 51.
2 S.K. Kesavan, A. Ghosh, M.E. Polasky, V. Parameswaran and S. Lee, Fuel. Sci. Technol. Int., 6 (1988) 505.
3 J.C. Monin, D. Barth, M. Perrut, M. Espitalié and B. Durand, Org. Geochem., 13 (1988) 1079.
4 G. Hopfgartner, J.-L. Veuthey, F.O. Gülacar and A. Buchs, Org. Geochem., 15 (1990) 397.
5 J. King, J. Chromatogr. Sci., 27 (1989) 355.
6 T. Greibrokk, M. Radke, M. Skurdal and H. Willsch, Org. Geochem., 18 (1992) 447.
7 A. Wilhelms, personal communication.

Analytica Chimica Acta, 284 (1993) 241–247
Elsevier Science Publishers B.V., Amsterdam

BOOK REVIEWS

K. Narahari Rao and Alfons Weber (Eds.), *Spectroscopy of the Earth's Atmosphere and Interstellar Medium*, Academic Press, London, 1992 (ISBN 0-12-580645-0). xi + 526 pp. Price US$ 129.50.

This volume is the fourth in the series *Molecular Spectroscopy: Modern Research,* which sets out to produce critical reviews and summaries in the field of high resolution spectroscopy. The primary subject area of the book is atmospheric spectroscopy. This reflects the present level of interest in, and investigation into, monitoring the levels of species such as carbon dioxide, chlorofluorocarbons, methane and ozone in the terrestrial atmosphere. From a practical and theoretical aspect the vibrational–rotational spectroscopy of a variety of molecules of atmospheric importance is presented with considerable detail in chapters one to five. Spectrochemical analysis of interstellar space is of great interest to those who probe the skies in their quest to understand the evolution of the universe. Chapter six deals with this topic from the perspective of radio-wave spectroscopy.

Chapter one looks at microwave and infrared spectroscopy, examining the problems of water vapour and spectral overlap due to trace level concomitant species. Discussion on high resolution instrumentation for both field and laboratory measurements is presented together with data analysis techniques. The second chapter begins with a historical perspective on the use of the mid-infrared region of the spectrum for the identification of atmospheric constituents. The remainder of the chapter deals with quantitative analysis of high resolution spectra employing the line-by-line calculation of simulated spectra using a model atmosphere; synthetic and observed spectra are then compared to obtain molecular concentrations as a function of altitude, the so-called volume mixing ratio. Chapter three is essentially a compilation of molecular parameters such as line strengths and line shift coefficients used for the line-by-line calculations in the previous chapter. Chapters four and five are concerned with the more theoretical facets of this area of spectroscopy namely collisional mixing and spherical top spectra, respectively. The final chapter covers four topics; carbon monoxide surveys, structure of molecular clouds, selected problems and astro-chemistry.

All the chapters are well written and supported with excellent spectra, diagrams and bibliographies. At the present time the market for this text will include physical spectroscopists, atmospheric researchers and astro-spectroscopists. However, as environmental analytical scientists are called upon routinely to monitor atmospheric parameters the technology and methodology will come from research efforts of the contributors to this book.

Neil W. Barnett

Robert Weinberger, *Practical Capillary Electrophoresis*, Academic Press, San Diego, CA, 1993 (ISBN 0-12-742355-9). 312 pp. Price US$ 69.95.

This monograph presents a broad overview of capillary electrophoresis as it is practised today. It represents a brief survey rather than an in-depth critique of the various approaches. There are extensive references to each topic for supplementary reading. In many ways, this is similar in style to the annual "critical reviews" published in *Analytical Chemistry*, but with a selected rather than comprehensive list of references and with actual diagrams and graphs from the technical publications. It is a useful guide for those who want to quickly get a sense for what has been done and where to look for information. Along these lines, the tables are quite useful for comparing the literature reports.

As the title indicates, this book is geared towards the users of the technique. It should be

0003-2670/93/$06.00 © 1993 – Elsevier Science Publishers B.V. All rights reserved

noted, however, that the brevity of the discussions means that other published sources are often needed to provide a complete picture. Because of the breadth of topics covered, there are also occasional errors. For example, it has long been established that indirect fluorescence detection typically offers 10 times lower detection limits than indirect absorption detection when there is no preconcentration step. Overall, this is a reasonable book for those who need general introductory information about this rapidly growing field.

Edward S. Yeung

S.A. Westwood (Ed.), *Supercritical Fluid Extraction and its use in Chromatographic Sample Preparation*, Blackie, Glasgow, 1993 (ISBN 07514 0089 0). 170 pp. Price £ 45.00.

The analytical chemistry literature continues to increase with the number and diversity of applications of supercritical fluids. This book, one of several now available in this new area of analytical research, focuses principally on the coupling of supercritical fluid extraction (SFE) with gas, liquid and supercritical fluid chromatography. While these are of no doubt important areas of research their use in the everyday workplace of an analytical laboratory must at the present time be rather specific and limited, not least owing to the lack of commercial equipment and manpower. These chapters (3–6) are, to me, rather nebulous concerning the merits of SFE at the present time (as in all cases exceptions no doubt will proliferate!). However, the features of the book are chapters 1 and 2. These chapters are concerned with the principles of and solubility in supercritical fluids, and methodology for off-line SFE. Both provide detailed practical knowledge concerned with the extraction process, current modelling techniques and guidelines for developing an extraction method. From this point of view the book provides an excellent introduction to this new and exciting field of analytical SFE.

John R. Dean

Martin J.J. Hetem, *Chemically Modified Silica Surfaces in Chromatography, A Fundamental Study*, Hüthig, Heidelberg, 1993 (ISBN 3-7785-2030-X). 175 pp. Price DM 198.00.

Silica, in different forms, is by far the most widely used support material for the stationary phase in chromatographic techniques. In this context, chemical modification of the surface is of crucial importance. In open tubular GC, modification is made in order to obtain deactivation and suitable wettability; for LC packing material, the modified surface constitutes the stationary phase. Several different methods and reagents have been applied for these modifications.

This book reports an investigation of the properties of silica modified in different ways. A model substrate, Cab–O–Sil, has thus been modified in various ways and the properties studied by means of ^{29}Si NMR spectroscopy.

The book contains seven chapters. The first is a short introduction (5 pp). Chapters two and three describe surface modification of fused silica capillaries for GC and the subsequent coating of the capillaries with stationary phase (44 pp.). In chapters four, five and six methods for preparation of surface modified silica particles for LC are described (114 pp.). Factors such as pretreatment of the silica, chain length of the modifying reagent, number of reactive groups on the reagent are discussed. Further, the properties of polymer coated-silica particles have been investigated. In the last chapter quantitative and qualitative aspects of solid state ^{29}Si NMR (9 pp.) are described.

The book is based on earlier published articles, and only the first and last chapters are newly written. The articles are from 1988–91, and papers published more recently are not referred to. Even though the material has been published previously, it is attractive to have it collected in a volume like this. The book would be of interest for those who want to have a deeper insight in the preparation of GC columns and packing material for LC.

Lars Blomberg

G. Szepesi, *How to use reverse-phase HPLC*, VCH, New York, 1992 (ISBN 0-89573-766-3). x + 356 pp. Price DM 168.00/£ 63.00.

The aim of this book is to provide the chromatographer with a practical companion on reversed-phase LC, with emphasis on the modes of interaction between solutes and stationary and mobile phases.

The introductory chapter discusses the advantages and disadvantages of reversed-phase LC and normal-phase LC and these are summarised in tabular form. A short chapter on chromatographic theory follows and column and eluent selection are covered in the next two chapters. The types of column and their uses are described, along with a review of solvent selection including the addition of masking agents, and the evaluation of column performance. Special methods and techniques are presented in chapter five, such as ion-pair, chiral, indirect detection, multi-column operation and protein separations. Phase system optimisation (combination of stationary and mobile phases) for maximum separation selectivity is described in chapter six, with emphasis on practical considerations. Finally, method validation techniques are discussed in chapter seven, with a review of the experimental considerations required for measurement of the performance of LC methods.

This book is a further addition to the extensive literature now available on LC, but would be a useful reference text particularly to those new in the field.

R.W. Abbott

J. Vindevogel and P. Sandra, *Introduction to Micellar Electrokinetic Chromatography*, Hüthig, Heidelberg, 1992 (ISBN 3-7785-2105-5). x + 231 pp. Price DM 88.00.

The emerging technique of micellar electrokinetic chromatography (MEKC) is a powerful combination of the selectivity of chromatography and electrokinetic propulsion. The advent of this monograph suggests that MEKC is now a mature technique but the authors suggest new developments that can be anticipated and discuss some of the current deficiencies.

The material is well presented, with clear diagrams and chromatograms throughout and extensive, up-to-date references accompanying each chapter. The contents are divided into four parts that cover fundamentals, instrumental aspects, resolution in MEKC and applications. The fundamentals section provides good coverage of various modes of electrokinetic analysis, including capillary zone electrophoresis, capillary electrochromatography and MEKC, and is particularly useful for readers unfamiliar with such techniques. Instrumentation is discussed in terms of columns, injection techniques, detection and thermal effects and the section on resolution provides a useful theoretical comparison with the van Deemter equation for conventional chromatography. The final section considers a wide range of general applications, including peptides, drugs, vitamins, steroids, natural products and metal chelates, and concludes with a timely discussion of chiral separations.

This is a thoughtful and well presented monograph that discusses all aspects of the technique of MEKC and is recommended to the specialist and the interested generalist alike.

P.J. Worsfold

M.R. Porter (Ed.), *Recent Developments in the Analysis of Surfactants*, Critical Reports on Applied Chemistry, Vol. 32, Society of Chemical Industry, Elsevier, London, 1991 (ISBN-1-85166-581-1). vi + 223 pp. Price £ 65.00.

This book provides a broad review and reference guide for the working laboratory undertaking surfactant analyses. Much of the content is clearly focussed towards cost effective and robust methods which are likely to be employed for rapid quality control and production analyses. Some contributors have captured the essence of current developments and indicated the direction for future research, whilst some are more di-

rected towards the best available proven methodologies.

The chapter on formulated products effectively updates most of the standard texts and reviews active areas of development such as electrochemical techniques, the separation sciences and infrared spectroscopy. An important conclusion is that new spectroscopic, multicomponent methods are developing rapidly and will become cost effective.

Trace component analysis in surfactants is reviewed in chapter 3. This chapter describes the standard approaches to analysis and their current limits of application.

The niche market of amphoteric surfactants is addressed in the fourth chapter. The author describes the principal types of amphoteric surfactants at some length and details the standard analytical requirements.

On-line techniques for surfactant analysis are addressed in the following chapter. This timely review makes interesting reading by addressing a wide field of new methods and technical advances and providing a practical and pragmatic commentary about their potential future applications as robust systems.

The growing area of analysis of test liquors and environmental samples is well covered by the final chapter. Much of the discussion in this section deliberates upon the difficulties placed before the analyst; in particular those derived from the matrices, sampling, detectability and analyte losses attributable to the methods.

C.J. Dowle

E.L. Charsley and S.B. Warrington (Eds.), *Thermal Analysis – Techniques and Applications*, The Royal Society of Chemistry, Cambridge, 1992 (ISBN 0-85186-375-2). 296 pp. Price £ 45.00.

Thermal analysis has been among the most rapidly developing methods in recent years as a result of the increase of applications. In comparison with other analytical techniques such as chromatography or spectroscopy to date there are only relatively few books on thermal analysis. The present book, based on a course organized by the Thermal Analysis Consultancy Service in Leeds, 12–13th September 1991, was written by twelve specialists in thermal analysis, some of them with world-wide reputations.

Thermal analysis deals with differential thermal analysis (DTA), differential scanning calorimetry (DSC), thermogravimetry (TG), simultaneous TG-DTA/DSC, thermomechanical analysis and dynamic mechanical analysis as the most important methods, as well as thermomicroscopy, high temperature x-ray diffraction, and evolved gas analysis. Besides these methods there are applications in various fields, such as of minerals, pharmaceuticals, polymers, materials science and quality assurance.

The book also offers a short introduction for beginners as well as for the experienced scientist and engineer. The added list of sources of information in thermal analysis and of addresses of companies supplying thermal analysis equipment in the U.K. could be helpful. In this book I have noted only a few mistakes, e.g., p. 189, Fig. 2, Form 1 and 2 are incorrectly interchanged.

Some double fractions (such as the one on p. 57), are difficult to read and understand. It is perhaps unfortunate in this age of desktop computers that the book has no uniform style as a result of the decision to employ camera ready manuscripts. As a whole the book can be recommended.

Erwin Wiederholt

S.N. Deming and S.L. Morgan, *Experimental Design: a Chemometric Approach, Second Edition*, Elsevier, Amsterdam, 1993 (ISBN 0-444-89111-0). 416 pp. US$ 177.25.

The first edition (1987) was the first full length text in this area aimed primarily at chemometricians. An appreciation of experimental design is important for effective research, but conceptual advances are often best presented in textbook and tutorial form rather than as original research papers.

The first 9 chapters, largely unchanged from the first edition, take the student through elementary systems theory, simple matrix concepts building up from one factor to three factors and then ANOVA and introducing concepts of degrees of freedom, coding and sums of squares. A new chapter 10 is introduced on regression analysis, largely involving sequential data. Chapter 11 provides a detailed analysis of a 10-factor experiment. Concepts of confidence intervals and uncertainty are stressed. Chapter 12 discusses a number of standard designs: a useful addition from the first volume is a section on mixture designs. A new Chapter 13 discusses the concepts of confidence, uncertainty and quality of information in substantial detail and Chapter 14 introduces factorial designs including the Taguchi design. Chapter 15, based largely on the original Chapter 12, discusses miscellaneous concepts such as confounding, blocking and randomization. There are extensive exercises, statistical appendices and a lengthy bibliography.

This book is definitely an excellent summary of state-of-the-art ideas in experimental design. Some of the explanations are rather personal to the authors, though, and there are alternative approaches to interpretation and planning of experiments. However, this book is a welcome addition to the libraries of research-active chemometricians and represents new material of substantial interest to the specialist.

Richard G. Brereton

H.-H. Perkampus, *UV–visible Spectroscopy and its Applications*, Springer, Berlin, 1992 (ISBN 3-540-55421-1). ix + 244 pp. Price DM 168.00.

A comprehensive and up-to-date account of UV–visible instrumentation and analytical applications would be a welcome contribution to the analytical chemistry literature. The title suggests that this book might be a suitable candidate but examination of the contents list and the text shows it to be something a little different.

The second half of the book is devoted to a very detailed discussion of the use of UV–visible spectrometry for the investigation of chemical equilibria and the kinetics of chemical reactions. It is therefore of more interest to physical organic chemists than to analytical chemists. The early chapters are of more direct relevance to analytical chemists with brief contributions on the origin of electronic spectra and instrumentation and substantial chapters on analytical applications and what are termed recent developments. These are specifically dual-wavelength, derivative, reflectance, photoacoustic and (surprisingly) luminescence spectroscopy. Recent advances in, e.g., chemometrics and solid state detection are only mentioned in passing. There are some useful summary tables in the applications chapter, e.g. of photometric determinations of elements, use of acidic and basic dyes, flotation methods and anionic determinations, but most of these have been reproduced from elsewhere.

I found the layout of the book, particularly the style of the equations and mathematical sections, tiring to read, and this was not helped by the technically correct but linguistically abrupt nature of the text. There are extensive reference lists for most of the chapters, but very few recent citations from the primary literature.

In summary the book contains some useful information for physical organic chemists and analytical chemists using molecular spectroscopy but it is not, in my view, appropriate as a teaching text.

P.J. Worsfold

K. Pfleger, H.H. Maurer and A. Weber, *Mass Spectral and GC Data of Drugs, Poisons, Pesticides, Pollutants and their Metabolites*, 2nd edn., VCH, Weinheim, 1992 (ISBN 3-527-26989-4). Part 1 xv + 1266 pp. Part 2 vii + 1004 pp. Part 3 vii + 1954 pp. Price DM 1290.00.

This compilation of mass spectra and retention indices is the second revised and enlarged edition of a well known reference work. Nearly three times as many spectra are now presented (4370) including new material on pesticides, pollutants, doping agents and designer drugs. The three vol-

umes provide a data base not only of use to clinical and forensic toxicologists but also to food scientists and chemists involved in any form of environmental monitoring. The data is presented in three major sections, the information in each section being deployed according to the problem addressed. The sections are, Tables of Measured Compounds (in order of name, category and retention index), Tables of Potential Poisons (in order of molecular mass, name and category) and CAS registry cross index (in order of common name, registry number and systematic CAS registry name). The standard of presentation of the data is extremely high particularly in relation to the (EI) spectra which are displayed both as mass/intensity listings and graphically. Metabolites of some drugs and poisons are listed under the parent compound.

There is little doubt that all laboratories involved in toxicological investigations should have access to this collection but many other GC–MS users will also find it an invaluable aid to the rapid identification of many compounds of current significance.

Alan D. Roberts

M. Hiraoka (Ed.), *Crown Ethers and Analogous Compounds*, Elsevier, Amsterdam, 1992 (ISBN 0-444-88191-3). 485 pp. Price US$ 228.50/Dfl. 400.00.

This is a timely publication, given the current level of interest in macrocyclic chemistry. It consists of eight chapters written by eleven Japanese authors. Each chapter covers a specific aspect of crown ether chemistry, and all are extensively referenced. Unfortunately, the references date mainly from the mid 1970s to the mid 1980s, and hence the more recent advances in this area are not covered at all. In addition, little reference is made to the extensive patent literature on the applications of crown and related compounds. This makes Hiroshi Tsukube's chapter on "Characteristics of New Crown Compounds" somewhat out of date.

The book commences with a very useful overview of the area by Michio Hiraoka, followed by a comprehensive review of synthetic strategies for making crown compounds by Mitsuo Okahara and Yohji Nakatsuji. The 4th chapter by Keiichi Kimura and Toshiyuki Shano covers applications of crown compounds in analytical and separation chemistry.

The fifth chapter by Shigeki Sasaki and Kenji Koga entitled "Enzyme Modelling with Crown Ethers" is a particularly interesting and important one for the future. Crown ethers can be modified to catalyse synthetic reactions in an enzyme-mimetic manner and may thus be useful tools in gaining an understanding of the very specific and often exceedingly rapid naturally occurring enzymatic reactions. Chapter 6 by Takahiro Kaneda describes the use of chromogenic and fluorescent acerands for selective amine detection. The chapter gives a useful summary of the principles of colour generation on complexation, and includes examples of chiral selective systems. In Chapter 7, Seiji Shinkai reviews progress in the development of 'Switched-on' crown ethers. These are materials with great potential, as the complexation ability of ligands bearing suitable substituent groups can be controlled via an external stimulus such as an electrical potential. Hence complexes with very large stability constants can still be made to release the encapsulated ion.

Finally, Eiichi Kimura reviews developments in macrocyclic polamine chemistry in Chapter 8 and discusses applications as metal and anion binders, chiral receptors, ATP sensors and systems with multiple chelate sites.

Overall, this book is a readable and useful volume reviewing crown ether work carried out up to the mid-to-late 1980s together with implications for the future. The enormous number of compounds cited, extensive references included with each chapter, and a comprehensive index, make this a very useful reference text for anyone working in macrocyclic chemistry.

Dermot Diamond and Stephen J. Harris

Helmward Zollner, *Handbook of Enzyme Inhibitors*, 2nd edn., VCH, Weinheim, 1993 (ISBN 3-527-28436-2). 520 pp. (Part A), 545 pp. (Part B). Price DM 525.00.

These two large volumes comprise almost entirely lists of enzyme inhibitors. In Part A, the lists are arranged in alphabetical order of the enzyme names, and include additional details such as K_i values, 50% or 100% inhibition levels, enzyme source and literature references. Part B comprises lists arranged in alphabetical order of the inhibitors, with only inhibition type and numerical constants included. Other details should be sought in Part A. It also has a glossary of common names of inhibitors, and a listing of enzymes in order of their EC numbers. There are numerous areas of science in which enzymes are involved, including analytical science. For those engaged in such activities this immense listing of inhibitors will be a greatly welcomed first port of call. At a cost of 1 DM for information on ca. 12 inhibitors and 4 enzymes, it also represents good value.

Alan Townshend

Guy Guelachvili and K. Narahari Rao, *Handbook of Infrared Standards II*, Academic Press, San Diego, CA, 1993 (ISBN 0-12-305362-5). ix + 715 pp.

The major part (571 pp) of this compilation records the detailed spectra and tables of wave number (accuracy better than 0.001 cm^{-1}) in the region 1.4 to 4 μm for a number of simple inorganic and organic molecules, as measured by the high resolution Fourier interferometer at the LPMA in Orsay, France. There follows tabulations of heterodyne frequency measurements for a range of simple molecules, collected from the recent literature (39 pp) and of the latest, high accuracy measurements for some OsO_4 lines (6 pp). The final chapter (99 pp) gives spectra and wave number data for methyl chloride in the range 6.2 μm to 7.7 μm.

R.J.H. Clark and R.E. Hester (Eds.), *Biomolecular Spectroscopy, Part B*, Wiley, Chichester, 1993 (ISBN 0-471-93832-7). xix + 344 pp. Price £ 110.00.

This is the second of a pair of books which demonstrates the power of modern spectroscopic techniques in unravelling the complexities of biological structures and processes. It contains chapters on ultrafast IR spectroscopy and protein dynamics, the use of resonance Raman spectroscopy in studies of retinoids, carotenoids and chlorophylls and of heme proteins, and on the spectroscopy, dynamics and function of cytochrome oxidases and other heme-copper oxidases. Two chapters deal with biomolecular chirality and vibrational spectroscopy, as related to amino acids, proteins, carbohydrates and nucleic acids. The final chapter discusses the use of x-ray absorption spectroscopy for locating transition metal sites in proteins.

Electrochemical and Electrocatalytic Reactions of Carbon Dioxide

edited by **B.P. Sullivan**, University of Wyoming, Laramie, WY, USA, **K. Krist**, Gas Research Institute, Chicago, IL, USA and **H.E. Guard**, Office of Naval Research, Department of the Navy, Arlington, VA, USA

The recycling of atmospheric molecules for use as fuels and chemicals is a goal which can only be achieved through a deeper understanding of catalytic processes, particularly electrocatalysis whereby redox transformations can be interfaced with solar or nuclear energy input. Carbon dioxide is a prototypical small molecule in many regards since it is chemically inert. In addition, because of the likely role of carbon dioxide in global temperature cycles, it will be imperative in the future to regulate the output from industrial processes. The purpose of this book is to present a unified discussion of the carbon dioxide chemistry which is necessary for the understanding and design of electrochemically-driven processes for the reduction of carbon dioxide and to provide an impetus for the further development of electrocatalytic carbon dioxide chemistry.

Contents:

1. Thermodynamic, Kinetic, and Product Considerations in Carbon Dioxide Reactivity *(F.R. Keene).*
2. Carbon Dioxide Binding to Transition-Metal Centers *(C. Creutz)*
3. Catalysis of the Water Gas Shift Reaction *(P.C. Ford).*
4. Electrochemical Concentration of Carbon Dioxide *(D.L. Dubois, A. Miedaner, W. Bell, J.C. Smart).*
5. Mechanisms of the Electrochemical Reduction of Carbon Dioxide Catalyzed by Transition Metal Complexes *(F.R. Keene, B.P. Sullivan).*
6. Electrochemical Reduction of CO_2 at Solid Electrodes *(K.W. Frese, Jr.).*
7. Electrocatalysis and Novel Electrodes for High Rate CO_2 Reduction under Ambient Conditions *(A.F. Sammells, R.L. Cook).*
8. Photochemical and Photoelectrochemical Reduction of Carbon Dioxide *(N.S. Lewis, G.A. Shreve).*
Index.

1993 xiv + 300 pages
Price: US $ 212.50 / Dfl. 340.00
ISBN 0-444-88316-9

ELSEVIER
SCIENCE PUBLISHERS

ORDER INFORMATION

For USA and Canada
ELSEVIER SCIENCE PUBLISHERS
Judy Weislogel
P.O. Box 945
Madison Square Station,
New York, NY 10160-0757
Tel: (212) 989 5800
Fax: (212) 633 3880

In all other countries
ELSEVIER SCIENCE PUBLISHERS
P.O. Box 211
1000 AE Amsterdam
The Netherlands
Tel: (+31-20) 5803 753
Fax: (+31-20) 5803 705

US$ prices are valid only for the USA & Canada and are subject to exchange rate fluctuations; in all other countries the Dutch guilder price (Dfl.) is definitive. Books are sent postfree if prepaid.

711/414\140\0001-00

Environmental Analysis

Techniques, Applications and Quality Assurance

Edited by **D. Barceló**

Techniques and Instrumentation in Analytical Chemistry Volume 13

Three aspects of environmental analysis are treated in this book:

- the use of various analytical techniques
- their applications to trace analysis of pollutants, mainly organic compounds
- quality assurance aspects, including the use of certified reference materials for quality control of the entire analytical process.

The book will serve as a general reference for post-graduate students as well as a practical reference for environmental chemists who need to use the analytical techniques for environmental studies. Analytical chemists needing information on the complexity of environmental sample matrices and interferences will also find this an invaluable reference.

Contents: Part 1. Field Sampling Techniques and Sample Preparation. 1. Sampling techniques for air pollutants (R. Niessner). 2. Sample handling strategies for the analysis of organic contaminants from environmental samples (M.-C. Hennion, P. Scribe). 3. Extraction, clean-up and recoveries of persistent trace organic contaminants from sediment and biota samples (D.E. Wells).
Part 2. Application Areas. 4. Current developments in the analysis of polychlorinated biphenyls (PCBs) including planar and other toxic metabolites in environmental matrices (D.E. Wells). 5. Official methods of analysis of priority pesticides in water using gas chromatographic techniques (D. Barceló). 6. Coupled-column reversed phase liquid chromatography as a versatile technique for the determination of polar pesticides (E.A. Hogendoorn, P. van Zoonen). 7. Liquid chromatographic determination of phenols and substituted derivatives in water samples (G. Marko-Varga). 8. HPLC methods for the determination of mycotoxins and phycotoxins (J.F. Lawrence, P.M. Scott). 9. Determination of radionuclides in environmental samples (V. Valkovic).
Part 3. Quality Assurance and Reference Materials. 10. Quality assurance in environmental analysis (W.P. Cofino). 11. Certified reference materials for the quality control of measurements in environmental monitoring (E.A. Maier). 12. Standard reference materials for the determination of trace organic constituents in environmental samples (S.A. Wise).
Part 4. Emerging Techniques. 13. Application of fluorescence spectroscopic techniques in the determination of PAHs and PAH metabolites (F. Ariese, C. Gooijer, N.H. Velthorst). 14. Characterization of surfactants in water by desorption ionization methods (F. Ventura). 15. Utilization of various LC-MS interfacing systems in environmental analysis; application to polar pesticides (M.H. Lamoree, R.T. Ghijsen, U.A.Th. Brinkman). 16. Hyphenated techniques applied to the speciation of organometallic compounds in the environment (O.F.X. Donard, R. Ritsema). 17. The potential of capillary electrophoresis in environmental analysis (M.W.F. Nielen).
Subject index.

© 1993 660 pages Hardbound
Price: Dfl. 465.00 (US $ 265.75)
ISBN 0-444-89648-1

ELSEVIER
SCIENCE PUBLISHERS

ORDER INFORMATION

For USA and Canada
ELSEVIER SCIENCE PUBLISHERS
P.O. Box 945
Madison Square Station
New York, NY 10160-0757
Fax: (212) 633 3880

In all other countries
ELSEVIER SCIENCE PUBLISHERS
P.O. Box 330
1000 AH Amsterdam
The Netherlands
Fax: (+31-20) 5862 845

US$ prices are valid only for the USA & Canada and are subject to exchange rate fluctuations; in all other countries the Dutch guilder price (Dfl.) is definitive. Customers in the European Community should add the appropriate VAT rate applicable in their country to the price(s). Books are sent postfree if prepaid.

414/143/0382

PUBLICATION SCHEDULE FOR 1994

	S'93	O'93	N'93	D'93	J	F	M	A	M			
Analytica Chimica Acta	281/1 281/2 281/3	282/1 282/2 282/3	283/1 283/2	283/3 284/1 284/2	284/3 285/1-2 285/3	286/1 286/2 286/3	287/1-2 287/3 288/1	288/2 288/3 289/1	289/2-3 290/1 290/2			
Vibrational Spectroscopy		6/1			6/2		6/3		7/1			

INFORMATION FOR AUTHORS

Detailed "Instructions to Authors" for *Analytica Chimica Acta* was published in Volume 256, No. 2, pp. 373–376. Free reprints of the "Instructions to Authors" of *Analytica Chimica Acta* and *Vibrational Spectroscopy* are available from the Editors or from: Elsevier Science Publishers B.V., P.O. Box 330, 1000 AH Amsterdam, The Netherlands. Telefax: (+31-20) 5862845.

Manuscripts. The language of the journal is English. English linguistic improvement is provided as part of the normal editorial processing. Authors should submit three copies of the manuscript in clear double-spaced typing on one side of the paper only. *Vibrational Spectroscopy* also accepts papers in English only.

Rapid publication Letters. *Letters* are short papers that describe innovative research. Criteria for letters are novelty, quality, significance, urgency and brevity. Submission data: max. of 2 printed pages (incl. Figs., Tables, Abstr., Refs.); short abstract (e.g., 3 lines); *no* proofs will be sent to the authors; submission on floppy disc; *no* revision will be possible.

Abstract. All papers and reviews begin with an Abstract (50–250 words) which should comprise a factual account of the contents of the paper, with emphasis on new information.

Figures. Figures should be prepared in black waterproof drawing ink on drawing or tracing paper of the same size as that on which the manuscript is typed. One original (or sharp glossy print) and two photostat (or other) copies are required. Attention should be given to line thickness, lettering (which should be kept to a minimum) and spacing on axes of graphs, to ensure suitability for reduction in size on printing. Axes of a graph should be clearly labelled, along the axes, outside the graph itself. All figures should be numbered with Arabic numerals, and require descriptive legends which should be typed on a separate sheet of paper. Simple straight-line graphs are not acceptable, because they can readily be described in the text by means of an equation or a sentence. Claims of linearity should be supported by regression data that include slope, intercept, standard deviations of the slope and intercept, standard error and the number of data points; correlation coefficients are optional.

Photographs should be glossy prints and be as rich in contrast as possible; colour photographs cannot be accepted. Line diagrams are generally preferred to photographs of equipment. Computer outputs for reproduction as figures must be good quality on blank paper, and should preferably be submitted as glossy prints.

Nomenclature, abbreviations and symbols. In general, the recommendations of IUPAC should be followed, and attention should be given to the recommendations of the Analytical Chemistry Division in the journal *Pure and Applied Chemistry* (see also *IUPAC Compendium of Analytical Nomenclature, Definitive Rules*, 1987).

References. The references should be collected at the end of the paper, numbered in the order of their appearance in the text (*not* alphabetically) and typed on a separate sheet.

Reprints. Fifty reprints will be supplied free of charge. Additional reprints (minimum 100) can be ordered. An order form containing price quotations will be sent to the authors together with the proofs of their article.

Papers dealing with vibrational spectroscopy should be sent to: Dr J.G. Grasselli, 150 Greentree Road, Chagrin Falls, OH 44022, U.S.A. Telefax: (+1-216) 2473360 (Americas, Canada, Australia and New Zealand) or Dr J.H. van der Maas, Department of Analytical Molecular Spectrometry, Faculty of Chemistry, University of Utrecht, P.O. Box 80083, 3508 TB Utrecht, The Netherlands. Telefax: (+31-30) 518219 (all other countries).

© 1993, ELSEVIER SCIENCE PUBLISHERS B.V. All rights reserved.

0003-2670/93/$06.00

No part of this publication may be reproduced, stored in a retrieval system or transmitted in any form or by any means, electronic, mechanical, photocopying, recording or otherwise, without the prior written permission of the publisher, Elsevier Science Publishers B.V., Copyright and Permissions Dept., P.O. Box 521, 1000 AM Amsterdam, The Netherlands.

Upon acceptance of an article by the journal, the author(s) will be asked to transfer copyright of the article to the publisher. The transfer will ensure the widest possible dissemination of information.

Special regulations for readers in the U.S.A.–This journal has been registered with the Copyright Clearance Center, Inc. Consent is given for copying of articles for personal or internal use, or for the personal use of specific clients. This consent is given on the condition that the copier pays through the Center the per-copy fee for copying beyond that permitted by Sections 107 or 108 of the U.S. Copyright Law. The per-copy fee is stated in the code-line at the bottom of the first page of each article. The appropriate fee, together with a copy of the first page of the article, should be forwarded to the Copyright Clearance Center, Inc., 27 Congress Street, Salem, MA 01970, U.S.A. If no code-line appears, broad consent to copy has not been given and permission to copy must be obtained directly from the author(s). All articles published prior to 1980 may be copied for a per-copy fee of US $2.25, also payable through the Center. This consent does not extend to other kinds of copying, such as for general distribution, resale, advertising and promotion purposes, or for creating new collective works. Special written permission must be obtained from the publisher for such copying.

No responsibility is assumed by the publisher for any injury and/or damage to persons or property as a matter of products liability, negligence or otherwise, or from any use or operation of any methods, products, instructions or ideas contained in the material herein.

Although all advertising material is expected to conform to ethical (medical) standards, inclusion in this publication does not constitute a guarantee or endorsement of the quality or value of such product or of the claims made of it by its manufacturer.

This issue is printed on acid-free paper.

PRINTED IN THE NETHERLANDS

Analytical Applications of Circular Dichroism

Edited by **N. Purdie** and **H.G. Brittain**

Techniques and Instrumentation in Analytical Chemistry Volume 14

Circular dichroism is a special technique which provides unique information on dissymmetric molecules. Such compounds are becoming increasingly important in a wide variety of fields, such as natural products chemistry, pharmaceutics, molecular biology, etc. The content of this book has been selected in order to feature the unique aspects of circular dichroism, and how these strengths can be of assistance to workers in the field.

Substantial discussions have been provided regarding the particular phenomena associated with dissymmetric compounds which give rise to the circular dichroism effect. Reviews are also given of the type of instrumentation available for the measurement of these effects. A number of chapters cover the wide range of applications illustrating the power of the method.

Owing to its broad appeal, the book will be of interest to workers in all areas of chemistry and pharmaceutical science.

Contents:

1. Introduction to chiroptical phenomena (H.G. Brittain).
2. Instrumentation for the measurement of circular dichroism; past, present and future developments (D.R. Bobbitt).
3. Instrumental methods of infrared and Raman vibrational optical activity (L.A. Nafie *et al.*).
4. Application of infrared CD to the analysis of the solution conformation of biological molecules (M. Diem).
5. Determination of absolute configuration by CD. Applications of the octant rule and the exciton chirality rule (D.A. Lightner).
6. Analysis of protein structure by circular dichroism spectroscopy (J.F. Towell III, M.C. Manning).
7. Chiroptical studies of molecules in electronically excited states (J.P. Riehl).
8. Analytical applications of CD to forensic, pharmaceutical, clinical, and food sciences (N. Purdie).
9. The use of circular dichroism as a liquid chromatographic detector (A. Gergely).
10. Applications of circular dichroism spectropolarimetry to the determination of steroids (A. Gergely).
11. Circular dichroism studies of the optical activity induced in achiral molecules through association with chiral substances (H.G. Brittain).
Subject index.

© 1994 360 pages Hardbound
Price: Dfl. 355.00 (US $ 202.75)
ISBN 0-444-89508-6

ORDER INFORMATION

For USA and Canada
ELSEVIER SCIENCE PUBLISHERS
P.O. Box 945
Madison Square Station
New York, NY 10160-0757
Fax: (212) 633 3880

In all other countries
ELSEVIER SCIENCE PUBLISHERS
P.O. Box 330
1000 AH Amsterdam
The Netherlands
Fax: (+31-20) 5862 845

US$ prices are valid only for the USA & Canada and are subject to exchange rate fluctuations; in all other countries the Dutch guilder price (Dfl.) is definitive. Customers in the European Community should add the appropriate VAT rate applicable in their country to the price(s). Books are sent postfree if prepaid.

ELSEVIER
SCIENCE PUBLISHERS

0003-2670(19931220)284:1;1-C